

**A study of transition from beam-like to
plate-like behaviour in the free vibration of free—
free and clamped-clamped beams and plates**

*A thesis submitted to the University of Manchester for the degree of Doctor of Philosophy
in the Faculty of Science and Engineering*

December 2002

Raad Ali

Dynamics and Aeroelasticity Research Group

Manchester School of Engineering

University of Manchester

ProQuest Number: 10758685

All rights reserved

INFORMATION TO ALL USERS

The quality of this reproduction is dependent upon the quality of the copy submitted.

In the unlikely event that the author did not send a complete manuscript and there are missing pages, these will be noted. Also, if material had to be removed, a note will indicate the deletion.



ProQuest 10758685

Published by ProQuest LLC (2018). Copyright of the Dissertation is held by the Author.

All rights reserved.

This work is protected against unauthorized copying under Title 17, United States Code
Microform Edition © ProQuest LLC.

ProQuest LLC.
789 East Eisenhower Parkway
P.O. Box 1346
Ann Arbor, MI 48106 – 1346

(EERQ4)

✕
TH 23327



JOHN BYLANDS
UNIVERSITY
LIBRARY OF
MANCHESTER

Contents

Abstract	9
Declaration	11
Copyright	11
Dedication	12
Acknowledgements	13

Chapter 1 General Introduction

1.1 Introduction	14
1.2 Historical background	15
1.3 Beam vibration	18
1.4 Plate vibration.....	19
1.5 Summary	21
1.6 Objectives of this thesis	22
1.7 Layout of thesis	23
1.8 Contributions to knowledge	25

Chapter 2 Theoretical vibration analysis of beams and plates.

2.1 Introduction	32
2.2 Vibration theories of beams.....	33
2.2.1 Euler-Bernoulli theory for beam bending vibration.	33
2.2.2 Timoshenko theory beam bending vibration.....	41

2.2.3 Comparison of frequency parameters obtained using Euler-Bernoulli and Timoshenko theories	44
2.2.4 Summary of Equations for bending vibration of beams	49
2.2.5 Torsional vibration of beam	58
2.3 Fundamental equations of classical plate theory	66
2.3.1 Solution of plate equation in rectangular co-ordinates	68
2.4 Comparison of frequency parameter for both free-free and clamped-clamped plate and beams	70
2.5 Summary	74

Chapter 3 Finite element analysis for free-free and clamped-clamped beams and plates

3.1 Introduction	75
3.2 Type of elements	77
3.2.1 Solid element	78
3.2.1 Thin shell element	78
3.2.3 Thick shell element	79
3.2.4 General purpose shell element	80
3.2.5 Full integration versus reduced integration	80
3.2.6 Linear versus quadratic interpolation	81
3.3 Method of the FEA procedure using ABAQUS	82
3.4 Element study	85
3.5 Mesh study	92
3.5.1 Variation of N_y at fixed values of N_x for clamped-clamped beam-plates.....	92
3.5.2 Variation of N_x at fixed value of N_y for clamped-clamped beam-plates.....	97

3.5.3	Variation of N_y at fixed values of N_x for free-free beam-plates.....	101
3.6	Prediction of natural frequencies and mode shapes	104
3.6.1	Deduction of frequency parameters from natural frequencies	105
3.7	Summary	106

Chapter 4 Study of the natural frequency parameters and mode shapes for clamped-clamped beams and plates.

4.1	Introduction	107
4.2	Variations of frequency parameters (λ_{ij}^2) and mode shapes with length-to-breadth ratios (a/b) and mode counters i and j	108
4.2.1	Relationship between frequency parameters and geometric ratios for fixed value of j for clamped-clamped beams and plates	109
4.2.2	Relationship between frequency parameters and geometric ratios for fixed value of i	121
4.3	Combined frequency parameter charts	136
4.4	Frequency parameter charts of other thickness to length ratio.....	141
4.5	Comparison of the frequency parameter charts for different thickness to length ratio with reference to the 1% thickness to length ratio	145
4.6	Summary	153

Chapter 5 Study of the natural frequency parameters and mode shapes for free-free beams and plates.

5.1	Introduction	154
5.2	Variations of frequency parameters (λ_{ij}^2) and mode shapes with length	

-to-breadth ratios and mode counters i and j	155
5.2.1 Relationship between frequency parameters and geometric ratios for fixed value of j	155
5.2.2 Relationship between frequency parameters and geometric ratios for fixed value of i	167
5.3 Combined frequency parameter chart	182
5.4 Effect of thickness to length ratio on frequency parameters.....	187
5.5 Comparison of the frequency parameter chart for different thickness to length ratio	191
5.6 Summary	197

Chapter 6 Defining the transition from beam-like to plate-like behaviour from one-dimensional bending modes of vibration.

6.1 Introduction	198
6.2 study of one-dimensional bending modes for free-free beam-plates.....	199
6.3 Derivation of transition curve based on one-dimensional bending behaviour for 1% thickness to length ratio free-free beam-plates.....	215
6.4 The effect of thickness to length ratio on transition curve obtained from one-dimensional bending modes.....	217
6.5 Study of one-dimensional bending modes for clamped-clamped beam-plates.....	222
6.6 Summary	225

Chapter 7 Deducing transition from beam-like to plate-like response using Symmetric modes of vibration

7.1 Introduction	226
------------------------	-----

7.2	Definition of symmetric and anti-symmetric modes	227
7.3	Obtaining the transition curve from symmetric modes for free-free boundary condition	229
7.3.1	Deduction from frequency parameter charts	229
7.3.2	Deduction from mode shapes	237
7.3.3	Derivation of transition curves and equations for thickness to length ratio 1% free-free beam-plates	246
7.3.4	Obtaining the transition curves from symmetric modes for free-free boundary conditions for other thickness to length ratio.....	249
7.4	Obtaining the transition curve from symmetric modes for clamped-clamped boundary conditions.....	256
7.4.1	Deduction from frequency parameter charts	256
7.4.2	Deduction from modes shapes	264
7.4.3	Derivation of transition curves and equations for 1% thickness to length ratio clamped-clamped beam-plates	273
7.4.4	Obtaining the transition curves from symmetric modes for clamped -clamped boundary conditions for other thickness to length ratio	276
7.5	Summary	282

Chapter 8 Deducing transition from beam-like to plate-like response using anti-symmetric modes of vibration

8.1	Introduction	283
8.2	Obtaining the transition curve from anti-symmetric modes for free-free boundary condition.....	284
8.2.1	Deduction from frequency parameter charts	284

8.2.2	Deduction from modes shapes	285
8.3	Transition curves and equations for free-free beam-plates	294
8.3.1	Tables of transition points.....	294
8.3.2	Transition equations.....	295
8.3.3	Transition curves.....	297
8.4	Obtaining the transition curve from anti-symmetric modes for clamped-clamped boundary conditions	302
8.4.1	Deduction from frequency parameter charts.....	302
8.4.2	Deduction from mode shapes	305
8.5	Transition curves and equations for clamped-clamped beam-plates.....	312
8.5.1	Tables of transition points.....	312
8.5.2	Transition equations.....	313
8.5.3	Transition curves.....	315
8.6	Summary	319

Chapter 9 Experimental and theoretical modal analysis of clamped-clamped and free-free beams and beams

9.1	Introduction	320
9.2	Finite element modal analysis	321
9.3	Experimental modal analysis	322
9.4	Comparison of measured and predicted modal characteristics	326
9.5	Comparison of measured and predicted FRFs	341
9.6	The use of frequency parameter chart to identify mode types from measured FRFs	350
9.7	Summary	355

Chapter 10 General summary, conclusions and recommendations

10.1 General summary.....	356
10.2 Conclusions	361
10.3 Recommendations for future work	363

References	364
-------------------------	------------

Appendix

Appendix 1 Linear Least-Square Method	370
Appendix 2 Solution of the Timoshenko beam equations for the free vibration of clamped-clamped and free-free boundary condition.	376

Abstract

This thesis is a study of the transition from beam-like to plate-like behaviour in the free vibration of free-free and clamped-clamped beams and plates. It is useful, when analysing the vibration behaviour of a beam-plate structure, which is a structure that is either a beam or plate, to classify the structure exactly either as a beam or a plate. If the structure is classified as a beam, then the exact analytical solutions for the bending and torsional vibrations of a beam can be used for the analysis. If the structure is classified as a plate, then an exact analytical solution can be obtained only for simply-supported (pinned) boundary conditions. However, for other boundary conditions, one of the approximate methods, like the finite element (FE) method, needs to be used.

Therefore, the focus of this work is on the classification of the vibration behaviour of beam-plates into beam-like and plate-like behaviour. This was developed by using the FE method to compute the frequency parameters of 160 free-free and clamped-clamped beam-plates of fixed lengths, variable breadths, aspect ratios (length/breadth) which varied from 0.25 to 20.0 and thickness-to-length ratio of 1%, 2%, 5% and 10%.

From the (FE) results generated, it was possible to produce a number of frequency parameter versus aspect ratio graphs. After a thorough investigation of these graphs and the associated mode shapes, transition curves between beam-like and plate-like behaviour were identified. These transition curves were plotted on the graphs of frequency parameter versus aspect ratio. The transition curves define two regions on the graph, namely: the regions of beam-like and plate-like behaviour.

The effect of beam-plate thickness on the transition curves is shown to be important. For each of the four thickness-to-length ratios investigated, a different transition curve and a corresponding transition equation were obtained. It was found that the frequency

parameter has an inverse relation to the thickness of the beam-plates. That is, the thicker the beam-plate the lower the frequency parameter becomes. This is due to the fact that the effect of the increase in stiffness of the beam-plate is less than the effect of the increased mass of the beam-plate. Because of this fact, the frequency parameter does not increase proportionately with the increase in the thickness-to-length ratio. For thickness-to-length ratios of 2% or less, the transition curves are very close. But for thickness-to-length ratios greater than 2%, there are increasing differences between the transition curves as the thickness-length increases.

Experimental modal analysis using the LMS Test System, was used to validate the natural frequencies and mode shapes for free-free beam-plates of aspect ratios 0.5, 2.0 and 3. The same was done for clamped-clamped beam-plates of aspect ratios 1, 2 and 3. A frequency chart was produced for each thickness of free-free and clamped-clamped beam-plates. The use of the frequency charts to identify mode types from measured frequency response functions is also illustrated.

Declaration

No portion of the work referred to in this thesis has been submitted in support of an application for another degree or qualification of this or any other university or other institute of learning.

Copyright

Copyright in text of this thesis rests with the Author. Copies (by any process) either in full, or of extracts, may be made only in accordance with instructions given by the Author and lodged in the John Rylands University Library of Manchester. Details may be obtained from the Librarian. This page must form part of any such copies made. Further copies (by any process) of copies made in accordance with such instructions may not be made without the permission (in writing) of the Author.

The ownership of any intellectual property rights which may be described in this thesis is vested in the University of Manchester, subject to any prior agreement to the contrary, and may not be made available for use by third parties without written permission of the University, which will prescribe the terms and conditions of any such agreement.

Further information on the conditions under which disclosures and exploitation may take place is available from the Head of the School of Engineering.

Dedication

**To my family, father, mother, brothers and sisters, my dear wife and
children**

Acknowledgements

I would like to acknowledge and to thank the following people whose contributions towards my work have been valuable.

Dr S O Oyadiji, for all his help, encouragement, care and invaluable advise during the period of my work. I have learnt much through his enthusiasm and excellent knowledge of dynamics and vibration.

All technicians in the Dynamics Laboratory of the Dynamics and Aeroelasticity Research Group for their help.

All of my friends for their kind help.

Many thanks to my family for their great support and encouragement.

Finally I would like to thank my wife, Mrs Surraya Ali, and my children, Mohamed, Jihad, Saja, Ibrahim and Sujood for their encouragement, moral support, patience and inspiration.

Chapter 1

General Introduction

1.1 Introduction

The distinction between a beam and a plate can sometimes be difficult. In general, a beam can be defined as a structure which has a length which is much longer than its breadth and thickness, whereas a plate is known to have its length and the breadth of the same order of magnitude while its thickness is much smaller than its planar dimensions.

But one can ask, what are the limits between the relative geometric dimensions of a beam and a plate? What are the determining factors for the limit between beam-like and plate-like behaviour? The aim of this thesis is to provide answers to these questions. This is done via the analyses of the vibration characteristics of free-free and clamped-clamped beam-plates. Then, the transition zones in their modal characteristics from beam-like to plate-like behaviour are investigated.

This study is important since there are several engineering applications where an engineering analyst or designer needs to ascertain whether a structural component is a beam or a plate. If the component is a beam or simply supported plate, then he can use analytical equations to compute the vibration characteristics of the component. But if the structure is a plate with other boundary conditions, then numerical methods, such as the finite element and finite difference methods need to be used. In general, it is usually much easier and quicker to use analytical equations to analyse the vibrations of a structure. This approach can be readily used by a designer as it relies on the use of a set of equations. But

the use of numerical methods is usually much more difficult and demanding. Often, it requires a trained analyst to operate sophisticated numerical codes such as commercially available finite element programs.

Previous work by Tangchichit [1,2,3] has involved investigating the transition zones from beam-like to plate-like behaviour for cantilevered beam-plates. The effect of thickness on the transition curves was also investigated. The thickness-to-length ratio considered in his work were 0.2%, 0.4%, 0.6%, 0.8% and 1.0%. He concluded that for this range of thickness-to-length ratio there is very small or no effect on the transition curves. The work covered also the effect of Poisson's ratio on the transition curves and found that Poisson's ratio had no significant effect on the transition curves. The aim of the work presented in this thesis is to extend the earlier work to free-free and clamped-clamped beam-plates of thickness-to-length ratio ranging from 1.0% to 10%.

In this chapter, a brief historical background of the study of the vibration of beams and plates is presented. This is followed by a brief review of the literature regarding beam and plate vibration theories, a description of the objectives of the work presented in the thesis, the layout of the chapters of the thesis. The chapter ends with a description of the contributions made to knowledge from the work presented in this thesis.

1.2 Historical background

The 1700s and early 1800s were productive periods, during which the mechanics of simple elastic structural elements were developed [4]. The theory of thin beam, supported and clamped in different ways, was first studied by Euler in 1744 and Daniel Bernoulli in 1751 [4]. The theory they developed independently is known as the Euler-Bernoulli or thin beam theory.

In 1784 Coulomb carried out both theoretical and experimental studies on the torsional oscillations of a metal cylinder suspended by a wire. He assumed that the

resisting torque of the twisted wire was proportional to the angle of twist. Thus, he derived the equation of motion for the torsional vibration of the suspended cylinder [5].

Stodola developed a method for analysing beam vibration that is applicable to turbine blades. Timoshenko developed a theory for thick beams, which includes the effects of rotary inertia and shear deformation [5]. These effects were not taken into account in the thin beam theory developed by Euler and Bernoulli. The thick beam theory is commonly known as the Timoshenko beam theory.

Similarly, the free vibration of plate has been under investigation for a long time. A brief historical account is provided by Szilard [6]. The story begins again with Euler, who in 1766, established the first mathematical approach to the membrane theory of plates [7]. He solved the problem of the free vibration of rectangular and circular elastic membranes using the idea of two systems of stretched strings placed perpendicular to each other. Euler's work was extended by his student, J. Bernoulli, JR., the great-nephew of the mathematician Bernoulli. Because the torsional resistance of plates was not taken into account in the differential equation of motion, Bernoulli found only similarity between theory and experiments but no general agreement.

The various modes of the free vibrations of plates was discovered by the German physicist, Chladni [8]. He carried out experiments on horizontal plates. He distributed powder evenly on the top of the plates, which formed regular patterns due to vibration. The powder was accumulated along the nodal lines, where no vertical displacements occurred.

Sophie Germain, the French mathematician, was one of several people who participated in a competition, to derive accurately the equations of vibrations of a plate organised by the French Academy in the early part of the 1900s. She established the differential equation for vibration of plates from the calculus of variations. But she

neglected to take account of the work done by warping of the middle surface of the plate in her derivation of the strain energy expression of the plate. She was awarded a prize by the French Academy in 1816. But the judges were not fully satisfied with her work because she did not explain properly the fundamentals. Later, Lagrange, who was one of the judges, corrected her work by adding the missing term. Thus Lagrange is the first to use the correct differential equation of the free vibration of plates.

Navier, the great engineer and bridge designer, was the originator of the modern theory of elasticity. He derived the correct differential equation of rectangular plates with flexural resistance and obtained solutions of various plate problems. He introduced an “exact” method, which transforms the differential equations into algebraic equations for certain boundary conditions. His method is based on the use of trigonometric series introduced by Fourier in the same decade. Poisson has extended Navier’s plate equation, to the lateral vibration of circular plates. His method was applicable only to thick plates.

Kirchhoff is the founder of the extended plate theory, which takes into account the combined bending and stretching of a plate [9]. He discovered the frequency equation of plates and introduced the virtual displacement methods in the solution of plate problems. Kirchhoff theory applies to thin plates. Love [10] and Mindlin [11] have extended Kirchhoffs work to thick plates via the introduction of rotary inertia and shear deformation terms into the thin plate theory. Due to the replacement of wood with structural steel in the construction of ships at the beginning of the 20th century, various plate theories were developed especially by the Russians. Krylov and his student Boobnav have developed extensively the theory of thin plates with flexural and extensional rigidities. Timoshenko exposed the western world to these developments in Russia on the theory of elasticity. and made numerous contributions to the free vibration of plate.

Von Karman developed the differential equation of the large-deflection theory of plates. His work included the problem of effective width and postbuckling behaviour of plates. Westergaard and Schleicher investigated problems of plates on elastic foundation. Reissner [12] has studied the deformations of plate caused by the transverse shear forces. Volmir and Panov considered the nonlinear problems of plate. Oniashvilli and Gontkevitch investigated the free and forced vibration of plates.

In 1956, Turner, Clough, Martin and Topp [13] introduced the finite element method (FE), as a numerical procedure for the solution of complex plate and shell problems. Argyis and Zienkiewicz have contributed extensively to the development of the FE method, which is now widely used in conjunction with computers for fast and efficient solution of plate vibration problems.

1.3 Beam Vibration

There are two main theories for analysing the bending vibrations of a beam. The first theory is the Euler-Bernoulli theory, which is used to study the bending vibrations of thin beams or slender beams. This ignores the effects of shear deformation and rotary inertia of the beam. The second theory is the Timoshenko theory, which considers the effects of shear deformation and rotary inertia of a beam cross section. There are exact, closed-form analytical solutions for the beam equations of motion based on these two theories

Of the two main theories of beam bending vibration, the Euler-Bernoulli is the more elementary. Its derivation is quite straight forward as can be found in several undergraduate texts, for example [14]. This derivation is also illustrated in the next chapter. However the Timoshenko theory is much more complicated. Levinson and

Cooke [15] have summarised this theory by two coupled equations of free motion. They obtained the frequency equation of Timoshenko free-free and clamped-clamped beams.

Ku [16] considered upper and lower bounds for the natural frequency of clamped-clamped beams. His results are summarised in Table 1.1. In his study he used the iterative method based on the Rayleigh and Timoshenko quotients.

Shastry and Rao [17] studied the vibration of short beams with various end conditions. One of these conditions was clamped-clamped boundary condition. They found the results shown in Table 1.2.

Hutchinson [18] studied the natural frequencies of transverse vibration of free beams with rectangular cross-section using the plane stress solution. In comparison to the Timoshenko beam theory the results were found to be accurate.

Torsional vibration of beam has been also considered in this work Blevins [25] has tabulated the torsional frequency parameter equation and the mode shape for various boundary condition of beams. Blevins has also tabulated the torsional constant of different cross section as this will be covered in chapter 2 in more detail.

1.4 Plate Vibration

There are two main theories of plate vibration, namely the Kirchhoff's thin plate theory and the Mindlin's thick plate theory. There are no exact closed form analytical equations to these equations of vibrating plates except in the case of simply-supported (pinned) boundary conditions. Therefore, approximate methods based on the Rayleigh-Ritz technique [19,20], Levy's series solution [21,22] and the finite difference and finite element approach [1,2,3,6] can be used. Some approaches based on the Rayleigh-Ritz method employ the mode shapes of beams or characteristic functions as shape functions to approximate the mode shapes of plates along the length and breadth of the plates.

Warburton [23], considered the free transverse vibrations of rectangular plates with all possible boundary conditions namely free, freely supported, and fixed edges. There are fifteen boundary conditions –all four edges free, freely supported, or fixed and the other twelve cases in which some of the edges have one condition and the rest another. In his paper Warburton stated and used the plate equation, which was originally derived by Love [24].

Warburton proposed an equation for determining the frequency of rectangular plates for all possible boundary conditions consisting of any combination of freely-supported, free, and fixed edges. The plate equation and solutions proposed by Warburton are summarised in Table 1.3.

Blevins [25] obtained results for a clamped-clamped and free-free plate for Poisson's ratio $\nu = 0.3$ as shown in Table 1.4 and Table 1.5. Leissa, Claassen and Thorne [25] studied the frequency parameters for a range of aspect ratios (a/b 0.4, 2/3, 1.0, 1.5, 2.5). Their results are summarised in Table 1.6 for free-free plates and Table 1.7 for clamped-clamped plates.

Sakata and Takahashi [27] studied the natural frequency of clamped-clamped rectangular plate and obtained Table 1.8. Young [19] studied the vibration of a square plate clamped at all four edges, two adjacent edges and one edge i.e. cantilevered plate. In his study he used the products of beam functions and Ritz method to obtain accurate frequencies.

Liew [28] provided a review of existing literature on the vibration of thick plates. Some of these papers, for example Cheung and Chakrabarti [29], considered the free vibration analysis of thick rectangular plates using a finite layer method. Al Janabi [30] studied the free vibration of square plates with different combinations of boundary conditions. Iyengar and Pandya [31] studied the vibration of thick orthotropic rectangular

plates using Vlasov's method of initial functions. Sivakumaran [32] studied the free vibration of thick laminated rectangular plates with free edges, and obtained the mode shapes and frequency parameters for free-free plates. Liew, Hung and Lim [33] studied the three-dimensional vibration of rectangular plates and the effects of thickness and edge constraints on the vibration responses of the plates

Mukhopadhyay [34] used a semi-analytical solution for the free vibration of rectangular plates having various boundary conditions. Bert and Malik [35] considered linear free vibrations of thin isotropic rectangular plates with combinations of boundary conditions. They showed possible analytical solutions for some of the plate boundary conditions. Also they stated that approximate or numerical methods need to be used to obtain solutions for some boundary conditions such as free-free and clamped-clamped. They presented tables of frequency parameters which were for only the first nine modes of vibration and for plate aspect ratios range from 0.4 to 2.5.

Liew, Kam and Chow [36] studied the free vibration analysis of rectangular plates using orthogonal plate functions for some of the plate boundary conditions including clamped-clamped boundary conditions. Tables of frequency parameters were presented for aspect ratios of 0.4 to 2.5.

1.5 Summary

A brief historical background and literature review on the study of vibrations of beams and plates have been presented in this chapter. It is important to be able to separate the behaviour of beam-plates into beam-like and plate-like behaviour so that one can apply the appropriate method or solution.

For all boundary conditions, beam-like bending behaviour is described by exact analytical equations based on Euler-Bernoulli for long slender beams or Timoshenko

theory for thick beams subjected to bending vibration. For beam-like torsional vibration, the torsional theory of beams is used. On the other hand, for plate-like behaviour exact analytical equations exist only for pinned-pinned boundary conditions. However for free-free and clamped-clamped plates, which are investigated in this thesis, approximate numerical methods need to be used. Frequency parameters for free-free and clamped-clamped plates available in the literature cover a small range of aspect ratios which includes 0.4 to 2.5 and a small number of modal frequencies. In the present work, the frequency range is considerably extended and the aspect ratios extend from 0.25 to 20.0. Also regions of transition from beam-like to plate-like behaviour are derived.

1.6 Objectives of this thesis

- To create frequency parameter charts which show the variation of natural frequency parameters with aspect ratios (length/breadth) for clamped-clamped and free-free beams and plates.
- To find the transition curves and transition equations which define the transition from beam-like to plate-like behaviour in the free vibration of clamped-clamped and free-free beam-plates.
- To study the effects of thickness on the frequency parameter charts and on the transition curves and equations.
- To compare natural frequencies, mode shapes and frequency response functions (FRFs) predicted using FEA with experimental results.
- To employ the frequency parameter charts to identify mode types from measured FRFs.

1.7 Layout of thesis

The analysis of the free vibrations of clamped-clamped and free-free beam-plates of thickness-to-length ratios 1%, 2%, 5% and 10% is covered in this thesis. Study of the transition curve from beam-like to plate-like behaviour is investigated. The thesis consist of 10 Chapters. Summaries of the contents of these chapters are as follows:

Chapter 1

In this chapter, a literature survey about the vibration of clamped-clamped and free-free beam-plates is presented. It also covers the objective of this thesis, and outlines the contributions to knowledge.

Chapter 2

The theoretical vibrations of beams and plates is presented in this chapter. This includes the Euler-Bernoulli and the Timoshenko theories for the bending vibration of beams, the torsional vibration theory of beams and the fundamental equations of classical plate theory.

Chapter 3

This chapter discusses the finite element (FE) procedure employed in this work for the analyses of the free vibration of clamped-clamped and free-free beam-plates using ABAQUS, a finite element programme. It includes an element study and a mesh study which were carried out in order to obtain an optimum mesh density and element type for the subsequent FE analyses from which the natural frequencies and mode shapes of the beam-plates were obtained.

Chapter 4

The natural frequency parameters and mode shapes of clamped-clamped beam-plates obtained from FE analyses are presented and discussed. The variations of frequency parameters and mode shapes with length-to-breadth ratios and mode counter

(i,j) are discussed. The discussion includes the relationships between frequency parameters and aspect ratios for fixed value of j , and the relationship between frequency parameters and aspect ratios for fixed value of i . Combined frequency parameter charts for clamped beam-plates are presented. The effect of thickness on the frequency parameters is also studied.

Chapter 5

This chapter is similar to chapter 4. But the focus here is on the modal characteristics of free-free beam-plates.

Chapter 6

This chapter consists of two parts. In the first part the transition curve from beam-like to plate-like behaviour from one-dimensional mode of free-free beam-plates are discussed. The effects of thickness on the transition curves are also covered. In the second parts the clamped-clamped beam-plates are considered. It is shown that it is not possible to obtain transition curves from the one-dimensional bending modes .

Chapter 7

The variation of frequency parameters with aspect ratios for symmetric modes for both free-free and clamped-clamped beam-plates are discussed. The transition curves and equations obtained from the symmetric modes are presented in this chapter. Selected modes shapes for the symmetric modes for both free-free and clamped-clamped beam-plates are also presented.

Chapter 8

Similar to chapter 7, this chapter discusses the anti-symmetric modal characteristics for both free-free and clamped-clamped beam-plates.

Chapter 9

This chapter covers the experimental and theoretical modal analysis of clamped-clamped and free-free beam-plates. The natural frequencies, mode shapes and the FRFs obtained for both free-free and clamped-clamped beam-plates from the FEA are compared with the corresponding experimentally measured modal properties. The use of the frequency parameter charts for the identification of mode types from measured FRFs is also discussed.

Chapter 10

This chapter covers the summary of the results obtained. It also includes the conclusions of the work presented in this thesis. Suggestions for future work are also covered.

1.8 Contributions to knowledge

1. The frequency parameter versus aspect ratio (length/breadth) charts obtained for free-free and clamped-clamped beam-plate boundary conditions cover a much wider range of aspect ratios than is currently available from the technical literature. These charts can be used by designers to determine the natural frequencies and mode shapes of beams and plates. They can also be used by experimental dynamicists to identify mode types present in measured FRFs.
2. The benefit of the use of the frequency parameter charts for the identification of mode types from a measured frequency response function (FRF). This approach is quicker and cheaper than the use of experimental modal analysis which requires the use of FRFs from many geometrical locations.
3. Application of the predominantly one-dimensional bending modes of vibration of free-free and clamped-clamped beams and plates to identify the boundary between beam-like and plate-like behaviour.

4. Derivation of transition curves and equations which express the boundary between beam-like and plate-like behaviour. These curves are plotted on the frequency parameter verses aspect ratio charts and divide the charts into two regions, namely: the beam-like and the plate-like regions. The right region of the transition curves are regions of beam-like behaviour in which one can use simple analytical solutions to predict the vibration behaviour of structures classified as beams. The left regions of the transition curves are regions of plate-like behaviour in which it is necessary to use approximate methods to predict the vibration behaviour of structures classified as plates.
5. Applications of symmetric and anti-symmetric mode shapes to identify the boundary between beam-like and plate-like behaviour in the vibration of clamped-clamped and free-free beams and plates. The transition boundary is expressed by transitions equations and transition curves which are plotted on the frequency parameter versus mode counter charts. The transition curves again define two regions. The region to the left is the beam-like region while the region to the right is the plate-like region.
6. The effect of increasing thickness to length ratio has been shown to reduce the frequency parameter of the beam-plate. This is due to the fact that as the thickness of the beam plate increases, the effect of the increase in stiffness of the beam-plate is less than the effect of the increased mass of the beam-plate. For thickness-to-length ratios of 2% or less, the transition curves are very close. But for thickness-to-length ratios greater than 2%, there is increase in difference in the transition curves.

Table 1.1 Comparison of Estimated frequency parameter for clamped-clamped [16]

Beam Configuration	Iteration	λ_R	λ_T	λ_I	λ_L
Clamp-Clamp	0	29.70	22.38	22.37	17.38
Beam	1	22.37	22.37	22.37	22.37

λ_R - frequency parameters from Rayleigh method $= \omega_R \sqrt{\frac{\rho l^4}{EI}}$, λ_T - frequency parameters from Timoshenko

method $= \omega_T \sqrt{\frac{\rho l^4}{EI}}$, λ_I - The exact frequency parameters $= \omega_I \sqrt{\frac{\rho l^4}{EI}}$ and λ_L - The lower bound eigenvalues

$= \omega_L \sqrt{\frac{\rho l^4}{EI}}$

Table 1.2 Frequency parameter λ found by Shastry and Rao [17]

Beam Configuration	Mode Number	L/R				
		10	25	50	100	500
Clamp-Clamp	1	3.739	4.468	4.656	4.711	4.729
	2	5.389	7.006	7.587	7.782	7.850
	3	6.828	9.260	10.384	10.822	10.989
	4	7.923	11.257	13.013	13.801	14.125
	5	8.287	13.052	15.477	16.710	17.261

L- Length of beam, R- Radius of gyration

Table 1.3 Warburton plate equation and [25] $\frac{\partial^4 w}{\partial x^4} + 2 \frac{\partial^4 w}{\partial x^2 \partial y^2} + \frac{\partial^4 w}{\partial y^4} + \frac{12\rho(1-\sigma^2)}{Egh^2} \frac{\partial^2 w}{\partial t^2} = 0$

Solution: $w = W \sin \alpha x = A \theta(x) \phi(y) \sin \omega t$

$$\lambda^2 = G_x^4 + G_y^4 \frac{a^4}{b^4} + \frac{2a^2}{b^2} (\sigma H_x H_y + (1-\sigma) J_x J_y)$$


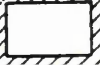

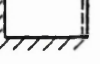
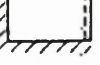


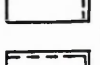
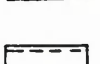

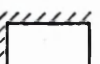
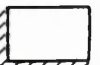



Boundary condition	m	G _x	H _x	J _x	n	G _y	H _y	J _y	Modes m/n ± n/n exist for a = b/2
1 	2, 3, 4, ...	m-1	(m-1) ²	(m-1) ²	2, 3, 4, ...	n-1	(n-1) ²	(n-1) ²	None
2 	2 3, 4, 5, ...	1.506 m-1/2	$\frac{1.248}{(m-1/2)^2} \left[1 - \frac{2}{(m-1/2)^2} \right]$	$\frac{1.248}{(m-1/2)^2} \left[1 - \frac{2}{(m-1/2)^2} \right]$	2 3, 4, 5, ...	1.506 n-1/2	$\frac{1.248}{(n-1/2)^2} \left[1 - \frac{2}{(n-1/2)^2} \right]$	$\frac{1.248}{(n-1/2)^2} \left[1 - \frac{2}{(n-1/2)^2} \right]$	m-n = ±2, 4, 6, ...
3 	0 1 2 3, 4, 5, ...	0 0 1.506 m-1/2	$\frac{0}{(m-1/2)^2} \left[1 - \frac{2}{(m-1/2)^2} \right]$	$\frac{12/\pi^2}{5.017} \left[1 + \frac{6}{(m-1/2)^2} \right]$	0 1 2 3, 4, 5, ...	0 0 1.506 n-1/2	$\frac{0}{(n-1/2)^2} \left[1 - \frac{2}{(n-1/2)^2} \right]$	$\frac{12/\pi^2}{5.017} \left[1 + \frac{6}{(n-1/2)^2} \right]$	m-n = ±2, 4, 6, ...
4 	2, 3, 4, ...	m-1/2	$(m-1/2)^2 \left[1 - \frac{1}{(m-1/2)^2} \right]$	$(m-1/2)^2 \left[1 - \frac{1}{(m-1/2)^2} \right]$	2 3, 4, 5, ...	1.506 n-1/2	$\frac{1.248}{(n-1/2)^2} \left[1 - \frac{2}{(n-1/2)^2} \right]$	$\frac{1.248}{(n-1/2)^2} \left[1 - \frac{2}{(n-1/2)^2} \right]$	None
5 	2, 3, 4, ...	m-1/2	$(m-1/2)^2 \left[1 - \frac{1}{(m-1/2)^2} \right]$	$(m-1/2)^2 \left[1 - \frac{1}{(m-1/2)^2} \right]$	2, 3, 4, ...	n-1/2	$(n-1/2)^2 \left[1 - \frac{1}{(n-1/2)^2} \right]$	$(n-1/2)^2 \left[1 - \frac{1}{(n-1/2)^2} \right]$	m ≠ n
6 	2 3, 4, 5, ...	1.506 m-1/2	$\frac{1.248}{(m-1/2)^2} \left[1 - \frac{2}{(m-1/2)^2} \right]$	$\frac{1.248}{(m-1/2)^2} \left[1 - \frac{2}{(m-1/2)^2} \right]$	2, 3, 4, ...	n-1	(n-1) ²	(n-1) ²	None
7 	2, 3, 4, ...	m-1/2	$(m-1/2)^2 \left[1 - \frac{1}{(m-1/2)^2} \right]$	$(m-1/2)^2 \left[1 - \frac{1}{(m-1/2)^2} \right]$	2, 3, 4, ...	n-1	(n-1) ²	(n-1) ²	None
8 	1 2, 3, 4, ...	0 m-1/2	$\frac{0}{(m-1/2)^2} \left[1 - \frac{1}{(m-1/2)^2} \right]$	$\frac{3/\pi^2}{(m-1/2)^2} \left[1 + \frac{3}{(m-1/2)^2} \right]$	0 1 2 3, 4, 5, ...	0 0 1.506 n-1/2	$\frac{0}{(n-1/2)^2} \left[1 - \frac{1}{(n-1/2)^2} \right]$	$\frac{3/\pi^2}{(n-1/2)^2} \left[1 + \frac{3}{(n-1/2)^2} \right]$	None
9 	1 2, 3, 4, ...	0 m-1/2	$\frac{0}{(m-1/2)^2} \left[1 - \frac{1}{(m-1/2)^2} \right]$	$\frac{3/\pi^2}{(m-1/2)^2} \left[1 + \frac{3}{(m-1/2)^2} \right]$	1 2, 3, 4, ...	0 n-1/2	$\frac{0}{(n-1/2)^2} \left[1 - \frac{1}{(n-1/2)^2} \right]$	$\frac{3/\pi^2}{(n-1/2)^2} \left[1 + \frac{3}{(n-1/2)^2} \right]$	m ≠ n
10 	0 1 2 3, 4, 5, ...	0 0 1.506 m-1/2	$\frac{0}{(m-1/2)^2} \left[1 - \frac{2}{(m-1/2)^2} \right]$	$\frac{12/\pi^2}{5.017} \left[1 + \frac{6}{(m-1/2)^2} \right]$	0 1 2 3, 4, 5, ...	0 0 1.506 n-1	(n-1) ²	(n-1) ²	None
11 	1 2, 3, 4, ...	0 m-1/2	$\frac{0}{(m-1/2)^2} \left[1 - \frac{1}{(m-1/2)^2} \right]$	$\frac{3/\pi^2}{(m-1/2)^2} \left[1 + \frac{3}{(m-1/2)^2} \right]$	1 2, 3, 4, ...	0 n-1	(n-1) ²	(n-1) ²	None
12 	1 2 3, 4, 5, ...	0.597 1.494 m-1/2	$\frac{-0.0870}{1.347} \left[1 - \frac{2}{(m-1/2)^2} \right]$	$\frac{0.471}{3.284} \left[1 + \frac{2}{(m-1/2)^2} \right]$	1 2 3, 4, 5, ...	0.597 1.494 n-1/2	$\frac{-0.0870}{1.347} \left[1 - \frac{2}{(n-1/2)^2} \right]$	$\frac{0.471}{3.284} \left[1 + \frac{2}{(n-1/2)^2} \right]$	None
13 	1 2 3, 4, 5, ...	0.597 1.494 m-1/2	$\frac{-0.0870}{1.347} \left[1 - \frac{2}{(m-1/2)^2} \right]$	$\frac{0.471}{3.284} \left[1 + \frac{2}{(m-1/2)^2} \right]$	1 2 3, 4, 5, ...	0.597 1.494 n-1/2	$\frac{-0.0870}{1.347} \left[1 - \frac{2}{(n-1/2)^2} \right]$	$\frac{0.471}{3.284} \left[1 + \frac{2}{(n-1/2)^2} \right]$	m ≠ n
14 	2 3, 4, 5, ...	1.506 m-1/2	$\frac{1.248}{(m-1/2)^2} \left[1 - \frac{2}{(m-1/2)^2} \right]$	$\frac{1.248}{(m-1/2)^2} \left[1 - \frac{2}{(m-1/2)^2} \right]$	0 1 2 3, 4, 5, ...	0 0 1.506 n-1/2	$\frac{0}{(n-1/2)^2} \left[1 - \frac{2}{(n-1/2)^2} \right]$	$\frac{12/\pi^2}{5.017} \left[1 + \frac{6}{(n-1/2)^2} \right]$	None
15 	1 2 3, 4, 5, ...	0.597 1.494 m-1/2	$\frac{-0.0870}{1.347} \left[1 - \frac{2}{(m-1/2)^2} \right]$	$\frac{0.471}{3.284} \left[1 + \frac{2}{(m-1/2)^2} \right]$	0 1 2 3, 4, 5, ...	0 0 1.506 n-1/2	$\frac{0}{(n-1/2)^2} \left[1 - \frac{2}{(n-1/2)^2} \right]$	$\frac{12/\pi^2}{5.017} \left[1 + \frac{6}{(n-1/2)^2} \right]$	None

Table 1.4 *Frequency parameters of clamped-clamped plates* [25]

Ratio a/b	$(\lambda_{ij}^2)_p, (i, j)^* , i = 1, 2, 3, \dots j = 1, 2, 3, \dots$					
	Mode Sequence					
	1	2	3	4	5	6
0.4	22.35	23.09	25.67	30.63	38.69	49.86
	(1,1)	(1,2)	(1,3)	(1,4)	(1,5)	(1,6)
2/3	22.31	24.31	31.70	46.82	61.57	64.34
	(1,1)	(1,2)	(1,3)	(1,4)	(2,1)	(2,2)
1.0	22.27	26.53	43.66	61.47	67.55	79.90
	(1,1)	(1,2)	(1,3)	(2,1)	(2,2)	(1,4)
1.5	22.21	30.90	61.30	70.96	74.26	118.30
	(1,1)	(1,2)	(2,1)	(1,3)	(2,2)	(2,3)
2.5	22.13	41.69	61.00	92.38	119.9	157.8
	(1,1)	(1,2)	(2,1)	(2,2)	(3,1)	(3,2)

Table 1.5 *Frequency parameters of free-free plates* [25]

ratio a/b	$(\lambda_{ij}^2)_p, (i, j)^* , i = 1, 2, 3, \dots j = 1, 2, 3, \dots$					
	Mode Sequence					
	1	2	3	4	5	6
0.4	3.463	5.288	9.622	11.44	18.79	19.10
	(1,3)	(2,2)	(1,4)	(2,3)	(1,5)	(2,4)
2/3	8.646	9.602	20.74	22.35	25.87	29.97
	(2,2)	(1,3)	(2,3)	(3,1)	(1,4)	(3,2)
1.0	13.49	19.79	24.43	35.02	35.02	61.53
	(2,2)	(1,3)	(3,1)	(3,2)	(2,3)	(4,1)
1.5	20.13	21.60	46.65	50.29	58.20	67.49
	(2,2)	(3,1)	(3,2)	(1,3)	(4,1)	(2,3)
2.5	21.64	33.05	60.14	71.48	117.5	119.4
	(3,1)	(2,2)	(4,1)	(3,2)	(5,1)	(4,2)

* i and j are defined by the number of half-sine waves along the lengthwise and breadthwise directions respectively. But in this thesis, i and j are defined by the number of nodal lines along the lengthwise and breadthwise directions respectively. a & b are length and width of beam.

Table 1.6 Frequency parameters λ for free-free plates (poission ratio=0.3) [26] a & b are length and width of beam

	Ratio a/b				
Mode sequence	0.4	2/3	1.0	1.5	2.5
1	13 3.4629 3.37%	22 8.9459 5.81%	22 13.489 5.26%	22 20.128 5.81%	31 21.643 3.37%
2	22 5.2881 7.40%	13 9.6015 3.56%	13 19.789 13.06%	31 21.603 3.56%	22 33.050 7.40%
3	14 9.6220 2.55%	23 20.735 4.37%	31 24.432 -8.43%	32 46.654 4.37%	41 60.137 2.55%
4	23 11.437 5.58%	31 22.353 0.09%	32 35.024 4.20%	13 50.293 0.09%	32 71.484 5.58%
5	15 18.793 2.94%	14 25.867 5.96%	23 35.024 4.20%	41 58.201 5.96%	51 117.45 2.94%
6	24 19.100 3.41%	32 29.973 -1.67%	41 61.526 0.24%	23 67.494 -1.67%	42 119.38 3.41%

Table 1.7 Frequency parameters λ for clamped-clamped plates (poission ratio=0.3) [26] a & b are length and width of beam

	Ratio a/b				
Mode sequence	0.4	2/3	1.0	1.5	2.5
1	11 22.346 0.12%	11 22.314 0.27%	11 22.272 0.46%	11 22.215 0.71%	11 22.130 1.10%
2	12 23.086 0.06%	12 24.309 0.13%	12 26.529 0.25%	12 30.901 0.56%	12 41.689 1.55%
3	13 25.666 0.42%	13 31.700 0.68%	13 43.664 0.98%	21 61.303 0.60%	21 61.002 1.10%
4	14 30.633 0.75%	14 46.820 1.01%	21 61.466 0.34%	13 70.960 1.20%	22 92.384 0.61%
5	15 38.687 0.33%	21 61.566 0.19%	22 67.549 0.16%	22 74.259 0.27%	31 119.88 0.85%
6	16 49.858 0.49%	22 64.343 0.09%	14 79.904 1.03%	23 118.33 0.99%	32 157.76 0.23%

Table 1.8 [27] Natural radian frequencies of orthotropic rectangular plates

(i, j)	H=D _x , D _y =D _x			H=0.5D _x , D _y =D _x			H=0.5D _x , D _y =0.5D _x		
	b=0.5a	b=a	b=2a	b=0.5a	b=a	b=2a	b=0.5a	b=a	b=2a
(1,1)	22.155	22.230	22.293	22.309	22.326	22.346	22.261	22.300	22.332
(2,1)	60.938	61.254	61.441	61.429	61.528	61.594	61.295	61.460	61.556
(3,1)	119.570	120.179	120.502	120.462	120.658	120.769	120.240	120.541	120.703
(1,2)	39.404	26.666	23.441	30.796	24.586	25.453	30.781	24.568	25.112
(2,2)	83.977	67.407	62.961	73.315	64.646	65.239	73.235	64.571	65.056
(3,2)	144.535	126.853	122.074	133.707	124.071	124.633	133.490	123.913	124.478
(1,3)	118.205	44.307	27.588	103.082	38.450	31.793	81.210	34.990	29.814
(2,3)	162.966	88.021	68.277	137.962	77.748	70.986	122.307	75.965	70.031
(3,3)	228.858	149.482	127.955	194.087	137.082	130.244	183.112	135.940	129.653

H, D_x, D_y flexural rigidities of the plate, a,b are length and width of plate

Chapter 2

Theoretical vibration analysis of beams and plates

2.1 Introduction

There are two main theories for the analysis of the bending vibration of a beam, as has been mentioned in Chapter One. The first theory is the Euler-Bernoulli theory which is for a thin or slender beam where the effects of shear deformation and rotary inertia of the beam are ignored. The second theory is the Timoshenko theory which considers the effects of shear deformation and rotary inertia of a beam whose cross sectional area is not small compared to its length. For plate vibrations, there are two main theories which account for both the bending and torsion of the plate. These are Kirchhoff theory which applies to thin plates for which $t/a < 0.1$, and Mindlin theory which applies to thick plates for which $t/a > 0.1$, where t is plate thickness and a is length of the plate.

This chapter is a review of the above beam theories and Kirchhoff's plate theory. The Cartesian co-ordinate system is used to derive the general solution of the equation

of vibration of thin plates. The solutions for this equation are infinite series expressions that contain arbitrary constants to be found from the boundary conditions of the plate. However, the value of these constants can only be found exactly for plates with simply-supported (pinned) boundary conditions. For other boundary conditions, there is no exact solution to the plate equation. In such cases, frequency parameters which are tabulated in texts on natural frequencies and mode shapes, such as the text by Blevins [24] can be used in conjunction with plate frequency formula. But as pointed out in chapter 1, the frequency parameters tabulated in such texts cover a very small range of aspect ratios. Therefore approximate numerical methods need to be used.

In general the equations of vibration of beams are relatively simple, whereas the plate equations are very complicated. Hence, it is important to classify the behaviour of a beam-plate structure as either beam-like or plate-like. If the behaviour of the beam-plate structure can be classified as beam-like, then the exact beam equations can be used to analyse the vibration of the structure. But if the behaviour of the beam-plate structure can only be classified as a plate-like, then it is easier to use the finite element method to analyse its vibration.

2.2 Vibration theories of beams

2.2.1 Euler –Bernoulli theory for beam bending vibration

Consider the cantilevered beam shown in Figure 2.1. The vibration of the beam in the direction perpendicular to its length is considered. This type of vibration is often called *transverse vibration* or *flexural vibration*, because points on the beam are displaced at right angles to the longitudinal axis of the beam. Figure 2.1 shows a cantilever beam with the transverse direction of vibration indicated (deflection, $w(x,t)$, is in the y direction). The beam is of cross section area $A(x)$, width b , thickness h , length a ,

mass density ρ , elastic modulus E , and flexural (bending) stiffness $EI(x)$, where $I(x)$ is the second moment of area of the cross-section about the z “axis”.

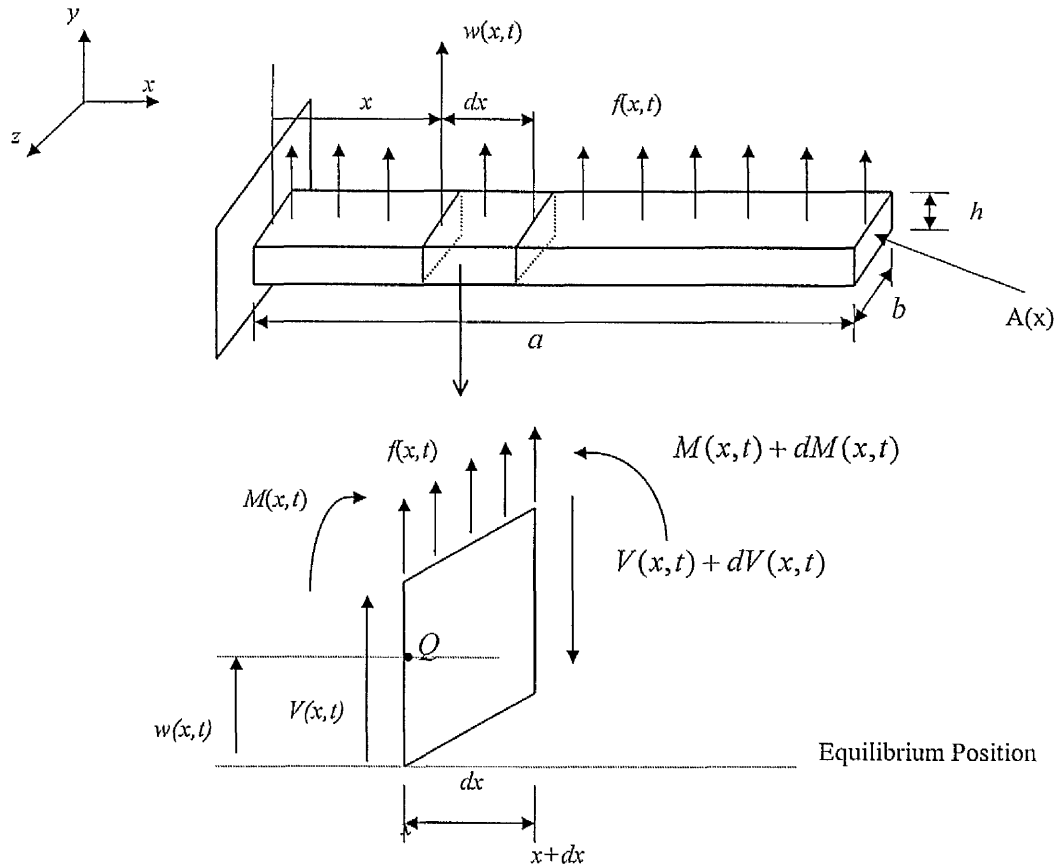


Figure 2.1 Beam in transverse vibration and a free-body diagram of a small element of the beam as it is deformed by a distributed force per unit length, enoted by $f(x,t)$

It is assumed that

- The beam is uniform along its length, and it is slender (b, h small compared to the length of the beam see Figure 2.1);
- It is composed of a linear, homogeneous, isotropic elastic material without axial loads;
- plane sections remain plane after bending deformation;

- plane of symmetry of the beam is also the plane of vibration so that rotation and translation are decoupled;
- rotary inertia and shear deformation can be neglected.

From the free-body diagram of an element of the beam shown in Figure 2.1 the inertia force acting on the element of the beam is

$$\rho A(x) dx \frac{\partial^2 w}{\partial t^2}(x, t) \quad (2.1)$$

From the force diagram of an infinitesimal element of the beam shown in Figure 2.1 we can write the equilibrium equation in y direction as,

$$-(V(x, t) + dV(x, t)) + f(x, t) dx + V(x, t) = \rho A(x) dx \frac{\partial^2 w(x, t)}{\partial t^2} \quad (2.2)$$

where; $V(x, t)$ is the shear force at the left end of the element dx ,

$V(x, t) + \frac{\partial V(x, t)}{\partial x} dx$ is the shear force at the right end of the element dx ,

$f(x, t)$ is the total external force applied to the element per unit length; on the right side of the equation is the inertial force of the element. The assumption of small shear deformation used in Equation (2.2) is true if $a/b \geq 10$ and $a/h \geq 10$ (i.e., for long slender beams) [14]. The moment equation of motion about the y axis passing through the point Q in Figure 2.1 is

$$[M(x, t) + dM(x, t)] - M(x, t) - [V(x, t) + dV(x, t)] dx + [f(x, t) dx] \frac{dx}{2} = 0 \quad (2.3)$$

Substituting; $dV = \frac{\partial V}{\partial x} dx$ and $dM = \frac{\partial M}{\partial x} dx$

and disregarding terms involving second powers in dx , Equation (2.2) and (2.3) can

be written as ;

$$-\frac{\partial V}{\partial x}(x, t) + f(x, t) = \rho A(x) \frac{\partial^2 w}{\partial t^2}(x, t) \quad (2.4)$$

$$\frac{\partial M}{\partial x}(x, t) - V(x, t) = 0 \quad (2.5)$$

Using the relation $V = \frac{\partial M}{\partial x}$ from Equation (2.5), Equation (2.4) becomes

$$-\frac{\partial^2 M}{\partial x^2}(x,t) + f(x,t) = \rho A(x) \frac{\partial^2 w}{\partial t^2}(x,t) \quad (2.6)$$

Also from Solid Mechanics, the beam sustains a bending moment $M(x,y)$ which is related to the beam deflection $w(x,t)$ by [14]

$$M(x,t) = EI(x) \frac{\partial^2 w(x,t)}{\partial x^2} \quad (2.7)$$

where , $M(x,y)$ = bending moment of beam,

E = Young's (elastic) modulus (N/m²),

I = Second moment of area (m⁴),

$w(x,t)$ = beam deflection (m).

From Equations (2.6) and (2.7) we can obtain the equation of motion for the forced lateral vibration of a non-uniform beam as

$$\frac{\partial^2}{\partial x^2} \left[EI(x) \frac{\partial^2 w}{\partial x^2}(x,t) \right] + \rho A(x) \frac{\partial^2 w}{\partial t^2}(x,t) = f(x,t) \quad (2.8)$$

For a uniform beam, Equation (2.8) reduces to

$$EI \frac{\partial^4 w}{\partial x^4}(x,t) + \rho A \frac{\partial^2 w}{\partial t^2}(x,t) = f(x,t) \quad (2.9)$$

For free vibration, $f(x,t) = 0$, and the equation of motion will be

$$c^2 \frac{\partial^4 w}{\partial x^4}(x,t) + \frac{\partial^2 w}{\partial t^2}(x,t) = 0 \quad (2.10)$$

$$\text{where } c = \sqrt{\frac{EI}{\rho A}} \quad (2.11)$$

A separation-of-variable solution, for solving Equation (2.10), is assumed to be of the form ;

$$w(x,t) = W(x)T(t).$$

Substituting this expression into equation (2.10) yields,

$$\frac{c^2}{W(x)} \frac{d^4 W(x)}{dx^4} = -\frac{1}{T(t)} \frac{d^2 T(t)}{dt^2} = a = \omega^2 \quad (2.12)$$

where $a = \omega^2$ is a positive constant

Equation (2.12) can be written as two equations:

$$\frac{d^4 W(x)}{dx^4} - \beta^4 W(x) = 0 \quad (2.13)$$

$$\frac{d^2 T(t)}{dt^2} + \omega^2 T(t) = 0 \quad (2.14)$$

where
$$\beta^4 = \frac{\omega^2}{c^2} = \frac{\rho A \omega^2}{EI} \quad (2.15)$$

The solution for Equation (2.14) can be expressed as

$$T(t) = A \cos \omega t + B \sin \omega t \quad (2.16)$$

where A and B are constant to be found from the initial conditions.

Assuming

$$W(x) = C e^{sx} \quad (2.17)$$

where C and s are constants, and substituting in Equation (2.13) gives the auxiliary equation as

$$s^4 - \beta^4 = 0 \quad (2.18)$$

The roots of this equation are

$$s_{1,2} = \pm \beta \quad s_{3,4} = \pm i\beta \quad (2.19)$$

Therefore the solution of Equation (2.13) becomes

$$W(x) = C_1 e^{\beta x} + C_2 e^{-\beta x} + C_3 e^{i\beta x} + C_4 e^{-i\beta x} \quad (2.20)$$

where C_1, C_2, C_3 and C_4 are constants

Equation (2.20) can also expressed as

$$W(x) = C_1 \cos \beta x + C_2 \sin \beta x + C_3 \cosh \beta x + C_4 \sinh \beta x \quad (2.21)$$

The natural frequencies of the beam can be computed from Equation (2.15) as

$$\omega = \beta^2 \sqrt{\frac{EI}{\rho A}} \quad (2.22)$$

where, the number β depends on the boundary condition.

A. Boundary conditions for a free-free beam.

At the free ends,

$$x = 0 \quad \text{and} \quad x = a$$

$$\text{Bending moment} = EI \frac{\partial^2 w}{\partial x^2} = 0 \quad \text{and} \quad \text{shear force} = \frac{\partial}{\partial x} \left(EI \frac{\partial^2 w}{\partial x^2} \right) = 0$$

From Equation (2.21);

$$\frac{\partial w}{\partial x} = \beta [C_1 \cos \beta x - C_2 \sin \beta x + C_3 \cosh \beta x + C_4 \sinh \beta x] \quad (2.23)$$

$$\frac{\partial^2 w}{\partial x^2} = \beta^2 [-C_1 \sin \beta x - C_2 \cos \beta x + C_3 \sinh \beta x + C_4 \cosh \beta x] \quad (2.24)$$

$$\frac{\partial^3 w}{\partial x^3} = \beta^3 [-C_1 \cos \beta x + C_2 \sin \beta x + C_3 \cosh \beta x + C_4 \sinh \beta x] \quad (2.25)$$

Substituting the boundary condition for free-free beam at $x = 0$ Equation (2.24) and (2.25) equal to zero.

From Equation (2.24)

$$0 = -C_2 + C_4 \quad \longrightarrow \quad C_2 = C_4 \quad (2.26)$$

Similarly from Equation (2.25)

$$0 = -C_1 + C_3 \quad \longrightarrow \quad C_1 = C_3 \quad (2.27)$$

Substituting Equations (2.26) and (2.27) into Equation (2.24) gives:

$$0 = [-C_1 \sin \beta a - C_2 \cos \beta a + C_1 \sinh \beta a + C_2 \cosh \beta a]$$

This can be simplified to:

$$C_1 (\sinh \beta a - \sin \beta a) + C_2 (\cosh \beta a - \cos \beta a) = 0 \quad (2.28)$$

Substituting Equations (2.26) and (2.27) into Equations (2.25) gives:

$$0 = [-C_1 \cos \beta a + C_2 \sin \beta a + C_1 \cosh \beta a + C_2 \sinh \beta a]$$

which can be simplified to:

$$C_1 (\cosh \beta a - \cos \beta a) + C_2 (\sinh \beta a + \sin \beta a) = 0 \quad (2.29)$$

Dividing Equation (2.28) and (2.29) gives,

$$\frac{\sinh \beta a - \sin \beta a}{\cosh \beta a - \cos \beta a} = \frac{\cos \beta a - \cosh \beta a}{-\sin \beta a - \sinh \beta a}$$

which simplifies to:

$$\cos \beta a \cdot \cosh \beta a - 1 = 0 \quad (2.30)$$

Note that in the case of the free-free beam vibration the first two modes are rigid body modes whose natural frequencies are zero.

The use of this frequency equation will be described after the treatment of the clamped-clamped boundary conditions.

B. Boundary conditions for a clamped-clamped beam.

The bending moment and shear force are unrestricted, but the deflection and slope are equal to zero at the ends; i.e.

$$\text{Deflection, } w = 0 \quad \text{at } x = 0, a \quad (2.31)$$

$$\text{Slope, } \frac{\partial w}{\partial x} = 0 \quad \text{at } x = 0, a \quad (2.32)$$

Substituting the boundary condition for a clamped-clamped beam, at $x = 0$ Equation (2.21) yields ;

$$W(a) = C_1 \sin \beta x + C_2 \cos \beta x + C_3 \sinh \beta x + C_4 \cosh \beta x = C_2 + C_4 = 0$$

$$\text{i.e. } C_2 = -C_4$$

Similarly substituting $x = 0$ in to Equation (2.23) gives;

$$\beta [C_1 \cos \beta x - C_2 \sin \beta x + C_3 \cosh \beta x + C_4 \sinh \beta x]_{x=0} = 0$$

$$(C_1 + C_3) = 0 \quad \rightarrow \quad C_1 = -C_3$$

For the other end of the clamped beam substituting for $x = a$ into Equation (2.21) yields:

$$W(a) = C_1 \sin \beta a + C_2 \cos \beta a + C_3 \sinh \beta a + C_4 \cosh \beta a = 0$$

Also,

$$\left. \frac{\partial W}{\partial x} \right|_{x=a} = \beta [C_1 \cos \beta a - C_2 \sin \beta a + C_3 \cosh \beta a + C_4 \sinh \beta a]_{x=a} = 0$$

Substituting for $C_1 = -C_3$ and $C_2 = -C_4$ into the above two equations gives;

$$C_1(\sin \beta a - \sinh \beta a) + C_2(\cos \beta a - \cosh \beta a) = 0 \quad \dots\dots\dots(A)$$

and

$$C_1(\cos \beta a - \cosh \beta a) - C_2(\sin \beta a + \sinh \beta a) = 0 \quad \dots\dots\dots(B)$$

Dividing (A) by (B) results gives,

$$\frac{\sin \beta a - \sinh \beta a}{\cos \beta a - \cosh \beta a} = \frac{-(\cos \beta a - \cosh \beta a)}{\sin \beta a + \sinh \beta a}$$

The above equation can be simplified to:

$$\cosh \beta a \cos \beta a - 1 = 0 \quad (2.33)$$

Notice that in both cases for free-free and clamped-clamped beams, the same frequency equation is obtained. This equation is satisfied by an infinite number of values of βa . The value of βa , denoted here as frequency parameters or λ , are presented in Table 2.1. From Equation (2.18)

$$\omega = \beta^2 \sqrt{\frac{EI}{\rho}}$$

Since $\omega = 2\pi f$

Therefore, $f = \frac{\omega}{2\pi} = \frac{\beta^2}{2\pi} \sqrt{\frac{EI}{\rho}}$

$$\text{or } f = \frac{(\beta a)^2}{2\pi a^2} \sqrt{\frac{EI}{\rho}} \quad (2.34)$$

where f is frequency (Hz)

Mode	βa
1	4.7300
2	7.8532
3	10.9956
4	14.1371
5	17.2787
for $n > 10$	$\frac{(2n+1)\pi}{2}$

Table 2.1 Frequency parameters for free-free and clamped-clamped boundary condition. n is mode number. [24]

2.2.2 Timoshenko theory for beam bending vibration

Unlike the Euler-Bernoulli theory, Timoshenko theory considers the effects of shear deformation and rotary inertia of the cross-section of the beam.

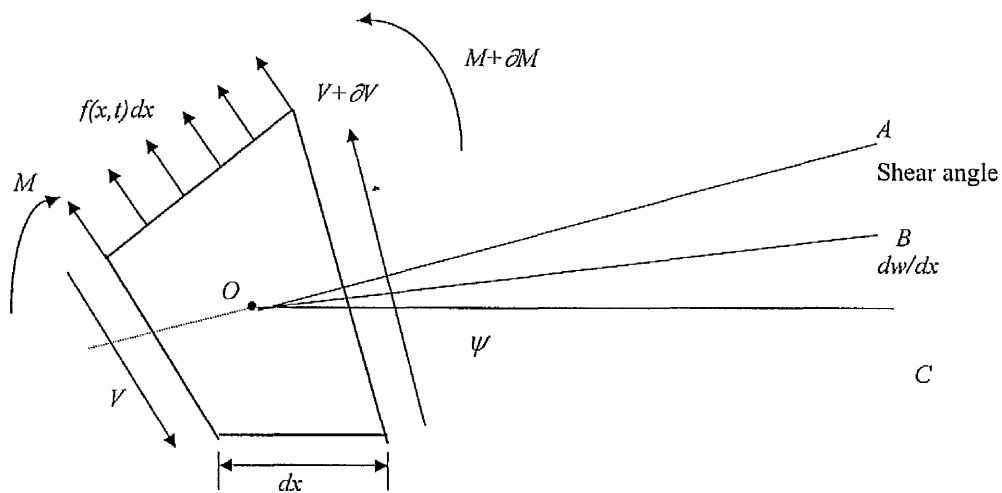


Figure 2.2 Shear deformation effect on an element of a bending beam

Figure 2.2 show the effects of shear deformation on an element of a bending beam. The line OA is a line through the centre of the element dx perpendicular to the face at the right side, line OB , is the line through the centre tangent to the centreline of

the beam, and line OC is the centreline of the beam while at rest. When the beam undergoes bending, the shear angle appears as the length a is decreased relative to the beam width. However in the case of a long beam, the lines OA and OB coincide. The higher shear force will cause the rectangular element shown in Figure 2.1 to distort almost to a diamond shape as shown in Figure 2.2. From Figure 2.1, the shear angle given by $\psi - dw/dx$ (the difference between the total angle due to bending, ψ and the slope of the centreline of the beam, dw/dx), represents the effect of shear deformation as it is shown in Figure 2.2. From Mechanics of Materials, the bending equation is [36]

$$EI \frac{d\psi(x,t)}{dx} = M(x,t) \quad (2.35)$$

Therefore the shear force equation becomes,

$$\kappa AG \left[\psi(x,t) - \frac{dw(x,t)}{dx} \right] = V(x,t) \quad (2.36)$$

where E = Young's modulus, I = Second moment of area, A = cross-sectional area, ψ = total angle due to bending, V = shear force (N), M = bending moment, G = shear modulus, κ = shear coefficient (dimensionless factor that depends on the shape of the cross-sectional area.), As in the case of Equation (2.2), The equation of motion is;

$$\rho A(x) dx \frac{\partial^2 w(x,t)}{\partial t^2} = - \left[V(x,t) + \frac{\partial V(x,t)}{\partial x} dx \right] + V(x,t) + f(x,t) dx \quad (2.37)$$

If rotary inertia is included, then the moment balance on dx previously given by Equation (2.3) becomes;

$$\begin{aligned} \rho I(x) dx \frac{\partial^2 \psi(x,t)}{\partial t^2} &= \left[M(x,t) + \frac{\partial M(x,t)}{\partial x} dx \right] - M(x,t) \\ &+ \left[V(x,t) + \frac{\partial V(x,t)}{\partial x} dx \right] dx + f(x,t) \frac{dx^2}{2} \end{aligned} \quad (2.38)$$

Substitution of Equation (2.35) and (2.36) into (2.37) and (2.38) yields the two coupled equations,

$$\frac{\partial}{\partial x} \left[EI \frac{\partial \psi}{\partial x} \right] + \kappa A G \left(\frac{\partial w}{\partial x} - \psi \right) = \rho I \frac{\partial^2 \psi}{\partial t^2} \quad (2.39)$$

and

$$\frac{\partial}{\partial x} \left[\kappa A G \left(\frac{\partial w}{\partial x} - \psi \right) \right] + f(x, t) = \rho A \frac{\partial^2 w}{\partial t^2} \quad (2.40)$$

Assuming constant value for all coefficients in the above equation and that there is no external force applied, the term $\psi(x, t)$ can be eliminated from the coupled equations which will reduce to one single equation for the free vibration of uniform beams:

$$EI \frac{\partial^4 w}{\partial x^4} + \rho A \frac{\partial^2 w}{\partial t^2} - \rho I \left(1 + \frac{E}{\kappa G} \right) \frac{\partial^4 w}{\partial x^2 \partial t^2} + \frac{\rho^2 I}{\kappa G} \frac{\partial^4 w}{\partial t^4} = 0 \quad (2.41)$$

This equation is known as the Timoshenko beam equation.

The boundary condition for **free-free** beams are

$$\kappa A G \left(\frac{\partial w}{\partial x} - \psi \right) = EI \frac{\partial \psi}{\partial x} = 0$$

Also the boundary conditions for both **clamped ends** of a beam are:

$$\psi(x, t) = w(0, t) = 0 \quad (2.42)$$

$$\psi(x, t) = w(a, t) = 0 \quad (2.43)$$

These equations can be solved by the methods suggested for the beam model given by Equation (2.9).

2.2.3 Comparison of frequency parameters obtained using Euler-Bernoulli and Timoshenko theories.

The coupled equations of free motion from Timoshenko beam theory are given by,

$$\left. \begin{aligned} \kappa \frac{\partial}{\partial x} AG \left(\psi + \frac{\partial w}{\partial x} \right) &= \rho A \frac{\partial^2 w}{\partial t^2} \\ \kappa AG \left(\psi + \frac{\partial w}{\partial x} \right) - \frac{\partial}{\partial x} \left(EI \frac{\partial \psi}{\partial x} \right) &= -\rho I \frac{\partial^2 \psi}{\partial t^2} \end{aligned} \right\} \quad (2.44)$$

- where A = the area of the beam section
 E = Young's modulus
 G = shear modulus
 I = second moment of area of the beam section
 t = time
 $w(x,t)$ = transverse deflection of the beam axis
 x = co-ordinate measured along the beam axis
 κ = Timoshenko shear coefficient
 ρ = mass density of the beam
 $\psi(x,y)$ = rotation of the beam section

From Equation (2.44), the frequency equation for the vibration of a **free-free** beam is [10]

$$2 + [(\lambda_1 \alpha_1 / \lambda_2 \alpha_2) - (\lambda_2 \alpha_2 / \lambda_1 \alpha_1)] \sinh \lambda_1 L \sin \lambda_2 L - 2 \cosh \lambda_1 L \cos \lambda_2 L = 0 \quad (2.45)$$

and for a **clamped-clamped** beam [15]

$$2 + [(\alpha_2^2 \lambda_1^2 - \alpha_1^2 \lambda_2^2) / \alpha_1 \alpha_2 \lambda_1 \lambda_2] \sinh \lambda_1 L \sin \lambda_2 L - 2 \cosh \lambda_1 L \cos \lambda_2 L = 0 \quad (2.46)$$

$$\text{where} \quad \alpha_{1,2} = \left(\frac{\rho \omega^2}{\kappa G} \pm \lambda_{1,2}^2 \right) \quad (2.47)$$

$$\lambda_{1,2}^2 = \sqrt{\left(\frac{\beta^4 \omega^4}{4} + \delta \omega^2 \right)} \mp \frac{\beta^2 \omega^2}{2} \quad (2.48)$$

$$\delta = \frac{\rho}{E} \left(\frac{A}{I} - \frac{\rho \omega^2}{\kappa G} \right) \quad (2.49)$$

$$\beta^2 = \frac{\rho}{E} \left(1 + \frac{E}{\kappa G} \right) \quad (2.50)$$

L = beam length

Consider a rectangular section free-free and clamped-clamped aluminium beam of length $L = 0.5\text{m}$, breadth $b = 0.05\text{ m}$ and thickness $t = 0.005\text{ m}$; $\rho = 2700\text{ kg/m}^3$, $\nu = 0.33$, $E = 70 \times 10^9\text{ N/m}^2$, $G = 26.3 \times 10^9\text{ N/m}^2$, $\kappa = 5/6$. Substitute these parameters into Equations (2.49) and (2.50). The value obtained for δ, β^2 was then substituted into Equations (2.47) and (2.48), and then back substituted for $\alpha_{1,2}$ and $\lambda_{1,2}^2$ into Equation (2.45) and (2.46). This was done using a MATLAB program as described in Appendix 3. The numerical values of ω and λ are shown in Table 2.2 for a free-free beam and Table 2.3 for a clamped-clamped beam.

ω_T = angular frequency from Timoshenko Beam equation.

ω_E = angular frequency from Euler-Bernoulli Beam equation, calculated from Equation (2.50) by using frequency parameters (λ_E) from Table (2.1)

λ_T = frequency parameters of Timoshenko Beam equation, calculated from Equation (2.52) by using ω_T .

λ_E = frequency parameters of Euler-Bernoulli Beam equation, from Table (2.1)

Table 2.2 Angular frequencies and frequency parameters of a free-free beam from Timoshenko and Euler-Bernoulli beam equations. Beam properties: $L=0.5$ m, $t=0.005$ m, $b=0.05$ m, $\rho=2700\text{kg/m}^3$, $\nu=0.33$, $E=70\times 10^9\text{N/m}^2$, $G=26.3\times 10^9\text{N/m}^2$, $\kappa=5/6$

Mode No.	ω_T	λ_T^2	ω_E	λ_E^2
1	104.63	22.35	104.69	22.273
2	288.20	61.58	288.61	61.672
3	564.34	120.59	565.76	120.903
4	931.44	199.04	935.23	199.859
5	1388.72	296.76	1397.06	298.553
6	1935.12	413.53	1951.28	416.99
7	2569.43	549.08	2597.87	555.165
8	3290.22	703.12	3336.87	713.079
9	4095.93	875.30	4168.14	890.732
10	4984.86	1065.26	5091.82	1088.123

Table 2.3 Angular frequencies and frequency parameters of a clamped-clamped beam from Timoshenko and Euler-Bernoulli beam equations. Beam properties: $L=0.5$ m, $t=0.005$ m, $b=0.05$ m, $\rho=2700\text{kg/m}^3$, $\nu=0.33$, $E=70\times 10^9\text{N/m}^2$, $G=26.3\times 10^9\text{N/m}^2$, $\kappa=5/6$

Mode No.	ω_T	λ_T^2	ω_E	λ_E^2
1	104.59	22.35	104.69	22.273
2	287.99	61.54	288.61	61.672
3	563.76	120.47	565.76	120.903
4	930.21	198.78	935.23	199.859
5	1386.49	296.29	1397.06	298.553
6	1931.46	412.75	1951.28	416.99
7	2563.85	547.89	2597.87	555.165
8	3282.18	701.40	3336.87	713.079
9	4084.82	872.92	4168.14	890.732
10	4970.03	1062.09	5091.82	1088.123

The frequency parameters of a beam are related to its natural frequencies and dimensions by,

$$\lambda^2 = \omega L^2 \sqrt{\frac{\rho A}{E I}} \quad (2.51)$$

For a rectangular beam , $I = \frac{1}{12}bh^3$ and $A = bh$. Therefore,

$$\lambda^2 = \omega L^2 \sqrt{\frac{12\rho}{Eh^2}} \quad (2.52)$$

The data shown in Tables 2.2 and 2.3 are for aspect ratio 10 for free-free and clamped-clamped boundary conditions. The frequency parameters were computed at other aspect ratios for the Timoshenko theory using Equation (2.45) and (2.46). For the Euler-Bernoulli theory, the frequency parameter is constant at all aspect ratio. These frequency parameters obtained from the Euler-Bernoulli and Timoshenko frequency equations are compared with finite element (FE) predictions in Figure 2.3 for the thickness to length ratio 1% (5 mm thick) free-free beam. The results show that the predictions of the Euler-Bernoulli theory are closer to the FE predictions for the first nine bending modes predicted. The predictions of the Timoshenko theory correlate closely with the FE predictions up to mode 6. For higher modes, slightly larger deviations are observed. This implies that the correction for rotary inertia and/or shear deformation effects is too much.

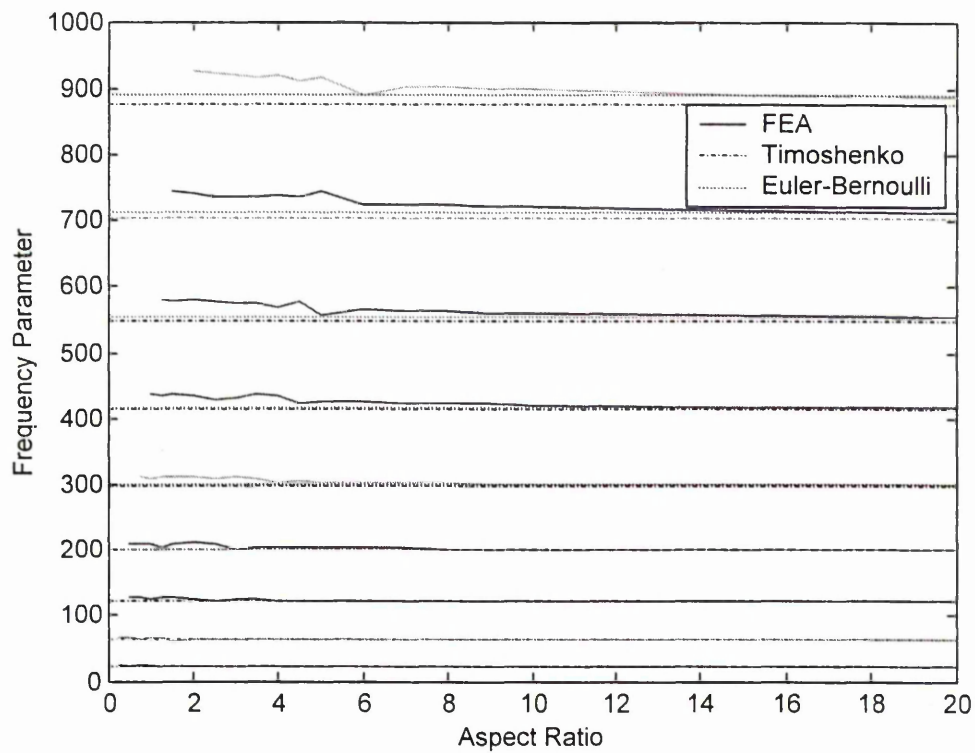


Figure 2.3 Comparison of predicted frequency parameters derived from the thickness to length ratio 1% (5 mm thick) free-free beam-plate.

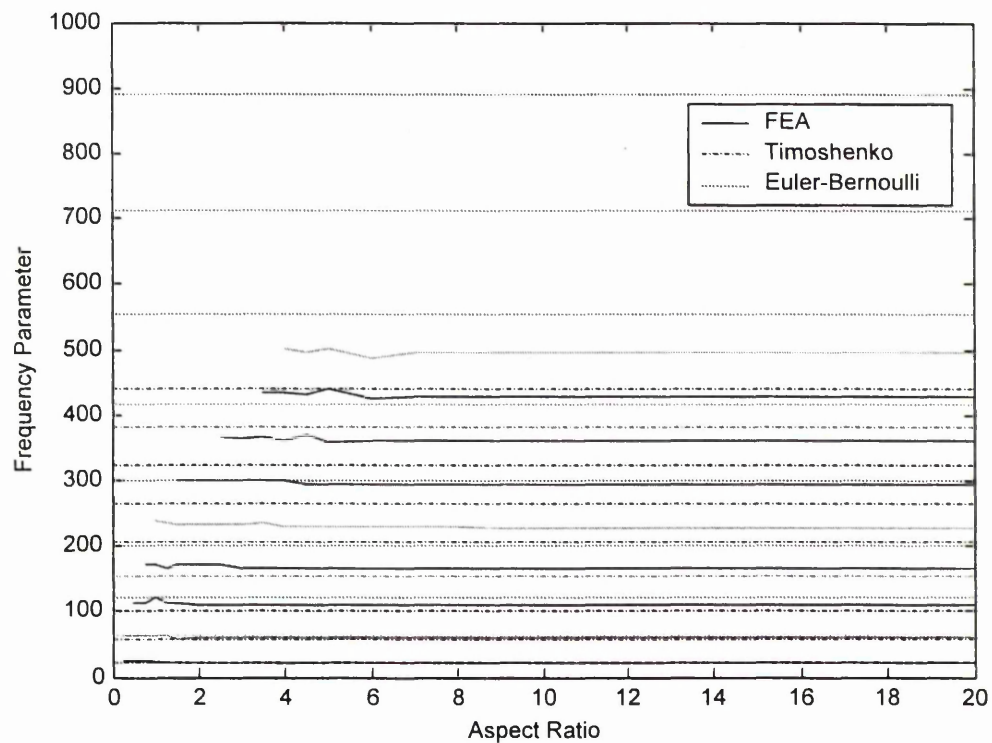
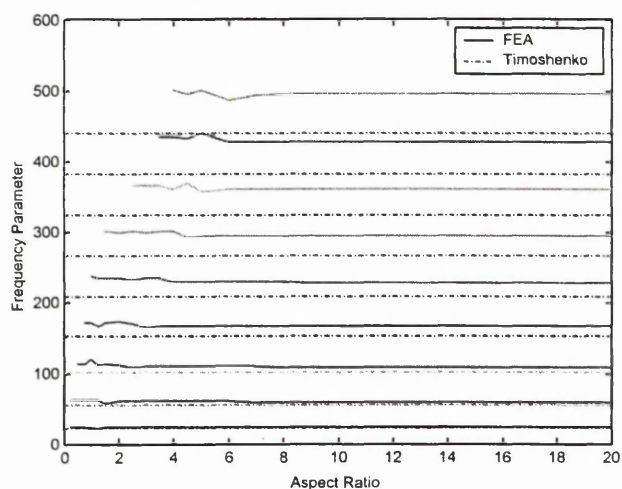
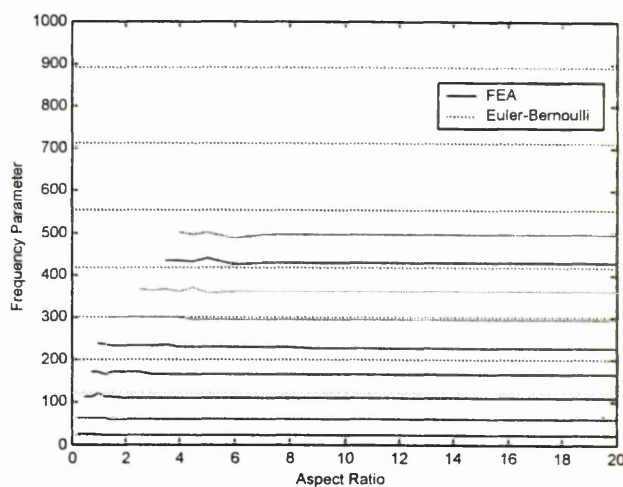


Figure 2.4(a) Comparison of predicted frequency parameters derived from the thickness to length ratio 10% (50 mm thick) free-free beam-plate.



(b)



(c)

Figure 2.4 Comparison of predicted frequency parameters derived from the thickness to length ratio 10% (50 mm thick) free-free beam-plate.

Similarly Figure 2.4(a) represent the combined frequency parameter results compute from the FE, Timoshenko and Euler-Bernoulli equation. Due to scale of this figure this figure was plotted again for FE and Timoshenko results as shown in Figure 2.4(b) and FE and Euler-Bernoulli as in Figure 2.4(c) The results show that the predictions of the Timoshenko theory are closer to the FE predictions for the first nine bending modes predicted. The predictions of the Euler-Bernoulli theory correlate closely with the FE predictions up to mode 3. For higher modes than 3 very larger deviations are observed between Euler-Bernoulli

2.2.4 Summary of Equations for Bending Vibration of Beams.

The effect of shear deformation and rotary inertia on the natural frequency of beams was investigated by Nash and Collar [37]. In one case they studied the effect of the rotary inertia in the equation of beam vibration. In another case, they demonstrated the effect of shear deformation alone. Finally they showed the effect of both shear deformation and rotary inertia on the original Euler-Bernoulli equation of beam

vibration. Their solution was presented in terms of the symmetric and anti-symmetric modes of vibration for various boundary conditions. The summarised equations for free-free and clamped-clamped conditions as follows. In these equations, 'Bending' denotes the elementary Euler-Bernoulli beam equation, 'Shear' denotes inclusion of shear deformation effects, while 'Rotary inertia' denotes inclusion of rotary inertia effects.

(1) Free-free beam: symmetric mode frequency equations

For Bending + Shear + Rotary Inertia ($\phi^2 \alpha \beta < 1$)

$$p(p^2 - \phi^2 \alpha) \cos p \sinh q + q(q^2 + \phi^2 \alpha) \sin p \cosh q = 0 \quad (2.53)$$

For Bending + Shear + Rotary Inertia ($\phi^2 \alpha \beta > 1$)

$$p(p^2 - \phi^2 \alpha) \cos p \sin r - r(r^2 - \phi^2 \alpha) \sin p \cos r = 0 \quad (2.54)$$

For Bending + Shear

$$q_1 \cos p_1 \sinh q_1 + p_1 \sin p_1 \cosh q_1 = 0 \quad (2.55)$$

For Bending + Rotary Inertia

$$p_2^3 \cos p_2 \sinh q_2 + q_2^3 \sin p_2 \cosh q_2 = 0 \quad (2.56)$$

For Bending

$$\cos \sqrt{\phi} \sinh \sqrt{\phi} + \sin \sqrt{\phi} \cosh \sqrt{\phi} = 0 \quad (2.57)$$

(2) Free-free beam: anti-symmetric mode frequency equations

For Bending + Shear + Rotary Inertia ($\phi^2 \alpha \beta < 1$)

$$p(p^2 - \phi^2 \alpha) \sin p \cosh q - q(q^2 + \phi^2 \alpha) \cos p \sinh q = 0 \quad (2.58)$$

For Bending + Shear + Rotary Inertia ($\phi^2 \alpha \beta > 1$)

$$p(p^2 - \phi^2 \alpha) \sin p \cos r - r(r^2 - \phi^2 \alpha) \cos p \sin r = 0 \quad (2.59)$$

For Bending + Shear

$$q_1 \sin p_1 \cosh q_1 - p_1 \cos p_1 \sinh q_1 = 0 \quad (2.60)$$

For Bending + Rotary Inertia

$$p_2^3 \sin p_2 \cosh q_2 - q_2^3 \cos p_2 \sinh q_2 = 0 \quad (2.61)$$

For Bending

$$\sin \sqrt{\phi} \cosh \sqrt{\phi} - \cos \sqrt{\phi} \sinh \sqrt{\phi} = 0 \quad (2.62)$$

(3) Clamped-clamped beam: symmetric mode frequency equations

For Bending + Shear + Rotary Inertia ($\phi^2 \alpha \beta < 1$)

$$q(p^2 - \phi^2 \alpha) \sin p \cosh q + p(q^2 + \phi^2 \alpha) \cos p \sinh q = 0 \quad (2.63)$$

For Bending + Shear + Rotary Inertia ($\phi^2 \alpha \beta > 1$)

$$r(p^2 + \phi^2 \alpha) \sin p \cos r - r(r^2 - \phi^2 \alpha) \cos p \sin r = 0 \quad (2.64)$$

For Bending + Rotary Inertia

$$p_1 \sin p_1 \cosh q_1 + q_1 \cos p_1 \sinh q_1 = 0 \quad (2.65)$$

For Bending + Shear

$$q_2^3 \sin p_2 \cosh q_2 + p_2^3 \cos p_2 \sinh q_2 = 0 \quad (2.66)$$

For Bending

$$\sin \sqrt{\phi} \cosh \sqrt{\phi} + \cos \sqrt{\phi} \sinh \sqrt{\phi} = 0 \quad (2.67)$$

(4) For clamped-clamped beam: anti-symmetric mode frequency equations

For Bending + Shear + Rotary Inertia ($\phi^2 \alpha \beta < 1$)

$$q(p^2 + \phi^2 \alpha) \sin p \cosh q - p(q^2 - \phi^2 \alpha) \cos p \sinh q = 0 \quad (2.68)$$

For Bending + Shear + Rotary Inertia ($\phi^2 \alpha \beta > 1$)

$$r(p^2 - \phi^2 \alpha) \sin p \cos r - r(p^2 + \phi^2 \alpha) \cos p \sin r = 0 \quad (2.69)$$

For Bending + Rotary Inertia

$$q_1 \sin p_1 \cosh q_1 - p_1 \cos p_1 \sinh q_1 = 0 \quad (2.70)$$

For Bending + Shear

$$p_2^3 \sin p_2 \cosh q_2 - q_2^3 \cos p_2 \sinh q_2 = 0 \quad (2.71)$$

For Bending

$$\sin \sqrt{\phi} \cosh \sqrt{\phi} - \cos \sqrt{\phi} \sinh \sqrt{\phi} = 0 \quad (2.72)$$

The parameters in the frequency equations are defined as follows:

$$\phi^2 = \sigma \omega^2 L^4 / B$$

$$\alpha = B / CL^2$$

$$\beta = k^2 / L^2$$

$$2p^2 = \phi^2(\alpha + \beta) + \sqrt{\phi^4(\alpha - \beta)^2 + 4\phi^2}$$

$$2q^2 = -\phi^2(\alpha + \beta) + \sqrt{\phi^4(\alpha - \beta)^2 + 4\phi^2}$$

ϕ = frequency parameter,

σ = mass per unit length of beam,

ω = circular frequency of vibration

α = parameter proportional to shear flexibility

β = parameter proportional to rotary inertia

k = radius of gyration of beam section

p, q, r = 'slave' parameters dependent on ϕ, α, β

B = bending stiffness

L = beam length

C = shear stiffness

MATLAB software was used to solve the above frequency equations. This was done by fixing the beam length at 0.5 m. and varying the breadth. The mode number against frequency was plotted as shown in Figures 2.5 and 2.6 for free-free and clamped-clamped beams of thickness to length ratios 1% and 10% respectively. Figures 2.5 (a), (b), (c) and Figures 2.6 (a), (b), (c) are for clamped-clamped boundary conditions while Figures 2.5 (d), (e), (f) and Figures 2.6 (d), (e), (f) are for free-free boundary conditions. In these figures BSRI denotes Bending + Shear + Rotary Inertia, BS denotes Bending + Shear, BRI denotes Bending + Rotary Inertia, and B denotes Bending.

From Figure 2.5 it is clearly seen that the effect of the rotary inertia and shear deformation on the natural frequency for 1% thickness to length ratio beam is very small for modes 1 to 30. For modes greater than 30, the effects of shear deformation and rotary inertia cause increasing decrease in the natural frequencies of the beam.

Figure 2.6 shows that for 10% thickness to length ratio, the effects of shear deformation and rotary inertia cause significant decrease in the value of the natural frequencies of the thicker beam for modes greater than 3. The figures also show that the shear deformation has a much greater effect (by factors of up to 3) in reducing the natural frequencies than rotary inertia. The combined effects of shear deformation and rotary inertia results in a reduction of the natural frequencies by factors of between 1 and 7.

Figures 2.7 and 2.8 represent the separate and combined effects of shear deformation and rotary inertia overlayed by the FE result obtained from the ABAQUS software for both 1% and 10% thickness to length ratio clamped-clamped and free-free and for aspect ratios 0.25 to 20. The FE results are presented at this stage only as reference data. They represent the true behaviour of the beam. Figures 2.7 shows that for beam thickness to length ratio 1% the FE results are close to those of the bending only i.e. ignoring the effect of shear deformation and rotary inertia. This suggests that as expected, the effect of shear deformation and rotary inertia for thin beam is very small. On the other hand Figure 2.8 shows that for the 10% thickness to length ratio beam, the FE predictions are closer to those of the beam including shear deformation and rotary inertia effects.

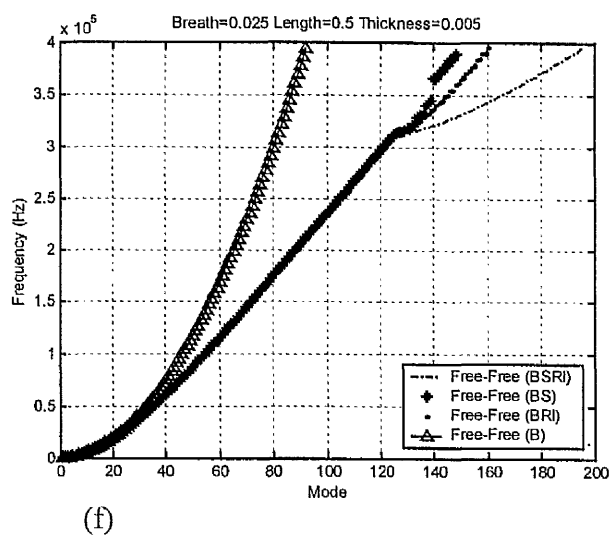
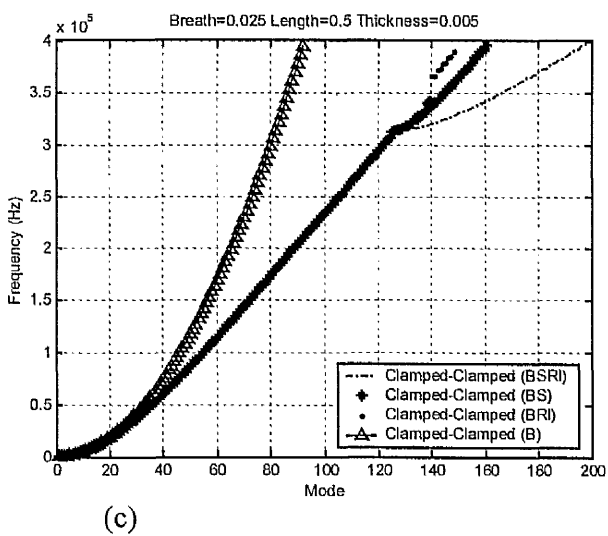
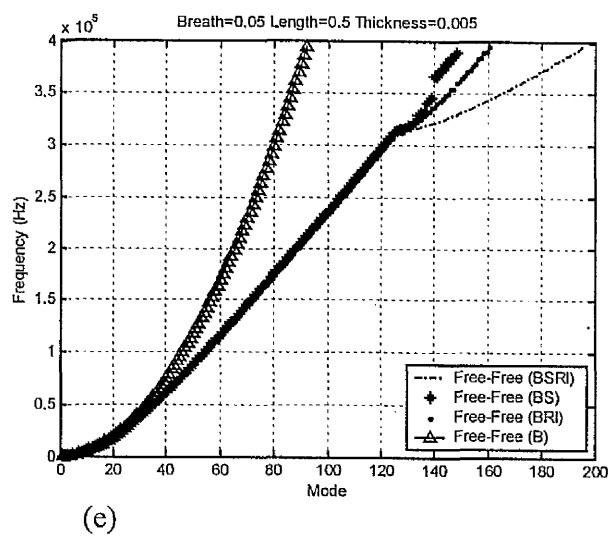
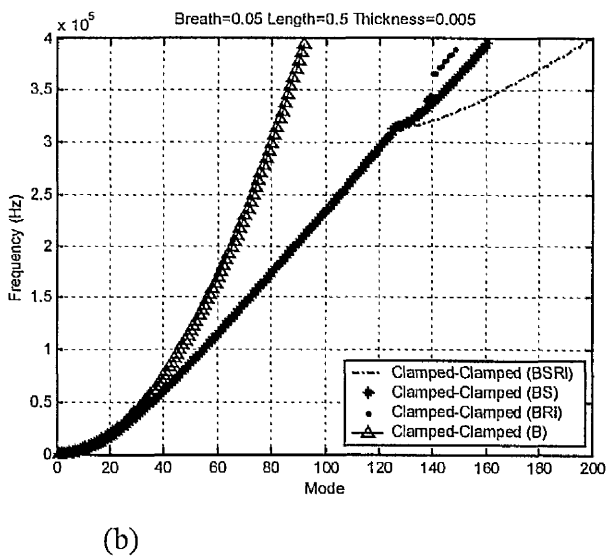
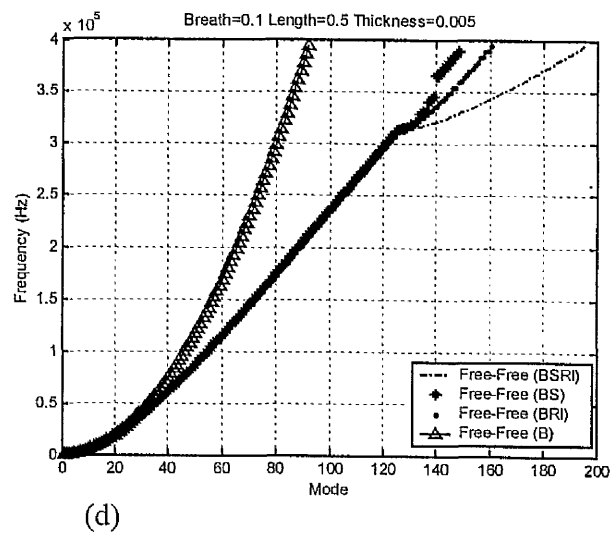
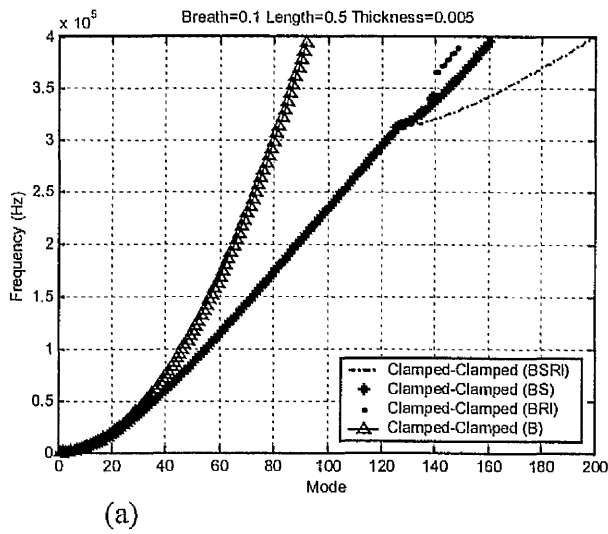
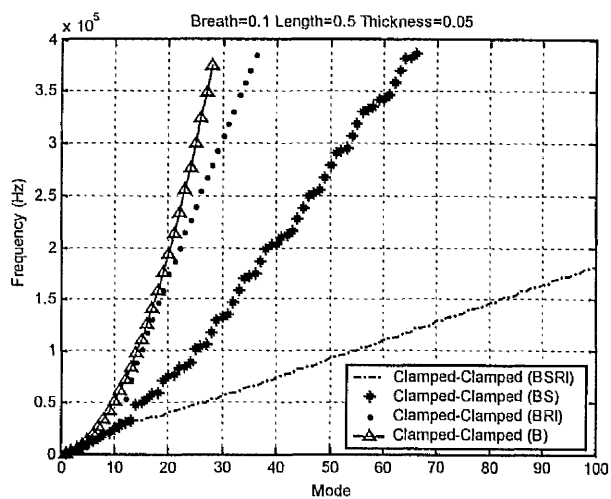
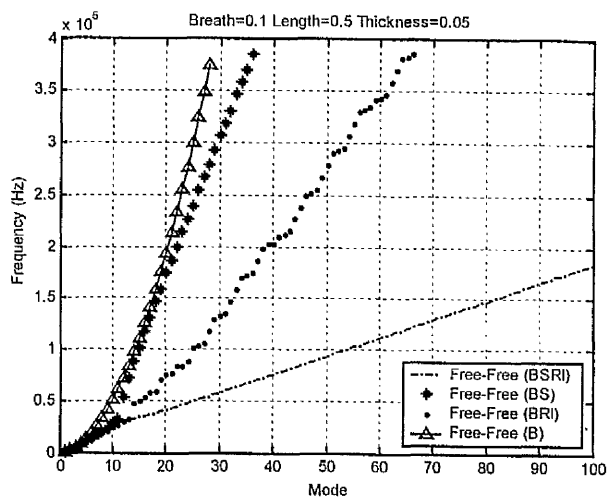


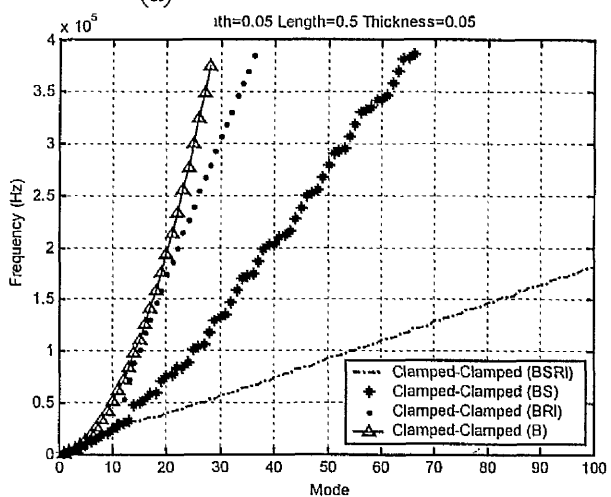
Figure 2.5 Effect of the rotary inertia and shear deformation on the natural frequency of beam for thickness to length ratio 1%



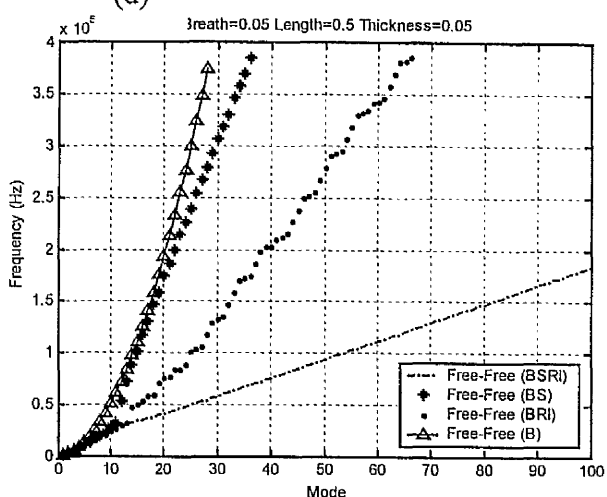
(a)



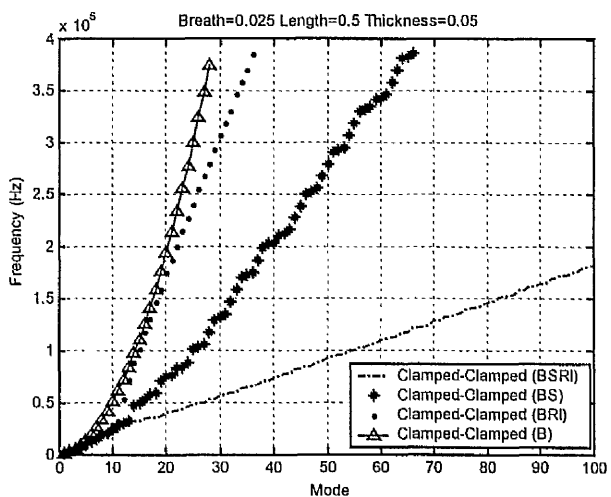
(d)



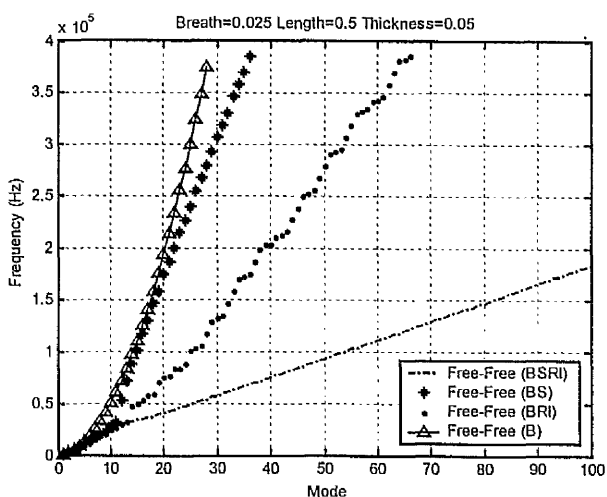
(b)



(e)



(c)



(f)

Figure 2.6 Effect of the rotary inertia and shear deformation on the natural frequency of beam for thickness to length ratio 10%

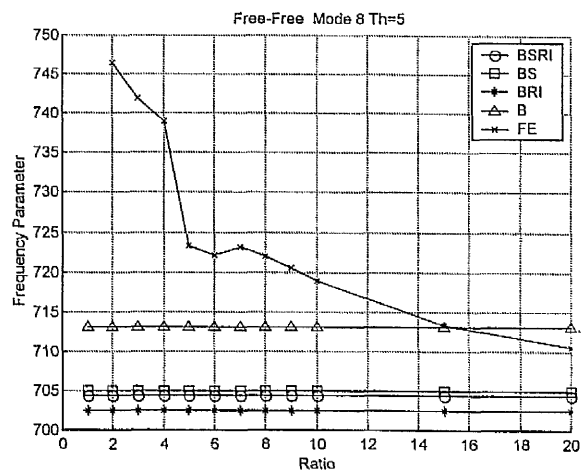
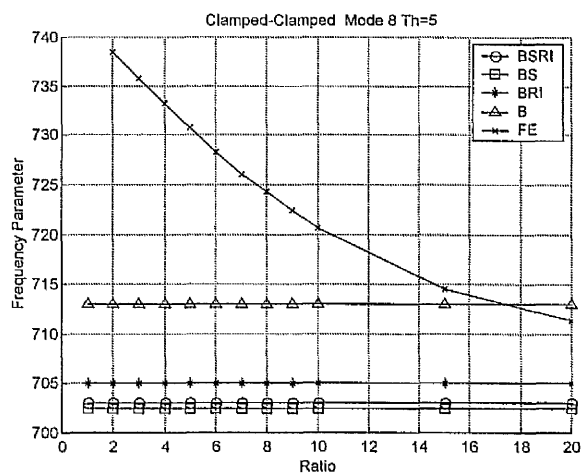
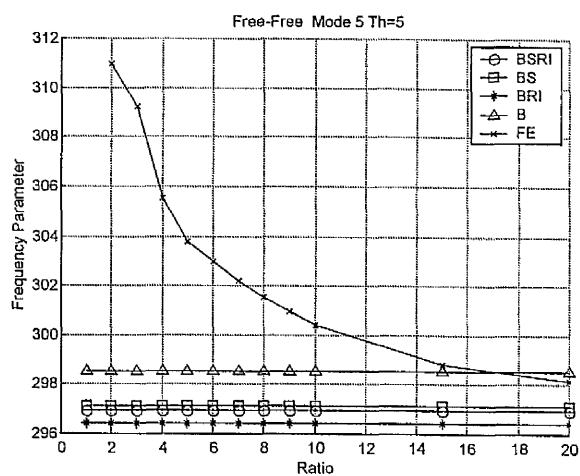
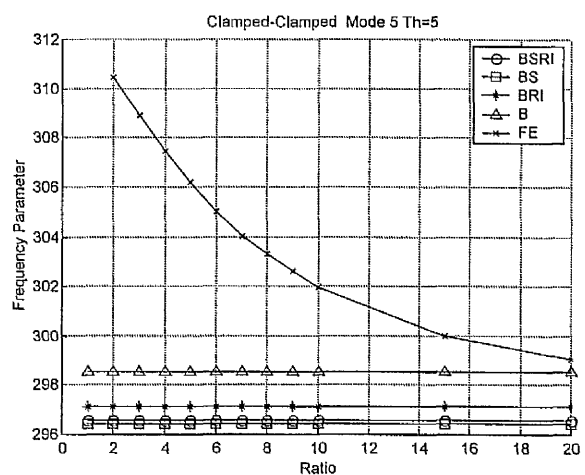
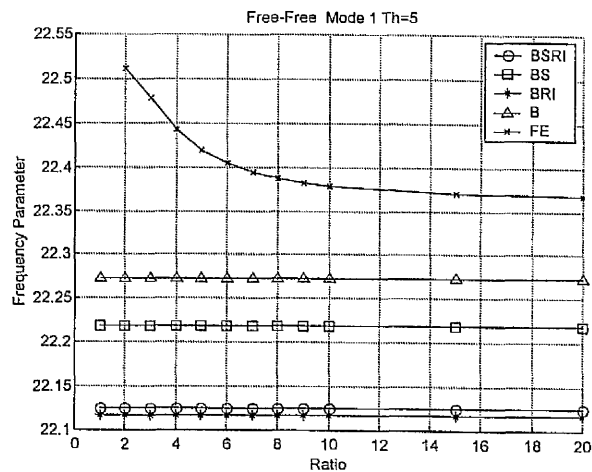
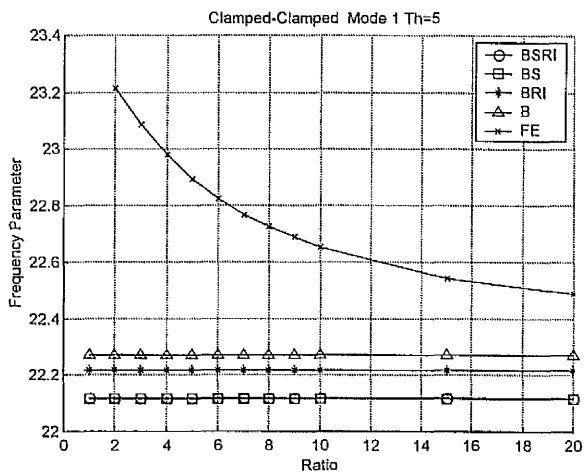


Figure 2.7 Effect of the rotary inertia and shear deformation on the frequency parameter of beam and plates for thickness to length ratio 1%

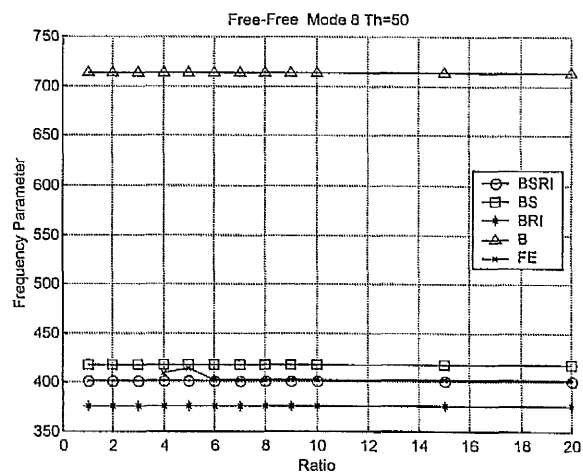
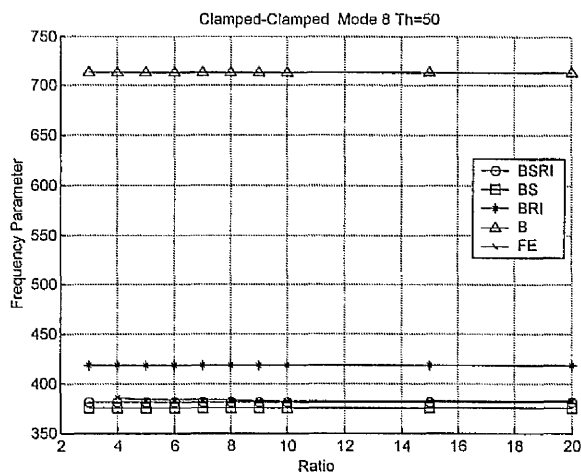
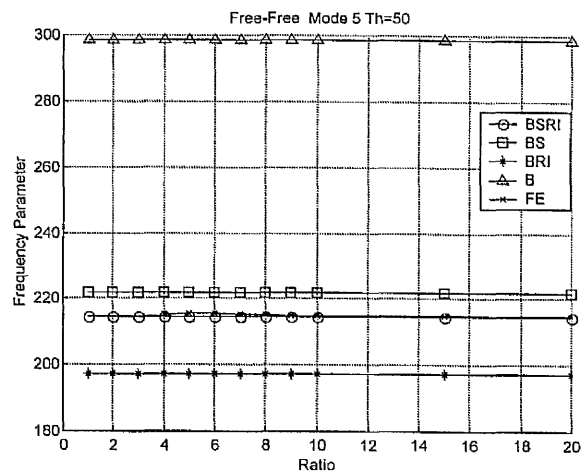
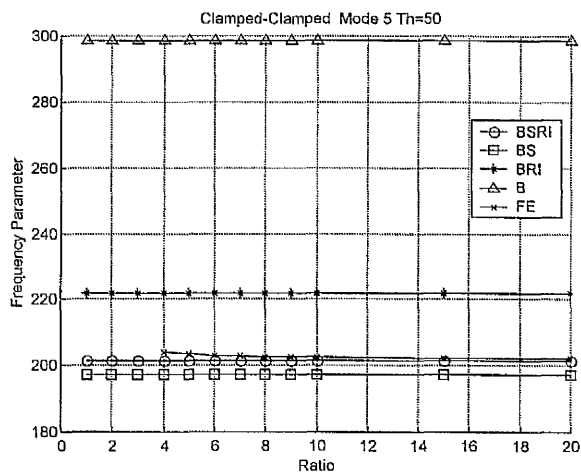
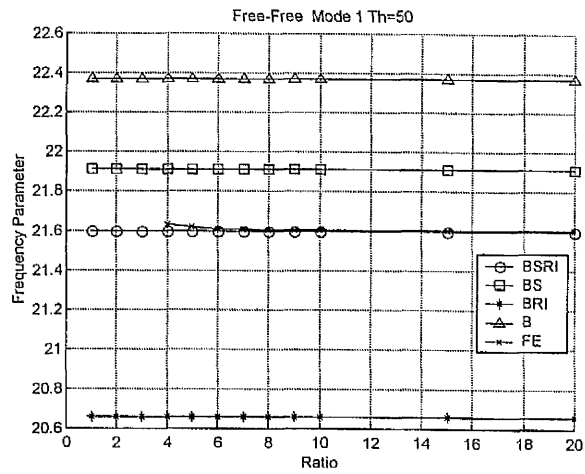
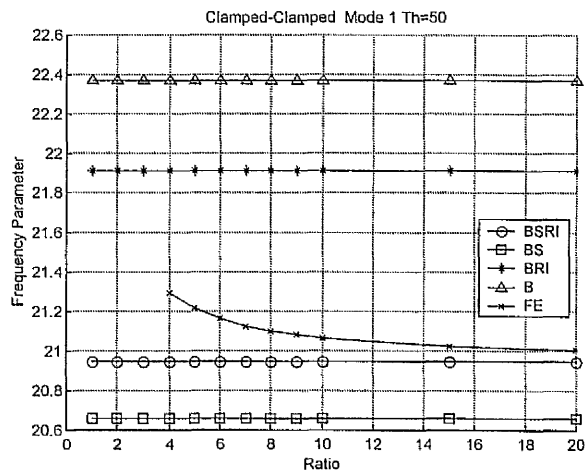


Figure 2.8 Effect of the rotary inertia and shear deformation on the frequency parameter of beam and plates for thickness to length ratio 10%

2.2.5 Torsional vibration of beam

The free-free and clamped-clamped beams may also vibrate in the torsional direction.

Therefore in this section, the theory of the torsional vibration of a beam is presented. The development of the theory is based on a circular-section rod or shaft. But the subsequent application is based on a rectangular-section beam. Consider the circular shaft of length l as shown in Figure 2.9. Torsional vibration occurs in an angular direction around the centre axis of the shaft in a plane parallel to the cross section of the shaft. The rotation of the shaft, θ , about the centre axis is a function of both position along the length of the shaft, x , and time, t . Thus θ is a function of two variables denoted $\theta(x,t)$. The equation of motion can be determined by considering a moment balance of an infinitesimal element of the shaft of length dx . The torque at the right face of the element, as shown in Figure 2.9, is τ , while that at the left end, at position $x+dx$, is $\tau + \frac{\partial \tau}{\partial x} dx$. From Mechanics of Solids, the applied torque is related to the torsional deflection by [14]

$$\tau = GI \frac{\partial \theta(x,t)}{\partial x} \quad (2.73)$$

where GI is the torsional stiffness composed of the shear modulus G and the polar moment of area I of the cross section. The polar moment of area could be a function of x as well but is considered constant here. The total torque acting on dx becomes [14]

$$\tau + \frac{\partial \tau}{\partial x} dx - \tau = I_o \frac{\partial^2 \theta}{\partial t^2} dx \quad (2.74)$$

where I_o is the polar moment of inertia of the shaft per unit length and $\frac{\partial^2 \theta}{\partial t^2}$ is the angular acceleration. If the shaft is of uniform circular cross section, I_o becomes simply

$I_o = \rho I$, where ρ is the shaft's material density. Substituting the torque given by Equation (2.73) into Equation (2.74) yields :

$$\frac{\partial}{\partial x} \left(GI \frac{\partial \theta}{\partial x} \right) = \rho I \frac{\partial^2 \theta}{\partial t^2} \quad (2.75)$$

Simplifying for the case of constant stiffness GI yields

$$\frac{\partial^2 \theta(x,t)}{\partial t^2} = \left(\frac{G}{\rho} \right) \frac{\partial^2 \theta(x,t)}{\partial x^2} \quad (2.76)$$

for the equation of twisting vibration of a circular shaft.

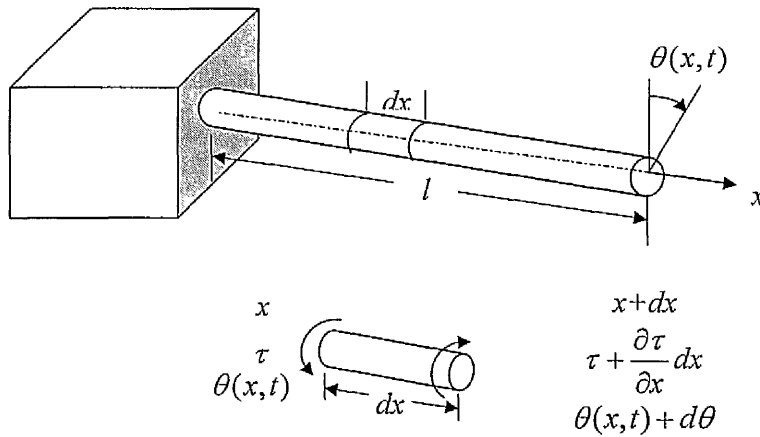


Figure 2.9 Circular shaft illustrating an angular motion, $\theta(x,t)$, as the result of a moment acting on a differential element dx of the shaft of density ρ , length l and given modulus G . The function $\theta(x,t)$ denotes the angle of twist.

For other types of cross sections, the torsional equation of a shaft can still be used to approximate the torsional motion by replacing I in Equation (2.73) with a torsional constant J defined to be the moment required to produce a torsional rotation of a rod of unit length divided by the shear modulus. Thus a shaft with noncircular cross section can be approximated by the equation [14]

$$\frac{\partial^2 \theta(x,t)}{\partial t^2} = \left(\frac{GJ}{\rho I} \right) \frac{\partial^2 \theta(x,t)}{\partial x^2} \quad (2.77)$$

Torsional constant, J , for rectangular cross section is presented in Table 2.4.

The solution of Equation (2.77) depends on two initial conditions in time, i.e. $\theta(x,0)$ and $\theta_t(x,0)$, and two boundary conditions, one at each end of the structure. For example the boundary conditions for clamped-clamped beams, are

$$(\text{deflection at } 0) \quad \theta(0,t) = 0,$$

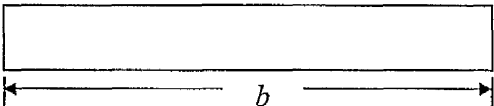
$$(\text{deflection at } x) \quad \theta_x(l,t) = 0$$

These boundary condition can then determine the solution to the above equation.

$$\frac{\partial^2 \theta(x,t)}{\partial t^2} = \left(\frac{GJ}{\rho I} \right) \frac{\partial^2 \theta(x,t)}{\partial x^2} = c^2 \frac{\partial^2 \theta(x,t)}{\partial x^2} \quad (2.78)$$

$$\text{where } c^2 = \frac{GJ}{\rho I}$$

Table 2.4 Torsional constant for rectangular cross section [25].

Cross section																	
Torsional constant	$J = \frac{c b^3 t^3}{b^2 + t^2}$ <table border="1"> <thead> <tr> <th>b/t</th><th>1</th><th>2</th><th>3</th><th>8</th><th>∞</th></tr> </thead> <tbody> <tr> <td>c</td><td>0.281</td><td>0.286</td><td>0.299</td><td>0.312</td><td>$\frac{1}{3}$</td></tr> </tbody> </table>					b/t	1	2	3	8	∞	c	0.281	0.286	0.299	0.312	$\frac{1}{3}$
b/t	1	2	3	8	∞												
c	0.281	0.286	0.299	0.312	$\frac{1}{3}$												

From Blevins' work [25], the torsional natural frequency is given by;

$$f_i = \frac{w_i}{2\pi} = \frac{\lambda_i}{2\pi L} \sqrt{\frac{JG}{\rho I_p}} \quad (2.79)$$

$$\text{where; } J = \frac{c b^3 t^3}{b^2 + t^2} \quad I_p = \frac{b^3 t}{12} + \frac{b t^3}{12} \quad (2.80)$$

From Equation (2.79) and (2.80),

$$\lambda_i^2 = \frac{\pi^2 f_i^2 \rho}{3Gc} \left(\frac{ab}{t}\right)^2 \left[1 + \left(\frac{t}{b}\right)^2\right]^2 \quad (2.81)$$

Similarly,

$$f_i = \frac{2\sqrt{3c}\lambda_i}{2\pi a} \sqrt{\frac{G}{\rho}} \frac{bt}{(1 + \frac{t^2}{b^2})} \quad (2.82)$$

For clamped-clamped and free-free beam-plates,

$$\lambda_i = i\pi$$

Therefore,

$$f_{iTorsion} = \frac{it\sqrt{3c}}{ab[1 + (\frac{t}{b})^2]} \sqrt{\frac{G}{\rho}}$$

$$\lambda_{iTorsion}^2 = 2\pi L^2 f_{iTorsion} \sqrt{\frac{12\rho(1-\nu^2)}{Eh^2}} \quad (2.83)$$

Figure 2.10 shows the comparison of the frequency parameter with aspect ratio obtained from torsion frequency equation for thickness to length ratio 10% shown in dashed line and 1% thickness to length ratio shown in solid line, this show that for 10% thickness to length ratio the frequency parameter is smaller than that of the 1% thickness to length ratio. In comparison this figure show a similar results obtained from the FE analysis i.e. the value of the frequency parameter for the 10% thickness to length ratio beam plate is significantly smaller than that for the 1% thickness to length ratio beam-plates in particle at higher aspect ratio.

The reason why the slope of the frequency parameter curves reduce as thickness increases, is that as the thickness increases, bending stiffness, torsional stiffness, mass and mass moment of inertia increase, but the effect of increase in bending and torsional stiffness are less than that effects of increase of mass and mass moment of inertia. i.e. bending k_b and torsional k_t stiffness do not increase at the same rate as thickness increases.

For bending, increases in thickness causes increase in rotary inertia effect which enhances the effects of mass

$$f_B \propto \sqrt{k_B/m}$$

$$f_T \propto \sqrt{k_B/I}$$

so as thickness increases, bending and torsional stiffness don't increase at the rate they should

Figures 2.11 and 2.12 shows comparison of the torsional frequency parameter and the FE frequency parameter for thickness to length ratio 1% and 10% beam with aspect ratio. From these figures it is clearly seen that the torsional frequency parameter agree with the FE in particular at low mode number

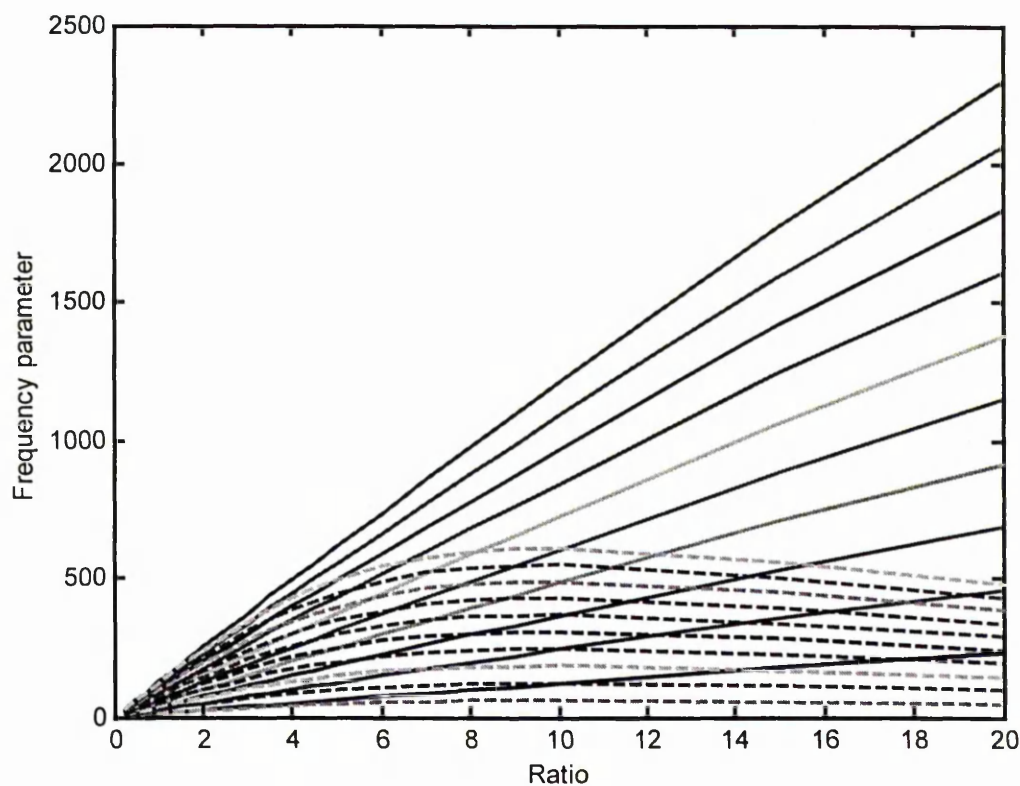


Figure 2.10 Comparison frequency parameter with aspect ratio obtained from torsion frequency equation for thickness to length ratio 10% shown in dashed line and 1% thickness to length ratio shown in solid line

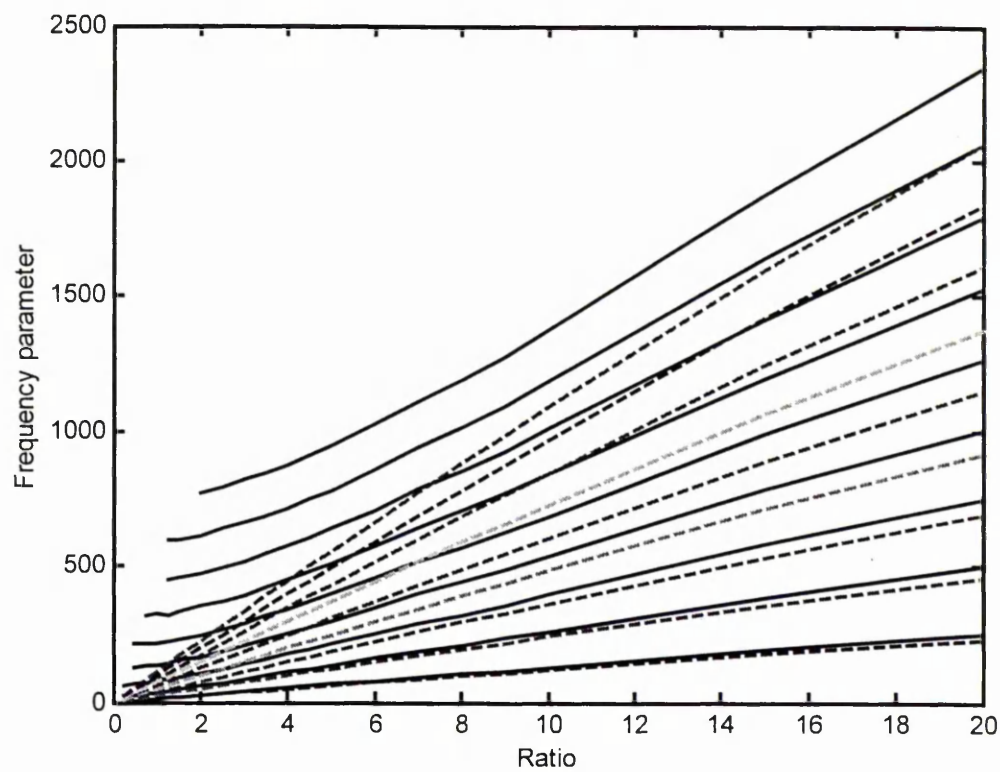


Figure 2.11 Comparison of the torsional mode for thickness to length ratio 1% obtained from FE analysis shown as a solid line and that obtained from torsional equation represented in dashed line

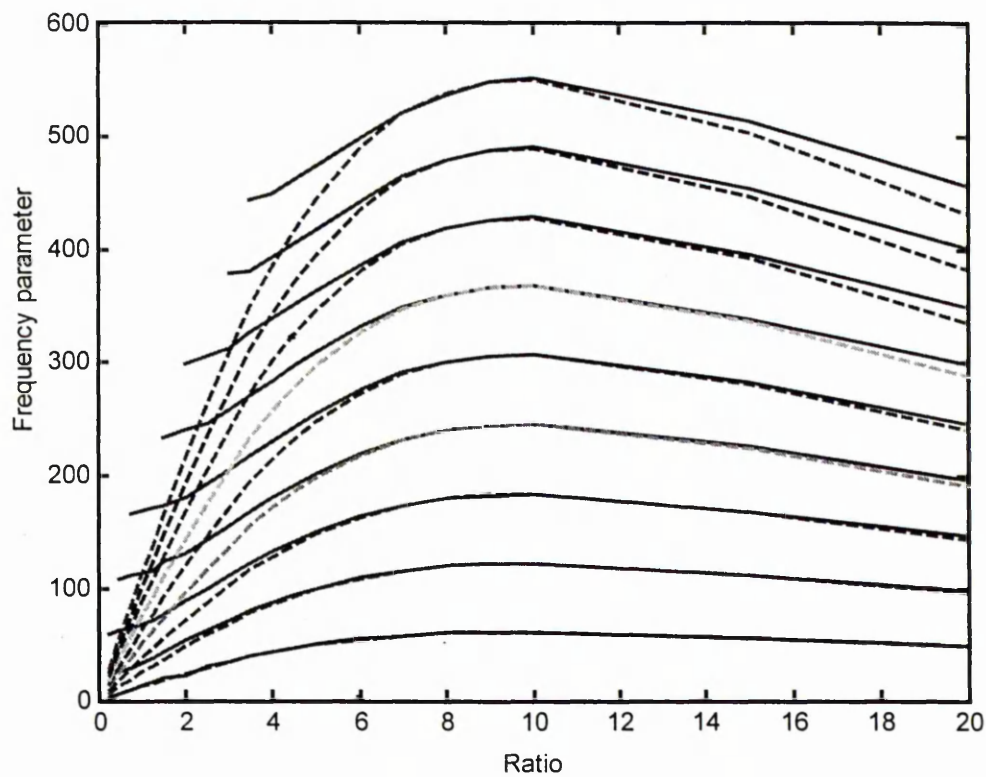


Figure 2.12 Comparison of the torsional mode for thickness to length ratio 10% obtained from FE analysis shown as a solid line and that obtained from torsional equation represented in dashed line

Table 2.5 to 2.8 show comparison between free-free and clamped-clamped for both bending and torsional modes for thickness to length ratio 1% and 10% of aspect ratio 10

Bending modes (ratio = 10, thickness to length ratio 1%)

	free-free	
mode number	mode identifier	frequency (Hz)
1	2,0	104
2	3,0	289
3	4,0	567
4	5,0	939
5	6,0	1405
6	7,0	1965
7	8,0	2618
8	9,0	3364
9	10,0	4200
10	11,0	5127

	clamped-clamped	
mode number	mode identifier	frequency (Hz)
1	0,0	106
2	1,0	291
3	2,0	572
4	3,0	945
5	4,0	1413
6	5,0	1973
7	6,0	2627
8	7,0	3372
9	8,0	4208
10	9,0	5133

Table 2.5 Comparison between the frequency obtained from the FE analysis (first 10 bending modes) for free-free and clamped-clamped beam-plates for ratio 10 and thickness to length ratio 1%

Torsional modes (ratio = 10, thickness to length ratio 1%)

	free-free	
mode number	mode identifier	frequency (Hz)
1	1,1	606
2	2,1	1222
3	3,1	1855
4	4,1	2515
5	5,1	3209
6	6,1	3943
7	7,1	4724
8	8,1	5557
9	9,1	6447
10	10,1	7397

	clamped-clamped	
mode number	mode identifier	frequency (Hz)
1	0,1	637
2	1,1	1285
3	2,1	1955
4	3,1	2656
5	4,1	3397
6	5,1	4186
7	6,1	5028
8	7,1	5928
9	8,1	6891
10	9,1	7919

Table 2.6 Comparison between the frequency obtained from the FE analysis (first 10 torsional modes) for free-free and clamped-clamped beam-plates for ratio 10 and thickness to length ratio 1%

Bending modes (ratio = 10, thickness to length ratio 10%)

	free-free	
mode number	mode identifier	frequency (Hz)
1	2,0	1010
2	3,0	2628
3	4,0	4793
4	5,0	7312
5	6,0	10054
6	7,0	12929
7	8,0	15879
8	9,0	18861
9	10,0	21844
10	11,0	24796

	clamped-clamped	
mode number	mode identifier	frequency (Hz)
1	0,0	985
2	1,0	2521
3	2,0	4550
4	3,0	6902
5	4,0	9469
6	5,0	12185
7	6,0	15002
8	7,0	17892
9	8,0	20834
10	9,0	23810

Table 2.7 Comparison between the frequency obtained from the FE analysis (first 10 bending modes) for free-free and clamped-clamped beam-plates for ratio 10 and thickness to length ratio 10%

Torsional modes (ratio = 10, thickness to length ratio 10%)

	free-free	
mode number	mode identifier	frequency (Hz)
1	1,1	2855
2	2,1	5712
3	3,1	8570
4	4,1	11430
5	5,1	14293
6	6,1	17158
7	7,1	20028
8	8,1	22901
9	9,1	25779
10	10,1	28662

	clamped-clamped	
mode number	mode identifier	frequency (Hz)
1	0,1	2860
2	1,1	5721
3	2,1	8584
4	3,1	11449
5	4,1	14317
6	5,1	17188
7	6,1	20063
8	7,1	22942
9	8,1	25827
10	9,1	28717

Table 2.8 Comparison between the frequency obtained from the FE analysis (first 10 torsional modes) for free-free and clamped-clamped beam-plates for ratio 10 and thickness to length ratio 10%

Tables show that the frequencies are very close for free-free and clamped-clamped beam-plate for the same aspect ratio, mode number and thickness.

2.3 Fundamental equations of classical plate theory

The general differential equation of motion for the transverse displacement w of a plate is given by [24]

$$D\nabla^4 w + \rho \frac{\partial^2 w}{\partial t^2} = 0 \quad (2.84)$$

where D is the flexural rigidity and is defined by ;

$$D = \frac{Eh^3}{12(1-\nu^2)} \quad (2.85)$$

E is Young's Modulus

h is the plate thickness

ν is Poisson's ratio

ρ is mass density per unit area of the plate

t is time

$$\nabla^4 = \nabla^2 \nabla^2$$

and $\nabla^2 = \partial^2 / \partial x^2 + \partial^2 / \partial y^2$ is the Laplacian operator

When free vibrations are assumed, the motion is expressed as

$$W(x,y,t) = W(x,y)\cos\omega t \quad (2.86)$$

where ω is the angular frequency (expressed in radians/unit time) and W is a function only of the position co-ordinates. Substituting Equation (2.84) into Equation (2.85) yields,

$$(\nabla^4 - k^4)W = 0 \quad (2.87)$$

where k is defined as,

$$k^4 = \frac{\rho\omega^2}{D} \quad (2.88)$$

It is usually convenient to factor Equation (2.56) into;

$$(\nabla^2 + k^2)(\nabla^2 - k^2)W = 0 \quad (2.89)$$

By the theory of linear differential equations, the complete solution to Equation (2.89) can be obtained by superimposing the solutions to the equations

$$\nabla^2 W_1 + k^2 W_1 = 0 \quad (2.90)$$

$$\nabla^2 W_2 - k^2 W_2 = 0 \quad (2.91)$$

In the case of a plate supported by a massless elastic medium (or foundation), Equation (2.81) becomes; [25]

$$D\nabla^4 w + Kw + \rho \frac{\partial^2 w}{\partial t^2} = 0 \quad (2.92)$$

where K is the stiffness of the foundation measured in unit length of deflection per unit area of contact. If the mass of the foundation is significant mass, then its differential equation must also be derived, and a coupled system of differential equations needs to be solved. However, this is beyond the scope of the present work.

Substituting Equation (2.86) into Equation (2.92) now gives,

$$k^4 = \frac{\rho\omega^2 - K}{D} \quad (2.93)$$

Therefore, all results presented in this thesis for the classical plate equation (Equation (2.84) can also apply to the case of elastic foundations by the simple use of Equation (2.93) in place of Equation (2.88).

2.3.1 Solution of plate equation in rectangular co-ordinates

A. Classical equation

The Laplacian operator in rectangular co-ordinates is [26]

$$\nabla^2 = \frac{\partial^2}{\partial x^2} + \frac{\partial^2}{\partial y^2} \quad (2.94)$$

Bending and twisting moments are related to the displacements by [26]

$$\left. \begin{aligned} M_x &= -D \left(\frac{\partial^2 w}{\partial x^2} + \nu \frac{\partial^2 w}{\partial y^2} \right) \\ M_y &= -D \left(\frac{\partial^2 w}{\partial y^2} + \nu \frac{\partial^2 w}{\partial x^2} \right) \\ M_{xy} &= -D(1-\nu) \frac{\partial^2 w}{\partial x \partial y} \end{aligned} \right\} \quad (2.95)$$

Transverse shearing forces are given by [26]

$$\left. \begin{aligned} Q_x &= -D \frac{\partial}{\partial x} (\nabla^2 w) \\ Q_y &= -D \frac{\partial}{\partial y} (\nabla^2 w) \end{aligned} \right\} \quad (2.96)$$

and Kelvin-Kirchhoff edge reactions are [26]

$$\left. \begin{aligned} V_x &= Q_x + \frac{\partial M_{xy}}{\partial y} \\ V_y &= Q_y + \frac{\partial M_{xy}}{\partial x} \end{aligned} \right\} \quad (2.97)$$

The strain energy of bending and twisting of a plate expressed in rectangular co-ordinates is [26]

$$U = \frac{D}{2} \int_A \left\{ \left(\frac{\partial^2 w}{\partial x^2} + \frac{\partial^2 w}{\partial y^2} \right)^2 - 2(1-\nu) \left[\frac{\partial^2 w}{\partial x^2} \frac{\partial^2 w}{\partial y^2} - \left(\frac{\partial^2 w}{\partial x \partial y} \right)^2 \right] \right\} dA \quad (2.98)$$

where $dA = dx dy$.

B. General solution

The general solutions to Equation (2.87) in rectangular co-ordinates may be obtained by assuming Fourier series in one of the variables, say x ; that is,[26]

$$W(x, y) = \sum_{m=1}^{\infty} Y_m(y) \sin \alpha x + \sum_{m=0}^{\infty} Y_m^*(y) \cos \alpha x \quad (2.99)$$

Substituting Equation (2.99) into Equation (2.90) and (2.91) yields [26]

$$\left. \begin{aligned} \frac{d^2 Y_{m1}}{dy^2} + (k^2 - \alpha^2) Y_{m1} &= 0 \\ \frac{d^2 Y_{m2}}{dy^2} - (k^2 + \alpha^2) Y_{m2} &= 0 \end{aligned} \right\} \quad (2.100)$$

and two similar equations for Y_m^* . Assuming that $k^2 > \alpha^2$, solutions to Equations (2.100) are [26]

$$\left. \begin{aligned} Y_{m1} &= A_m \sin(\sqrt{k^2 - \alpha^2} y) + B_m \cos(\sqrt{k^2 - \alpha^2} y) \\ Y_{m2} &= C_m \sinh(\sqrt{k^2 + \alpha^2} y) + D_m \cosh(\sqrt{k^2 + \alpha^2} y) \end{aligned} \right\} \quad (2.101)$$

where A_m, \dots, D_m are arbitrary coefficients determining the mode shape and are obtained from the boundary conditions. If $k^2 < \alpha^2$, it is necessary to rewrite Y_{m1} as [26]

$$Y_{m1} = A_m \sinh(\sqrt{\alpha^2 - k^2} y) + B_m \cosh(\sqrt{\alpha^2 - k^2} y) \quad (2.102)$$

Therefore, the complete solution to equation (2.87) may be written as [26]

$$\begin{aligned} W(x, y) = & \sum_{m=1}^{\infty} \left(A_m \sin(\sqrt{k^2 - \alpha^2} y) + B_m \cos(\sqrt{k^2 - \alpha^2} y) + \dots \right. \\ & \left. C_m \sinh(\sqrt{k^2 + \alpha^2} y) + D_m \cosh(\sqrt{k^2 + \alpha^2} y) \right) \sin \alpha x + \dots \\ & \sum_{m=0}^{\infty} \left(A_m^* \sin(\sqrt{k^2 - \alpha^2} y) + B_m^* \cos(\sqrt{k^2 - \alpha^2} y) + \dots \right. \\ & \left. C_m^* \sinh(\sqrt{k^2 + \alpha^2} y) + D_m^* \cosh(\sqrt{k^2 + \alpha^2} y) \right) \cos \alpha x \end{aligned} \quad (2.103)$$

2.4 Comparison of frequency parameters for both free-free and clamped-clamped beams and plates.

Blevins [25] obtained results for a clamped-clamped plate for $\nu = 0.3$ as shown in Table (1.9) in Chapter 1. For convenience, this table is reproduced in this Chapter as Tables 2.9 and 2.10.

Table 2.9 *The square of frequency parameter for free-free plate [24]*

a/b	$(\lambda_{ij}^2)_p, (i, j), I = 1, 2, 3, \dots \quad j = 1, 2, 3, \dots$					
	Mode			Sequence		
	1	2	3	4	5	6
0.4	3.463 (1,3)	5.288 (2,2)	9.622 (1,4)	11.44 (2,3)	18.79 (1,5)	19.10 (2,4)
2/3	8.946 (2,2)	9.602 (1,3)	20.74 (2,3)	22.35 (3,1)	25.87 (1,4)	29.97 (3,2)
1.0	13.49 (2,2)	19.79 (1,3)	24.43 (3,1)	35.02 (3,2)	35.02 (2,3)	61.53 (4,1)
1.5	20.13 (2,2)	21.60 (3,1)	46.65 (3,2)	50.29 (1,3)	58.20 (4,1)	67.49 (2,3)
2.5	21.64 (3,1)	33.05 (2,2)	60.14 (4,1)	71.48 (3,2)	117.5 (5,1)	119.4 (4,2)

Table 2.10 *The square of frequency parameter for clamped-clamped plate [24]*

A/b	$(\lambda_{ij}^2)_p, (i, j), I = 1, 2, 3, \dots \quad j = 1, 2, 3, \dots$					
	Mode			Sequence		
	1	2	3	4	5	6
0.4	22.35 (1,1)	23.09 (1,2)	25.67 (1,3)	30.63 (1,4)	38.69 (1,5)	49.86 (1,6)
2/3	22.31 (1,1)	24.31 (1,2)	31.70 (1,3)	46.82 (1,4)	61.57 (2,1)	64.34 (2,2)
1.0	22.27 (1,1)	26.53 (1,2)	43.66 (1,3)	61.47 (2,1)	67.55 (2,2)	79.90 (1,4)
1.5	22.21 (1,1)	30.90 (1,2)	61.30 (2,1)	70.96 (1,3)	74.26 (2,2)	118.30 (2,3)
2.5	22.13 (1,1)	41.69 (1,2)	61.00 (2,1)	92.38 (2,2)	119.90 (3,1)	157.80 (3,2)

The natural frequencies of a plate are given by [25]

$$f_{ij} = \frac{\lambda_{ij}^2}{2\pi L^2} \left[\frac{Eh^3}{12\gamma(1-\nu^2)} \right]^{1/2} \quad (2.104)$$

where $i = 1, 2, 3, \dots$ and $j = 1, 2, 3, \dots$ and λ_{ij} is the frequency parameter

Equation (2.73) can be written as

$$\lambda_{ij}^2 = 2\pi L^2 f_{ij} \left[\frac{12\gamma(1-\nu^2)}{Eh^3} \right]^{1/2} \quad (2.105)$$

Substituting $\gamma = \rho h$, into Equation (2.105) gives the frequency parameters of a plate as

$$(\lambda_{ij}^2)_p = 2\pi L^2 f_{ij} \left[\frac{12\rho(1-\nu^2)}{Eh^2} \right]^{1/2} \quad (2.106)$$

The natural frequencies of a beam are given by

$$f_i = \frac{\lambda_i^2}{2\pi L^2} \left[\frac{Eh^3}{12\gamma} \right]^{1/2} \quad (2.107)$$

$$i = 1, 2, 3, \dots$$

Equation (2.76) can be written as

$$\lambda_i^2 = 2\pi L^2 f_i \left[\frac{12\gamma}{Eh^3} \right]^{1/2} \quad (2.108)$$

Substituting $\gamma = \rho h$, then Equation (2.77) can be written as

$$(\lambda_i^2)_B = 2\pi L^2 f_i \left[\frac{12\rho}{Eh^2} \right]^{1/2} \quad (2.109)$$

where $(\lambda_i^2)_B$ = frequency parameter for beam

$(\lambda_{ij}^2)_P$ = frequency parameter for plate

f_{ij} = natural frequency (Hz)

λ_{ij}^2 = square of frequency parameters

γ = mass per unit area of plate (kg/m^2)

ρ = density (kg/m^3)

ν = Poisson's ratio

E = Young modulus (Pa)

L = length of plate (m)

h = thickness of plate (m)

i = number of half-waves in mode shape along horizontal axis

j = number of half-waves in mode shape along vertical axis

Dividing Equation (2.109) by Equation (2.106) yields:

$$\frac{(\lambda_i^2)_B}{(\lambda_{ij}^2)_P} = \frac{1}{\sqrt{1-\nu^2}}$$

or

$$(\lambda_i^2)_B = \left(\frac{1}{\sqrt{1-\nu^2}} \right) (\lambda_{ij}^2)_P \quad (2.110)$$

From Table 2.9 and 2.10 we can obtain $(\lambda_i^2)_B$ for beam-like behaviour from $(\lambda_{ij}^2)_P$ for plate-like behaviour by using Equation (2.110). The values of $(\lambda_i^2)_B$ obtained are compared with those of $(\lambda_{ij}^2)_P$ in Table 2.11 and 2.12. The tables show that values of $(\lambda_{ij}^2)_P$ are smaller than those of $(\lambda_i^2)_B$. These values of frequency parameters which have been derived from the literature cover a small range of aspect ratio a/b ranging from 0.4 to 2.5. These frequency parameters will be compared with those derived from the work presented in this thesis in subsequent chapters.

Table 2.11 Comparison of the square of frequency parameter for a free-free plate and free-free beam

a/b	$(\lambda_{ij}^2)_p, (\lambda_i^2)_B, (i, j) \quad i = 1, 2, 3, \dots \quad j = 1, 2, 3, \dots$					
	Mode			Sequence		
	1	2	3	4	5	6
0.40	3.463	5.288	9.622	11.44	18.79	19.10
	3.630	5.543	10.086	11.99	19.69	20.02
	(1,3)	(2,2)	(1,4)	(2,3)	(1,5)	(2,4)
2/3	8.946	9.602	20.74	22.35	25.87	29.97
	9.378	10.066	21.74	23.43	27.12	31.42
	(2,2)	(1,3)	(2,3)	(3,1)	(1,4)	(3,2)
1.0	13.49	19.79	24.43	35.02	35.02	61.53
	14.14	20.76	25.61	36.72	36.72	64.40
	(2,2)	(1,3)	(3,1)	(3,2)	(2,3)	(4,1)
1.5	20.13	21.60	46.65	50.29	58.20	67.49
	21.02	22.63	48.90	52.72	61.01	70.75
	(2,2)	(3,1)	(3,2)	(1,3)	(4,1)	(2,3)
2.5	21.64	33.05	60.14	71.48	117.5	119.4
	22.68	34.64	63.04	74.93	123.17	125.17
	(3,1)	(2,2)	(4,1)	(3,2)	(5,1)	(4,2)

Table 2.12 Comparison of the square of frequency parameter for a clamped-clamped plate and clamped-clamped beam

a/b	$(\lambda_{ij}^2)_p, (\lambda_i^2)_B, (i, j) \quad i = 1, 2, 3, \dots \quad j = 1, 2, 3, \dots$					
	Mode			Sequence		
	1	2	3	4	5	6
0.40	22.35	23.09	25.67	30.63	38.69	49.86
	23.43	24.20	26.91	32.11	40.56	52.27
	(1,1)	(1,2)	(1,3)	(1,4)	(1,5)	(1,6)
2/3	22.31	24.31	37.70	46.82	61.57	64.34
	23.39	25.48	39.52	49.10	64.54	67.45
	(1,1)	(1,2)	(1,3)	(1,4)	(2,1)	(2,2)
1.0	22.27	26.53	43.66	61.47	67.55	79.90
	23.36	27.81	45.77	64.44	70.81	83.76
	(1,1)	(1,2)	(1,3)	(2,1)	(2,2)	(1,4)
1.5	22.21	30.90	61.30	70.96	74.26	118.30
	23.28	32.39	64.26	74.39	77.85	124.01
	(1,1)	(1,2)	(2,1)	(1,3)	(2,2)	(2,3)
2.5	22.13	41.69	61.00	92.38	119.90	157.80
	23.20	43.70	63.94	96.84	125.69	165.42
	(1,1)	(1,2)	(2,1)	(2,2)	(3,1)	(3,2)

Note: In each cell of Tables 2.11 and 2.12, the top number is $(\lambda_{ij}^2)_p$, the middle number is $(\lambda_i^2)_B$ and the bottom pair of numbers denote mode number (i, j) .

2.5 Summary

This chapter has covered the classical theories of the vibrations of beams and plates. There are two classical beams theories that are used for the analysis of bending vibration of beams, namely: Euler-Bernoulli and Timoshenko beam theories. The Euler-Bernoulli theory is used for long slender beams vibration while Timoshenko theory is used for short beams. For torsional vibration of beams, the torsion theory of beams is used. On the other hand Kirchhoff theory is used for the analysis of the vibration of thin plates and Mindlin theory for the vibration of thick plates. However, there is only an exact solution for simply-supported (pinned) plate boundary condition. i.e. there are no exact solutions for other boundary conditions of a plate. Therefore approximate numerical methods, such as the Finite Element Method (FEM) have to be used to predict the vibration of plates with general boundary conditions. The natural frequencies and the frequency parameters for the torsional vibration of beams predicted using the torsion theory shown to be very close to these predicted using the FE method. The frequency parameters derived for the vibrations of beams and those derived from the literature for the vibrations of plates will be compared to those derived in this thesis in subsequent chapters.

Chapter 3

Finite element analysis for free-free and clamped-clamped beams and plates

3.1 Introduction

The finite element method is a sophisticated and complex technique, which is based on simple and easily understood fundamental principles [38]. However, the finite element method is an approximate method of analysis. The way an object is modelled, such as the choice of element or the representation of the loading and constraint conditions, is important in order to obtain good results [38].

This chapter considers the finite element analysis of the vibration of free-free and clamped-clamped beams and plates using ABAQUS, a finite element programme which runs on the HP 700 work stations at the Manchester School of Engineering and the Silicon Graphics Origin 2000 supercomputer of the Manchester Computing Centre. The program was used to calculate the first 50 natural frequencies and mode shapes for

free-free and clamped-clamped beams and plates.

Figure 3.1 shows the dimensions of the beams and plates analysed. The length of the beam was $a = 500$ mm, while the breadth b was varied correspondingly with the variation of the aspect ratio a/b . Twenty (20) aspect ratios were used, namely; 0.25, 0.50, 0.75, 1.0, 1.25, 1.5, 2.0, 2.5, 3.0, 3.5, 4.0, 4.5, 5.0, 6.0, 7.0, 8.0, 9.0, 10.0, 15.0 and 20.0. The thickness to length ratios of the beams and plates used were 1%, 2%, 5% and 10%. The beams and plates assumed to be made of aluminium. However, other engineering materials such as steel and brass could have been used. Figure 3.2 shows the boundary conditions of the beams and plates analysed.

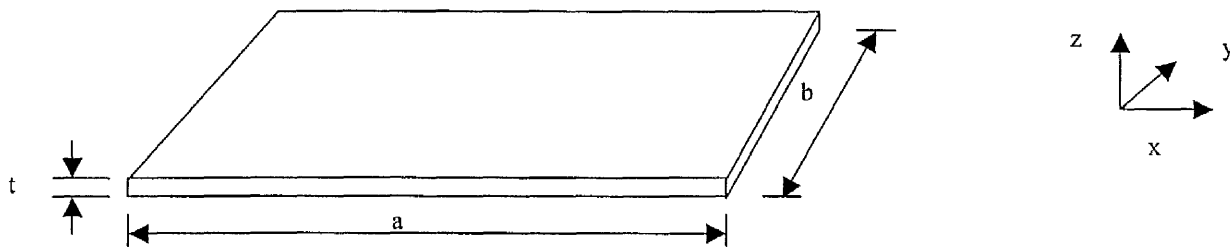


Figure 3.1 Beam/ plate geometry

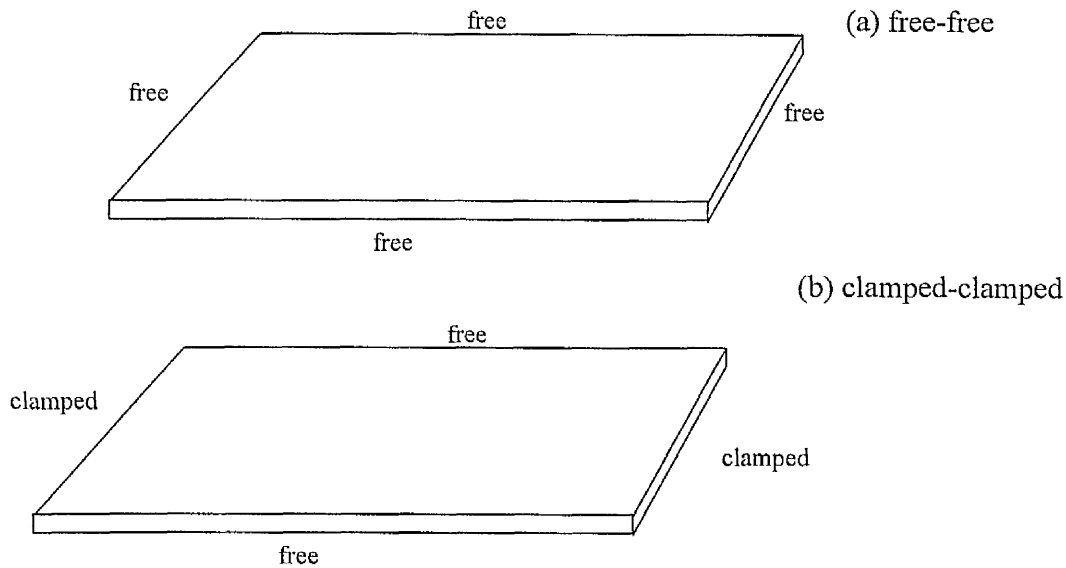


Figure 3.2 Beam/ plate boundary conditions

The analysis for the clamped-clamped and free-free plate was done using both shell and solid finite elements. The frequency parameters and mode shapes predicted by the FE analysis were investigated to predict the transition curve from beam-like behaviour to plate-like behaviour for different plate thicknesses. A mesh study was also carried out in order to obtain an optimum mesh size for the FE analyses. Also, an element study was carried out to find the most suitable element for the structure.

3.2 Types of elements

The finite element analysis (FEA) program ABAQUS [39-44] which was used to analyse the beams and plates has many element types available for use for different engineering applications. The element types used in this work were solid element C3D20R, thin shell element S8R5, and general purpose shell element S4R.

3.2.1 Solid element

Solid elements of type C3D20R were used in the FE analyses. The element node numbering convention is shown in Figure 3.3 C3D20R stands for continuum stress/displacement (C), three dimensional (3D), 20R denotes 20 nodes and reduced integration (R) respectively [40]. Each node of this element has 3 degree of freedom (DOF) which are the three translational degrees of freedom in the x, y and z directions. Therefore the element has a total of 60 DOFs. The solid element type C3D20R was used in the FE analysis for the thicker beam. The element has mid-side nodes in addition to the corner nodes. It uses quadratic interpolation of the nodal shape functions and therefore gives a more accurate interpolation than solid elements of type C3D8 and C3D8R, which use linear interpolation.

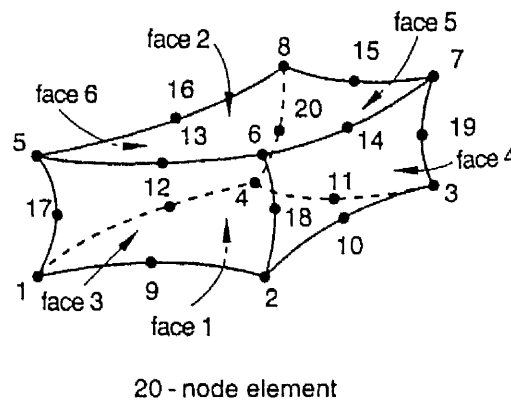


Figure 3.3 Node ordering of 20 nodes solid element [40]

3.2.2 Thin shell element

Thin shells are needed in cases where there is no transverse shear deformation. Thin shell element type S8R5 was used in the FE analysis in this section and other

chapters of this thesis for thickness-to-length ratios of 1% or less. S8R5 stands for stress/displacement shell (S), 8 nodes, reduced integration (R), and 5 degrees of freedom per node [40] that is, a total of 40 DOFs is calculated for this type of element the element is intended to be used for thin shells. It uses quadratic interpolation for solving and finding solutions. The element node numbering convention is shown in Figure 3.4

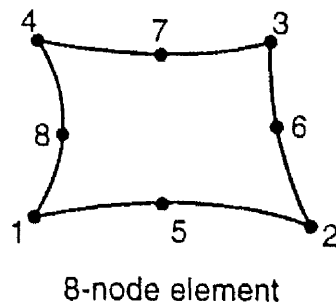


Figure 3.4 Node ordering of 8 nodes shell element [40]

3.2.3 Thick shell elements

Thick shells are needed in cases where transverse shear deformation is important. One of the thick shell elements in the ABAQUS element library is denoted as S8R. This element has 6 DOFs for each node and a total of 64 DOFs. S8R stands for stress/displacement thick shell (S), 8 nodes and reduced integration (R) [40] It uses quadratic interpolation for solving and finding solutions. The element node numbering convention is shown in Figure 3.4. This element S8R should be used only for thick shells.

3.2.4 General purpose shell element

General purpose elements are also based on transverse shear deformation theory. They use thick shell theory as the shell thickness increases and become discrete Kirchhoff thin shell elements as the thickness decreases; the transverse shear deformation becomes very small as the shell thickness decreases. S4R, general purpose shell element is used in the FE analysis in this section. The S4R stands for stress/displacement shell (S), 4 nodes and reduced integration (R). It has 6 DOFs per node and a total of 24 DOFs. It uses linear interpolation for solving and finding solutions Figure 3.5 [40] shows the node numbering convention for element type S4R.

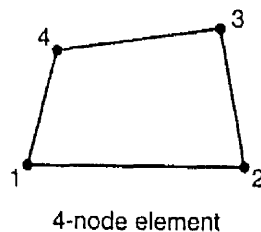


Figure 3.5 Node ordering of 4 nodes shell element [40]

3.2.5 Full integration versus reduced integration

Reduced integration elements are available for quadrilateral and hexahedral (brick) elements. These types of elements use a lower-order integration to form the element stiffness matrix. The mass matrix and distributed loading use full integration. Reduced integration means reduced running time, especially in three dimensional problems. Element type C3D20 has 27 integration points, while C3D20R has only 8; therefore, element assembly is roughly 3.5 times more costly for C3D20 than for C3D20R.

It is also important to know that the second-order reduced-integration elements generally yield more accurate results than the corresponding fully integrated elements. However, for first-order elements the accuracy achieved with full versus reduced integration is largely dependent on the nature of the problem [40].

3.2.6 Linear versus Quadratic interpolation

Displacements or other degrees of freedom are calculated at the nodes of the element. At any other point in the element, the displacements are obtained by interpolating from the nodal displacements. Usually the interpolation order is determined by the number of nodes used in the element. Elements that have nodes only at their corners, such as the 8-node brick elements use linear interpolation in each direction and are often called linear elements or first-order elements. Elements with midside nodes, such as the 20-node brick elements use quadratic interpolation and are often called quadratic elements or second-order elements. The number of nodes in an element is clearly identified in its name. The 8-node brick element is called C3D8, and the 8-node three-dimensional shell element is called S8R.

The beam element family uses a slightly different convention: the order of interpolation is identified in the name. Thus, a first-order, three-dimensional beam element is called B31, whereas a second-order, three-dimensional beam element is called B32. A similar convention is used for axisymmetric shell and membrane elements.

ABAQUS provides two basic truss elements: a 2-node straight truss, which uses linear interpolation for position and displacement and has a constant stress, and a 3-node curved truss, which uses quadratic interpolation for position and displacement so that the strain varies linearly along the element.

In addition, hybrid versions of the stress/displacement trusses, coupled temperature-displacement trusses, and piezoelectric trusses are available.

The solid element library includes first-order (linear) interpolation elements and second-order (quadratic) interpolation elements in one, two, or three dimensions. Triangles and quadrilaterals are available in two dimensions; and tetrahedra, triangular prisms, and hexahedra ("bricks") are provided in three dimensions. Curved (parabolic) edges can be used on the second-order elements but are not recommended for pore pressure or coupled temperature-displacement elements.

Second-order elements provide higher accuracy than first-order elements for "smooth" problems that do not involve complex contact conditions, impact, or severe element distortions. They capture stress concentrations more effectively and are better for modelling geometric features: they can model a curved surface with fewer elements. Finally, second-order elements are very effective in bending-dominated problems.

First-order triangular and tetrahedral elements should be avoided as much as possible in stress analysis problems; the elements are overly stiff and exhibit slow convergence with mesh refinement, which is especially a problem with first-order tetrahedral elements. If they are required, an extremely fine mesh may be needed to obtain results of sufficient accuracy [40]

3.3 Method of the FEA procedure using ABAQUS

The work presented in this thesis was carried out using the ABAQUS FE (finite element), a commercial finite element program. A complete ABAQUS analysis usually consists of three main stages: pre-processing, simulation and post processing. These three stages are linked together by files as shown in Figure 3.6.

Pre-processing (ABAQUS/Pre)

The first stage in the FE method is to define the model of the physical problem and create an ABAQUS input file. The model can be created graphically using ABAQUS/CAE or other pre-processor, e.g. Patran. For simple structures, the ABAQUS input file may be created directly using ABAQUS/Pre commands such as NODE, NGEN, NFILL, ..., ELEMENT, ELGEN, ELCOPY, ..., SECTION, ..., ELASTIC, DENSITY, ..., and STEP, FREQUENCY, ... to define the nodes, elements, section properties, material properties and perturbation step respectively. Because the geometry of the beam or plate is simple, the ABAQUS/Pre commands and ABAQUS/CAE were used to generate the ABAQUS input files in this work [35]

Simulation (ABAQUS/Standard)

A job is run usually in batch or background mode. ABAQUS/Standard solves the numerical problem defined by the programme in the input file. The output files, containing the required data, are stored in binary format, ready for post processing. Depending on the complexity of the model being analysed and the computer being used for the analysis, it may take any thing from seconds to days to achieve a solution. The work in this thesis was carried out using the ABAQUS FE program on the HP 700 workstations of the Manchester School of Engineering and on the Silicon Graphics Origin 2000 super computer of the Manchester Computing Centre.

Post-processing

Once an ABAQUS job has run successfully, the graphical results can be viewed using ABAQUS/Post or ABAQUS/CAE or another post-processor, which reads the binary output files, from which a hard copy on the model can be printed and stored.

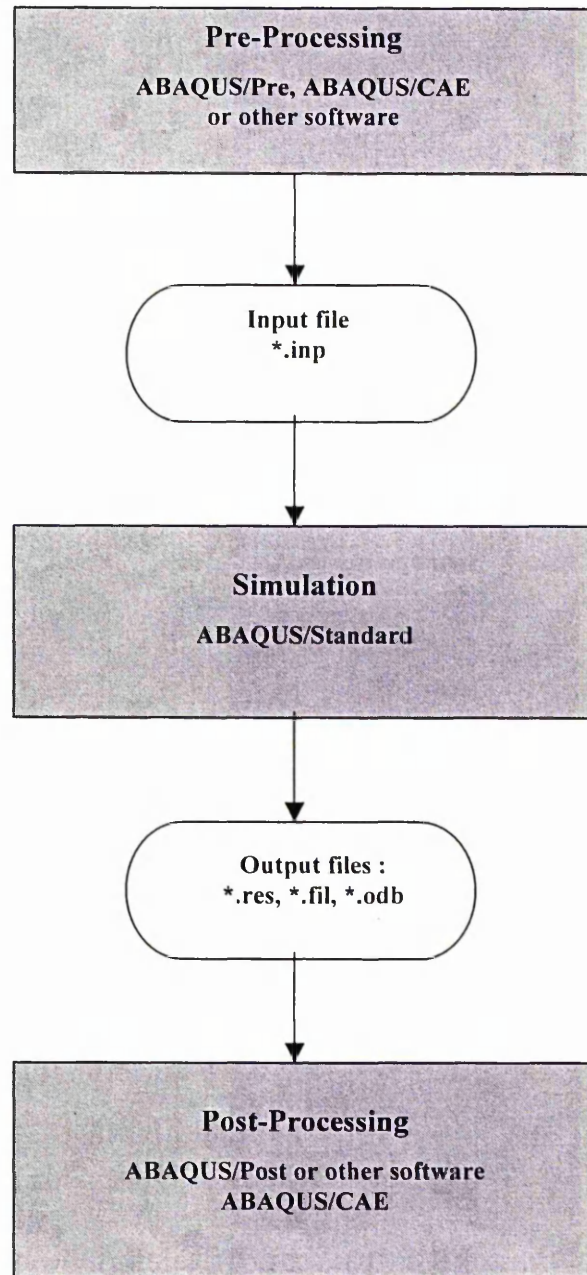


Figure 3.6 Flow chart showing the three stages of a complete ABAQUS analysis [39]

3.4 Element study

In any FE analysis it is important to select the appropriate element type for the analysis in order to obtain the best results. In this work, FE analysis was performed for different beams and plates of thickness to length ratio of 1%, 2%, 5% and 10%. Therefore it was important to find the appropriate element type to suite the plate thickness taking into consideration the time required for the job to run using the ABAQUS FE program and the results file sizes created by the programme.

A previous study by Tangchaichit [3] involved thickness to length ratio 0.2% to 1% (1 to 5 mm thick) cantilevered beams and plates. He considered different types of solid and shell elements and concluded that the thin shell rigid elements S8R5 should be used in the FE analysis. The choice of using the S8R5 element type was based on the accuracy of the results obtained, output file sizes and time for the job to run in comparison to the solid element C3D20R.

However, the work presented in this thesis shows that the S8R5 element type was not suitable to be used for thicker beam-plate sizes thickness to length ratio 2%, 5% and 10% (10, 25, 50 mm thick), so a number of element types (S4R, S8R5, S8R, C3D20R) were investigated in order to find the most appropriate element type which can be used for thicker beam or plate. This element study was carried out on beams and plates of 10% thickness to length ratio and for all aspect ratios ranging from 0.25 to 20.0.

Table 3.2 shows the natural frequencies predicted by the four element types for the clamped-clamped beam and plate for aspect ratio 0.5 and 15. The table clearly shows that the maximum deviation of the natural frequencies is about 1.0%. Similarly, Figures 3.7 shows that at small aspect ratios of 0.25, 0.5 and 1.0 the deviations between the frequency parameters derived from the natural frequencies predicted using the four

element types is insignificant. However for higher aspect ratios there is significant deviation between the natural frequencies predicted using the four element types. This is shown, for example, by Table 3.3 clamped-clamped beams and plates of aspect ratio 15. The table shows that the largest deviations occur at the higher modes of vibration. This is also illustrated in Figure 3.8 for aspect ratios 2.0 to 20.0. The figure shows that at higher aspect ratios and higher modes of vibration, the predictions of element types S8R and S8R5 are inaccurate and the percentage errors increase dramatically in comparison to the predictions of element types S4R and C3D20R. The natural frequencies predicted by element types S4R and C3D20R are seen to be close. Based on this analysis it was decided to use element type S4R because it gives very good results in less time and produces smaller output files in comparison to the solid element C3D20R.

Table 3.2 First 50 natural frequencies (Hz) of vibration of a clamped-clamped plate of aspect ratio 0.5 and thickness to length ratio 10% ($L=0.5$ m, $b=1$ m, $t=50$ mm)

Mode No	C3D20R	S4R	S8R	S8R5
1	22.08	21.9	21.89	21.95
2	22.98	22.8	22.79	22.88
3	26.66	26.47	26.46	26.62
4	34.02	33.81	33.81	34.14
5	45.87	45.62	45.61	46.26
6	56.35	55.8	55.75	56.25
7	57.4	56.86	56.8	57.36
8	61.72	61.14	61.09	61.78
9	62.06	61.75	61.72	62.88
10	63.87	63.87	63.84	63.82
11	69.07	68.45	68.4	69.36
12	79.77	79.08	79.05	80.42
13	81.99	81.56	81.49	82.1
14	82.2	82.13	82.01	83.38
15	93.95	93.16	93.11	95.07
16	101.52	100.39	100.21	101.7
17	102.4	101.29	101.12	102.69
18	104.94	104.35	104.22	107.03
19	106.7	105.53	105.37	107.11
20	111.4	110.52	110.45	110.93
21	111.46	110.97	110.81	111.87
22	112.32	111.92	111.8	113.18
23	113.7	112.46	112.31	114.39
24	117.63	117.35	117.1	117.3
25	122.54	122.26	121.91	122.49
26	123.6	122.61	122.13	124.68
27	124.94	124.88	124.59	124.85
28	130.32	129.49	129.27	133.19
29	131.96	130.83	130.72	134.39
30	136.45	134.96	134.84	138.03
31	138.97	138.79	138	138.71
32	140.41	140.27	139.71	140.19
33	152.14	150.47	150.35	154.31
34	153.7	151.82	151.42	154.4
35	154.41	152.56	152.16	155.27
36	155.04	153.66	153.48	158.21
37	157.58	156.48	156.14	159.5
38	158.57	156.62	156.24	161.27
39	163.87	163.02	162.67	163.64

Mode No	C3D20R	S4R	S8R	S8R5
40	165.07	163.72	162.76	166.28
41	169.28	168.6	168.37	169.18
42	170.4	169.25	168.45	170.19
43	170.5	170.29	169.05	170.25
44	174.18	172	171.68	173.33
45	180.2	178.53	178.25	175.77
46	185.89	183.53	183.24	184.15
47	186.34	184.9	184.15	186.68
48	186.73	187	184.28	186.81
49	186.82	187.14	184.4	187.95
50	191.27	189.1	188.91	190.82

Table 3.3 First 50 natural frequencies (Hz) of vibration of a clamped-clamped plate of aspect ratio 15 and thickness to length ratio 10% ($L=0.5$ m, $b=1$ m, $t=50$ mm)

Mode No	C3D29R	S4R	S8R	S8R5
1	14.66	14.26	14.32	14.38
2	21.19	21.05	21.05	21.11
3	38.97	37.99	37.64	38.27
4	54.3	53.87	53.84	48.97
5	57.48	56.55	56.73	54.34
6	73.07	71.46	69.49	71.84
7	98.14	97.25	97.15	81.97
8	109.63	109.17	107.07	98.62
9	114.87	112.69	109.18	109.15
10	115.04	113.21	113.57	113.05
11	149.05	147.53	147.29	124.4
12	162.62	160.08	147.9	150.3
13	172.75	170.11	170.59	160.24
14	204.74	202.46	189.66	164.12
15	214.92	212.27	201.99	206.94
16	218.84	218.26	218.22	212
17	230.65	227.33	227.89	218.19
18	263.69	260.55	230.11	227.52
19	270.69	268.23	259.75	246.55
20	288.81	284.96	267.18	266.88
21	324.89	320.85	285.54	267.26
22	327.18	327.18	299.17	314.86
23	329.07	327.23	319.63	325.22
24	347.28	343.08	325.3	326.97
25	387.68	382.7	326.86	328.75

Mode No	C3D20R	S4R	S8R	S8R5
26	389.48	388.52	343.56	329.26
27	406.07	401.74	345.78	351.88
28	434.1	435.94	361.49	385.22
29	451.43	445.63	373.54	392.22
30	451.56	451.8	380.94	412.08
31	465.19	460.96	382.89	435.32
32	514.56	509.34	390.29	446.81
33	516.13	516.68	396.26	456.42
34	524.64	520.75	401.21	491.3
35	538.83	544.27	402.02	494.75
36	578.61	573.54	405.38	509.64
37	581.07	581.12	408.98	521.13
38	584.43	582.94	412.14	543.07
39	640.27	637.85	414.97	573.39
40	643.35	642.06	417.54	576.77
41	644.57	650.35	419.89	585.7
42	645.89	652.04	422.12	625.33
43	679.32	683.94	424.19	637.85
44	704.02	700.21	426.18	642.02
45	705	703.59	428.11	649.96
46	708.6	718.72	429.95	650.54
47	717.54	718.78	430.1	657.62
48	736.57	757.41	430.12	702.86
49	753.32	758.93	430.27	715.3
50	765.71	765.65	430.31	736.7

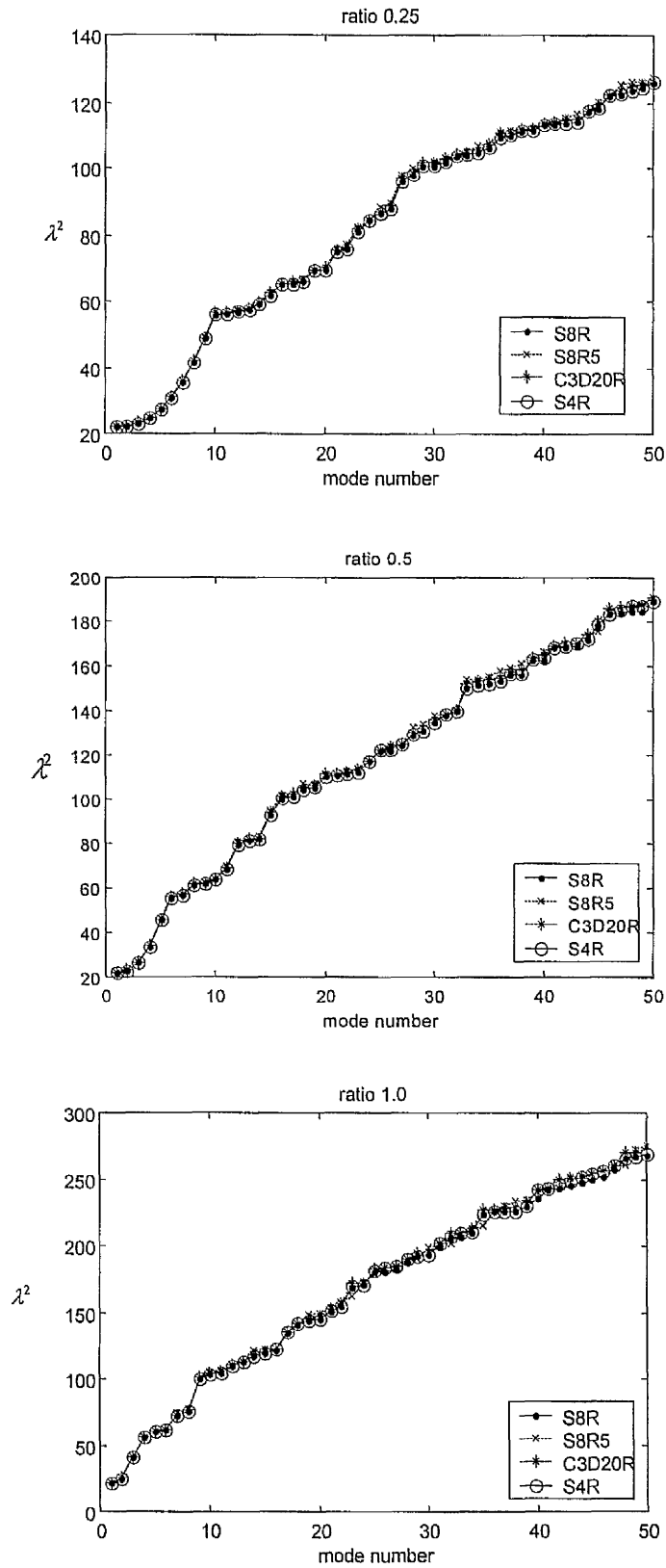


Figure 3.7 Variation of frequency parameters with mode number using element types (S8R, S8R5, C3D20R, S4R) for 10% thickness to length ratio

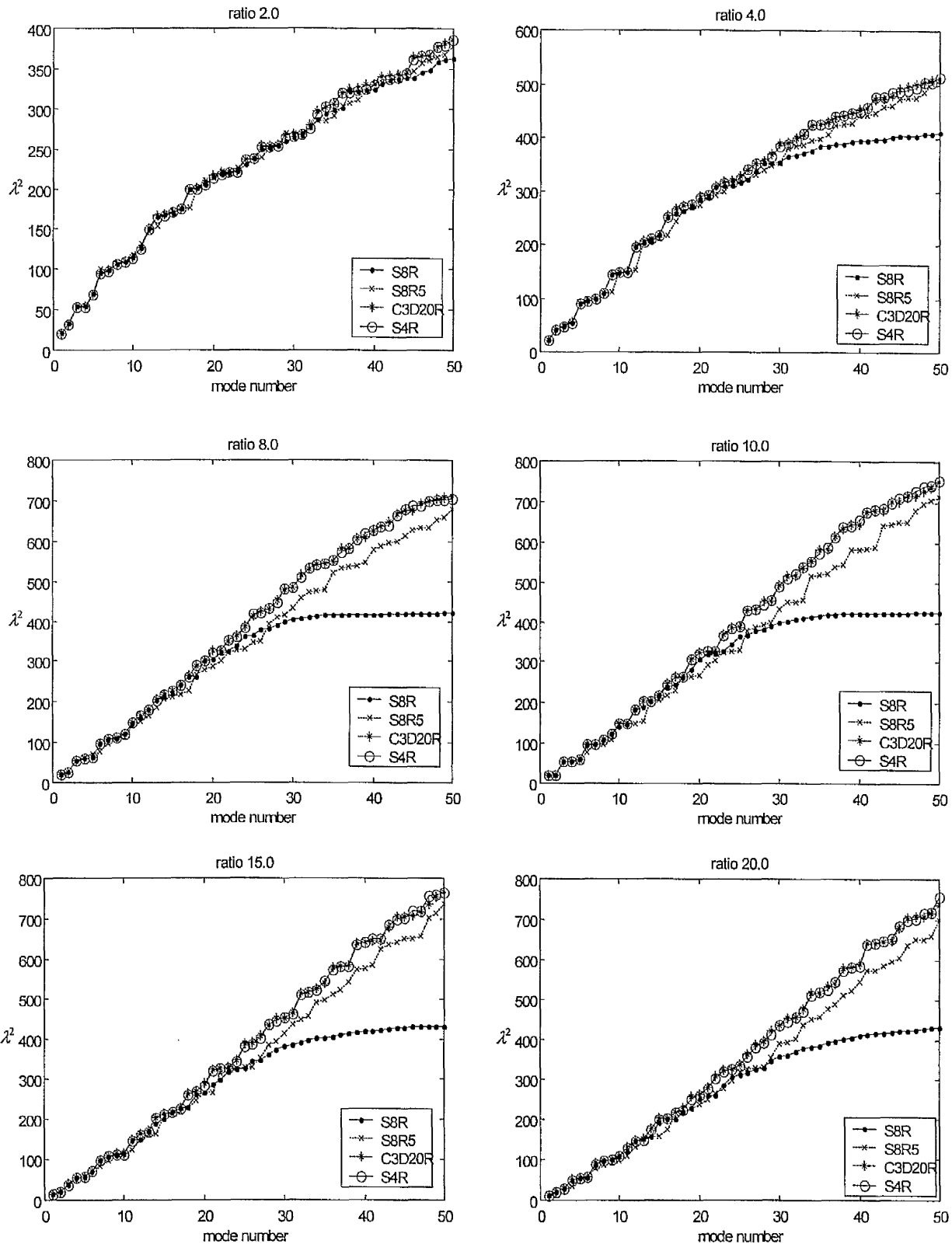


Figure 3.8 Variation of frequency parameters with mode number using element types (S8R, S8R5, C3D20R, S4R) for 10% thickness to length ratio

3.5 Mesh study

To obtain the best results from an FE analysis, the choice of the mesh density is equally as important as the choice of the element type. A previous study by Tangchaichit [3] involved a mesh study on 1% thickness to length ratio for cantilevered beams and plates. He considered different numbers of elements along the lengthwise and breathwise directions of the cantilevered beams and plates. He concluded that the minimum number of elements to be used along the x -axis is $N_x = 50$ in the finite element analysis while the number of elements along the y -axis varied with the aspect ratios of the beam-plates.

The work presented in this section investigates the optimum number of elements to be used for thicker beam-plates. For the mesh study, the ABAQUS FEA program was used to obtain the natural frequencies and mode shapes of clamped-clamped and free-free beam-plates of aspect ratio 1.0. The length (a) was 0.5 m, the breath (b) was 0.5 m and the thickness (t) was 0.05 m. The number of elements along the x -axis (N_x) were 5, 10, 20, 50 and 100 while the number of elements along the y -axis (N_y) were 5, 10, 20, 50 and 100. Each value of N_x was used in conjunction with each of the 5 values of N_y . The solid element type C3D20R was used in the analyses.

3.5.1 Variation of N_y at fixed values of N_x for clamped-clamped beam-plates.

Figures 3.9 to 3.13 show the effect of the mesh density on the frequency parameters for selected modes 1, 5, 10, 15 and 20 of the clamped-clamped beam-plate of aspect ratio 1.0. The figures show the variation of the frequency parameters with the number of elements along the y -axis (N_y), while number of elements along the x -axis (N_x) were fixed at 5, 10, 20, 50 and 100. The definition of the symbols and lines types used in these figures are defined as follows:

- * and solid line denote the frequency parameters using $N_x = 5$,
- o and dash line denote the frequency parameters using $N_x = 10$,
- o and solid line denote the frequency parameters using $N_x = 20$,
- * and dash line denote the frequency parameters using $N_x = 50$,
- + and dashdot line denote the frequency parameters using $N_x = 100$,

Figure 3.9 shows that the predicted frequency parameters for mode 1 are very close in value when $N_x > 20$ and $N_y > 5$. The percentage error in the predicted frequency parameters using $N_x = 5$, $N_y = 5$ compared to using $N_x = 100$, $N_y = 100$ is about 12%, which is not acceptable. The percentage error for the predicted frequency parameter using $N_x = 10$, $N_y = 5$ compared to using $N_x = 100$, $N_y = 100$ is about 4 %. But the percentage error for the predicted frequency parameter using for $N_x = 20$, $N_y = 5$ compared to using $N_x = 100$, $N_y = 100$ is about 0.2%. Therefore, for mode 1, the values of $N_x \geq 20$ and $N_y \geq 5$ is acceptable.

Figure 3.10 shows the percentage error in the predicted frequency parameter for mode 5 using $N_x = 5$, $N_y = 10$ compared to using $N_x = 100$, $N_y = 100$ is about 20%. For $N_x = 10$, $N_y = 10$ the percentage error is about 3 % with respect to $N_x = 100$, $N_y = 100$. But for $N_x = 20$, $N_y = 10$ the percentage error is about 1% with respect to $N_x = 100$, $N_y = 100$. Therefore, for mode 5 the value of $N_x \geq 20$ and $N_y \geq 5$ is acceptable.

For mode 10, It can be deduced from Figure 3.11 that when $N_x = 5$, $N_y = 20$ the predicted frequency parameters are in error by about 10% in comparison to $N_x = 100$, $N_y = 100$. Similarly, when $N_x = 10$, $N_y = 20$ and when $N_x = 20$, $N_y \geq 20$ the errors in the predicted frequency parameters are about 5% and 0.5%, respectively in comparison to the use of $N_x = 100$, $N_y = 100$. Thus, for mode 10, $N_x \geq 20$ and $N_y \geq 20$ is acceptable.

From Figure 3.12 in the same way it can be seen that the predicted frequency parameters for mode 15 are close when $20 < N_x \leq 100$ if $N_y \geq 20$. Similarly, for mode

20, Figure 3.13 shows that the acceptable number's of elements to use for accurate predictions are given by $20 < N_x < 100$ and $N_y \geq 20$.

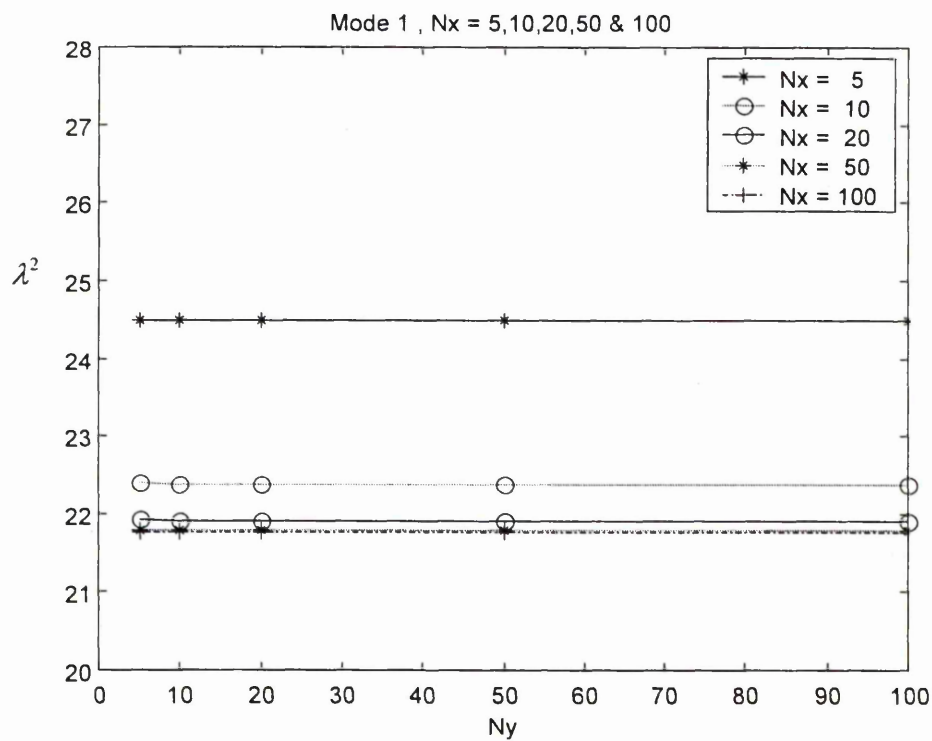


Figure 3.9 Variation of frequency parameter for mode 1 with number of elements in y -axis (N_y) and number of elements in x -axis (N_x) varied from 5 to 100

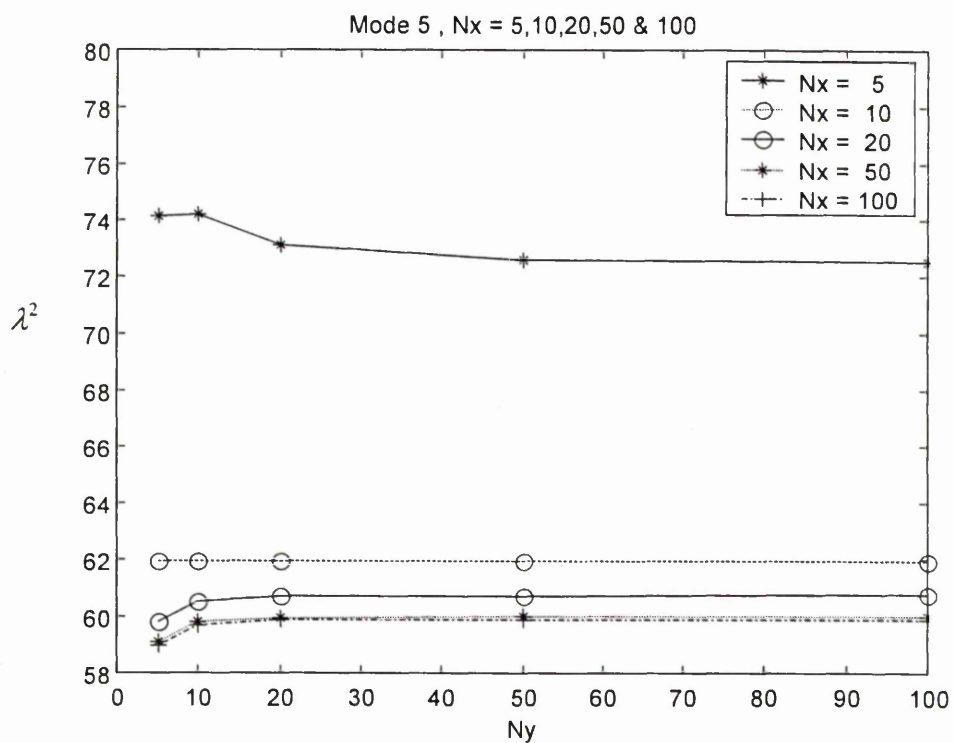


Figure 3.10 Variation of frequency parameter for mode 5 with number of elements in y -axis (N_y) and number of elements in x -axis (N_x) varied from 5 to 100

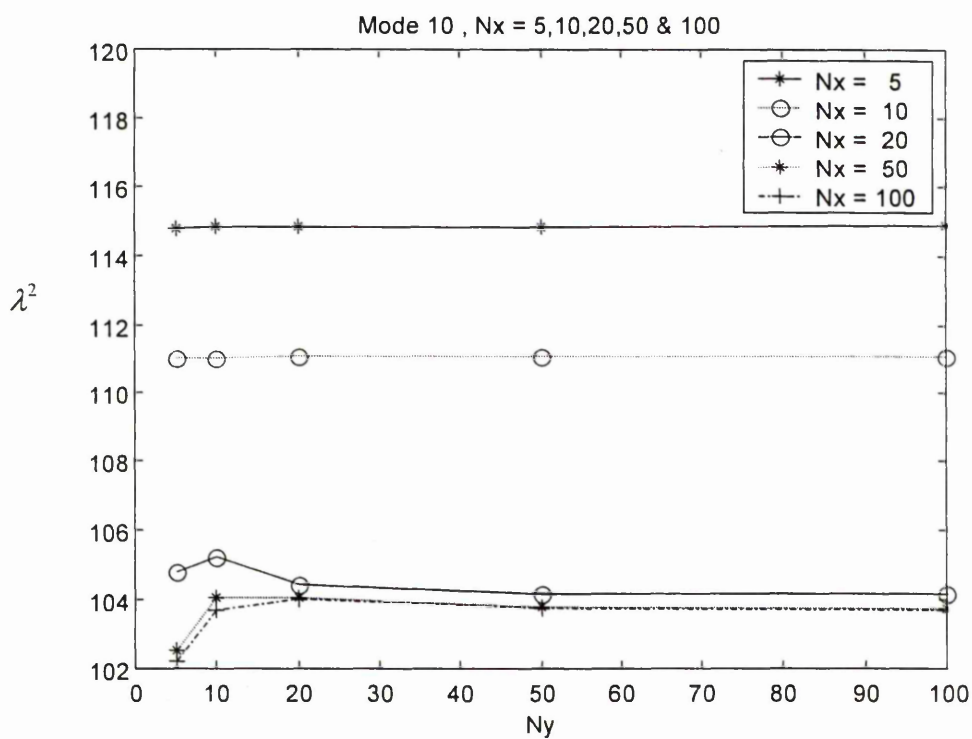


Figure 3.11 Variation of frequency parameter for mode 10 with number of elements in y -axis (N_y) and number of elements in x -axis (N_x) varied from 5 to 100

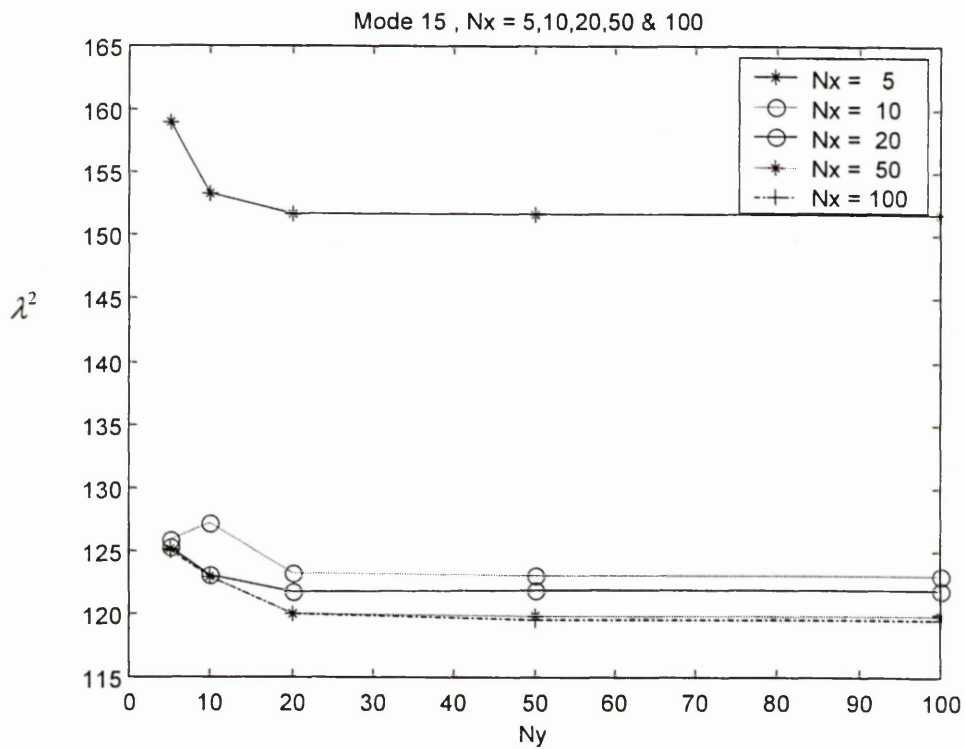


Figure 3.12 Variation of frequency parameter for mode 15 with number of elements in y -axis (N_y) and number of elements in x -axis (N_x) varied from 5 to 100

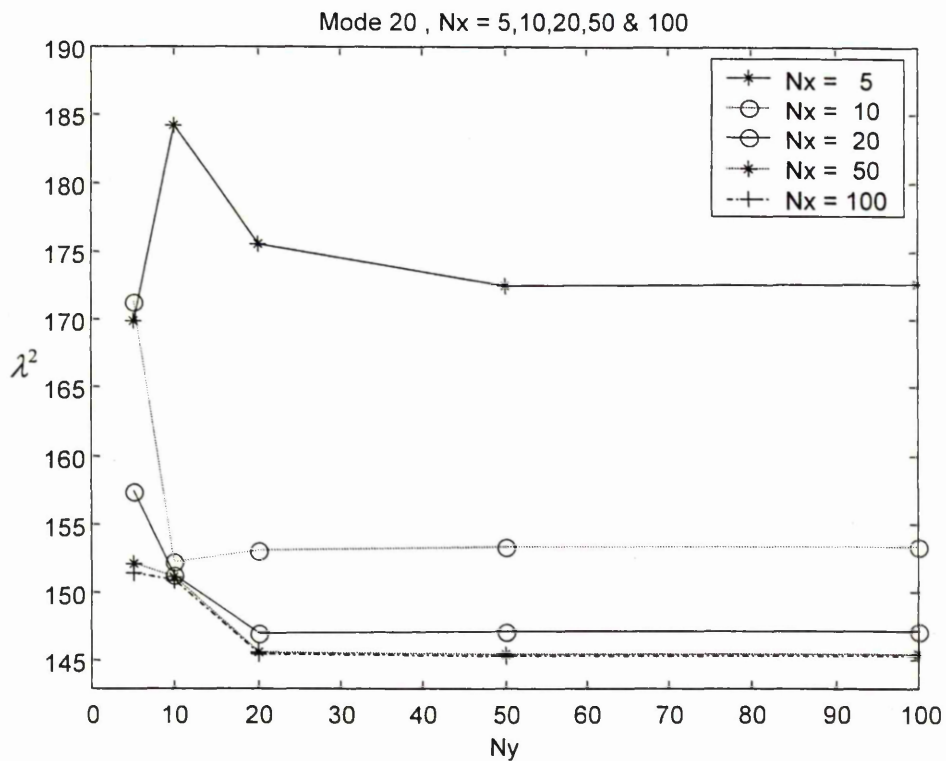


Figure 3.13 Variation of frequency parameter for mode 20 with number of elements in y -axis (N_y) and number of elements in x -axis (N_x) varied from 5 to 100

3.5.2 Variation of N_x at fixed value of N_y for clamped-clamped beam-plates.

Figures 3.14 to 3.17 show the variation of the frequency parameters for modes 1, 5, 10, 15 and 20 of the clamped-clamped plate of aspect ratio 1.0 with the number of elements along the x -axis (N_x) while the number of elements along the y -axis (N_y) was fixed at 5, 10, 20, 50 and 100. The definition of the symbols and line types in these figures are as follows:

- * and solid line denote the frequency parameters using $N_y = 5$,
- o and dash line denote the frequency parameters using $N_y = 10$,
- o and solid line denote the frequency parameters using $N_y = 20$,
- * and dash line denote the frequency parameters using $N_y = 50$,
- + and dashdot line denote the frequency parameters using $N_y = 100$,

Figure 3.14 shows the variation of the frequency parameter for mode 1 with the number of elements in the x -axis (N_x). It can be seen that the frequency parameters predicted are very close for all the values of N_x and N_y used. Therefore the range of values of $N_x \geq 5$ and $N_y \geq 5$ are acceptable.

From Figure 3.15 for mode 5, it is seen that for values of $N_x \geq 10$ and $N_y \geq 5$, the errors in the predicted frequency parameters are less than 4%. For errors of less than 0.5% the number of elements used should be $N_x \geq 20$, $N_y \geq 10$.

For mode 10, Figure 3.16 shows that $N_x \geq 50$ and $20 < N_y < 100$ will predict frequency parameters within an error bound of less than 0.2 %. Similarly, for mode 15, Figures 3.17 shows that when $N_x > 20$ and $20 < N_y < 100$, the errors in the predicted frequency parameters are negligibly small.

Finally, in Figure 3.18 the predicted frequency parameters are very close for $20 < N_y < 100$ and $N_x \geq 20$. The percentage error of the predicted frequency parameter at $N_x = 20$ is less than 0.1%.

It can be concluded from the study of Figures 3.9 to 3.18, that the minimum suitable number of elements to be used in the ABAQUS FEA program for a beam-plates of aspect ratio 1.0 are $N_x = N_y = 20$. However it was decided for more accurate results to use minimum number of elements $N_x = N_y = 100$, that is five times the minimum required. This is because the subsequent analysis will be carried out for 50 modes of vibration and in order to obtain very accurate results. For the other aspect ratio the number of elements along the y -axis (N_y) was varied according to the aspect ratios (r).

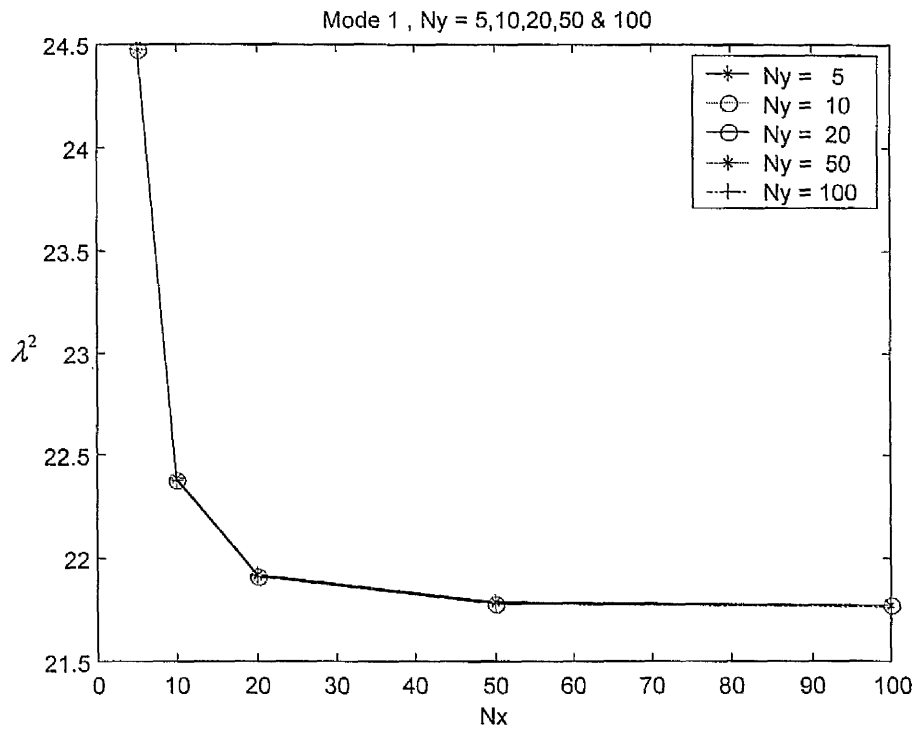


Figure 3.14 Variation of frequency parameter for mode 1 with number of elements in x -axis (N_x) and number of elements in y -axis (N_y) varied from 5 to 100

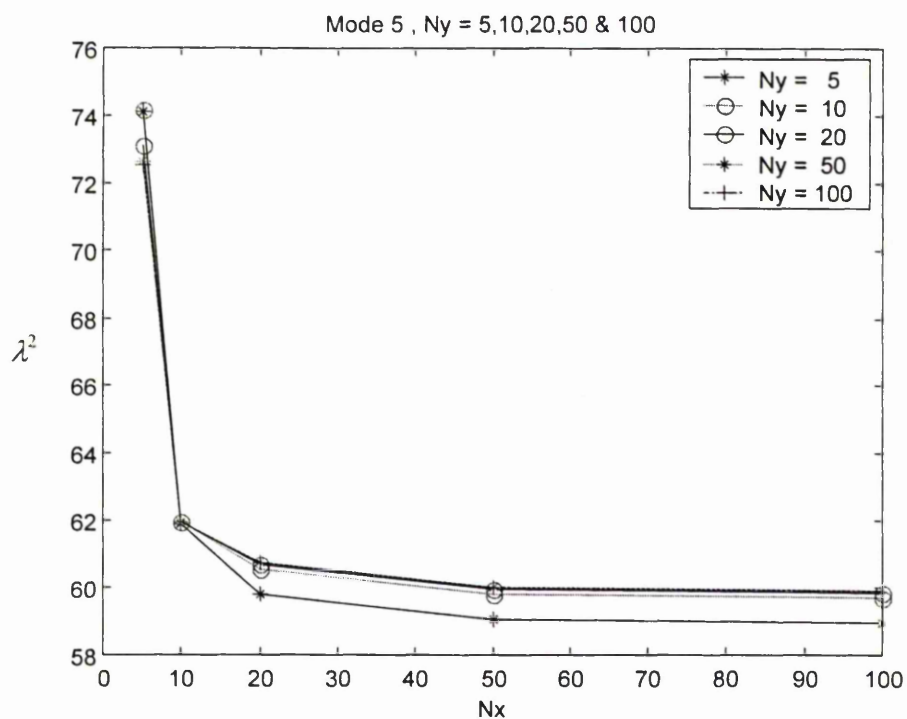


Figure 3.15 Variation of frequency parameter for mode 5 with number of elements in x -axis (N_x) and number of elements in y -axis (N_y) varied from 5 to 100

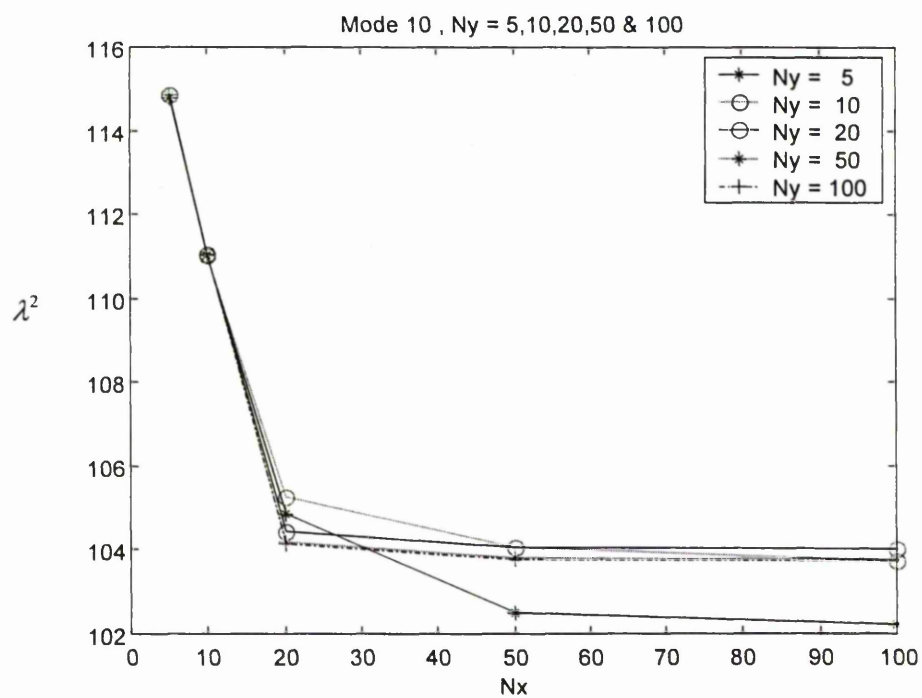


Figure 3.16 Variation of frequency parameter for mode 10 with number of elements in x -axis (N_x) and number of elements in y -axis (N_y) varied from 5 to 100

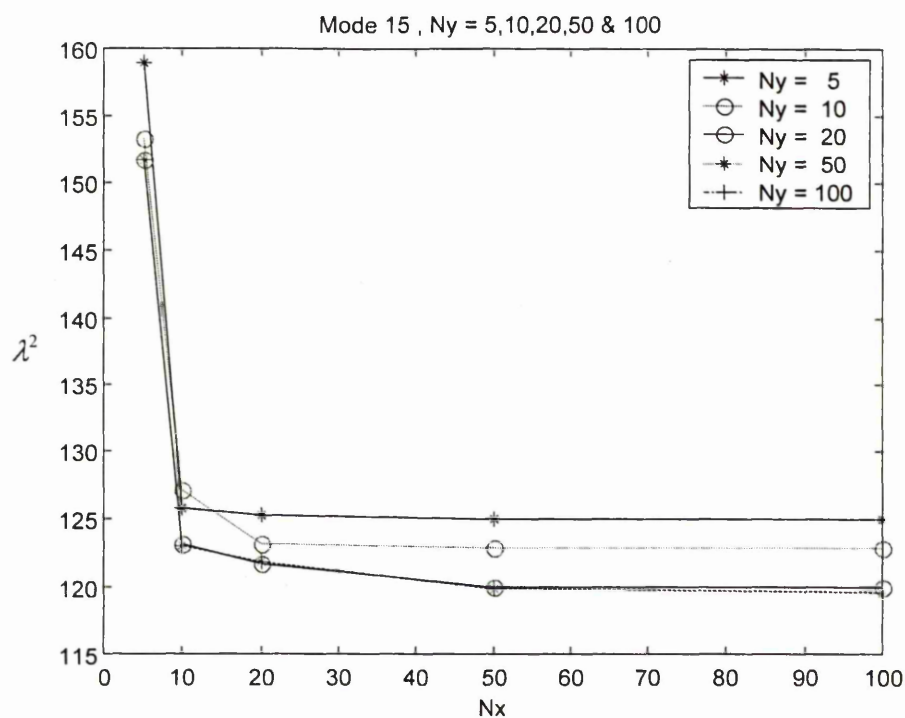


Figure 3.17 Variation of frequency parameter for mode 15 with number of elements in x -axis (N_x) and number of elements in y -axis (N_y) varied from 5 to 100

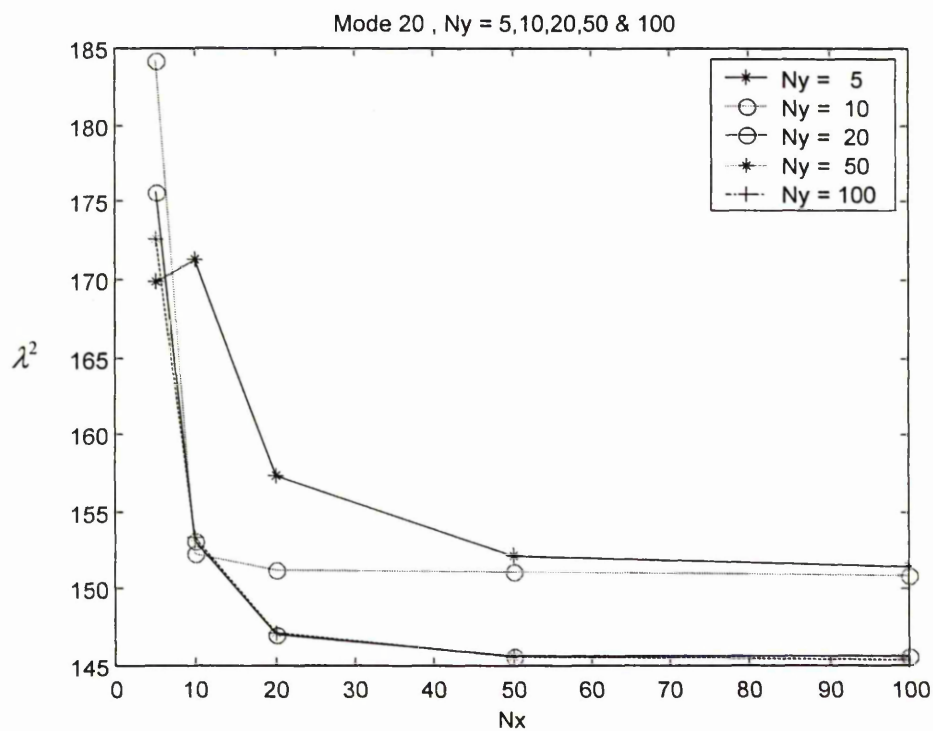


Figure 3.18 Variation of frequency parameter for mode 20 with number of elements in x -axis (N_x) and number of elements in y -axis (N_y) varied from 5 to 100.

3.5.3 Variation of N_y at fixed values of N_x for free-free beam-plates

A similar analysis was carried out on the free-free boundary conditions Figures 3.19 to 3.23 show the variation of the frequency parameter with mode number N_y . Due to the symmetry of the free-free beam-plates, variation of N_x or N_y will produce similar results. It can be deduced from Figure 3.19 that $N_x = 5$ and $N_y = 5$ give errors of about 3%, $N_x = 10$, $N_y = 5$ give errors of about 1%, while $N_x = 20$, $N_y = 5$ give errors of about 0.1% in comparison to $N_x = 100$, $N_y = 100$. Therefore, for mode 1, values of $N_x \geq 20$ and $N_y \geq 5$ are acceptable.

For mode 5, Figure 3.20 indicates that the errors in the predicted frequency parameters are about 5%, 1% or 0.2% when $N_x = 5$, $N_y = 10$ or $N_x = 10$, $N_y = 10$ or $N_x = 20$, $N_y = 10$ are used instead of $N_x = 100$, $N_y = 100$. Therefore, for mode 5 the values of $N_x \geq 20$ and $N_y \geq 5$ are acceptable. Similarly, Figure 3.21 to 3.23 indicate that for negligibly small errors, numbers of elements to use in the analysis are given by $N_x \geq 20$, $N_y \geq 20$ for modes 10, 15 and 20.

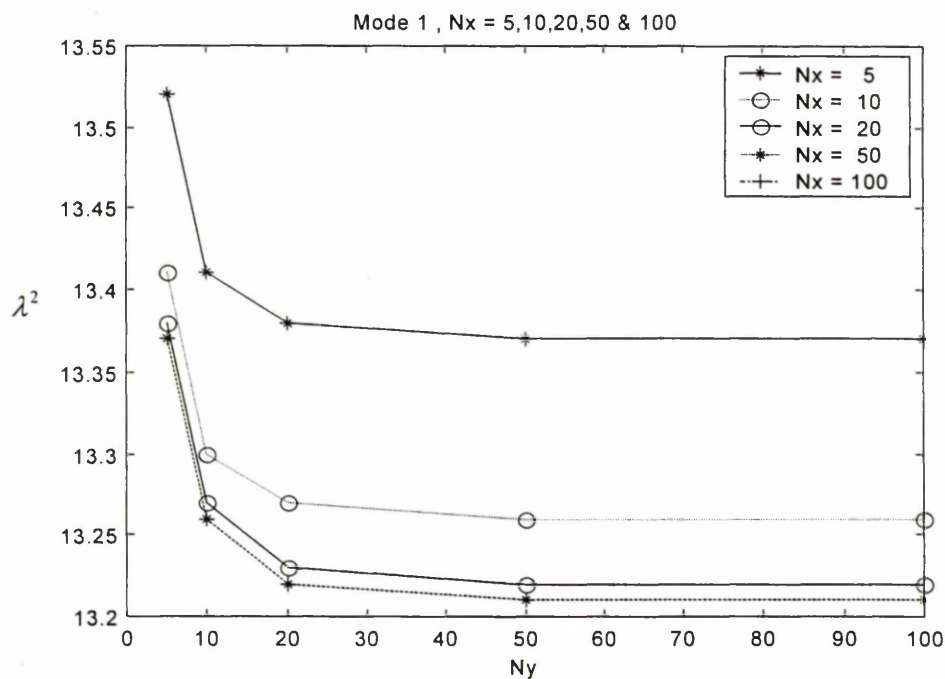


Figure 3.19 Variation of frequency parameter for mode 1 with number of elements in y-axis (N_y) and number of elements in x-axis (N_x) varied from 5 to 100

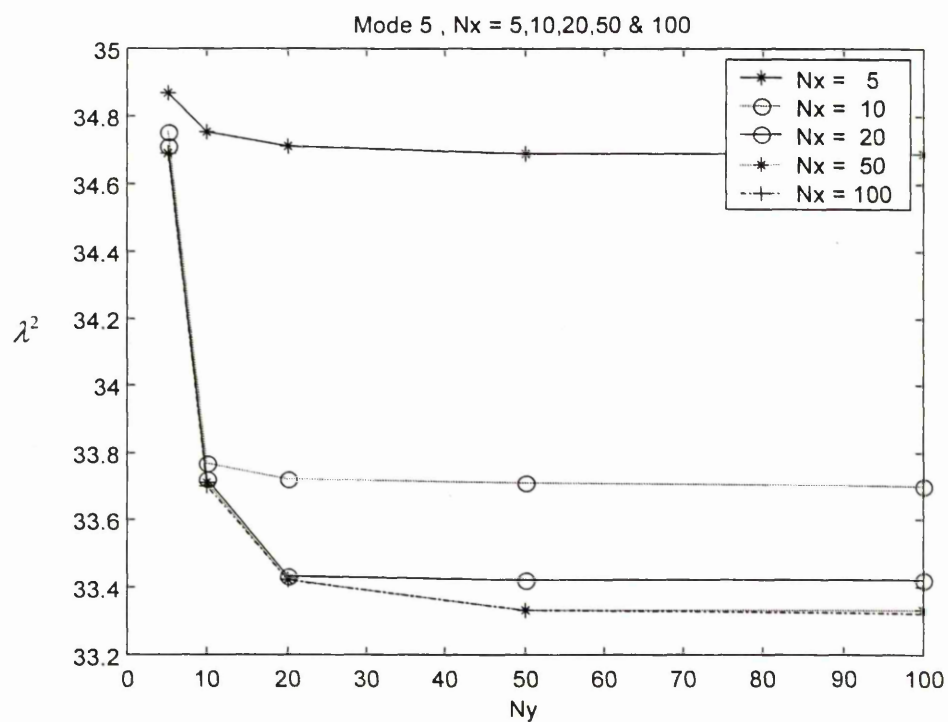


Figure 3.20 Variation of frequency parameter for mode 5 with number of elements in y -axis (N_y) and number of elements in x -axis (N_x) varied from 5 to 100

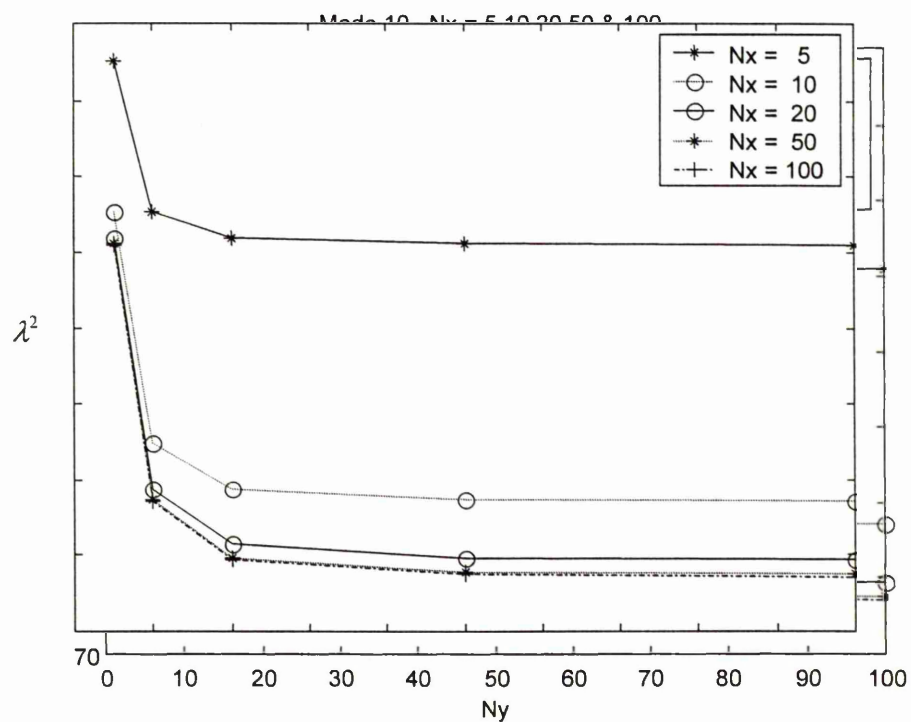


Figure 3.21 Variation of frequency parameter for mode 10 with number of elements in y -axis (N_y) and number of elements in x -axis (N_x) varied from 5 to 100

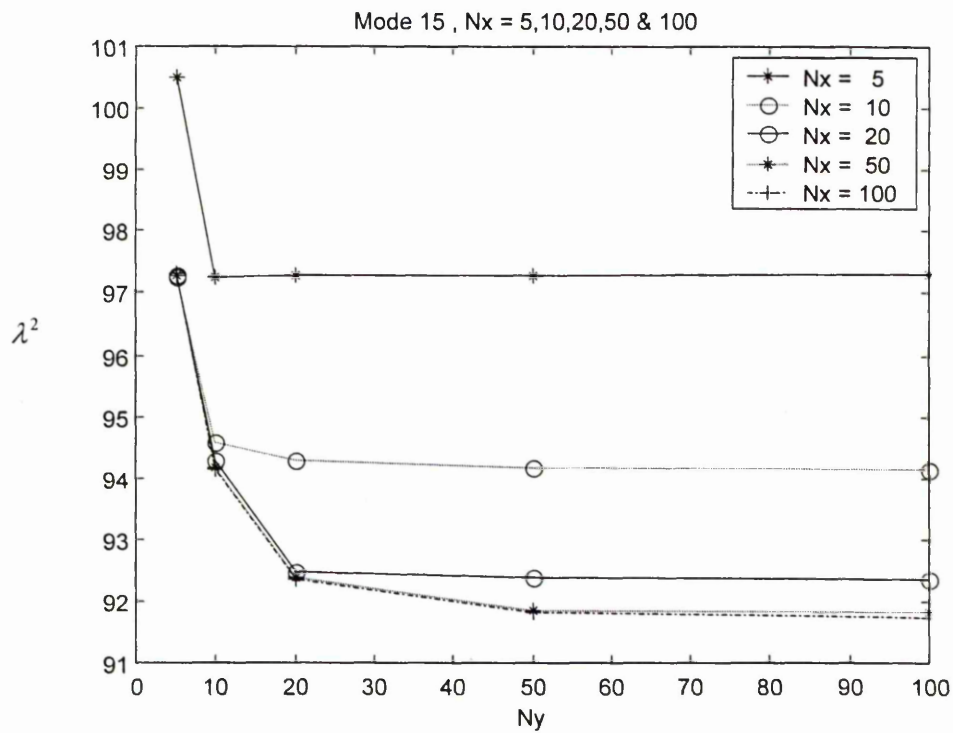


Figure 3.22 Variation of frequency parameter for mode 15 with number of elements in y-axis (N_y) and number of elements in x-axis (N_x) varied from 5 to 100

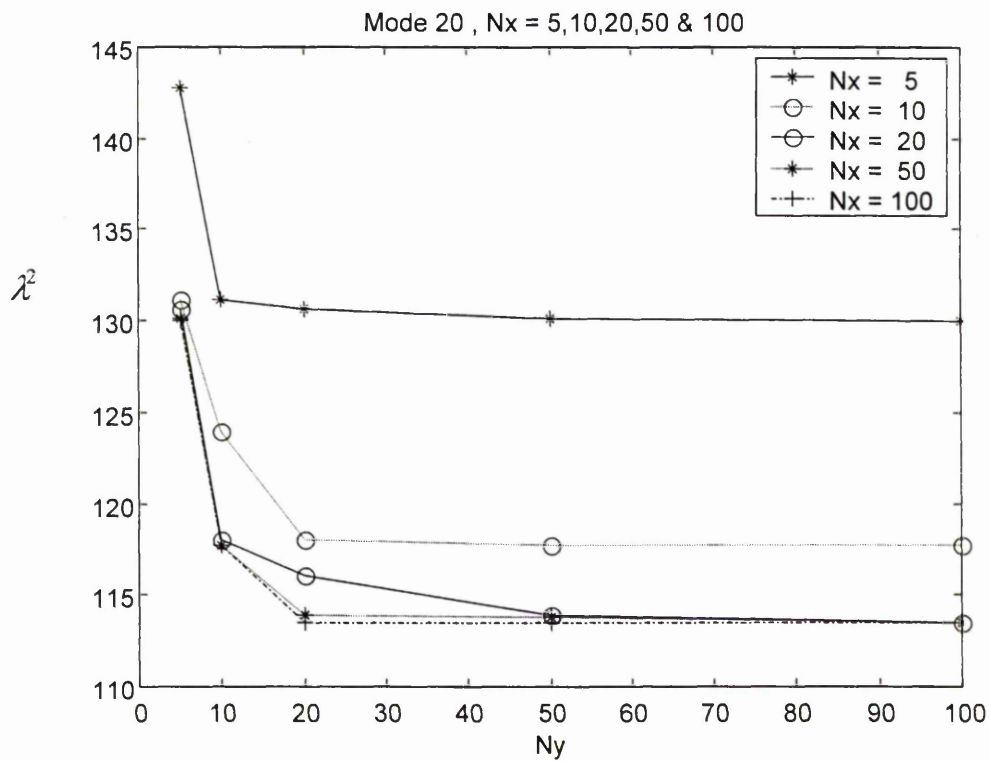


Figure 3.23 Variation of frequency parameter for mode 20 with number of elements in y-axis (N_y) and number of elements in x-axis (N_x) varied from 5 to 100

3.6 Prediction of natural frequencies and mode shapes

The ABAQUS FE program was used to calculate the natural frequencies for the free-free and clamped-clamped beam-plates for 20 ratios (a/b) which are 0.25, 0.5, 0.75, 1.00, 1.25, 1.50, 1.75, 2.00, 2.5, 3.0, 3.5, 4.0, 4.5, 5.0, 6.0, 7.0, 8.0, 9.0, 10.0, 15.0 and 20.0. The number of elements along the x-axis (N_x) for aspect ratio 0.25 was 60 and for aspect ratio 0.5 was 80 and for aspect ratio greater than 0.75 (N_x) was fixed to 100 elements. The reason for using fewer elements for small aspect ratio is to minimise the results file size and the time to solve the finite element analysis. However the number of elements along the y-axis, (N_y) varied according to the ratio a/b , and this ratio varied as the breadths (b) varied. Table 3.1 shows the values of a/b , a , b , N_x , N_y used in this analysis

Table 3.1 Ratio(a/b), length(a), number of elements in x axis (N_x) and number of elements in y axis (N_y).

Ratio(a/b)	Length a (m)	Breath b (m)	N_x	N_y
0.25	0.50	2.00	60	240
0.50	0.50	1.00	80	160
0.75	0.50	0.667	100	133
1.00	0.50	0.50	100	100
1.25	0.50	0.40	100	80
1.50	0.50	0.333	100	67
2.00	0.50	0.25	100	50
2.50	0.50	0.20	100	40
3.00	0.50	0.167	100	33
3.5	0.50	0.143	100	29
4.00	0.50	0.125	100	25
4.50	0.50	0.111	100	22
5.00	0.50	0.10	100	20
6.00	0.50	0.083	100	17
7.00	0.50	0.071	100	14
8.00	0.50	0.063	100	13
9.00	0.50	0.056	100	11
10.00	0.50	0.05	100	10
15.00	0.50	0.033	100	7
20.00	0.50	0.025	100	5

3.6.1 Deduction of the frequency parameters from natural frequencies

From Equations (2.70) and (2.73) of the previous chapter, the frequency parameters for plate-like behaviour and beam-like behaviour are related to the natural frequency, respectively, by

$$(\lambda^2_{ij})_p = 2\pi a^2 f_{ij} \left[\frac{12\rho(1-\nu^2)}{Eh^2} \right]^{1/2} \quad (3.1)$$

$$(\lambda^2_{ij})_b = 2\pi a^2 f_{ij} \left[\frac{12\rho}{Eh^2} \right]^{1/2} \quad (3.2)$$

where;

$(\lambda^2_{ij})_p$ = square of frequency parameters calculated from plate equation

$(\lambda^2_{ij})_b$ = square of frequency parameters calculated from beam equation

f_{ij} = natural frequency (Hz)

λ^2_{ij} = square of frequency parameters

γ = mass per unit area of plate (ke/m²)

ρ = density of aluminium (kg/m³)

ν = Poisson's ratio of aluminium

E = Young modulus of aluminium (pa)

a = Length of plate (m)

h = thickness of plate (m)

i = number of half-wave in mode shape along horizontal axis

j = number of half-wave in mode shape along vertical axis

Substituting f_{ij} (from FE results), $\rho = 2700 \text{ kg/m}^3$, $\nu = 0.33$, $E = 70 \times 10^9 \text{ N/m}^2$, $a = 0.50 \text{ m}$ and $h = 0.005, 0.01, 0.025$ and 0.05 m into Equations (3.1) and (3.2), the square of frequency parameters of plate-like and beam-like vibration, can be calculated from the predicted natural frequencies.

3.7 Summary

The work discussed in this chapter has covered an important part of the finite element analysis. This is the selection of element type and the number of elements which can be used along the length and breadth of the beam-plates in order to produce the best result. This was done through the study of element type and mesh density using the ABAQUS FEA programme. The general purpose shell element S4R was found to be the best economical element to use for thicker beam-plates. This study was based on the comparisons of these elements with the 20-noded solid element C3D20R in terms of the accuracy of the results, time for the job to run, the sizes of the output files. From the mesh study, the minimum number of elements required along the x -axis and y -axis for accurate results are 20, 20 respectively for a beam-plate of aspect ratio 1.0 and for the first 20 natural frequencies and mode shapes. But in the rest of the work presented in subsequent chapters, the first 50 natural frequencies and mode shapes of beam-plates are computed. Therefore for high accuracy up to mode 50, it was decided that the number of elements along the x -axis be $N_x = 100$, while the number of elements along the y -axis was varied with the aspect ratios (r) according to the formula: $N_y = N_x/r$.

Chapter 4

Study of the natural frequency parameters and mode shapes for clamped-clamped beams and plates

4.1 Introduction

This chapter is focused on the natural frequencies and mode shapes of clamped-clamped beams and plates predicted by the finite element method using the ABAQUS FEA program. The natural frequency parameters are derived from the natural frequencies and used as a basis for investigating the presence or absences of a distinct transition from beam-like to plate-like behaviour in the vibration characteristics of clamped-clamped beams and plates.

The first 50 natural frequencies and mode shapes of clamped-clamped aluminium alloy beams and plates were obtained from the ABAQUS FEA program

Aluminium alloy was used in the analysis. However, other engineering materials such as steel and brass could be used. The important material properties to consider are young's modulus (E), density (ρ) and poisson's ratio (ν). In previous work, Tangchaichit [1,2,3] showed that poisson's ratio does not have a significant effect on the frequency parameters. The effects of the other two parameters can be examined in terms of wave velocity $C = \sqrt{E/\rho}$. For example, the wave velocity of aluminium alloy and steel are considered. For aluminium alloy, $E = 70\text{Gpa}$, $\rho = 2700\text{ kg/m}^3$ and $C_{al} = 5090\text{ m/s}$. For steel, $E = 210\text{ Gpa}$, $\rho = 7850\text{ kg/m}^3$ and $C_{st} = 5170\text{ m/s}$. Because the wave velocities of aluminium alloy and steel are very close the results obtained from the FE analyses for aluminium alloy beams and plates are directly applicable to steel beams and plates. The beams and plates were of a fixed length $a = 500\text{ mm}$ and thickness to length ratio thickness 1%, 2%, 5% and 10% (thickness, $t = 5, 10, 25$ and 50 mm). The breadths were varied from 25 mm to 2000 mm to give 20 values of the aspect ratios, a/b , which varied from 0.25 to 20. These values of aspect ratios were 0.25, 0.5, 0.75, 1.0, 1.25, 1.50, 2.0, 2.5, 3.0, 3.5, 4.0, 4.5, 5.0, 6.0, 7.0, 8.0, 9.0, 10.0, 15.0 and 20.0. The finite element analysis was carried out using the thin shell element S8R5 for thickness to length ratio of 1%. The general purpose shell element S4R was used for thickness to length ratio of 2%, 5% and 10%. The number of elements in the lengthwise or x -axis (N_x) direction was fixed at 60 and 80 for ratio 0.25 and 0.5 respectively, and 100 elements for all other aspect ratios, while the number of elements in the breadthwise or y -axis (N_y) direction was varied with the aspect ratios a/b .

4.2 Variations of frequency parameters ($\lambda_{i,j}^2$) and mode shapes with length to-breadth ratios (a/b) and mode counter i and j

The natural frequencies, calculated using the ABAQUS FEA program, and the frequency parameters of the clamped-clamped beams and plates, obtained from the FEA results using Equations (3.3) and (3.6), for beam frequency parameters $(\lambda_{ij}^2)_b$ and plate frequency parameters $(\lambda_{ij}^2)_p$. The difference in value between these two sets of frequency parameters is due to the Poisson's ratio as shown in Equation (2.74) or Equations (3.1) and (3.2). In this chapter, and throughout the thesis, the frequency parameters $(\lambda_{ij}^2)_b$ for beam-like behaviour is used in all the various plots generated and discussed. This is to enable easy comparison with frequency parameters obtained using the Euler-Bernoulli, Timoshenko and torsional beam equations.

4.2.1 Relationship between frequency parameters and aspect ratios for fixed values of j for the clamped-clamped beams and plates.

Figures (4.1) to (4.7) shows the relationship between frequency parameters $(\lambda_{ij}^2)_b$ and aspect ratios (a/b) for fixed values of the breadthwise mode counters j . In these figures, the x -axis defines the aspect ratios while the y -axis represents the frequency parameters.

Predominantly bending modes along lengthwise direction ($j=0$)

The variations of the frequency parameters with aspect ratios are shown in Figure 4.1a, which consists of 10 curves. These curves are for $j = 0$ and $i = 0, 1, 2, 3, 4, 5, 6, 7, 8$ and 9 from the bottom-most curve to the top-most curve, respectively. The 10 curves represent the first 10 predominantly bending modes along the longitudinal (x) axis of the clamped-clamped beams and plates. Due to the scale of the graph, all curves

look like straight lines. But in reality, the curves show a decaying exponential behaviour with increasing aspect ratio. Figure 4.1b shows the mode shapes of the first ($i = 0, j = 0$) and the sixth ($i = 5, j = 0$) modes for aspect ratios 1, 5 and 10. For a particular mode, e.g. mode 1 ($i = 0$), the figure shows that the natural frequencies decrease in value as the aspect ratio increases. This indicates that the natural frequencies of the bending modes of the plates along their x-axis are greater than the corresponding natural frequencies of the beams. It suggests that the effect of the increase in bending stiffness of the plates compared to the beams is greater than the effect of the increased mass of the plates compared to the beams.

Predominantly torsional modes about lengthwise axis ($j=1$)

The trends of the frequency parameters with respect to the aspect ratios for values of $j = 1$ and $i = 0$ to 10 are shown in Figure 4.2a. This figure consists of 11 curves that correspond to values of $j = 1$ and $i = 0, 1, 2, 3, 4, 5, 6, 7, 8, 9$ and 10 from the bottom-most curve to the top-most curve, respectively. These curves show the first 11 predominantly torsion modes of the clamped-clamped beams and plates. From the graph, it is clearly seen that the frequency parameters increase in value as the aspect ratio increases and as the lengthwise mode counter i of the beam-plate increases. Figure 4.2b show the mode shapes of the first ($i = 0, j = 1$) and the sixth ($i = 5, j = 1$) modes for aspect ratios 1, 5 and 10. For a selected mode, e.g. mode 1 ($i = 0$) or mode 6 ($i = 5$), the natural frequencies (shown in brackets) of the plates are less than those of the beams. This suggests that the effect of the increase in torsional stiffness of the plates compared to the beams is less than the effect of the increased mass moment of inertia of the plates compared to the beams.

First bending deformation along breadthwise direction ($j=2$)

In Figure 4.3a is shown the variation of the frequency parameters with aspect ratios for values of $j = 2$ and $i = 0$ to 8. This figure contains 9 curves which correspond to values of $j = 2$ and $i = 0$ for the bottom-most curve to values of $j = 2$ and $i = 8$ for the top-most curve, respectively. From the figure it is clearly shown that λ_{i2}^2 increases exponentially as the aspect ratio increases. The 9 curves correspond to the first 9 combination modes for which the lengthwise bending modes are coupled with the first breadthwise bending modes. Figure 4.3b shows the mode shapes of the first ($i = 0, j = 2$) and the sixth ($i = 5, j = 2$) modes for aspect ratios 1, 5 and 10. In addition to the lengthwise bending, this figure clearly shows the breadthwise bending of the beams and plates. It is seen that for a selected mode, e.g. mode 1 ($i = 0$) and mode 6 ($i = 5$), the natural frequencies of the beams are greater than the natural frequencies of the plates. Again, this suggests that the effect of increases in the breadthwise bending stiffness is less than the effect of increases in the mass moment of inertia.

Second bending deformation along breadthwise direction ($j=3$)

Figure 4.4a shows the variation of the frequency parameters with aspect ratios for values of $j = 3$ and $i = 0$ to 7. This figure consists of 8 curves which correspond to values of $j = 3$ and $i = 0, 1, 2, 3, 4, 5, 6, 7$ and 8 from the bottom-most curve to the top-most curve, respectively. It is obvious from the figure that the frequency parameters, λ_{i3}^2 , increase exponentially as the aspect ratio increases. The 8 curves shown in this figure correspond to the first 8 combination modes for which the lengthwise bending modes are coupled with the second breadthwise bending modes. The mode shapes of the first ($i = 0, j = 3$) and the fourth ($i = 3, j = 3$) modes for aspect ratios 1 and 5 are

shown in Figure 4.4*b*. The deductions made concerning the separate effects of bending stiffness and mass moment of inertia when $j=2$ are seen to hold.

Third bending deformation along breadthwise direction ($j=4$)

The variation of the frequency parameters, λ_{i4}^2 with aspect ratios for values of $j = 4$ and $i = 0$ to 5 are shown in Figure 4.5*a*. The curves shown in this figure are for $j = 4$ and $i = 0, 1, 2, 3, 4, 5$ from the bottom-most curve to the top-most curve, respectively. From the figure it is clearly that λ_{i4}^2 increases exponentially as the aspect ratio increases, and as the lengthwise mode counter i of the plate increases.

The curves in this figure correspond to the first 6 combination modes for which the lengthwise bending modes are coupled with the third breadthwise bending modes. The mode shapes of the first ($i = 0, j = 4$) and the fourth ($i = 3, j = 4$) modes for aspect ratios 1 and 2 are shown in Figure 4.5*b*. Again, the previous deductions made when $j=2$ that the effects of mass moment of inertia are greater than the effects of breadthwise bending stiffness are seen to apply.

Fourth bending deformation along breadthwise direction ($j=5$)

Figure 4.6*a* show 5 curves which represent the variation of the frequency parameters with aspect ratios for values of $j = 5$ and $i = 0, 1, 2, 3, 4$ from the bottom-most curve to the top-most curve, respectively. The figure shows that the frequency parameters increase as the aspect ratio increase and as the mode counter i increase. The 5 curves in this figure correspond to the first 5 combination modes for which the lengthwise bending modes are coupled with the fourth breadthwise bending modes. Figure 4.6*b* shows the mode shapes of the first ($i = 0, j = 5$) and the fourth ($i = 3, j = 5$) modes for aspect ratios 0.50 and 1. Since, the natural frequencies at the higher aspect

ratios of 1 are higher than those of aspect ratio $r = 0.5$, it can be implied that the previous deductions of the case $j=2$ also apply here.

Fifth bending deformation along breadthwise direction ($j=6$)

The variations of frequency parameters with aspect ratios for the values of $j = 6$ and $i = 0$ to 4 are shown in Figure 4.7a. This figure consist of 5 curves which correspond to values of $j = 6$ and $i = 0, 1, 2, 3$ and 4 from the bottom-most curve to the top-most curve, respectively. These 5 curves show that the frequency parameters increase as the aspect ratios and as the mode counter i increases. These curves correspond to the first 5 combination modes for which the lengthwise bending modes are coupled with the sixth breadthwise bending modes. Figure 4.7b show the mode shapes of the first ($i = 0, j = 6$) and the fourth ($i = 3, j = 6$) modes for aspect ratios 0.50 and 1. As in the previous case of $j=5$, it can be deduced from the frequencies that the effect of increased mass moment of inertia is greater than the effect of increased bending stiffness.

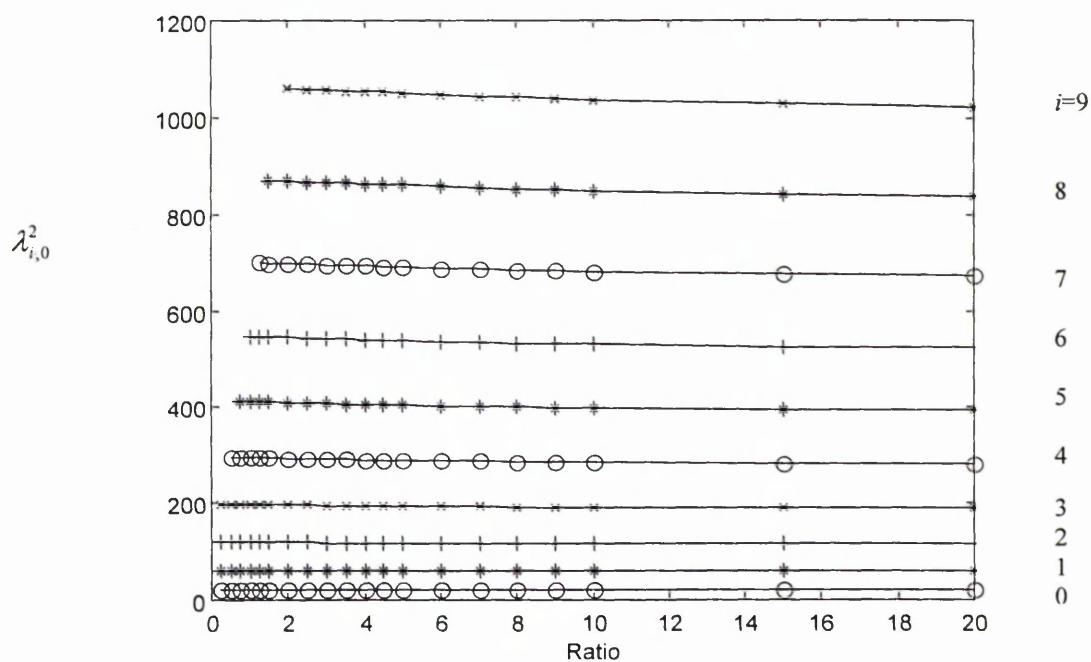


Figure 4.1a Variation of frequency parameters with aspect ratios for $j = 0$ and $i=0$ to 9

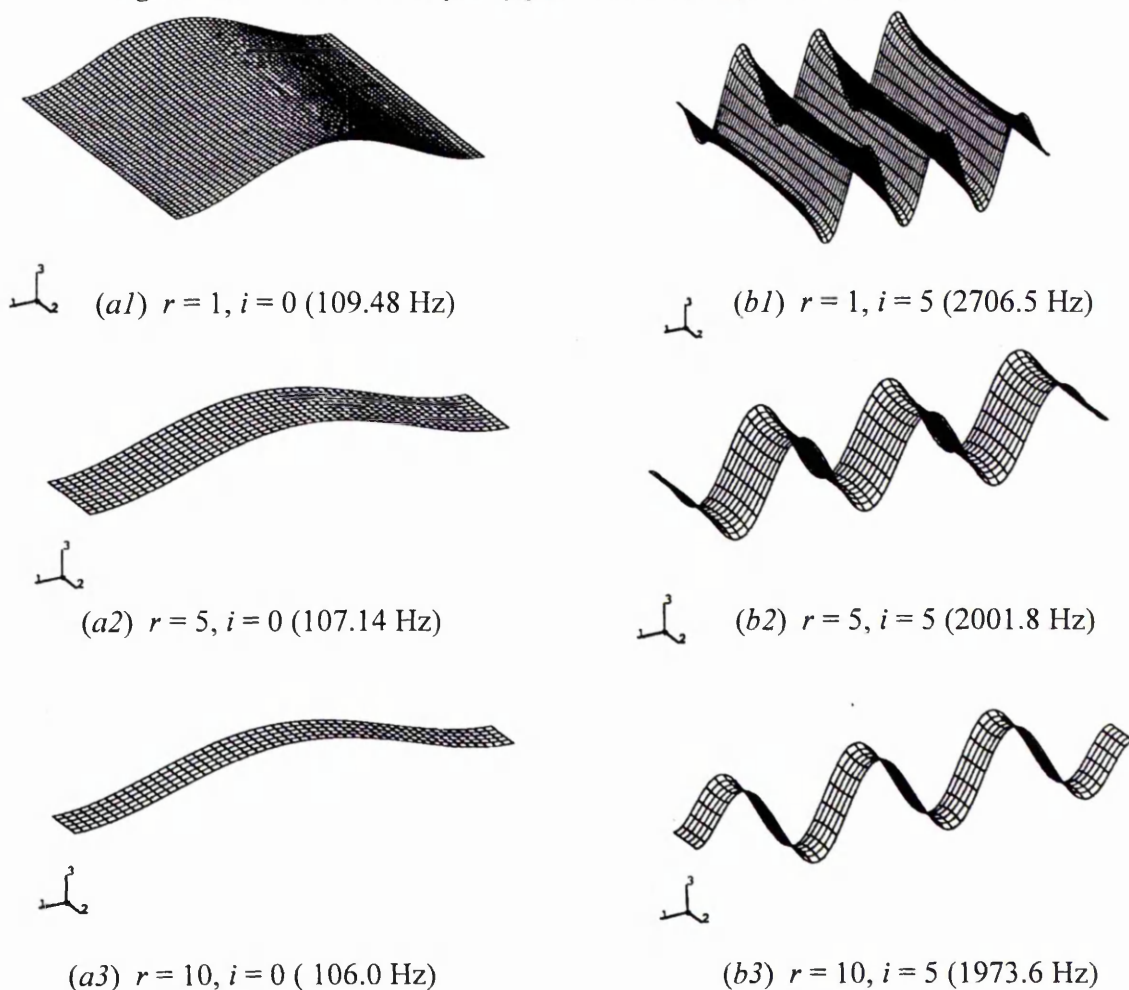


Figure 4.1b Mode shapes of beam-plates for mode counter $j = 0$

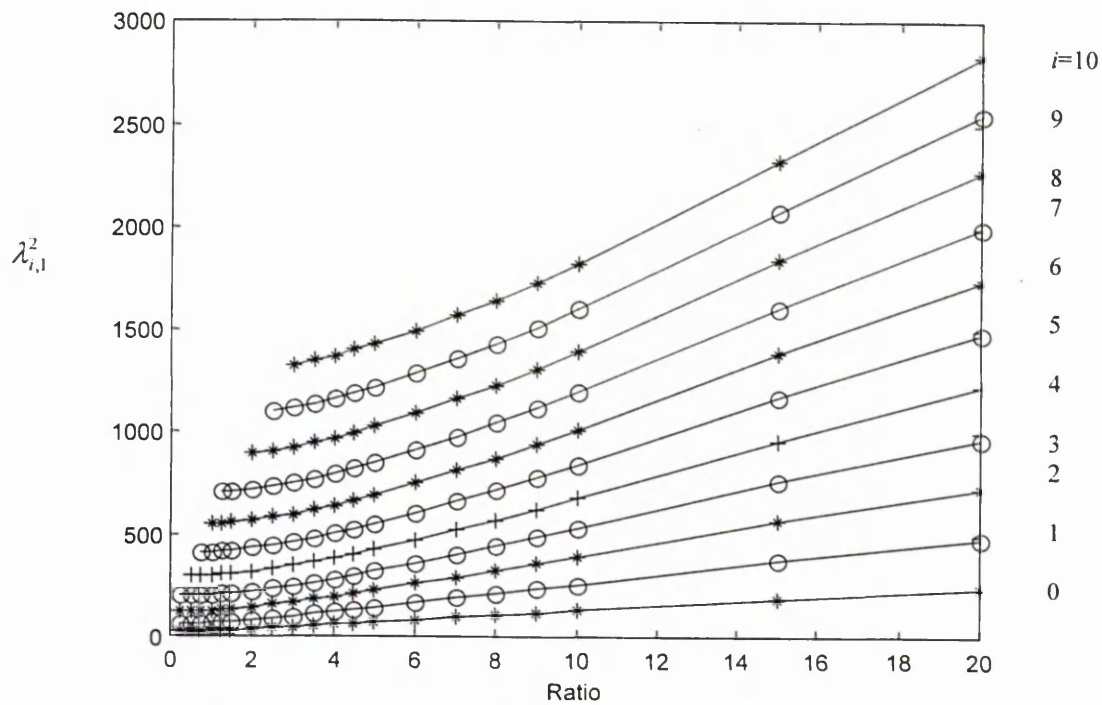


Figure 4.2a Variation of frequency parameters with aspect ratios for $j = 1$

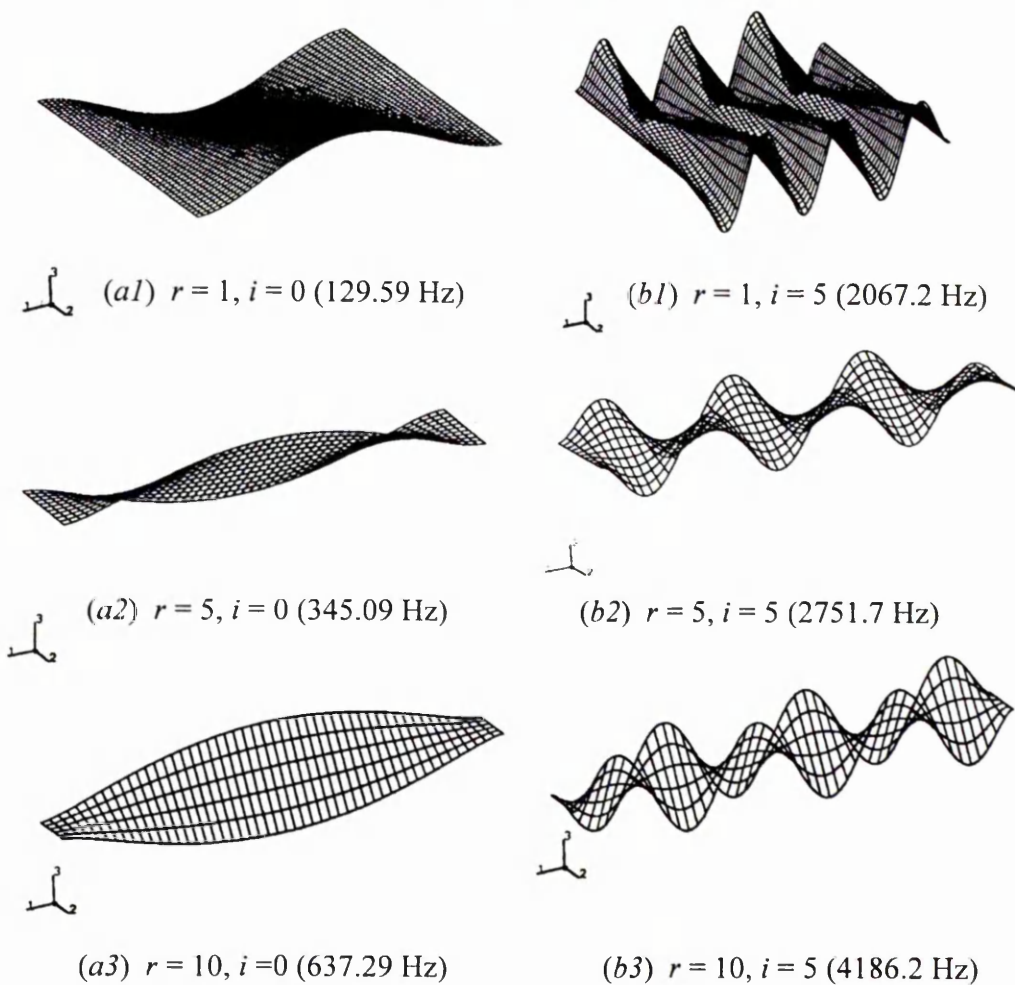


Figure 4.2b Mode shapes of beam-plates for mode counter $j = 1$

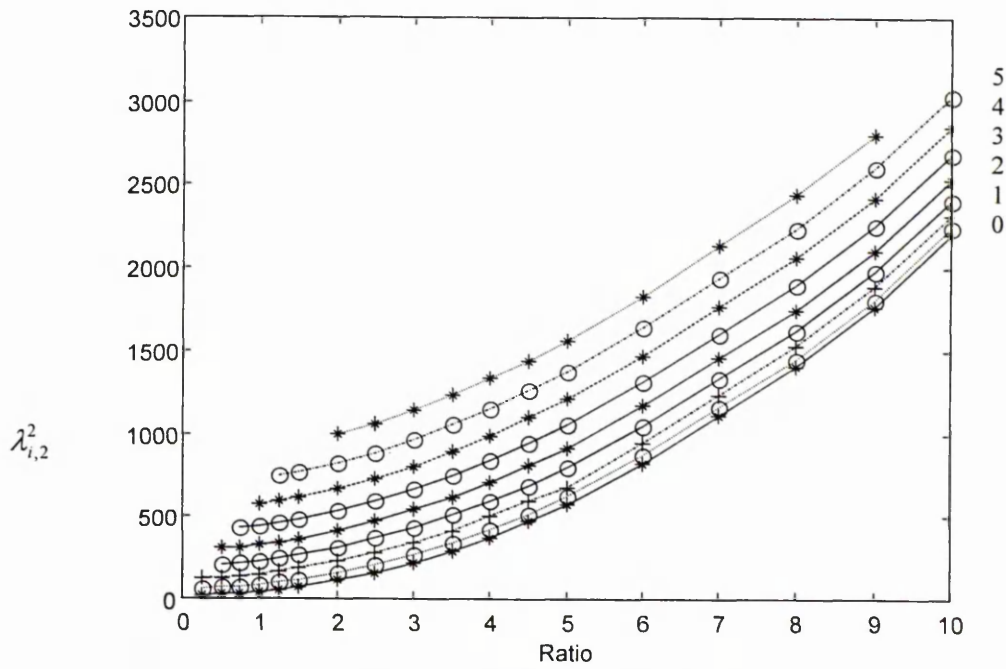


Figure 4.3a Variation of frequency parameters with aspect ratios for $j = 2$

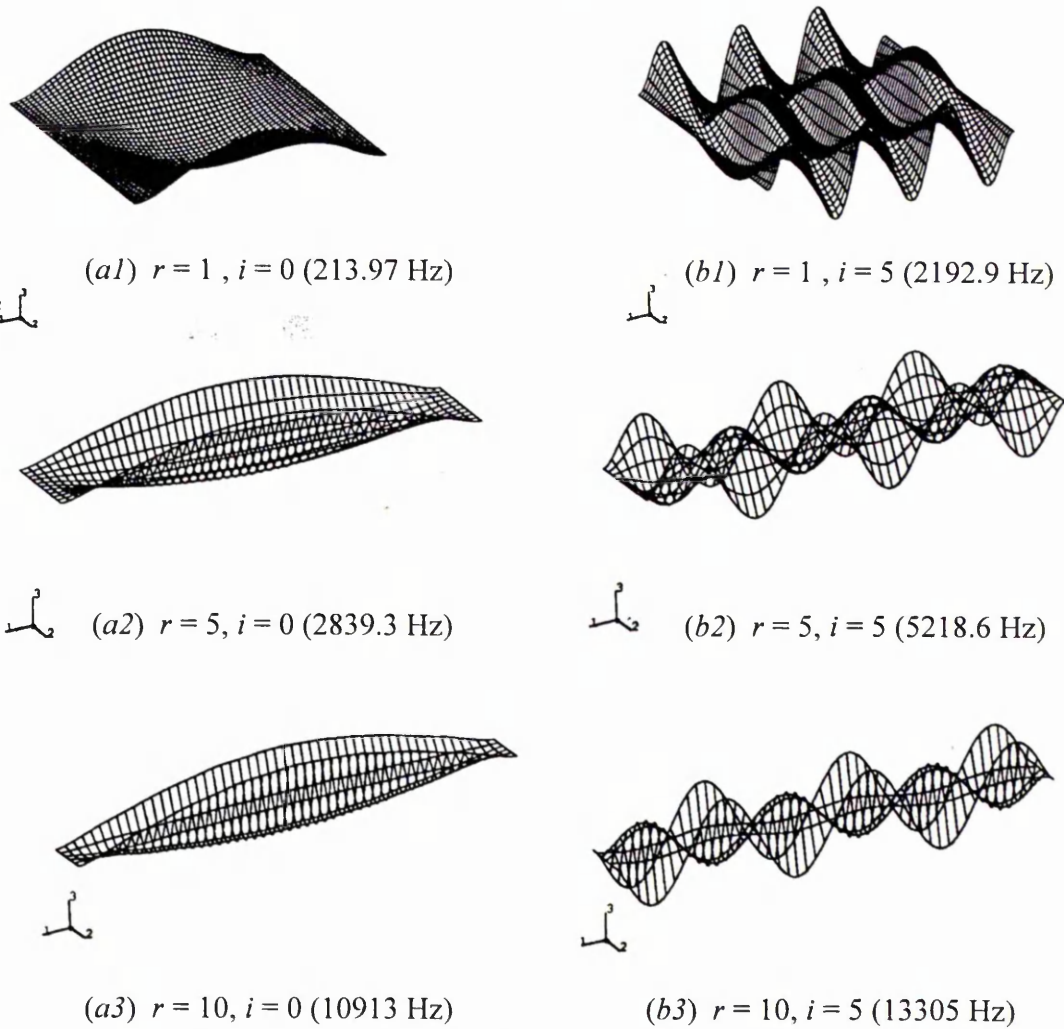


Figure 4.3b Mode shapes of beam-plates for mode counter $j = 2$

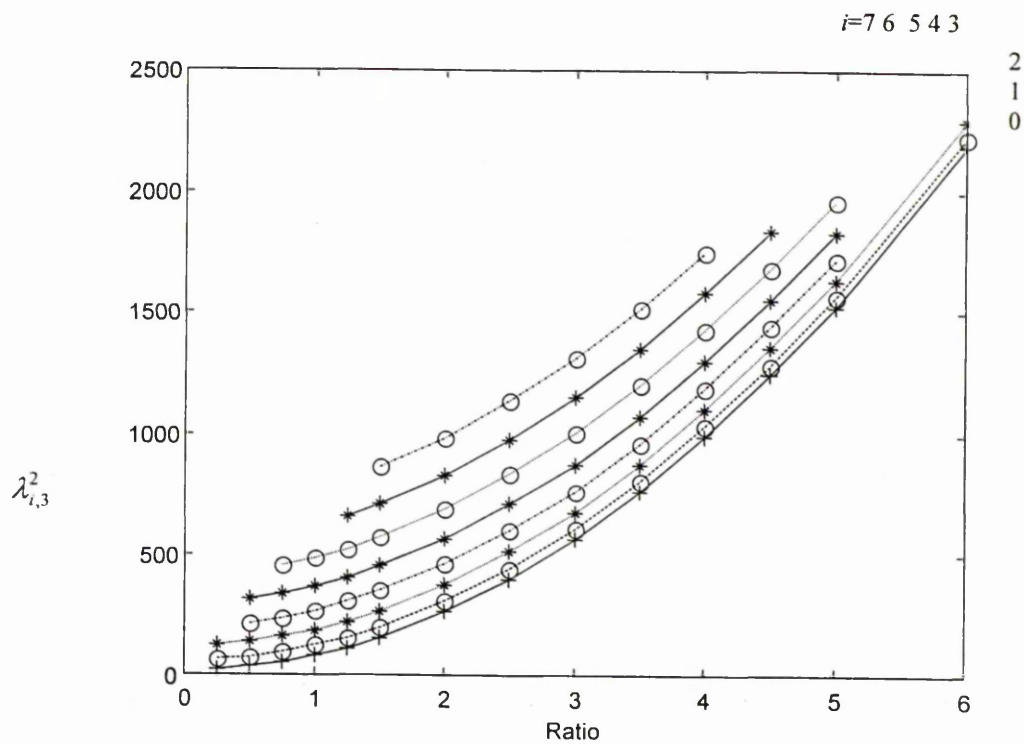


Figure 4.4a Variation of frequency parameters with aspect ratios for $j = 3$

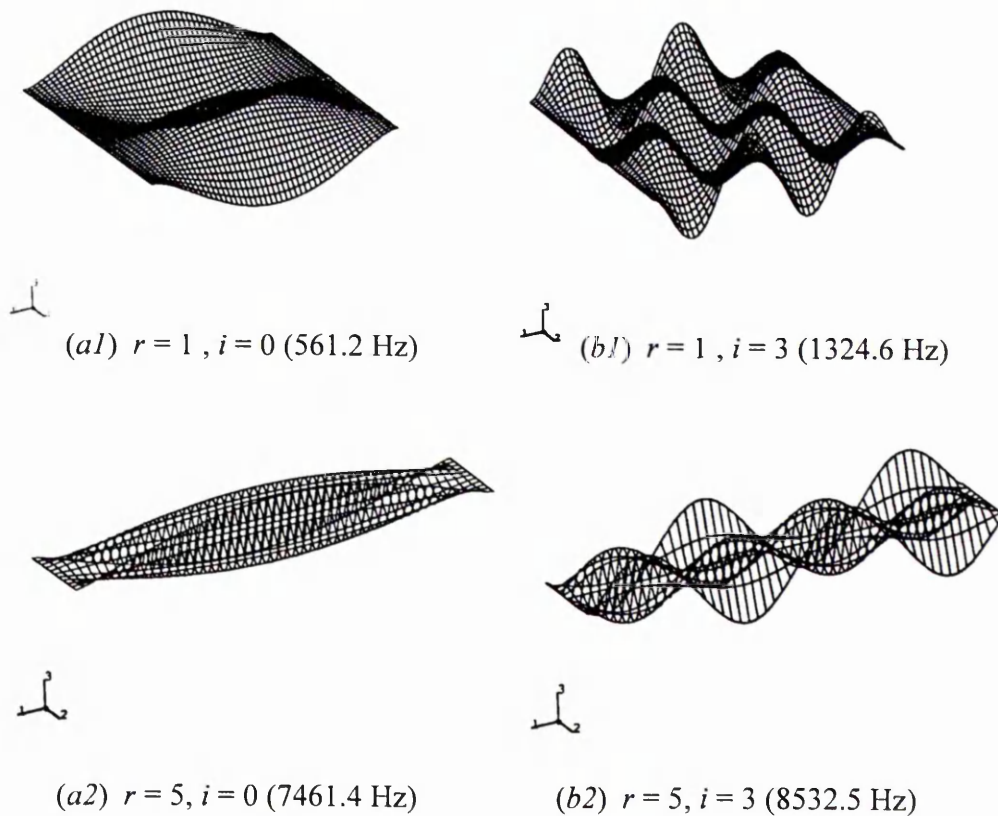


Figure 4.4b Mode shapes of beam-plates for mode counter $j = 3$

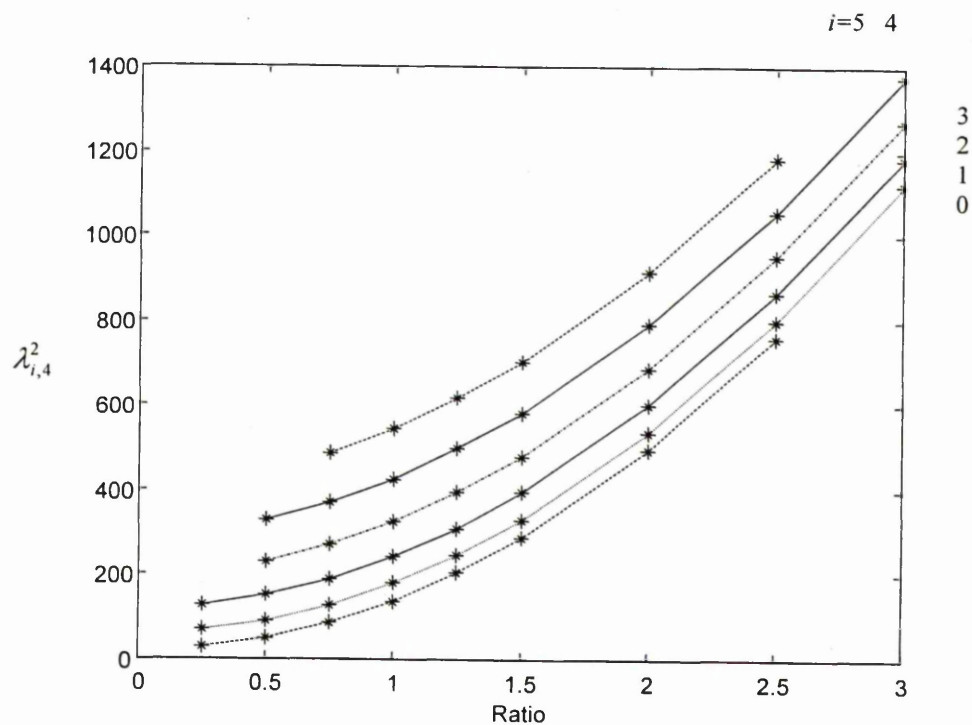


Figure 4.5a Variation of frequency parameters with aspect ratios for $j = 4$

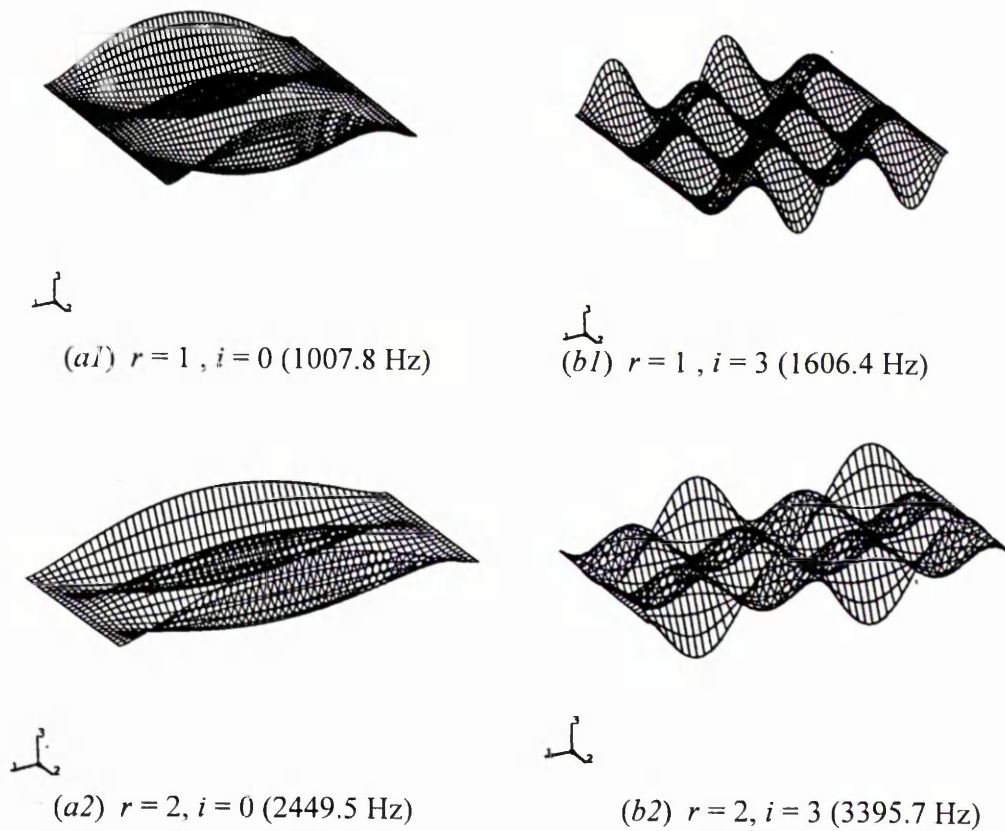


Figure 4.5b Mode shapes of beam-plates for aspect ratio 0.75, $j = 4$

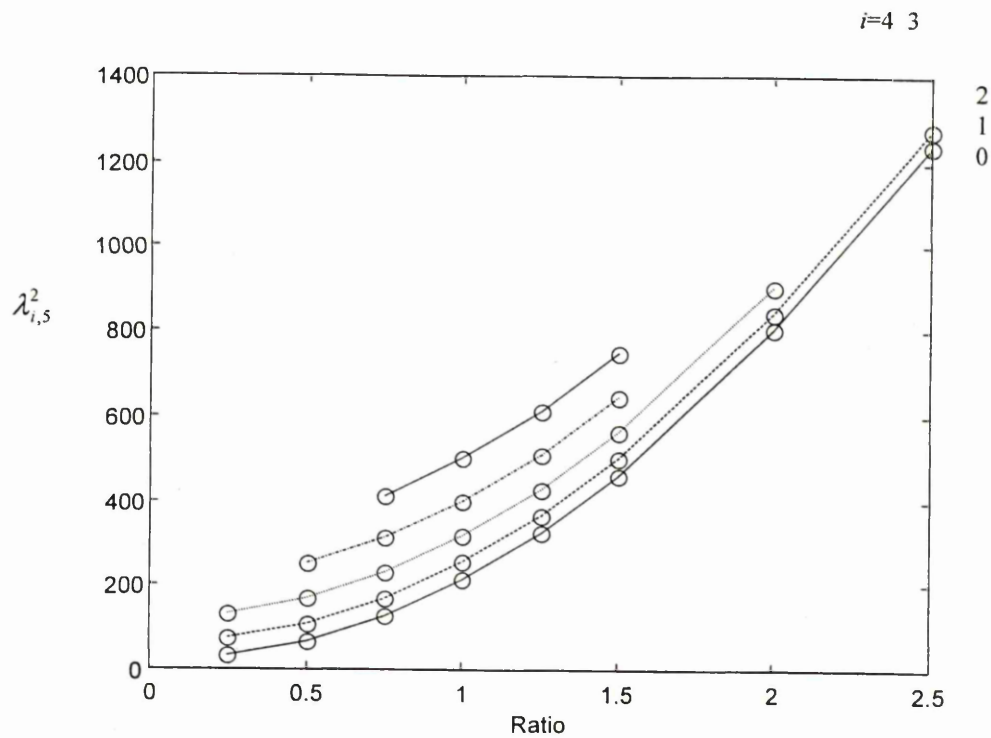


Figure 4.6a Variation of frequency parameters with aspect ratios for $j = 5$

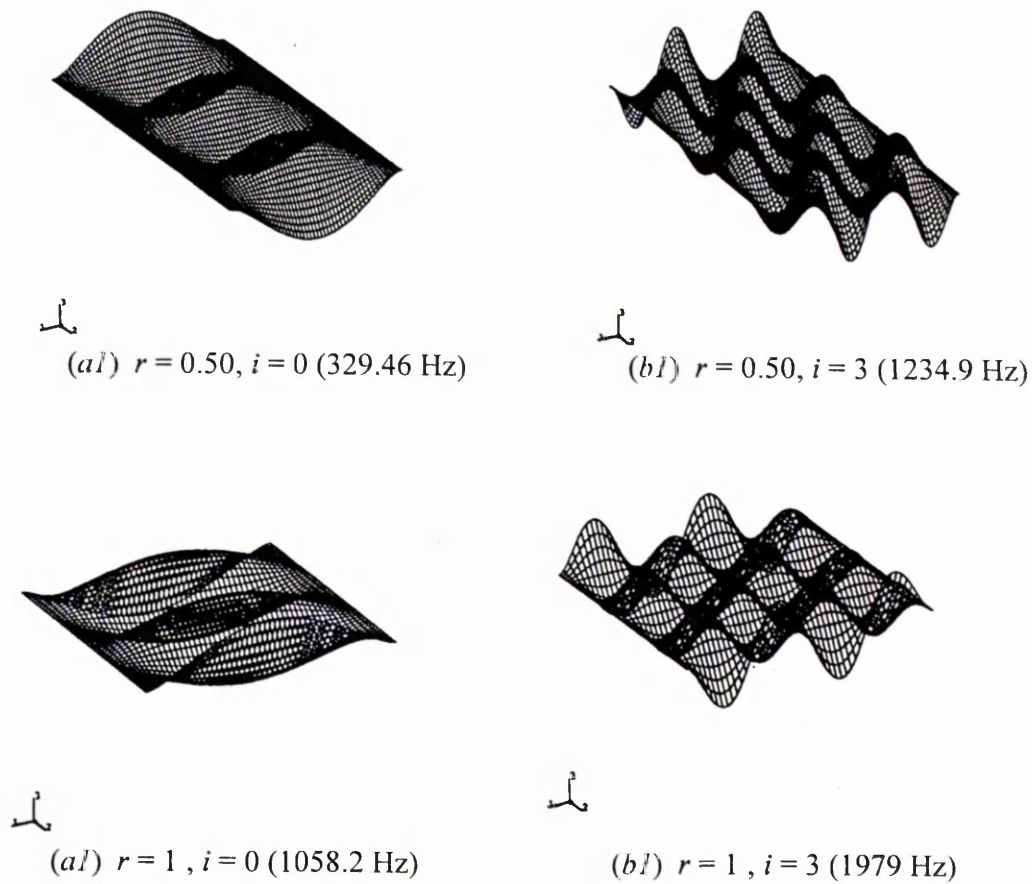


Figure 4.6b Mode shapes of beam-plates for mode counter $j = 5$

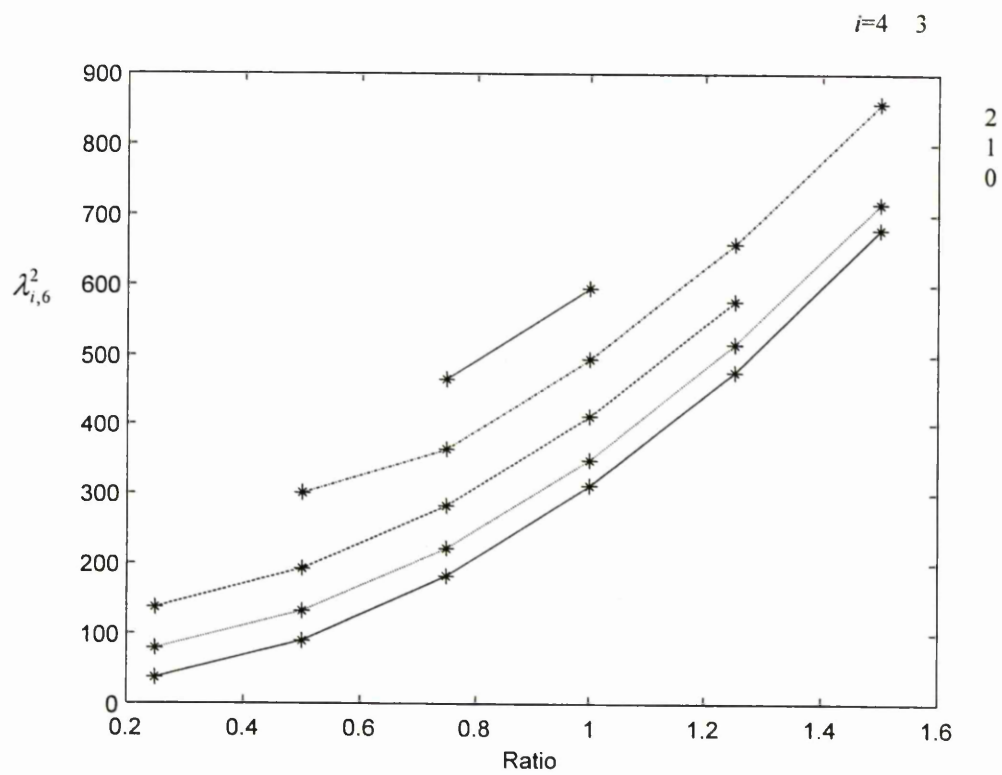


Figure 4.7a Variation of frequency parameters with aspect ratios for $j = 6$

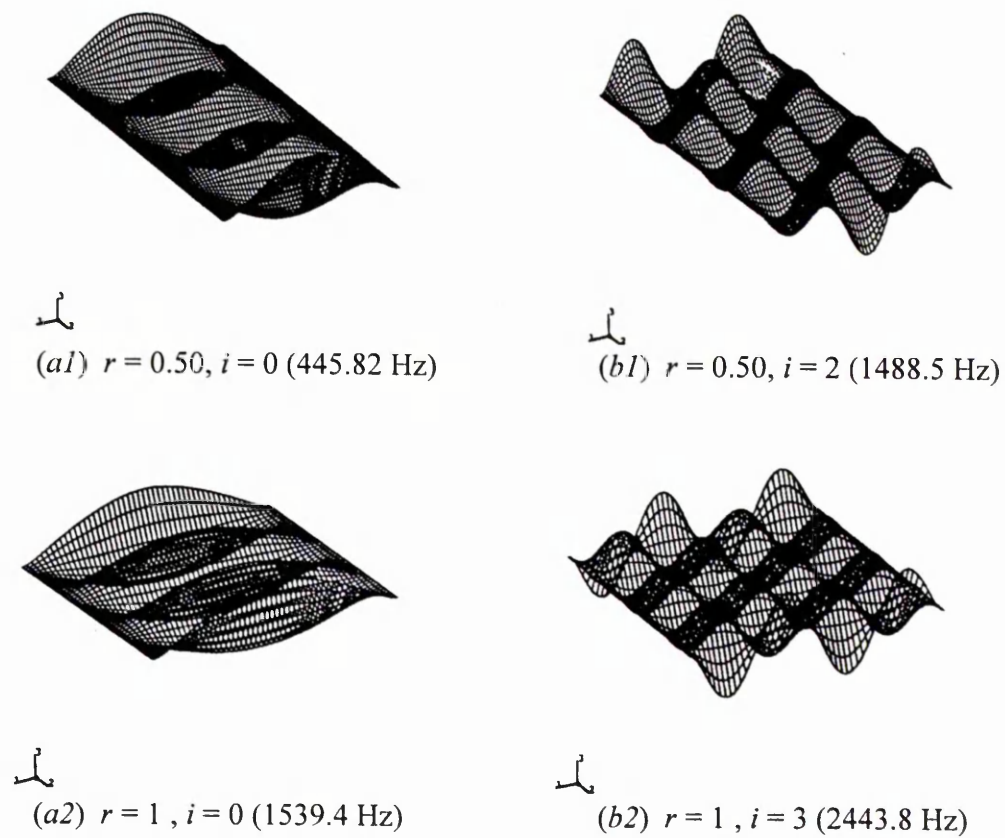


Figure 4.7b Mode shapes of beam-plates for mode counter $j = 6$

4.2.2 Relationship between frequency parameters and aspect ratios for fixed values of i

The graphical results presented in previous section show the deformation in the breadthwise direction (denoted by j) kept constant, while the deformation in the lengthwise direction (denoted by i) varied. This section covers the case when the lengthwise deformation is kept constant while the breadthwise deformation is varied. This approach will enable a close study and comparison of the purely one-dimensional beam modes of vibration, for which $j = 0$ (pure bending), and $j = 1$ (pure torsion), with the two-dimensional plate modes of vibration, for which $j \geq 2$.

Figures 4.8a to 4.15a show the relationship between frequency parameters and aspect ratios for fixed values of i . In these figures, the x -axis denotes the aspect ratios while the y -axis denotes the frequency parameters. Figures 4.8b to 4.15b show the corresponding mode shapes.

First bending deformation along lengthwise direction ($i=0$)

The variation of the frequency parameters with the aspect ratios for values of $i = 0$ and $j = 0$ to 6 are shown in Figure 4.8a shows. The 7 curves shown in this figure correspond to the first bending deformation along the lengthwise direction for which $i=0$, that is there is no nodal line (in the mode shape) along the lengthwise direction. The curve for which $i = 0$ and $j = 0$ is almost a constant straight line. This suggests that the frequency parameters do not change significantly when the aspect ratio changes. The mode shapes in Figures 4.8b (a1) and (b1) show that this curve corresponds to the fundamental mode of pure bending vibration. The curve for which $i = 0$ and $j = 1$ shows that $\lambda_{0,j}^2$ increases smoothly, gradually and linearly when the aspect ratio increases.

This curve corresponds to the fundamental mode of pure torsional vibration as illustrated by the mode shapes presented in Figures 4.8*b* (a2) and (b2).

When $i = 0$ and $j = 2$ to 6 , the frequency parameter increases rapidly as the aspect ratio increases. The trend of $\lambda_{0,j}^2$ with aspect ratio becomes a parabola or an exponential curve. The other frequency parameter curves from $j = 2$ to $j = 6$ represent the fundamental modes of vibration for increasing degrees of deformation in the breadthwise direction. Other typical mode shapes, which correspond to the frequency parameter curves, are shown in Figure 4.8*b* for aspect ratios 1 and 5. It is seen that as j increase from $j = 0$ to $j = 3$, the breadthwise deformation increases.

When $j \geq 2$, the figure shows that at the higher aspect ratio of 5, the 'beam' appears to be more distorted than the plate of aspect ratio 1 although both structures have the same corresponding values of the mode counters i and j . Also, when $j=1$ the natural frequency of the 'beam' is more than twice greater than the natural frequency of the plate. But when $j>2$, the natural frequencies of the 'beam' are more than an order of magnitude greater than the natural frequencies of the plate. This indicates that the effect on natural frequency of the increased mass moment of inertia of the plate in comparison to the beam is more than the effect of increased breadthwise stiffness.

Second bending deformation along lengthwise direction ($i=1$)

The variation of the frequency parameters with the aspect ratios for values of $i = 1$ and $j = 0$ to 6 are shown in Figure 4.9*a*. The 7 curves presented in this figure correspond to values of $i = 1$ and $j = 0$ for the bottom-most to values of $i = 1$ and $j = 6$ for the top-most curves, respectively. The curve for which $i = 1$ and $j = 0$ is nearly a constant straight line. This suggests that the frequency parameters of this mode of vibration do not change significantly when the aspect ratio changes. This curve denotes

the second mode of pure bending vibration as shown by the mode shapes presented in Figures 4.9b (a1) and (b1). The curve for which $i = 1$ and $j = 1$ shows that $\lambda_{1,j}^2$ increases smoothly, gradually and linearly when the aspect ratio increases. This curve denotes the second mode of pure torsional vibration as can be seen from the mode shapes in Figure 4.9b (a2) and (b2).

When $i = 1$ and $j = 2$ to 6, the frequency parameter increases rapidly as the aspect ratio increases. The frequency parameters $\lambda_{1,j}^2$, increase parabolically or exponentially as the aspect ratios increase. Figure 4.9b show the mode shapes which correspond to the frequency parameter curve for aspect ratios 1 and 5, and mode counters $i = 1, j = 0$ to 3. While Figure 4.9b (b1) and (b2) show the pure bending and pure torsional modes of vibration, Figures 4.9b (a1) and (a2) show that the plate does not really deform purely in bending about the y -axis and torsion about the x -axis. There is some bending about the x -axis as well in both cases. In general, Figure 4.9b shows that the breadthwise deformation increases as j increases. Also, it is important to notice that when $j=1$ the natural frequency of the 'beam' is more than twice greater than the natural frequency of the 'plate'. But when $j \geq 2$, the natural frequencies of the 'beam' are more than an order of magnitude greater than the natural frequencies of the plate. This suggests that the effect of increased mass moment of inertia on the natural frequency is more significant for the plate than for the beam.

Third bending deformation along lengthwise direction ($i=2$)

The relationships between the frequency parameters and the aspect ratios for values of $i = 2$ and $j = 0$ to 6 shown in Figure 4.10a. this figure show the bottom-most curve for which $i = 2$ and $j = 0$ is almost a straight line this corresponds to the third pure bending modes of the beams and plates. The curve for which $i = 2$ and $j = 1$ shows that

when the aspect ratio increases, the frequency parameter $\lambda_{2,j}^2$ increases smoothly, gradually and linearly. This curve corresponds to the third pure torsional modes. When $i = 2$ and $j = 2$ to $j = 6$, the frequency parameter increases rapidly with the increases of the aspect ratio. The variation of $\lambda_{2,j}^2$ with ratio becomes an exponential curve. Figure 4.10b show the mode shapes for aspect ratios 1 and 5, and for $i = 2, j = 0$ to 3. From this figure clearly show the breadthwise deformation increases when the mode counter j increases. Also show that when $j \geq 2$, the deformation of the beam ($r = 5$) is much more complex than the deformation of the plate ($r = 1$). Again, as in the previous case of $i=1$, it can be deduced that the effect of increased mass moment of inertia is greater than the effect of increased bending stiffness

Fourth bending deformation along lengthwise direction ($i=3$)

Figure 4.11a show the variation of the frequency parameters with the aspect ratios for values of $i = 3$ and $j = 0$ to 6. These curves correspond to values of $i = 3$ and $j = 0$ for the bottom-most curve to values of $i = 3$ and $j = 6$ for the top-most curve respectively. The curve for which $i = 3$ and $j = 0$ is almost a constant straight line. This suggests that the frequency parameters of this mode of vibration do not change a lot when the aspect ratio changes. This curve corresponds to the fourth bending mode. The curve for which $i = 3$ and $j = 1$ is approximately a straight line and corresponds to the fourth torsion mode. While $i = 3$ and $j \geq 2$, the frequency parameters increase rapidly as the aspect ratio increases. The frequency parameters, $\lambda_{3,j}^2$, increase parabolically as the aspect ratios increase. Figure 4.11b show the mode shapes for $i = 3, j = 0$ to 3 and for aspect ratios 1 and 5. It is also clear that when the mode counter j increases, the breadthwise deformation increases. Also, it is seen from Figure 4.11b (b1) and (b2) that when $i = 3$ and $j = 0, 1$ the beam ($r = 5$) has a practically straight edge and is, therefore,

undergoing pure bending and pure torsional modes of vibration. Also it is seen that when $j \geq 2$ the natural frequency of beam increases considerably compared to that of plate. This suggests, as in previous cases, that the increased mass moment of inertia of the plate affects its natural frequency much more than its stiffness in comparison to the beam.

Fifth bending deformation along lengthwise direction ($i=4$)

The variation of the frequency parameters with aspect ratios for values of $i = 4$ and $j = 0$ for the bottom-most curve to $i = 4$ and $j = 6$ for top-most curve are shown in Figure 4.12a. From the graph the bottom-most curve, which is almost a constant straight line represents the fifth bending mode. The curve for which $i = 4$ and $j = 1$ represents the fifth torsional mode of vibration. The curves at higher values of j involve increasing degrees of deformation in the breadthwise direction of the beam and plate. Figure 4.12b show typical mode shapes of the beam ($r = 5$) and plate ($r = 1$) It is obvious that the deformation of breadthwise increases when the mode counter j increases. The figure also shows that for $j = 0$ and $j = 1$, the mode shapes of the beam ($r = 5$) are true pure bending and pure torsional modes of vibration, whereas the mode shapes of the corresponding plate ($r = 1$) are highly distorted. When $j \geq 2$, the natural frequency of beam is twice as that for plate, which suggests that the natural frequency is affected more by mass moment of inertia than stiffness.

Sixth bending deformation along lengthwise direction ($i=5$)

The variation of the frequency parameters with aspect ratios for values of $i = 5$ and $j = 0$ to 4 are shown in Figure 4.13a. The bottom-most curve for which $i = 5$ and $j = 0$ corresponds to the sixth bending mode. The next curve for which $i = 5$ and $j = 1$

corresponds to the sixth torsional mode. The curves for which $i = 5$ and $j = 2$ to 4 correspond to increasing degrees of deformation in the breadthwise direction. Figure 4.13b show the mode shapes for $i = 5, j = 0, 1$ and 2 and for aspect ratios 1 and 5. From this figure clearly seen that when mode counter j increases, the breadthwise deformation increases and the mode shapes of the plate are more distorted than the corresponding mode shapes of the beam. It also seen from this figure when $j \geq 2$ the natural frequency for beams is twice as much as that for plates.

Seventh bending deformation along lengthwise direction ($i=6$)

Figure 4.14a shows the variation of the frequency parameters with aspect ratios for values of $i = 6$ and $j = 0$ to 3. The 4 curves in this figure correspond to values of $i = 6$ and $j = 0$ for the bottom-most curve to values of $i = 6$ and $j = 3$ for the top-most curve, respectively. The bottom-most curve represents the seventh bending mode, while the next curve ($j = 1$) represents the seventh torsional mode, etc. The corresponding mode shapes for values of $j = 1, 2$ and 3, and for a beam ($r = 5$) and plate ($r = 1$) are shown in Figure 4.14b. The figure shows that the mode shapes of the plate are more complicated than those of the beam for the same value of the breadthwise mode counter j . Previous observations on different effects of mass moment of inertia and stiffness on natural frequencies of the beam and plate apply.

Eighth bending deformation along lengthwise direction ($i=7$)

In Figure 4.15a is shown the variation of the frequency parameters with aspect ratios for values of $i = 7$ and $j = 0$ to 3. The bottom-most curve corresponds to values of $i = 7$ and $j = 0$, while the top-most curve corresponds to values of $i = 7$ and $j = 3$, respectively. Also, the bottom-most curve is associated with the eighth mode of bending

vibration, while the curve ($j = 1$) immediately above is the eighth mode of torsional vibration. However these two modes of vibration are not pure modes because there is considerable deformation in the breadthwise direction for both the beam and the plate. When $j \geq 2$ the natural frequency is twice as much for the beam as for the plate. As in previous cases, this indicates that the natural frequency of the plate is much more affected by increased mass moment of inertia than by increased stiffness.

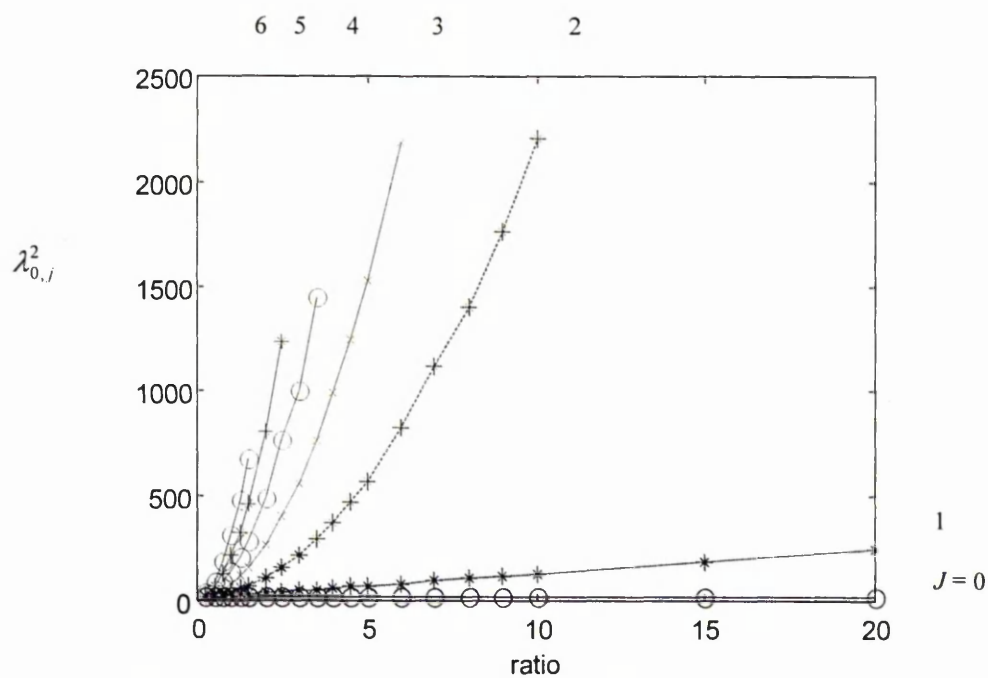


Figure 4.8a Variation of the frequency parameters with aspect ratios for $i = 0$

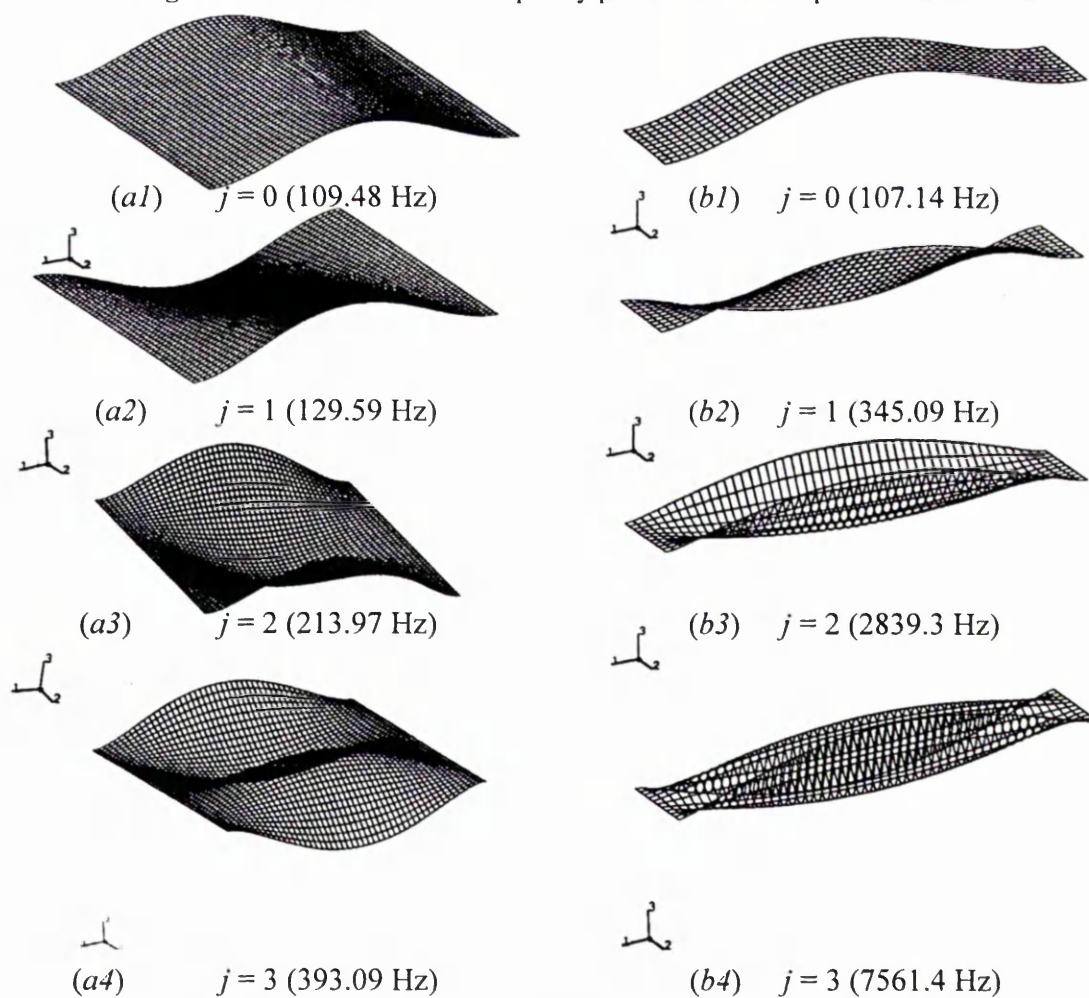


Figure 4.8b Mode shapes for $i = 0$ (a) aspect ratio 1, (b) aspect ratio 5

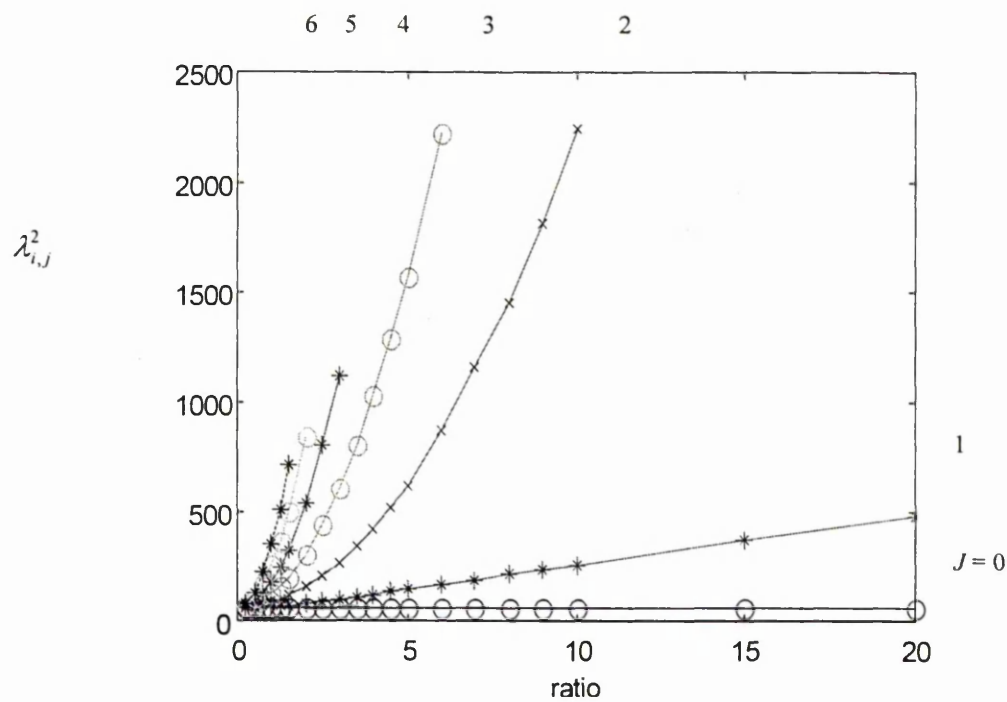


Figure 4.9a Variation of the frequency parameters with aspect ratios for $i = 1$

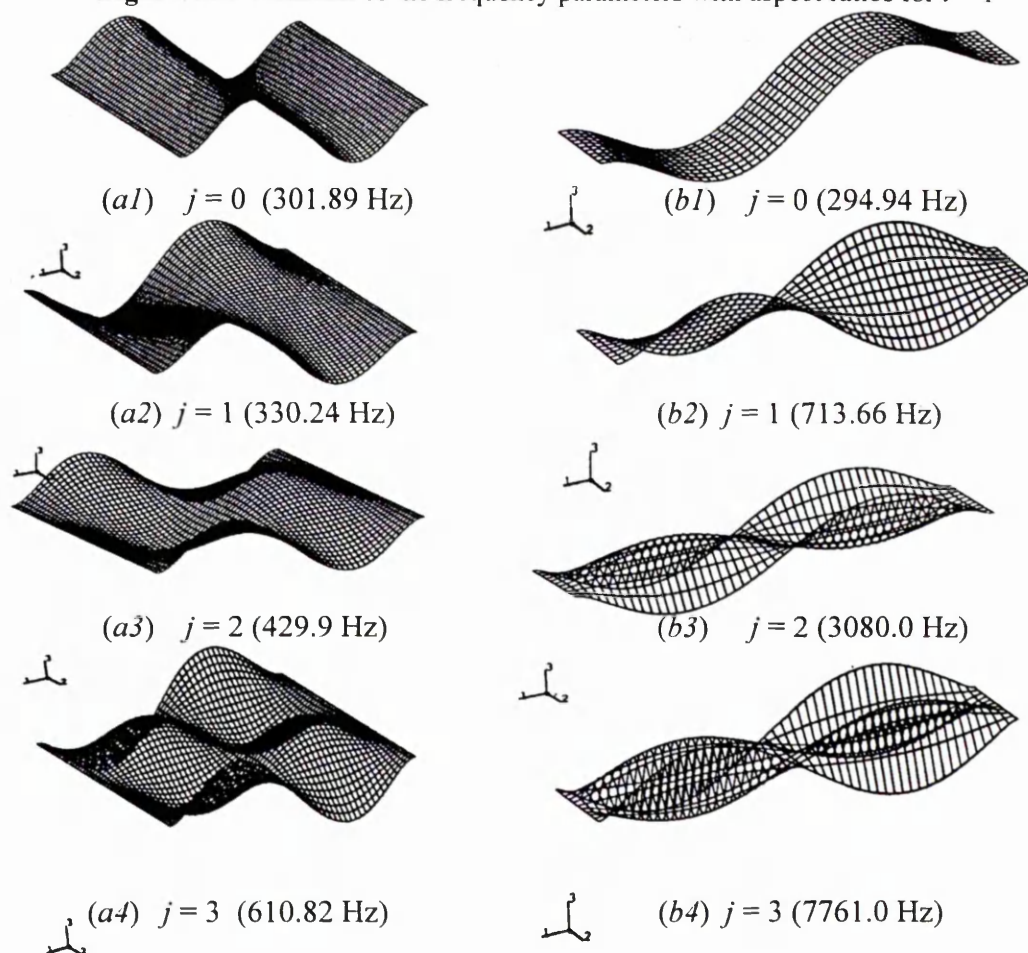


Figure 4.9b Mode shapes for $i = 1$ (a) aspect ratio 1, (b) aspect ratio 5

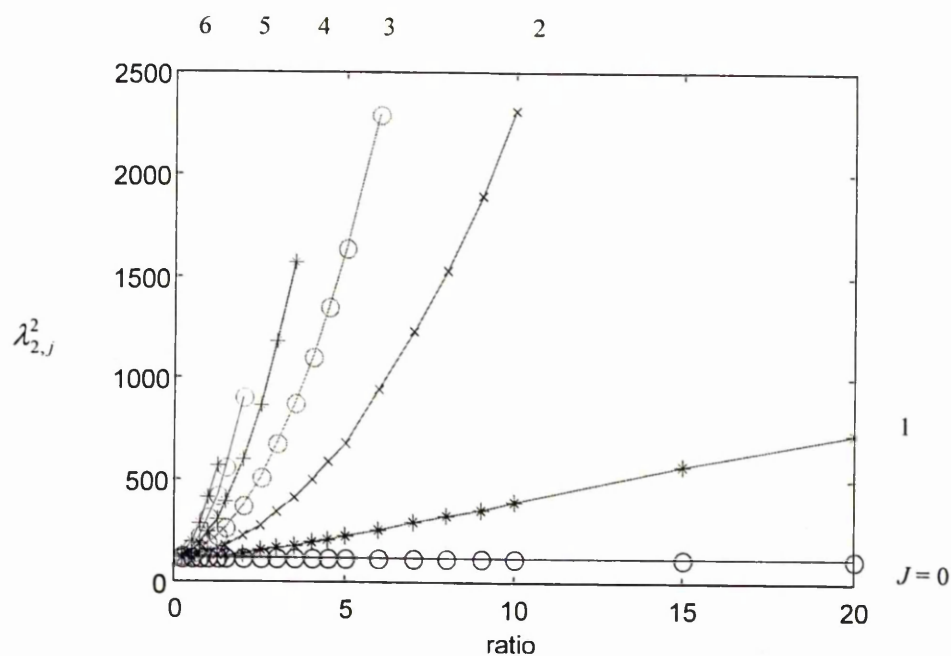
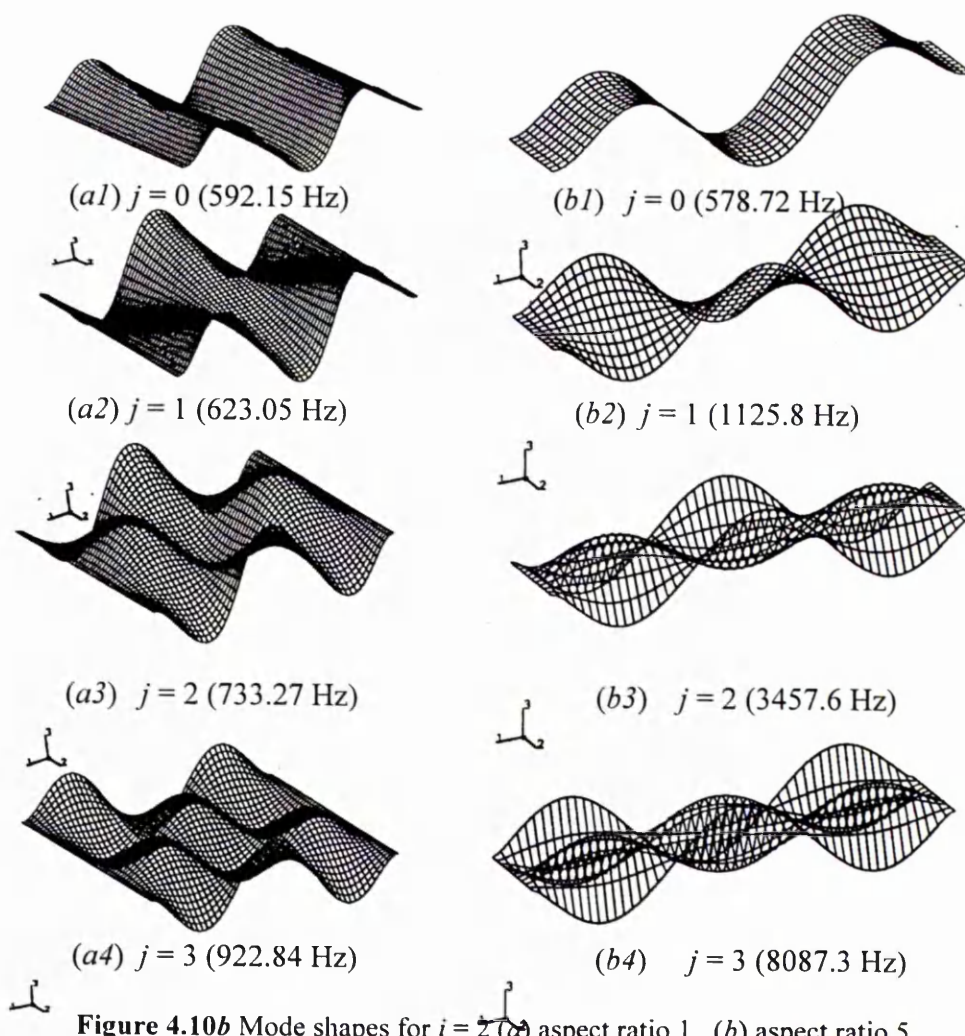


Figure 4.10a Variation of the frequency parameters with aspect ratios $i = 2$



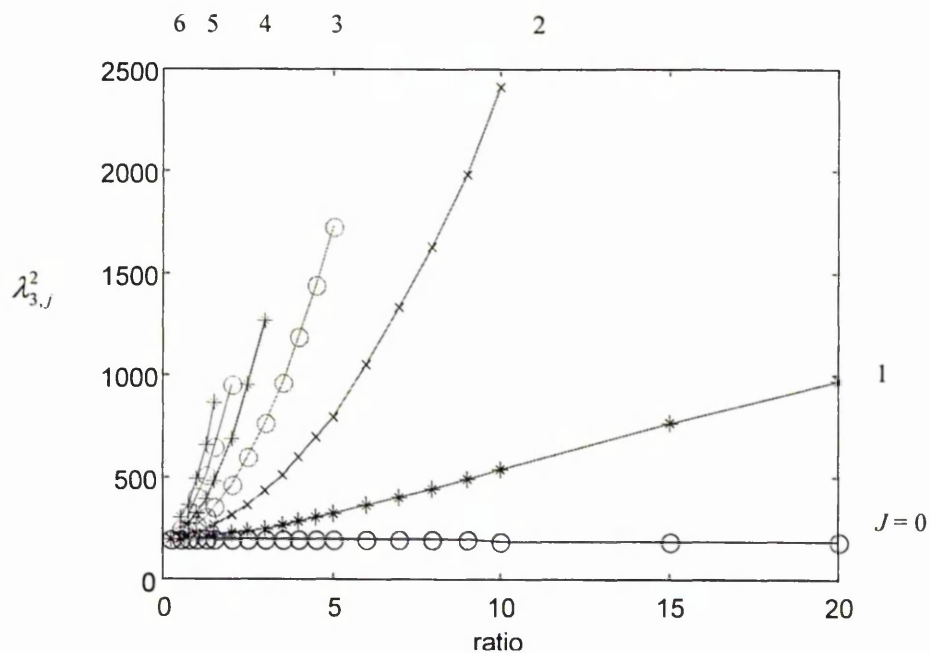


Figure 4.11a Variation of the frequency parameters with aspect ratios for $i = 3$

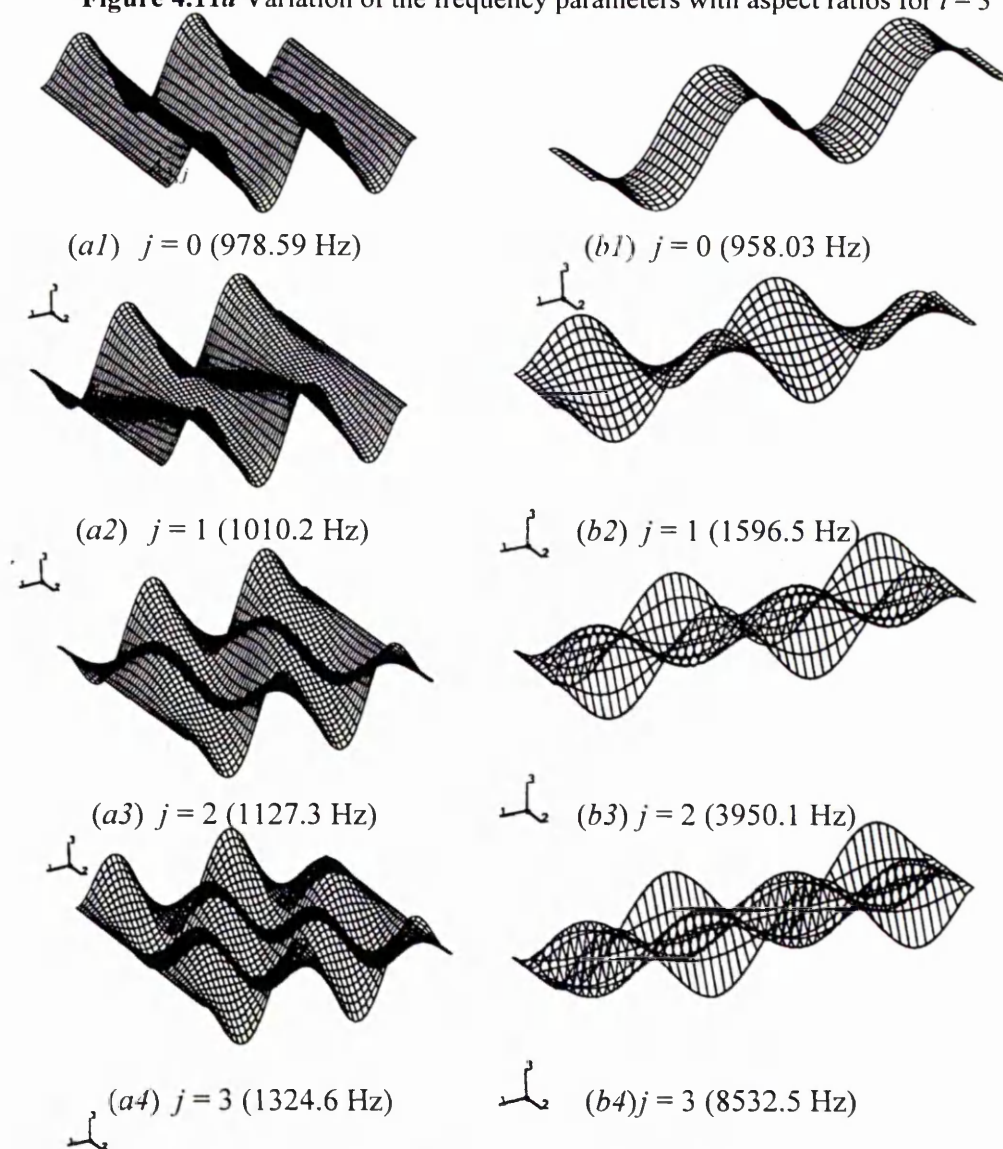


Figure 4.11b Mode shapes for $i = 3$ (a) aspect ratio 1, (b) aspect ratio 5

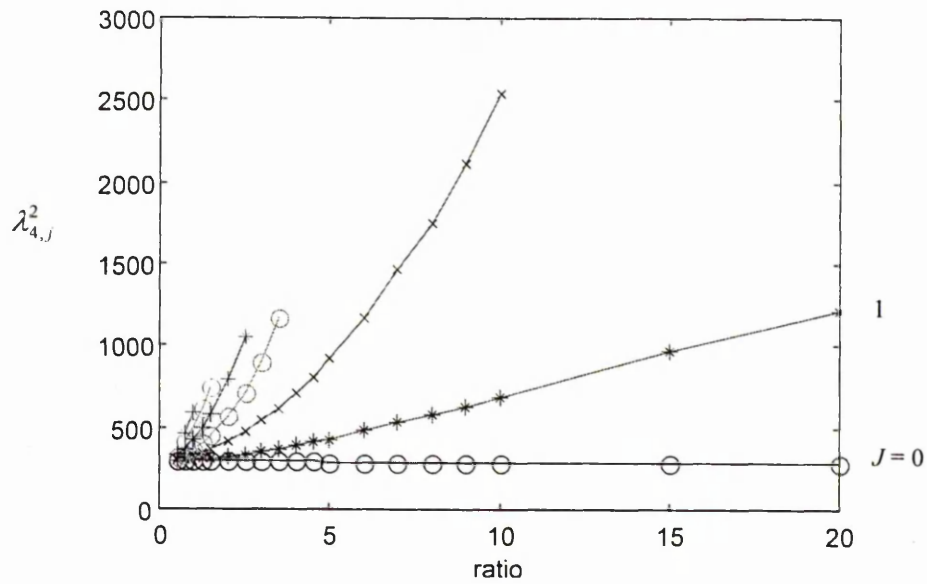


Figure 4.12a Variation of the frequency parameters with aspect ratios for $i = 4$

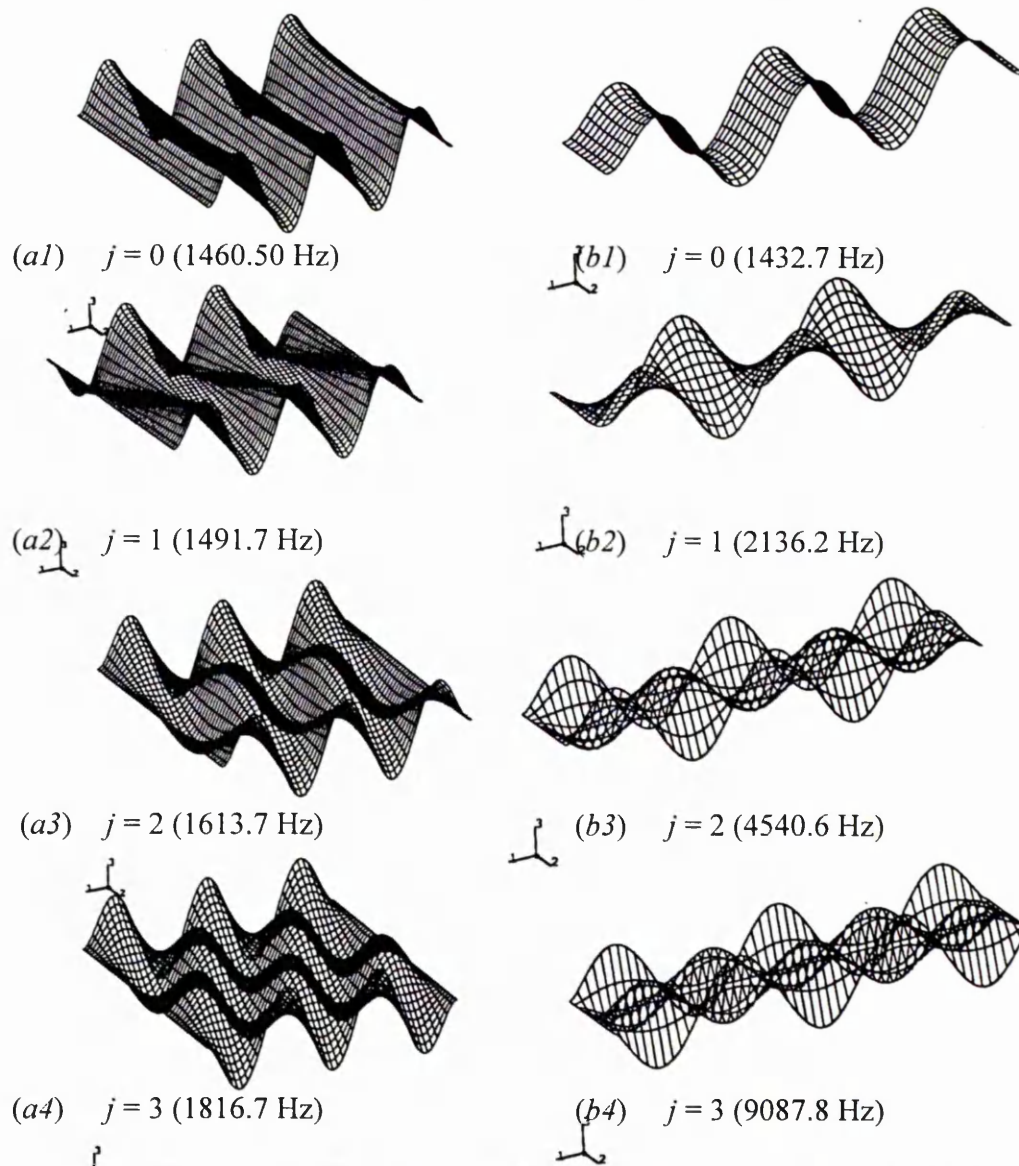


Figure 4.12b Mode shapes for $i = 4$ (a) aspect ratio 1, (b) aspect ratio 5

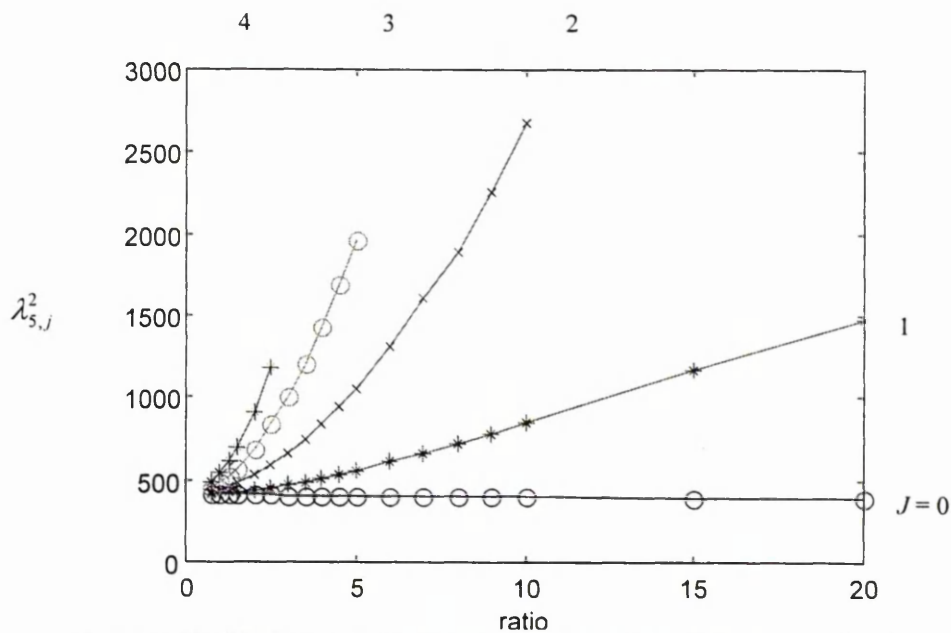


Figure 4.13a Variation of the frequency parameters with aspect ratios for $i = 5$

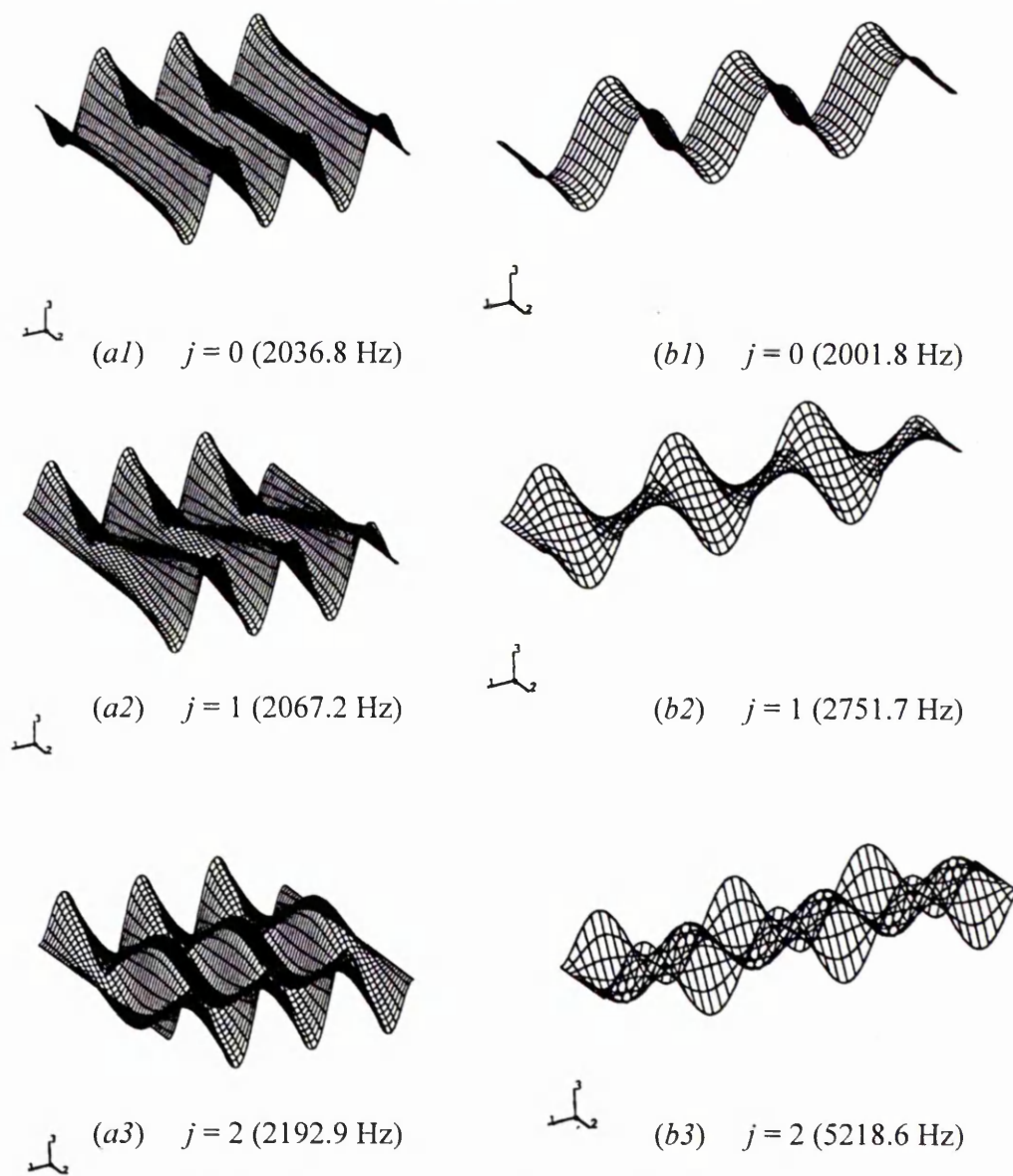


Figure 4.13b Mode shapes for $i = 5$ (a) aspect ratio 1, (b) aspect ratio 5

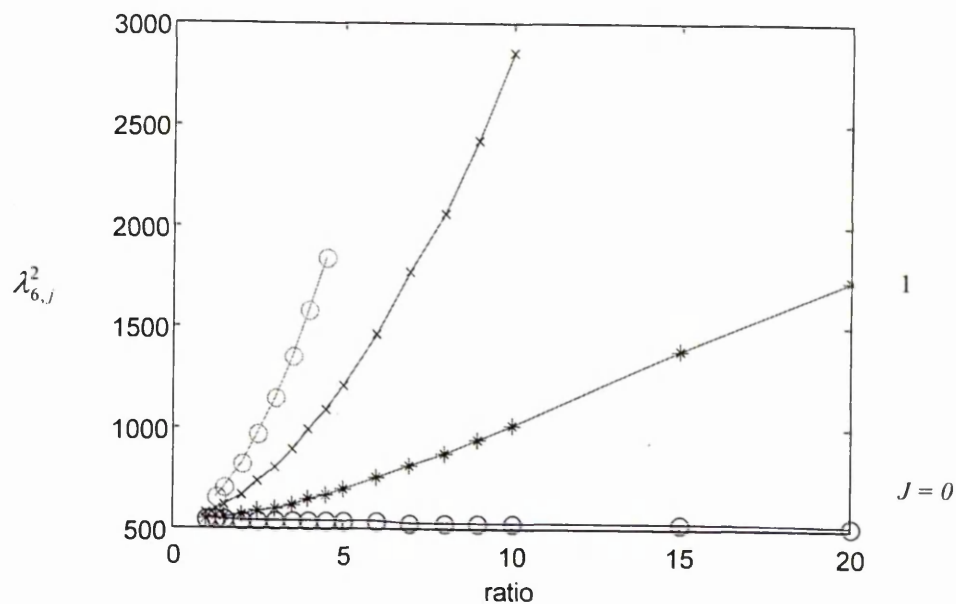


Figure 4.14a Variation of the frequency parameters with aspect ratios for $i = 6$

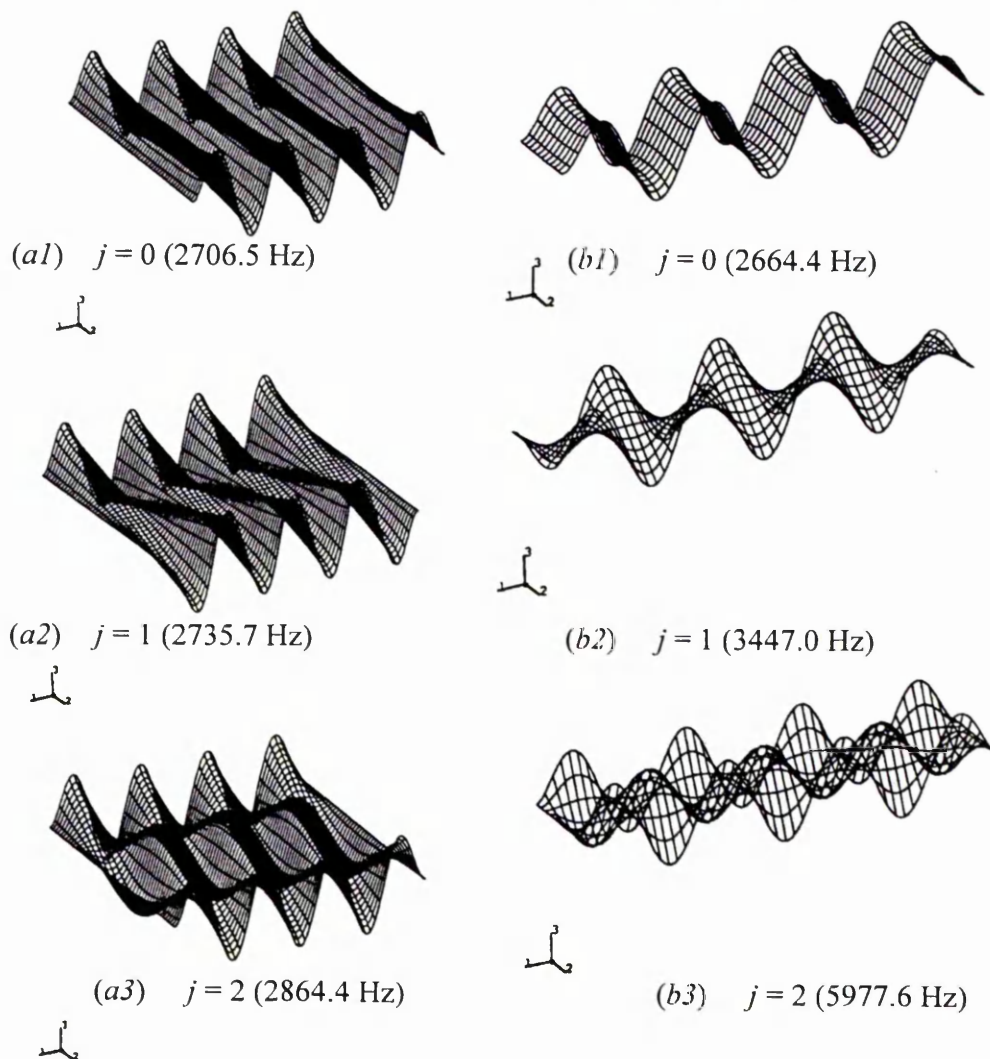


Figure 4.14b Mode shapes for $i = 6$ (a) aspect ratio 1, (b) aspect ratio 5

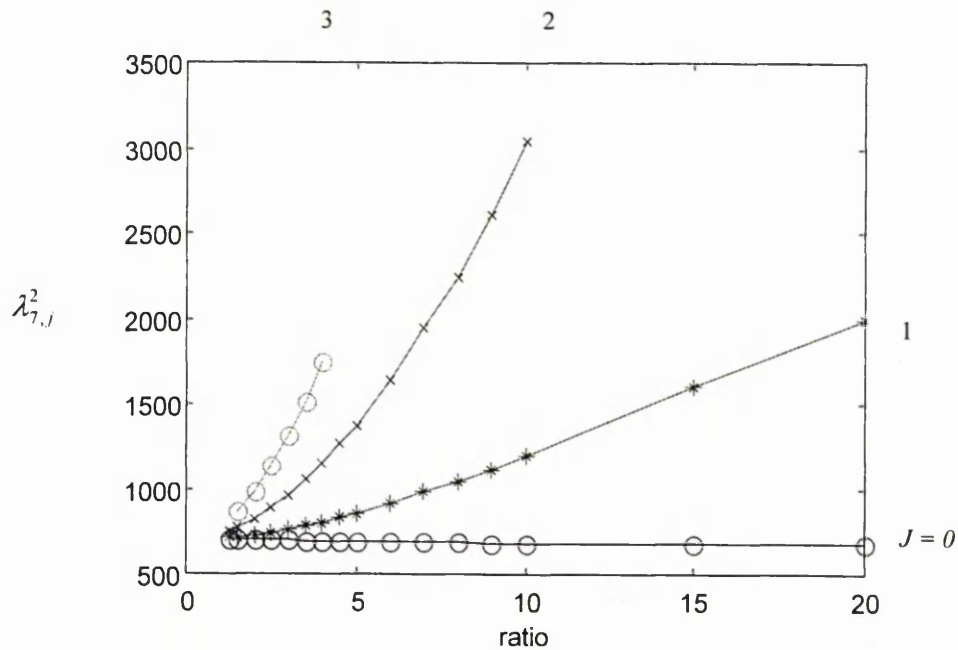


Figure 4.15a Variation of the frequency parameters with aspect ratios for $i = 7$

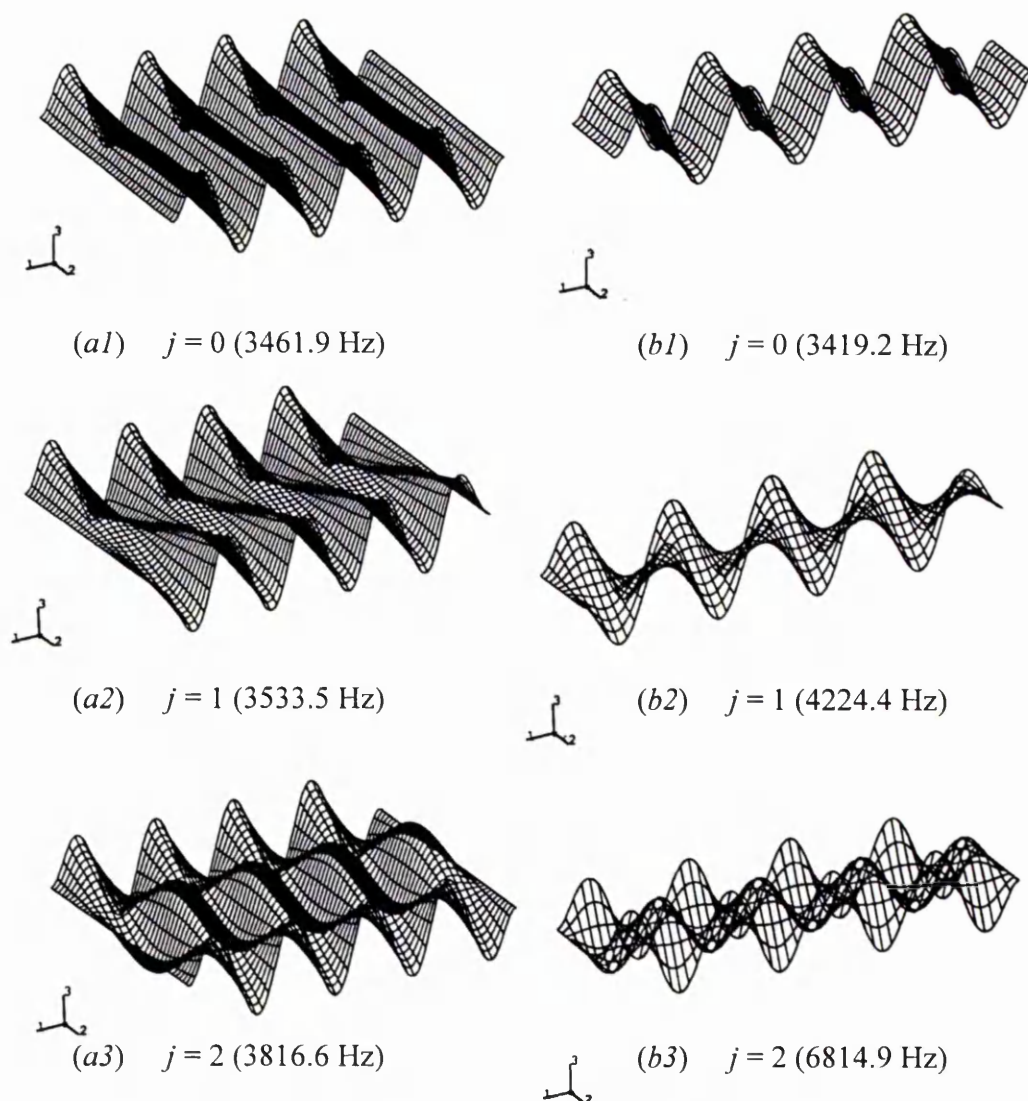


Figure 4.15b Mode shapes for $i = 7$ (a) aspect ratio 1.50, (b) aspect ratio 5

4.3 Combined frequency parameter chart

The combination of all the graphical results presented earlier in this chapter is now shown in a single chart in Figure 4.16*a*. The first and the second enlargements of this chart are shown in Figures 4.16*b* and 4.16*c* respectively. The line types used for families of curves in these graphs correspond to different values of the breadthwise mode counter j . As an example, the almost horizontal solid lines shown in the graph correspond to $j = 0$. These are the different modes of bending vibration. The next family of line type shown as slanting chain-dashed lines are for $j = 1$ and correspond to different modes of torsional vibration. Proceeding in an anticlockwise direction, the next family of line type shown as dotted curves are for $j = 2$ and correspond to the combination modes of vibration involving first bending deformation in the breadthwise direction. These curves are followed in the anticlockwise direction by a group of chain-dashed curves which correspond to values of $j = 3$. This is followed by the solid line which correspond to $j = 4$.

For aspect ratios equal to or greater than 10, and for $\lambda^2 \leq 2200$, Figure 4.16*a* shows that there are 2 types of modes of vibration. The two modes are denoted on the graphs by the horizontal solid lines for which $j = 0$ and by the slanting dotted lines for which $j = 1$. They correspond to the bending and torsion modes of vibration respectively. But for aspect ratios less than 10, there are more than 2 types of modes of vibration. Each type of vibration is represented by a different line type and is associated with a value of $j \geq 2$. As stated earlier, Figures 4.16*b* and 4.16*c* are enlargements of Figure 4.16*a*. Figure 4.16*b* shows the variation of the frequency parameters between 0 to 2000 and aspect ratios from 0 to 10, while Figure 4.16*c* shows the variation of the frequency parameters from 0 to 1500 with the aspect ratios from 0 to 5.

Figures 4.16(a),(b) and (c) can be used to determine the first 50 natural frequencies and types of mode of vibration of a clamped-clamped beam-plate for aspect ratios of between 0.25 to 20. For example, consider the determination of first six natural frequencies and types of modes of a clamped-clamped plate of aspect ratio 4. From Figure 4.16 (c), at aspect ratio 4.0. The frequency parameters of the first six modes of vibration can be estimated at aspect ratio 4.0 using Figure 4.16c. The estimated values can then be substituted in Equation (3.2) together with the material and geometric properties of the plate in order to determine the first six natural frequencies. It is also important to notice that from Figure 4.16(c) the mode types are as follows; the first mode is B1, then B2, T1, B3, T2 and B4 for the second mode to the sixth mode respectively where B denotes bending mode and T denotes torsion mode. B1 denotes first bending mode, T1 denotes first torsion mode, etc. It is also important to note that the aspect ratios and frequency parameters presented in Figure 4.16 are about an order of magnitude greater than those available in current technical literature.

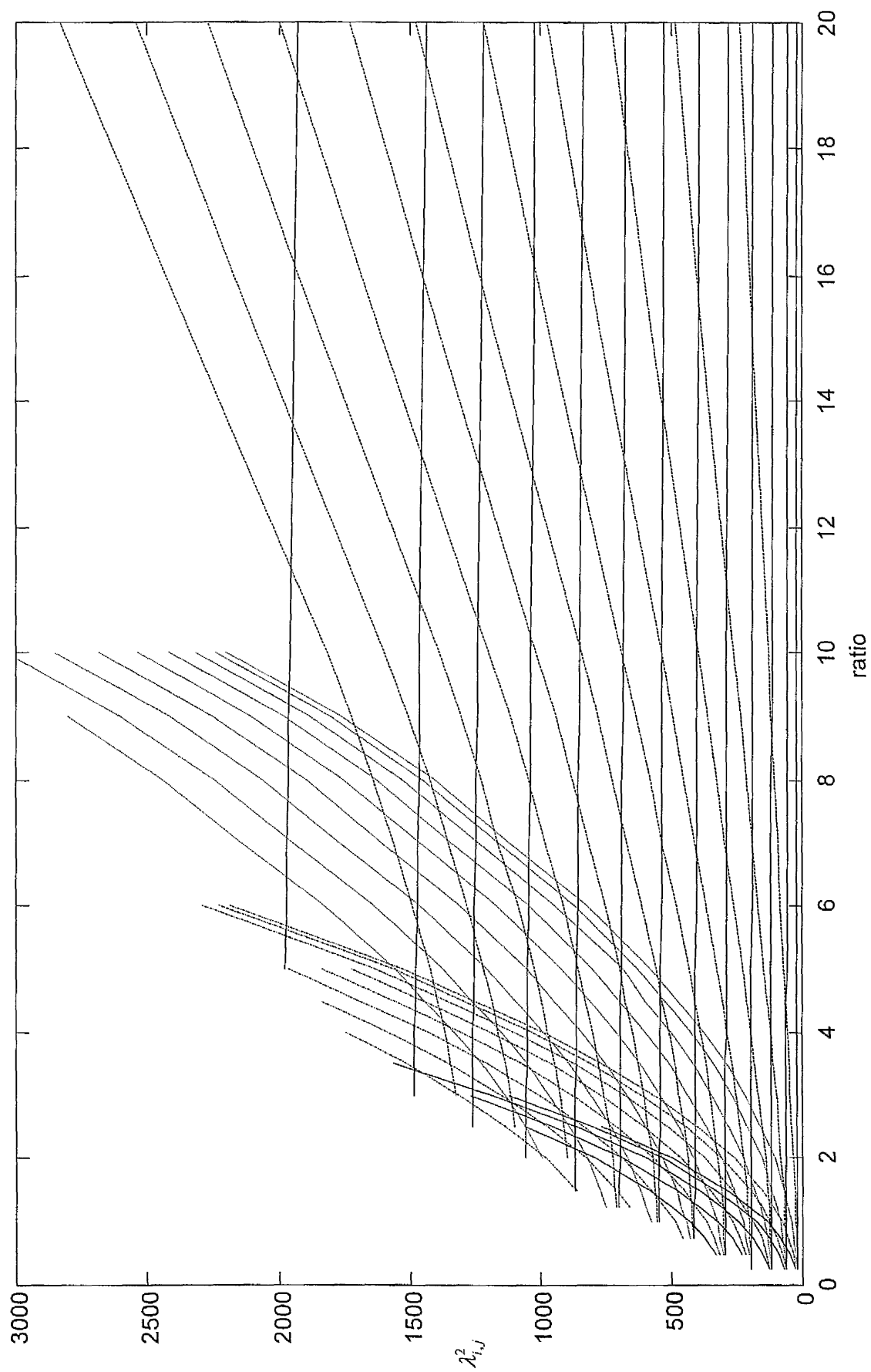


Figure 4.16 (a) Variation of frequency parameter with aspect ratio for clamped-clamped beams and plates of thickness to length ratio of 1%

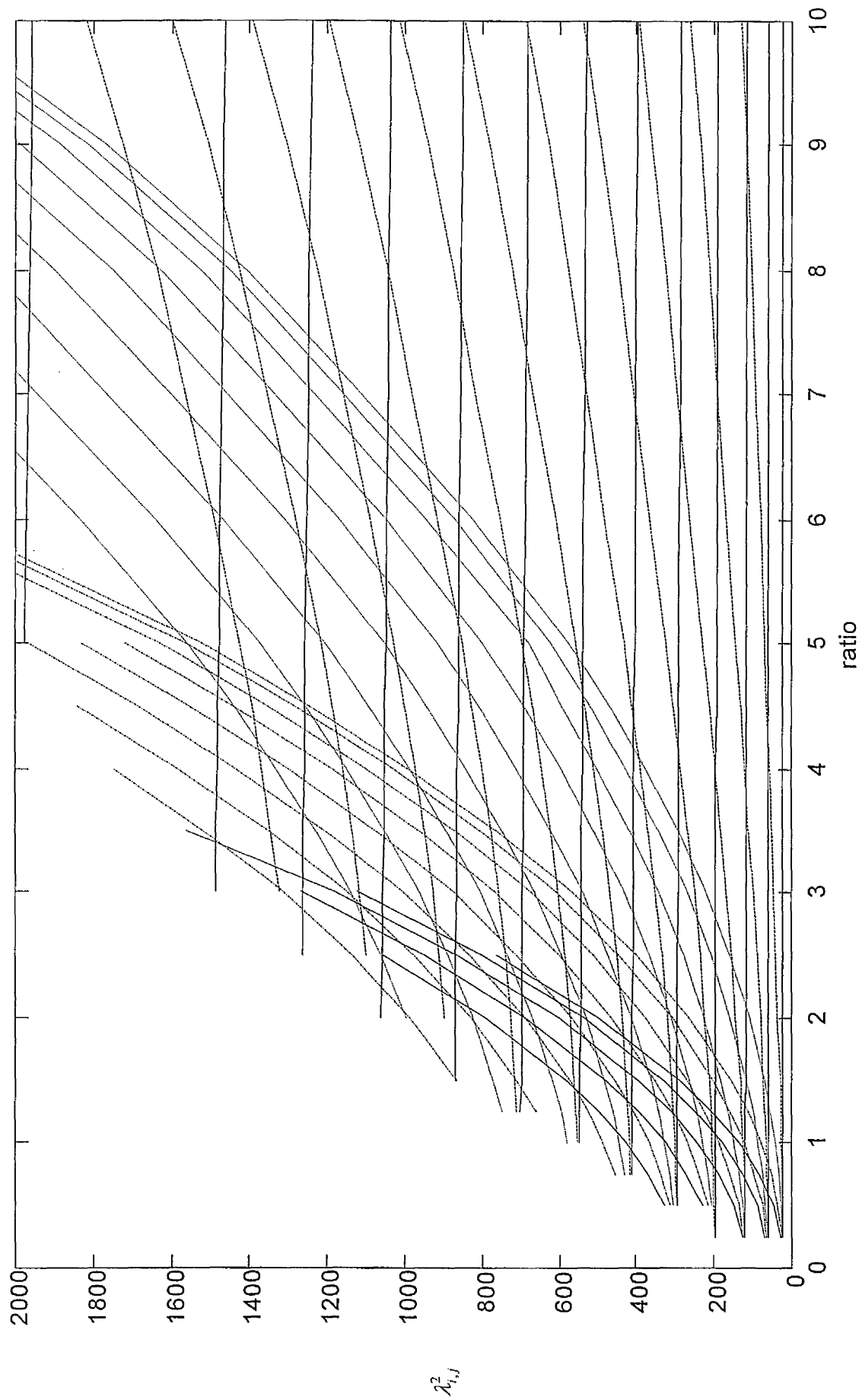


Figure 4.16 (b) First enlargement of figure 4.16 (a)

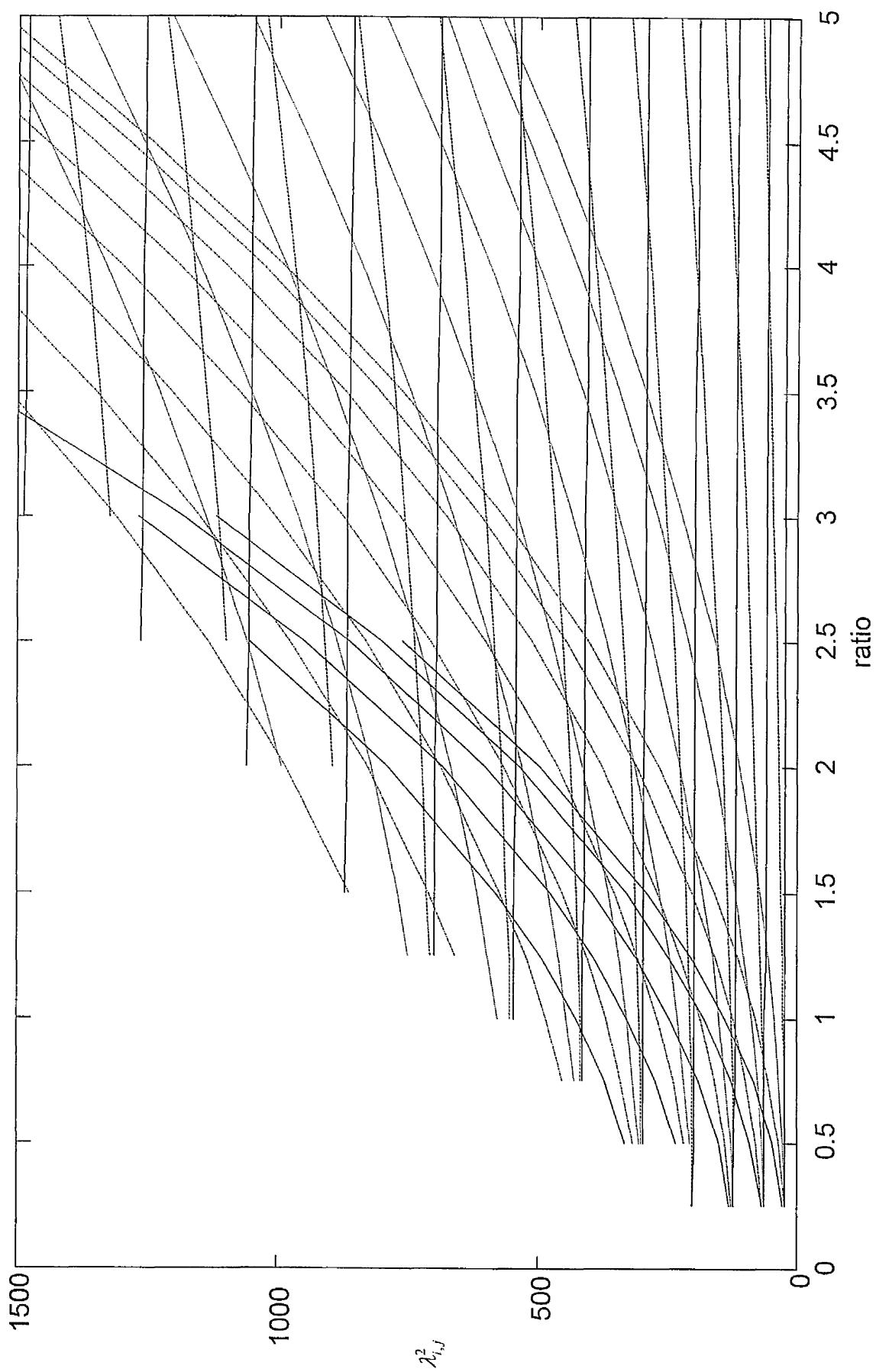


Figure 4.16 (c) Second enlargement of figure 4.16 (a)

4.4 Frequency parameter charts of other thickness to length ratio

All the work presented early in this chapter and the frequency parameter chart presented in Figure 4.16 is for thickness to length ratio of 1%. This section covers the frequency parameter charts for the other three thickness to length ratio 2%, 5% and 10% and for 20 aspect ratios. The value of the natural frequency obtained from the ABAQUS FE program was found to increase with the increase of the thickness whereas the frequency parameter reduced in value as the thickness increased. The frequency parameters were derived from Equations (3.1) and (3.2).

Figures 4.17, 4.18 and 4.19 show the frequency parameter charts for beam-plates of thickness to length ratio of 2%, 5% and 10%. Comparing these figures, it is clearly seen that the frequency parameters reduce in value with increase of the thickness to length ratios. This shows that plate thickness to length ratio has a significant effect on the magnitudes of the frequency parameter of clamped-clamped beams and plates. The line types used in this graph are as follows: solid line type is for $j = 0$ which represents predominantly beam bending modes, dashed lines represent $j = 1$ which are predominantly the torsion modes of beams, dotted lines represent $j = 2$ and are for modes of vibration in which the beam or plate bends in the breadthwise direction.

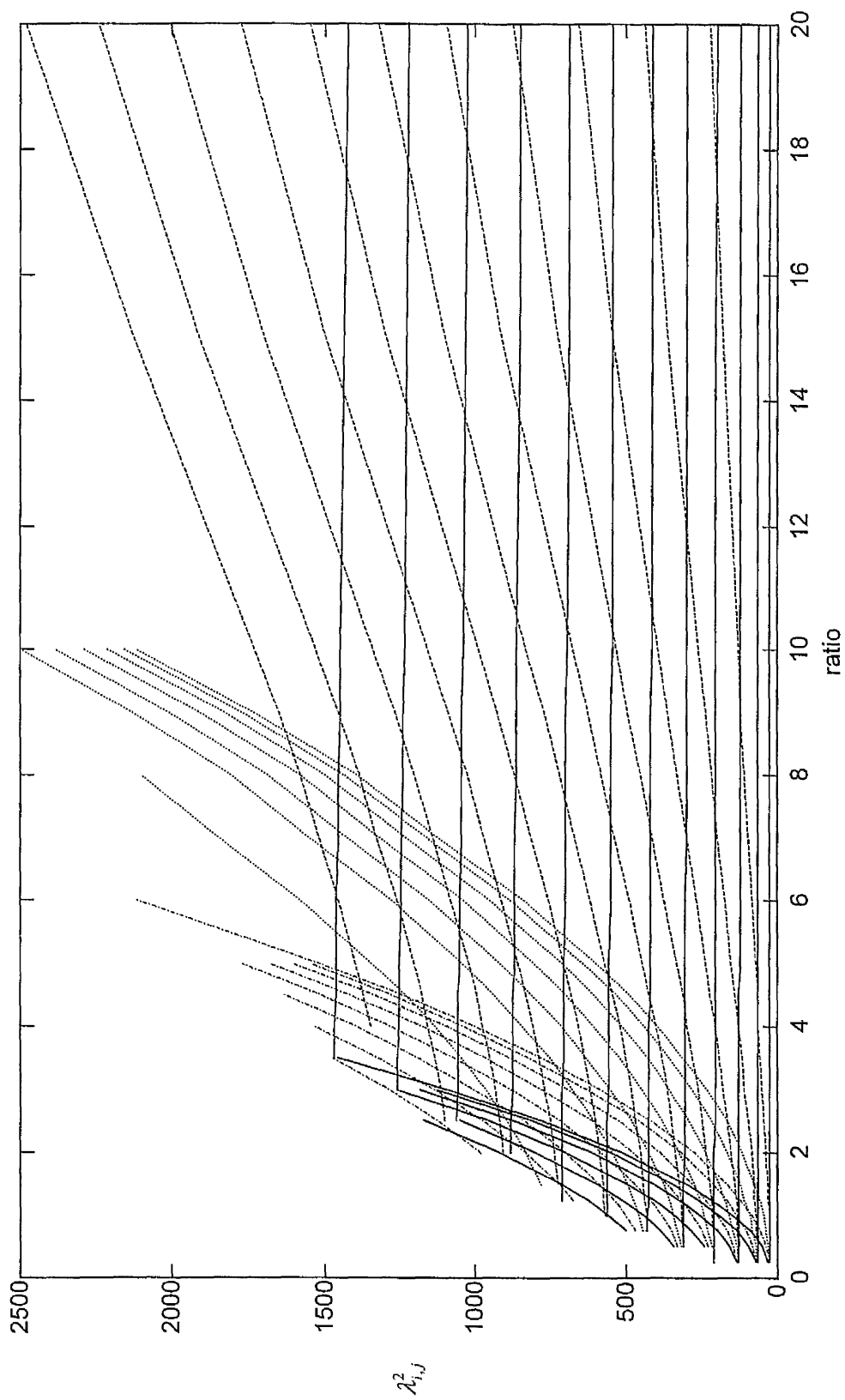


Figure 4.17 Variation of frequency parameter with aspect ratio for clamped-clamped thickness to length ratio of 2%

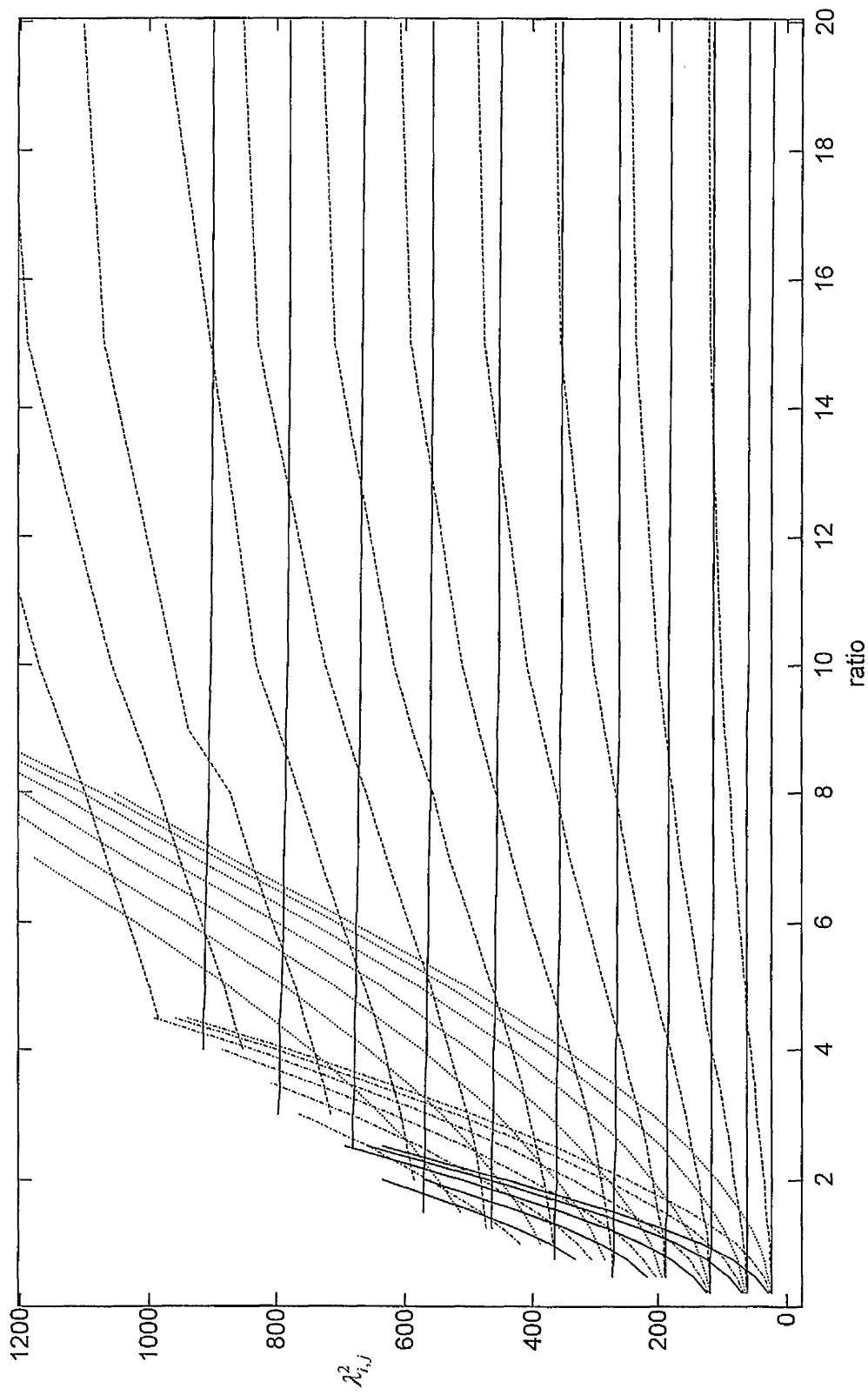


Figure 4.18 Variation of frequency parameter with geometric ratio for clamped-clamped thickness to length ratio of 5%

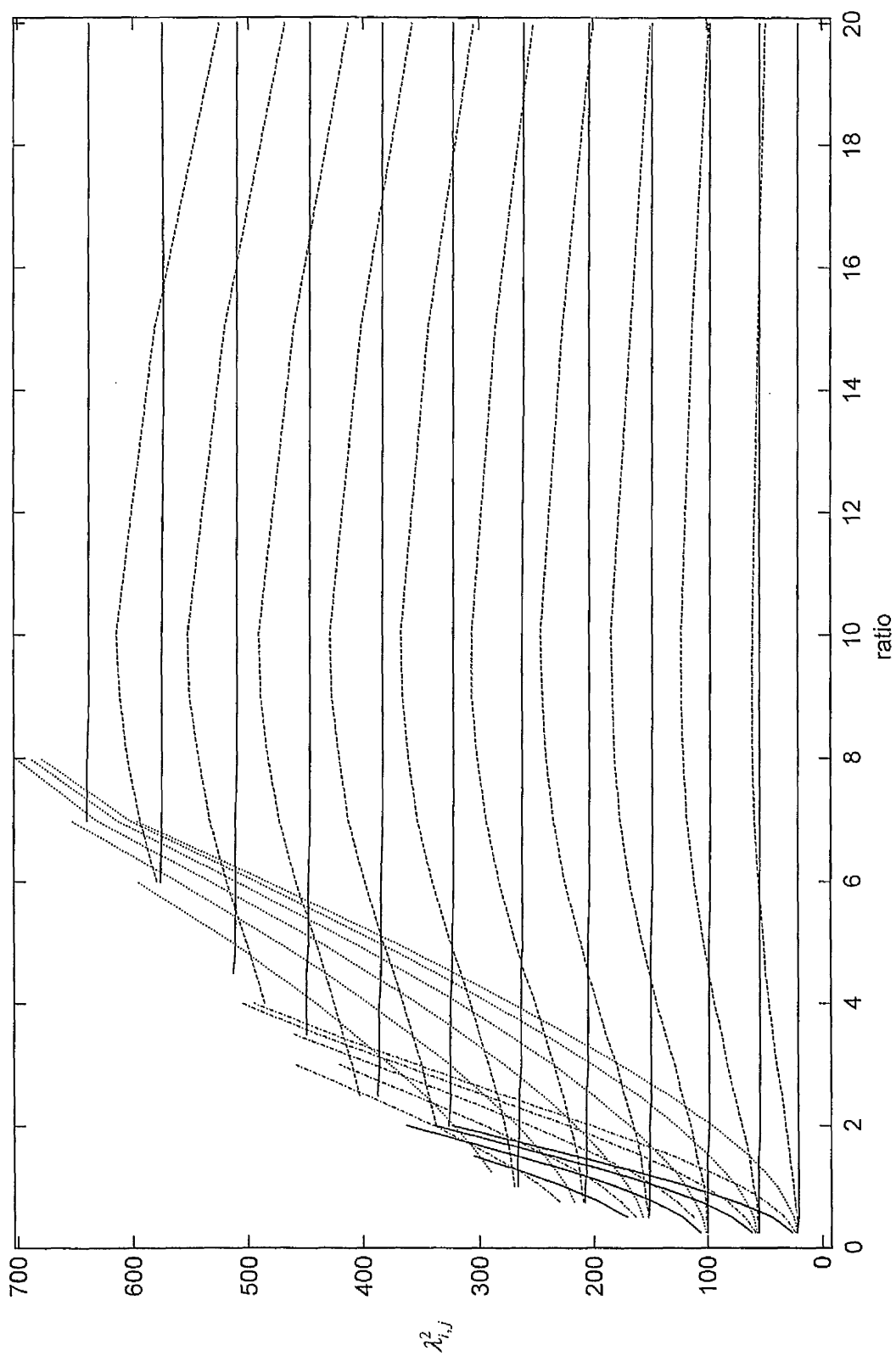


Figure 4.19 Variation of frequency parameter with geometric ratio for clamped-clamped thickness to length ratio of 10%

4.5 Comparison of the frequency parameter charts for different thickness to length ratio with reference to the 1% thickness to length ratio.

In this section, the effect of thickness on the frequency parameter charts is examined more in detail. Figures 4.20 (a), 4.21 (a) and 4.22 (a) show the comparison subsets of the frequency parameter charts of beam-plates of thickness to length ratio of 2%, 5% and 10% with respect to that of the 1% thickness to length ratio. These figures are for the predominately bending mode $j=0$. It is clearly show that from figure 4.20 (a) these lines are very close and the percentage error about 10 % for thickness to length ratio of 1% and 2%. Figure 4.21 (a) show the lines are apart and the percentage error about 25 % for thickness to length ratio of 1% and 5%. The percentage error is greater for thickness to length ratio 1% and 10%, which is about 50 %. The dashed lines in these figures represent data for 1% thickness to length ratio and the solid line is for 2%, 5% and 10% respectively.

Figures 4.20 (b), 4.21 (b) and 4.22 (b) show the comparison of the frequency parameter against the aspect ratio for thickness to length ratio 2%, 5% and 10% with respect to 1% thickness to length ratio for $j=1$ which represent predominantly torsional modes again the dashed lines in these figures represent data for 1% thickness to length ratio and the solid line is for 2%, 5% and 10% respectively.

Figures 4.20 (c), 4.21 (c) and 4.22 (c) show the comparison of the frequency parameter against the aspect ratio for thickness to length ratio 2%, 5% and 10% with respect to 1% thickness to length ratio for $j=2$. Similarly for Figures 4.20 (d), 4.21 (d) and 4.22 (d) show the comparison of the frequency parameter against the aspect ratio for thickness to length ratio 2%, 5% and 10% with respect to 1% thickness to length ratio for $j=3$.

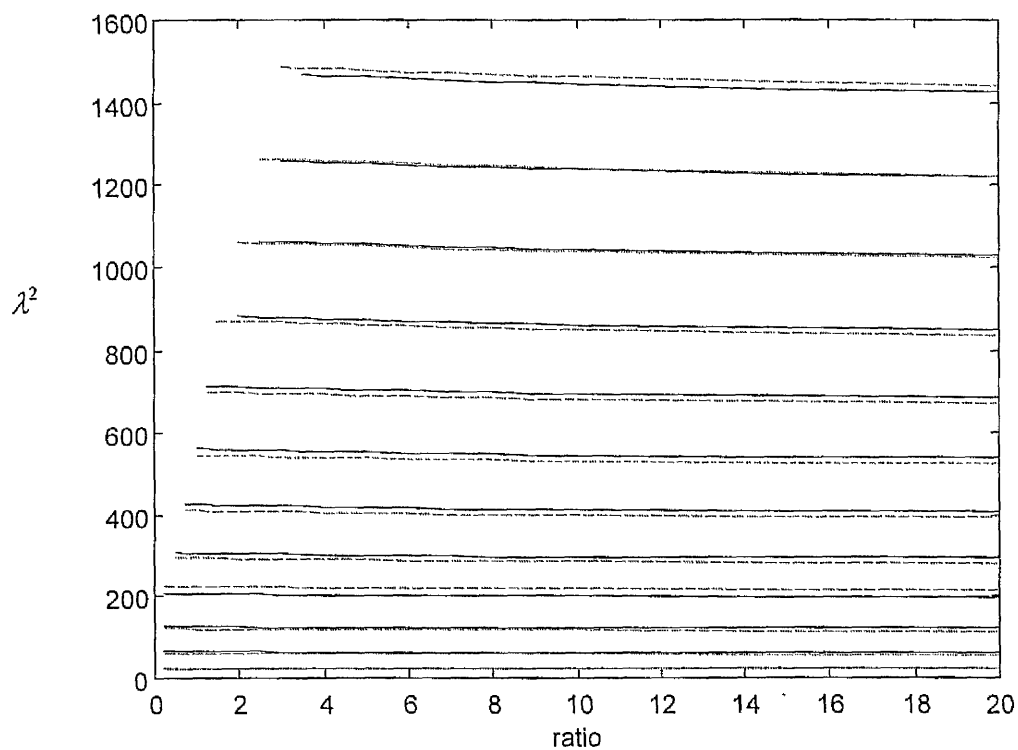


Figure 4.20 (a) Comparison of variation frequency parameter with aspect ratio for clamped-clamped beam-plate of thickness to length ratio 1% and 2%, $j=0$; dashed line:1%, solid line:2%

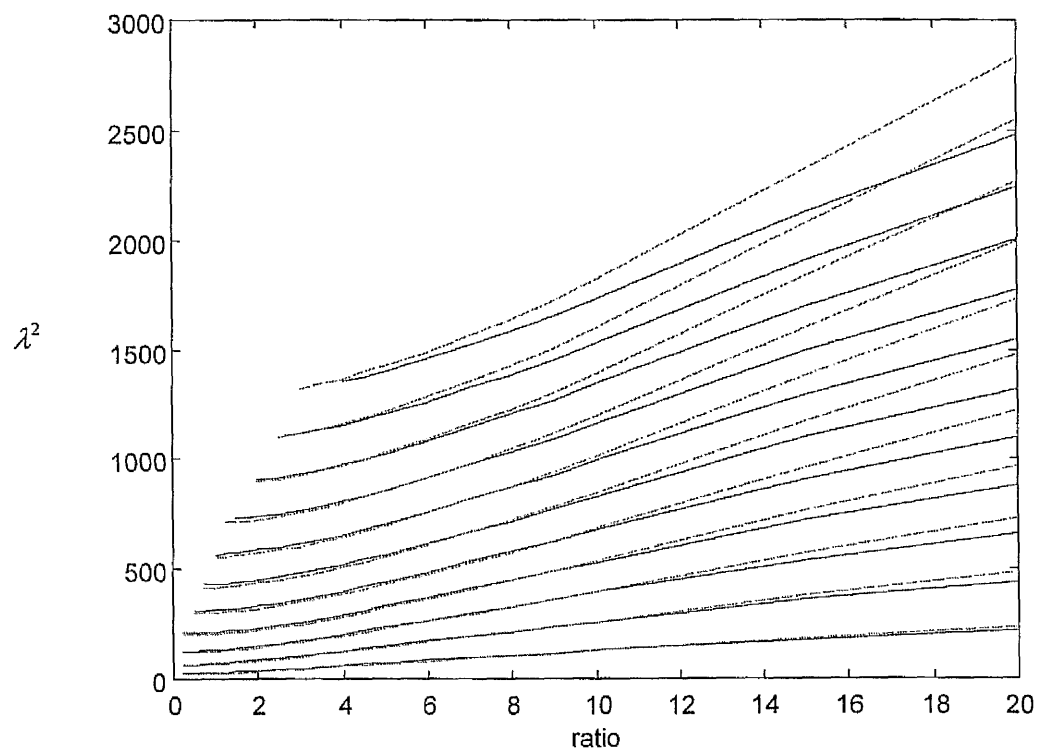


Figure 4.20 (b) $j=1$; dashed line:1%, solid line:2%

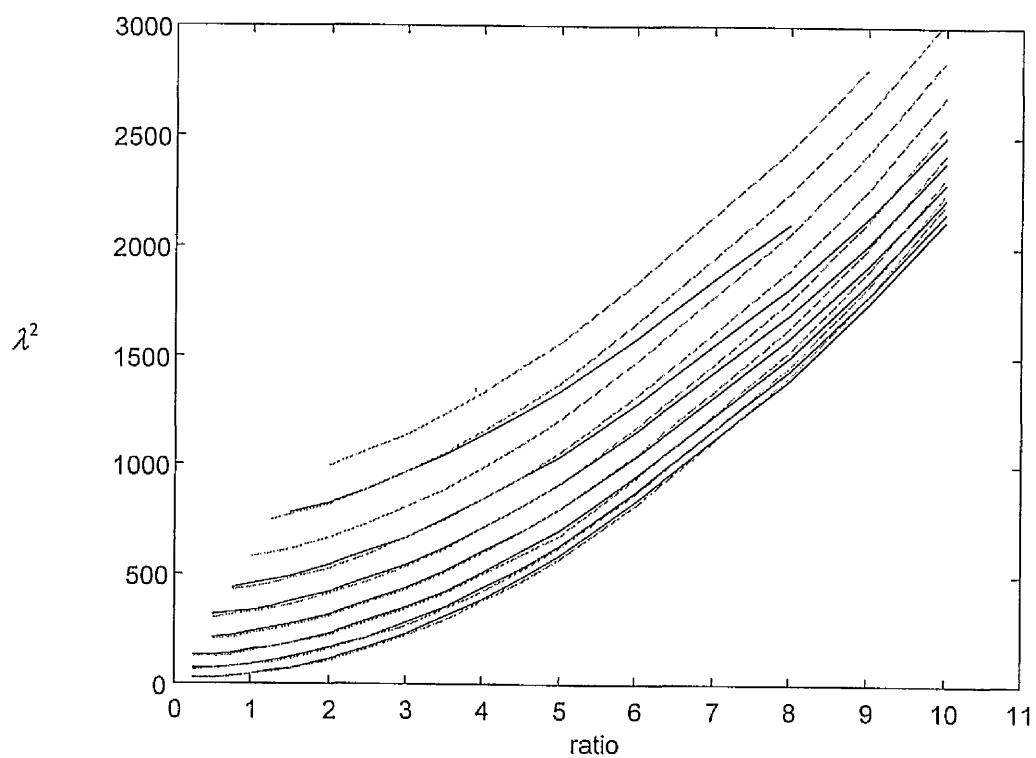


Figure 4.20 (c) $j=2$; dashed line:1%, solid line:2%

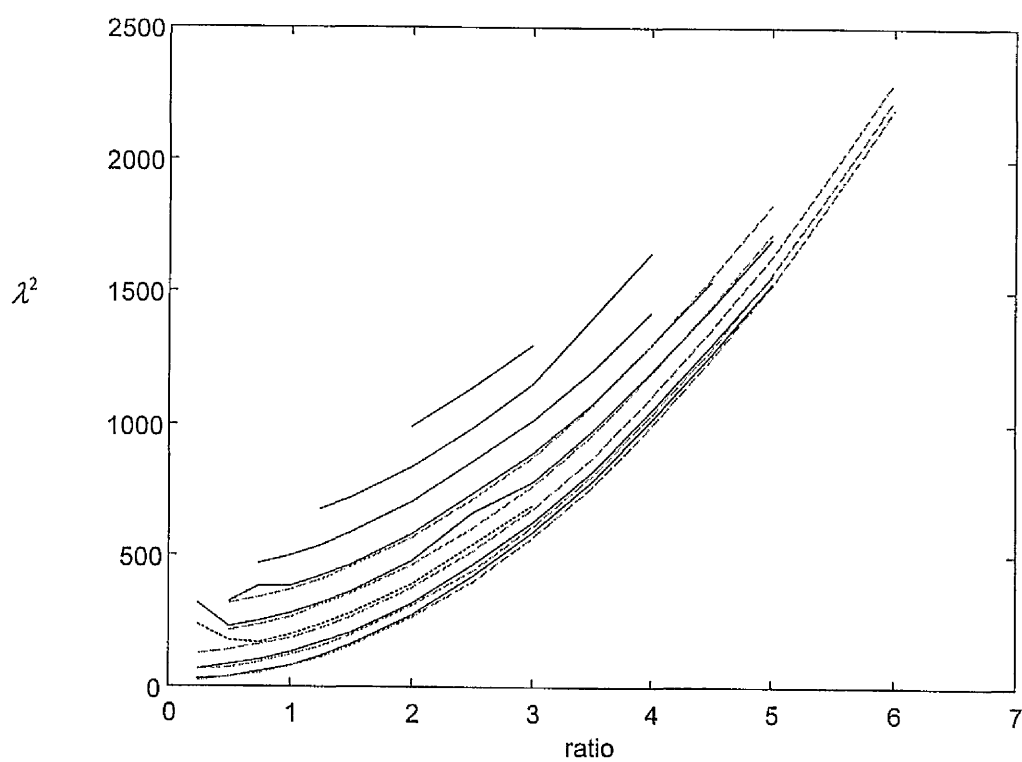


Figure 4.20 (d) $j=3$; solid line:1%, dashed line:2%

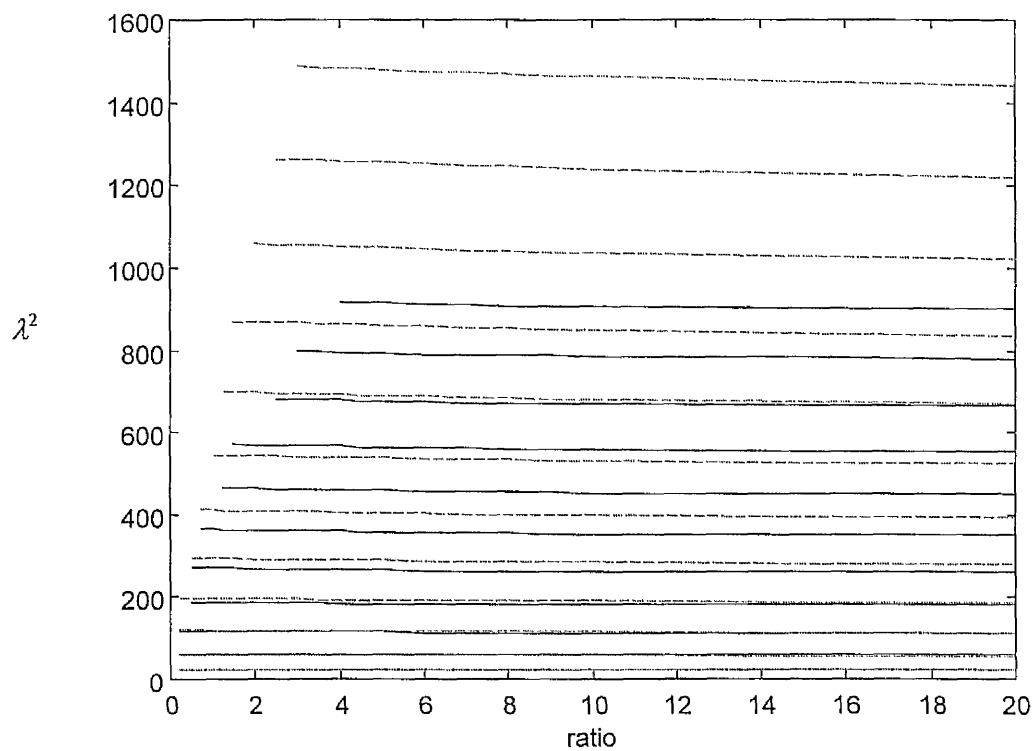


Figure 4.21 (a) Comparison of variation frequency parameter with aspect ratio for clamped-clamped beam-plate of thickness to length ratio 1% and 5%, $j=0$; dashed line:1%, solid line:5%

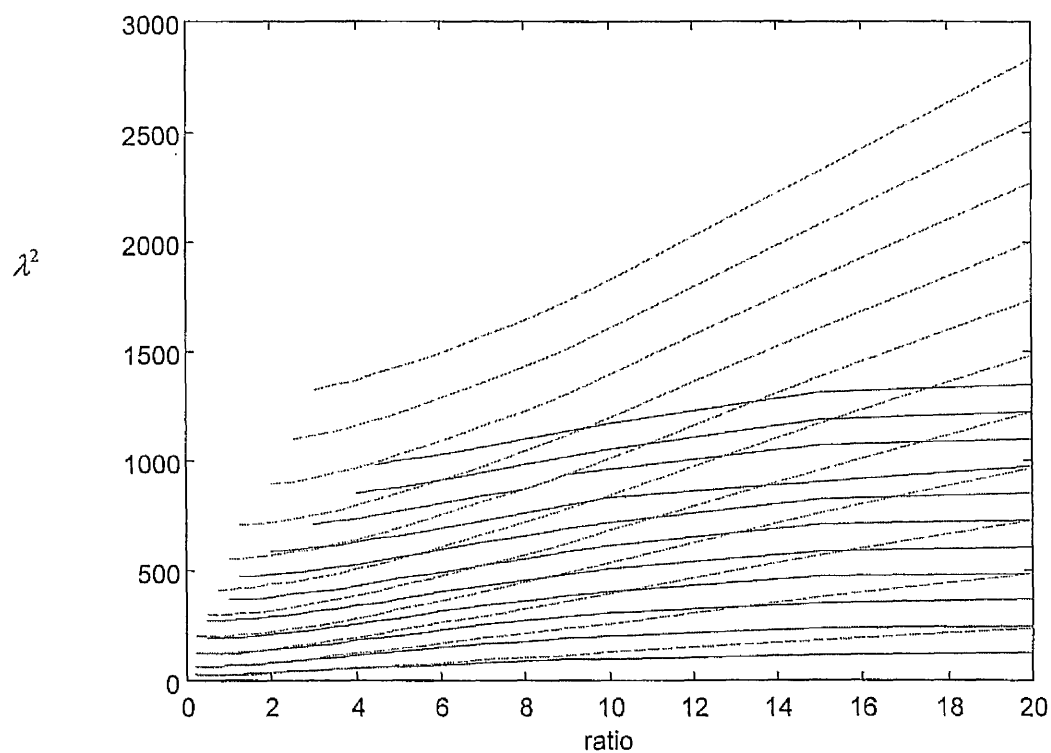


Figure 4.21 (b) $j=1$ dashed line:1%, solid line:5%

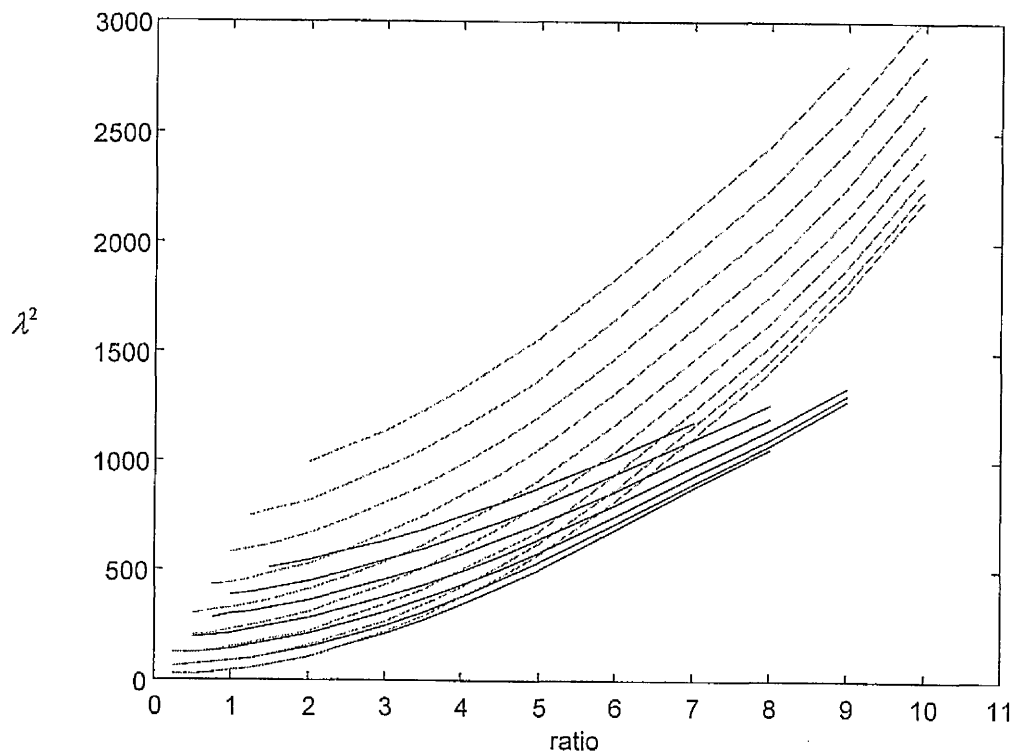


Figure 4.21 (c) $j=2$; dashed line:1%, solid line:5%

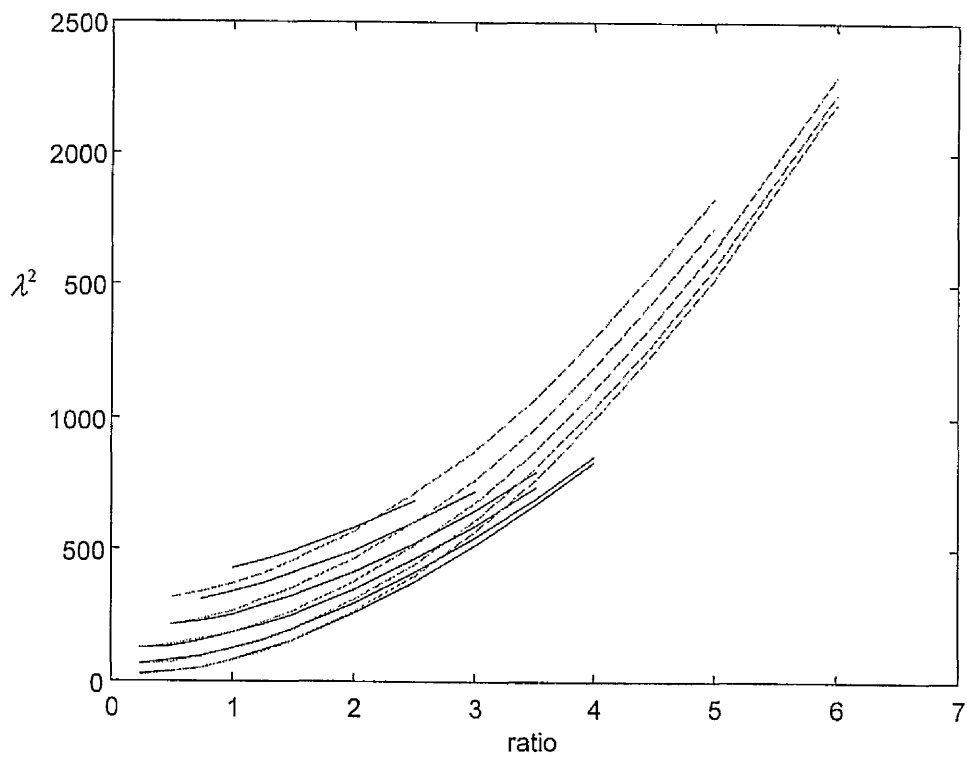


Figure 4.21 (d) $j=3$; dashed line:1%, solid line:5%

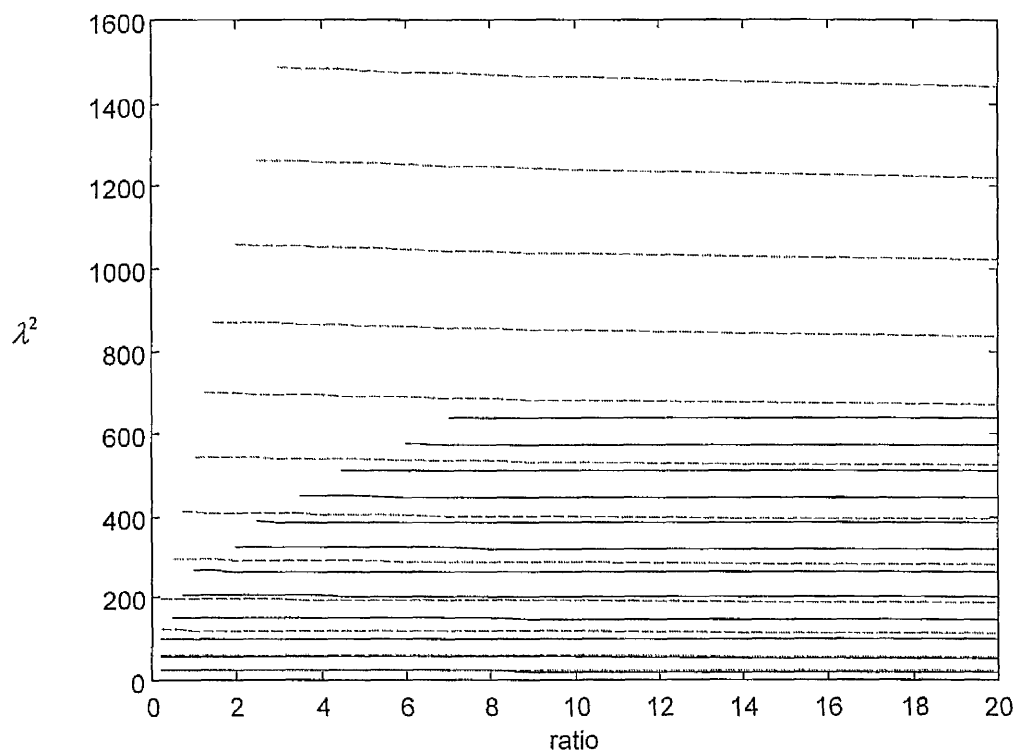


Figure 4.22 (a) Comparison of variation frequency parameter with aspect ratio for clamped-clamped beam-plate of thickness to length ratio 1% and 10%, $j=0$; dashed line: 1%, solid line: 10%

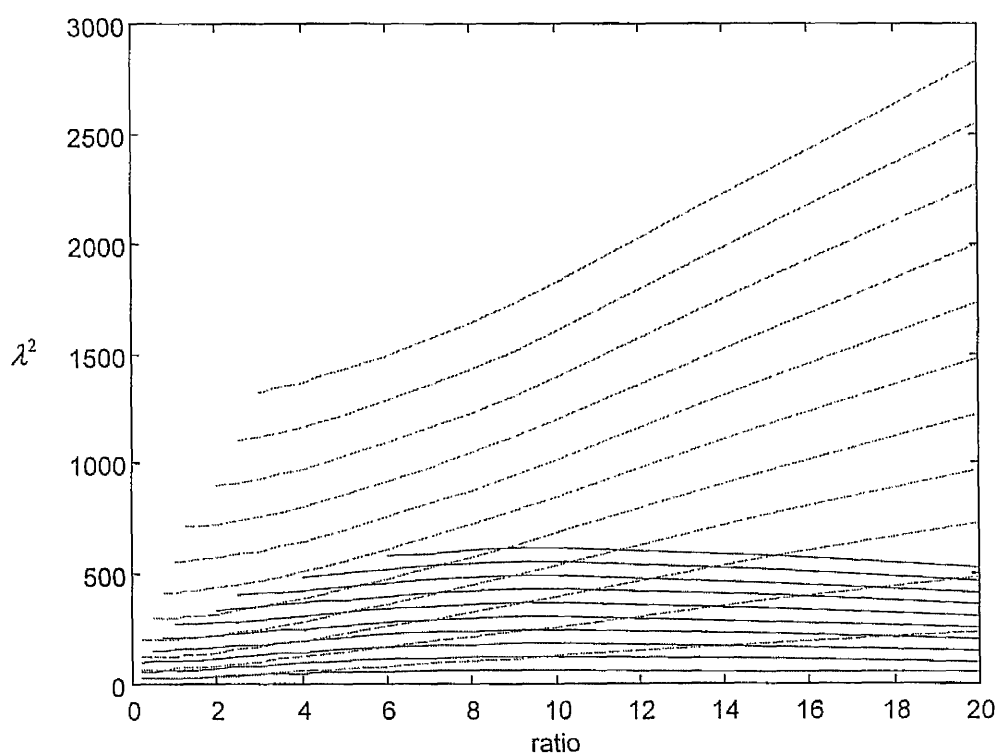


Figure 4.22 (b) $j=1$; dashed line: 1%, solid line: 10%

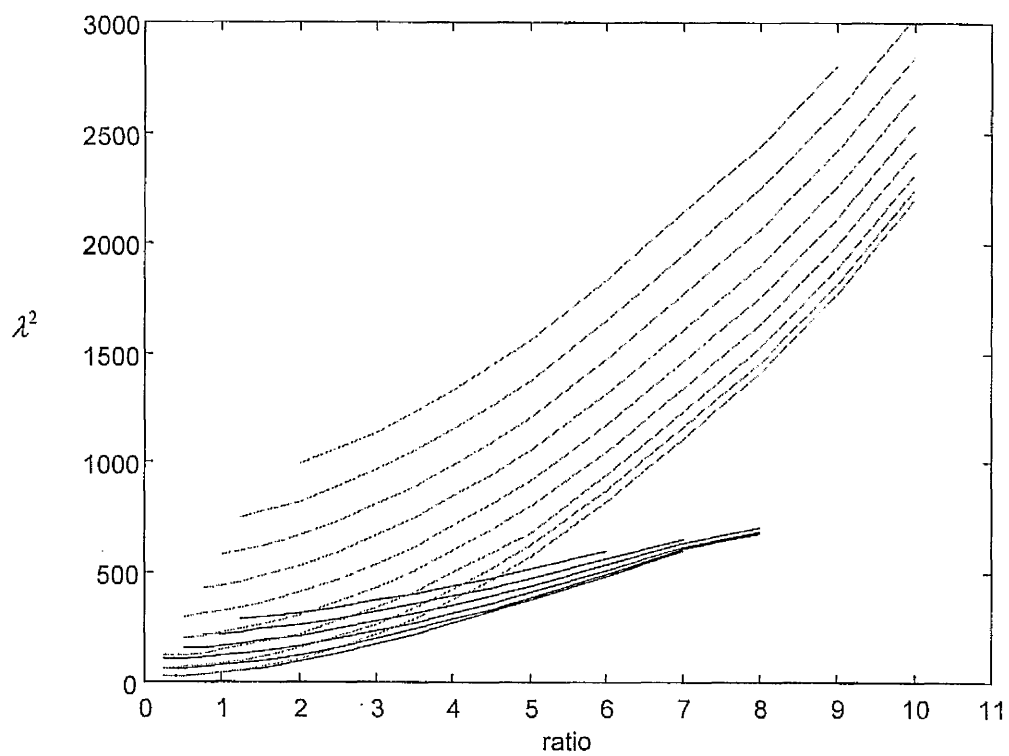


Figure 4.22 (c) $j=2$; dashed line:1%, solid line:10%

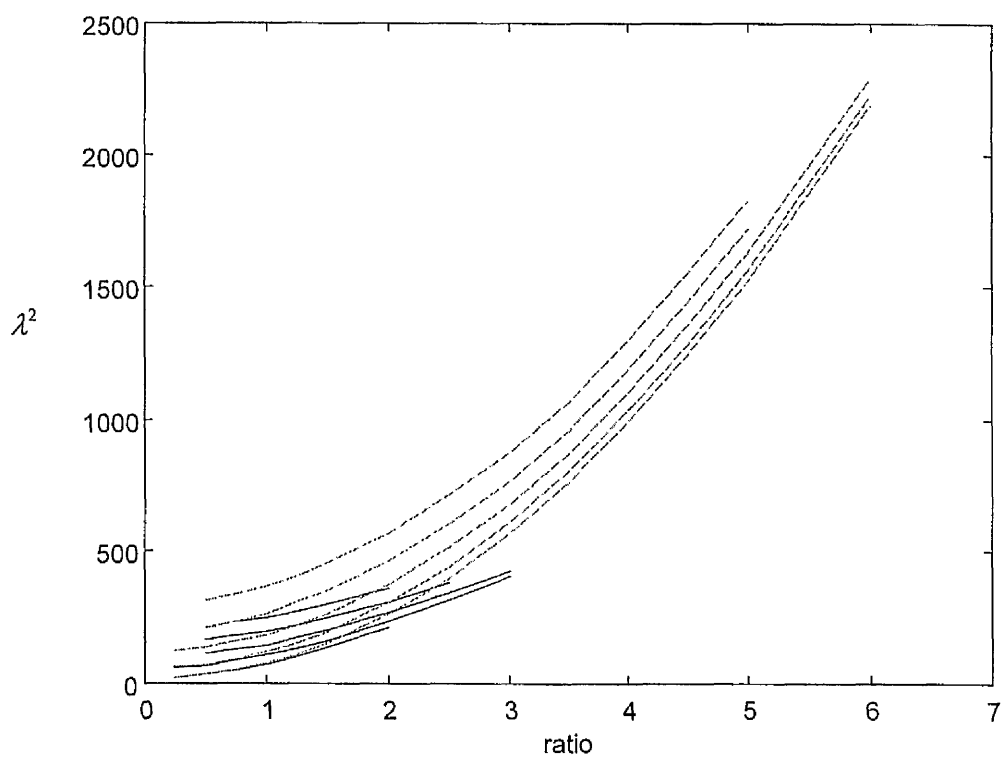


Figure 4.22 (d) $j=3$; dashed line:1%, solid line:10%

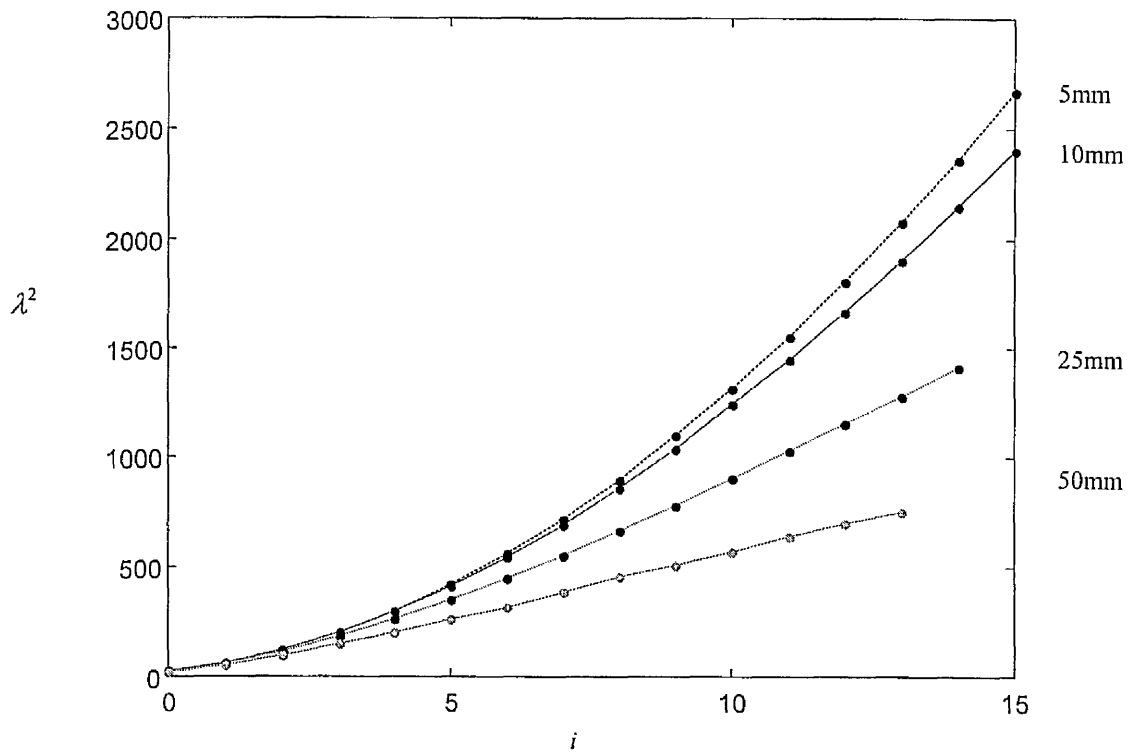


Figure 4.23 Variation of frequencies parameter for aspect ratio 10 for thickness to length ratio 1%, 2%, 5% and 10% for $j=0$ and i varies

Figure 4.23 shows the variation of frequency parameter for selected aspect ratio 10, and for thickness to length ratio 1%, 2%, 5% and 10%. These curves, which are for $j=0$ and varying i , represent the bending modes for beam-plate of aspect ratio 10 where it can be seen that the frequency parameter in the first 3 bending modes for the four thickness to length ratio are very close and the % error is small. However, the error increases rapidly for higher bending modes especially in the case of the 5% and 10% thickness to length ratio. This is due to the fact that the frequency parameter calculated from the formula $\lambda^2 = 2\pi L^2 f \sqrt{\frac{12\rho}{Eh^2}}$, where h is the beam plate thickness, and as the thickness increases the frequency parameter decreases as this shown in Figure 4.23.

4.6 Summary

In this chapter the frequency parameter charts, which show the variation of frequency parameter with aspect ratio for fixed values of i and j were produced and discussed in more detail for thickness to length ratio 1%. The frequency parameter charts for thickness to length ratio 2%, 5% and 10% were also obtained in this chapter. From all these charts the variation of the frequency parameters with aspect ratios for $j = 0$ are nearly constant while the frequency parameters for $j = 1$ to 6 increase as the aspect ratios increase and as the lengthwise mode number i increases. The variation of the frequency parameters for fixed value of i , for $i = 0$, with aspect ratio are almost constant and for $i = 1$, the frequency parameters increase gradually as the aspect ratio increases while for $i \geq 2$, the frequency parameter changes rapidly as the aspect ratio changes. The effect of beam and plate thickness has been proven to have significant effect on the value of the frequency parameter.

Chapter 5

Study of the natural frequency parameters and mode shapes for free-free beams and plates

5.1 Introduction

In the previous chapter, the ABAQUS FEA software was used to calculate the first 50 natural frequencies and mode shapes of aluminium alloy beams and plates of clamped-clamped boundary conditions. This chapter considers the free-free boundary conditions. The beams and plates were of a fixed length $a = 500$ mm, and different thickness to length ratio of 1%, 2%, 5% and 10% (thickness $t = 5, 10, 25$, and 50 mm). The breadths were varied from 25 mm to 2000 mm to generate 20 values of the aspect ratios ($r=a/b$) for analysis. These aspect ratios were 0.25, 0.5, 0.75, 1.0, 1.25, 1.50, 2.0, 2.5, 3.0, 3.5, 4.0, 4.5, 5.0, 6.0, 7.0, 8.0, 9.0, 10.0, 15.0 and 20.0. The analysis was carried out using the thin shell element S8R5 for 1% thickness to length ratio, while the

general shell element S4R was used for the beams and plates of the other three thickness to length ratio. The number of elements in the lengthwise or x -axis (N_x) direction was fixed at 60 and 80 for ratio 0.25 and 0.5 respectively, and 100 elements for the other aspect ratios, while the number of elements in the breadthwise or y -axis (N_y) direction was varied with the aspect ratios a/b .

5.2 Variations of frequency parameters ($\lambda_{i,j}^2$) and mode shapes with length to-breadth ratios (a/b) and mode counter i and j

From the calculated natural frequencies of the free-free beam-plates the frequency parameters $(\lambda_{ij}^2)_B$ and $(\lambda_{ij}^2)_P$ for beam-like and plate-like behaviour were derived in the same way as the clamped-clamped boundary condition as described in the previous chapter.

5.2.1 Relationship between frequency parameters and aspect ratios for fixed values of j

The relationship between frequency parameters (λ_{ij}^2) and aspect ratios (a/b) for fixed values of the breadthwise mode counters j are shown in Figures 5.1 to 5.7. In these figures, the x -axis denotes the aspect ratios while the y -axis denotes the frequency parameters.

Predominantly bending modes along lengthwise direction ($j=0$)

Figure 5.1a shows the variation of the frequency parameters with aspect ratios. This figure consists of 10 curves representing values of $j = 0$ and $i = 2, 3, 4, 5, 6, 7, 8, 9, 10$ and 11 from the bottom-most curve to the top-most curve, respectively. In this figure

the 10 curves represent the first 10 predominantly bending modes along the longitudinal (x) axis of the free-free beams and plates. All the curves look like straight lines due to the scale of this graph, but in fact, the curves show erratic behaviour at small aspect ratios and decrease fairly exponentially at moderate to high aspect ratios. Figure 5.1b shows the mode shapes for the first ($i = 2, j = 0$) and the fifth mode ($i = 6, j = 0$) modes for aspect ratios 1.25, 5 and 10. It should be noted that the actual first two modes for which $i=0, 1$ is a rigid body mode which occur for the free-free boundary condition, this behaviour known as anticlastic behaviour where there is bending along x -axis accompanied by bending along the y -axis. The first elastic mode occurs at $i=2$. Similarly, $i=6$ is the fifth elastic mode. It is seen that for a particular mode, e.g. mode 1 ($i = 2$) the natural frequencies decrease in value as the aspect ratio increases. This implies that the natural frequencies of the bending modes of the plates along their x -axis are greater than the corresponding natural frequencies of the beams. This suggests that the effect of the increase in bending stiffness of the plates compared to the beams is greater than the effect of the increased mass moment of inertia of the plate compared to the beams.

Predominantly torsional modes about lengthwise axis ($j=1$)

For $j = 1$ and $i = 1$ to 13 Figure 5.2a show the variation of the frequency parameters with respect to the aspect ratios. There are 13 curves in this figure which correspond to values of $j = 1$ and $i = 1, 2, 3, 4, 5, 6, 7, 8, 9, 10, 11, 12$ and 13 from the bottom-most curve to the top-most curve, respectively. All these curves represent the behaviour of the first 13 predominantly torsion modes of the free-free beams and plates. The graph also shows that the frequency parameters increase in value as the aspect ratio increases and as the lengthwise mode counter i of the beam-plate increases. Figure 5.2b

show the mode shapes of the first ($i = 1, j = 1$) and the fifth ($i = 5, j = 1$) modes for aspect ratios 1.25, 5 and 10. It is important to notice that the natural frequencies of the beams are greater than those of the plates, which suggests that the mass moment of inertia of the plates are greater than those of beams.

First bending deformation along breadthwise direction ($j=2$)

The variation of the frequency parameters with aspect ratios for values of $j = 2$ and $i = 0$ to 9 is shown in Figure 5.3a. There are 10 curves in this figure. These curves correspond to values of $j = 2$ and $i = 0$ for the bottom-most curve to values of $j = 2$ and $i = 9$ for the top-most curve, respectively. Clearly λ_{i2}^2 increases parabolically as the aspect ratio increases. Also, λ_{i2}^2 increases as the lengthwise mode counter i of the beam-plate increases. The 10 curves correspond to the first 10 combinational modes for which the lengthwise bending modes are coupled with the first breadthwise bending modes. The mode shapes of the first ($i = 0, j = 2$) and the sixth ($i = 5, j = 2$) modes for aspect ratios 1, 5 and 10 are illustrated in Figure 5.3b. From this figure it is clearly shown that the natural frequencies of the beams are greater than the natural frequencies of the plates for the selected mode 1 ($i = 0$) and mode 6 ($i = 5$). Again, this suggests that the effect of increase in the breadthwise bending stiffness is less than the effect of increase in the mass moment of inertia.

Second bending deformation along breadthwise direction ($j=3$)

There are 8 curves in the variation of the frequency parameters with aspect ratios for values of $j = 3$ and $i = 0$ to 7 as shown in Figure 5.4a. These correspond to values of $j = 3$ and $i = 0, 1, 2, 3, 4, 5, 6$ and 7 from the bottom-most curve to the top-most curve, respectively. From this figure it is seen that the frequency parameters, λ_{i3}^2 , increase

parabolically as the ratio increases and as the lengthwise mode number i of the plate increases. These 8 curves correspond to the first 8 combination modes for which the lengthwise bending modes are coupled with the second breadthwise bending modes. Figure 5.4b shows the mode shapes of the first ($i = 0, j = 3$) and the sixth ($i = 5, j = 3$) modes for aspect ratios 1.25 and 5. Again as previous, the natural frequencies of the beams are greater than those for plates which suggests that the relative effects of the bending stiffness and of the mass moment of inertia described previously when $j=2$ are seen to hold.

Third bending deformation along breadthwise direction ($j=4$)

Figure 5.5a show the variation of the frequency parameters, λ_{is}^2 , with aspect ratios for values of $j = 4$ and $i = 0$ to 6. The frequency parameter data are presented for $j = 4$ and $i = 0, 1, 2, 3, 4, 5$ and 6 from the bottom-most curve to the top-most curve, respectively. This figure shows that λ_{i4}^2 increases parabolically as the aspect ratio increases and as the lengthwise mode counter i of the plate increases. The curves correspond to the first 7 combination modes for which the lengthwise bending modes are coupled with the third breadthwise bending modes. The mode shapes of the first ($i = 0, j = 4$) and the fourth ($i = 3, j = 4$) modes for aspect ratios 1.25 and 2 are illustrated in Figure 5.5b. Again, the previous deductions made when $j=2$ that the effect of mass moment of inertia are greater than the effect of breadthwise bending stiffness are seen to apply here.

Fourth bending deformation along breadthwise direction ($j=5$)

The 6 curves shown in Figure 5.6a represent the variation of the frequency parameters with aspect ratios for values of $j = 5$ and $i = 0, 1, 2, 3, 4$ and 5 from the

bottom-most curve to the top-most curve, respectively. The figure shows that the frequency parameters increase as the aspect ratios increase and as the mode counter i increases. These 6 curves correspond to the first 6 combination modes for which the lengthwise bending modes are coupled with the fourth breadthwise bending modes. Figure 5.6b shows the mode shapes of the first ($i = 0, j = 5$) and the fourth ($i = 3, j = 5$) modes for aspect ratios 0.50 and 1. The figure shows that the natural frequency increases as the aspect ratio increases, which implies that the previous deduction when $j=2$ also applies here.

Fifth bending deformation along breadthwise direction ($j=6$)

The variations of frequency parameters with aspect ratios for the value of $j = 6$ and $i = 0$ to 4 are shown in Figure 5.7a. This figure show there are 5 curves which correspond to values of $j = 6$ and $i = 0, 1, 2, 3$ and 4 from the bottom-most curve to the top-most curve, respectively. These curves show clearly that the frequency parameters increase as the aspect ratios and mode counter i of the beam-plate increase. These curves correspond to the first 5 combination modes for which the lengthwise bending modes are coupled with the fifth breadthwise bending modes. The mode shapes of the first ($i = 0, j = 6$) and the fourth ($i = 3, j = 6$) modes for aspect ratios 0.50 and 1.25 are shown in Figure 5.6b. Again the natural frequency increases with the increase of aspect ratio, which again implies that the deduction from the case $j=2$ is also applicable here.

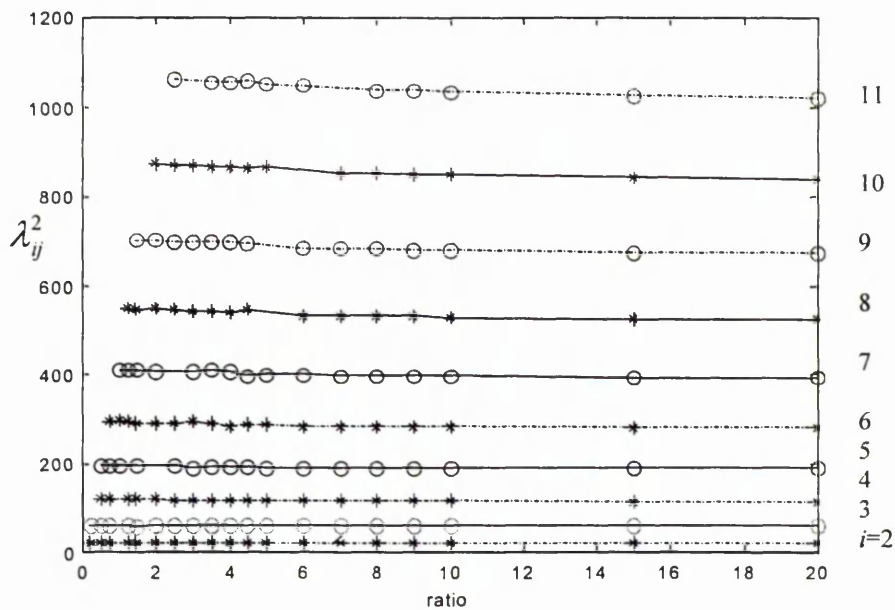


Figure 5.1a Variation of frequency parameters with aspect ratios for $j = 0$

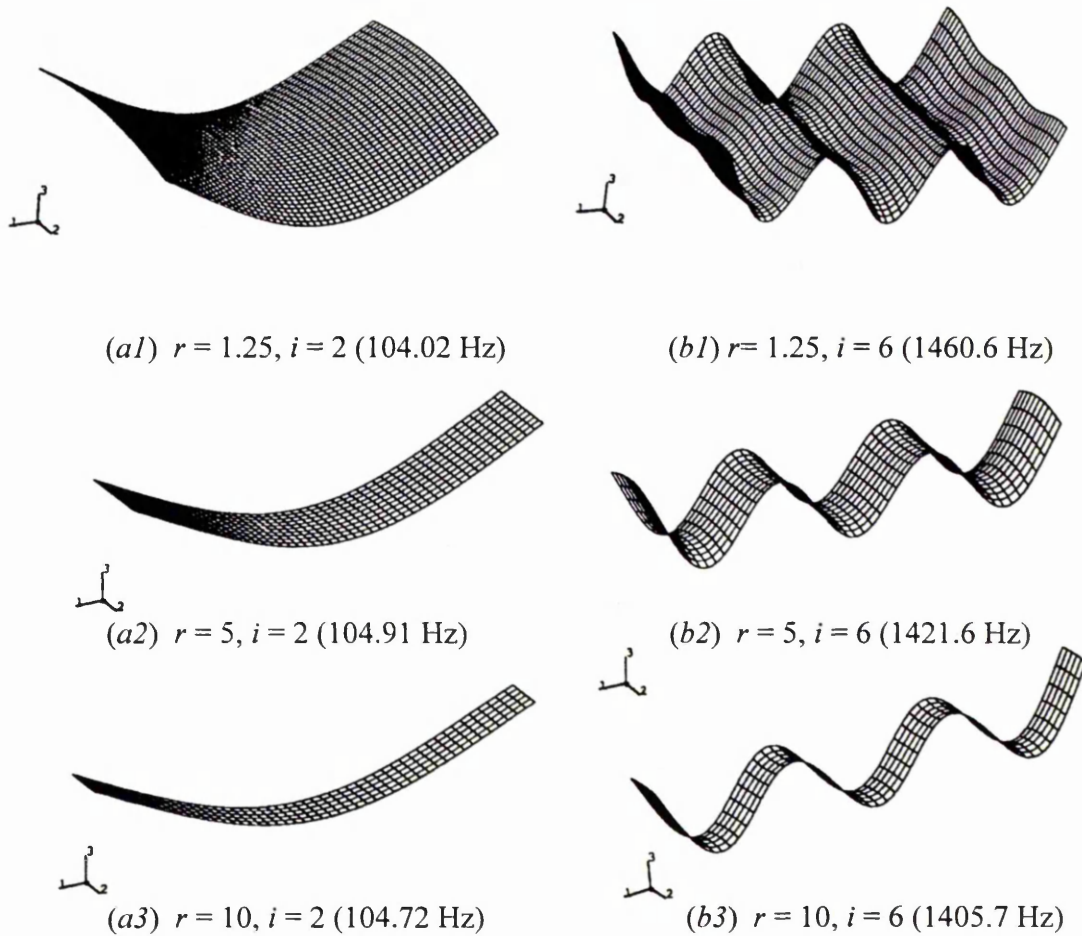


Figure 5.1b Mode shapes of beam-plates for mode counter $j = 0$

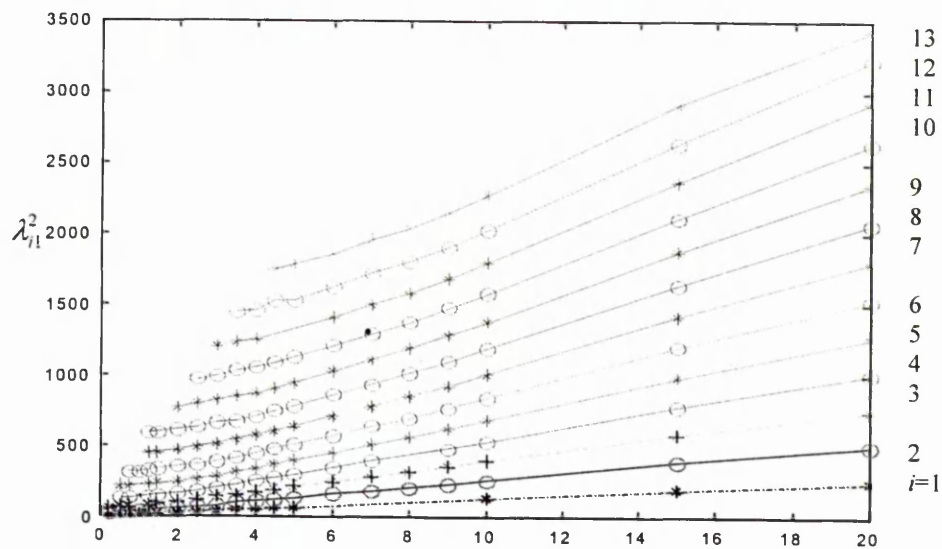


Figure 5.2a Variation of frequency parameters with aspect ratios for $j = 1$

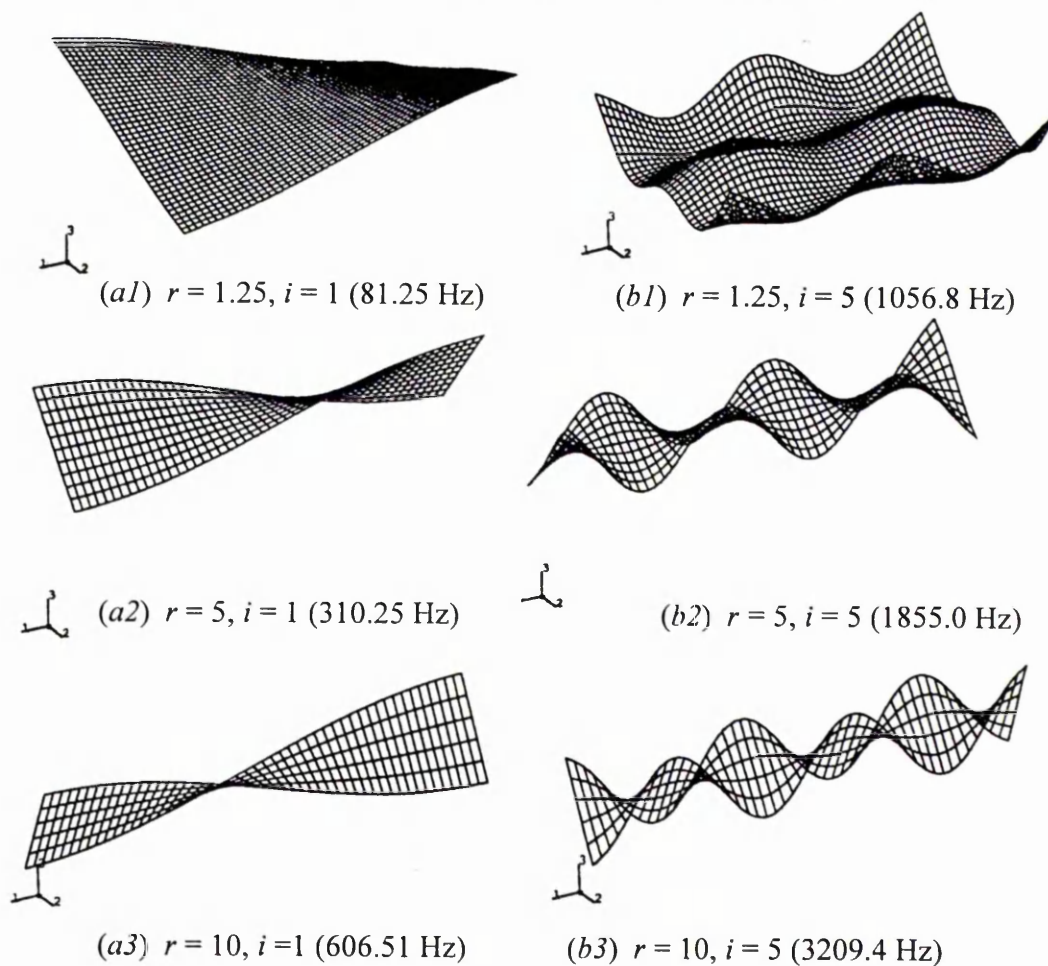


Figure 5.2b Mode shapes of beam-plates for mode counter $j = 1$

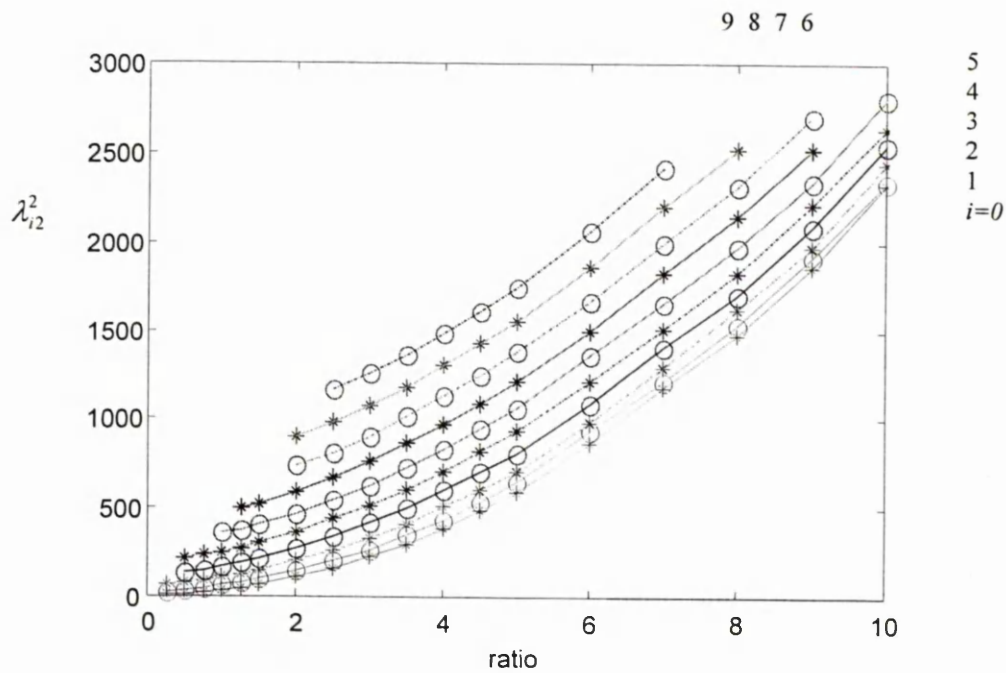


Figure 5.3a Variation of frequency parameters with aspect ratios for $j = 2$

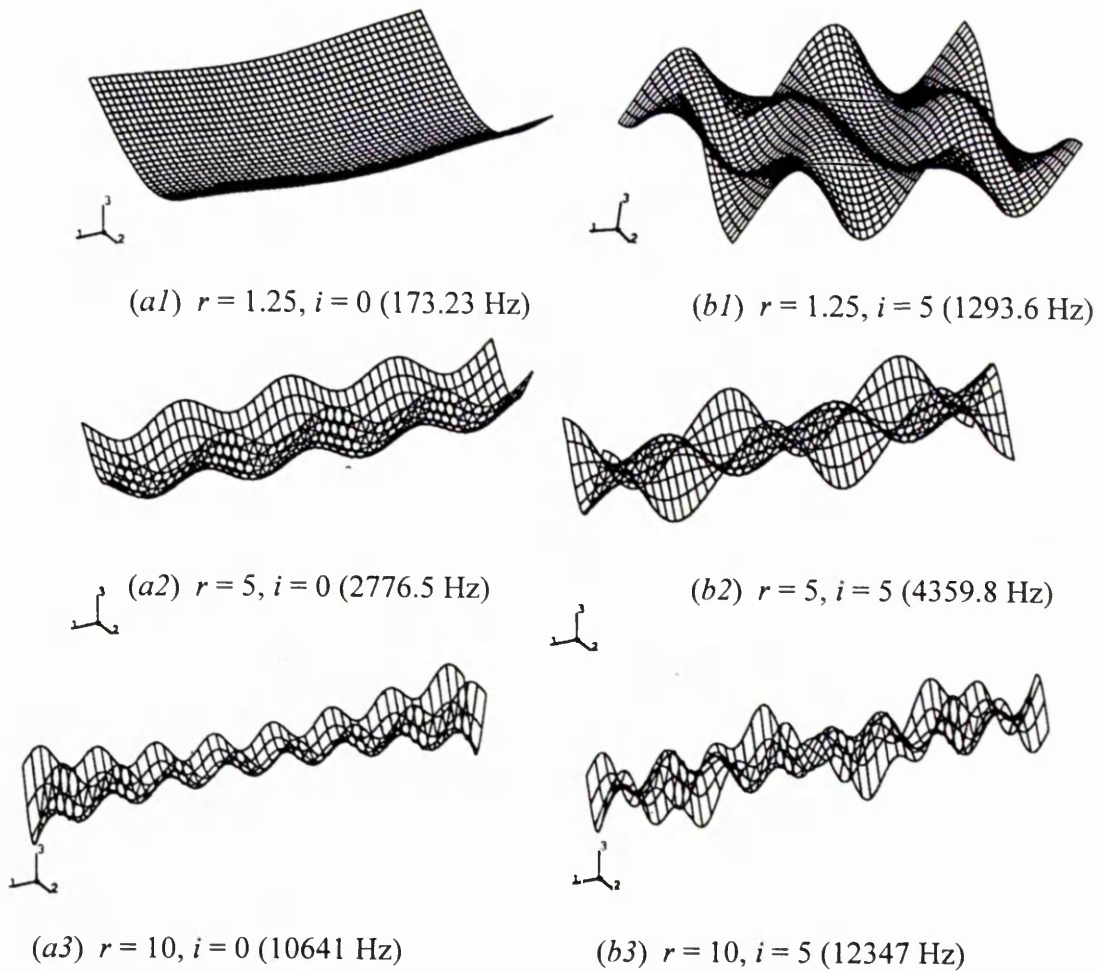


Figure 5.3b Mode shapes of beam-plates for mode counter $j = 2$

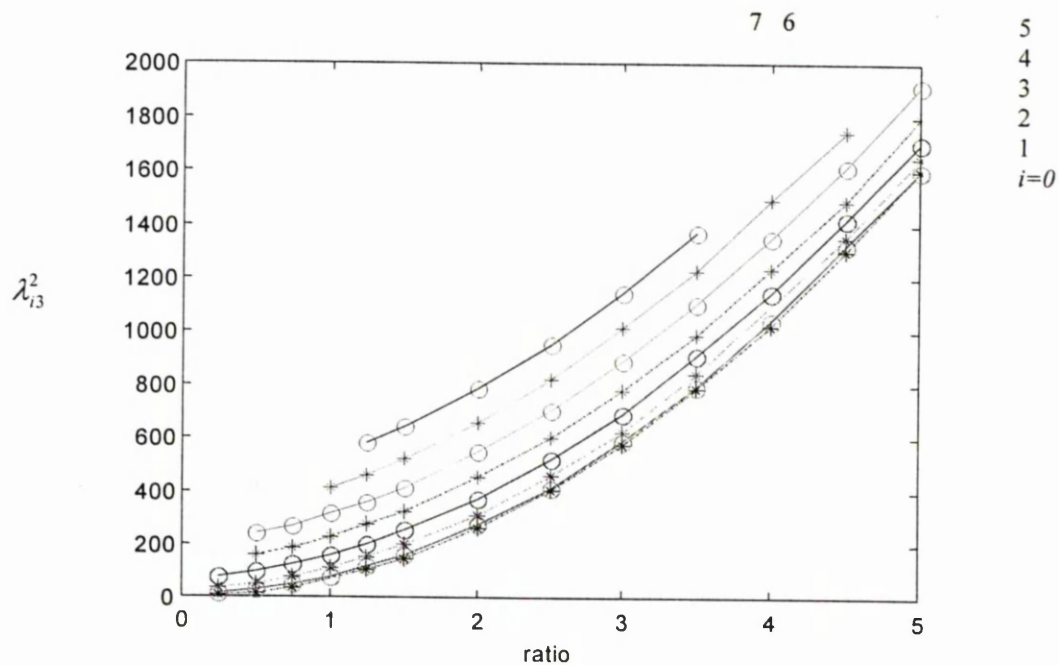
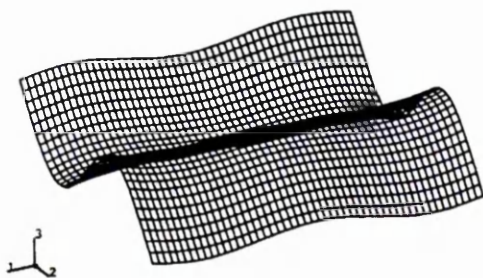
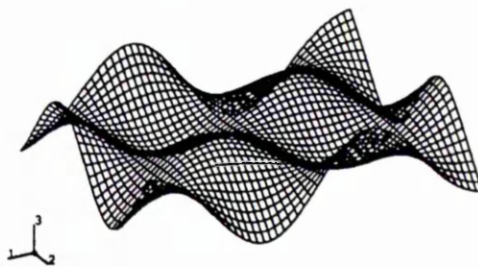


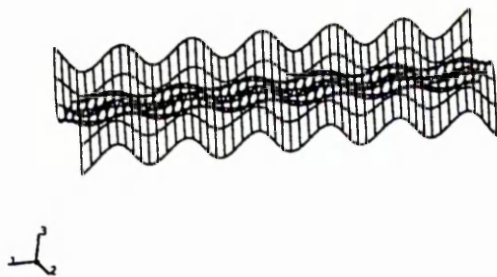
Figure 5.4a Variation of frequency parameters with aspect ratios for $j = 3$



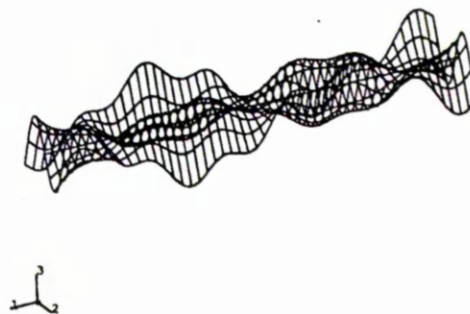
(a1) $r = 1.25, i = 0$ (469.73 Hz)



(b1) $r = 1.25, i = 3$ (942.66 Hz)



(a2) $r = 5, i = 0$ (7495.2 Hz)



(b2) $r = 5, i = 3$ (7975.3 Hz)

Figure 5.4b Mode shapes of beam-plates for mode counter $j = 3$

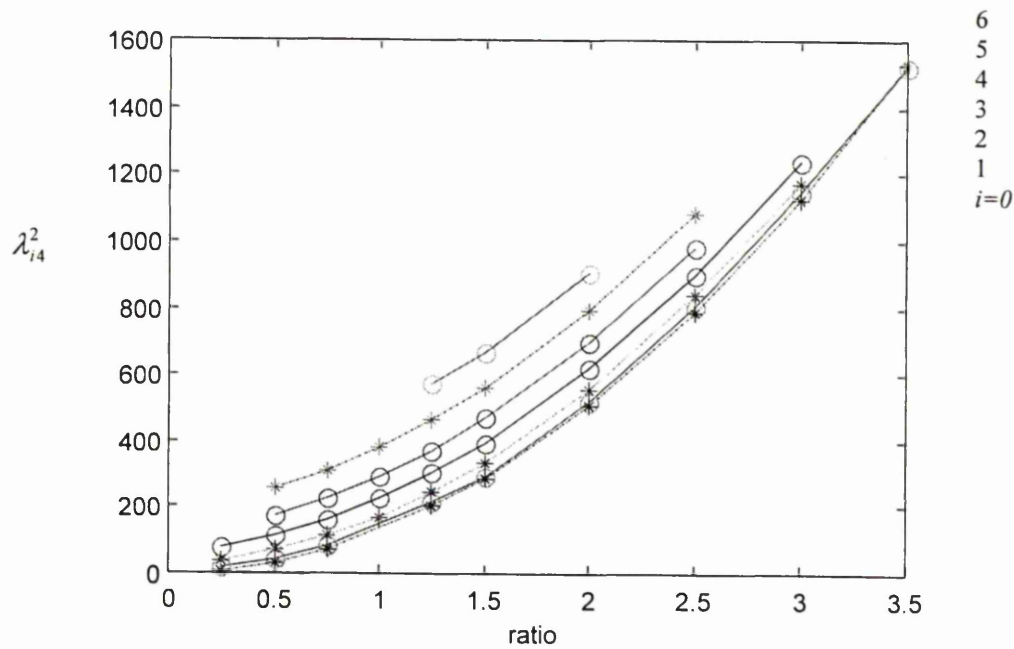


Figure 5.5a Variation of frequency parameters with aspect ratios for $j = 4$

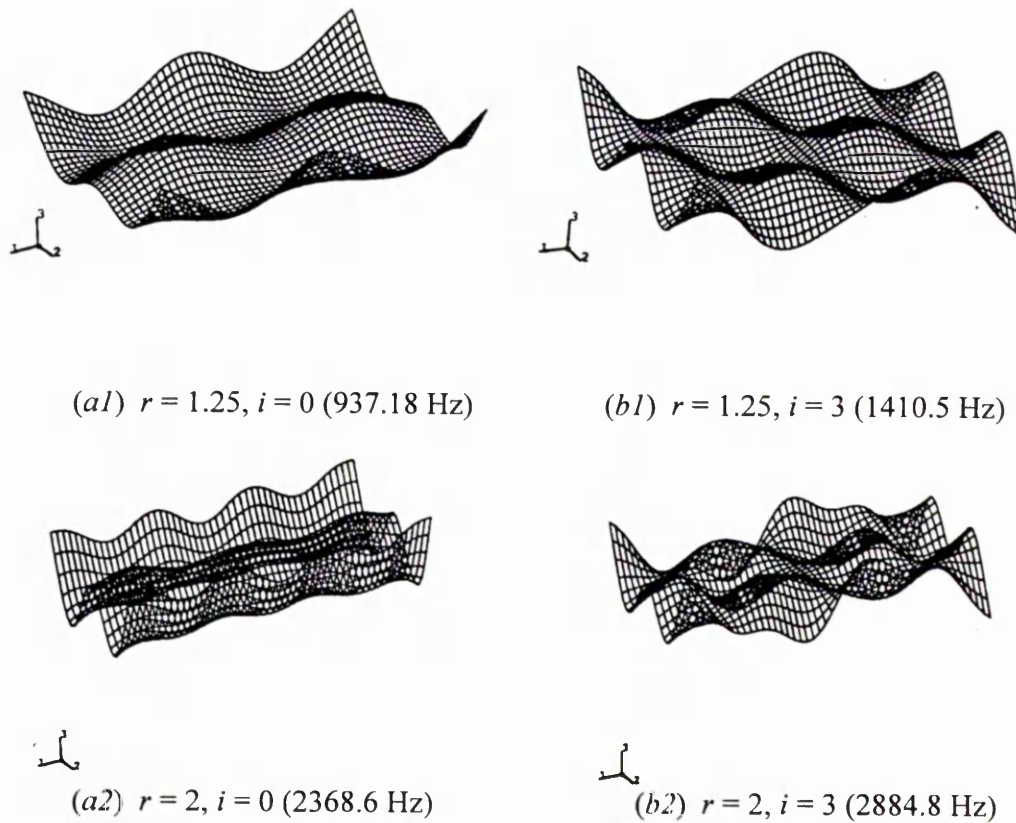


Figure 5.5b Mode shapes of beam-plates for aspect ratio 0.75, $j = 4$

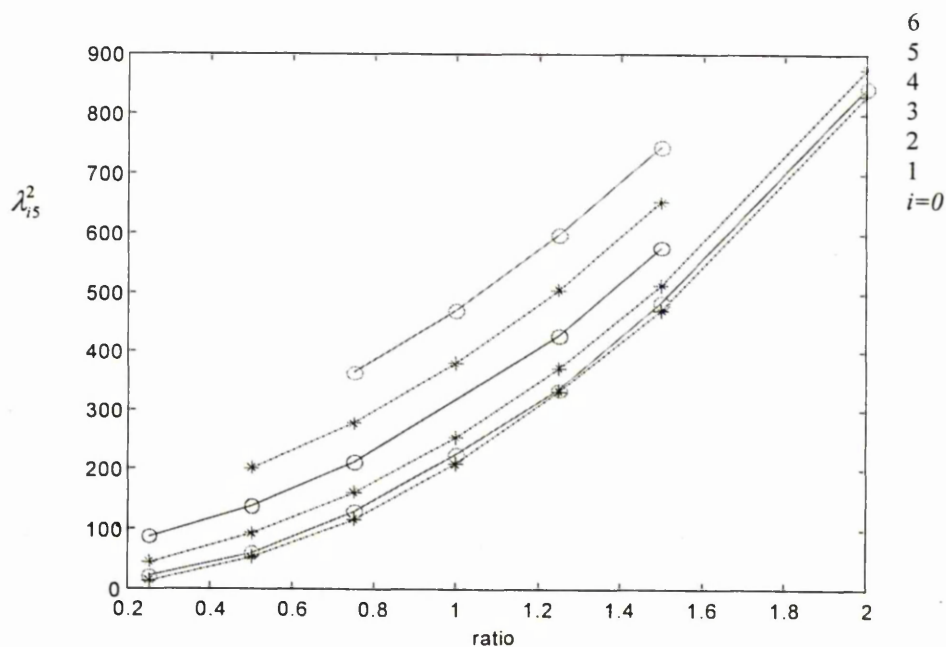


Figure 5.6a Variation of frequency parameters with aspect ratios for $j = 5$

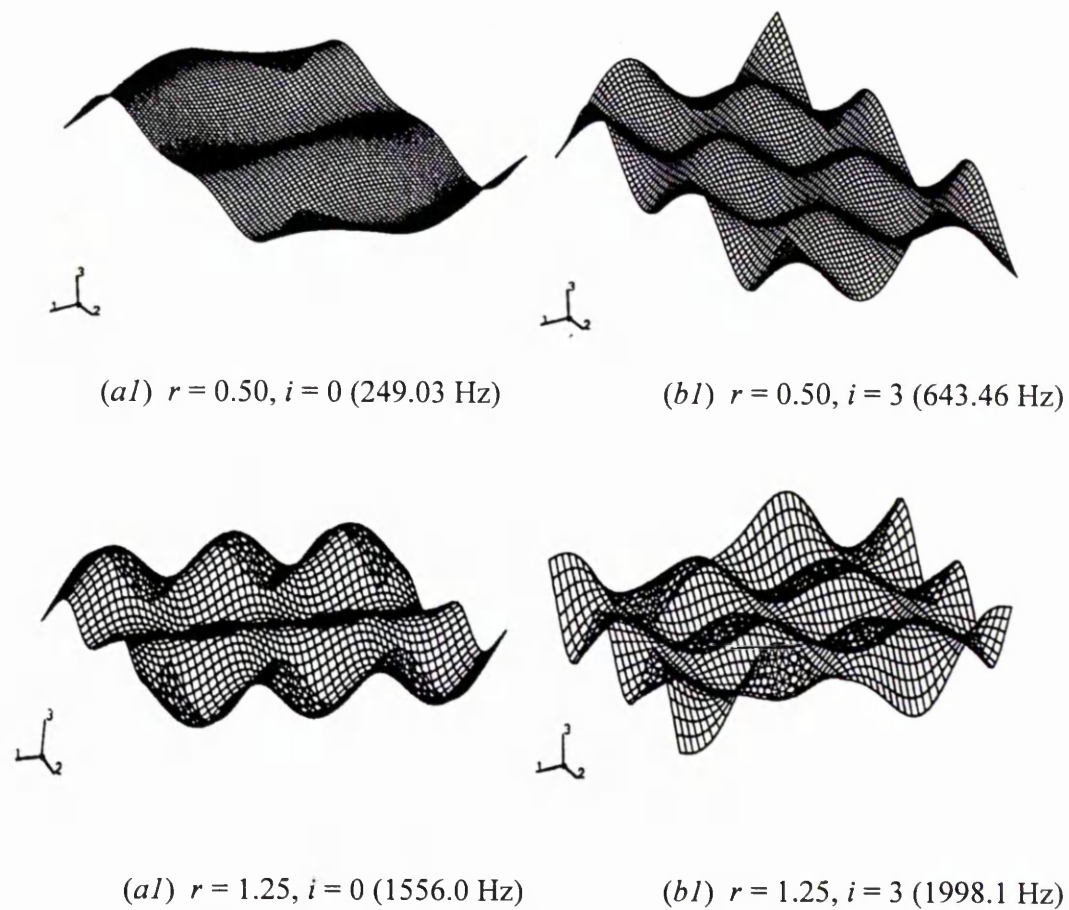


Figure 5.6b Mode shapes of beam-plates for mode counter $j = 5$

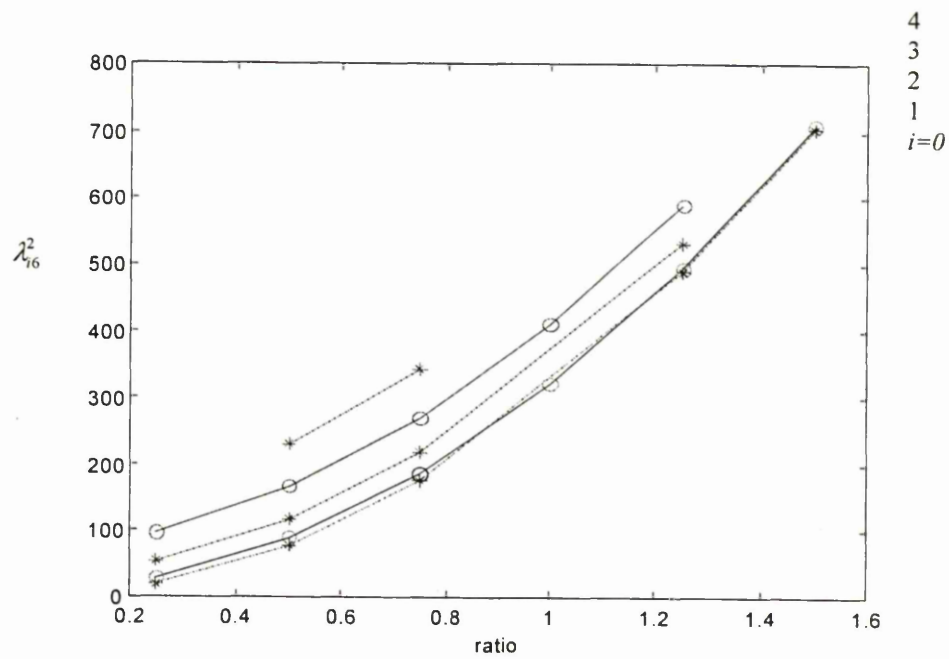
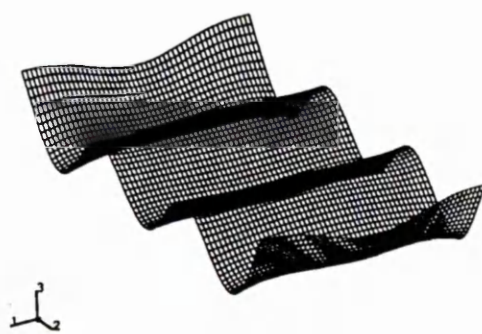
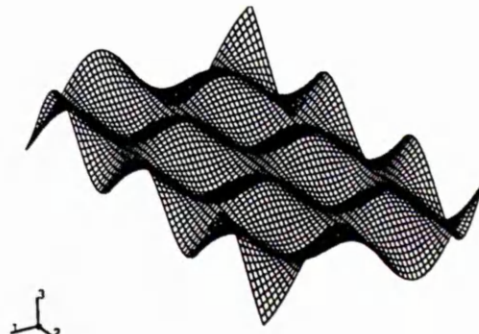


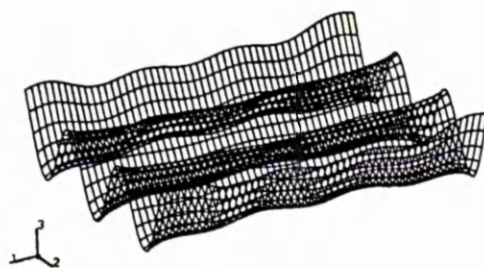
Figure 5.7a Variation of frequency parameters with aspect ratios for $j = 6$



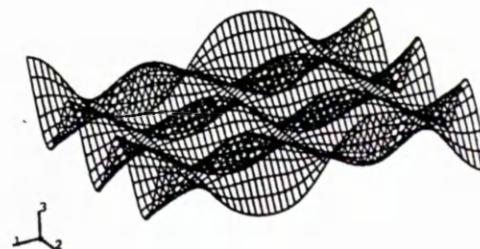
(a1) $r = 0.50, i = 0$ (365.07 Hz)



(b1) $r = 0.50, i = 3$ (776.02 Hz)



(a2) $r = 1.25, i = 0$ (2281.1 Hz)



(b2) $r = 1.25, i = 3$ (2749.7 Hz)

Figure 5.7b Mode shapes of beam-plates for mode counter $j = 6$

5.2.2 Relationship between frequency parameters and aspect ratios for fixed values of i

The results and discussion in the previous section 5.2.1, were for constant deformation in the breadthwise direction (denoted by j) while the deformation in the lengthwise direction (denoted by i) varied. In this section, the lengthwise deformation is kept constant while the breadthwise deformation is varied. This will enable a close study and comparison of the purely one-dimensional beam modes of vibration, for which $j = 0$ (pure bending) and $j = 1$ (pure torsion), with the two-dimensional plate modes of vibration, for which $j \geq 2$.

Figures 5.8a to 5.15a show the relationship between frequency parameters and aspect ratios for fixed values of i . The x -axis denotes the aspect ratios while the y -axis denotes the frequency parameters. The corresponding typical mode shapes are shown in Figures 5.8b to 5.15b.

Bending deformation along breadthwise direction ($i=0$)

In Figure 5.8a, the variations of the frequency parameters with the aspect ratios for values of $i = 0$ and $j = 2$ to 6 are presented. The figure shows that the frequency parameter curve for which $i = 0$ and $j = 2$ increases rapidly as the aspect ratio increases. The next curves for which $j = 2$ to $j = 6$ represent the fundamental modes of vibration for increasing degrees of deformation in the breadthwise direction. Generally, the variation of $\lambda_{0,j}^2$ with aspect ratio is a parabolic or exponential curve. Figure 5.8b shows typical mode shapes, which correspond to the frequency parameter curves. The 5 curves shown in this figure correspond to the first bending deformation along the lengthwise direction for which $i=0$; there is no nodal line (in the mode shape), along the lengthwise direction.

Torsional deformation about lengthwise direction ($i=1$)

The variation of the frequency parameters with the aspect ratios for values of $i = 1$ and $j = 1$ to 6 shown in Figure 5.9a. This figure consists of 6 curves which correspond to values of $i = 1$ and $j = 1$ for the bottom-most to values of $i = 1$ and $j = 6$ for the top-most curves, respectively. The figure shows that when $i = 1$ and $j = 1$, $\lambda_{1,j}^2$ increases smoothly, gradually and linearly as the aspect ratio increases. This curve denotes the first mode of pure torsional vibration as can be seen from the mode shapes in Figure 5.9b (a1) and (b1).

When $i = 1$ and $j = 2$ to 5, the frequency parameter increases rapidly as the aspect ratio increases. The frequency parameters, $\lambda_{1,j}^2$, increase parabolically or exponentially as the aspect ratios increase. The mode shapes which correspond to the frequency parameter curve for aspect ratios 1.25 and 5, and mode counters $i = 1, j = 1$ to 3 are shown in Figure 5.9b. While Figure 5.9b (a1) and (a2) show pure torsional modes of vibration about the lengthwise axis, Figures 5.9b (b1) and (b2) show a combination of torsional vibration about the lengthwise axis and the first bending deformation along the breadthwise axis. Similarly, Figure 5.9(b) shows that when $i=1$ and $j=3$, the mode of vibration is a combination of torsional vibration about the lengthwise axis and the second bending deformation along the breadthwise direction.

In general, when $i=1$, the modes of vibration are a combination of torsional modes about the lengthwise direction and bending deformation of increasing order in the breadthwise direction. It is also important to notice that the natural frequency for beams is much greater than that for plates. This suggests that the bending and torsional stiffnesses of the beams are higher than those for plates, while the mass moment of inertia of the plates are greater than those of the beams.

First bending deformation along lengthwise direction ($i=2$)

The relationships between the frequency parameters and the aspect ratios for values of $i = 2$ and $j = 0$ to 6 are shown in Figure 5.10a. The bottom-most curve for which $i = 2$ and $j = 0$ is almost a constant straight line and it corresponds to the first pure bending modes of the beams and plates. The curve for which $i = 2$ and $j = 1$ shows that when the aspect ratio increases, the frequency parameter $\lambda_{2,j}^2$ increases smoothly, gradually and linearly. This curve corresponds to the second pure torsional modes.

When $i = 2$ and $j = 2$ to $j = 6$, the frequency parameter increases rapidly as the aspect ratio increases. The variation of $\lambda_{2,j}^2$ with ratio becomes an exponential curve. Typical mode shapes for aspect ratios 1.25 and 5, and for $i = 2, j = 0$ to 3 are shown in Figure 5.10b. It can be seen clearly from this figure that the breadthwise deformation increases when the mode counter j increases. Also it is seen that when $j \geq 2$, the deformation of the 'beam' ($r = 5$) is much more complex than the deformation of the plate ($r = 1$) as shown in figure 5.10b.

Furthermore, the natural frequency for the beam is more than an order of magnitude greater than that for the natural frequency of the plate. This suggests that the effect on the natural frequency of the increase mass moment of inertia of the plate in comparison to the beam is more than the effect of the increase in the stiffness.

Second bending deformation along lengthwise direction ($i=3$)

The variation of the frequency parameters with the aspect ratios for values of $i = 3$ and $j = 0$ to 6 are shown in Figure 5.11a. These curves correspond to values of $i = 3$ and $j = 0$ for the bottom-most curve to values of $i = 3$ and $j = 6$ for the top-most curve respectively. The curve for which $i = 3$ and $j = 0$ is almost a constant straight line. This indicates that the frequency parameters of this mode of vibration do not change

significantly when the aspect ratio changes. This curve corresponds to the second bending mode. The curve for which $i = 3$ and $j = 1$ is approximately a straight line and corresponds to the third torsion mode. When $i = 3$ and $j \geq 2$, the frequency parameters increase rapidly as the aspect ratio increases. The frequency parameters, $\lambda_{3,j}^2$, increase parabolically as the aspect ratios increase.

Figure 5.11*b* shows the mode shapes for $i = 3, j = 0$ to 3 for aspect ratios 1.25 and 5. It is clearly seen that the mode shapes consist of a combination of predominately second bending mode of deformation along the lengthwise direction but of different degree of deformation in the breadthwise direction. The degree of deformation in the breadthwise direction increases as the mode counter j increases. Also, it is seen from Figure 5.11*b* (*b1*) and (*b2*) that when $i = 3$ and $j = 0, 1$, the beam ($r = 5$) has a practically straight edge and is, therefore, undergoing pure bending and pure torsional modes of vibration. However, from Figures 5.11*b* (*a1*) and (*a2*), it is evident that the edge of the plate is slightly deformed into a wavy pattern instead of being straight. Thus these modes are not truly pure bending and torsional modes of vibration. Again, it is seen that the natural frequencies of the beams are greater than those of the plates for the same reasons stated previously.

Third bending deformation along lengthwise direction ($i=4$)

Figure 5.12*a* represents the variation of the frequency parameters with aspect ratios for values of $i = 4$ and $j = 0$ for the bottom-most curve to $i=4$ and $j=6$ for top-most curve. The bottom-most curve, which is almost a constant straight line represents the third bending mode. The curve for which $i = 4$ and $j = 1$ represents the fourth torsional mode of vibration. The curves at higher values of j involve increasing degrees of deformation in the breadthwise direction of the beam-plate. Typical mode shapes of the

beam ($r = 5$) and plate ($r = 1.25$) are shown in Figure 5.12*b*. It is clearly seen from the figure that the deformation of the beams and plates in the breadthwise direction increases when the mode counter j increases. This figure also shows that for $j = 0$ and $j = 1$, the mode shapes of the beam ($r = 5$) are true pure bending and pure torsional modes of vibration, whereas the corresponding mode shapes of the plate ($r = 1.25$) are highly distorted. This indicates that either the combined stiffness of the beams is higher than that of the plates and/or the mass moment of inertia of the plates is higher than that of the beam. This is reflected by the fact that the natural frequencies of the beams are much greater than the natural frequencies of the plates.

Fourth bending deformation along lengthwise direction ($i=5$)

The variation of the frequency parameters with aspect ratios for values of $i = 5$ and $j = 0$ to 5 are shown in Figure 5.13*a*. The bottom-most curve for which $i = 5$ and $j = 0$ corresponds to the fourth bending mode. The curve for which $i = 5$ and $j = 1$ corresponds to the fifth torsional mode. The curves for which $i = 5$ and $j = 2$ to 5 correspond to increasing degrees of deformation in the breadthwise direction.

The mode shapes for $i = 5$, $j = 0, 1$ and 2 and for aspect ratios 1.25 and 5 are shown in Figure 5.13*b*. It is evident that the mode shapes consist of combinations of second bending deformation along the lengthwise direction but of different degrees of deformation in the breadthwise direction. The degree of deformation in the breadthwise direction increases as the mode counter j increases. This figure shows that the mode shapes of the plate are more distorted than the corresponding mode shapes of the beam. It is important to notice that the edge of the beam is no longer straight in the first two modes ($j = 0, j = 1$) of vibration. This suggests that these lowest two modes are no longer truly pure bending and pure torsional modes of vibration. It is also seen from this

figure that the natural frequencies of the beams are greater than those of the plates for the same reason stated previously.

Fifth bending deformation along lengthwise direction ($i=6$)

Figure 5.14a shows the variation of the frequency parameters with aspect ratios for values of $i = 6$ and $j = 0$ to 4. There are 5 curves in this figure which correspond to values of $i = 6$ and $j = 0$ for the bottom-most curve to values of $i = 6$ and $j = 4$ for the top-most curve, respectively. The bottom-most curve represents the fifth bending mode, while the next curve ($j = 1$) represents the sixth torsional mode. The corresponding mode shapes for values of $j = 1, 2$ and 3 , and for a beam ($r = 5$) and plate ($r = 1.25$) are shown in Figure 5.14b. The figure shows that the mode shapes of the plate are more complicated than those of the beam for the same value of the breadthwise mode counter j . Also, this figure shows that the edge of the beam is slightly curved when $j = 0$ and $j = 1$. This suggests that the corresponding modes are not truly pure bending and pure torsional modes of vibration. Also it is important to notice that the value of the natural frequency of the beams is much higher than that for the plates. This suggests that the effect of increase in mass moment of inertia of the plates compared to the beams is greater than the effect of increasing bending stiffness of the plates compared to the beams.

Sixth bending deformation along lengthwise direction ($i=7$)

In Figure 5.15a is shown the variation of the frequency parameters with aspect ratios for values of $i = 7$ and $j = 0$ to 3. The bottom-most curve corresponds to values of $i = 7$ and $j = 0$, while the top-most curve corresponds to values of $i = 7$ and $j = 3$, respectively. Also, the bottom-most curve corresponds with the sixth mode of bending

vibration, while the next curve ($j = 1$) represents the seventh torsional mode of vibration. Again the previous statement for $i=6$ that the edge of the beam is curved, when $j=0$ and $j=1$ holds. This suggests that these modes do not truly show pure bending and pure torsional of vibration for the same reason stated previously.

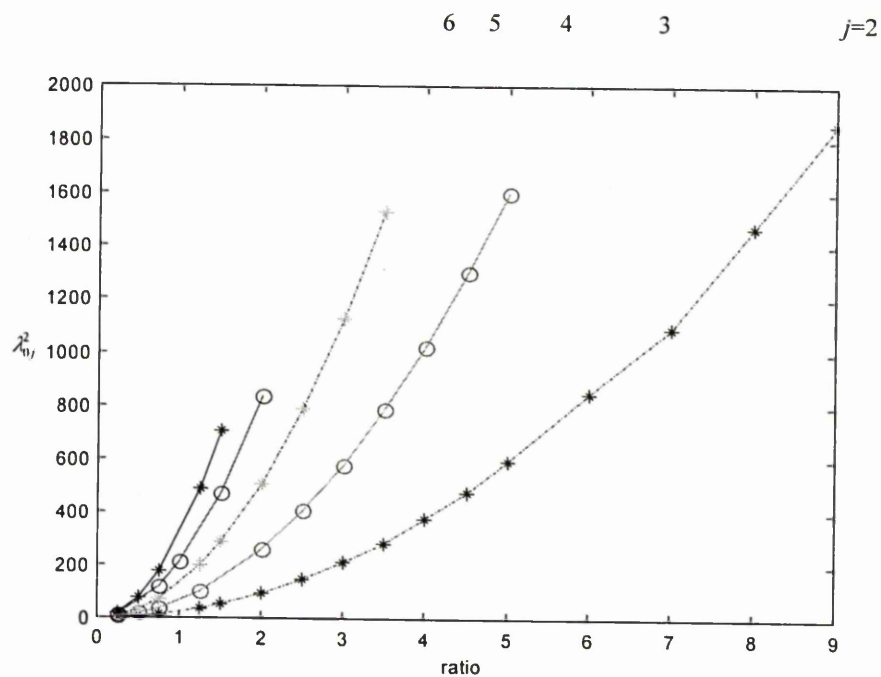


Figure 5.8a Variation of the frequency parameters with aspect ratios for $i = 0$

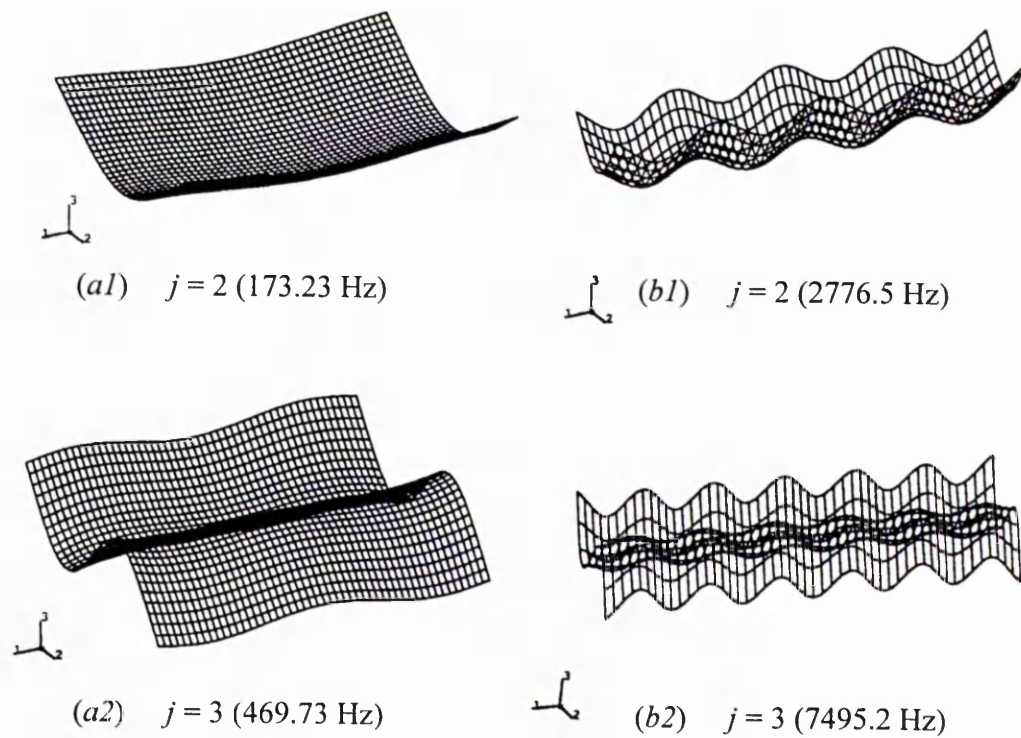


Figure 5.8b Mode shapes for $i = 0$ (a) aspect ratio 1.25, (b) aspect ratio 5

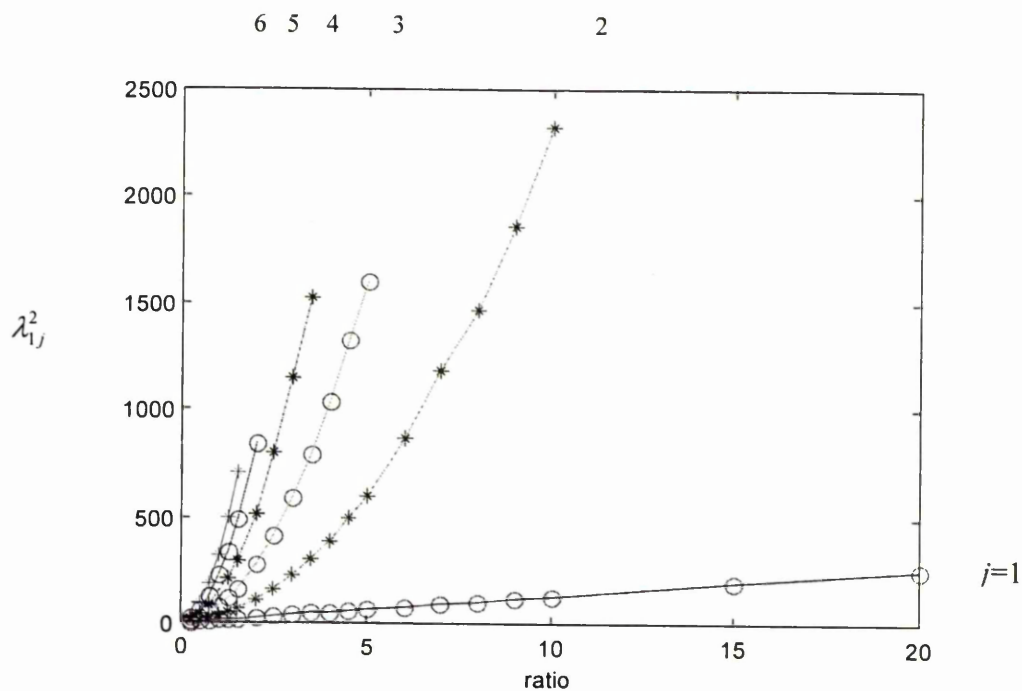


Figure 5.9a Variation of the frequency parameters with aspect ratios for $i = 1$

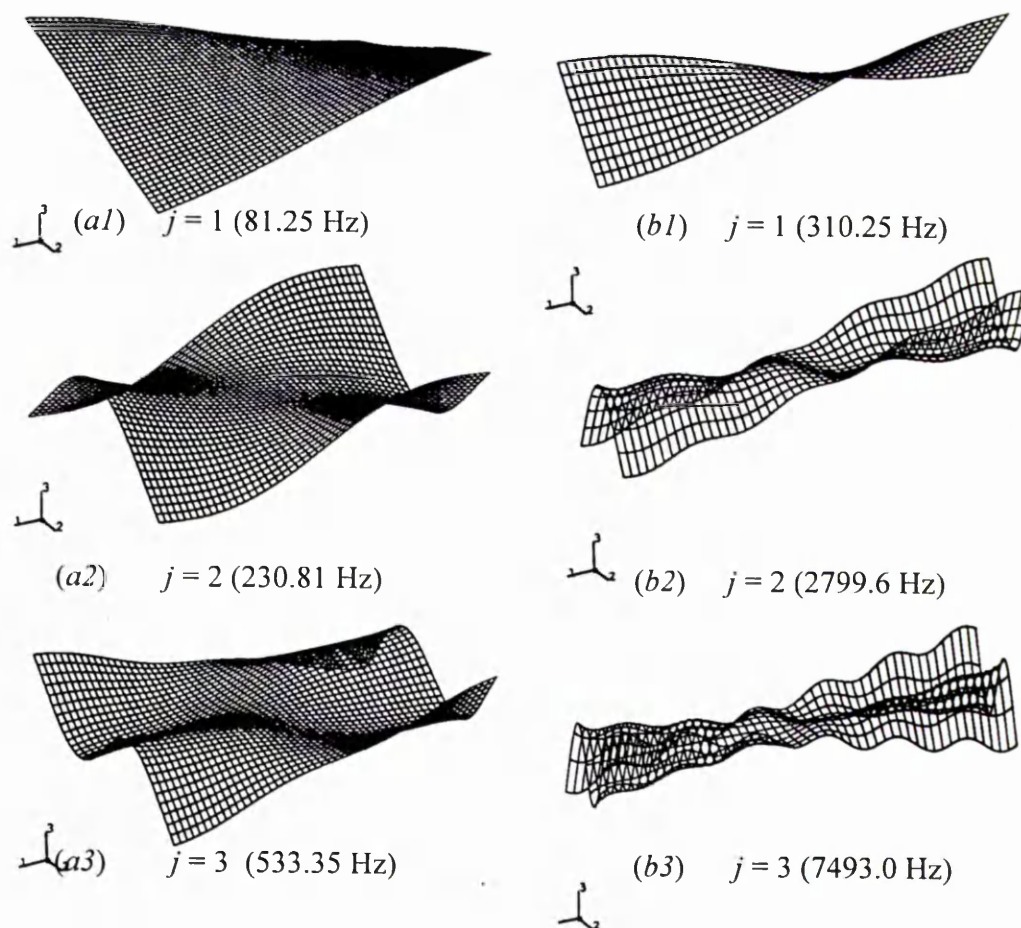


Figure 5.9b Mode shapes for $i = 1$ (a) aspect ratio 1.25, (b) aspect ratio 5

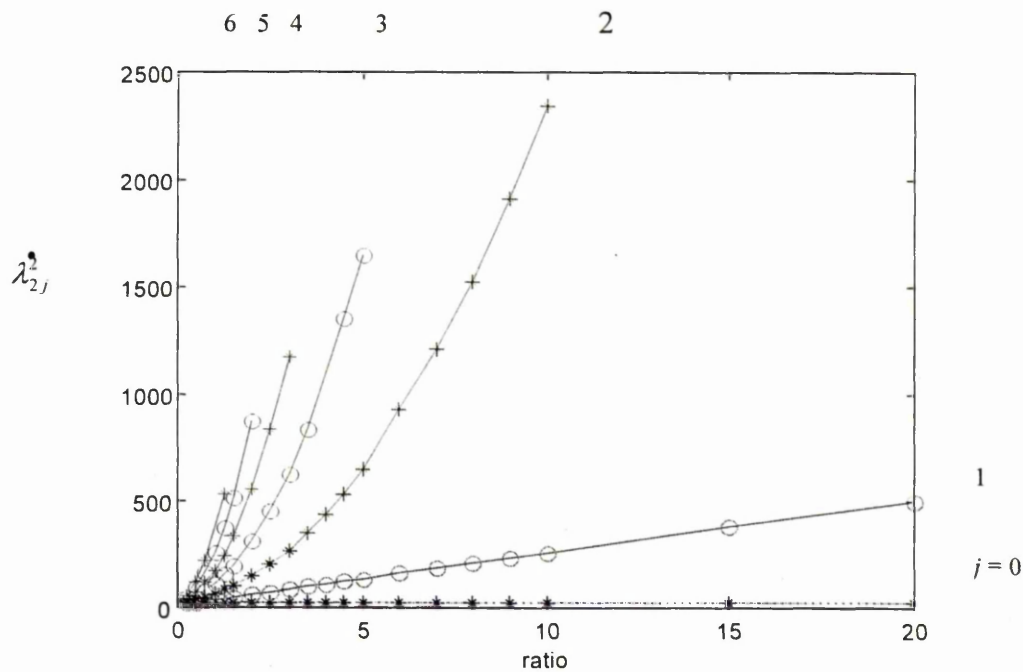


Figure 5.10a Variation of the frequency parameters with aspect ratios $i = 2$

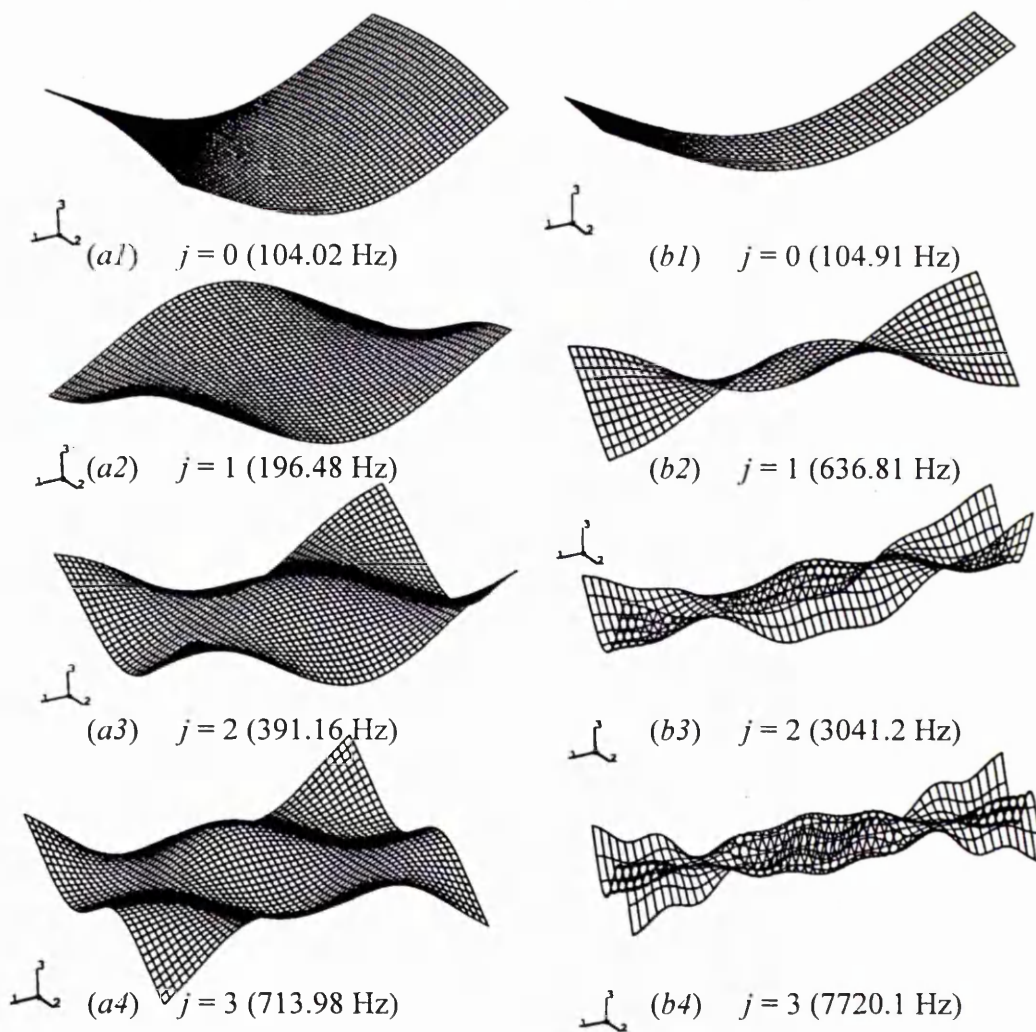


Figure 5.10b Mode shapes for $i = 2$ (a) aspect ratio 1.25, (b) aspect ratio 5

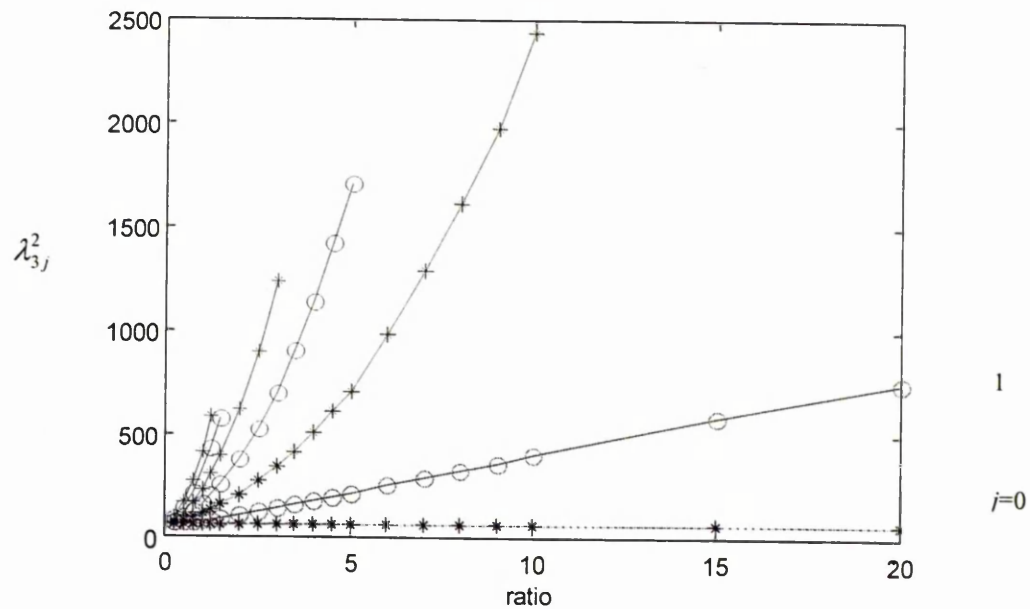


Figure 5.11a Variation of the frequency parameters with aspect ratios for $i = 3$

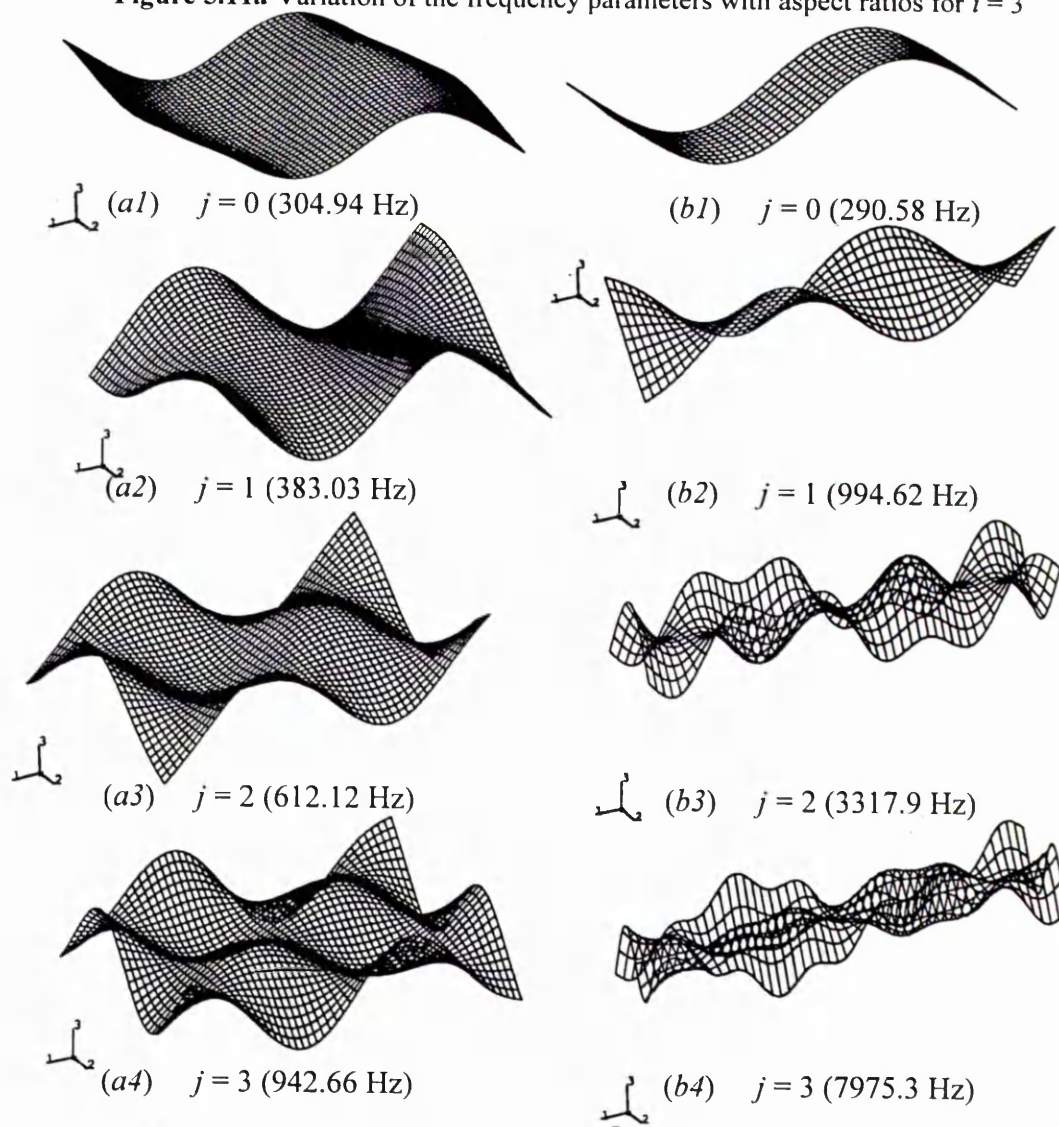


Figure 5.11b Mode shapes for $i = 3$ (a) aspect ratio 1.25, (b) aspect ratio 5

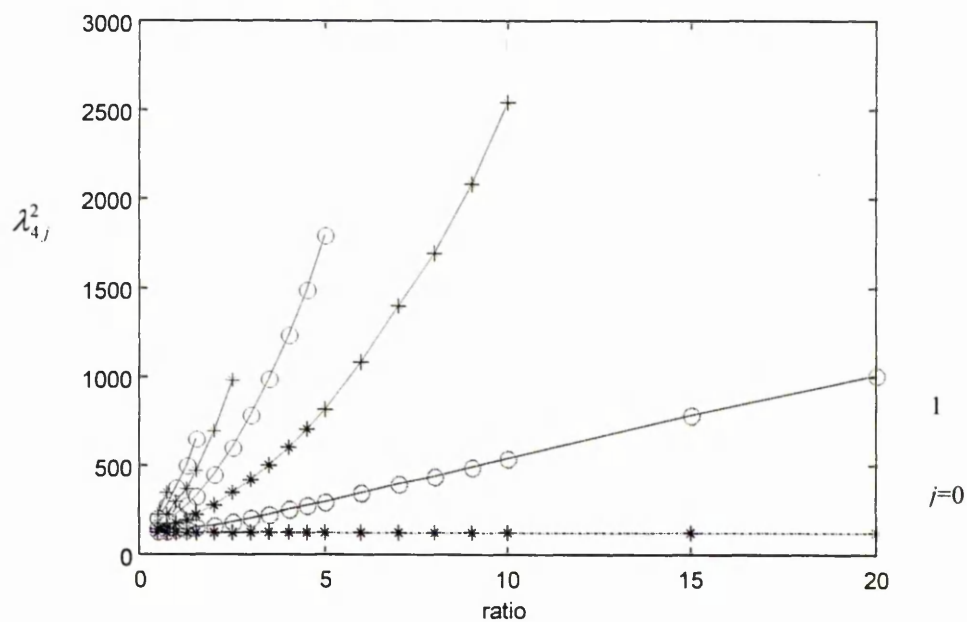


Figure 5.12a Variation of the frequency parameters with aspect ratios for $i = 4$

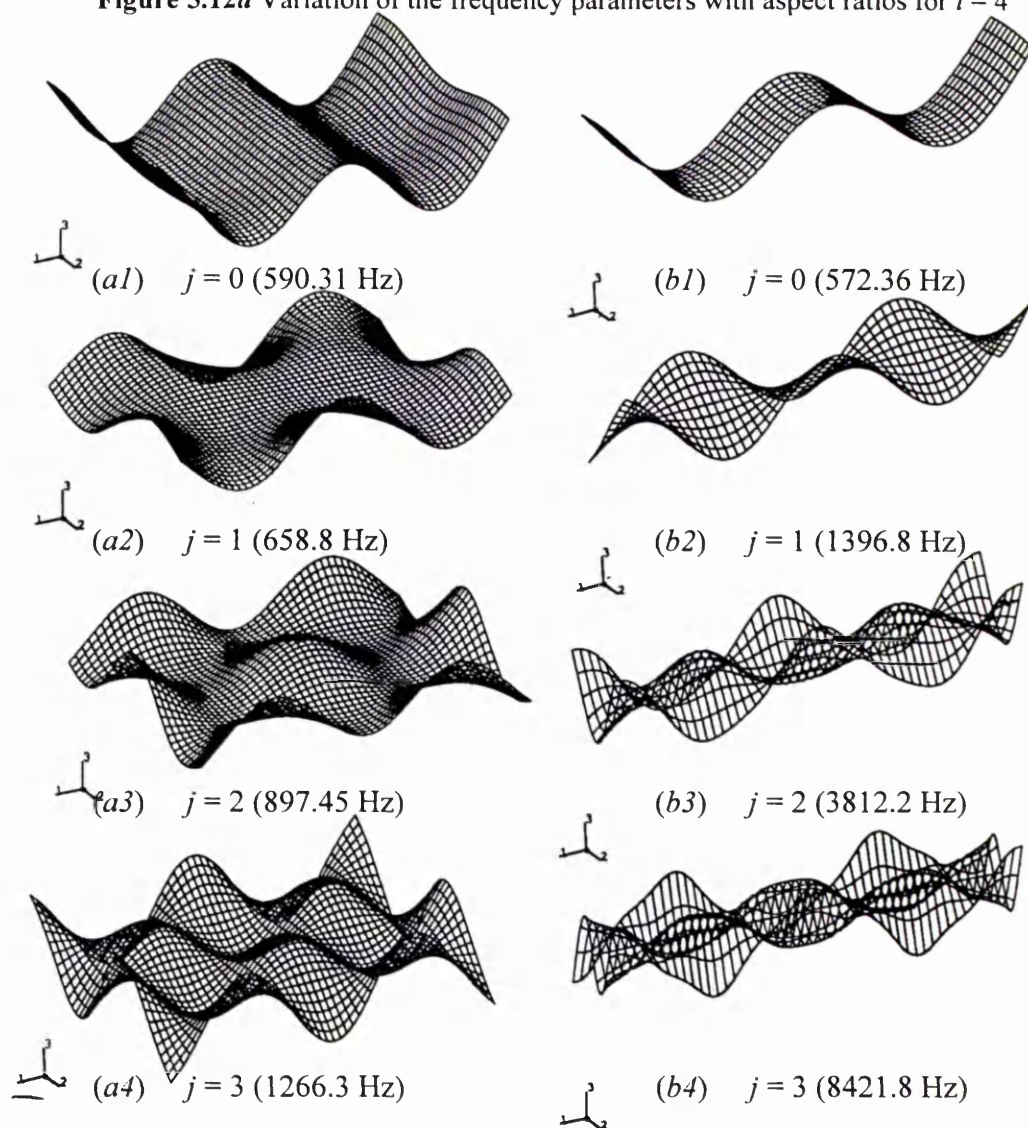


Figure 5.12b Mode shapes for $i = 4$ (a) aspect ratio 1.25, (b) aspect ratio 5

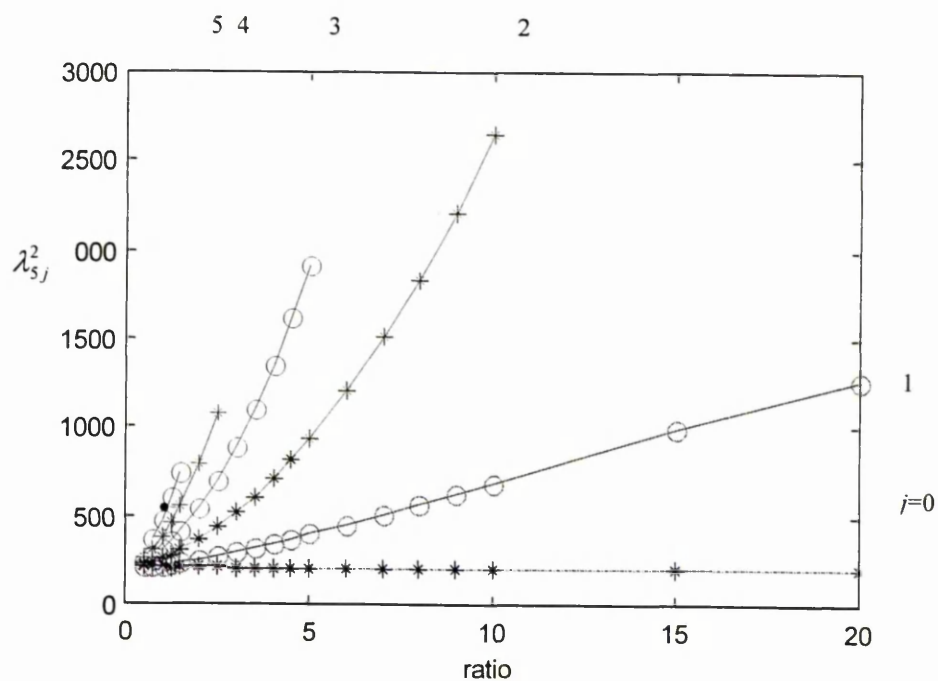


Figure 5.13a Variation of the frequency parameters with aspect ratios for $i = 5$

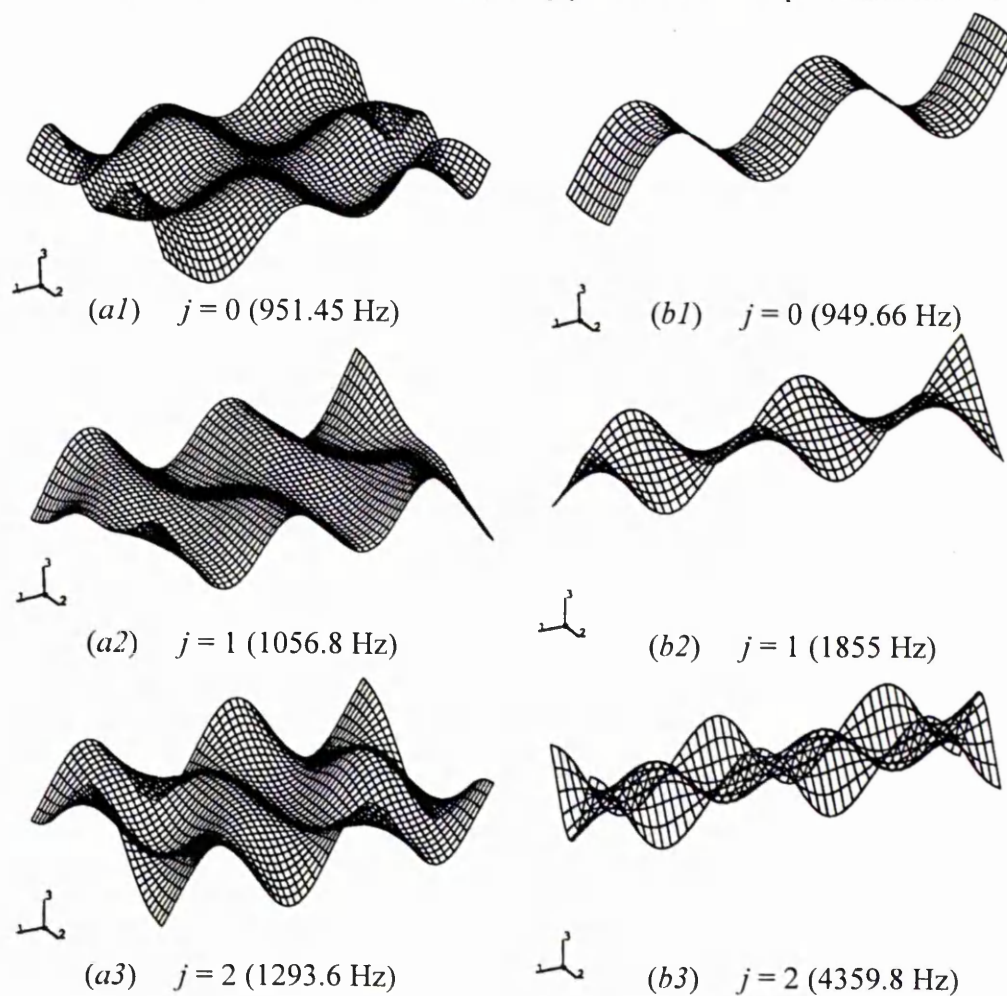


Figure 5.13b Mode shapes for $i = 5$ (a) aspect ratio 1.25, (b) aspect ratio 5

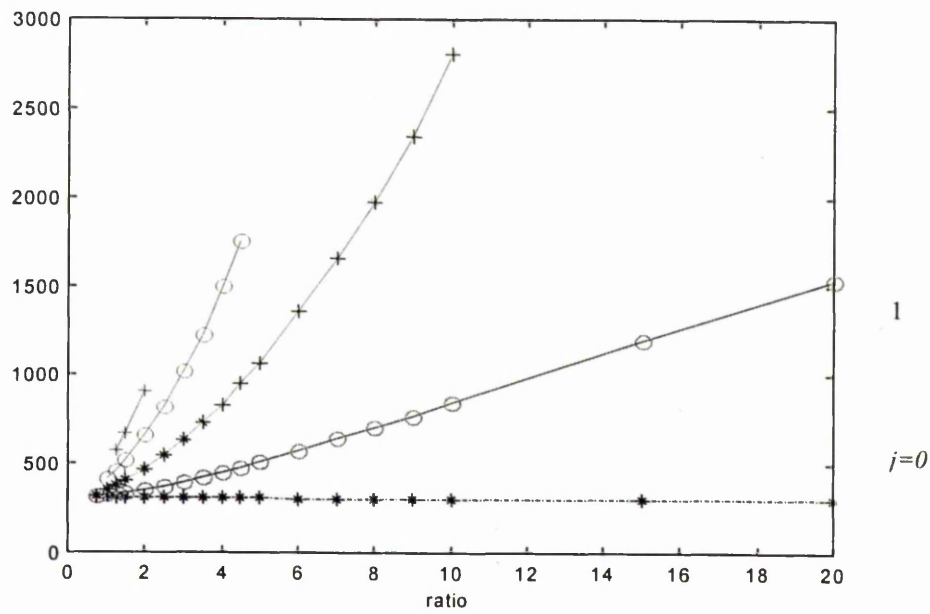


Figure 5.14a Variation of the frequency parameters with aspect ratios for $i = 6$

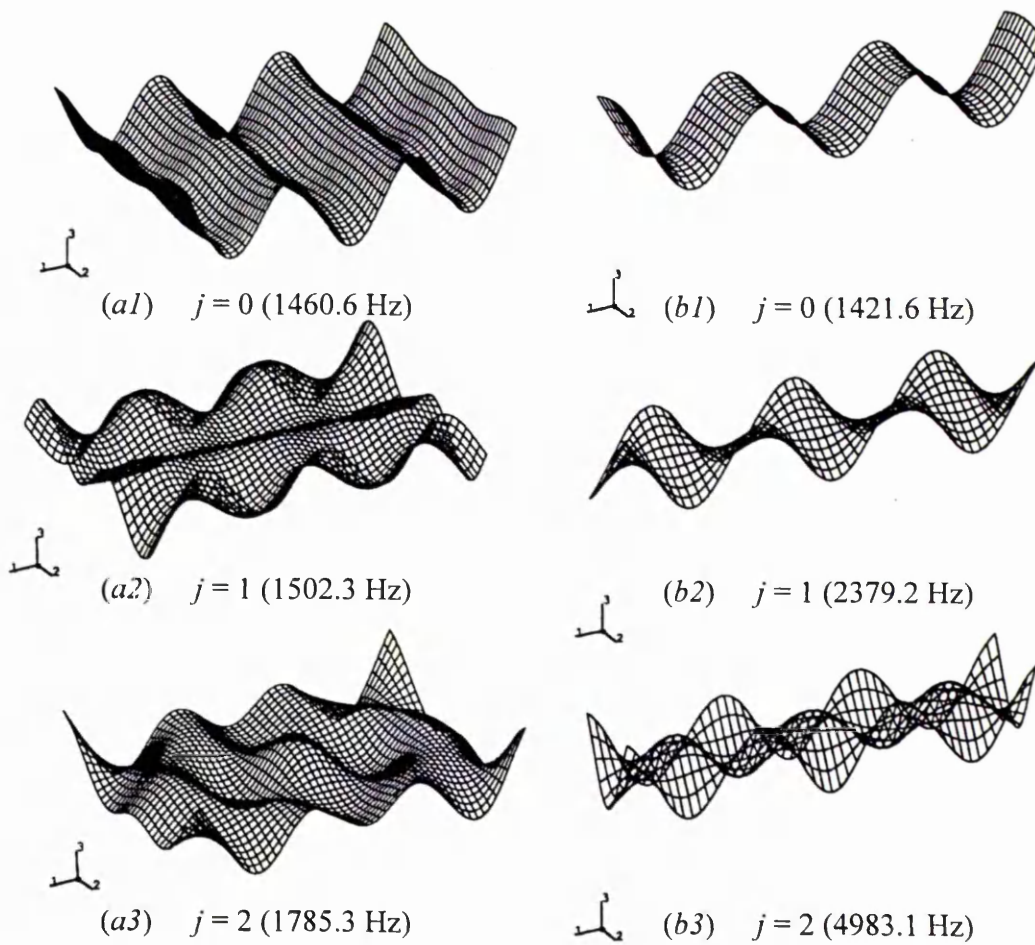


Figure 5.14b Mode shapes for $i = 6$ (a) aspect ratio 1.25, (b) aspect ratio 5

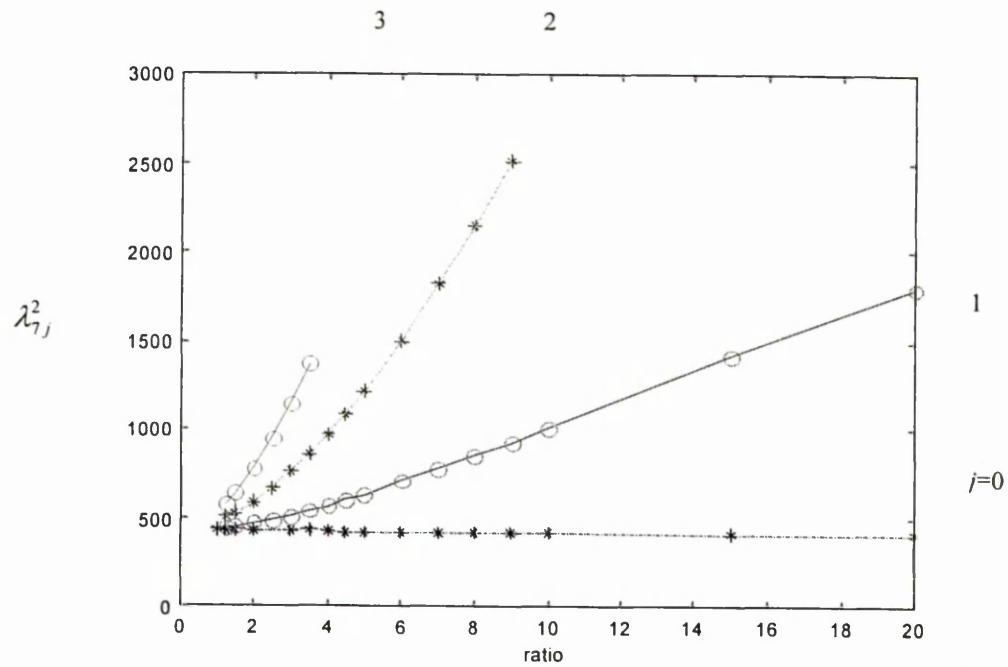


Figure 5.15a Variation of the frequency parameters with aspect ratios for $i = 7$

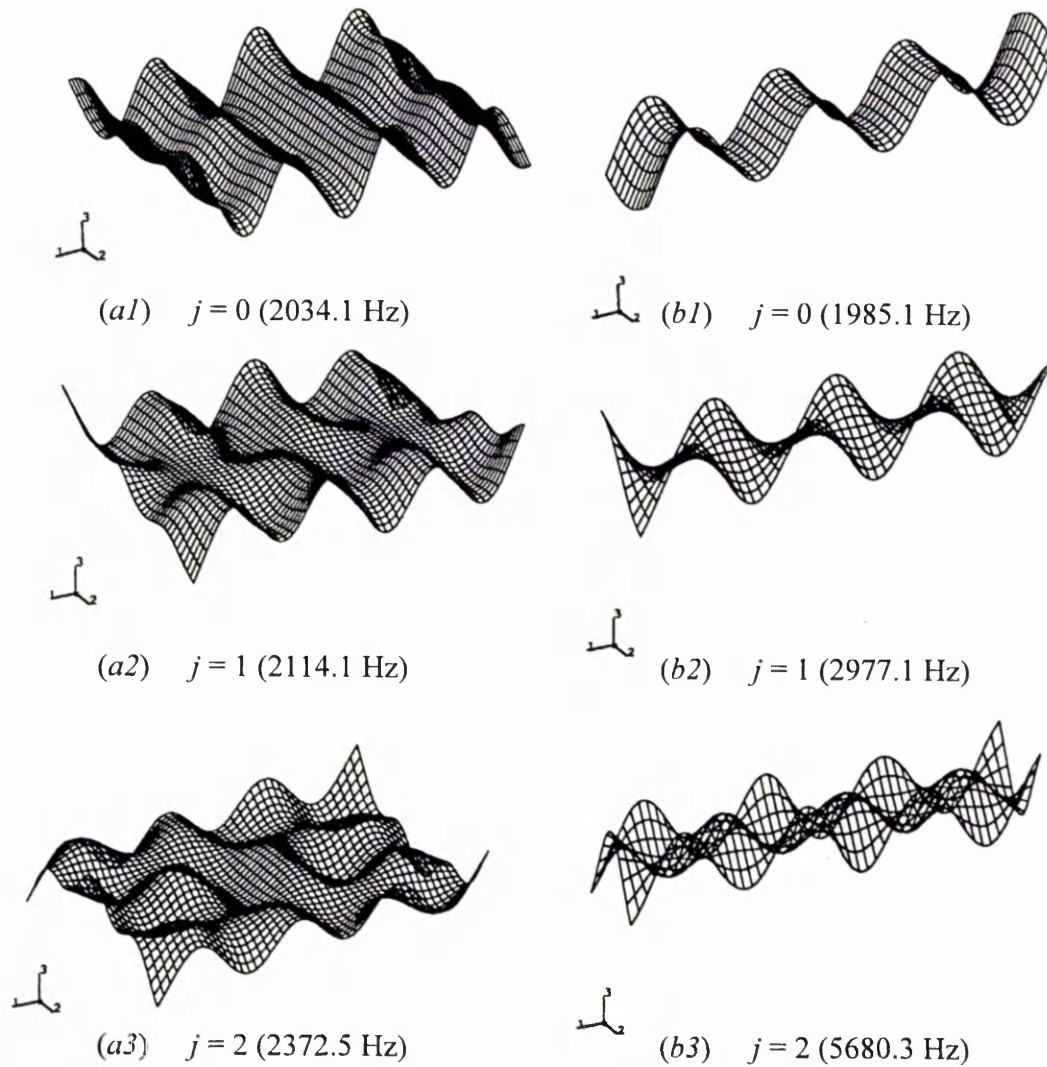


Figure 5.15b Mode shapes for $i = 7$ (a) aspect ratio 1.50, (b) aspect ratio 5

5.3 Combined frequency parameter chart

The combined frequency chart and its enlargements are shown in Figure 5.16(a), (b) and (c) these charts were formed by combining all the results shown separately in Figures 5.8*a* to 5.15*a*. The family of curves presented in this chart correspond to different values of the breadthwise mode counter j and are indicated by different line types. These curves are in groups or families. The first group of curves, which are shown as almost horizontal solid lines, correspond to $j = 0$ and represent the different modes of bending vibration. The following next group of slanting dashed lines are for $j = 1$ which correspond to different modes of torsional vibration. The next group of dotted curves are for $j = 2$ and correspond to the combinational modes of vibration involving first bending mode in the breadthwise direction. These curves are followed in anticlockwise direction by a group of chain-dashed and solid lines, which correspond to values of $j = 3$ and $j=4$ respectively.

From the graphs, it seen that for aspect ratios equal to or greater than 10, there are 2 types of modes of vibration. These modes are denoted on the graphs by the horizontal solid lines for which $j = 0$ and by the slanting dashed lines for which $j = 1$. They correspond to the bending and torsion modes of vibration respectively. However for aspect ratios less than 10, there are more than 2 types of modes of vibration. Each type of vibration is represented by different line type and is associated with a value of $j \geq 2$. Figures 5.16*b* and 5.16*c* are the enlargements of Figure 5.16*a*. Figure 5.16*b* shows the variation of the frequency parameters between 0 to 2000 and aspect ratios from 0 to 10, and Figure 5.16*c* shows the variation of the frequency parameters from 0 to 2000 with the aspect ratios from 0 to 5.

This chart can be used to find the natural frequencies and mode types of vibration for free-free beam and plate for aspect ratios of between 0.25 to 20. As an

example, to find the first six natural frequencies and mode types of free-free beam-plate of aspect ratio 3.5. The frequency parameters of the first six modes of vibration can be estimated for aspect ratio 3.5 from Figure 5.16 (c). The estimated values can then be used in Equation (3.2) together with the material and geometric properties of the plate in order to determine the required first six natural frequencies. It is also important to notice that from Figure 5.16(c) the mode types are as follows. The first mode is B1, then T1, B2, T2, B3 and T3 for the second mode to the sixth mode respectively where B denotes bending mode and T denotes torsion mode.

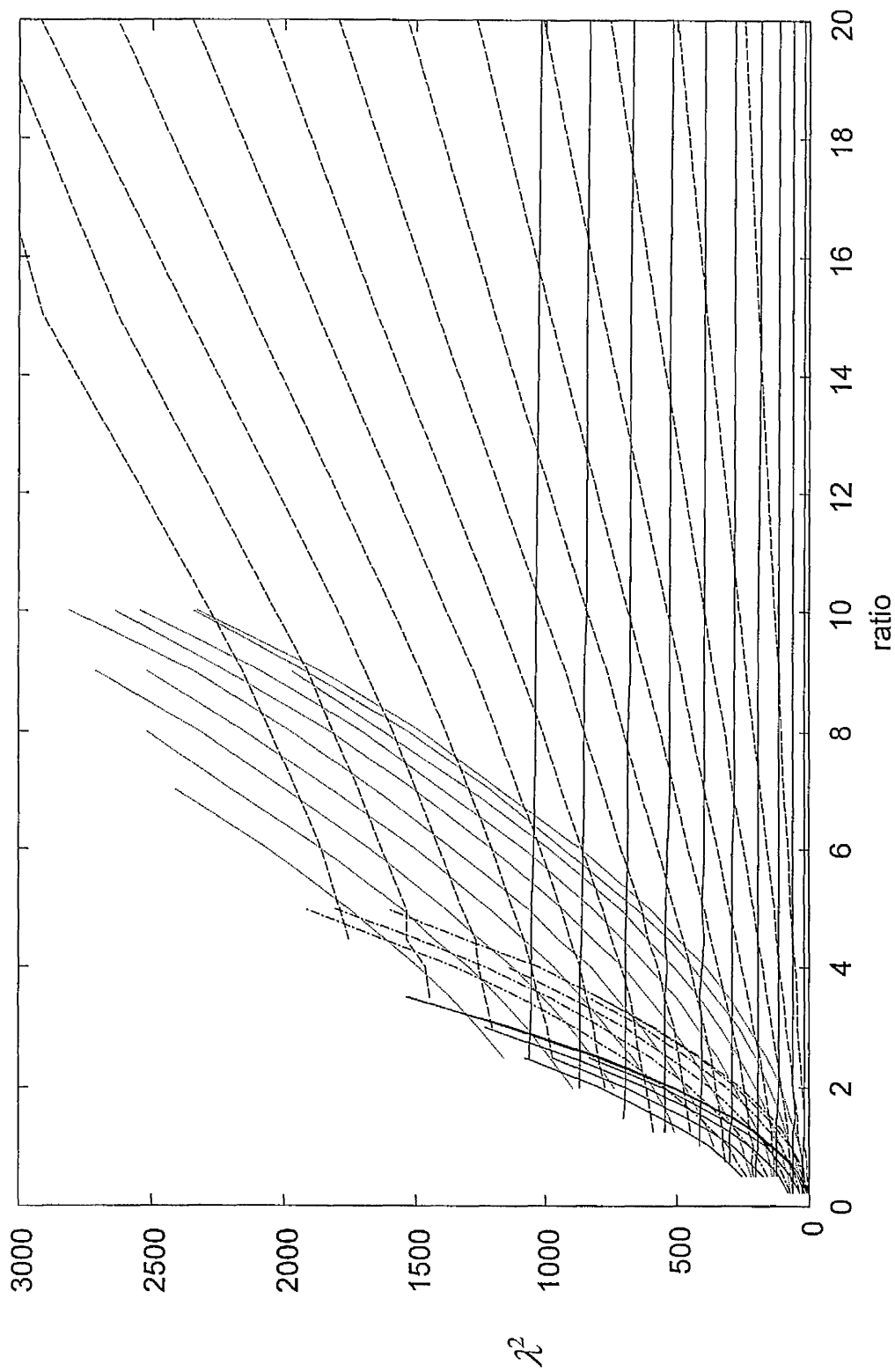


Figure 5.16 (a) Variation of frequency parameters with aspect ratio for free-free beam-plate of 1% thickness to length ratio

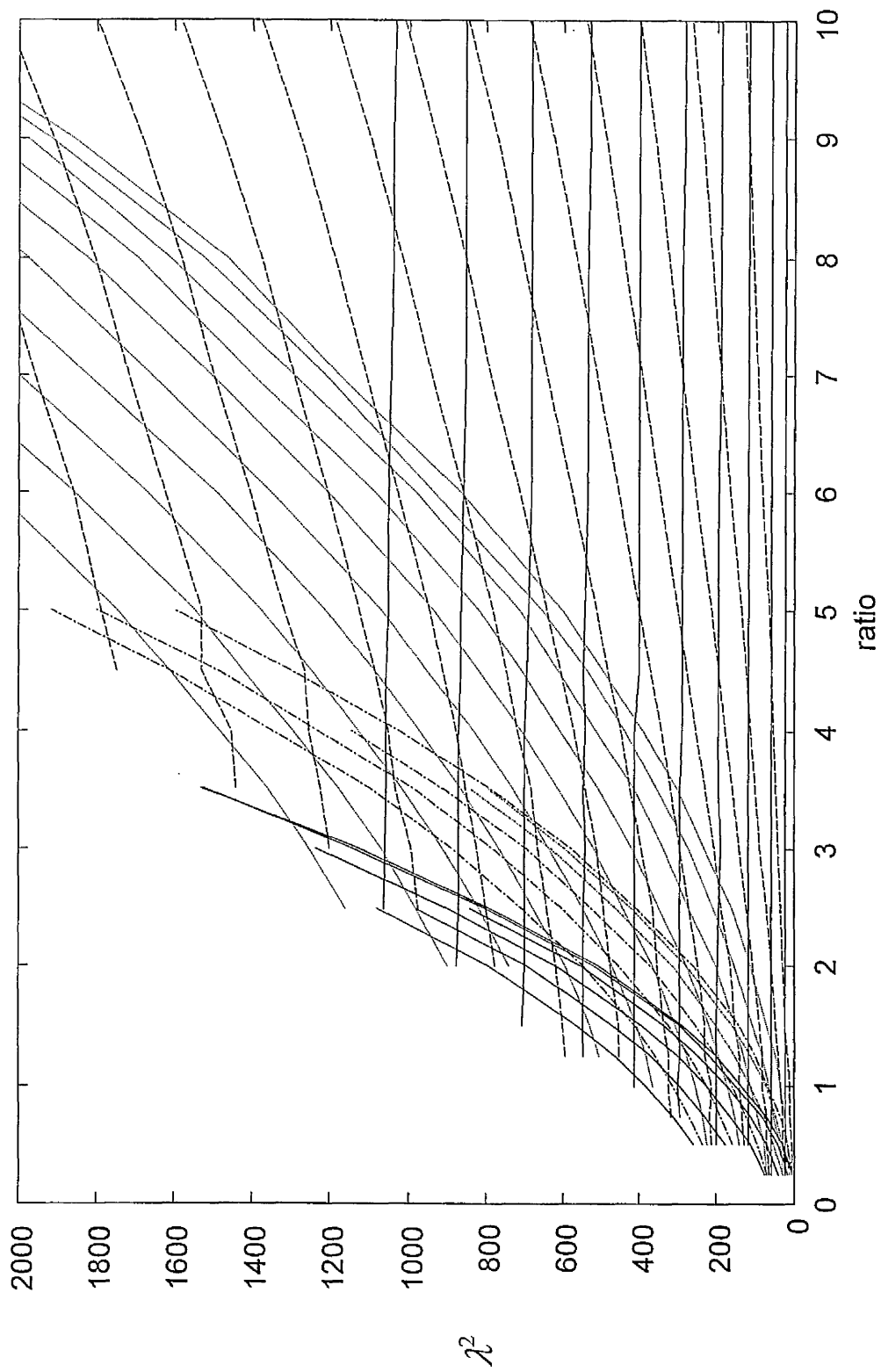


Figure 5.16 (b) First enlargement of figure 5.16 (a)

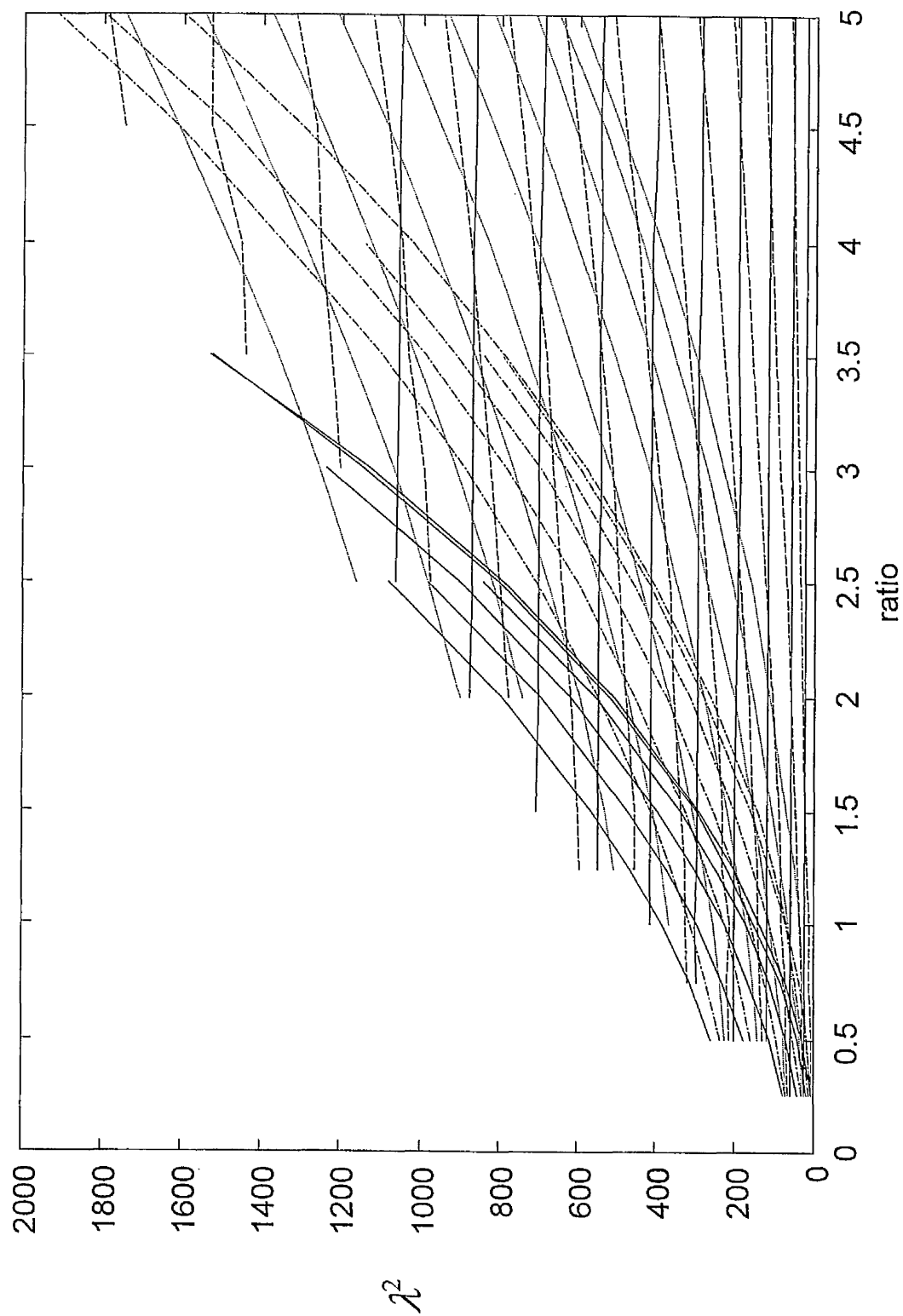


Figure 5.16 (c) Second enlargement of figure 5.16 (a)

5.4 Effects of thickness to length ratio on frequency parameters

The effects of thickness on the frequency parameter for free-free beams and plates are considered in this section. The frequency parameters were computed for free-free beams and plates of thickness to length ratio of 2%, 5% and 10%, Young's modulus $E=70\text{Gpa}$ and Poisson's ratio $\nu = 0.33$. The graph of the combined charts of the variation of frequency parameters with aspect ratio for thickness to length ratio 2%, 5% and 10% were plotted as in Figures 5.17, 5.18 and 5.19 respectively. In these figures, there are group or families of line types, which correspond to different mode types. The solid horizontal lines are for the mode type for which $j = 0$. These are predominantly beam bending modes. The next group of line types are the dotted lines for $j = 1$, which represent the predominantly torsional modes of beams. These are followed by chain lines for $j = 2$ which are for modes of vibration in which the beam or plate bends in the breadthwise direction. The next group of line types are solid lines for $j = 3$. In this case, the beam or plate is subjected to the second mode of bending deformation in the breadthwise direction. Figures 5.17, 5.18 and 5.18 show there are 10 almost constant straight lines. These curves are for $j=0$ and $i =0$ to 9 from the bottom-most curve to the top-most curve respectively. These curves represent the first 10 predominantly bending modes along the longitudinal (x) axis. However all these curves show erratic behaviour at small aspect ratios between the range 0.25 to 8 and decrease fairly exponentially at high aspect ratios. From these figures it is clearly seen that as the thickness increases the frequency parameter decreases. For example, the values of the frequency parameter for the first 10 bending modes for thickness to length ratio 2% (Figure5.17) are in the range 0-1100, and that for thickness to length ratio 5% (Figure5.18) are in the range 0-900, and for thickness to length ratio 10% (Figure5.19), the range is 0-600.

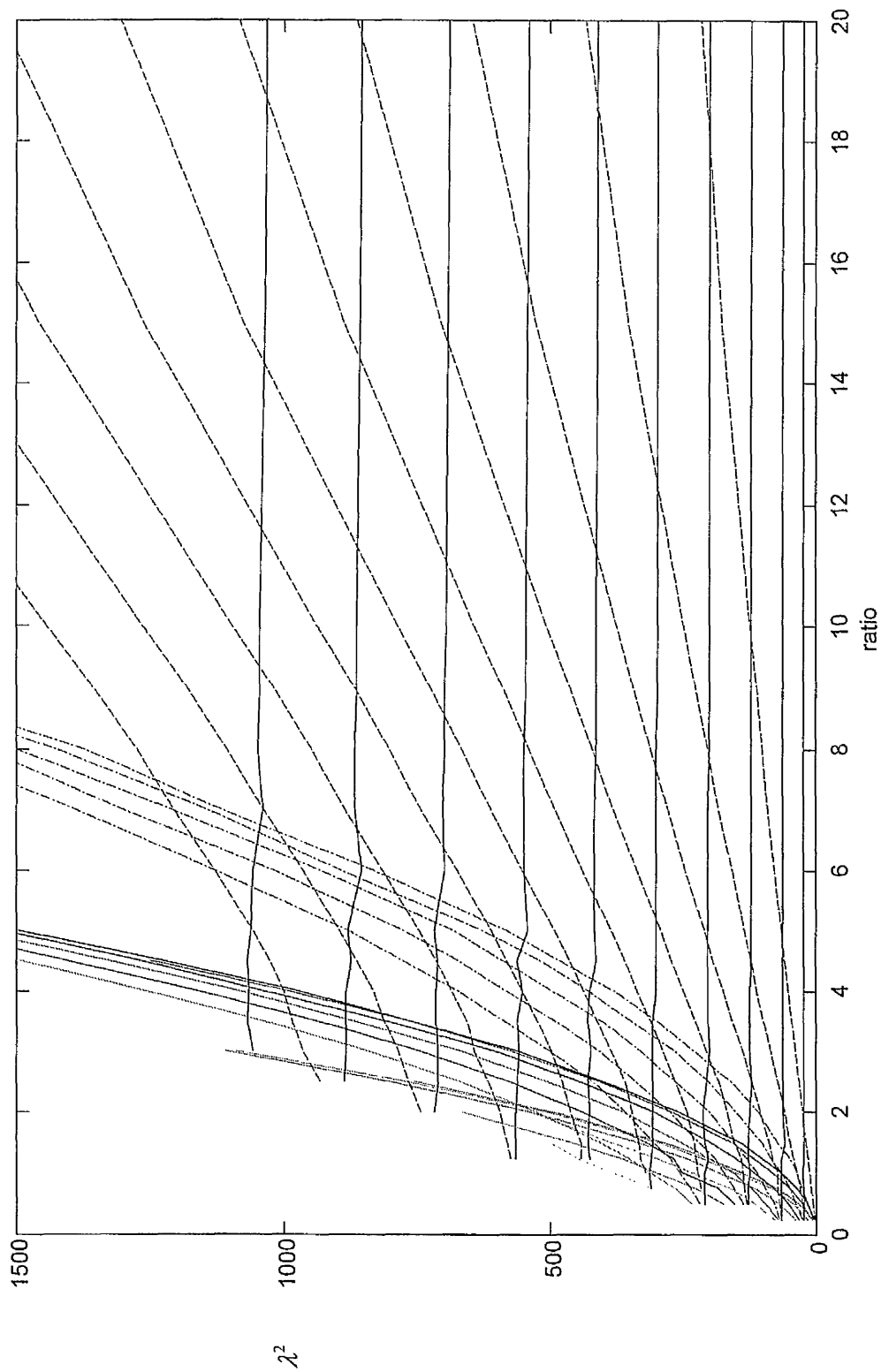


Figure 5.17 Variation of frequency parameter with aspect ratio for free-free thickness to length ratio 2%

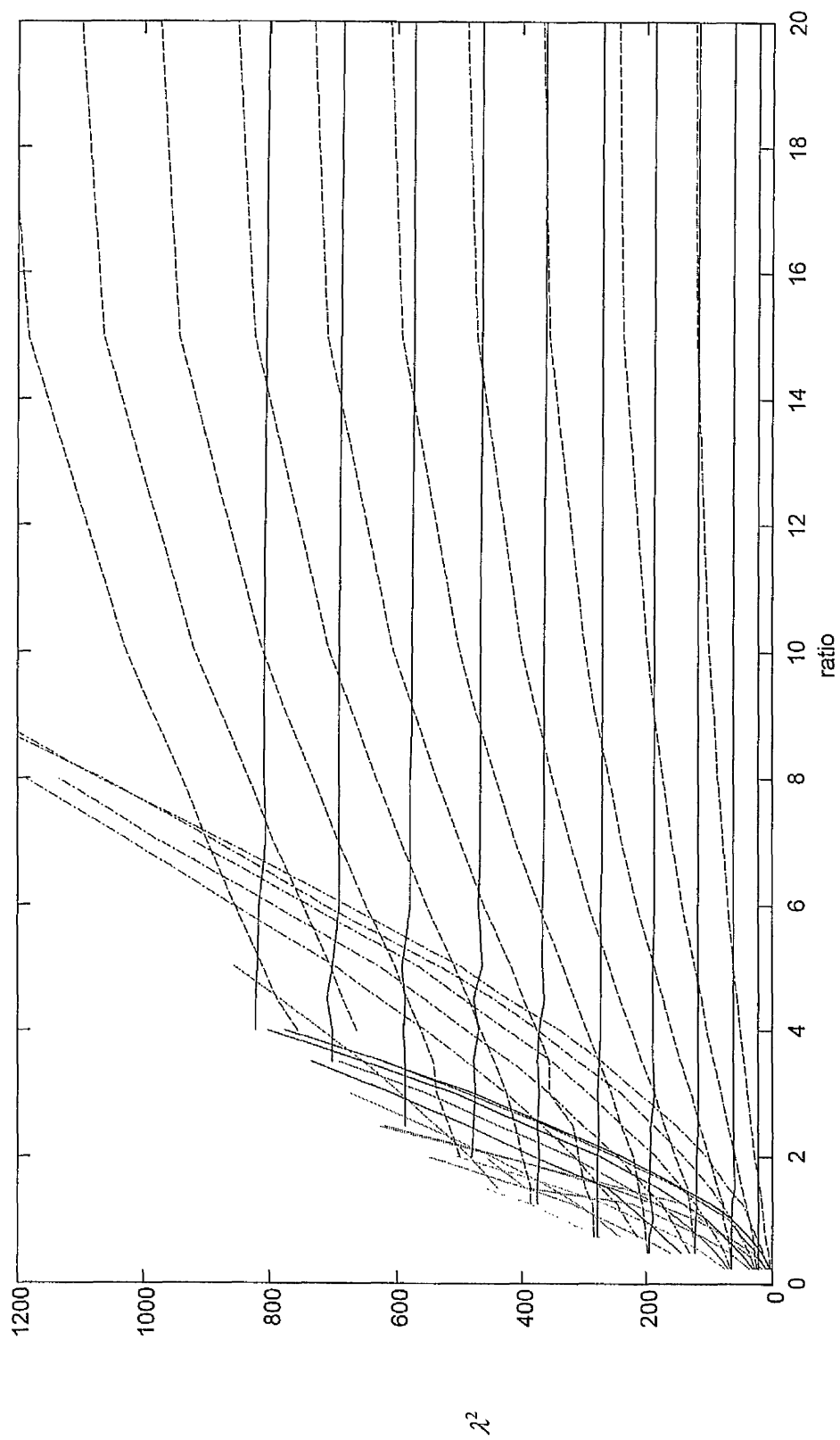


Figure 5.18 Variation of frequency parameter with aspect ratio for free-free thickness to length ratio 5%

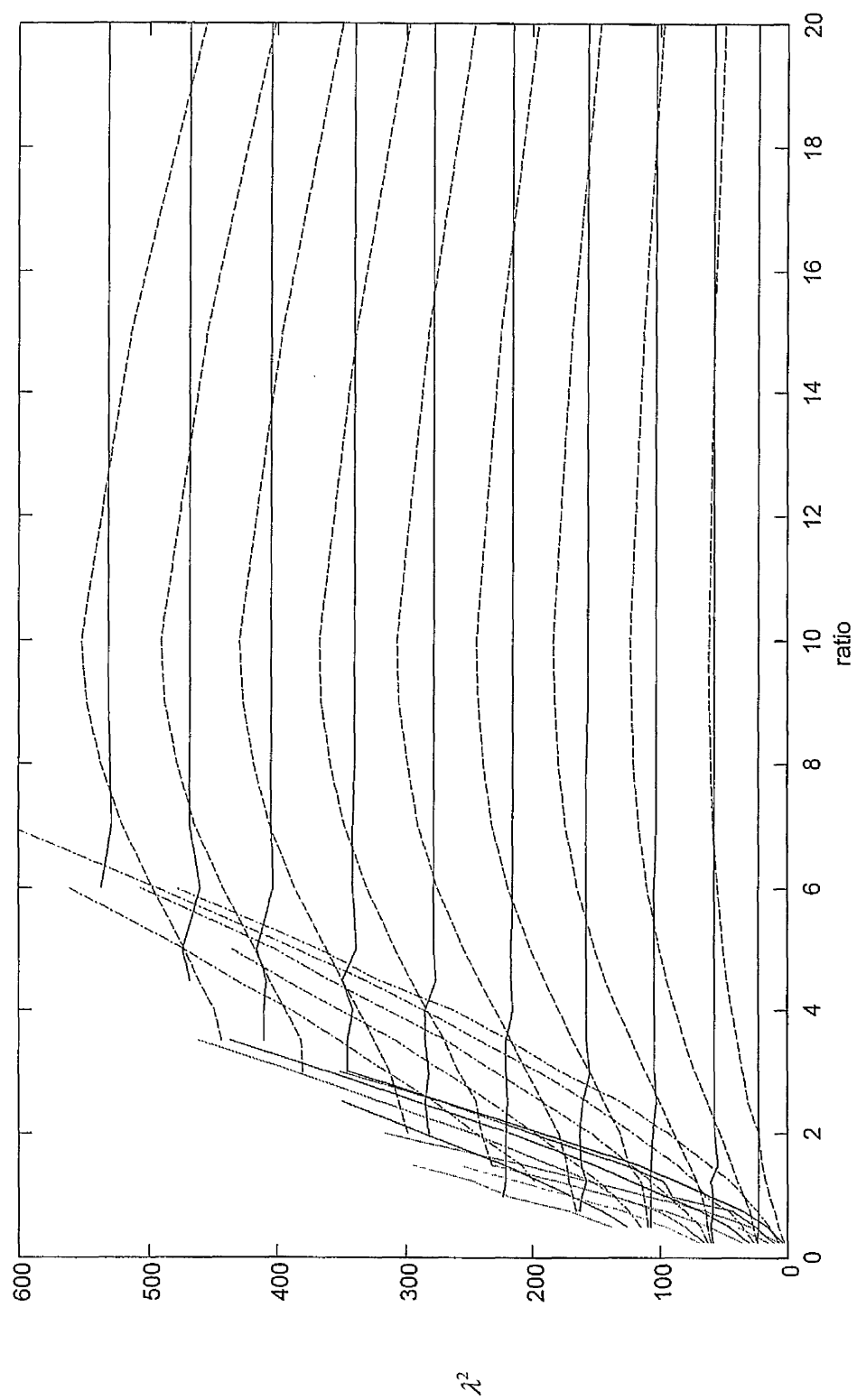


Figure 5.19 Variation of frequency parameter with aspect ratio for free-free thickness to length ratio 10%

5.5 Comparison of the frequency parameter charts for beam-plates of different thickness to length ratio.

Figures 5.20(a), 5.21(a) and 5.22(a) show the comparisons of the frequency parameter charts of the thickness to length ratio 2%, 5% and 10%, respectively, with those of the 1% thickness to length ratio. In these figures, the dotted line represents the characteristics of 1% thickness to length ratio, while the solid line represents the characteristics of 2%, 5% and 10%. These figures show the first 10 predominantly bending modes for these thickness to length ratio which correspond to the values of $j=0$ and $i=0$ to 9.

It is important to notice that the characteristics of the first 2 bending modes shown in these figures are very close to each other and the percentage difference is very small. But the figures show that for modes of vibration greater than 2, the percentage difference between the frequency parameters of thickness to length ratio 2%, 5% and 10%, and those of the 1% thickness to length ratio increase as the mode increases and as the thickness increases. For example Figure 5.20(a), which represents the comparison between the characteristics of the 1% and 2% thickness to length ratio, the difference in the frequency parameters is in the range 0-10% from the lowest modes (bottom curves) to the highest modes (top curves).

Similarly, Figure 5.21(a) shows that the difference in the frequency parameters of the 5% thickness to length ratio compared to those of the 1% thickness to length ratio is between 0% (lowest modes) and 30% (highest modes). However, for the 10% thickness to length ratio, Figure 5.22(a) shows that its frequency parameters deviate from those of the 1% thickness to length ratio by up to 50% at the highest modes. Thus, it can be concluded that the frequency parameter of the beam-plate reduces as its thickness increases.

Figures 5.20(b), 5.21(b) and 5.22(b) show the comparisons of the frequency parameters for the predominantly torsional modes of vibration, for which $j=1$, of thickness to length ratio 2%, 5% and 10% with those of the 1% thickness to length ratio. At small aspect ratios and lower mode of torsional vibration ($i \geq 7$), the percentage difference is small. But at high aspect ratios and higher modes of torsional vibration ($i > 7$), the percentage difference is large. In general, the percentage difference between the frequency parameters of those of the thicker beam-plates and those of the reference 1% thickness to length ratio increases as the aspect ratio increases and as the torsional mode number increases.

Figure 5.20(b) shows that the frequency parameter of both the 1% thickness to length ratio (reference) and 2% thickness to length ratio increase as the aspect ratio and mode number increases. However, compared to the frequency parameters of thickness to length ratio 1% it is seen that the rate of increase of the frequency parameter of the 2% thickness to length ratio decreases as the torsional mode number increases. The difference in the two sets of frequency parameters ranges from 0% to 12%. In the case of the 5% thickness to length ratio, Figure 5.21(b) shows that the frequency parameters increase as aspect ratio increases up to aspect ratio 15. As the aspect ratio increases further, the frequency parameter remains constant. The difference between these frequency parameters and those of the 1% thickness to length ratio is very large being between 0% and 52%.

For the 10% thickness to length ratio, the frequency parameter increases as the aspect ratio increases up to aspect ratio 10. Then it decreases as the aspect ratio increase further. The difference between the frequency parameters and those of the 1% thickness to length ratio is now exceeding large. It ranges from 0% at the smallest aspect ratios

and lowest torsional modes of vibration to more than 80% at high aspect ratios and highest torsional modes of vibration.

Similarly for $j=2$ and 3, Figures 5.20(c),(d), 5.21(c),(d) and 5.22(c),(d) show increasing deviations between the frequency parameters of the reference 1% thickness to length ratio and those of the 2%, 5% and 10% thickness to length ratio.

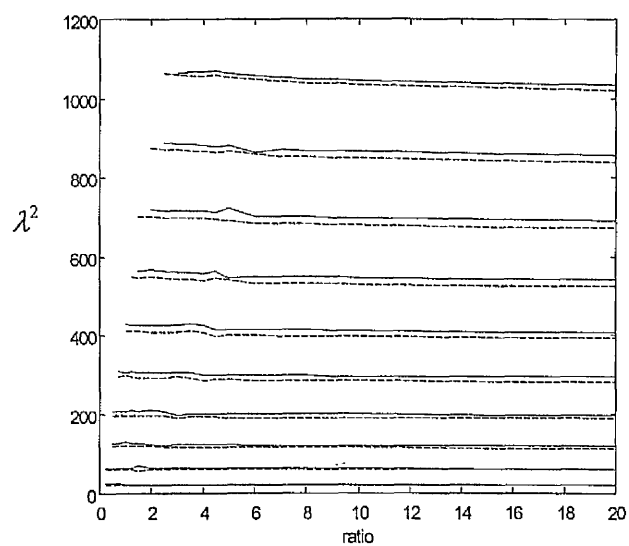


Figure 5.20(a) $j=0$

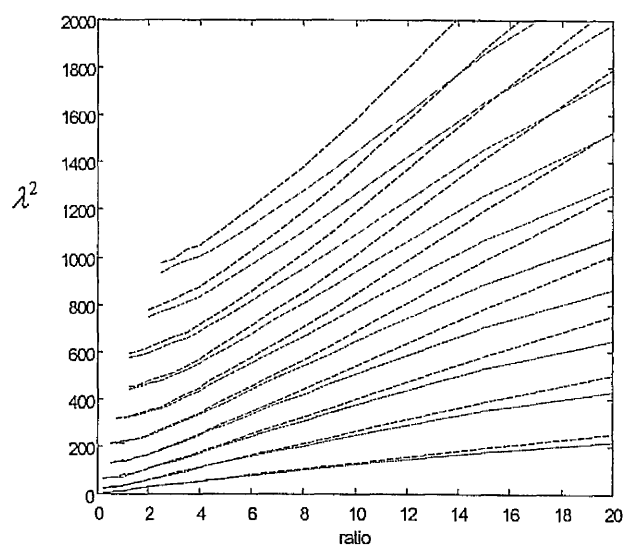


Figure 5.20(b) $j=1$

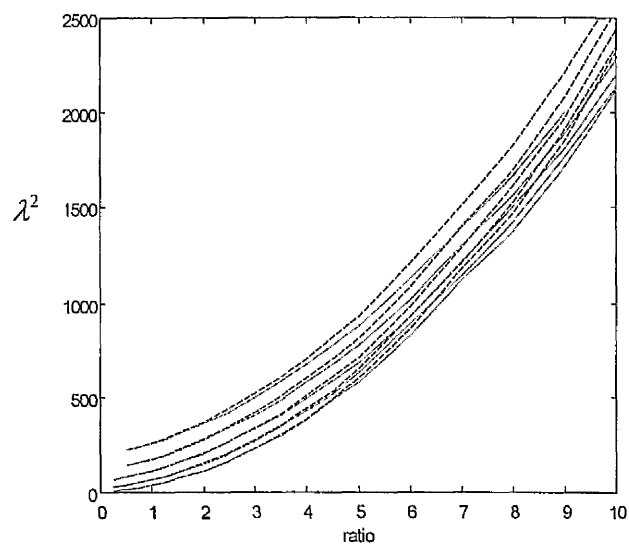


Figure 5.20(c) $j=2$

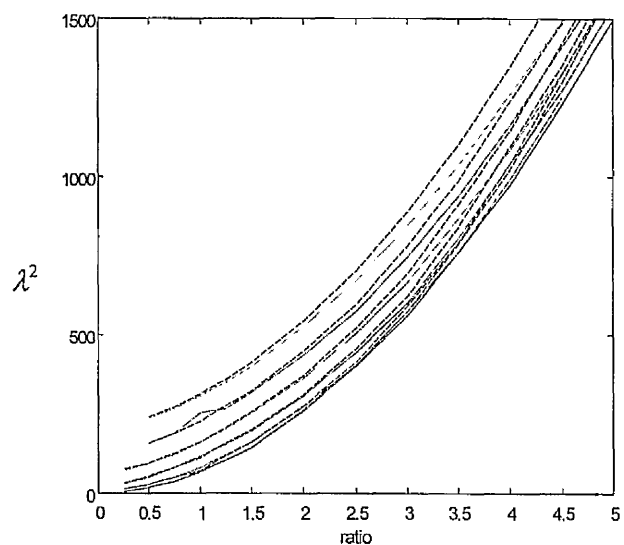


Figure 5.20(d) $j=3$

Figure 5.20 Comparison of variation frequency parameter with aspect ratio for free-free beam-plate of thickness to length ratio 1% and 2%, $j=0-3$; dashed line: thickness to length ratio 1%, solid line: thickness to length ratio 2%

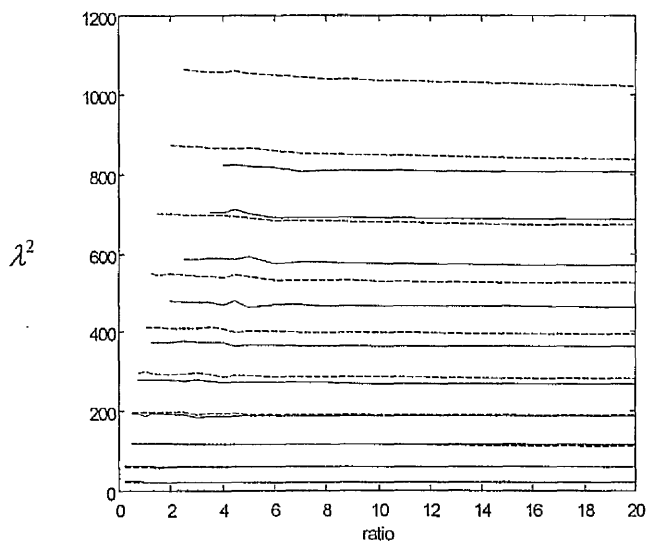


Figure 5.21(a) $j=0$

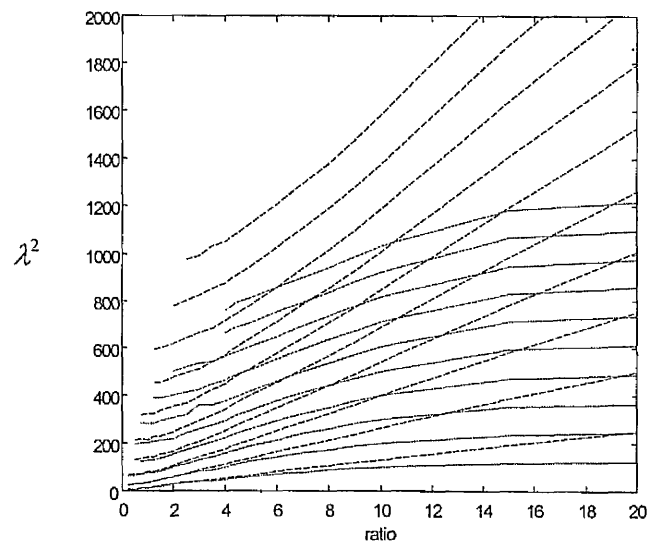


Figure 5.21(b) $j=1$

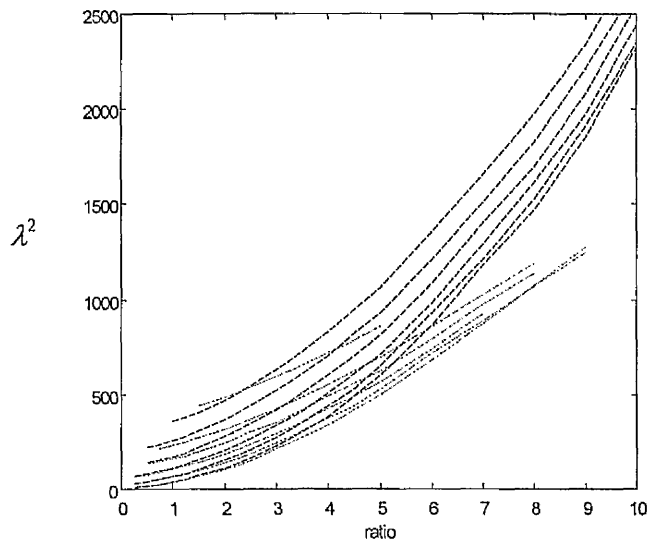


Figure 5.21(c) $j=2$

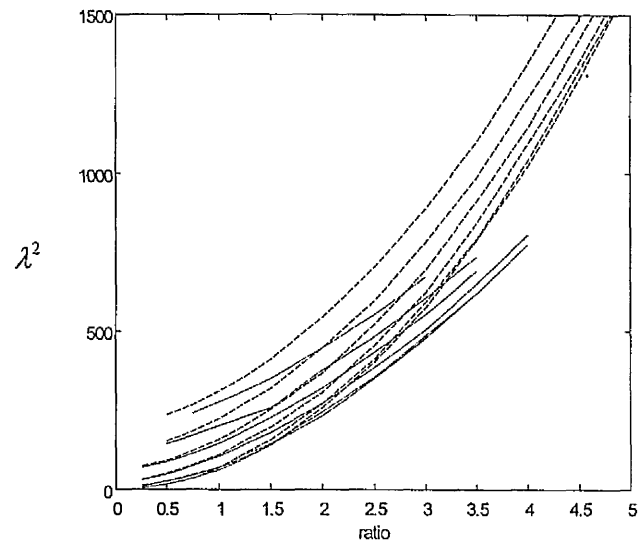


Figure 5.21(d) $j=3$

Figure 5.21 Comparison of variation frequency parameter with aspect ratio for free-free beam-plate of thickness to length ratio 1% and 5%, $j=0-3$; dashed line: thickness to length ratio 1%, solid line: thickness to length ratio 5%

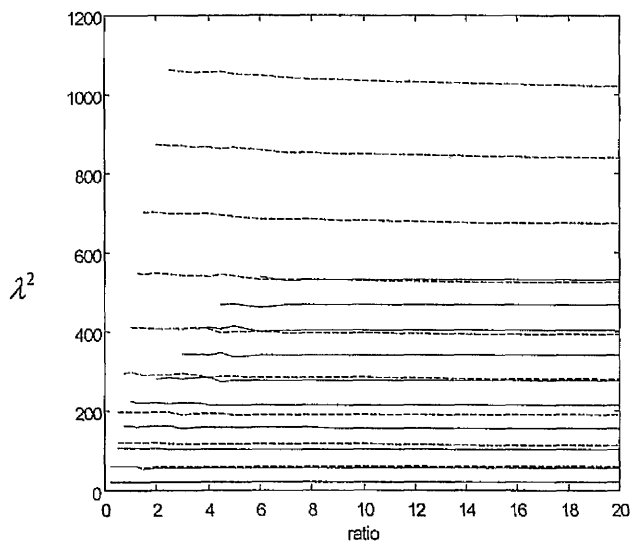


Figure 5.22(a) $j=2$

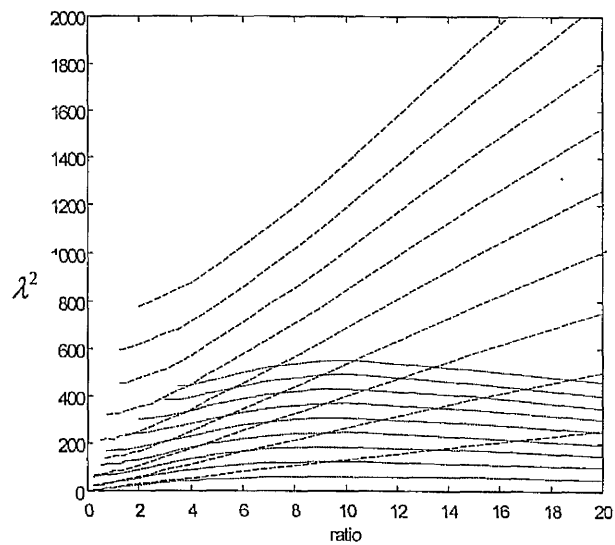


Figure 5.22(b) $j=3$

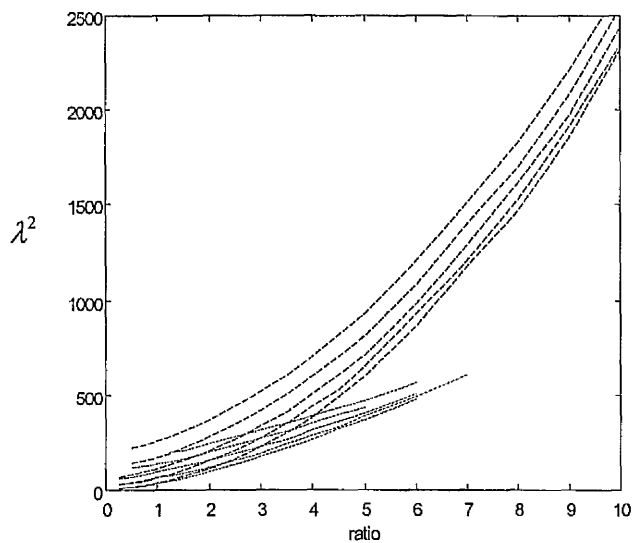


Figure 5.22(c) $j=2$

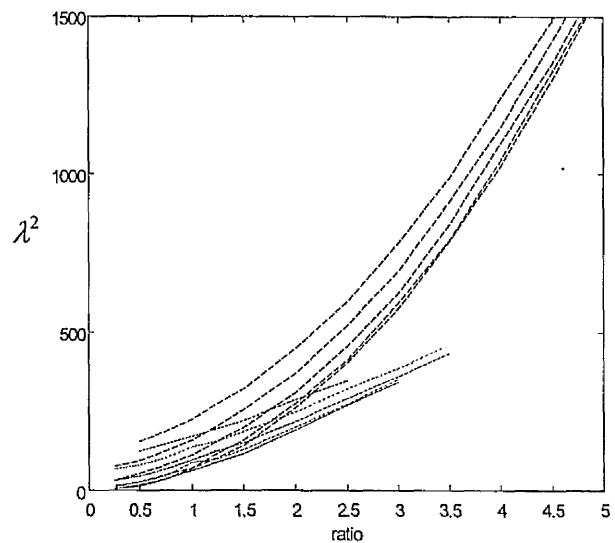


Figure 5.22(d) $j=3$

Figure 5.22 Comparison of variation frequency parameter with aspect ratio for free-free beam-plate of thickness to length ratio 1% and 10%, $j=0-3$; dashed line: thickness to length ratio 1%, solid line: thickness to length ratio 10%

5.6 Summary

The variation of frequency parameters of the thickness to length ratio 1%, 2%, 5% and 10% with aspect ratio for fixed values of i and j were discussed in this chapter. For the 1% and 2% thickness to length ratio variations of the frequency parameter with aspect ratio for $j = 0$ are nearly constant, while the frequency parameters increase with aspect ratio increases for $j = 1$ to 6. The variation of the frequency parameters with aspect ratio for fixed values of i , for $i=0, j=2$ to 6 are almost parabolic. For $i=1, j=1$ the frequency parameters increase gradually as straight lines with the increases of the aspect ratio, while for $i \geq 2$, the frequency parameter changes rapidly as the aspect ratio changes. The comparison of the frequency parameters for 5% and 10% thickness to length ratio with reference to 1% thickness to length ratio show that the differences range for 5% thickness to length ratio between 0% to 52%, and 0% to 80% for 10% thickness to length ratio. The results presented in this chapter have proven that the beam-plates thickness has a significant effect on the frequency parameter value of the beam-plates.

Chapter 6

Defining the transition from beam-like to plate-like behaviour from one-dimensional bending modes of vibration

6.1 Introduction

From the general beam vibration analysis, it is possible to find exact, analytical solutions using either the Euler-Bernoulli or Timoshenko theories. However there is no exact, closed-form analytical solution for the vibration analysis of plates, of any general boundary conditions. The only exception to this is the vibration of plates with simply supported (pinned) boundary conditions. Consequently, approximate methods such as the finite element and the finite difference methods are used to analyse the vibration behaviour of plates. Therefore, to analyse the vibration of a beam-like or plate-like structure, it is useful to be able to place the structure in the beam or plate category so as to be able to use either the exact beam equations or the approximate plate methods to calculate its response.

This chapter will study the natural frequencies and mode shapes for free-free and clamped-clamped beams and plates, which were presented in Chapters 4 and 5, in order to obtain the transition curve or boundary between beam-like and plate-like behavior.

6.2 Study of one-dimensional bending modes for free-free beam-plates

Figures 6.1a to 6.9a show the relationships between the frequency parameters and aspect ratios for fixed values of $j = 0$ and for $i = 2$ to 10 respectively for the 5 mm thick free-free beam-plates. In the same way Figures 6.1b to 6.9b show the results for the 50 mm thick beam-plates. In these figures the x -axis represents the aspect ratios and the y -axis represents the frequency parameters. The line types and symbols used in these figures denote the following:

1. Solid line with circles denotes the frequency parameters from the finite element analysis
2. Dash-dot line with stars denotes the analytical frequency parameters (derived from Tables 1.2 and 1.3) using $\lambda_B^2 = \lambda_p^2 / \sqrt{1 - \nu^2}$
3. Dash-dot line denotes the frequency parameters from Timoshenko beam theory (obtained from Table 2.2 and Table 2.3)
4. Solid line denotes the frequency parameters from Euler-Bernoulli beam theory (obtained from Table 2.2 and Table 2.3)

First bending mode of beam-plates

Figures 6.1a and 6.1b show the variations of the frequency parameters ($\lambda_{2,0}^2$) for mode (2,0) against aspect ratios 0.25 – 20. It should be noted that for the free-free beam, the first elastic mode (i.e. non-rigid body mode) is the mode (2,0). The figures show that

the analytical plate results, which cover a small range of ratios of between 0.40 and 2.5, agree closely with the FEA results. However, the two sets of beam results, obtained from the Timoshenko and Euler-Bernoulli equations, have constant values of 22.359 and 22.37 for the 1% thickness to length ratio and 21.53, 22.37 for the 10% thickness to length ratio respectively. From these figures it is seen that the error between the FEA and the analytical results in comparison to the Timoshenko and Euler-Bernoulli equations are very close for the 1% thickness to length ratio beam and plates. Figure 6.1b shows that the Timoshenko equation predicts better results for 10% thickness to length ratio as expected due to the fact that a higher shear deformation occurs with the thicker beam and plates.

The relative errors between the FEA, analytical, Timoshenko and Euler-Bernoulli results can be expressed as;

$$\varepsilon_1 = \left(\frac{\lambda_{Anal}^2 - \lambda_{FEA}^2}{\lambda_{FEA}^2} \right) \times 100\% \quad (6.1)$$

$$\varepsilon_2 = \left(\frac{\lambda_{Timo}^2 - \lambda_{FEA}^2}{\lambda_{FEA}^2} \right) \times 100\% \quad (6.2)$$

$$\varepsilon_3 = \left(\frac{\lambda_{Euler}^2 - \lambda_{FEA}^2}{\lambda_{FEA}^2} \right) \times 100\% \quad (6.3)$$

where

ε_1 percent error between the analytical plate frequency parameters and the frequency parameters obtained from finite element analysis.

ε_2 percent error between the frequency parameters obtained from Timoshenko beam equation and the frequency parameters obtained from finite element analysis.

ε_3 percent error between the frequency parameters obtained from Euler-Bernoulli beam equation and the frequency parameters obtained from finite element

analysis.

λ_{FEA}^2	frequency parameters obtained from finite element analysis.
λ_{Anal}^2	analytical plate frequency parameters obtained from Table 1.9
λ_{Timo}^2	frequency parameters obtained from Timoshenko beam equation
λ_{Euler}^2	frequency parameters obtained from Euler-Bernoulli beam equation

Tables 6.1(a) and (b) show the percentage errors in the frequency parameters for selected aspect ratios of 0.25, 0.50, 1.00, 1.50, 2.50, 5.00 for mode (2, 0) and for beam-plate thickness to length ratio 1% and 10% respectively. The analytical value of the frequency parameters for aspect ratio 5.00 was estimated from the limited analytical results. Figures 6.1(a) and (b) show that the error between the analytical and FEA results is generally less than 2% with the exception of aspect ratios less than 1.0. Also the relative error between Timoshenko and Euler-Bernoulli beam results and the FEA results are small. The maximum absolute error is approximately 5 % at small aspect ratios of between 0.25 and 1.00. But at these small aspect ratios, the structure is, without doubt, a plate.

A selection of mode shapes for aspect ratios of between 0.25 and 5.0 are shown in Figure 6.1c. These mode shapes show that both the beams and the plates exhibit the fundamental classical one-dimensional bending mode of vibration.

Second bending mode of beam-plates

The comparisons of the variations of the frequency parameter $\lambda_{3,0}^2$ for mode (3,0) with aspect ratios are shown in Figures 6.2(a) and (b) for 1% and 10% thickness to length ratio respectively. These figures show the FEA results, analytical plate results, Timoshenko and Euler-Bernoulli beam results. The figures shows that there is close correlation between

the FEA and analytical plate results for the 1% thickness to length ratio. However, there is considerable difference between the FEA, the analytical and the Euler-Bernoulli beam results for the 10% thickness to length ratio. The calculated percentage errors from these figures are presented in Tables 6.2 (a) and (b). The tables show that the absolute relative errors between the frequency parameters obtained from the FEA and the Timoshenko beam equations are between 1 % to 5 % and the percentage error between the results of the FEA and the Euler-Bernoulli beam equation are between 5 % to 13 % for the 10% thickness to length ratio.

The relationship between the variation of the frequency parameters and aspect ratios for modes (4,0) to (10,0) are shown in Figures 6.3 (a) and (b) to 6.9 (a) and (b). From these figures it is clearly shown that there is a large difference between the FEA results and Euler-Bernoulli beam results especially at higher aspect ratios for the 10% thickness to length ratio. The FEA results and Timoshenko beam results are closer for the 10% thickness to length ratio. The figures also show that for the 1% thickness to length ratio for aspect ratios less than 3.5, 4.0, 4.5, 5.0, 6.0, 7.0 and 8.0 for modes (4,0), (5,0), (6,0), (7,0), (8,0), (9,0) and (10,0), respectively, the frequency parameters behave vary erratically in a non-monotonic fashion. However, as the aspect ratio increases from 3.5, 4.0, 4.5, 5.0, 6.0, 7.0 and 8.0 for modes (4,0), (5,0), (6,0), (7,0), (8,0), (9,0) and (10,0), respectively, the variation of the frequency parameters with aspect ratio becomes smooth and monotonic. Therefore, aspect ratios 3.5, 4.0, 4.5, 5.0, 6.0, 7.0 and 8.0 appear to be transition points from beam-like to plate-like behaviour for modes (4,0), (5,0), (6,0), (7,0), (8,0), (9,0) and (10,0) respectively. This will be discussed further later in this chapter.

Table 6.1a *Percentage errors in frequency parameters of mode (2,0) for 1% thickness to length ratio free-free beam-plates.*

Aspect ratios a/b	Relative errors in frequency parameters (%)		
	ε_1	ε_2	ε_3
0.25	-	-5.44	-5.39
0.50	-	-3.69	-3.64
1.00	9.44	9.5	9.6
1.50	1.86	-0.45	-0.40
2.50	1.83	-0.67	-0.62
5.00	-	-0.32	-0.27

Table 6.1b *Percentage errors in frequency parameters of mode (2,0) for 10% thickness to length ratio free-free beam-plates*

Aspect ratios a/b	Relative errors in frequency parameters (%)		
	ε_1	ε_2	ε_3
0.25	-	-5.61	-1.93
0.50	-	-3.83	-0.08
1.00	17.12	-2.55	1.24
1.50	5.58	-0.64	3.23
2.50	5.58	-0.83	3.03
5.00	-	-0.55	3.32

Table 6.2a *Percentage errors in frequency parameters of mode (3,0) for 1% thickness to length ratio free-free beam-plates*

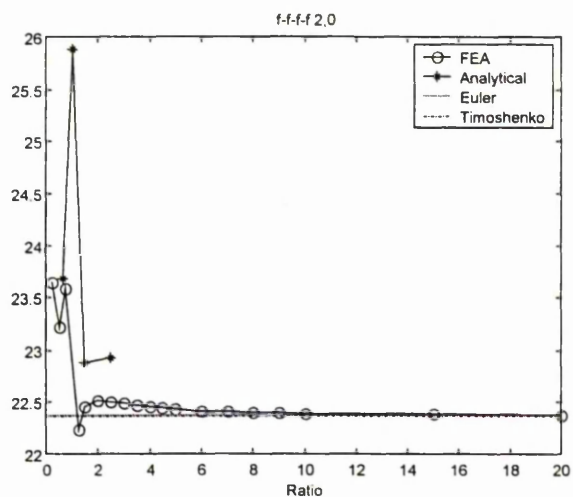
Aspect ratios a/b	Relative errors in frequency parameters (%)		
	ε_1	ε_2	ε_3
0.25	-	-4.54	-4.42
0.50	-	-4.88	-4.75
1.00	1.02	-4.54	-4.42
1.50	2.45	2.32	2.48
2.50	1.75	-1.56	-1.43
5.00	-	-0.87	-0.74

Table 6.2b *Percentage errors in frequency parameters of mode (3,0) for 10% thickness to length ratio free-free beam-plates*

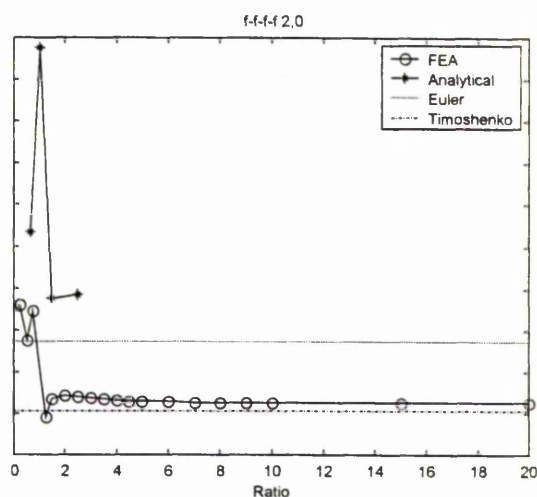
Aspect ratios a/b	Relative errors in frequency parameters (%)		
	ε_1	ε_2	ε_3
0.25	-	-4.56	5.84
0.50	-	-5.25	5.08
1.00	11.51	-4.87	5.51
1.50	13.84	2.66	13.87
2.50	12.35	-1.82	8.89
5.00	-	-1.39	9.36

From the investigation of the mode shapes presented in Figures 6.3c to 6.9c it is possible to determine the transition point. The figures show the mode shapes of modes (4,0), (5,0), (6,0), (7,0), (8,0), (9,0) and (10,0) respectively. It can be seen in these figures that for ratios 3.5, 4.0, 4.5, 5.0, 6.0, 7.0 and 8.0 (and greater) for modes (4,0), (5,0), (6,0),

(7,0), (8,0), (9,0) and (10,0), respectively, the free breadthwise edges of the beam-plates remain practically straight. Therefore, these modes are pure bending modes and they indicate beam-like behaviour. However for aspect ratios less than 3.5, 4.0, 4.5, 5.0, 6.0, 7.0 and 8.0 for modes (4,0), (5,0), (6,0), (7,0), (8,0), (9,0) and (10,0), respectively, the figures show that in addition to the bending of the plates along the x -axis, the other free edges of the plates are also bent. This indicates plate-like behaviour. Therefore the aspect ratios 3.5, 4.0, 4.5, 5.0, 6.0, 7.0 and 8.0 are the transition points for beam-like to plate-like behaviour for modes (4,0), (5,0), (6,0), (7,0), (8,0), (9,0) and (10,0) respectively.

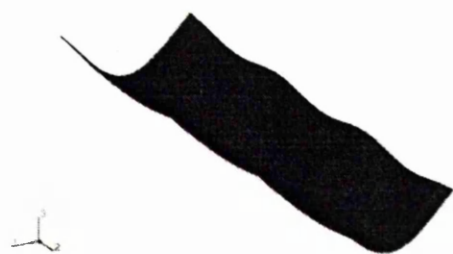
$\lambda_{2,0}^2$


(a) 1% thickness to length ratio

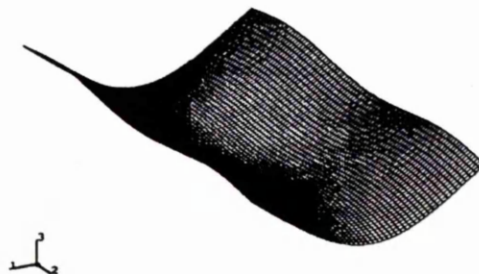


(b) 10% thickness to length ratio

Figure 6.1 Variation of frequency parameters with aspect ratios for mode (2,0)



(a) $r = 0.25$ (23.646 Hz)



(b) $r = 0.50$ (23.217 Hz)



(c) $r = 0.75$ (23.582 Hz)



(d) $r = 1.25$ (22.242 Hz)

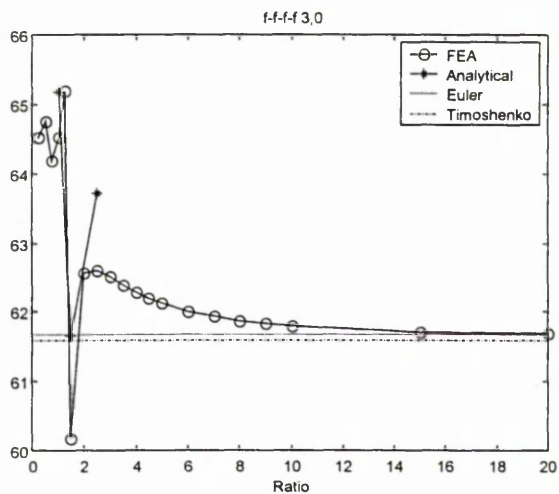


(e) $r = 2.0$ (22.523 Hz)

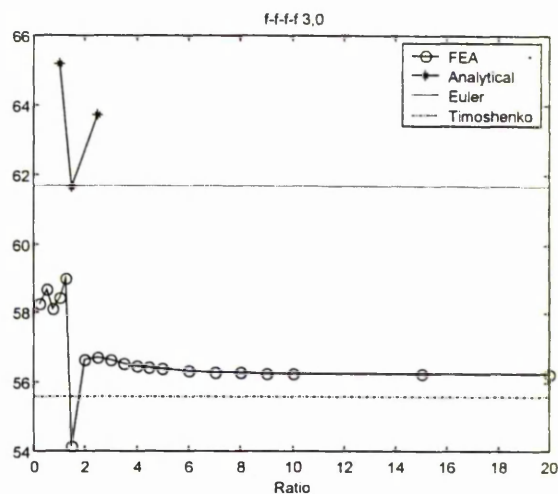


(f) $r = 5.0$ (22.431 Hz)

Figure 6.1c Selected mode shapes for mode (2,0) and various aspect ratios.

$\lambda_{3,0}^2$


(a) 1% thickness to length ratio

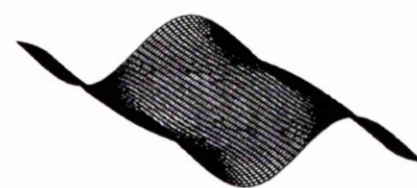


(b) 10% thickness to length ratio

Figure 6.2 Variation of frequency parameters with aspect ratios for mode (3,0)



(a) $r = 0.50$ (64.75 Hz)



(b) $r = 0.75$ (64.19 Hz)



(c) $r = 1$ (64.52 Hz)



(d) $r = 2.5$ (62.61 Hz)

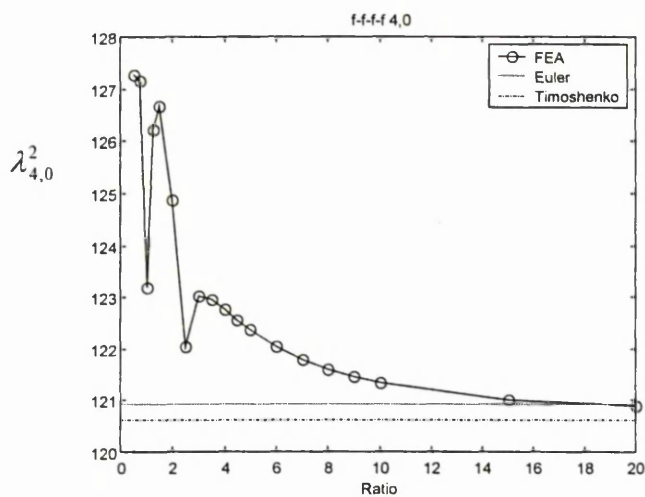


(e) $r = 5.0$ (62.13 Hz)

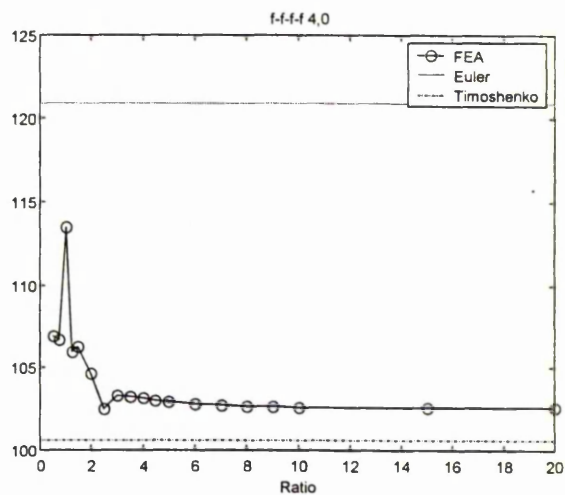


(f) $r = 8.0$ (62.01 Hz)

Figure 6.2c Selected mode shapes for mode (3,0) and various aspect ratios.

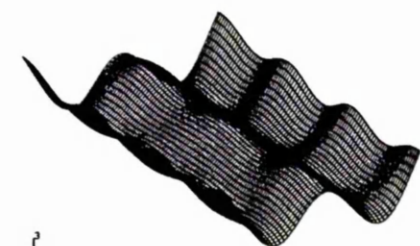


(a) 1% thickness to length ratio

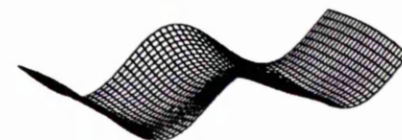


(b) 10% thickness to length ratio

Figure 6.3 Variation of frequency parameters with aspect ratio for mode (4,0).



(a) $r = 0.50$ (127.27 Hz)



(b) $r = 2.0$ (124.89 Hz)



(c) $r = 2.50$ (122.04 Hz)



(d) $r = 3.50$ (122.96 Hz)

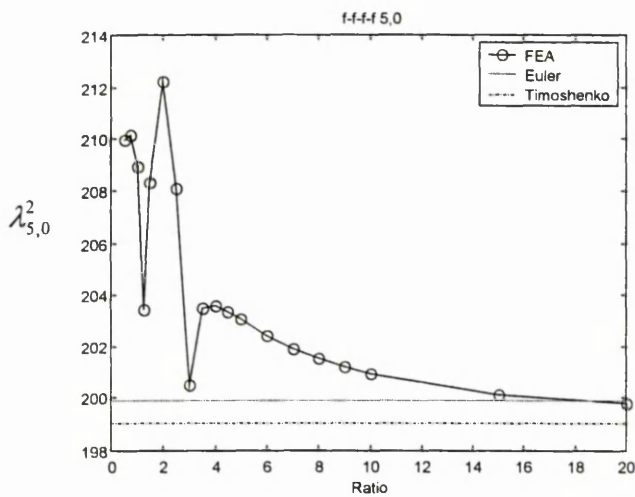


(e) $r = 4.0$ (122.77 Hz)

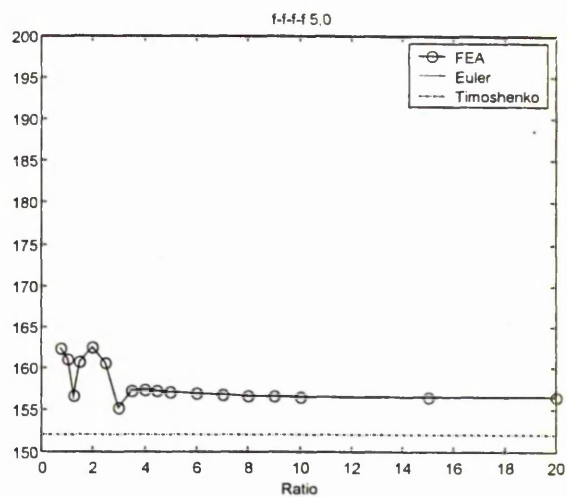


(f) $r = 9.0$ (121.46 Hz)

Figure 6.3c Selected mode shapes for mode (4,0) and various aspect ratios.

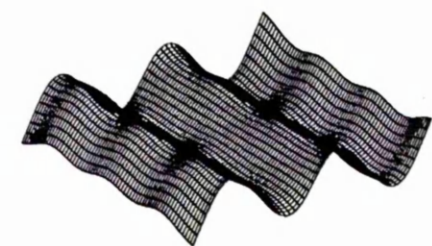


(a) 1% thickness to length ratio



(b) 10% thickness to length ratio

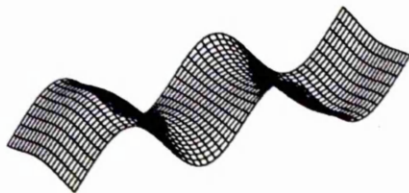
Figure 6.4a Variation of frequency parameters with geometric for mode (5,0).



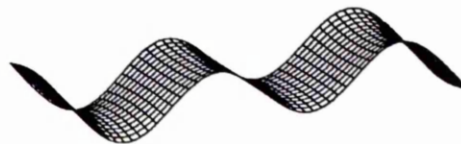
(a) $r = 0.75$ (210.16 Hz)



(b) $r = 1.5$ (208.33 Hz)



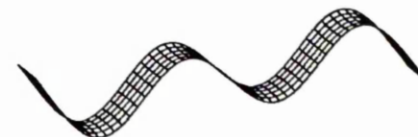
(c) $r = 2.5$ (208.10 Hz)



(d) $r = 4.0$ (203.58 Hz)

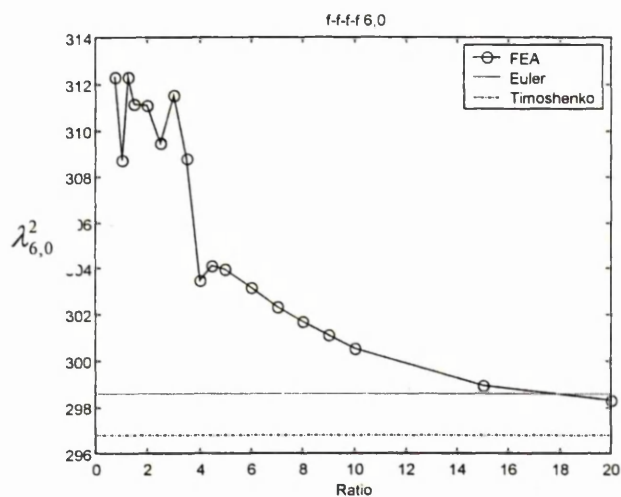


(e) $r = 5.0$ (203.06 Hz)

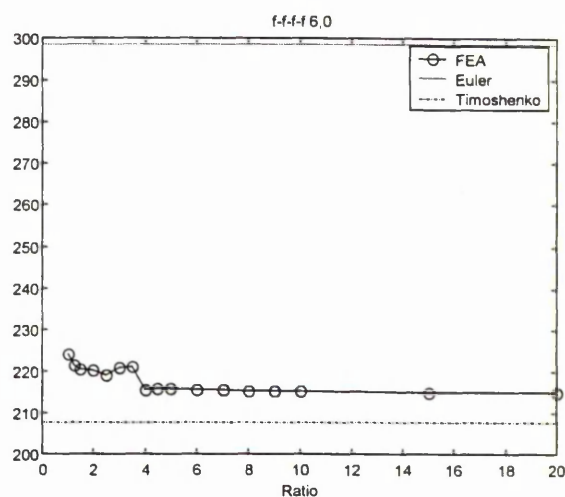


(f) $r = 10.0$ (200.90 Hz)

Figure 6.4c Selected mode shapes for mode (5,0) and various aspect ratios.



(a) 1% thickness to length ratio



(b) 10% thickness to length ratio

Figure 6.5 Variation of frequency parameters with aspect ratios for mode (6,0).

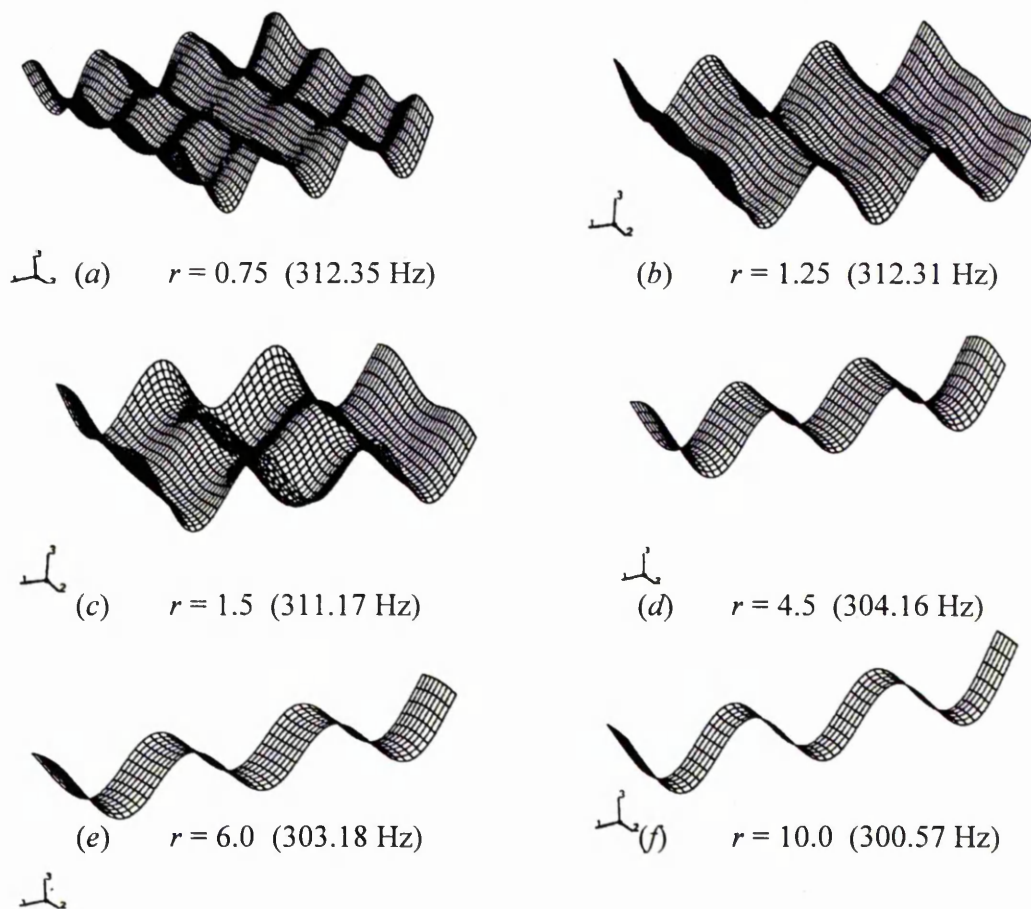
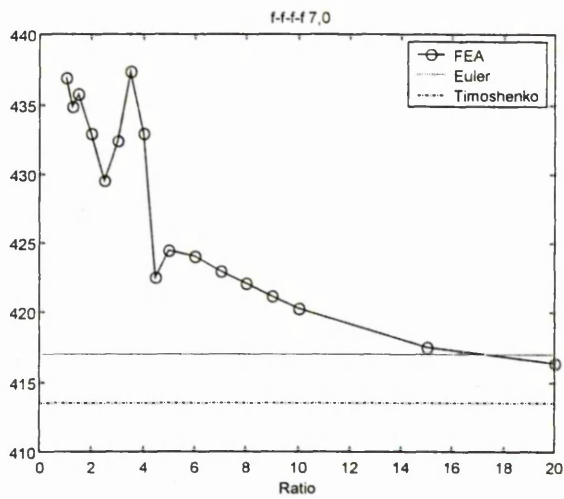
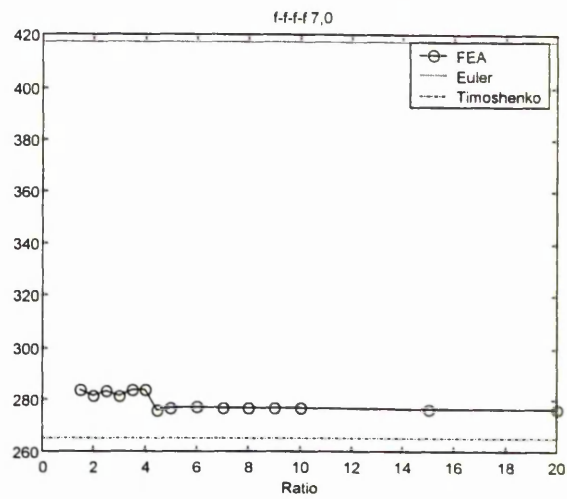


Figure 6.5c Selected mode shapes for mode (6,0) and various aspect ratios.

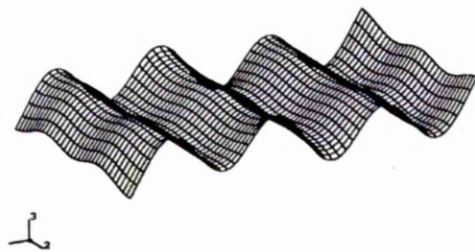
$\lambda_{7,0}^2$ 

(a) 1% thickness to length ratio

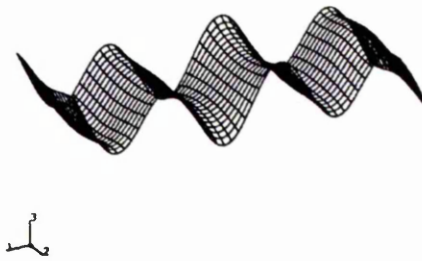


(b) 10% thickness to length ratio

Figure 6.6 Variation of frequency parameters with aspect ratio for mode (7,0).



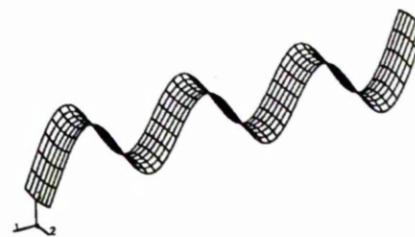
(a) $r = 1.50$ (435.81 Hz)



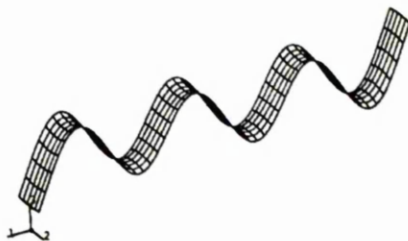
(b) $r = 3.0$ (432.47 Hz)



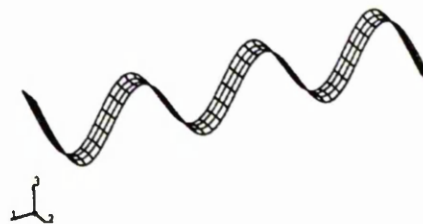
(c) $r = 6.0$ (424.03 Hz)



(d) $r = 8.0$ (422.06 Hz)

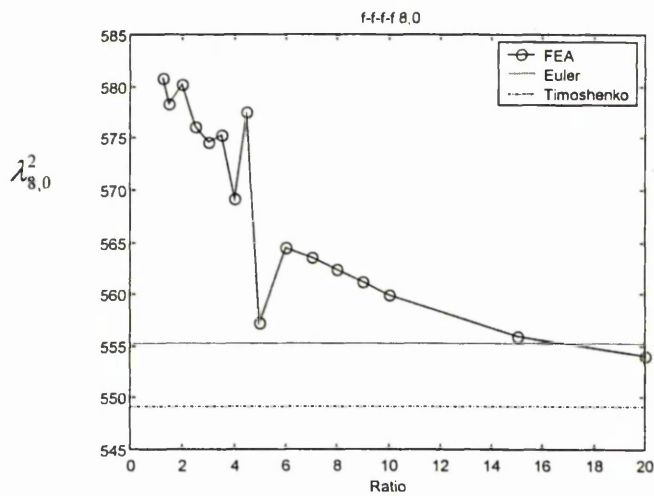


(e) $r = 10.0$ (420.28 Hz)

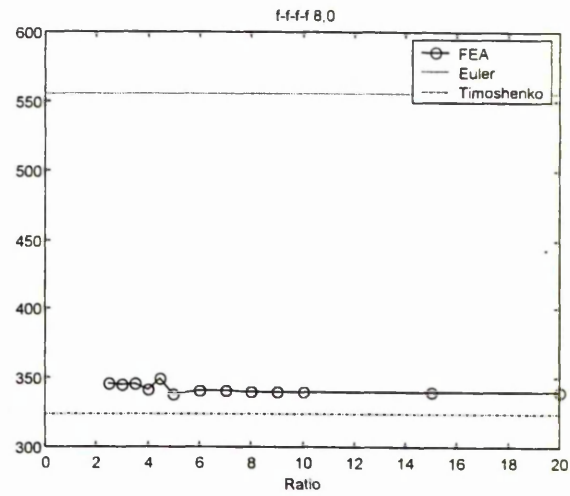


(f) $r = 15.0$ (417.63 Hz)

Figure 6.6c Selected mode shapes for mode (7,0) and various aspect ratios.

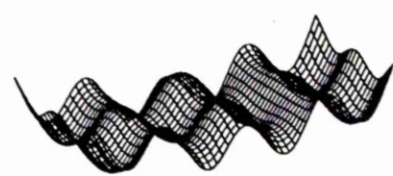


(a) 1% thickness to length ratio

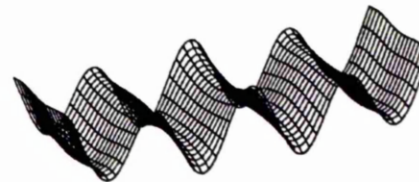


(b) 10% thickness to length ratio

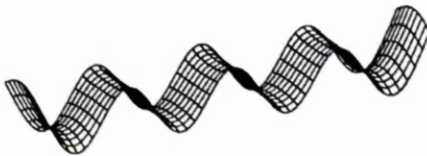
Figure 6.7 Variation of frequency parameters with aspect ratio for mode (8,0).



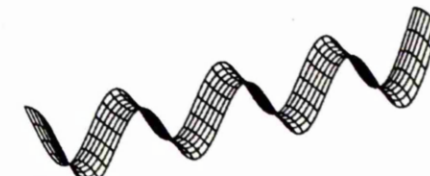
(a) $r = 2.0$ (580.26 Hz)



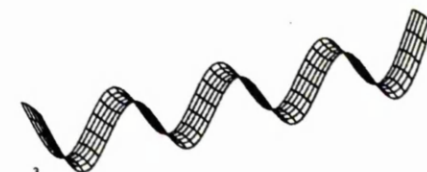
(b) $r = 3.0$ (574.60 Hz)



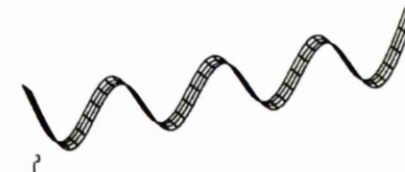
(c) $r = 6.0$ (564.44 Hz)



(d) $r = 8.0$ (562.39 Hz)

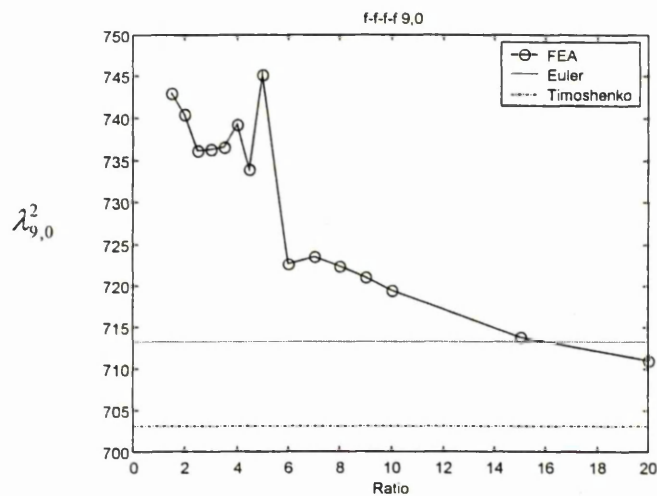


(e) $r = 10.0$ (559.95 Hz)

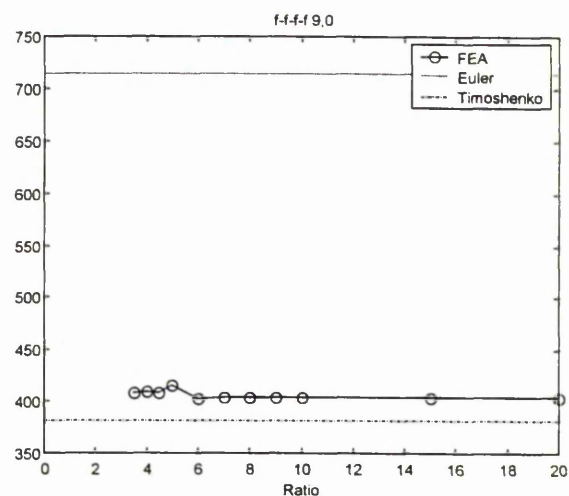


(f) $r = 20.0$ (554.05 Hz)

Figure 6.7c Selected mode shapes for mode (8,0) and various geometric.



(a) 1% thickness to length ratio

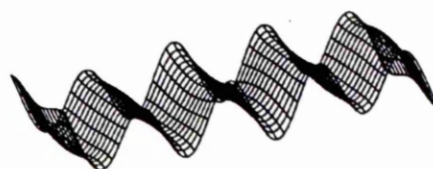


(b) 10% thickness to length ratio

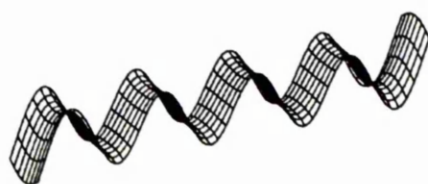
Figure 6.8 Variation of frequency parameters with aspect ratio for mode (9,0).



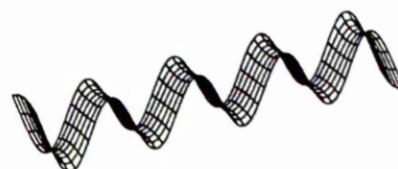
(a) $r = 2.0$ (740.44 Hz)



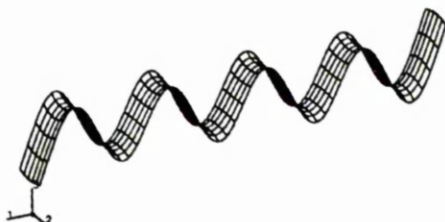
(b) $r = 3.5$ (736.72 Hz)



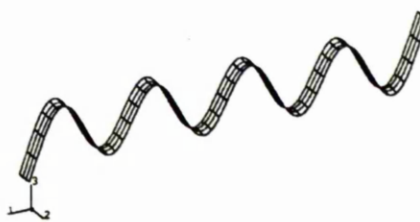
(c) $r = 7.0$ (723.52 Hz)



(d) $r = 8.0$ (722.39 Hz)

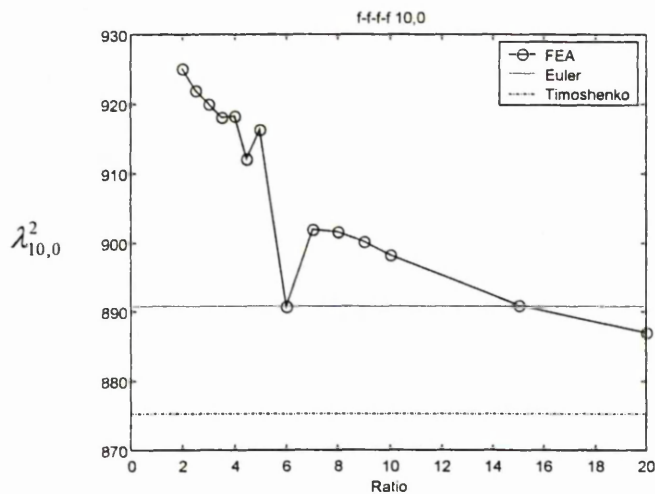


(e) $r = 10.0$ (719.35 Hz)

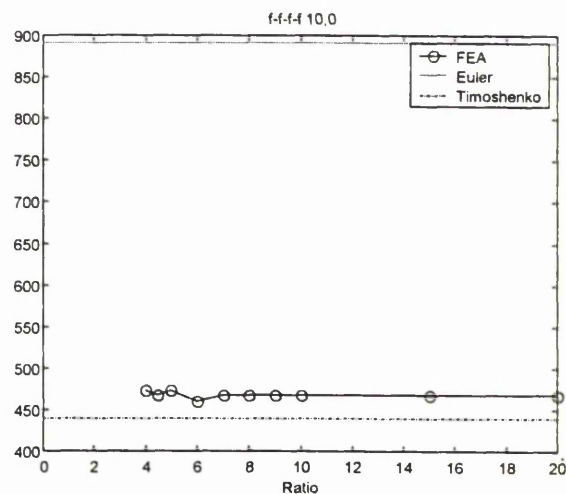


(f) $r = 20.0$ (710.97 Hz)

Figure 6.8c Selected mode shapes for mode (9,0) and various aspect ratios.

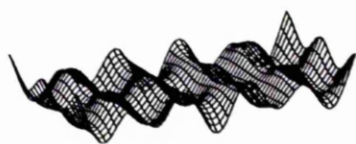


(a) 1% thickness to length ratio

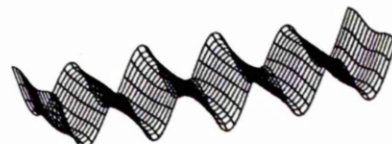


(b) 10% thickness to length ratio

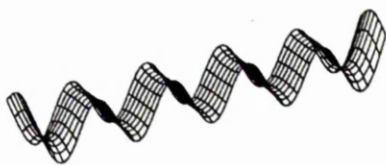
Figure 6.9 Variation of frequency parameters with aspect ratio for mode (10,0).



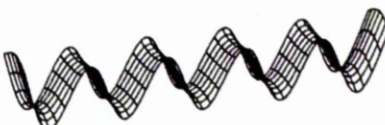
(a) $r = 2.0$ (925.20 Hz)



(b) $r = 3.5$ (920.07 Hz)



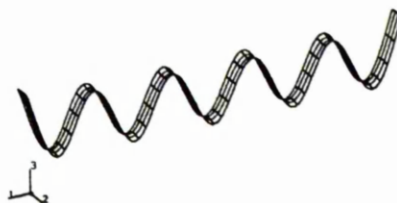
(c) $r = 7.0$ (901.98 Hz)



(d) $r = 8.0$ (901.61 Hz)



(e) $r = 10.0$ (898.24 Hz)



(f) $r = 20.0$ (887.03 Hz)

Figure 6.9c Selected mode shapes for mode (10,0) and various aspect ratios.

6.3 Derivation of transition curve based on one-dimensional bending behaviour for the 1% thickness to length ratio free-free beam-plates

From the previous section it was possible to generate Table 6.4. which represent the mode number, aspect ratio and frequency parameter at the transition points for the one-dimensional bending mode, Figures 6.1a to 6.9a. Using the least-square curve-fitting method, these transition points can be expressed by the following polynomial equation:

$$\lambda^2 = 5.64r^2 + 91.44r - 190.56 \quad (6.4)$$

where λ^2 = frequency parameter

r = aspect ratio

Table 6.4 Mode number, aspect ratio and frequency parameter at the transition points for 1% thickness to length ratio beam-plates.

Mode	Ratio	λ^2
(2,0)	2.0	22.52
(3,0)	3.0	62.61
(4,0)	3.5	123.03
(5,0)	4.0	203.60
(6,0)	4.5	304.2
(7,0)	5.0	424.03
(8,0)	6.0	564.01
(9,0)	7.0	723.5
(10,0)	8.0	901.06

From the modal data presented in Figures 6.1a to 6.9a for selected modes (2,0) to (10,0) it was possible to plot Figure 6.10 which shows the transition curve obtained from the one-dimensional bending modes.

The empirical equation, Equation (6.4), for the transition from beam-like to plate-like behaviour is also found from Figure 6.10. It is seen that the transition equation is a curve which delineates the boundary between beam-like to plate-like characteristics. The transition curve defines two regions namely,

1. The right region of the transition curve is a region of beam behaviour in which one can use the simple beam equations.
2. The left region of the transition curve is a region of plate behaviour where it is important to use finite element analysis to calculate the behaviour/response of the beam-plate structure.

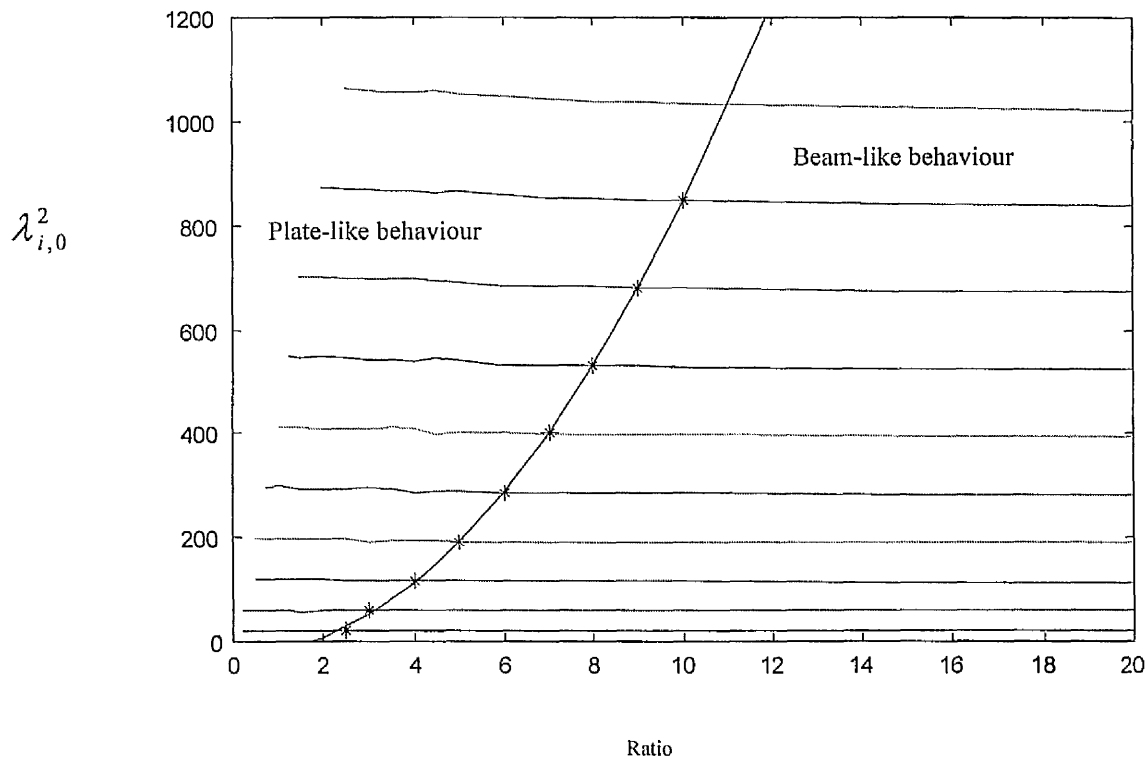


Figure 6.10 Variation of $\lambda_{i,0}^2$ with aspect ratios for modes (2,0) to (10,0). The transition curve from plate-like to beam-like behaviour is overlaid

6.4.1 The effect of thickness to length ratio on transition curve obtained from one-dimensional bending modes

The previous work was focused on finding the transition curve for beam-like to plate-like behaviour for the 1% thickness to length ratio, which is represented in Figure 6.10. This section will study the effect of the thickness of beams-plates on their frequency parameters and, hence, on the transition curve for beam-like to plate-like behaviour.

The ABAQUS FEA program was used to calculate the first 50 natural frequencies of the free-free beam-plates for 3 values of thickness to length ratios namely: 2%, 5%, 10% (thickness 10, 25, 50 mm), and for 20 values of aspect ratios, a/b , using the general purpose rigid shell element, S4R. These values of aspect ratios were 0.25, 0.5, 0.75, 1.0, 1.25, 1.50, 2.0, 2.5, 3.0, 3.5, 4.0, 4.5, 5.0, 6.0, 7.0, 8.0, 9.0, 10.0, 15.0 and 20.0. The beams and plates were of fixed length $a = 500$ mm and their breadths (b) were varied from 25 mm to 2000 mm. The number of elements along the x-axis (N_x) was fixed for ratios 0.75 - 20 at 100 elements. The smaller ratio 0.25 used 60 elements and ratio 0.5 used 80 elements this was done to minimise the results file size and the time to solve the finite element analysis. The number of elements along the y axis, (N_y) varied according to the ratio a/b , and this ratio varied as the breadths (b) varied, i.e. the analysis done on these thickness to length ratios was identical to the analysis for 1% thickness to length ratio.

From the computed natural frequencies, the frequency parameters were calculated for each of the 3 thickness to length ratio using Equations (3.1) and (3.2). For each thickness, the frequency parameters were plotted against the aspect ratios and the graphical data was analysed as in the previous section for each mode in order to determine the transition point. The transition points for each mode were found to occur at the same aspect

ratio for all the thickness to length ratio (2%, 5% and 10%). The transition points for the four thicknesses to length ratios are tabulated in Table 6.5. From the transition points, a transition curve was determined empirically for each thickness to length ratio by means of the least-square curves fitting method.

Table 6.5 Mode numbers, aspect ratios and frequency parameters at transition points of thicknesses to length ratio 1%, 2%,5% and 10%.

Mode	r_t	λ_t^2 thickness			
		1%	2%	5%	10%
(2,0)	2.0	22.52	22.49	22.27	21.72
(3,0)	3.0	62.61	62.37	60.81	56.70
(4,0)	3.5	123.03	122.12	116.63	103.25
(5,0)	4.0	203.60	201.40	187.53	157.29
(6,0)	4.5	304.20	299.50	271.00	215.88
(7,0)	5.0	424.03	415.70	364.77	277.10
(8,0)	6.0	564.01	549.54	467.09	340.08
(9,0)	7.0	723.50	697.01	576.06	403.71
(10,0)	8.0	901.06	865.00	690.00	467.38

r_t = value of aspect ratio at transition point, λ_t^2 = value of frequency parameters at transition point

Figure 6.11 shows the variation of frequency parameter, $\lambda_{t,0}^2$, with aspect ratio for modes (2,0) to (11,0) for free-free beam-plates of thicknesses to length ratios 2%, 5% and 10%. The corresponding transition curves are overlaid. The transition points are tabulated in Table 6.5 Using the linear least-square curve fitting method, these transition points can be expressed for the thicknesses to length ratios 2%,5% and 10% respectively by the following equations :

$$\lambda^2 = 7.53r^2 + 71.17r - 171.33 \quad (\text{for thickness to length ratio } 2\%) \quad (6.5)$$

$$\lambda^2 = 2.73r^2 + 87.45r - 186.87 \quad (\text{for thickness to length ratio } 5\%) \quad (6.6)$$

$$\lambda^2 = 1.16r^2 + 89.27r - 164.39 \quad (\text{for thickness to length ratio } 10\%) \quad (6.7)$$

where λ^2 = frequency parameter and r = aspect ratio

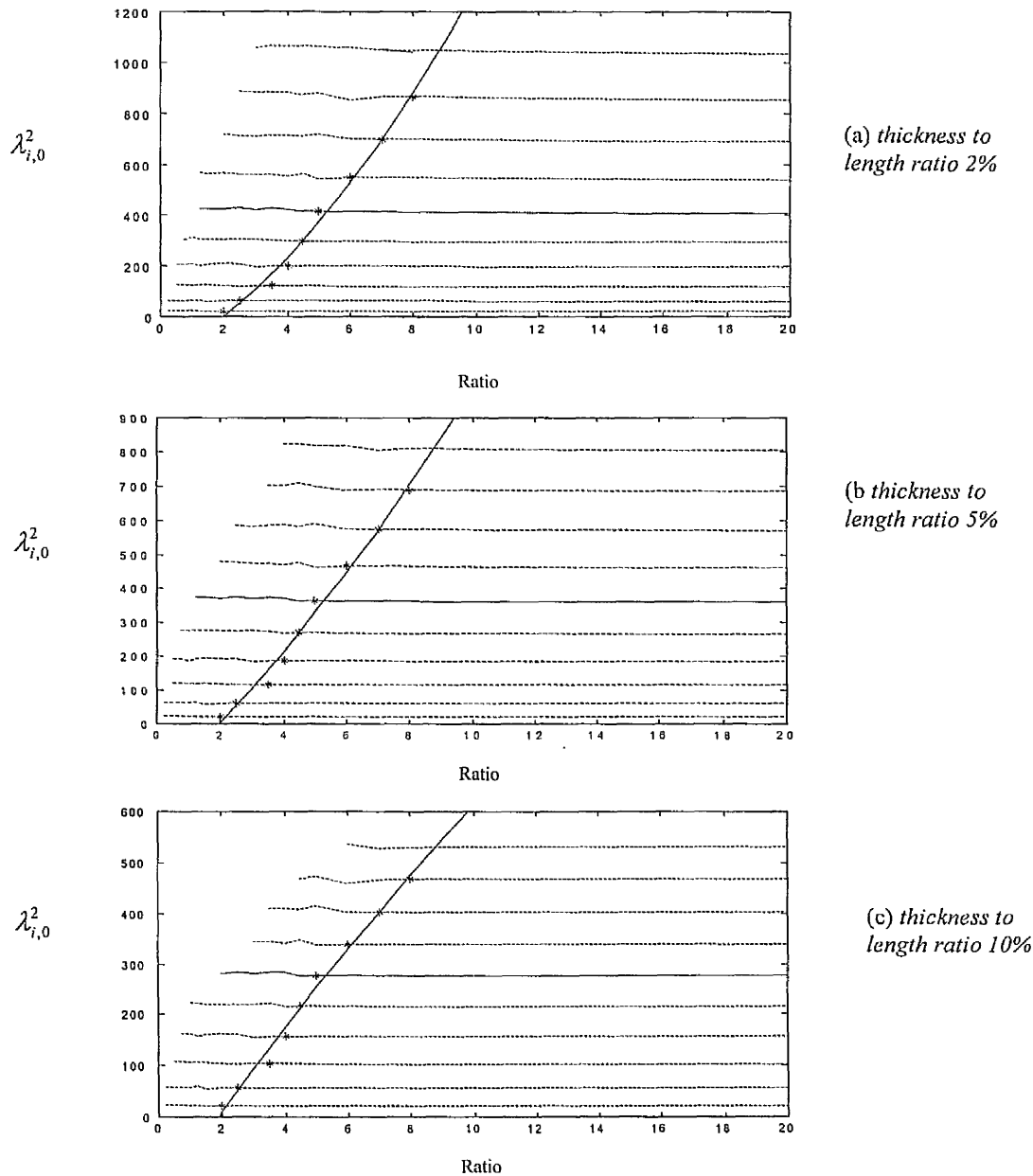


Figure 6.11 Variation of frequency parameter with aspect ratio for mode (2,0) to (11,0) of free-free beams and plates of thicknesses to length ratio (a) 2%, (b) 5%, (c) 10%. The transition curve for beam-like to plate-like behaviour are overlaid.

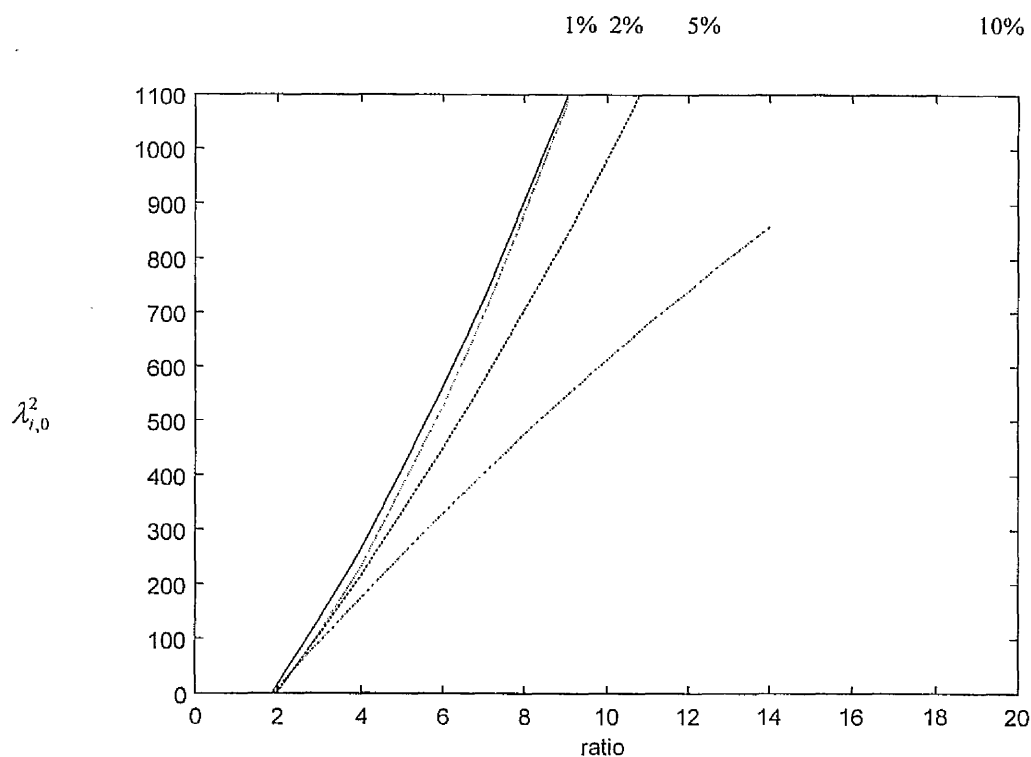


Figure 6.12 Comparisons of transition curves for free-free beam-plates of thickness to length ratios 1%, 2%, 5% and 10%

Figure 6.12 represent the combined transition curves for all thicknesses to length ratios considered. The top curves is the transition curve for beam-plate thickness to length ratio 1%, while the bottom curve is the transition curve for beam-plate thickness to length ratio 10%. It can be seen that the transition curves of beam-plates of thicknesses to length ratio 1%, 2% are relatively close, and as the beam-plate becomes thicker the slope of the transition curve decreases.

Table 6.6 shows the percentage relative deviation between the frequency parameters at the transition points for beam-plates of thicknesses to length ratio 2%, 5% and 10% and

those of the 1% thickness to length ratio. The average relative deviations for the 2% thickness to length ratio is about 10 %, and for 5% thickness to length ratio about 20 % and for the 10% thickness to length ratio 35 %.

Using the least square method, shown in Appendix 1, the transition curves for free-free beam-plates of thickness to length ratios 1%, 2%, 5% and 10% can be presented mathematically as

$$\lambda^2 = (-181 - 115r + 8r^2) + (-205 + 7116r - 77r^2)\tau + (3611 - 51186r - 1045r^2)\tau^2 \quad (6.8)$$

where λ^2 = frequency parameter, r = aspect ratio

$\tau = \frac{t}{a}$ = thickness to length ratio, t = thickness, a = length

Table 6.6 Mode numbers, aspect ratios and relative deviations of frequency parameters at transition points for beam-plates of thickness to length ratio 2%, 5%, 10%.

Mode	r_t	Relative Deviation (%)		
		Thickness		
		2%	5%	10%
(1,0)	2.0	32.00	80.00	93.00
(2,0)	3.0	16.32	19.23	28.76
(3,0)	3.5	15.01	20.00	32.50
(4,0)	4.0	11.53	19.23	33.60
(5,0)	4.5	9.46	19.4	34.50
(6,0)	5.0	7.75	19.50	37.35
(7,0)	6.0	6.36	18.19	39.69
(8,0)	7.0	5.41	21.22	42.30
(9,0)	8.0	3.27	22.12	44.77

$$\text{Relative deviation} = \frac{\lambda_{ts}^2 - \lambda_t^2}{\lambda_{ts}^2} \times 100\%$$

λ_{ts}^2 = value of frequency parameter at transition point of the 1% thickness to length ratio

6.5 Study of one dimensional bending modes for clamped-clamped beam-plates

The previous section covers the study of the one-dimensional bending modes for free-free beam-plates. This section will study the one-dimensional bending modes for clamped-clamped beams-plates.

Figures 6.13 and 6.14 show the variation of frequency parameters with aspect ratios for modes (0,0) to (9,0). The definition of line type is the same as for the beam-plates with free-free boundary conditions. The figures show that the frequency parameters vary smoothly with aspect ratio at all the modes of one-dimensional bending examined. Unlike the frequency parameter curves of the free-free beam-plates, which show discontinuities, the frequency parameter curves of the clamped-clamped beam-plates do not show any discontinuities. Due to the smoothness of the frequency parameter curves it is not possible to find the point of transition from the one-dimensional bending modes for the clamped-clamped beam-plates, the reasons for this is due to the anticlastic behaviour of the clamped-clamped beam-plates. However, it is shown in chapter 7 and 8 that the use of symmetric and anti-symmetric modes helps in identification of the transition zone in the frequency chart of clamped-clamped beam-plates. Furthermore, Figures 6.13 and 6.14 show that for the range of thicknesses of beam-plates studied, the Timoshenko beam equation predicts more accurate results than the Euler-Bernoulli equations.

The errors between the FE results and the predictions of the Euler-Bernoulli and Timoshenko beam equations range between 5% and 2% and between 5.5% and 2.5%, respectively, for the 1% thickness to length ratio. But for the 10% thickness to length ratio, the errors range between 5% and 70% for the Euler-Bernoulli beam equation and between 4% and 7% for the Timoshenko beam equations.

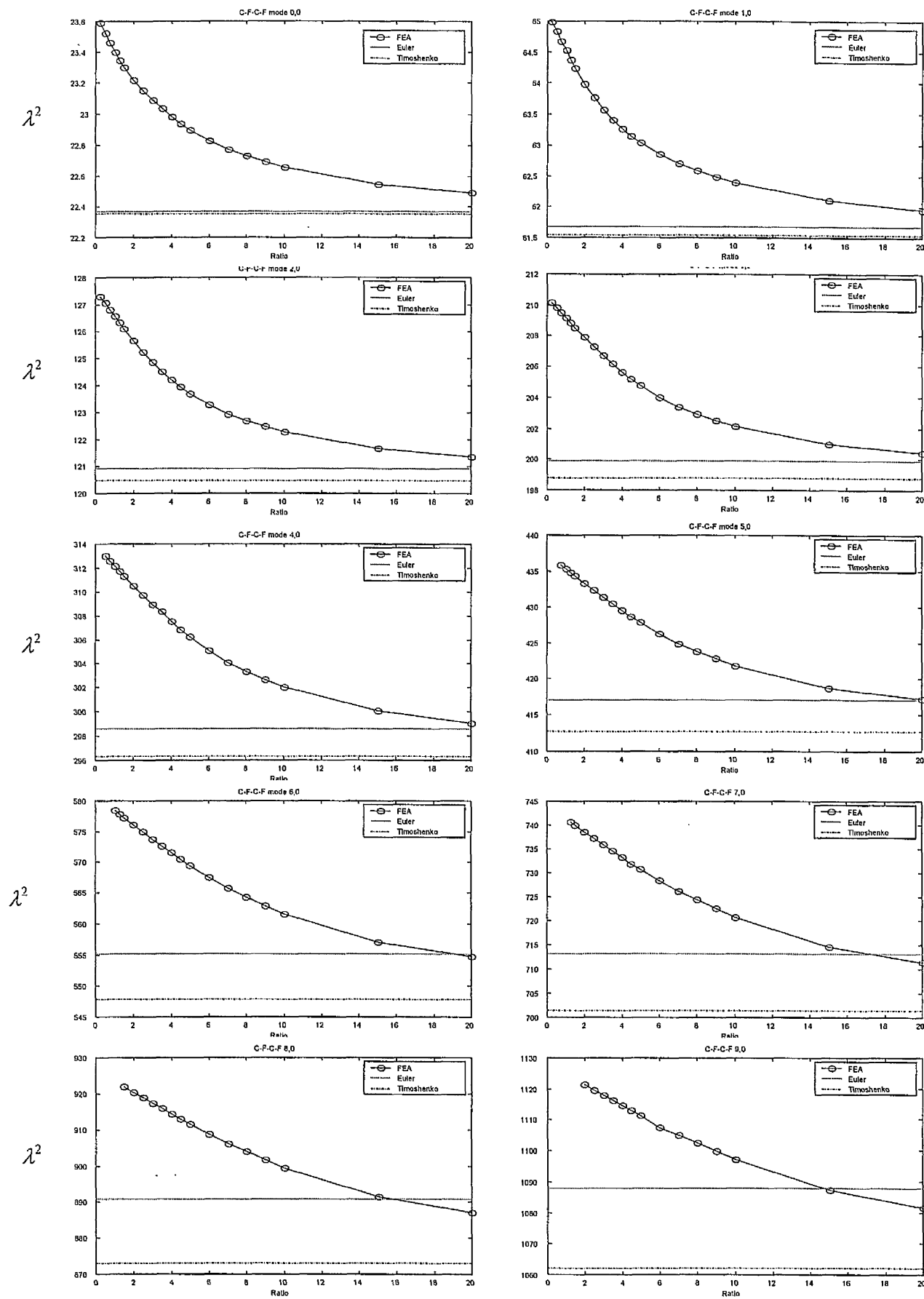


Figure 6.13 Variation of frequency parameters with aspect ratios for the 1% thickness to length ratio clamped-clamped

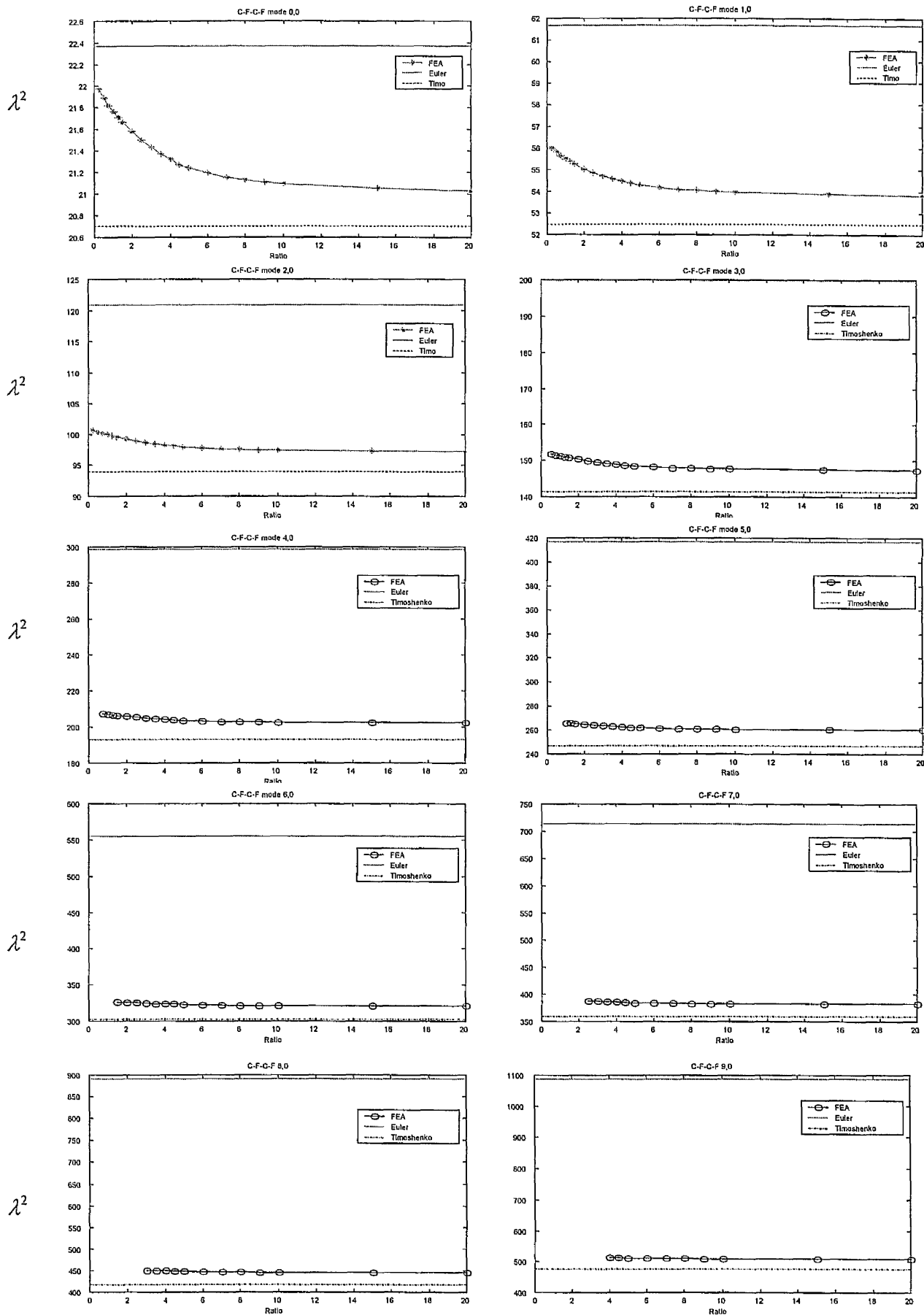


Figure 6.14 Variation of frequency parameters with aspect ratios for the 10% clamped-clamped

6.6 Summary

This chapter investigated the transition from beam-like to plate-like behaviour from the one-dimensional bending modes for both free-free and clamped-clamped beam-plates. It was possible to determine transition curves and equations for the free-free beam-plates from the discontinuities in the trends of the frequency parameter curves. On the contrary, frequency parameter curves of the clamped-clamped beam-plates were smooth. They did not exhibit any erratic behaviour. Therefore, it was not possible to deduce any transition points using the approach presented in this chapter. The data obtained from both the Euler-Bernoulli and the Timoshenko beam equations were compared to the FEA results.

Chapter 7

Deducing transition from beam-like to plate-like behaviour using symmetric modes of vibration

7.1 Introduction

In the previous chapter it was possible to determine the transition curve from beam-like to plate-like behaviour from the one dimensional bending modes. It was easy to determine the transition curve for the free-free boundary condition. This was achieved by plotting the frequency parameter against the aspect ratio. The curves obtained were smooth except at the transition zone where the curve became zigzag. But for the clamped-clamped boundary conditions, the plots of frequency parameter versus aspect ratio were very smooth without any section of the curve showing discontinuity. Therefore, it was not possible to determine the transition curve. However this chapter will consider the symmetric mode for both free-free and clamped-clamped beam-plates in order to determine the transition curves.

7.2 Definition of symmetric and anti-symmetric modes

The definition of a symmetric mode is a mode shape, which is symmetric with respect to the centreline line of a beam or a plate, as shown in Figure 7.1. The definition of mode shape as (i,j) , where i denotes the number of nodal lines in the lengthwise (x) direction, and j denotes the number of nodal lines in the breadthwise (y) direction. A value of $j = 0$ means that there is no nodal line in the breadthwise direction. Therefore all points at the same axial location from the centreline c-c will vibrate with the same amplitude and phase. This mode will be a one-dimensional bending mode which is define as a symmetric mode. When $j = 1$, there will be one nodal line in the breadthwise direction. All points at the same axial location from the centreline c-c vibrate with the same amplitude but with opposite phase. The mode is, therefore, a one-dimensional torsional mode, which is defined as an anti-symmetric mode. In general, the mode shapes for which the mode counter j is even numbers are symmetric modes. Anti-symmetric modes are the mode shapes for which j are odd numbers. Symmetric and anti-symmetric modes for free-free and clamped-clamped beam-plates are shown in Figure 7.2 (a) and (b) respectively.

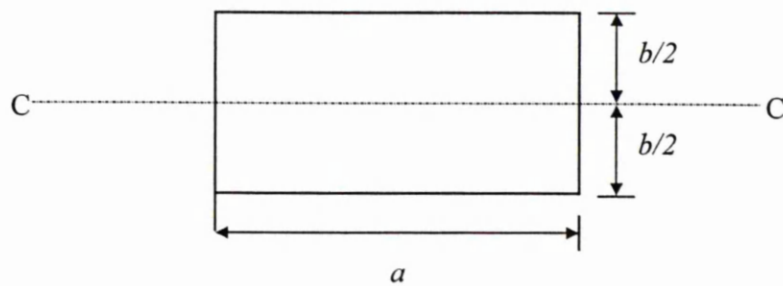


Figure. 7.1 Centreline of plate c-c.

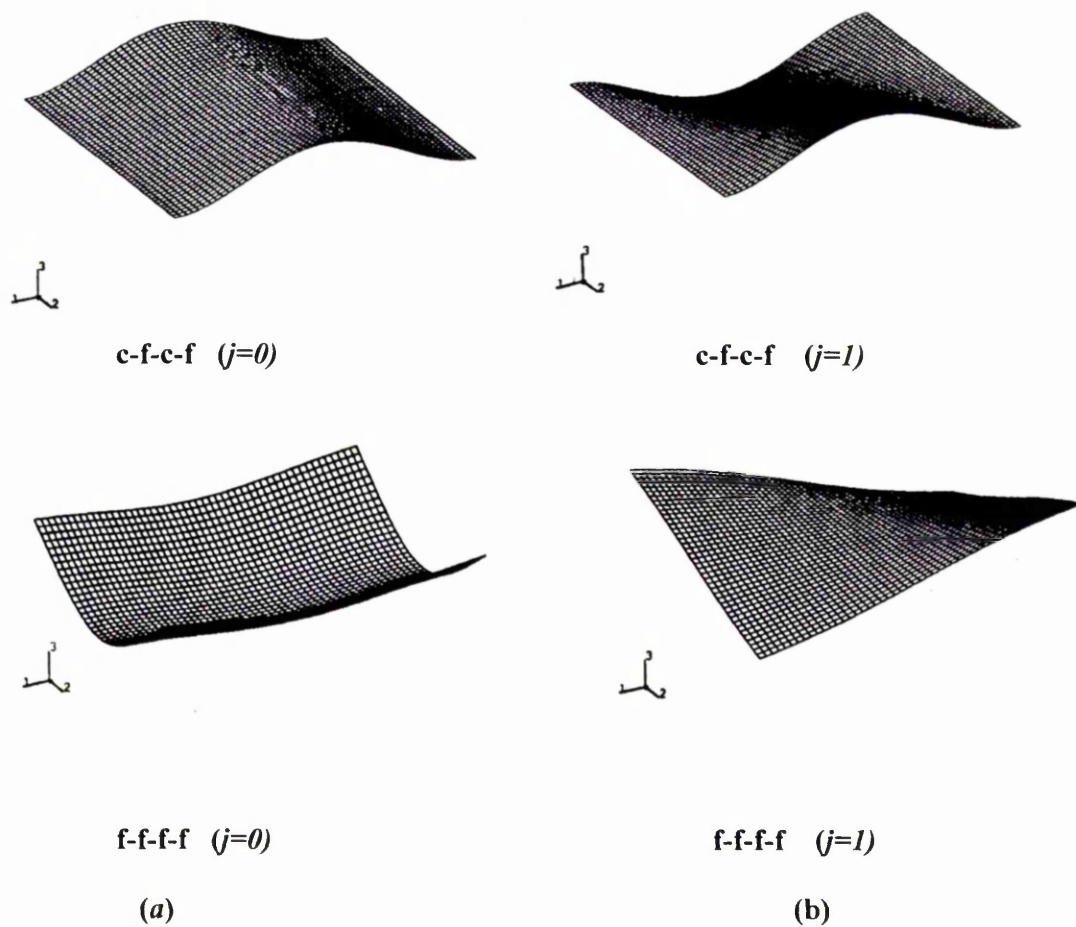


Figure 7.2 (a) symmetric mode shape (b) anti-symmetric mode shape.

for clamped-clamped (c-f-c-f) and free-free (f-f-f-f) beam-plate

7.3 Obtaining the transition curve from symmetric modes for free-free boundary condition

7.3.1 Deduction from frequency parameter charts

This section will investigate the transition curve from the frequency parameter charts, which are presented in Figures 7.3 to 7.7 that show the variation of the frequency parameters of the symmetric modes (λ_{sm}^2) with the symmetric mode counter (m) for aspect ratios of 0.25 to 20 for thickness to length ratio 1%. By examining these figures, it is possible to deduce for each curve, the symmetric mode counter (m) at which the curve shows a transition from being smooth to being zigzag or wavy. This is noted as the transition point for the curve.

From Figures 7.3 to 7.7, it is clearly seen that the graphs are zigzag wavy lines for small aspect ratios, but from aspect ratio 2.5 to 10 the figures show that the lines are smooth at the start and then become zigzag wavy lines. This is because as the mode counter m increases, different types of modes are traversed. The smooth parts of the line represent bending vibration, hence, beam behavior, the zigzag line represents plate behavior.

Figure 7.3 shows the variations of the frequency parameters of the symmetric modes λ_{sm}^2 with the lengthwise symmetric mode counter m for aspect ratios of 0.25 to 1.0. It is seen that all the curves are zigzag lines. Therefore, this represents plate-like behavior. The variation of the frequency parameters of the symmetric modes (λ_{sm}^2) with the symmetric mode counter (m) for aspect ratios of 1.25, 1.50, 2.00 and 2.50 is shown by Figure 7.4 when considering aspect ratio 2.50, Figure 7.4 shows that λ_{sm}^2 varies smoothly

with m as m increases from 1 to 3. This section of the curve exhibits beam-like behavior. However, at $m = 3$, there is a discontinuity in the curve. And as the value of m increases from 3 to 27 the curve become "zigzag". This part of the curve exhibits plate-like behavior. From this we can deduce that at $m = 3$ is the transition point from beam-like to plate-like behavior for ratio 2.50. This value of $m=3$ represents an upper bound for the transition point. A lower (conservative) bound for the transition point can be define at a value of $m=2$.

Figure 7.5 shows the variations of the frequency parameters of the symmetric modes λ_{sm}^2 with the lengthwise symmetric mode counter m for aspect ratios of 3.00 to 4.50. Considering aspect ratio of 3.00, the figure shows that λ_{sm}^2 varies smoothly with m as m increases from 1 to 4. The corresponding values of i, j are $(i, j) = (2, 0), (3, 0), (4, 0)$ and $(5, 0)$, while the mode types are B_{x2}, B_{x3}, B_{x4} and B_{x5} respectively where B_{xi} denotes the i^{th} bending mode along the x -axis of the beam. Thus, this section of the curve denotes beam-like behavior. But when $m = 4$, there is a discontinuity in the curve, followed by a "zigzag" variation of λ_{sm}^2 with m as m increases from 4 to 25. This part of the curve denotes plate-like behavior. Therefore, the transition point from beam-like to plate-like behavior for aspect ratio 3.0 occurs at $m = 4$ (upper bound) or $m = 3$ (lower bound). Similarly, for aspect ratios of 3.50, 4.00 and 4.50, the transition points are found to occur at $m = 5, m = 6$ and $m = 7$ (upper bound) or $m = 4, m = 5$ and $m = 6$ (lower bound) respectively.

In Figures 7.6 and 7.7 is seen the variations of the frequency parameters of the symmetric modes λ_{sm}^2 with the lengthwise symmetric mode counter m for aspect ratios 5.0 to 20.0. These figures show that for aspect ratios of between 5.0 and 10.0 (inclusive), the curve of variation of frequency parameters λ_{sm}^2 with m can be divided into 2 parts. In the

first part, when $1 \leq m \leq m_t$, where m_t is the value of m at the transition from beam-like to plate-like behavior, λ_{sm}^2 varies smoothly with m . This section of the curve denotes beam-like behavior. In the second part of the curve, when $m > m_t$, λ_{sm}^2 varies in a somewhat zigzag, wavy manner as m increases. This part of the curve denotes plate-like behaviour. From this we can deduce that the lower bound values of m at the transition point from beam-like to plate-like behavior are 7, 8, 9, 11, 12 and 14 for aspect ratios of 5.0, 6.0, 7.0, 8.0, 9.0 and 10.0 respectively, and the corresponding upper bound values of m are 8, 9, 10, 12, 13 and 15. Also it is important to notice from Figures 7.7 that there are no transition points for aspect ratios 15.0 and 20.0. This is because at these aspect ratios, the first 20 symmetric modes shown in these figures are bending modes of vibration.

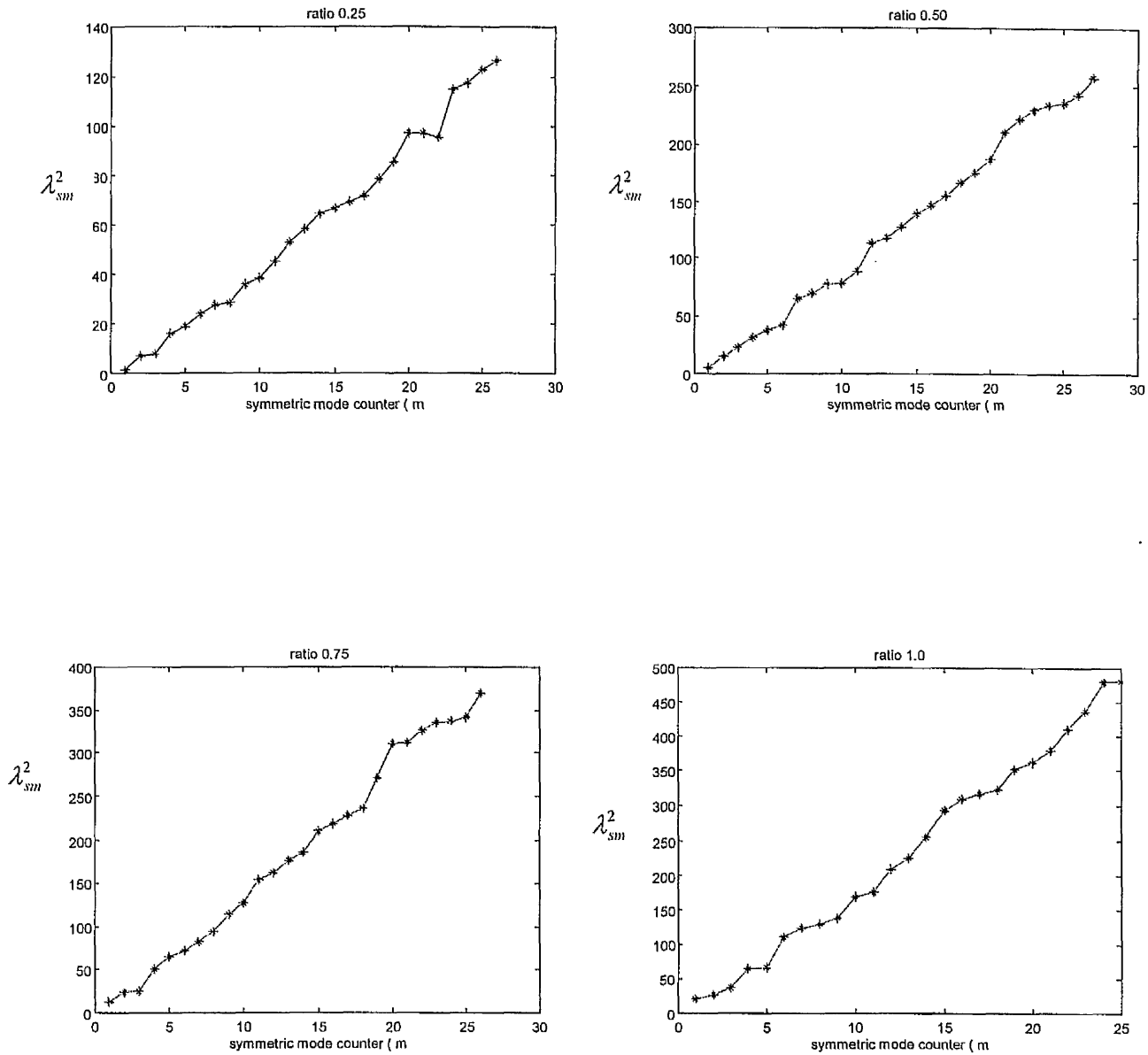


Figure 7.3 Variation of the frequency parameters of symmetric modes with symmetric mode counter (m) for ratio 0.25, 0.5, 0.75 and 1.0, for free-free beam-plate of thickness to length ratio 1%

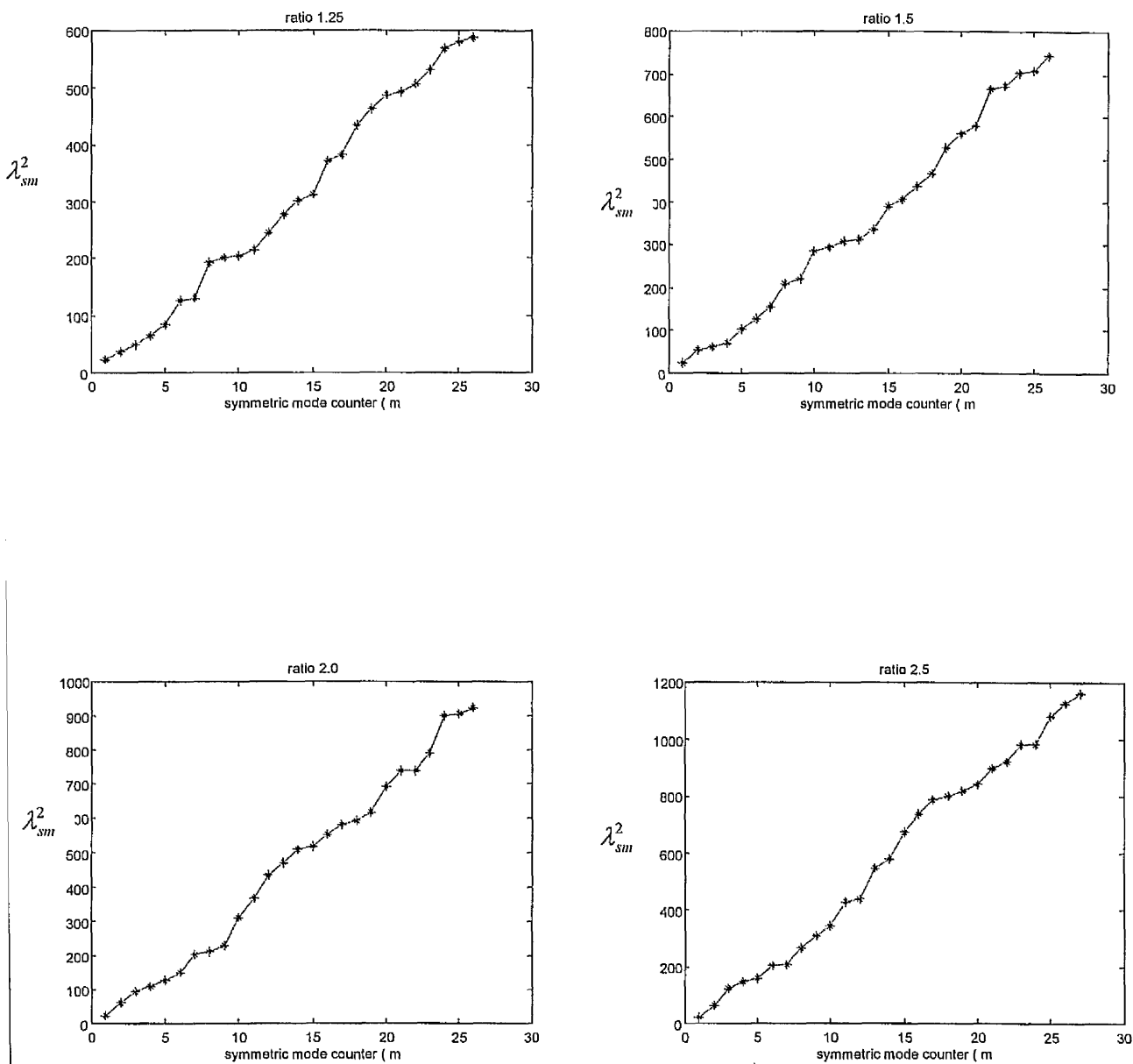
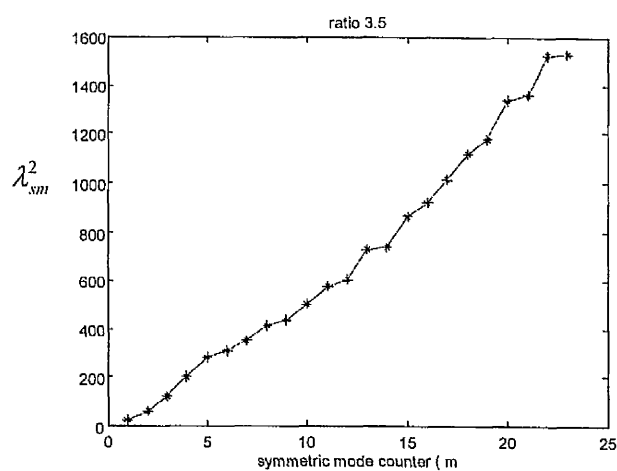
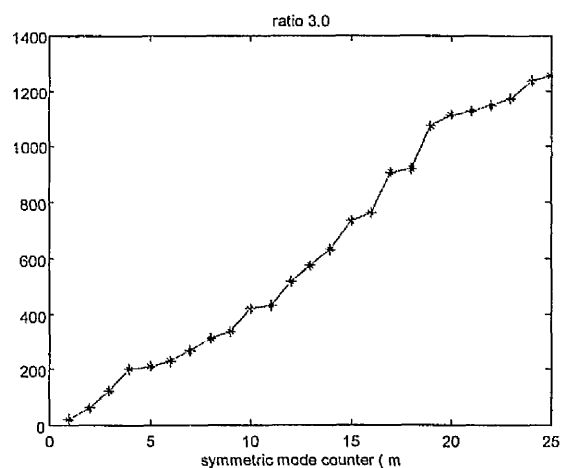


Figure 7.4 Variation of the frequency parameters of symmetric modes with symmetric mode counter (m) for ratio 1.25, 1.5, 2.0 and 2.5, for free-free beam-plate of thickness to length ratio 1%

2
SM



1
m

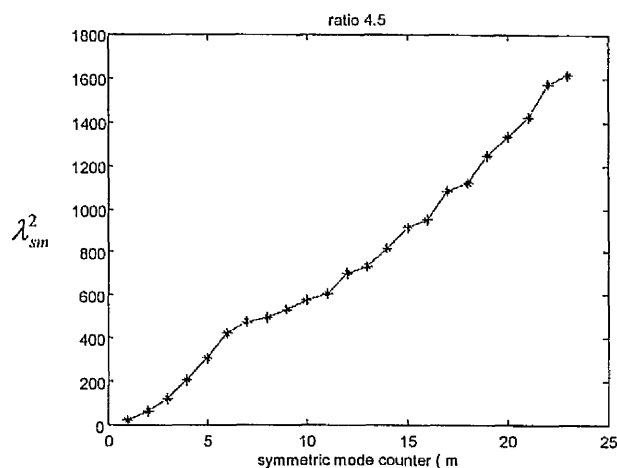
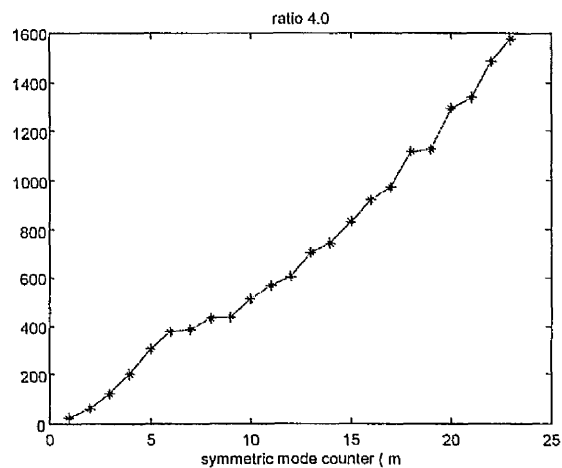


Figure 7.5 Variation of the frequency parameters of symmetric modes with symmetric mode counter (m) for ratio 3.0, 3.5, 4.0 and 4.5, for free-free beam-plate of thickness to length ratio 1%

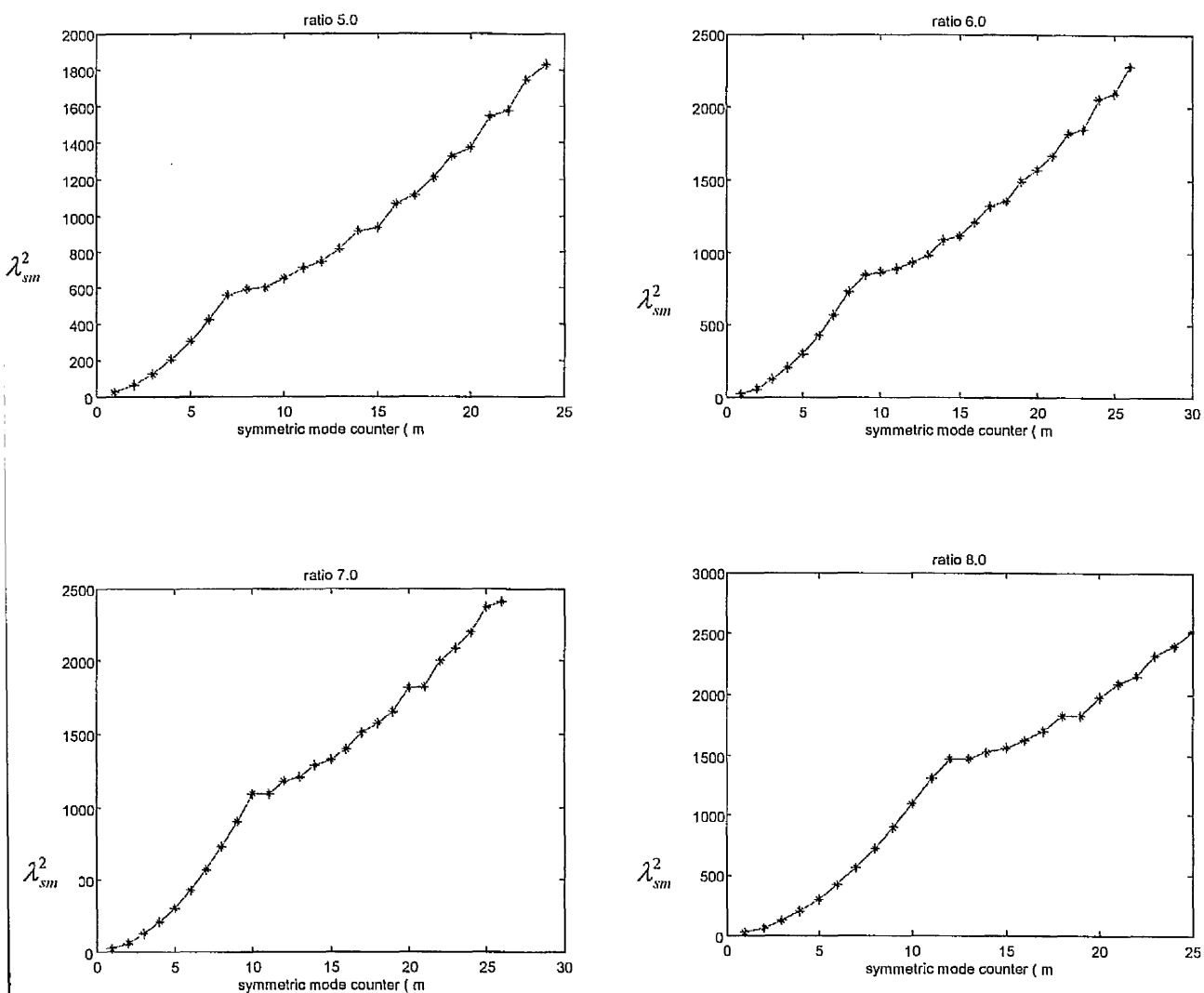


Figure 7.6 Variation of the frequency parameters of symmetric modes with symmetric mode counter (m) for ratio 5.0, 6.0, 7.0 and 8.0 for free-free beam-plate of thickness to length ratio 1%

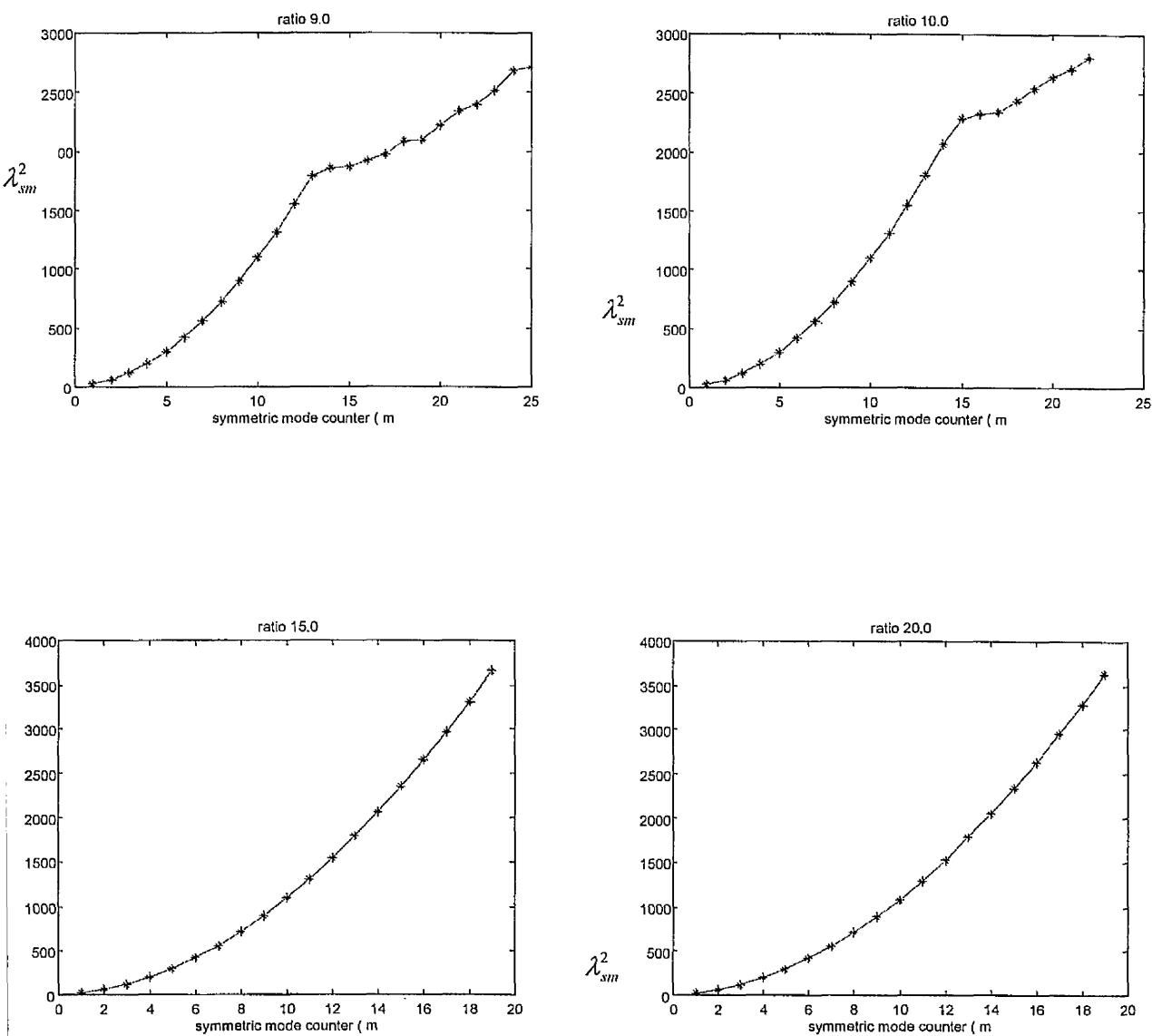


Figure 7.7 Variation of the frequency parameters of symmetric modes with symmetric mode counter (m) for ratio 9.0, 10, 15 and 20 for free-free beam-plate of thickness to length ratio 1%

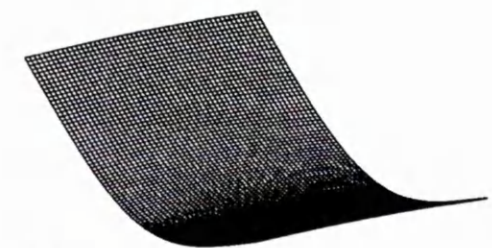
7.3.2 Deduction from mode shapes

The previous section has covered the study of the transition curves using the symmetric modes from the frequency parameter charts. This section is on the determination of the transition curves based on the mode shapes for selected aspect ratios. The procedure involves examination of the deformation of the breadthwise edges of the beam-plates, which are parallel to the y -axis (2-axis) or j direction at different modes of vibration. Modes of vibration for which these edges are straight are classed as beam behaviour, while modes for which these edges are significantly deformed are classed as plate behaviour. Figures 7.8 to 7.14 show the selected mode shape for aspect ratios 0.5, 1.25, 2.5, 3.0, 5.0, 10.0 and 20.0 respectively. By close examinations of these selected mode shapes, it can be seen from Figure 7.8, which represents aspect ratio 0.5 that the edge of the plate in the (j) direction is not a straight line for all the mode shapes. That is, there is considerable deformation in the j direction of the plate. This indicates a plate-like behavior. This deduction is confirmed from Figure 7.3, which shows a zigzag variation of the frequency parameters and indicates plate-like behavior. The same deductions apply for aspect ratio 1.25 as can be seen from Figure 7.9 and 7.4.

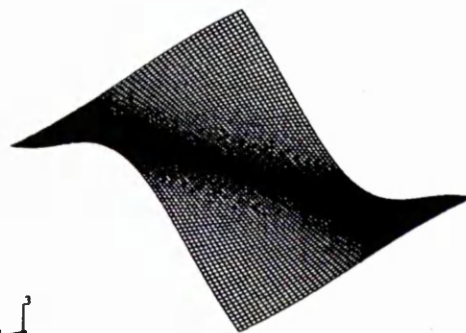
Selected mode shapes for aspect ratio 2.5 shown in Figure 7.10. The figure shows that for $m=1$ to $m=3$, the free breadthwise edges of the beam-plate are straight which indicates beam-like behaviour. However, the figure shows that for $m = 4$ to $m = 8$, the free breadthwise edges of the beam-plate is curved which indicate plate-like behavior. This statement also agrees with Figure 7.4 which shows that the data points corresponding to the first 3 modes lie on a smooth curve but when $m>3$ the modal points form a zigzag pattern

which indicates plate-like behavior. The selected mode shape for aspect ratio 3.0 is shown in Figure 7.11 the transition is at breadthwise edges, it is seen that the transition is at mode 4, which again agrees with the deductions from Figure 7.5.

Figure 7.12 shows selected symmetric mode shapes for aspect ratio 5.0. Which contain the transition mode shape at mode 7 again, this agrees with Figure 7.6. Figure 7.13 shows the mode shapes of 9 to 16 for aspect ratio 10. The first 5 modes in this figure represent beam behavior and at mode 14 and over the mode shapes represent plate-like behavior. This is also confirmed by Figure 7.7 which shows a smooth curve up to mode 15 and becomes a zigzag pattern for modes greater than 15. Finally, Figure 7.14 which represents the symmetric modes for aspect ratio 20, shows that there is no transition mode due to the fact that there is no deformation in the breadthwise direction of the beam-plate, that is, the edge of the beam is straight. This indicates beam-like behavior. Again, this agrees with deduction from Figure 7.7 which shows that the modal data points from a smooth curve and there is no transition point.



(a) mode 1



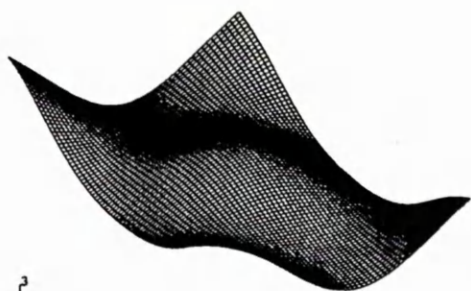
(b) mode 2



(c) mode 3



(d) mode 4



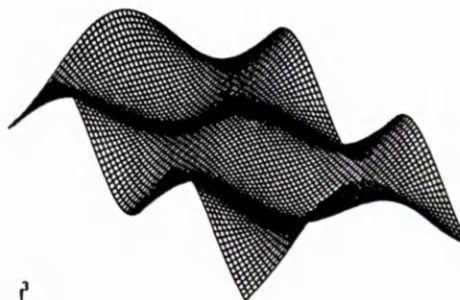
(e) mode 5



(f) mode 6

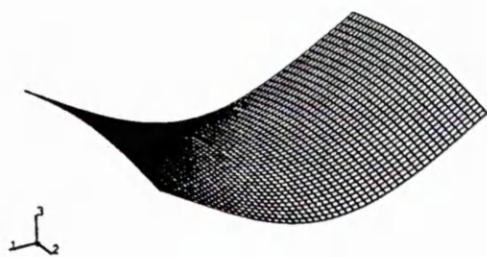


(g) mode 7



(h) mode 8

Figure 7.8 Symmetric mode shapes for aspect ratio 0.50, for free-free beam-plate thickness to length ratio 1%



(a) mode 1



(b) mode 2



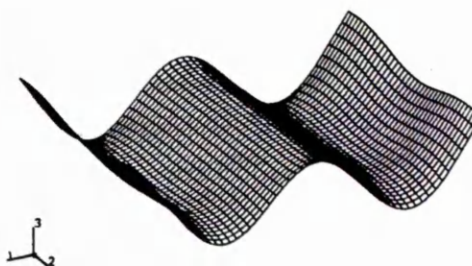
(c) mode 3



(d) mode 4



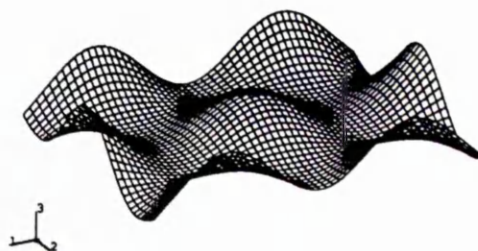
(e) mode 5



(f) mode 6



(g) mode 7

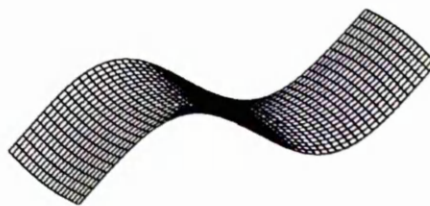


(h) mode 8

Figure 7.9 symmetric mode shapes for aspect ratio 1.25, for free-free beam-plate thickness to length ratio 1%



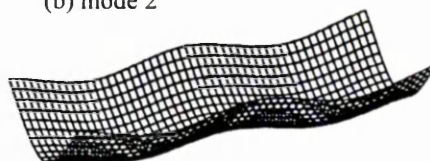
(a) mode 1



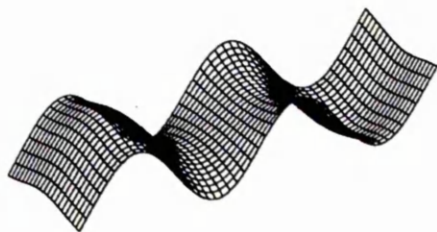
(b) mode 2



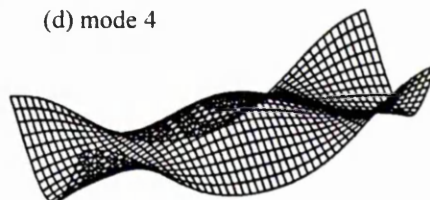
(c) mode 3



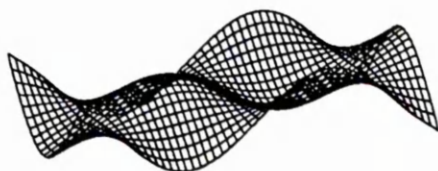
(d) mode 4



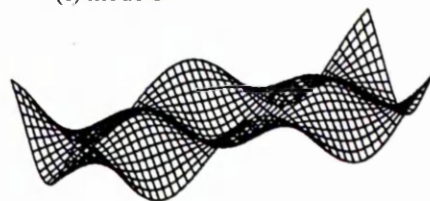
(e) mode 5



(f) mode 6



(g) mode 7

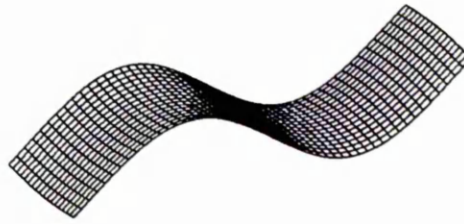


(h) mode 8

Figure 7.10 Symmetric mode shapes for aspect ratio 2.5, for free-free beam-plate thickness to length ratio 1%



(a) mode 1



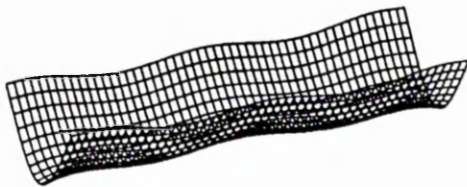
(b) mode 2



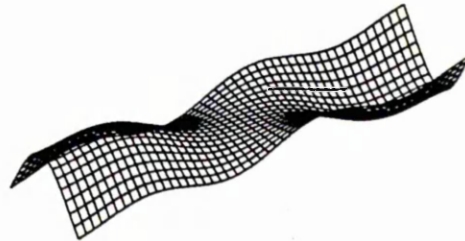
(c) mode 3



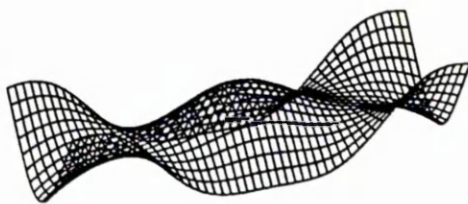
(d) mode 4



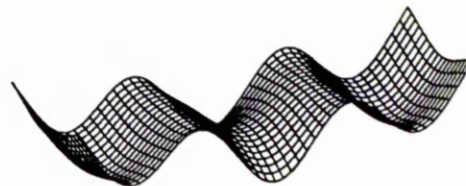
(e) mode 5



(f) mode 6



(g) mode 7

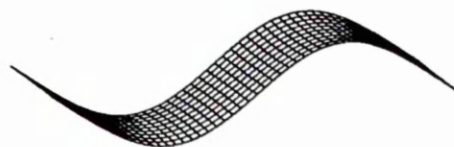


(h) mode 8

Figure 7.11 Symmetric mode shapes for aspect ratio 3.0, for free-free beam-plate thickness to length ratio 1%



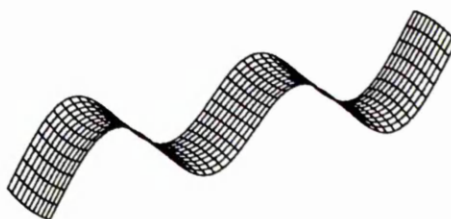
(a) mode 1



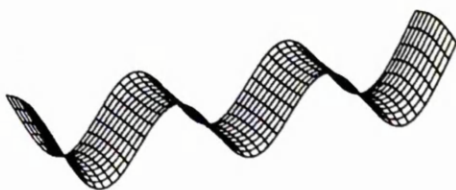
(b) mode 2



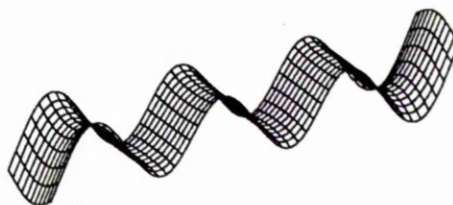
(c) mode 3



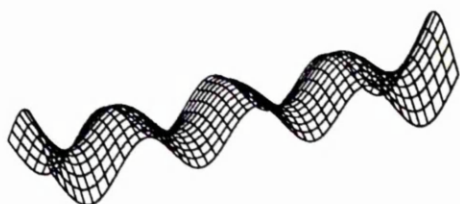
(d) mode 4



(e) mode 5



(f) mode 6



(g) mode 7



(h) mode 8

Figure 7.12 Symmetric mode shapes for aspect ratio 5.0, for free-free beam-plate thickness to length ratio 1%

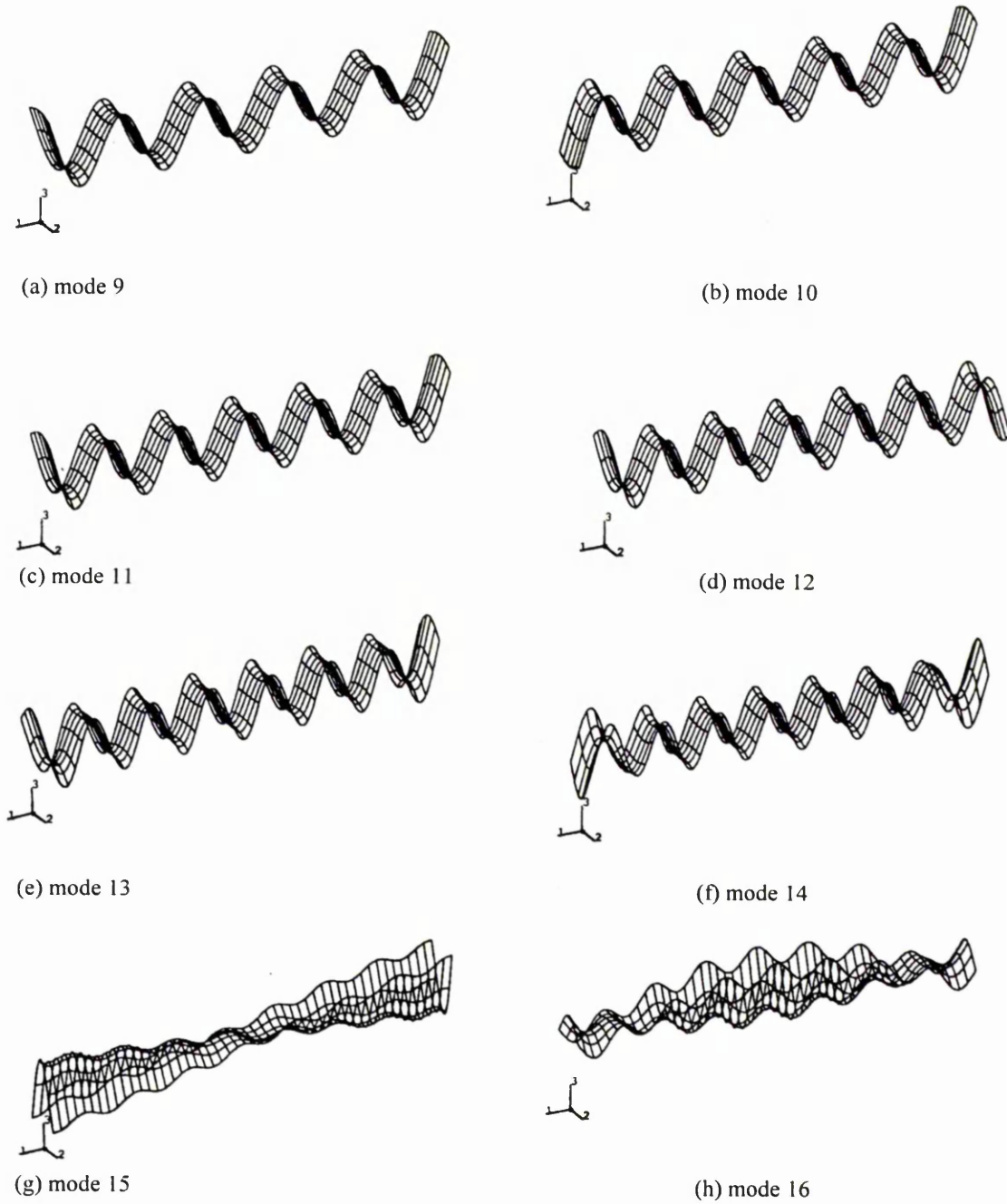
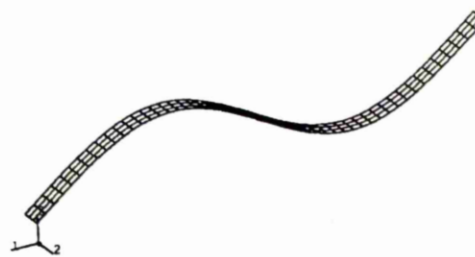


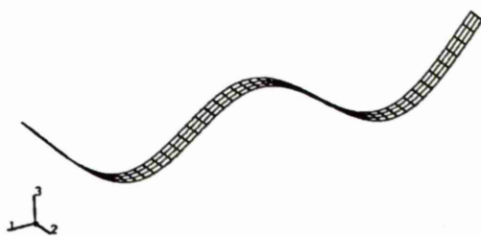
Figure 7.13 Symmetric mode shapes for aspect ratio 10.0, for free-free beam-plate thickness to length ratio 1%



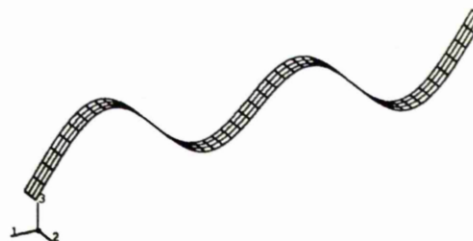
(a) mode 1



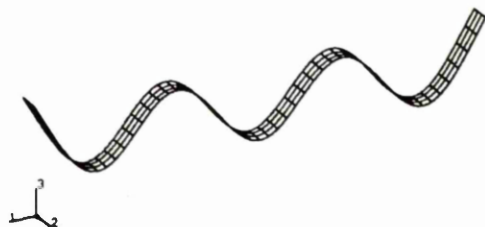
(b) mode 2



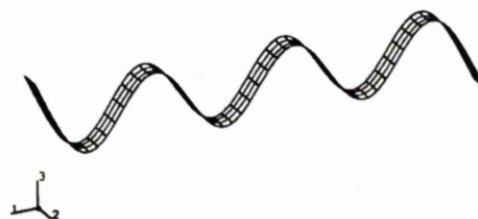
(c) mode 3



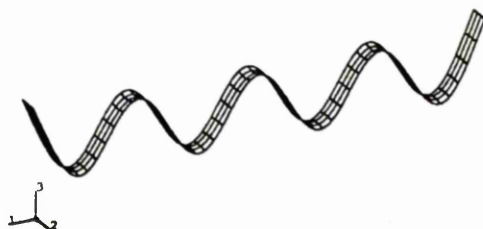
(d) mode 4



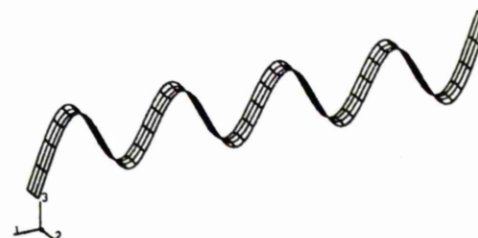
(e) mode 5



(f) mode 6



(g) mode 7



(h) mode 8

Figure 7.14 Symmetric mode shapes for aspect ratio 20.0, for free-free beam-plate thickness to length ratio 1%

7.3.3 Derivation of transition curves and equations for thickness to length ratio 1% free-free beam-plates

Table 7.1 shows the lower and upper bound values of m and λ_{sm}^2 at the transition points for all the aspect ratios considered. By using the linear least-square method, the lower bound values of the frequency parameters of the symmetric modes and the symmetric mode counter at the transition from beam-like to plate-like behaviour can be represented by the following equation:

$$\lambda_{ll}^2 = 11.42 m_{ll}^2 - 9.97 m_{ll} + 30.21 \quad (7.1)$$

Similarly, the upper bound values can be expressed as

$$\lambda_{lu}^2 = 9.69 m_{lu}^2 - 0.55 m_{lu} + 12.18 \quad (7.2)$$

Also, the values of the symmetric mode counter at the lower and upper transition points can be related to the aspect ratio, by equations which are derived using the least squares method, as follows:

$$m_{ll} = 1.39 r - 0.61 \text{ (lower bound)} \quad (7.3)$$

$$m_{lu} = 1.40 r + 0.17 \text{ (upper bound)} \quad (7.4)$$

Equations (7.1) and (7.2) show the equations for the two transition curves in Figure 7.15 which represent the variations of the limiting values of the frequency parameters of the symmetric modes with the symmetric mode counters at the lower and upper transition points. The comparison between the lower and upper bound values of the symmetric mode counters predicted by Equations (7.3) and (7.4) are shown in Figure 7.16. It is seen that the 2 sets of curves are close. When applying these equations, it is better to use Equations (7.1) and (7.3) which provide conservative (lower bound) estimates of the transition values of frequency parameter and number of pure bending modes that occur before plate-like behaviour for a particular aspect ratio. For example,

for a beam-plate structure of aspect ratio 5.5, which has not been investigated, Equations (7.1) and (7.3) can be used to obtain conservative estimates of $m_t = 6$ and $\lambda_t = 398.86$. This implies that the first six symmetric modes of this structure are one-dimensional beam bending modes. Therefore, the one-dimensional wave equations for the transverse vibrations of beams can be used to analyze these six symmetric modes.

Table 7.1 *Mode counter and frequency parameter of symmetric modes at transition points deduced from frequency parameter charts*

Aspect ratio	Lower bound values		Upper bound values	
	Mode counter	λ_{sm}^2	Mode counter	λ_{sm}^2
2.50	2	59.10	3	115.20
3.00	3	116.13	4	189.28
3.50	4	192.10	5	266.71
4.00	5	286.53	6	355.82
4.50	6	398.86	7	448.29
5.00	7	526.00	8	560.41
6.00	8	682.10	9	796.64
7.00	9	851.44	10	1030.82
8.00	11	1238.60	12	1384.50
9.00	12	1461.20	13	1684.50
10.00	14	1950.20	15	2162.30

Figure 7.17 shows the variation of the frequency parameters of the symmetric modes with the symmetric mode counter m for all the aspect ratios. This combined graph shows the curve OA , which represents the boundary region between beam-like and plate-like behaviour. However, all points on the curve OA denote beam-like behaviour

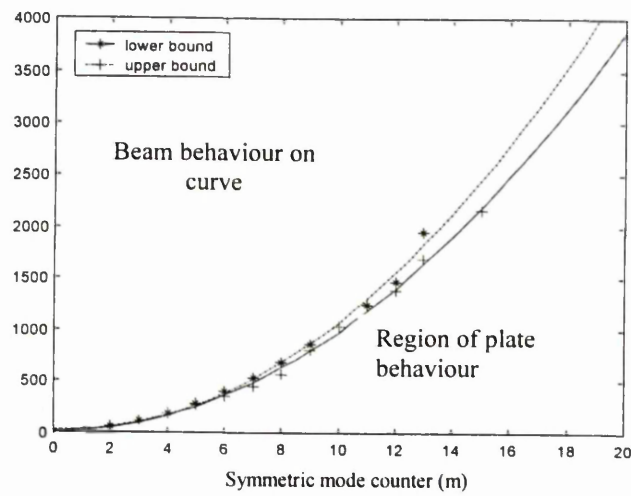
λ_{sm}^2 

Figure 7.15 Variation of frequency parameter of symmetric modes with symmetric mode counter, for free-free beam-plates of thickness to length ratio 1%

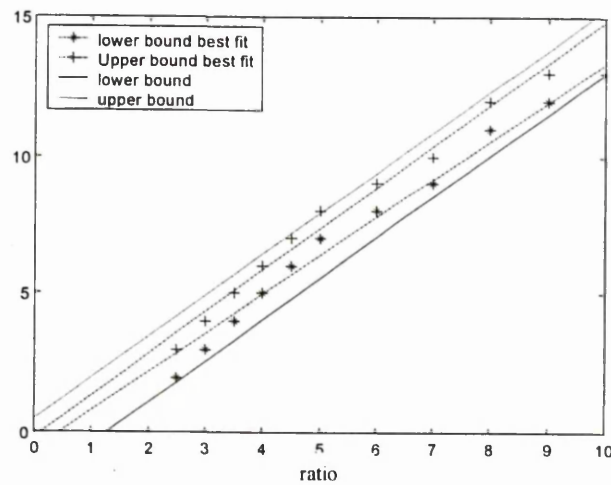
 m 

Figure 7.16 Variation of symmetric mode counter at transition point with aspect ratio, for free-free beam-plate thickness to length ratio 1%

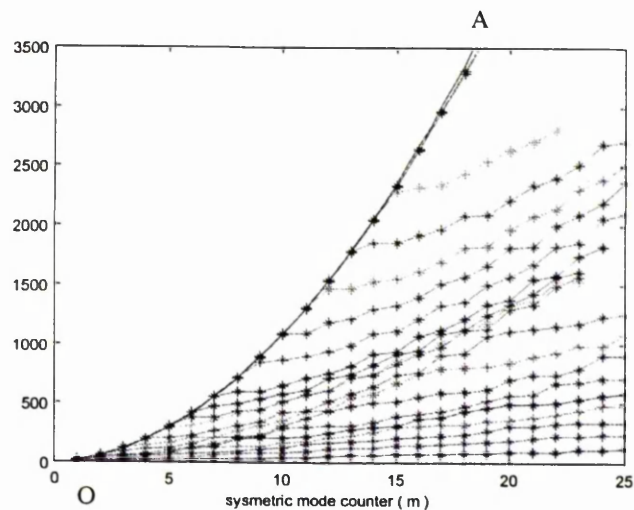
 λ_{sm}^2 

Figure 7.17 Variation of the frequency parameters of symmetric modes with symmetric mode counter (m) for aspect ratio 0.25 to 20.00, for free-free beam-plates of thickness to length ratio 1%

This curve is to be used to calculate the frequency parameters for beam-like behaviour only. The right region of the curve is a region of plate-like behaviour where it is necessary to use finite element analysis to calculate the frequency parameters.

Based on the least squares method, an equation can be derived from the points which lie on the beam-like behaviour curve OA as:

$$\lambda_{sm}^2 = (75.89 - 11.75r + 0.364r^2) + (-51.367 + 10.728r - 0.372r^2)m + (15.178 - 0.886r + 0.0284r^2)m^2 \quad (7.5)$$

where

λ_{sm}^2 = frequency parameters of symmetric modes

r = aspect ratio

m = symmetric mode counter

7.3.4 Obtaining the transition curve from symmetric modes for free-free boundary condition for other thickness to length ratio

All the work presented early in this chapter was for 1% thickness to length ratio beam-plates. In addition beam-plates of thickness to length ratios 2%, 5% and 10% were also considered. The transition points, transition curves and transition equation were derived for each of these thickness to length ratios as was done for the 1% thickness to length ratio beam-plates. The results are presented in the following Tables 7.2 to 7.4, and Figures 7.18 to 7.26.

Transition points, curves and equations for 2% thickness to length ratio beam-plate

Table 7.2 *Mode counter and frequency parameter of symmetric modes at transition points for 2% thickness to length ratio beam-plates.*

Aspect ratio	Lower bound values		Upper bound values	
	Mode counter	λ_{sm}^2	Mode counter	λ_{sm}^2
2.50	2	58.87	3	113.94
3.00	3	115.33	4	187.14
3.50	4	190.02	5	262.88
4.00	5	282.09	6	349.40
4.50	5	382.70	6	390.53
5.00	6	392.38	7	511.86
6.00	8	659.56	9	765.83
7.00	9	817.57	10	981.75
8.00	10	988.98	11	1170.74
9.00	12	1370.22	13	1564.35
10.00	13	1580.29	14	1797.63

The transition equations, corresponding to transition curves shown in Figure 7.18, are

$$\lambda_{II}^2 = 7.684 m_{II}^2 + 24.057 m_{II} - 26.017 \quad (7.6)$$

$$\lambda_{III}^2 = 7.99 m_{III}^2 + 18.342 m_{III} - 19.805 \quad (7.7)$$

The symmetric mode counter equations (corresponding to Figure 7.19)

$$m_{II} = 1.446r - 1.214 \quad (\text{lower bound}) \quad (7.8)$$

$$m_{III} = 1.446r - 0.214 \quad (\text{upper bound}) \quad (7.9)$$

$$\lambda_{sm}^2 = (5.401 - 0.871r - 0.0579r^2) + (10.629 + 0.372r - 0.0298r^2)m + (9.109 - 0.0866r + 0.008r^2)m^2 \quad (7.10)$$

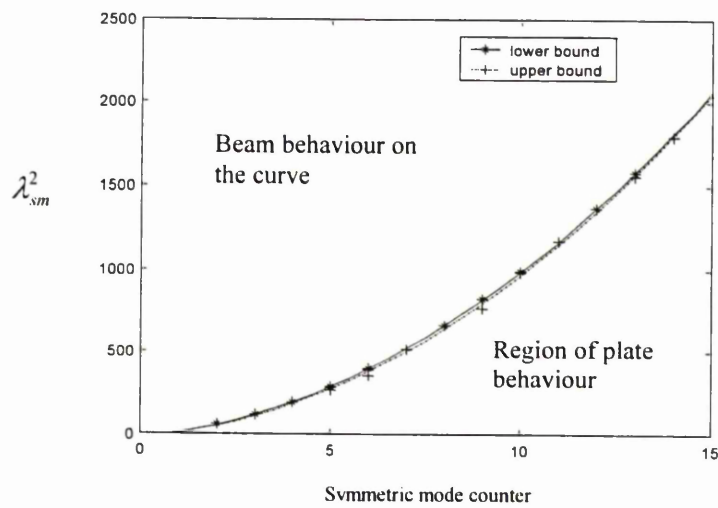


Figure 7.18 Variation of frequency parameter of symmetric modes with symmetric mode counter at transition point for 2% thickness to length ratio free-free beam-plates.

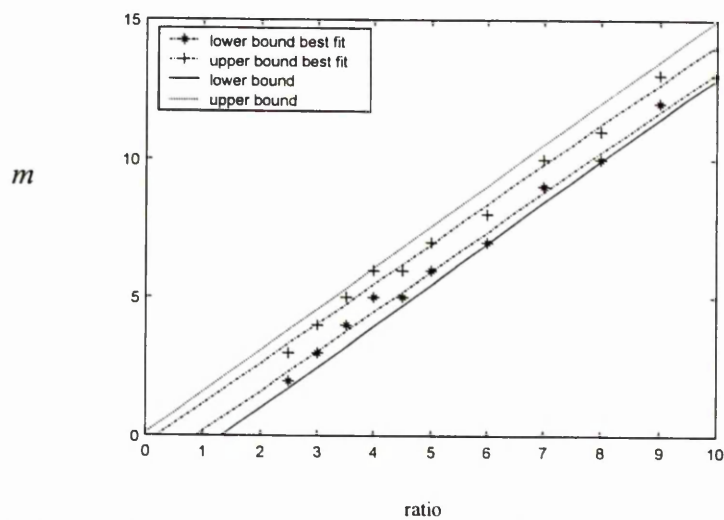


Figure 7.19 Variation of symmetric mode counter at transition point with aspect ratio for 2% thickness to length ratio free-free beam-plates.

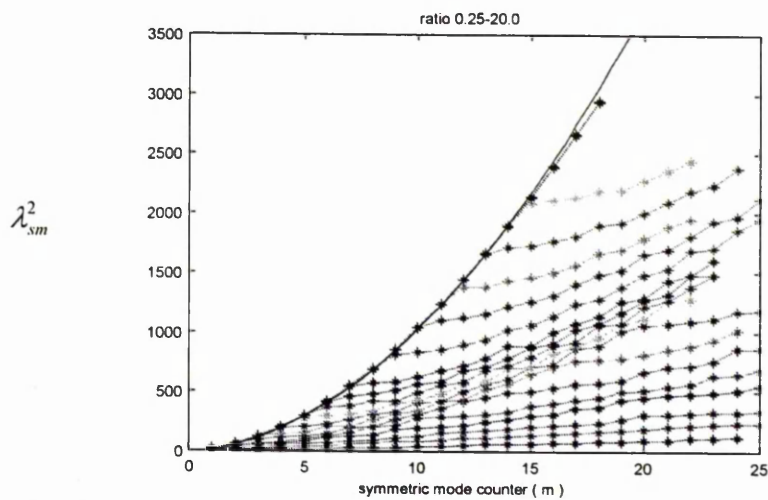


Figure 7.20 Variation of the frequency parameters of symmetric modes with symmetric mode counter (m) for aspect ratio 0.25 to 20.00, for free-free beam-plates of thickness to length ratio 2%.

Transition points, curves and equations for 5% thickness to length ratio beam-plate

Table 7.3 Mode counter and frequency parameter of symmetric modes at transition points for 5% thickness to length ratio beam-plates.

Aspect ratio	Lower bound values		Upper bound values	
	Mode counter	λ_{sm}^2	Mode counter	λ_{sm}^2
2.50	2	57.53	3	109.55
3.00	3	110.40	4	174.72
3.50	4	177.34	5	241.38
4.00	4	177.42	5	255.88
4.50	5	256.41	6	343.64
5.00	6	345.12	7	437.41
6.00	8	544.23	9	628.14
7.00	9	653.23	10	761.74
8.00	11	879.55	12	974.25
9.00	12	998.93	13	1113.75
10.00	14	1239.87	15	1351.58

The transition equations, corresponding to transition curves shown in Figure 7.21

$$\lambda_{ll}^2 = 2.917 m_{ll}^2 + 54.158 m_{ll} - 78.292 \quad (7.11)$$

$$\lambda_{lm}^2 = 2.536 m_{lm}^2 + 59.721 m_{lm} - 104.749 \quad (7.12)$$

The symmetric mode counter equations (corresponding to Figure 7.22)

$$m_{ll} = 1.576r - 1.866 \quad (\text{lower bound}) \quad (7.13)$$

$$m_{lm} = 1.576r - 0.866 \quad (\text{upper bound}) \quad (7.14)$$

$$\lambda_{sm}^2 = (16.423 - 7.817r - 0.184r^2) + (9.151 + 4.554r - 0.116r^2)m + (7.116 - 0.469r + 0.0127r^2)m^2 \quad (7.15)$$

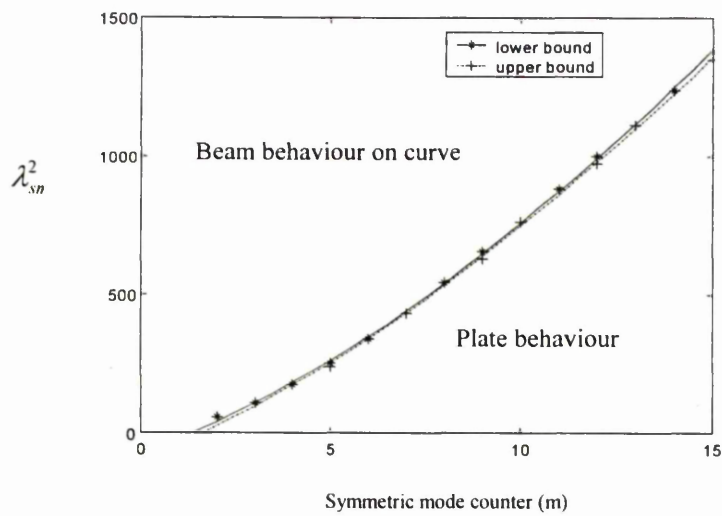


Figure 7.21 Variation of frequency parameter of symmetric modes with symmetric mode counter at transition point for 5% thickness to length ratio free-free beam-plates.

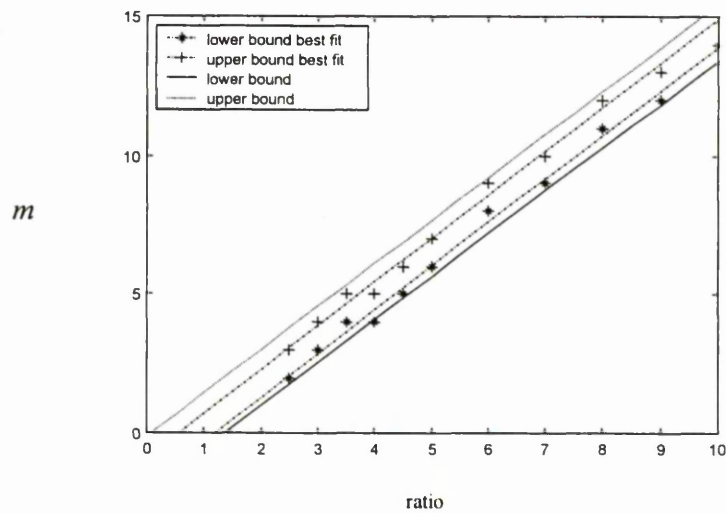


Figure 7.22 Variation of symmetric mode counter at transition point with aspect ratio for 5% thickness to length ratio free-free beam-plates.

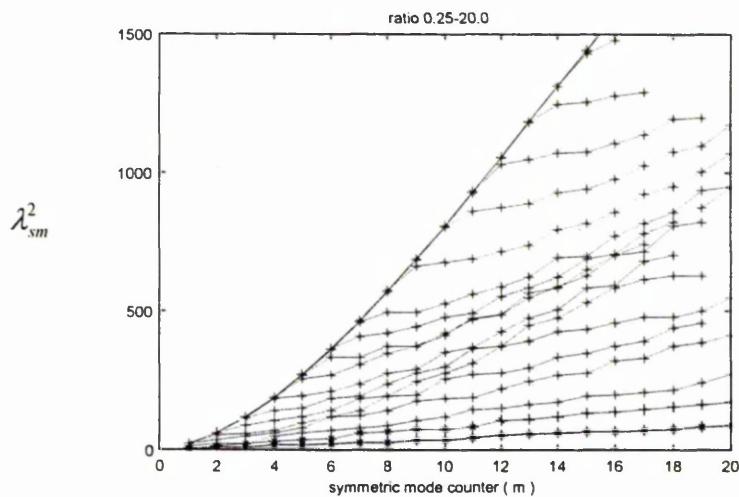


Figure 7.23 Variation of the frequency parameters of symmetric modes with symmetric mode counter (m) for aspect ratio 0.25 to 20.00 for 5% thickness to length ratio free-free beam-plates.

Transition points, curves and equations for 10% thickness to length ratio beam-plate

Table 7.4 Mode counter and frequency parameter of symmetric modes at transition points for 10% thickness to length ratio beams-plates.

Aspect Ratio	Lower bound values		Upper bound values	
	Mode counter	λ_{sm}^2	Mode counter	λ_{sm}^2
2.50	2	53.52	3	96.77
3.00	3	97.48	4	146.39
3.50	4	148.35	5	195.80
4.00	4	148.47	5	203.33
4.50	5	203.78	6	260.56
5.00	6	261.57	7	318.55
6.00	8	380.24	9	433.81
7.00	10	498.52	11	545.26
8.00	11	557.50	12	609.33

The transition equations, corresponding to transition curves shown in Figure 7.24

$$\lambda_{ll}^2 = 0.796 m_{ll}^2 + 46.487 m_{ll} - 47.312 \quad (7.16)$$

$$\lambda_{lu}^2 = 0.324 m_{lu}^2 + 52.392 m_{lu} - 66.928 \quad (7.17)$$

The symmetric mode counter equations (corresponding to Figure 7.25)

$$m_{ll} = 1.684 r - 2.255 \quad (\text{lower bound}) \quad (7.18)$$

$$m_{lu} = 1.684 r - 1.255 \quad (\text{upper bound}) \quad (7.19)$$

$$\lambda_{sm}^2 = (22.820 - 9.477 r - 0.218 r^2) + (7.107 + 6.015 r - 0.156 r^2) m + (4.851 - 0.637 r + 0.0178 r^2) m^2 \quad (7.20)$$

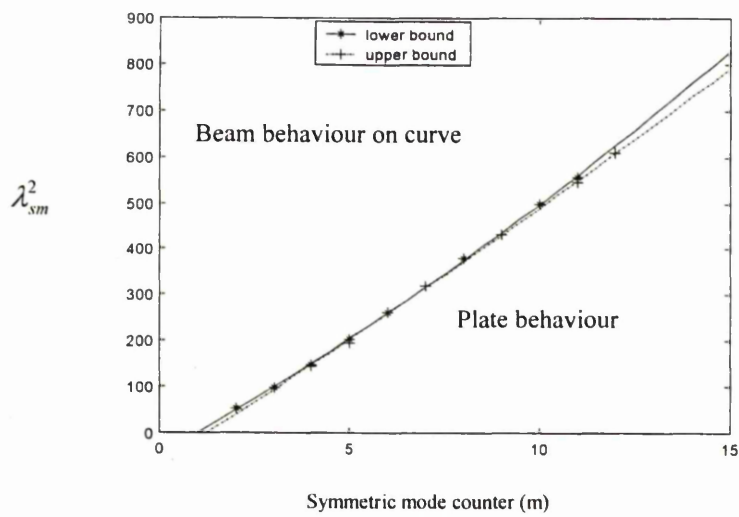


Figure 7.24 Variation of frequency parameter of symmetric modes with symmetric mode counter at transition point for 10% thickness to length ratio free-free beam-plates

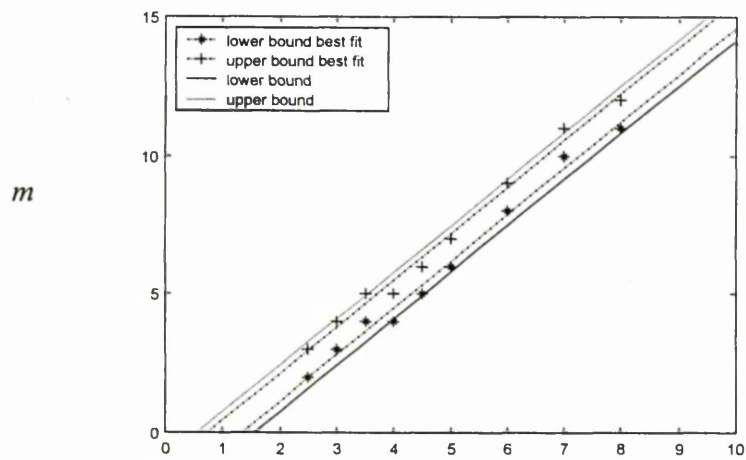


Figure 7.25 Variation of symmetric mode counter at transition point with aspect ratio for 10% thickness to length ratio free-free beam-plates.

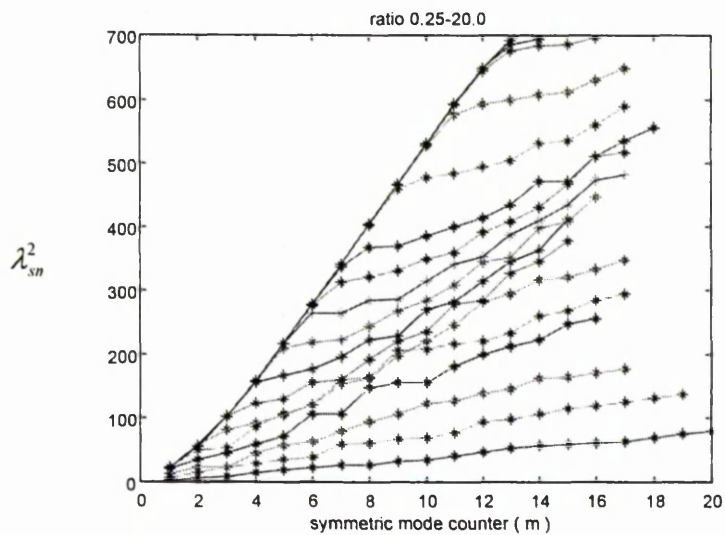


Figure 7.26 Variation of the frequency parameters of symmetric modes with symmetric mode counter (m) for aspect ratio 0.25 to 20.00 for 10% thickness to length ratio free-free beam-

7.4 Obtaining the transition curve from symmetric modes for clamped-clamped boundary condition

7.4.1 Deduction from frequency parameter charts

Figures 7.27 to 7.31 show the relationship between the frequency parameters of symmetric modes (λ_{sm}^2) and symmetric mode counter (m) for all aspect ratios examined in this work for clamped-clamped beam-plates of thickness to length ratio 1%. A similar approach as in the case of free-free beam-plates is adopted in obtaining the transition curve for 1% thick to length ratio clamped-clamped beam-plates. From Figures 7.27 to 7.31 it is clearly seen that the graphs are zigzag wavy lines for small aspect ratios but for aspect ratios 2.5 to 10, the figures show that the lines are smooth at the start and subsequently they become zigzag wavy lines. Therefore, a transition zone between beam-like and plate-like behavior can be found from the symmetric mode data for clamped-clamped beam-plates.

Figure 7.27 shows the variations of the frequency parameters of the symmetric modes λ_{sm}^2 with the lengthwise symmetric mode counter m for aspect ratios of 0.25 to 1.0. It is seen that all the curves are zigzag lines. Therefore, this represents plate-like behavior. The variation of the frequency parameters of the symmetric modes (λ_{sm}^2) with the symmetric mode counter (m) for aspect ratios of 1.25, 1.50, 2.00 and 2.50 is shown by Figure 7.28. When considering aspect ratio 2.50, Figure 7.28 shows that λ_{sm}^2 varies smoothly with m as m increases from 1 to 3. This section of the curve exhibits beam-like behavior. However, at $m = 3$, there is a discontinuity in the curve. And as the value of m

increases from 3 to 29 the curve becomes "zigzag. This part of the curve exhibits plate-like behavior. From this we can deduce that at $m = 3$ is the transition point from beam-like to plate-like behavior for ratio 2.50. This value of $m=3$ represents an upper bound for the transition point. A lower (conservative) bound for the transition point can be defined at a value of $m=2$.

Figure 7.29 shows the variations of the frequency parameters of the symmetric modes λ_{sm}^2 with the lengthwise symmetric mode counter m for aspect ratios of 3.00 to 4.50. Considering aspect ratio of 3.00, the figure shows that λ_{sm}^2 varies smoothly with m as m increases from 1 to 4. The corresponding values of i, j are $(i, j) = (2, 0), (3, 0), (4, 0)$ and $(5, 0)$, while the mode types are B_{x2}, B_{x3}, B_{x4} and B_{x5} respectively where B_{xi} denotes the i^{th} bending mode along the x -axis of the beam. Thus, this section of the curve denotes beam-like behavior. But when $m = 4$, there is a discontinuity in the curve, followed by a "zigzag" variation of λ_{sm}^2 with m as m increases from 4 to 27. This part of the curve denotes plate-like behavior. Therefore, the transition point from beam-like to plate-like behavior for aspect ratio 3.0 occurs at $m = 4$ (upper bound) or $m = 3$ (lower bound). Similarly, for aspect ratios of 3.50, 4.00 and 4.50, the transition points are found to occur at $m = 5, m = 6$ and $m = 7$ (upper bound) or $m = 4, m = 5$ and $m = 6$ (lower bound) respectively.

In Figures 7.30 and 7.31 is seen the variations of the frequency parameters of the symmetric modes λ_{sm}^2 with the lengthwise symmetric mode counter m for aspect ratios 5.0 to 20.0. These figures show that for aspect ratios of between 5.0 and 10.0 (inclusive), the curve of variation of frequency parameters λ_{sm}^2 with m can be divided into 2 parts. In the first part, when $1 \leq m \leq m_t$ where m_t is the value of m at the transition from beam-like to

plate-like behavior, λ_{sm}^2 varies smoothly with m . This section of the curve denotes beam-like behavior. In the second part of the curve, when $m > m_t$, λ_{sm}^2 varies in a somewhat zigzag, wavy manner as m increases. This part of the curve denotes plate-like behaviour. From this we can deduce that the lower bound values of m at the transition point from beam-like to plate-like behavior are 6, 7, 9, 11, 12 and 14 for aspect ratios of 5.0, 6.0, 7.0, 8.0, 9.0 and 10.0 respectively, and the corresponding upper bound values of m are 7, 8, 10, 12, 13 and 15. Also it is important to notice that from Figures 7.31 that there are no transition points for aspect ratios 15.0 and 20.0. This is because at these aspect ratios, the first 20 symmetric modes shown in these figures are bending modes of vibration.

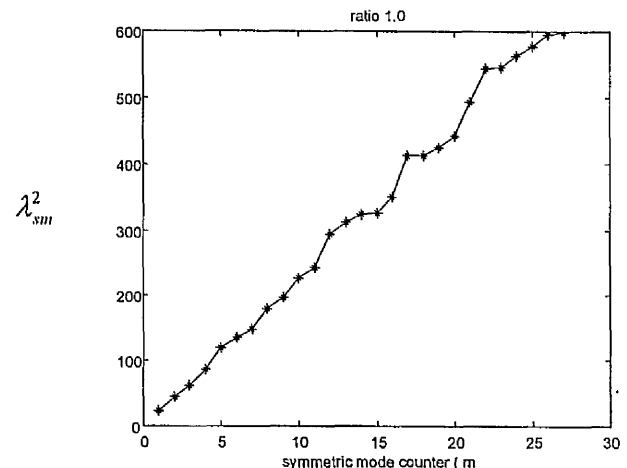
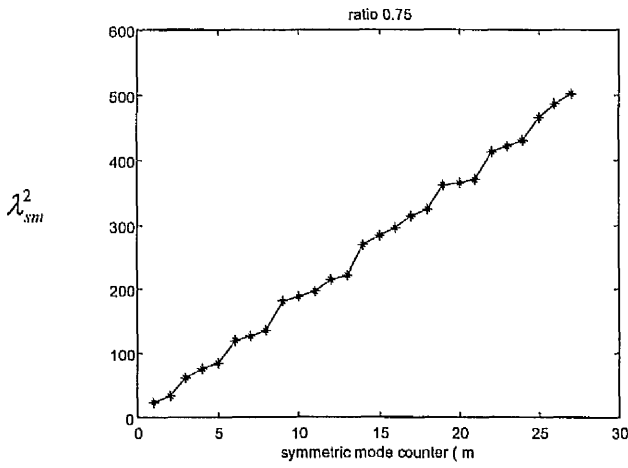
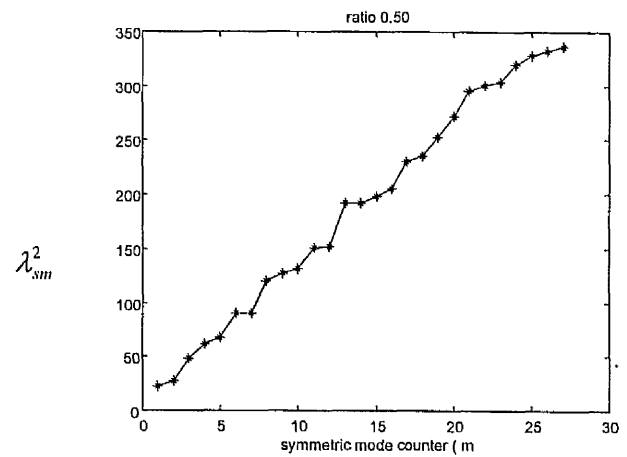
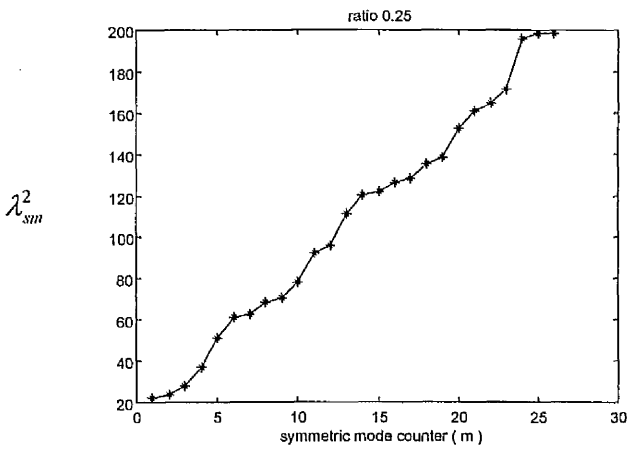


Figure 7.27 Variation of the frequency parameters of symmetric modes with symmetric mode counter (m) for ratio 0.25, 0.5, 0.75 and 1.0 for 1% thickness to length ratio clamped-clamped beams and plates.

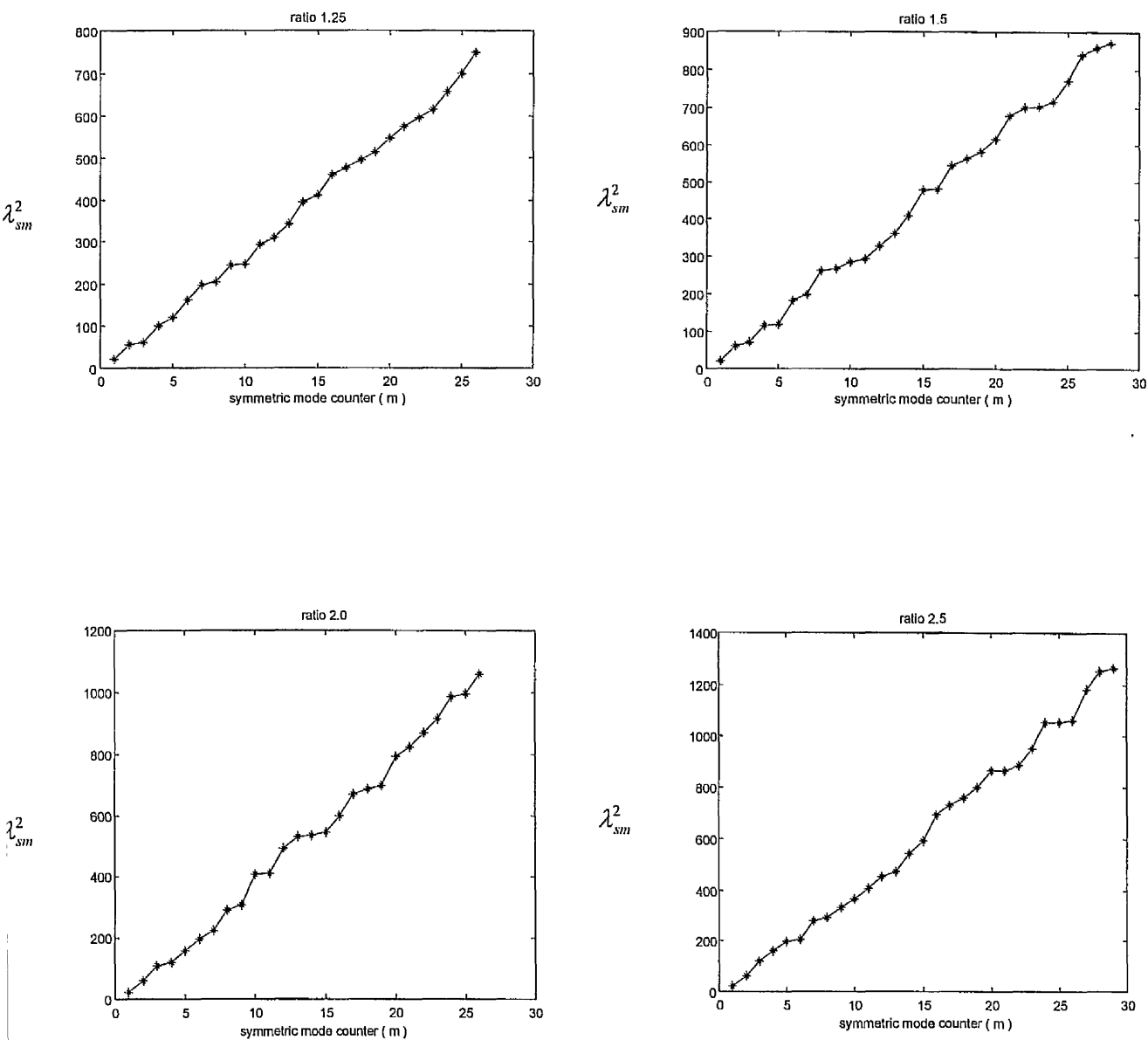


Figure 7.28 Variation of the frequency parameters of symmetric modes with symmetric mode counter (m) for ratio 1.25, 1.5, 2.0 and 2.5 for 1% thickness to length ratio clamped-clamped beams and plates.

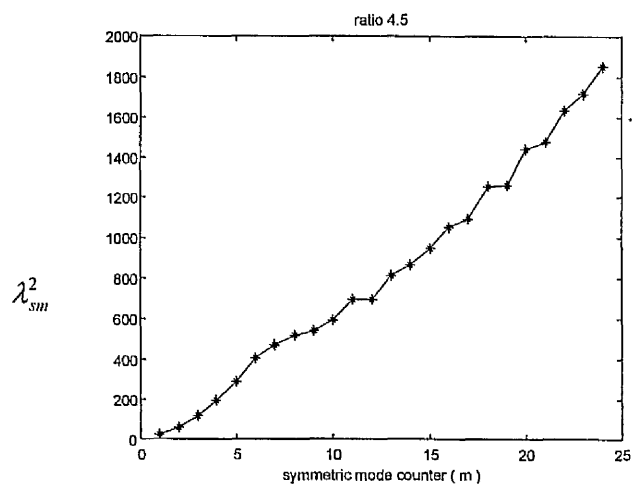
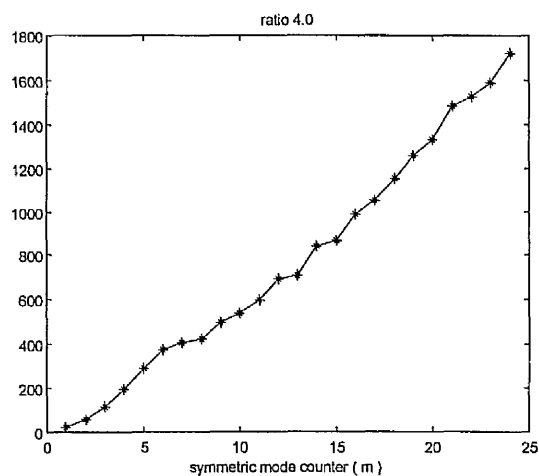
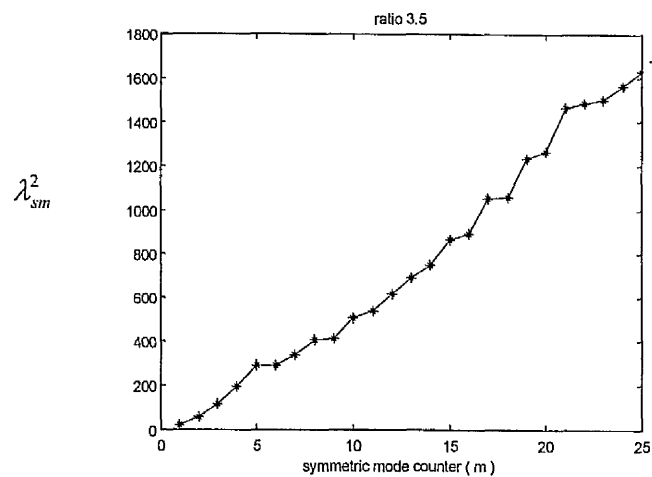
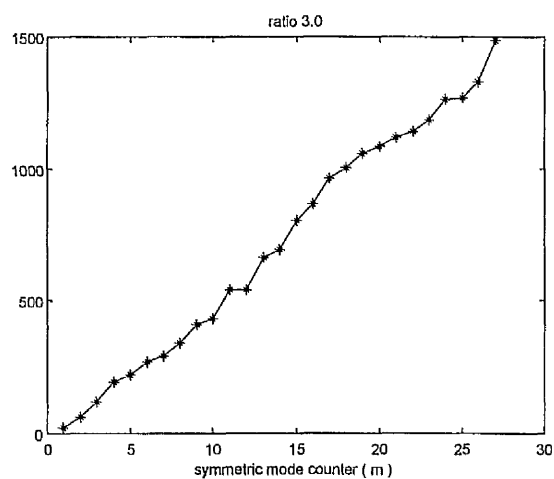


Figure 7.29 Variation of the frequency parameters of symmetric modes with symmetric mode counter (m) for ratio 3.0, 3.5, 4.0 and 4.5 for 1% thickness to length ratio clamped-clamped beams and plates.

2
sm

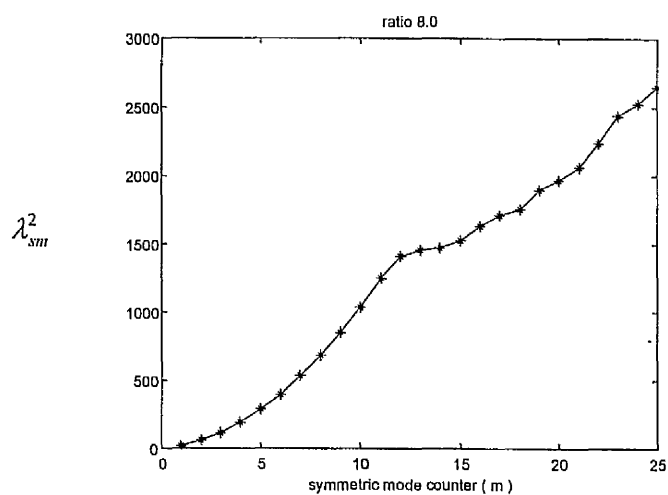
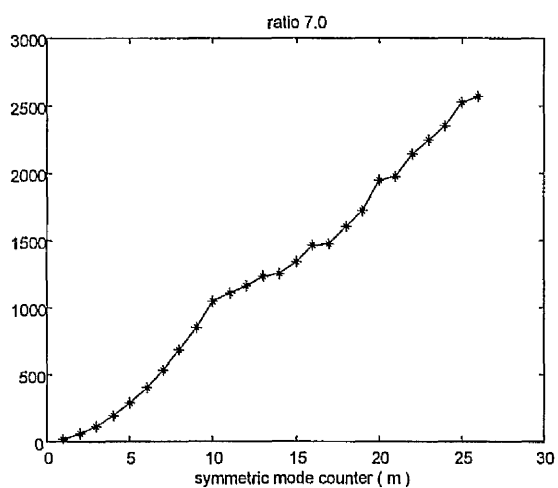
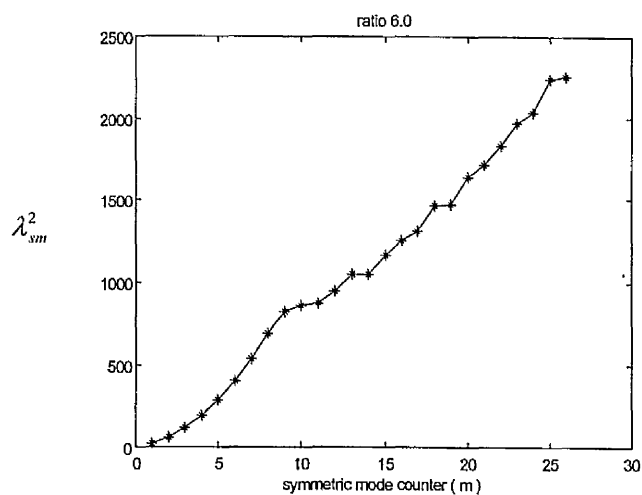
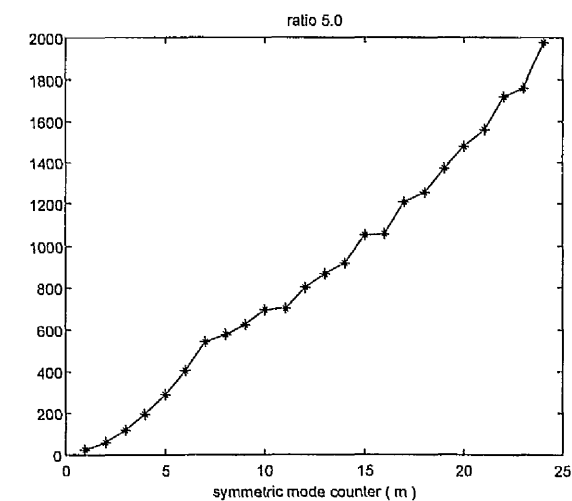


Figure 7.30 Variation of the frequency parameters of symmetric modes with symmetric mode counter (m) for ratio 5.0,6.0,7.0 and 8.0 for 1% thickness to length ratio clamped-clamped beams and plates.

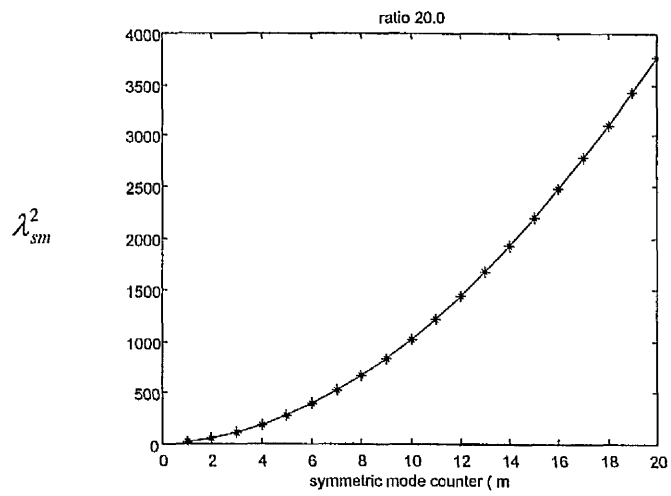
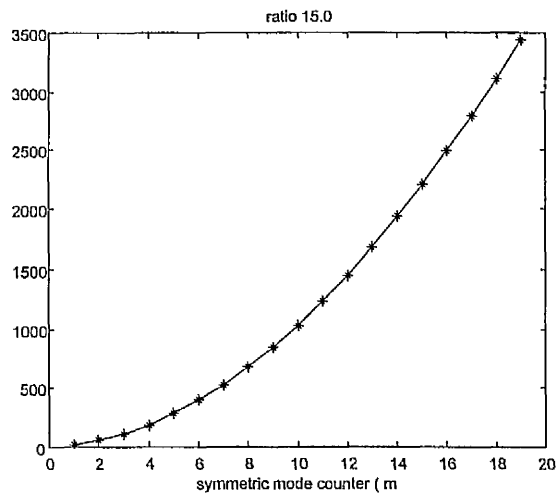
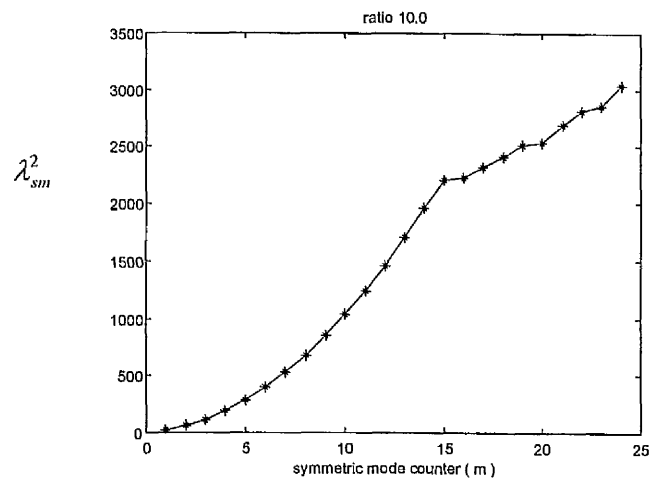
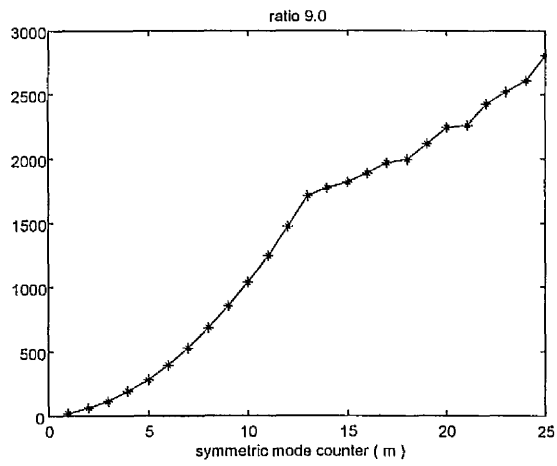


Figure 7.31 Variation of the frequency parameters of symmetric modes with symmetric mode counter (m) for ratio 9.0, 10, 15 and 20.0 for 1% thickness to length ratio clamped-clamped beams and plates.

7.4.2 Deduction from mode shapes

This section is on determination of transition curves from the mode shapes of the clamped-clamped beam-plates. Figures 7.32 to 7.38 show the selected mode shapes for aspect ratios 0.50, 1.25, 2.5, 3.0, 5.0, 10.0 and 20.0 respectively. On examining these mode shapes, transition points can be deduced.

Figure 7.32 shows that for aspect ratio 0.50, there is considerable deformation in the j direction of the plate, which indicates plate-like behavior. This deduction is confirmed from Figure 7.27 which a zigzag variation of the frequency parameters and indicates plate-like behavior. The same deduction applies to aspect ratio 1.25 as can be seen from Figures 7.33 and 7.28.

The next set of selected mode shapes are for aspect ratio 2.5 which are shown in Figure 7.34. The figure shows that for $m=1$ to $m=3$, there is no significant deformation in the breadthwise (j) direction. This indicates beam-like behaviour. However, the figure shows that for $m = 4$ to $m = 8$, there is significant deformation in the breadthwise (j) direction which indicates plate-like behavior. These observations also agree with Figure 7.28 which shows that the data points corresponding to the first 3 modes lie on a smooth curve but when $m>3$ the modal points form a zigzag pattern which indicates plate-like behavior.

The selected mode shapes for aspect ratio 3 are shown in Figure 7.35. This figure shows that for $m = 4$ to $m = 8$, there is deformation in the breadthwise (j) direction which indicates plate-like behavior. It is seen that the transition is at mode 4, which again agrees with Figure 7.29.

Figure 7.36 shows selected symmetric mode shapes for aspect ratio 5.0. This figure shows the mode shapes of modes 1 to 8. It is seen that there is significant deformation in the breadthwise (j) direction from modes 5 to 8. Therefore, mode 5 appears to be a transition point. Figure 7.30 actually shows that the transition point is more likely at mode 7.

Figure 7.37 shows the mode shapes of modes 8 to 15 for aspect ratio 10.0. The first 4 modes in this figure represent beam-like behavior. From mode 12 and over, there is significant deformation in the breadthwise (j) direction of the beam-plates which indicates plate-like behavior. On the other hand a transition point at mode 14. Therefore, mode 12 represents the lower transition point whereas mode 14 represents the upper transition point. Finally, Figure 7.38 shows the symmetric mode shapes for aspect ratio 20. The figure indicates that there is no transition mode due to the fact that there is no deformation in the breadthwise (j) direction. This suggests beam-like behavior. Again this is in agreement with the deduction from Figure 7.31.

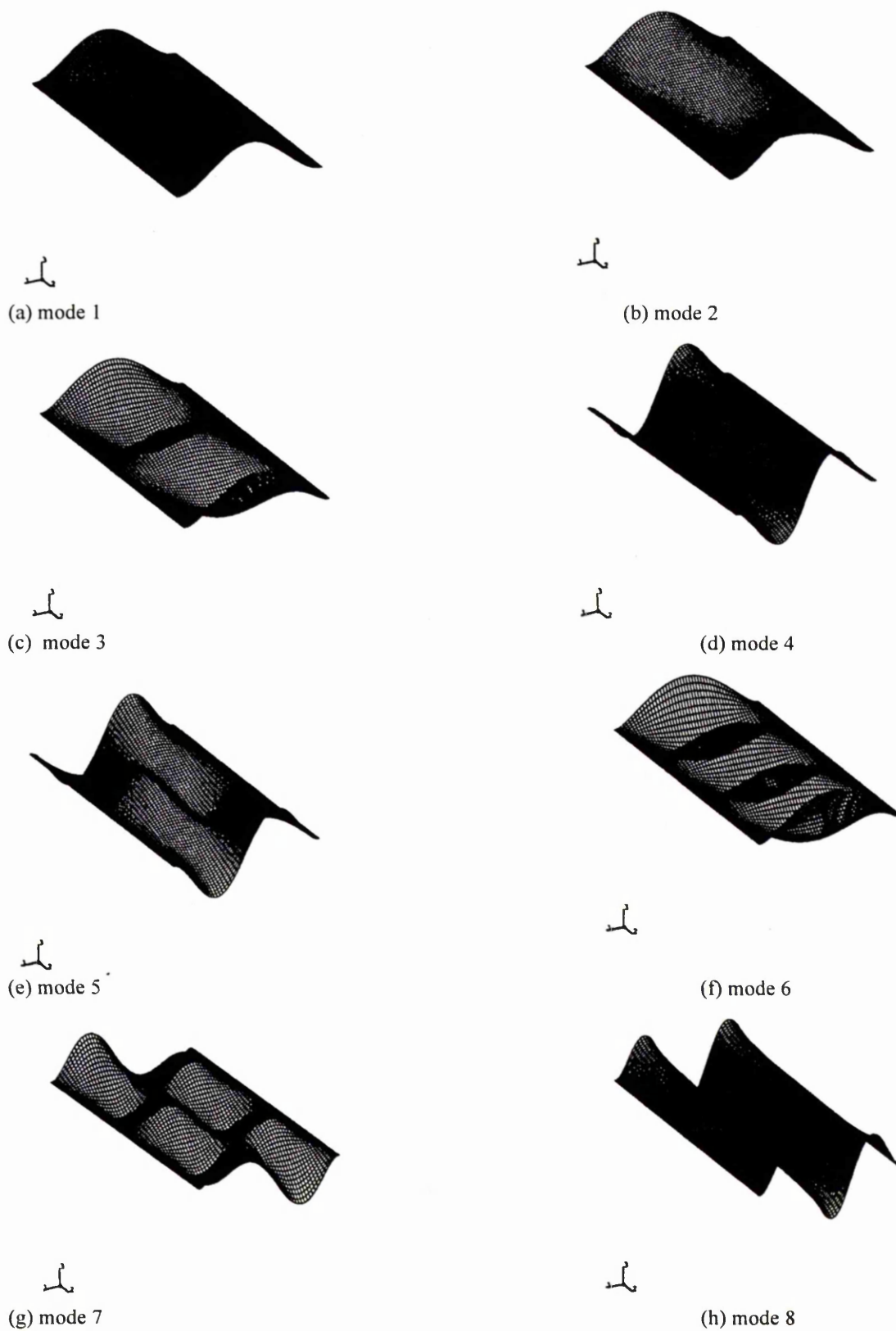


Figure 7.32 Symmetric mode shape for aspect ratio 0.50, for clamped-clamped beam-plate of 1% thickness to length ratio

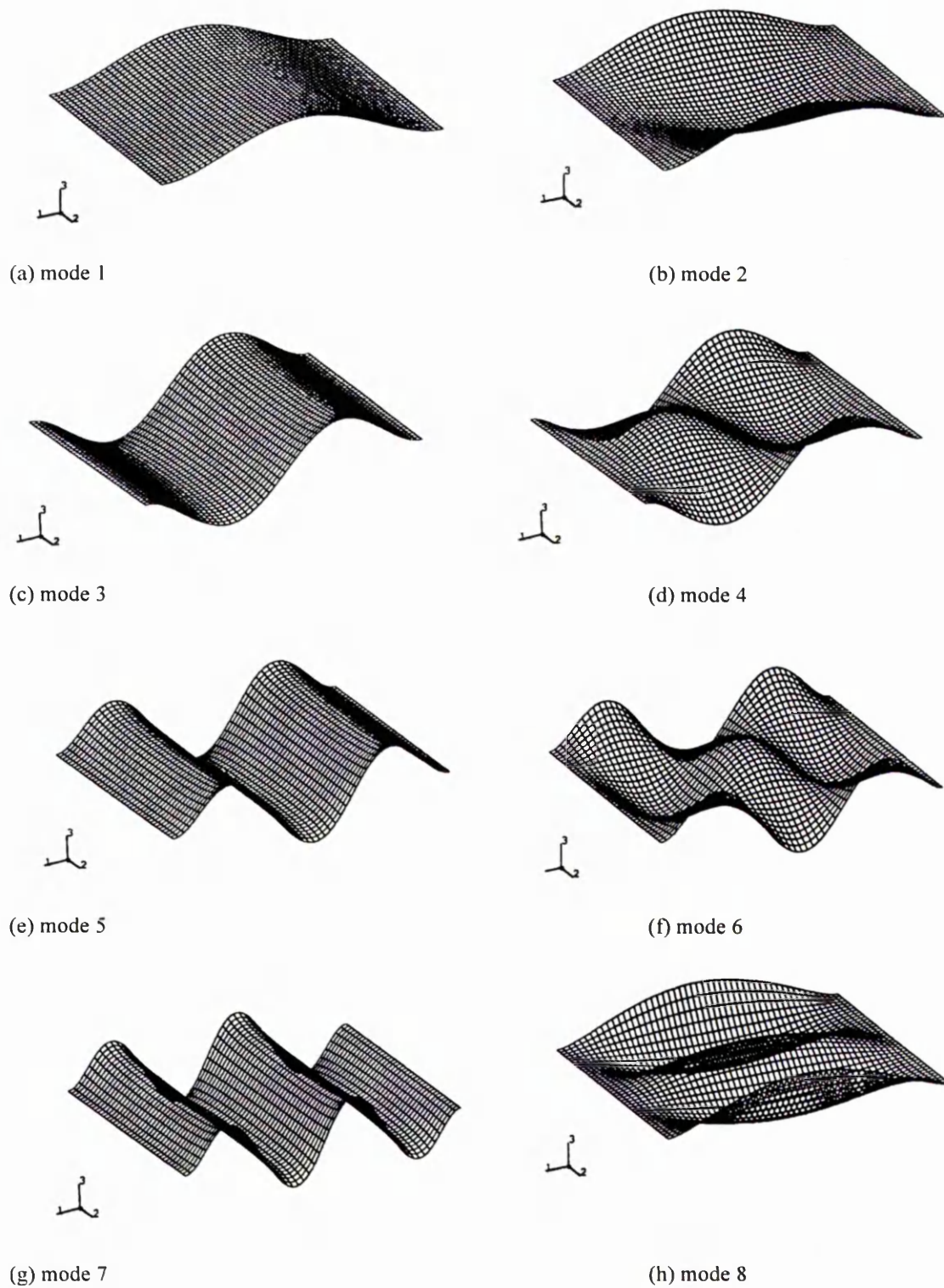


Figure 7.33 Symmetric mode shape for aspect ratio 1.25, for clamped-clamped beam-plate of 1% thickness to length ratio

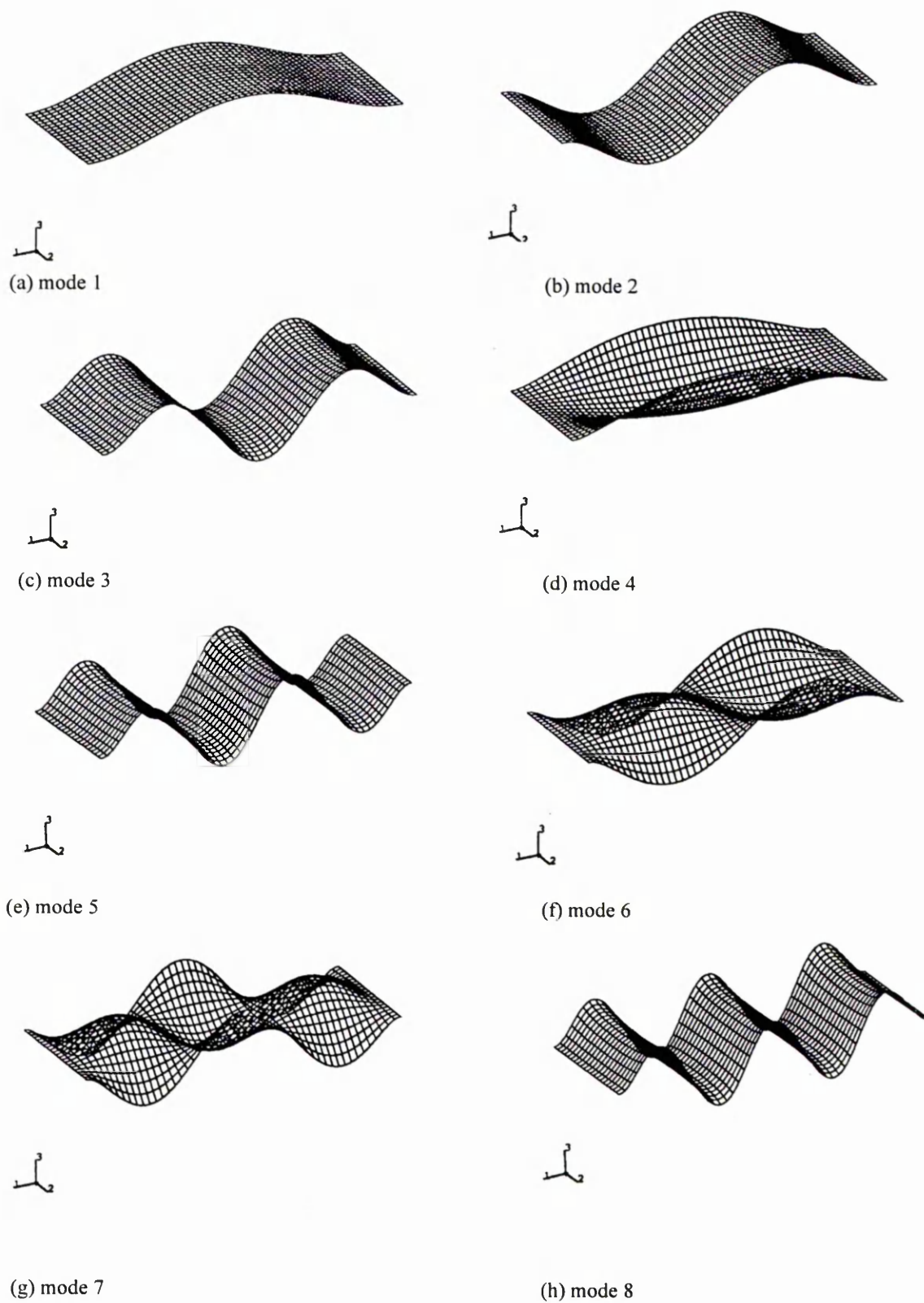
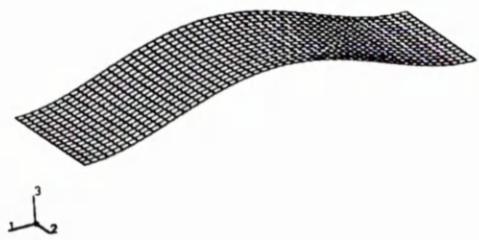
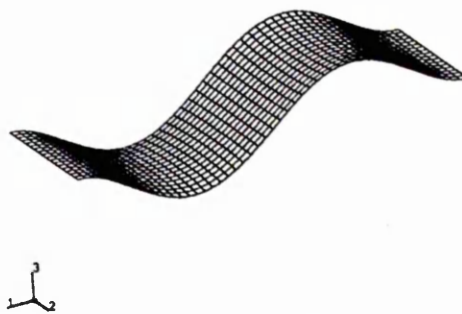


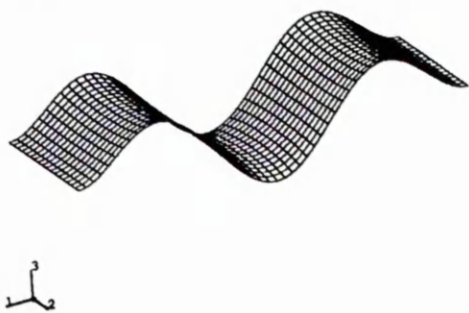
Figure 7.34 Symmetric mode shape for aspect ratio 2.5, for clamped-clamped beam-plate of 1% thickness to length ratio



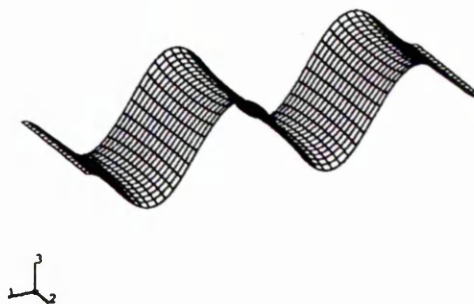
(a) mode 1



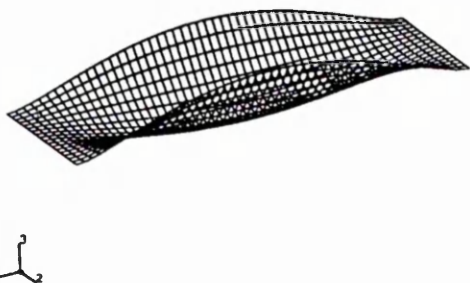
(b) mode 2



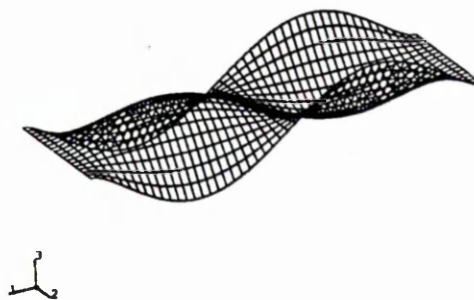
(c) mode 3



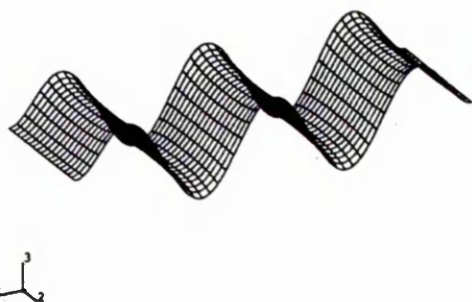
(d) mode 4



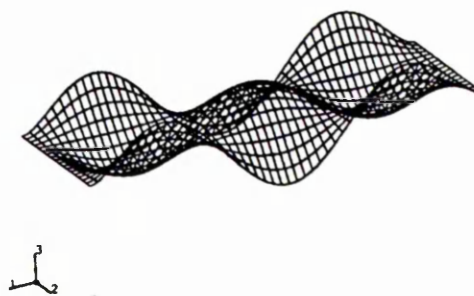
(e) mode 5



(f) mode 6



(g) mode 7



(h) mode 8

Figure 7.35 Symmetric mode shape for aspect ratio 3.0, for clamped-clamped beam-plate of 1% thickness to length ratio

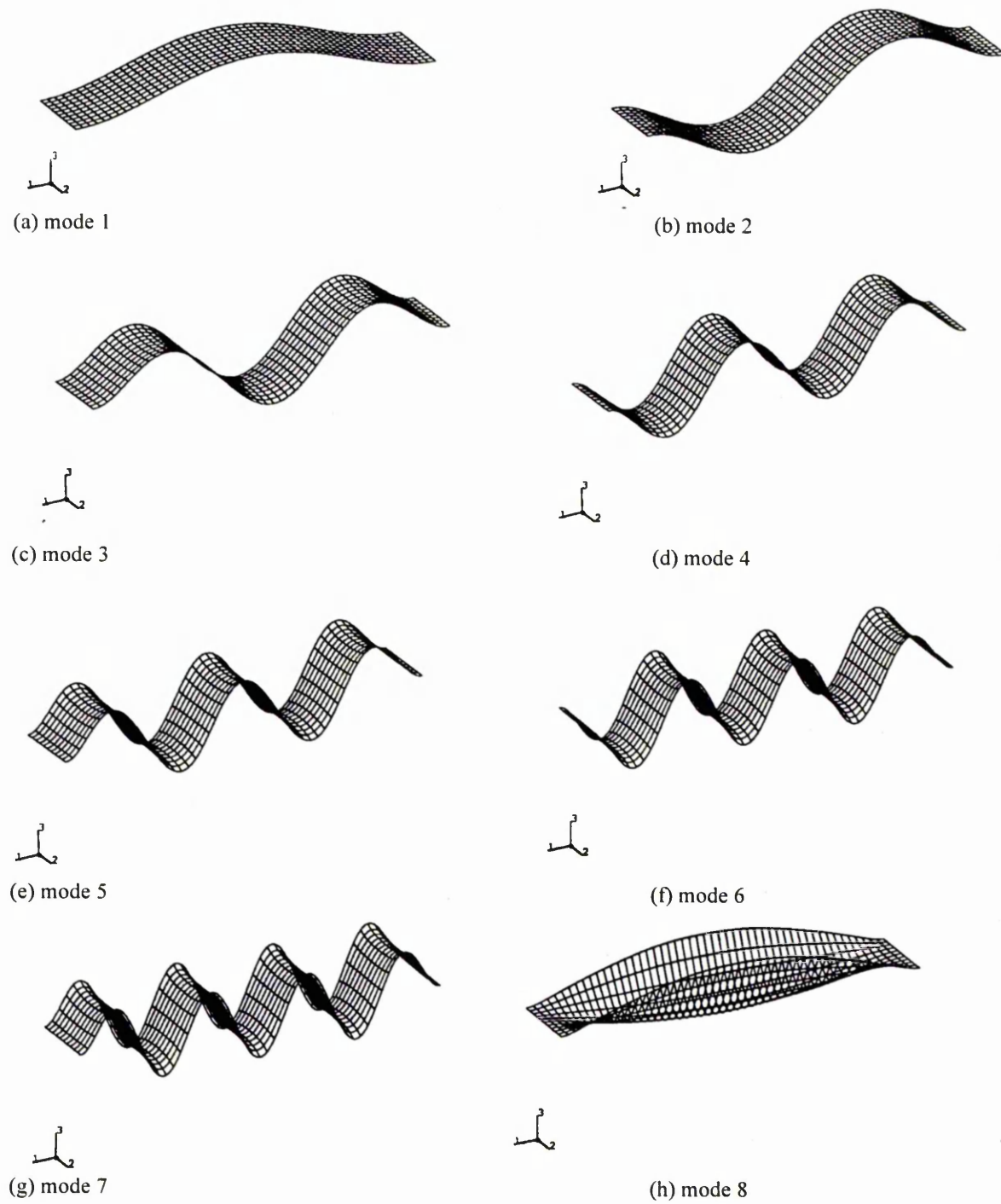
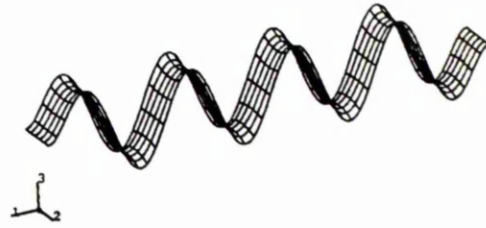


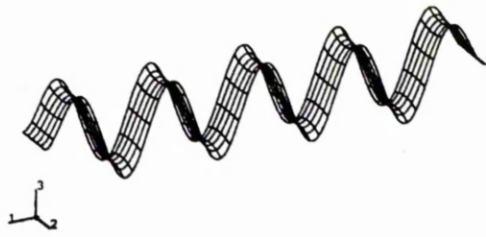
Figure 7.36 Symmetric mode shape for aspect ratio 5.0, for clamped-clamped beam-plate of 1% thickness to length ratio



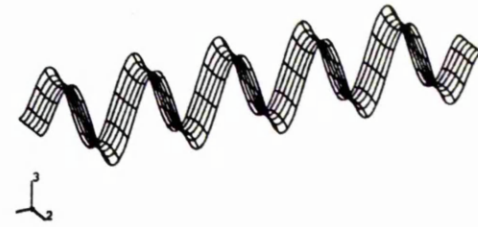
(a) mode 8



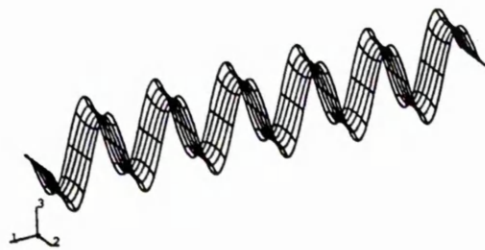
(b) mode 9



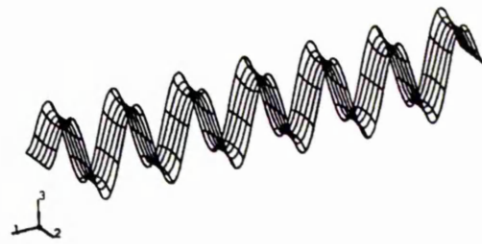
(c) mode 8



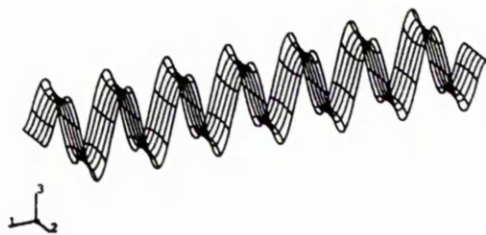
(d) mode 9



(e) mode 12



(f) mode 13



(g) mode 14



(h) mode 15

Figure 7.37 Symmetric mode shape for aspect ratio 10.0, for clamped-clamped beam-plate of 1% thickness to length ratio

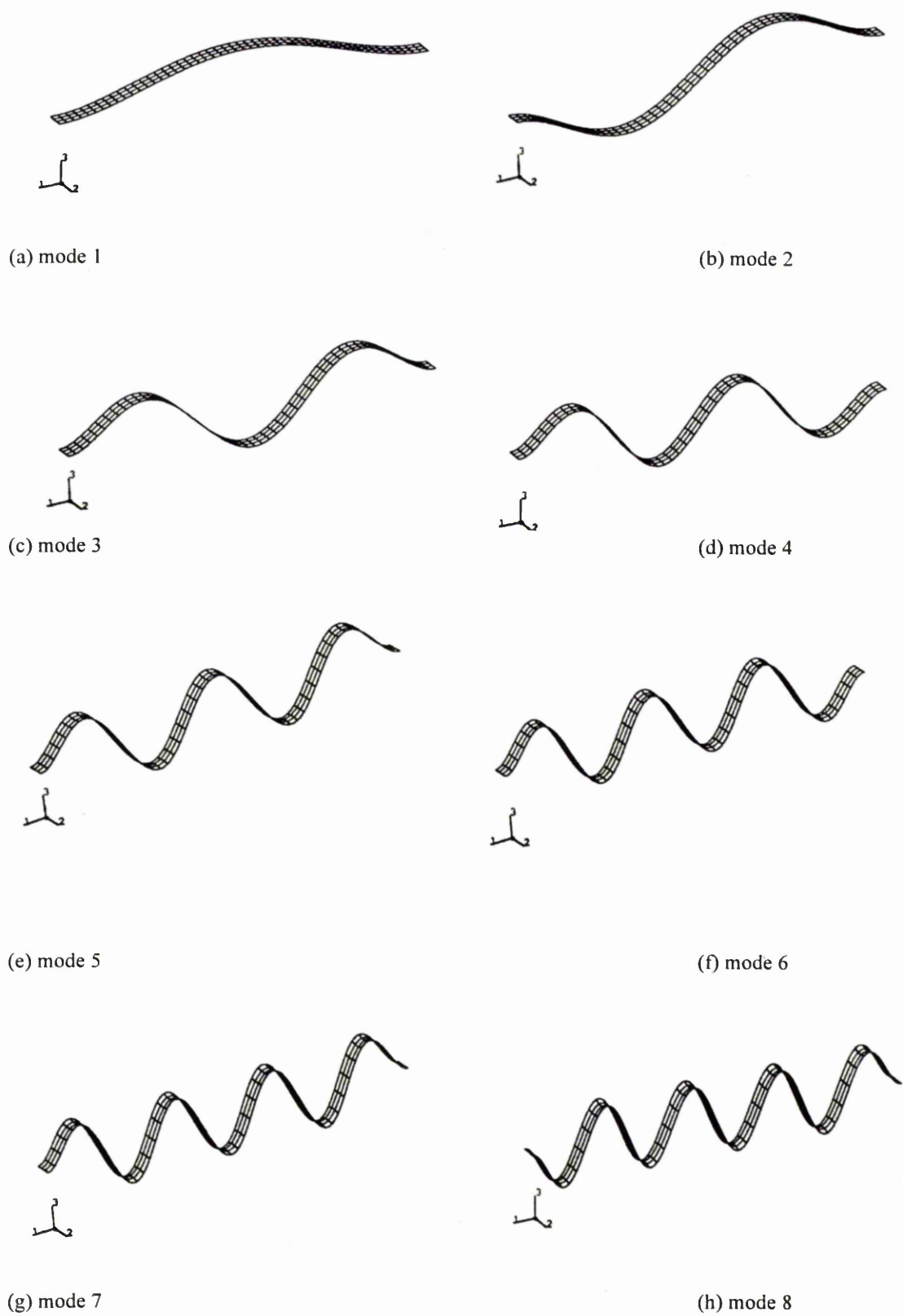


Figure 7.38 Symmetric mode shape for aspect ratio 20.0, for clamped-clamped beam-plate of 1% thickness to length ratio

7.4.3 Derivation of transition curves and equations for 1% thickness to length ratio clamped-clamped beam-plates

Table 7.5 shows the lower and upper bound values of m and λ_{sm}^2 at the transition points for all the aspect ratios considered for clamped-clamped beam-plate of 1% thickness to length ratio.

Table 7.5 Mode counter and frequency parameter of symmetric modes at transition points for 1% thickness to length ratio clamped-clamped beam- plates.

Aspect ratio	Lower bound values		Upper bound values	
	Mode counter	λ_{sm}^2	Mode counter	λ_{sm}^2
2.50	2	60.21	3	118.26
3.00	3	117.91	4	195.20
3.50	4	194.68	5	290.41
4.00	5	290.39	6	374.13
4.50	5	289.76	6	404.83
5.00	6	404.04	7	537.78
6.00	7	535.91	8	687.85
7.00	9	855.66	10	1043.55
8.00	11	1246.40	12	1405.00
9.00	12	1465.80	13	1705.00
10.00	14	1956.60	15	2202.70

Using the linear least-square method, the lower bound values of the frequency parameters of the symmetric modes and the symmetric mode counter at the transition from beam-like to plate-like behaviour can be represented by the following equation:

$$\lambda_{ll}^2 = 9.223 m_{ll}^2 + 11.625 m_{ll} + 0.732 \quad (7.21)$$

Similarly, the upper bound values can be expressed as:

$$\lambda_{uu}^2 = 8.846 m_{uu}^2 + 15.01 m_{uu} - 8.071 \quad (7.22)$$

Also, the values of the symmetric mode counter at the lower and upper transition points can be related to the aspect ratio, by an equations which are derived using the least square method, as follows:

$$m_{ll} = 1.512r - 1.574 \quad (\text{lower bound}) \quad (7.23)$$

$$m_{lu} = 1.512r - 0.574 \quad (\text{upper bound}) \quad (7.24)$$

$$\begin{aligned} \lambda_{sm}^2 = & (17.746 - 3.005r - 0.068r^2) + (2.517 + 1.398r - 0.032r^2)m + \\ & (10.339 - 0.165r + 0.004r^2)m^2 \end{aligned} \quad (7.25)$$

Equations (7.21) and (7.22) show the equations for the two transition curves in Figure 7.39 which represent the variations of the limiting values of the frequency parameters of the symmetric modes with the symmetric mode counters at the lower and upper transition points. The comparison between the lower and upper bound values of the symmetric mode counters predicted by Equations (7.23) and (7.24) are shown on Figure 7.40 when applying these equations, it is better to use Equations (7.21) and (7.23) which provide conservative (lower bound) estimates of the transition values of frequency parameter and number of pure bending modes that occur before plate-like behaviour for a particular aspect ratio.

Figure 7.41 shows the variation of the frequency parameters of the symmetric modes with the symmetric mode counter m for all the aspect ratios. This combined graph shows the curve OA which represents the boundary region between beam-like and plate-like behaviour. However, all points on the curve OA denote beam-like behaviour. This curve is to be used to calculate the frequency parameters for beam-like behaviour only. The right region of the curve is a region of plate-like behaviour where it is necessary to use finite element analysis to calculate the frequency parameters.

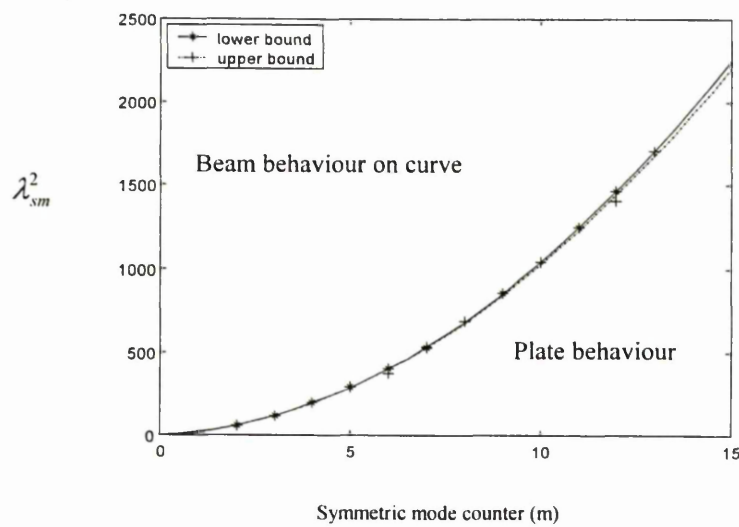


Figure 7.39 Variation of frequency parameter of symmetric modes with symmetric mode counter at transition point for 1% thickness to length ratio clamped-clamped beams and plates.

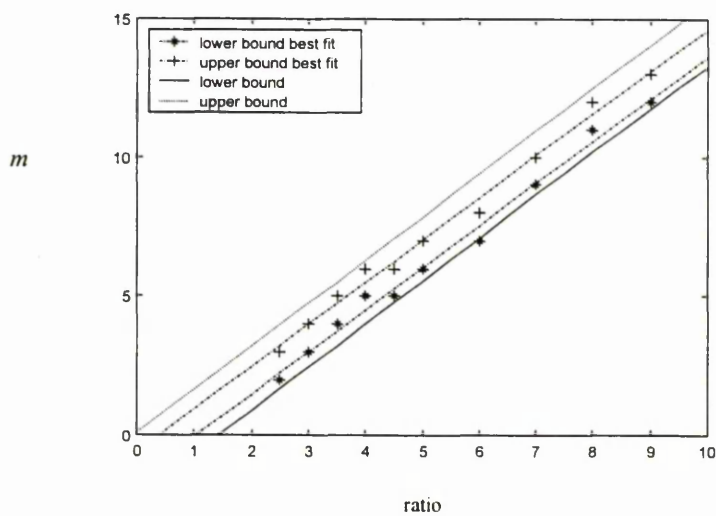


Figure 7.40 Variation of symmetric mode counter at transition point with aspect ratio for 1% thickness to length ratio clamped-clamped beams and plates.

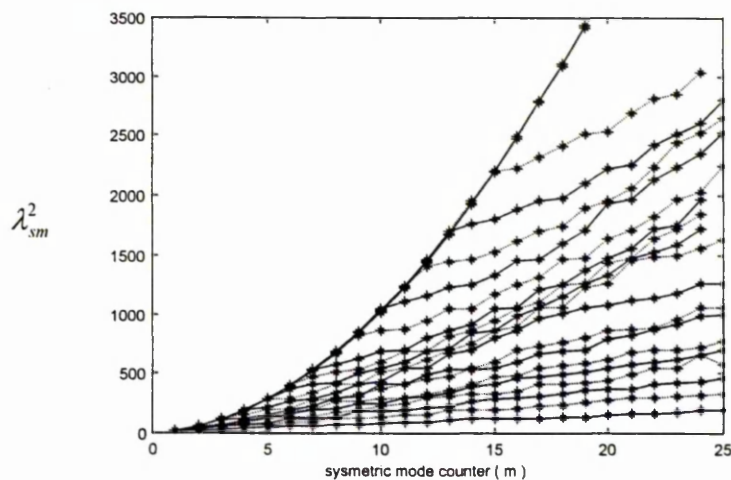


Figure 7.41 Variation of the frequency parameters of symmetric modes with symmetric mode counter (m) for aspect ratio 0.25 to 20.00 for 1% thickness to length ratio clamped-clamped beams and plates.

7.4.4 Obtaining the transition curve from symmetric modes for clamped-clamped boundary condition for other thickness to length ratio

The work presented earlier was for 1% thickness to length ratio clamped-clamped beam-plates. In addition beam-plates of thickness to length ratios 2%, 5% and 10% were also considered. The transition points, transition curves and transition equation were derived for each of these thicknesses to length ratios as was done for the 1% thickness to length ratio. The results are presented in the following Tables 7.6 to 7.8, and Figures 7.42 to 7.50.

Transition points, curves and equations for 2% thickness to length ratio beam-plate

Table 7.6 *Mode counter and frequency parameter of symmetric modes at transition points for 2% thickness to length ratio clamped-clamped beam-plates.*

Aspect ratio	Lower bound values		Upper bound values	
	Mode counter	λ_{sm}^2	Mode counter	λ_{sm}^2
2.50	2	59.87	3	117.19
3.00	3	116.83	4	192.58
3.50	4	192.06	5	331.58
4.00	5	285.02	6	366.27
4.50	5	284.37	6	395.05
5.00	6	394.27	7	521.45
6.00	8	662.33	9	788.51
7.00	9	817.79	10	989.63
8.00	11	1172.46	12	1316.10
9.00	12	1367.29	13	1576.76
10.00	14	1793.80	15	2005.28

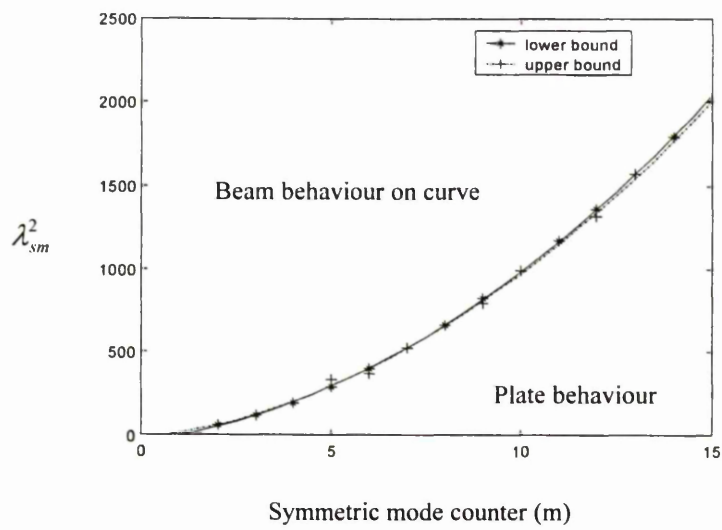


Figure 7.42 Variation of frequency parameter of symmetric modes with symmetric mode counter at transition point for 2% thickness to length ratio clamped-clamped

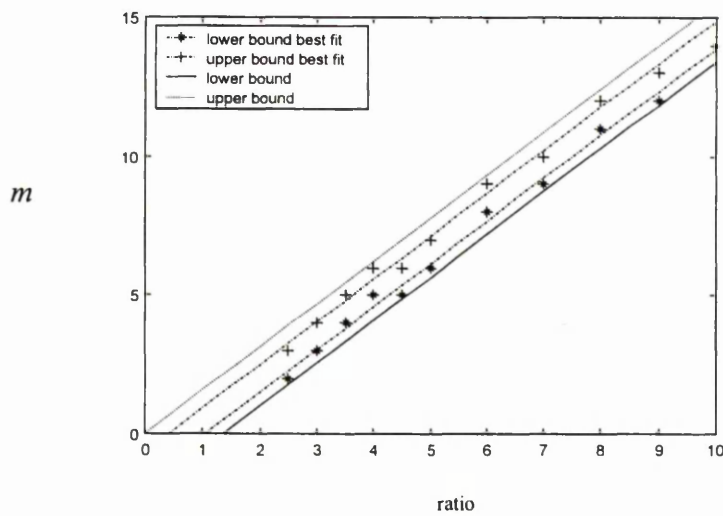


Figure 7.43 Variation of symmetric mode counter at transition point with aspect ratio for 2% thickness to length ratio clamped-clamped beam-plates.

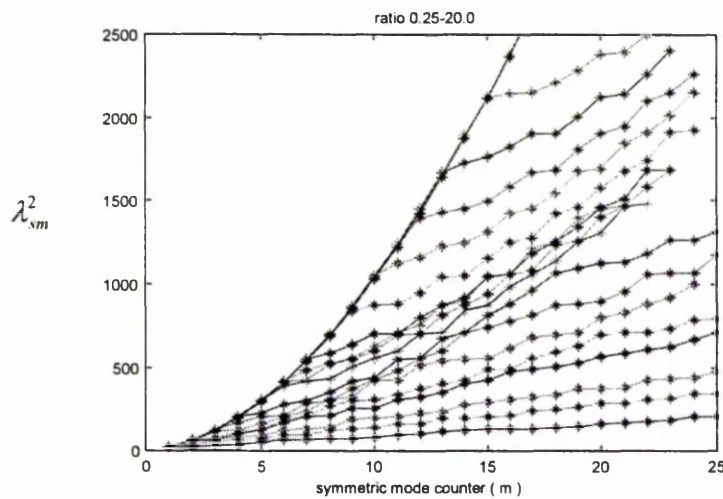


Figure 7.44 Variation of the frequency parameters of symmetric modes with symmetric mode counter (m) for aspect ratio 0.25 to 20.00 for 2% thickness to length ratio clamped-clamped beam-plates.

The transition equations, corresponding to transition curves shown in Figure 7.42, are

$$\lambda_{ll}^2 = 7.386 m_{ll}^2 + 27.661 m_{ll} - 33.161 \quad (7.26)$$

$$\lambda_{lu}^2 = 7.319 m_{lu}^2 + 25.768 m_{lu} - 20.987 \quad (7.27)$$

The symmetric mode counter equations (corresponding to Figure 7.43)

$$m_{ll} = 1.55r - 1.625 \quad (\text{lower bound}) \quad (7.28)$$

$$m_{lu} = 1.55r - 0.625 \quad (\text{upper bound}) \quad (7.29)$$

$$\lambda_{sm}^2 = (21.315 - 4.508r - 0.049r^2) + (0.433 - 2.647r - 0.045r^2)m + (10.193 - 0.315r + 0.007r^2)m^2 \quad (7.30)$$

Transition points, curves and equations for 5% thickness to length ratio beam-plate

Table 7.7 Mode counter and frequency parameter of symmetric modes at transition points for 5% thickness to length ratio clamped-clamped beam-plates.

Aspect ratio	Lower bound values		Upper bound values	
	Mode counter	λ_{sm}^2	Mode counter	λ_{sm}^2
2.50	2	57.74	3	110.27
3.00	3	109.93	4	176.10
3.50	4	175.63	5	253.21
4.00	5	252.66	6	327.02
4.50	5	252.13	6	339.00
5.00	6	338.39	7	432.92
6.00	8	532.23	9	637.99
7.00	10	788.84	11	877.27
8.00	11	914.13	12	974.24
9.00	13	1091.04	14	1207.96

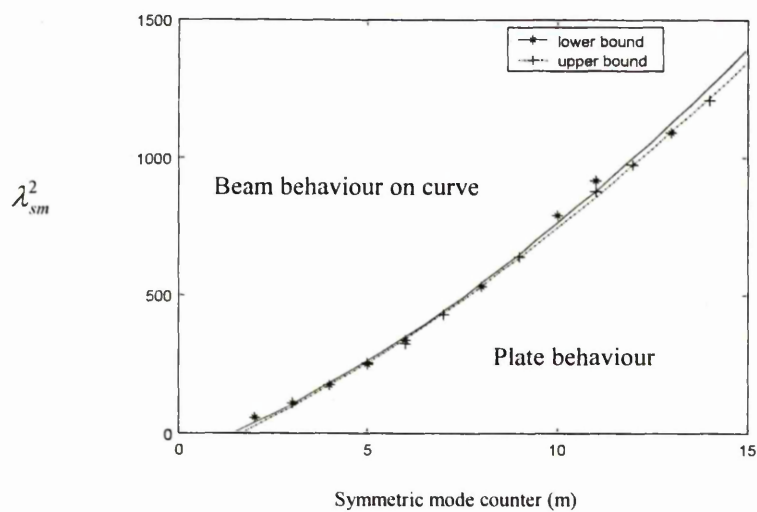


Figure 7.45 Variation of frequency parameter of symmetric modes with symmetric mode counter at transition point for 5% thickness to length ratio clamped-clamped

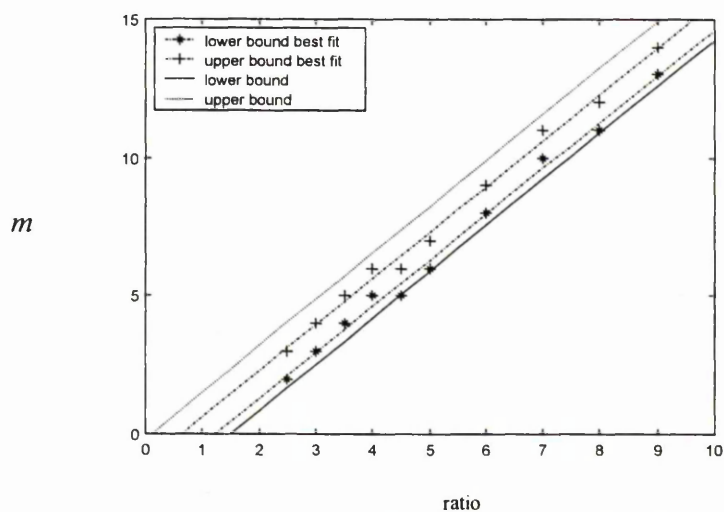


Figure 7.46 Variation of symmetric mode counter at transition point with aspect ratio for 5% thickness to length ratio thick clamped-clamped beam-plates.

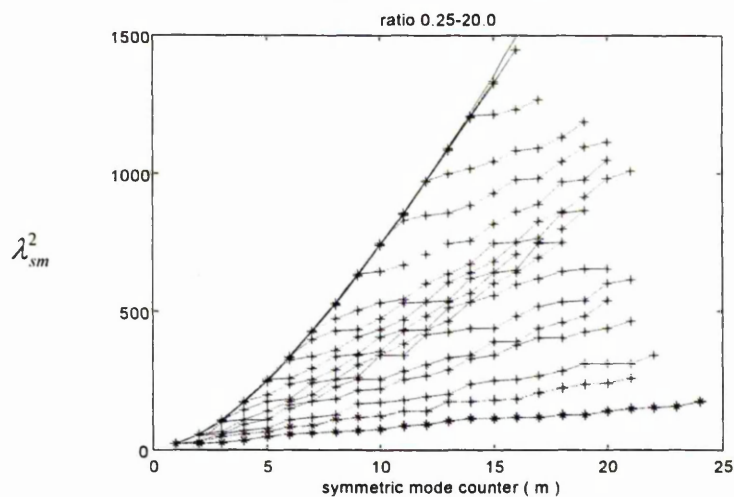


Figure 7.47 Variation of the frequency parameters of symmetric modes with symmetric mode counter (m) for aspect ratio 0.25 to 20.00 for 5% thickness to length ratio clamped-clamped beams and plates.

The transition equations, corresponding to transition curves shown in Figure 7.45

$$\lambda_{ll}^2 = 2.908 m_{ll}^2 + 55.266 m_{ll} - 84.523 \quad (7.31)$$

$$\lambda_{mm}^2 = 2.499 m_{mm}^2 + 59.559 m_{mm} - 103.246 \quad (7.32)$$

The symmetric mode counter equations (corresponding to Figure 7.46)

$$m_{ll} = 1.663 r - 2.034 \quad (\text{lower bound}) \quad (7.33)$$

$$m_{mm} = 1.663 r - 1.034 \quad (\text{upper bound}) \quad (7.34)$$

$$\lambda_{sm}^2 = (10.637 - 7.618 r - 0.206 r^2) + (12.571 + 4.351 r - 0.122 r^2) m + (7.268 - 0.529 r + 0.0154 r^2) m^2 \quad (7.35)$$

Transition points, curves and equations for 10% thickness to length ratio beam-plate

Table 7.8 Mode counter and frequency parameter of symmetric modes at transition points for 10% thickness to length ratio clamped-clamped beam-plates.

Aspect ratio	Lower bound values		Upper bound values	
	Mode counter	λ_{sm}^2	Mode counter	λ_{sm}^2
2.50	2	51.78	3	93.39
3.00	3	93.12	4	141.15
3.50	4	130.85	5	193.16
4.00	5	192.84	6	248.05
4.50	6	247.71	7	303.52
5.00	7	304.59	8	353.03
6.00	8	362.57	9	422.09
7.00	10	481.81	11	542.33
8.00	11	542.06	12	602.78

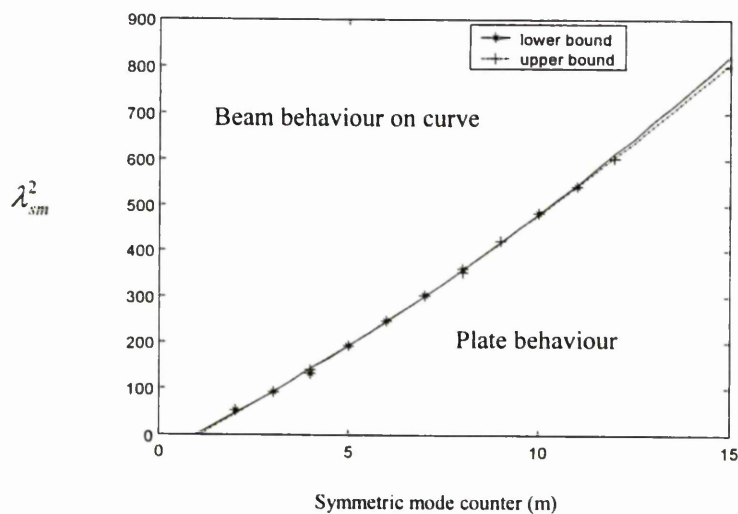


Figure 7.48 Variation of frequency parameter of symmetric modes with symmetric mode counter at transition point for 10% thickness to length ratio clamped-clamped beam-plates.

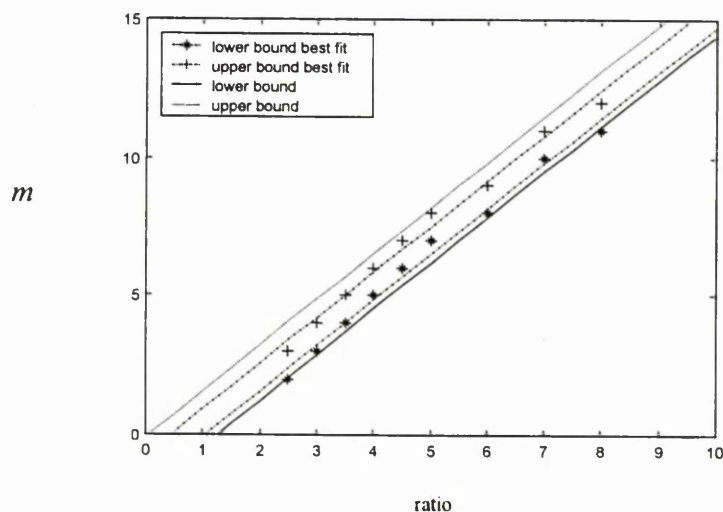


Figure 7.49 Variation of symmetric mode counter at transition point with aspect ratio for 10% thickness to length ratio clamped-clamped beam-plates.

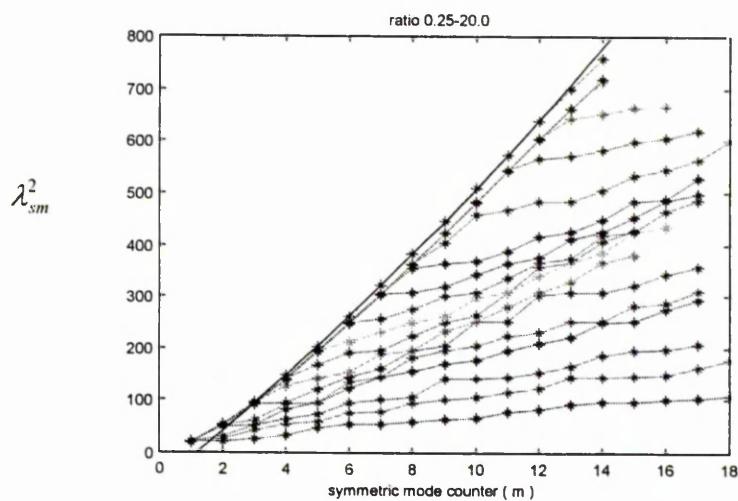


Figure 7.50 Variation of the frequency parameters of symmetric modes with symmetric mode counter (m) for aspect ratio 0.25 to 20.00 for 10% thickness to length ratio clamped-clamped beam-plates.

The transition equations, corresponding to transition curves shown in Figure 7.42

$$\lambda_{ll}^2 = 1.089 m_{ll}^2 + 41.227 m_{ll} - 40.382 \quad (7.36)$$

$$\lambda_{lu}^2 = 0.893 m_{lu}^2 + 43.514 m_{lu} - 46.188 \quad (7.37)$$

The symmetric mode counter equations (corresponding to Figure 7.43)

$$m_{ll} = 1.648 r - 1.745 \quad (\text{lower bound}) \quad (7.38)$$

$$m_{lu} = 1.648 r - 0.745 \quad (\text{upper bound}) \quad (7.39)$$

$$\lambda_{sm}^2 = (10.616 - 4.072 r + 0.102 r^2) + (9.840 + 3.308 r - 0.093 r^2) m + (5.978 - 0.663 r + 0.021 r^2) m^2 \quad (7.40)$$

7.5 Summary

The definitions of symmetric and anti-symmetric vibration modes have been given in this chapter. Based on these definitions, transition curves for beam-like to plate-like behaviour for both free-free and clamped-clamped beam-plates have been derived from the symmetric vibration modes. Using the least squares method, transition equations were derived to represent the transition curves. The beam-plate thicknesses to length ratio considered were 1%, 2%, 5% and 10%. The transition curves divide the frequency parameter versus symmetric mode counter charts in to 2 regions. The first region, which is the beam-like region, coincides with the transition curve. The second region, which is to the right of the transition curve, is the plate-like region.

Chapter 8

Deducing transition from beam-like to plate-like response using anti-symmetric modes of vibration

8.1 Introduction

Chapter 7 has covered the study of the symmetric modes of vibration for both free-free and clamped-clamped beams-plates and deduces the transition curve from beam-like to plate-like behaviour for beam-plate of thickness to length ratio 1%, 2%, 5% and 10%. This chapter will consider the anti-symmetric modes of vibration for both free-free and clamped-clamped beam-plates and deduce the possible transition curves, based on the study of the frequency parameter charts and examination of the mode shapes. The examination of the mode shapes is important to prove and confirm the results obtained from the frequency parameter charts, and so that the reader can see clearly the behaviour of the beam-plates at the transition from beam-like to plate-like behaviour. Beam-like behaviour is considered to be the fundamental twist or first torsional deformation about the lengthwise axis of the beam-plates. Higher order of torsional deformation about the lengthwise axis or bending along the breadthwise direction are regarded as plate-like behaviour.

8.2 Obtaining the transition curve from anti-symmetric modes for free-free boundary condition

8.2.1 Deduction from frequency parameter charts

Figures 8.1 and 8.2 show the relationship between the frequency parameters of the anti-symmetric modes (λ_{sn}^2) and the anti-symmetric mode counter (n) for aspect ratios (0.25 to 20.0) respectively for free-free beam-plates of thickness to length ratio 1%. The figures show clearly that it is possible to obtain the transition from beam-like to plate-like behaviour from the anti-symmetric modes. The transition point is located in most of the graphs at the intersection of the smooth part of the frequency parameter curve with the zigzag part.

Figure 8.1 shows the variation of the frequency parameters of the anti-symmetric modes (λ_{sn}^2) with the anti-symmetric mode counter (n) for aspect ratios of 0.25 to 3.5. The figure shows zigzag wavy lines for aspect ratios 0.25 to 1, which indicate plate-like behaviour. However as the aspect ratio increases, the chart develops a smooth curve at low values of n . But as n increases, the chart becomes a zigzag wavy line. For example, consider the beam-plate of aspect ratio of 1.25. It is seen that λ_{sn}^2 varies smoothly with n as n increases from 1 to 3. This section of the curve is associated with beam-like behaviour. However, at $n = 3$, there is a discontinuity in the curve. And as the value of n increases from 3 to 22 the curve becomes a zigzag line. This part of the curve suggest a plate-like behaviour. Therefore we can conclude from this that at $n = 3$ is the transition point from beam-like to plate-like behaviour for ratio 1.25. This value of $n = 3$ represents an upper

bound for the transition point. A lower (conservative) bound for the transition point can be defined at a value of $n = 2$.

Figures 8.1 and 8.2 show that for aspect ratios between 3.0 and 6.0 (inclusive), the curve of variation of frequency parameters λ_{an}^2 with n can be divided into 2 sections. In the first section, when $1 \leq n \leq n_t$, where n_t is the value of n at the transition from beam-like to plate-like behaviour, λ_{an}^2 varies smoothly with n . This section of the curve denotes beam-like behaviour. In the second section of the curve, when $n > n_t$, λ_{an}^2 varies in a somewhat zigzag, wavy manner as n increases. This latter section of the curve denotes plate-like behaviour. The upper bound values of n at the transition point from beam-like to plate-like behaviour are deduced from these figures as 7, 8, 10, 11, 12 and 14 for aspect ratios of 3.00, 3.50, 4.00, 4.50, 5.0 and 6.0 respectively. The corresponding lower bound values of n are 6, 7, 9, 10, 11 and 13.

For aspect ratios greater than 7.0 the figures show that there is no discontinuity in the line, and there are no transition points. This is because at these aspect ratios, the first 20 anti-symmetric modes shown in these figures are torsional modes of vibration.

8.2.2 Deduction from mode shapes

The previous section has covered the study of the transition curves using the anti-symmetric modes from the frequency parameter charts. This section is on the determination of the transition curves based on the study of the mode shapes for selected aspect ratios. The procedure involves examination of the deformation of the breadthwise edges of the beam-plates, which are parallel to the y -axis (2-axis), or j direction at different modes of vibration.

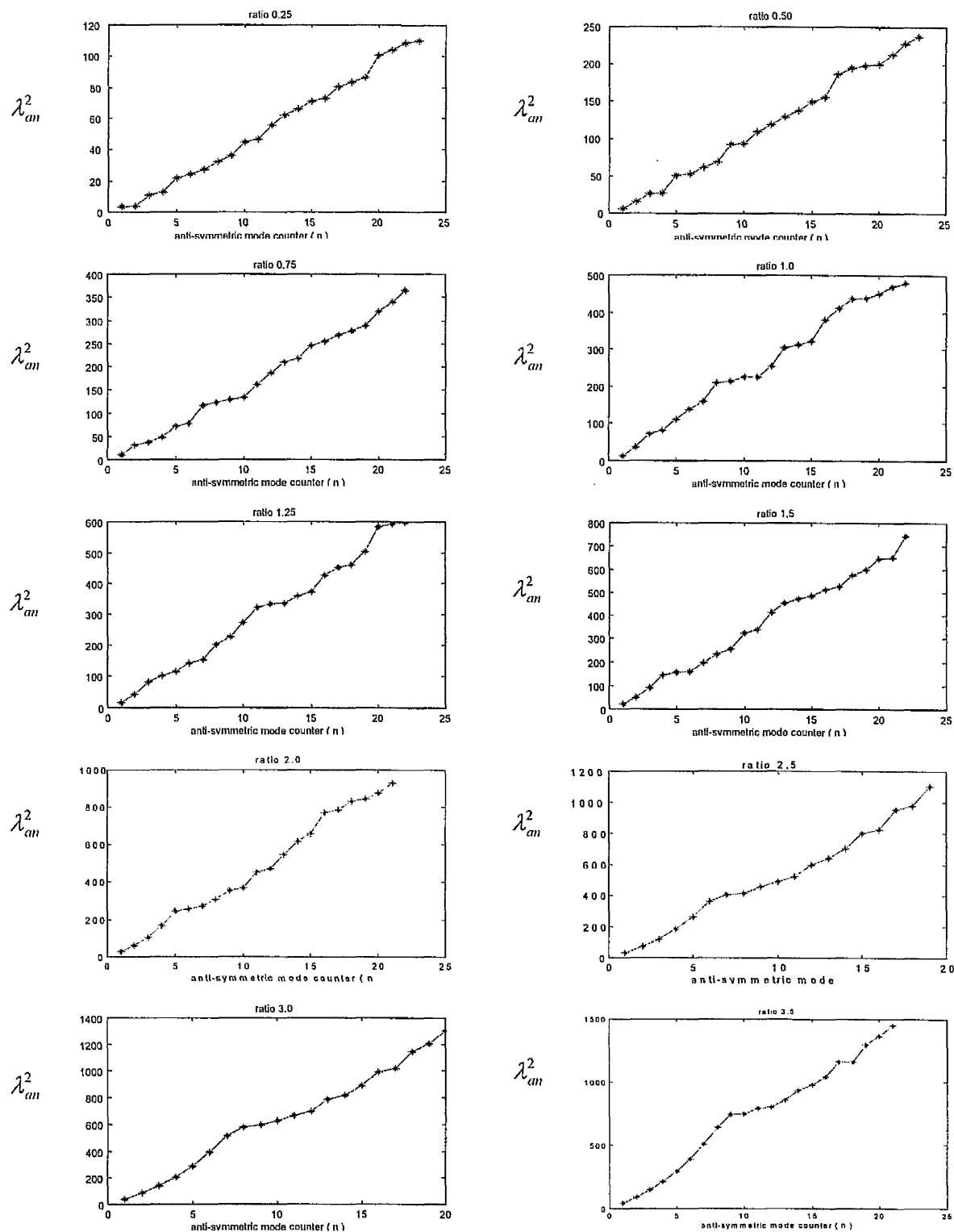


Figure 8.1 Variation of the frequency parameters of anti-symmetric modes with anti-symmetric mode counter (n) for aspect ratios 0.25 to 3.5 for 1% thickness to length ratio free-free beam-plates.

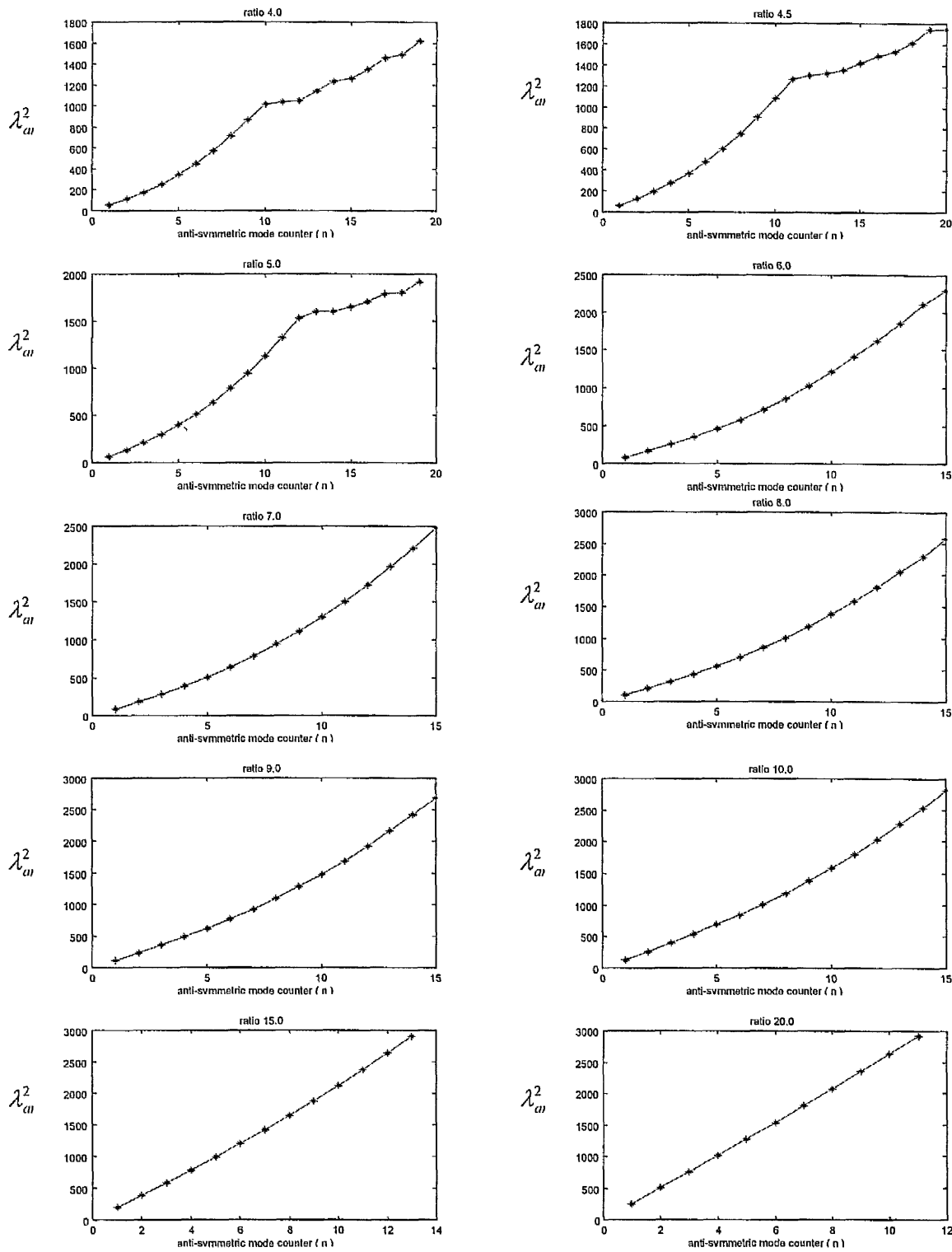


Figure 8.2 Variation of the frequency parameters of anti-symmetric modes with anti-symmetric mode counter (n) for aspect ratios 4 to 20 for 1% thickness to length ratio free-free beam-plates.

The modes of vibration for which there is a torsional vibration about the lengthwise direction are classed as beam-like behaviour, while modes for which there is a twist or higher order of torsional deformation about the lengthwise axis or bending along the breathwise direction are classed as plate-like behaviour. Figures 8.3 to 8.7 shows the selected mode shapes for aspect ratios 0.5, 1.25, 2.5, 5.0 and 20.0 respectively. On examination of these modes, it is seen clearly that there is a transition mode.

Consider Figure 8.3 that represent aspect ratio 0.5. This figure shows clearly that there is bending along the breathwise direction (j). This indicates a plate-like behavior. This deduction is also confirmed from Figure 8.1, which shows a zigzag variation of the frequency parameters.

Selected mode shapes for aspect ratio 1.25 are shown in Figure 8.4. The figure shows that for $n=1$ to $n=2$, the free breadthwise edges of the beam-plate are almost straight which indicates beam-like behaviour. However, the figure shows that for $n=3$ to $n=8$, the free breadthwise edges of the beam-plate is curved which indicate plate-like behaviour. This statement also agrees with Figure 8.1 which shows that the data points corresponding to the first 2 modes lie on a smooth curve but when $n>2$ the modal points form a zigzag pattern which indicates plate-like behaviour. The selected mode shapes for aspect ratio 2.50 are shown in Figure 8.5. It is seen that the transition is at mode 6, which again agrees with the deductions from Figure 8.1.

Figure 8.6 shows selected anti-symmetric mode shapes for aspect ratio 5.0. The figure contains the transition mode shape at mode 12 again, which agrees with Figure 8.2. Figure 8.7 shows the mode shapes of modes 1 to 8 for aspect ratio 20.0. All modes in this figure are pure torsional modes and there is no bending in the (j) direction. This represents beam-like behaviour. This is also confirmed by Figure 8.2 which shows a smooth curve.

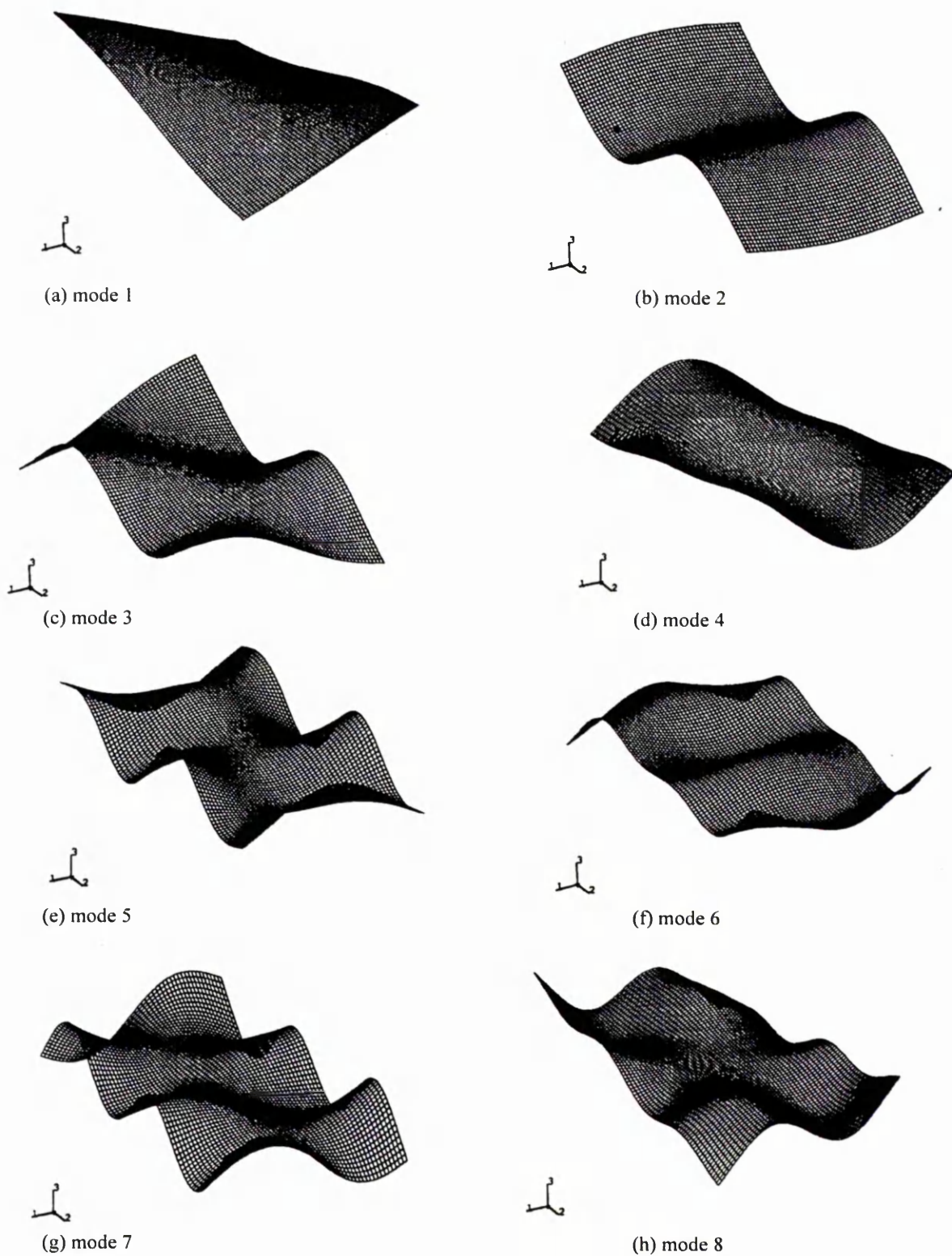


Figure 8.3 Anti-symmetric mode shape for aspect ratio 0.50 for 1% thickness to length ratio free-free beam-plates.

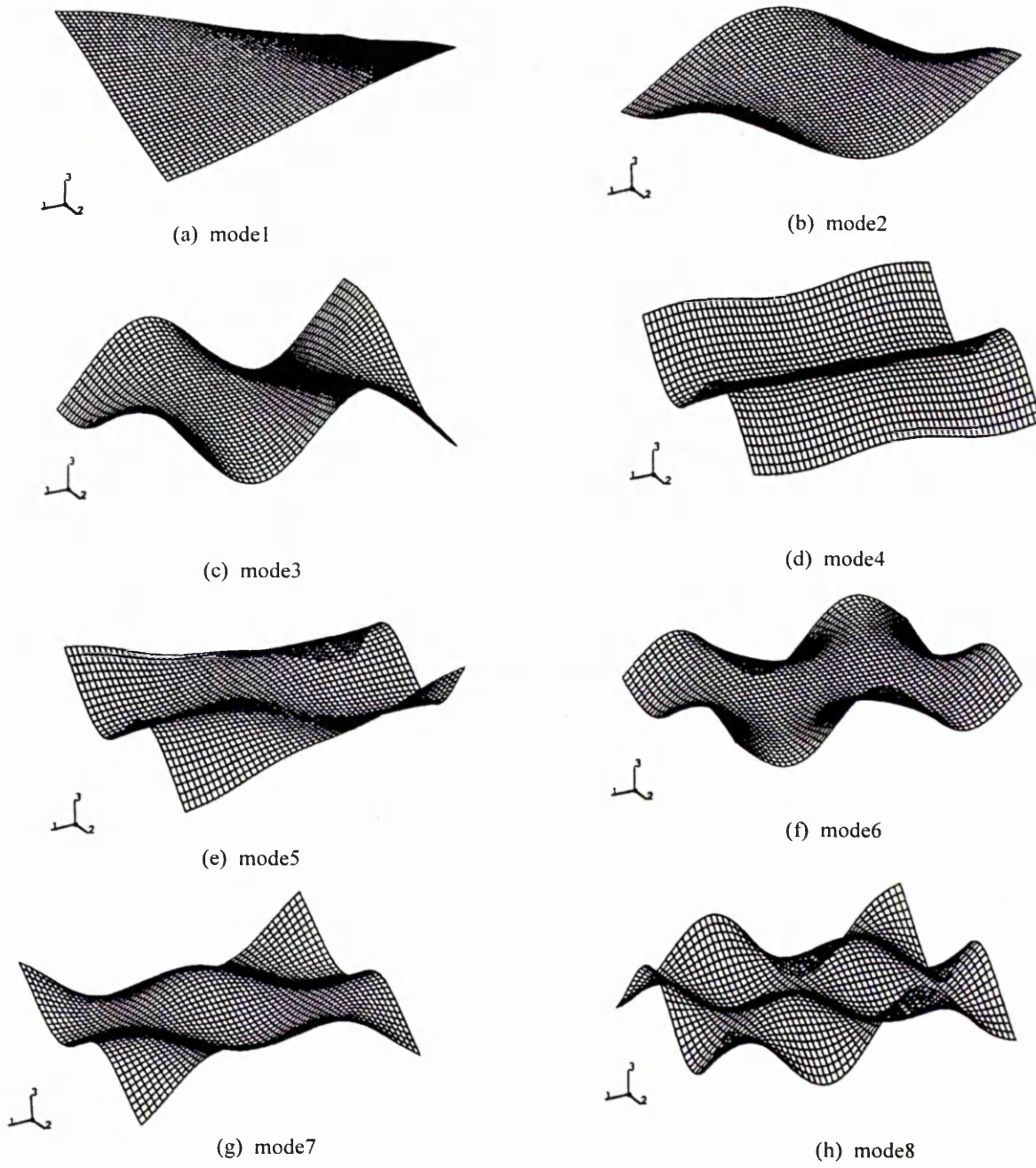


Figure 8.4 Anti-symmetric mode shape for aspect ratio 1.25 for 1% thickness to length ratio free-free beam-plates.

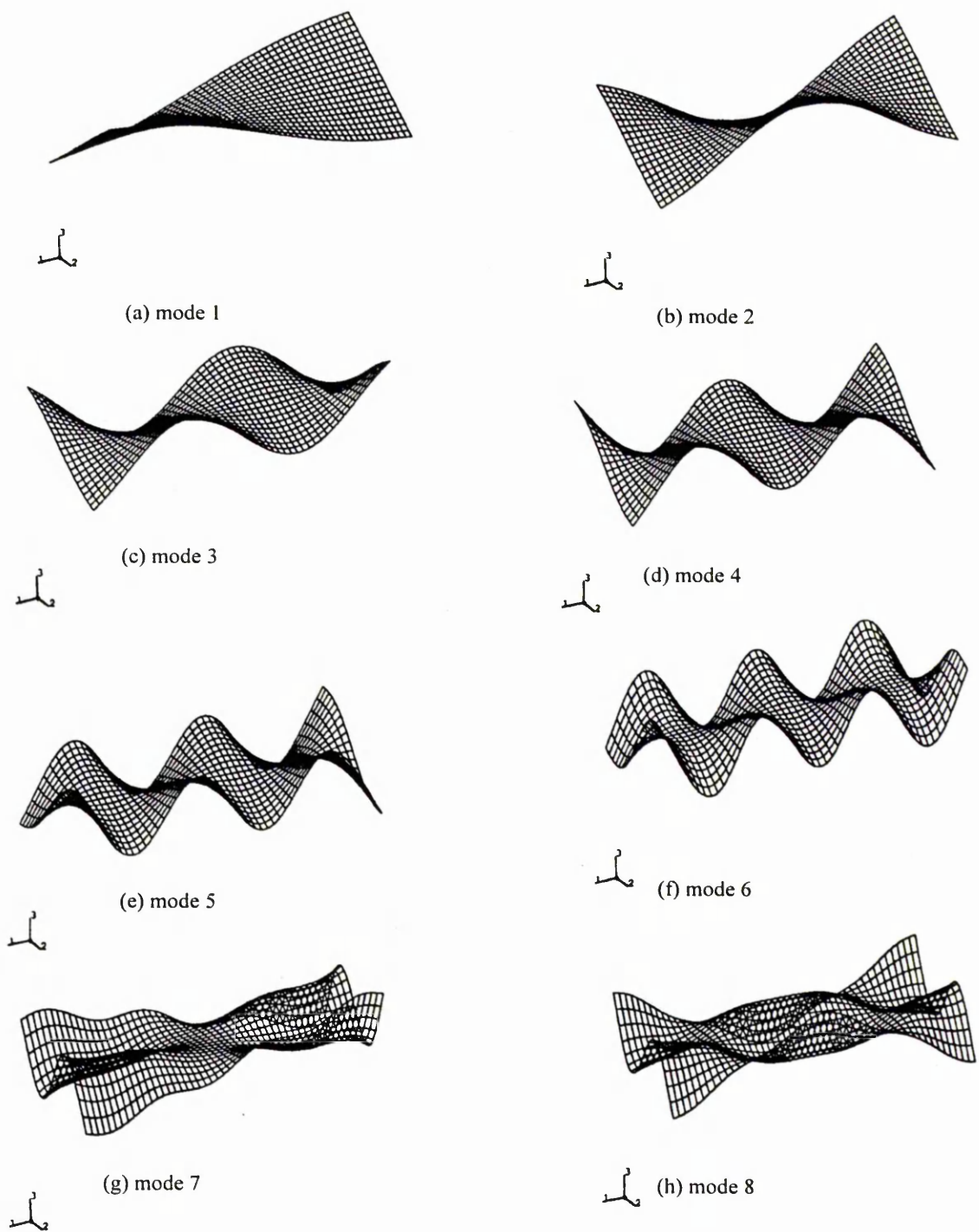


Figure 8.5 Anti-symmetric mode shape for aspect ratio 2.50 for 1% thickness to length ratio free-free beam-plates.

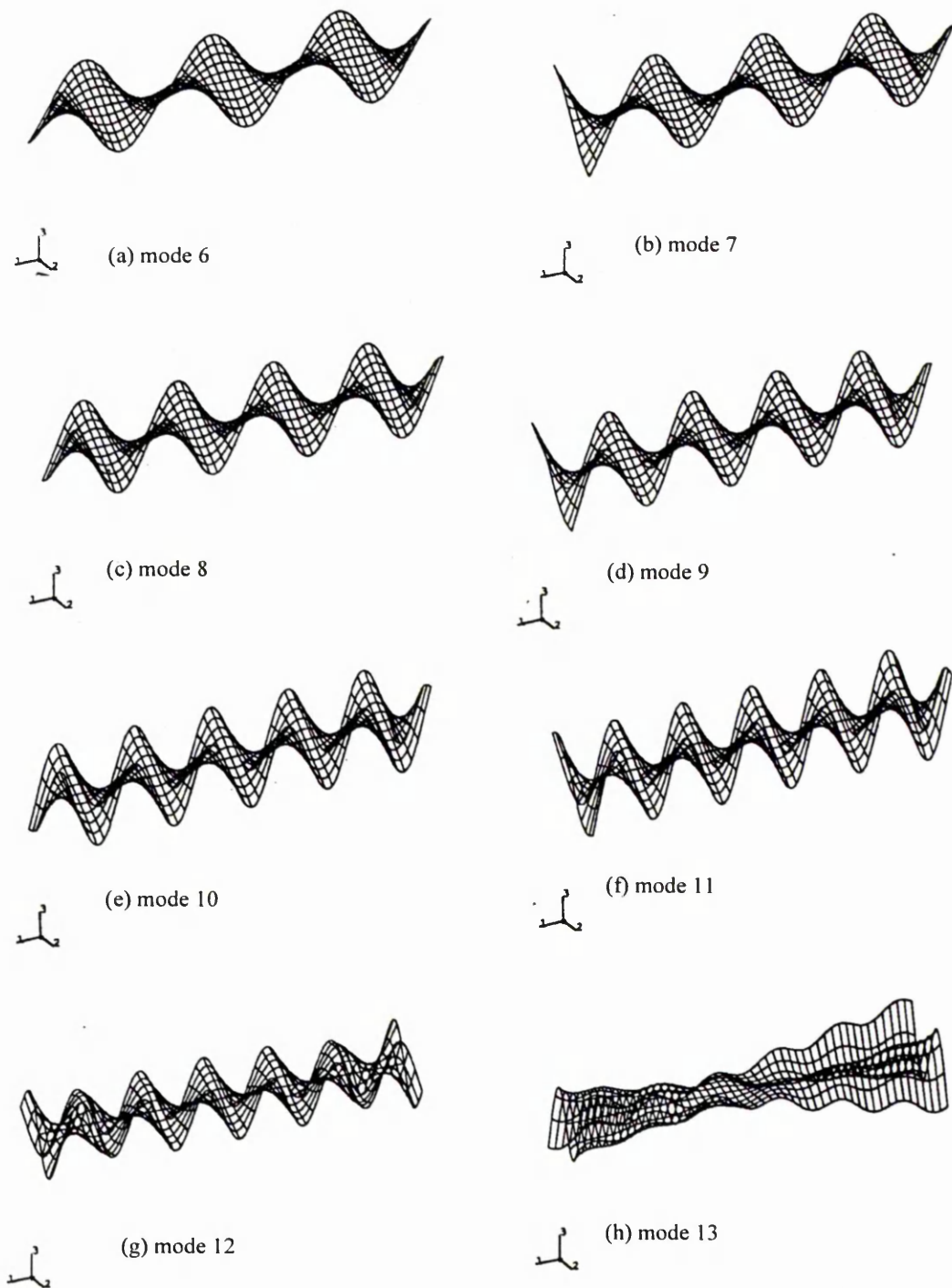


Figure 8.6 Anti-symmetric mode shape for aspect ratio 5.0 for 1% thickness to length ratio free-free beam-plates.

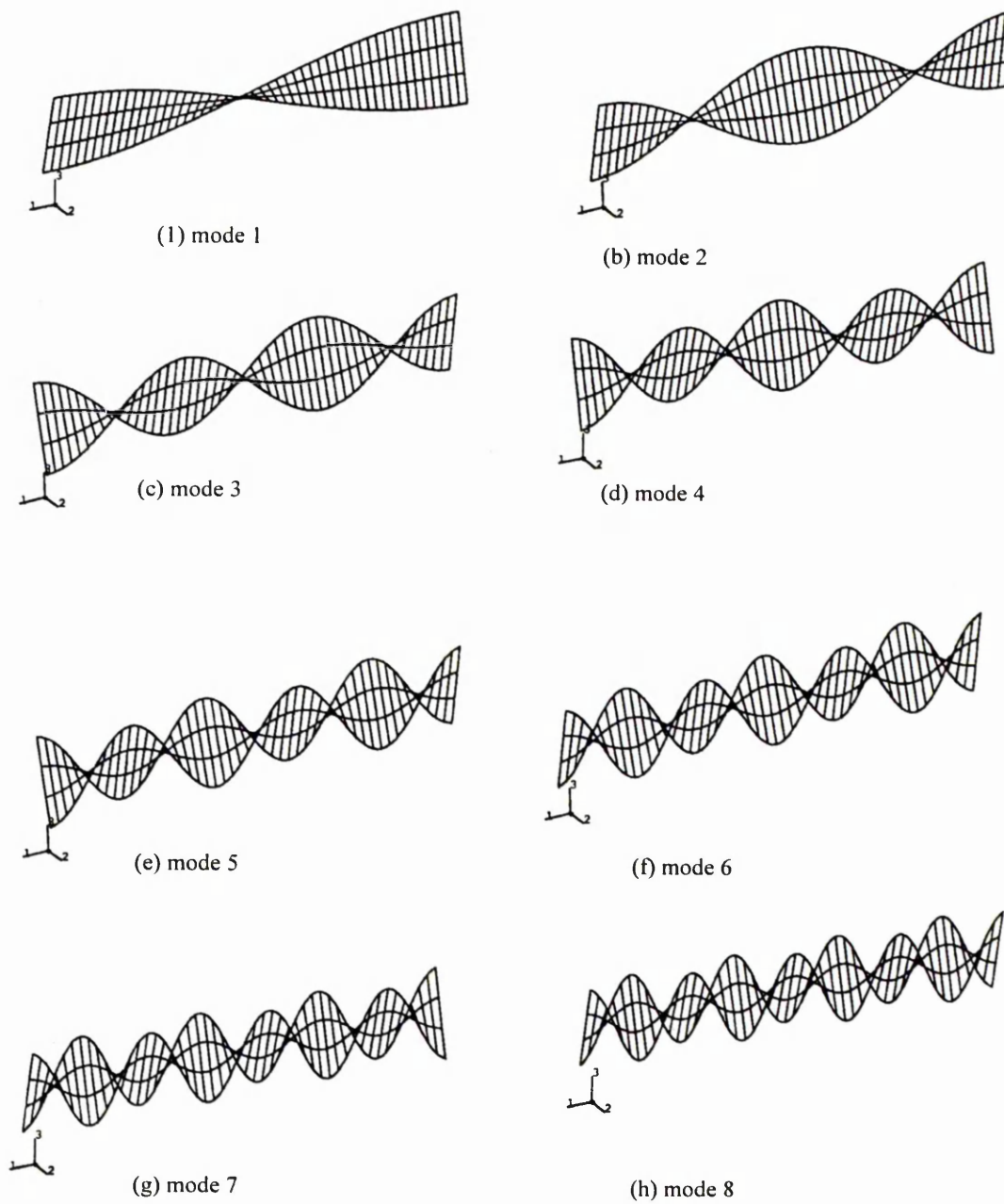


Figure 8.7 Anti-symmetric mode shape for aspect ratio 20.0 for 1% thickness to length ratio free-free beam-plates.

8.3 Transition curves and equations for free-free beam-plates

8.3.1 Tables of transition points

Tables 8.1 to 8.4 show the transition points for thickness to length ratios 1%, 2%, 5% and 10%

Table 8.1 *Mode counter and frequency parameter of anti-symmetric modes at transition points for 1% thickness to length ratio free-free beam- plates*

Aspect ratio	Lower bound values		Upper bound values	
	Mode counter	λ_{am}^2	Mode counter	λ_{am}^2
1.25	2	39.65	3	77.31
1.50	3	84.39	4	133.88
2.00	4	157.31	5	230.78
2.50	5	252.91	6	345.95
3.00	6	370.62	7	483.04
3.50	7	510.84	8	642.28
4.00	9	823.10	10	961.30
4.50	10	1025.19	11	1198.30
5.00	11	1247.30	12	1443.10
6.00	13	1754.80	14	1988.90

Table 8.2 *Mode counter and frequency parameter of anti-symmetric modes at transition points for 2% thickness to length ratio free-free beam-plates.*

Aspect ratio	Lower bound values		Upper bound values	
	Mode counter	λ_{am}^2	Mode counter	λ_{am}^2
1.50	3	83.62	4	132.67
2.00	4	155.17	5	226.97
2.50	5	248.11	6	338.11
3.00	6	361.27	7	468.70
3.50	7	494.38	8	681.27
4.00	9	785.53	10	934.66
4.50	10	969.41	11	1126.55
5.00	11	1168.22	12	1342.17

Table 8.3 Mode counter and frequency parameter of anti-symmetric modes at transition points for 5% thickness to length ratio free-free beam-plates.

Aspect Ratio	Lower bound values		Upper bound values	
	Mode counter	λ_{an}^2	Mode counter	λ_{an}^2
1.50	3	80.25	4	125.95
2.00	4	145.22	5	207.98
2.50	5	225.43	6	299.84
3.00	6	317.83	7	401.58
3.50	7	420.40	8	511.50
4.00	8	530.77	9	627.65
4.50	10	748.57	11	847.63

Table 8.4 Mode counter and frequency parameter of anti-symmetric modes at transition points for 10% thickness to length ratio free-free beam-plates.

Aspect Ratio	Lower bound values		Upper bound values	
	Mode counter	λ_{an}^2	Mode counter	λ_{an}^2
1.50	3	72.19	4	109.29
2.00	4	123.51	5	169.19
2.50	5	181.37	6	231.07
3.00	6	242.87	7	294.68
3.50	7	306.49	8	359.05
4.00	8	370.79	9	422.72

8.3.2 Transition equations

By means of the linear least-square method, transition equations were obtained as follows:

Transition equation for 1% thickness to length ratio beam-plates.

$$\lambda_{ll}^2 = 10.55 n_{ll}^2 - 2.74 n_{ll} - 1.86 \quad (\text{lower bound, Figure 8.8}) \quad (8.1)$$

$$\lambda_{lu}^2 = 10.66 n_{lu}^2 - 8.43 n_{lu} + 7.04 \quad (\text{upper bound, Figure 8.8}) \quad (8.2)$$

$$n_{ll} = 2.32 r - 0.74 \quad (\text{lower bound, Figure 8.9}) \quad (8.3)$$

$$n_{tu} = 2.32r + 0.25 \quad (\text{upper bound, Figure 8.9}) \quad (8.4)$$

$$\begin{aligned} \lambda_{an}^2 = & (-24.85 + 14.139r - 0.724r^2) + (-5.624 + 4.272r + 0.407r^2)n + \\ & (5.532 + 0.361r - 0.034r^2)n^2 \quad (\text{curve } OA, \text{ Figure 8.10}) \end{aligned} \quad (8.5)$$

Transition equation for 2% thickness to length ratio beam-plates.

$$\lambda_{tl}^2 = 8.546n_{tl}^2 + 15.782n_{tl} - 42.127 \quad (\text{lower bound, Figure 8.11}) \quad (8.6)$$

$$\lambda_{tu}^2 = 6.071n_{tu}^2 + 53.667n_{tu} - 187.43 \quad (\text{upper bound, Figure 8.11}) \quad (8.7)$$

$$m_{tl} = 2.357r - 1.786 \quad (\text{lower bound, Figure 8.12}) \quad (8.8)$$

$$m_{tu} = 2.357r - 0.214 \quad (\text{upper bound, Figure 8.12}) \quad (8.9)$$

$$\begin{aligned} \lambda_{an}^2 = & (7.070 + 4.665r - 0.231r^2) + (-15.792 + 11.08r - 0.018r^2)n + \\ & (7.559 - 0.373r + 0.0024r^2)n^2 \quad \text{Curve } OA, \text{ Figure 8.13} \end{aligned} \quad (8.10)$$

Transition equation for 5% thickness to length ratio beam-plates.

$$\lambda_{tl}^2 = 3.696n_{tl}^2 + 48.849n_{tl} - 105.30 \quad (\text{lower bound, Figure 8.14}) \quad (8.11)$$

$$\lambda_{tu}^2 = 2.428n_{tu}^2 + 67.970n_{tu} - 189.75 \quad (\text{upper bound, Figure 8.14}) \quad (8.12)$$

$$m_{tl} = 2.214r - 0.5 \quad (\text{lower bound, Figure 8.15}) \quad (8.13)$$

$$m_{tu} = 2.214r + 0.5 \quad (\text{upper bound, Figure 8.15}) \quad (8.14)$$

$$\begin{aligned} \lambda_{an}^2 = & (-5.791 + 1.725r - 0.065r^2) + (-2.090 + 12.402r - 0.331r^2)n + \\ & (5.030 - 0.607r + 0.0185r^2)n^2 \quad (\text{curve } OA, \text{ Figure 8.16}) \end{aligned} \quad (8.15)$$

Transition equation for 10% thickness to length ratio beam-plates.

$$\lambda_{tl}^2 = 1.570n_{tl}^2 + 42.824n_{tl} - 71.44 \quad (\text{lower bound, Figure 8.17}) \quad (8.16)$$

$$\lambda_{m_u}^2 = 0.514 n_{m_u}^2 + 56.178 n_{m_u} - 124.06 \quad (\text{upper bound, Figure 8.17}) \quad (8.17)$$

$$m_{m_l} = 2.00 r - 0.002 \quad (\text{lower bound, Figure 8.18}) \quad (8.18)$$

$$m_{m_u} = 2.00 r + 1.002 \quad (\text{upper bound, Figure 8.18}) \quad (8.19)$$

$$\lambda_{m_u}^2 = (-12.070 + 1.776 r - 0.057 r^2) + (14.753 + 7.832 r - 0.326 r^2) n + (2.243 - 0.442 r + 0.018 r^2) n^2 \quad (\text{curve } OA, \text{ Figure 8.19}) \quad (8.20)$$

where: λ^2 = frequency parameters of anti-symmetric modes, r = aspect ratio

n = anti-symmetric mode counter, subscript t = denoted transition, subscript l, u denoted lower and upper bound.

8.3.3 Transition curves

The variation of the anti-symmetric mode verses the anti-symmetric mode counter for the free-free beam-plates are presented in Figures 8.8 to 8.19, for thickness to length ratio 1%, 2%, 5% and 10%. These figures show there are two distinct regions, the beam-like and plate-like behaviour, Figures 8.10, 8.13, 8.16 and 8.19 show clearly these regions and the transition line OA is the line that separates the two regions. It is important to notice the difference between the anti-symmetric mode and that for the symmetric mode studied in the previous chapter. This show that for aspect ratio higher than 7 the anti-symmetric mode verses anti-symmetric mode counter show smooth lines in the beam-like behaviour region, where as in the case of the symmetric modes aspect ratios higher than 15 show smooth line in the beam behaviour region.

Transition curves for 1% thickness to length ratio beam-plates.

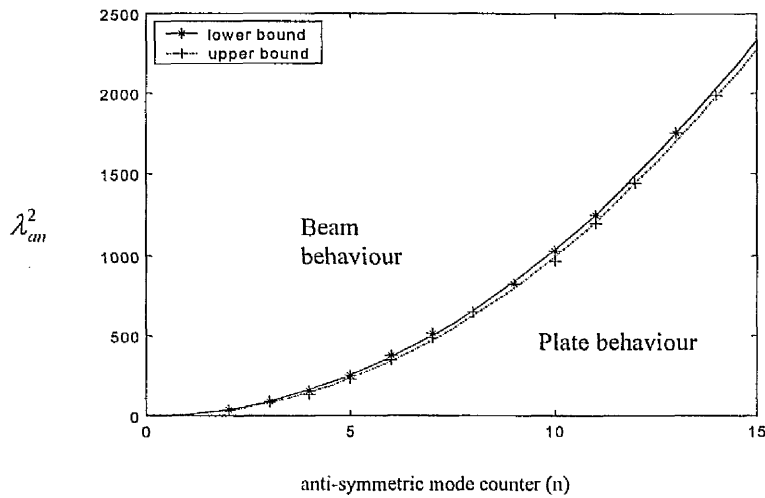


Figure 8.8 Variation of frequency parameter of anti-symmetric modes with anti-symmetric mode counter at transition point for 1% thickness to length ratio free-free beam-plates.

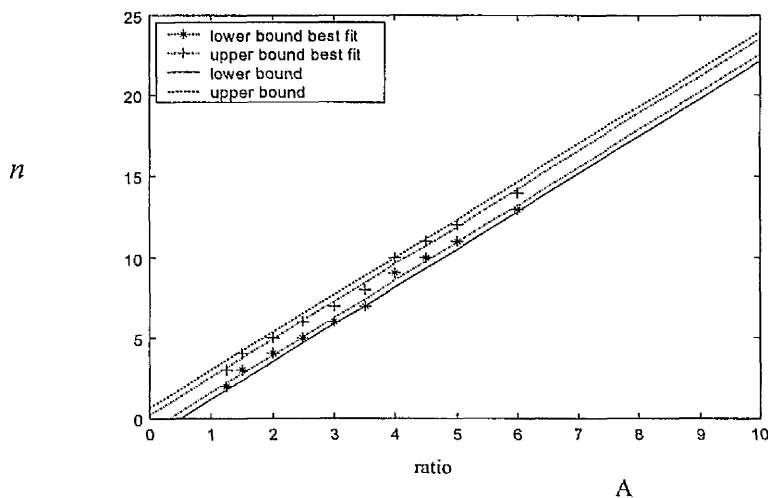


Figure 8.9 Variation of anti-symmetric mode counter at transition point with aspect ratio for 1% thickness to length ratio free-free beam-plates.

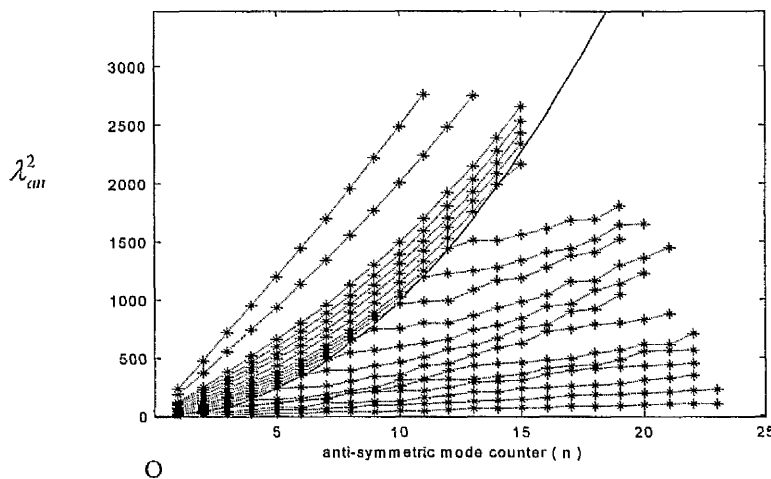


Figure 8.10 Variation of the frequency parameters of anti-symmetric mode with anti-symmetric mode counter (n) for aspect ratios 0.25 to 20.00 for 1% thickness to length ratio free-free beam-plates.

Transition curves for 2% thickness to length ratio beam-plates.

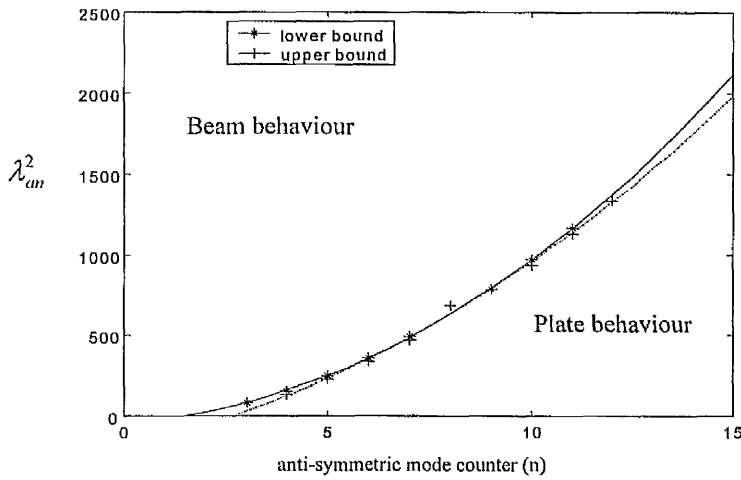


Figure 8.11 Variation of frequency parameter of anti-symmetric modes with anti symmetric mode counter at transition point for 2% thickness to length ratio free-free beam-plates.

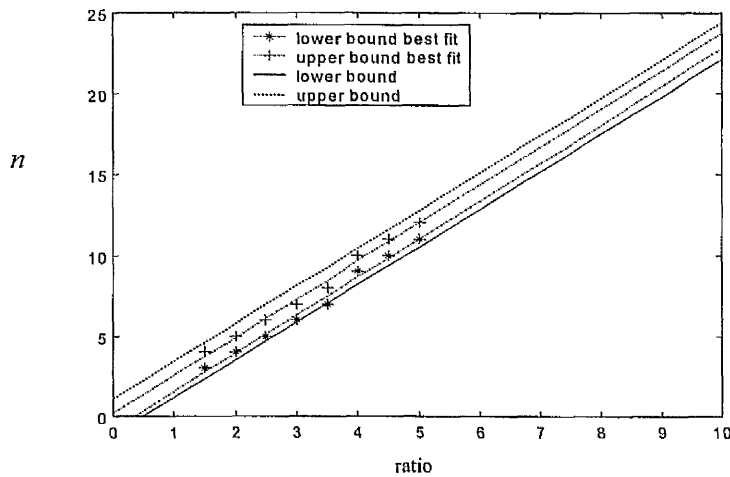


Figure 8.12 Variation of anti-symmetric mode counter at transition point with aspect ratio for 2% thickness to length ratio free-free beam-plates.

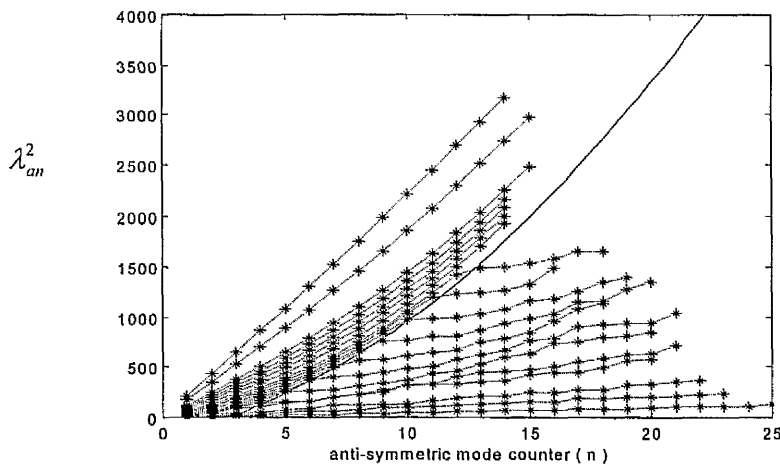


Figure 8.13 Variation of the frequency parameters of anti-symmetric mode with anti-symmetric mode counter (n) for aspect ratios 0.25 to 20.00 for 2% thickness to length ratio free-free beam-plates.

Transition curves for 5% thickness to length ratio beam-plates.

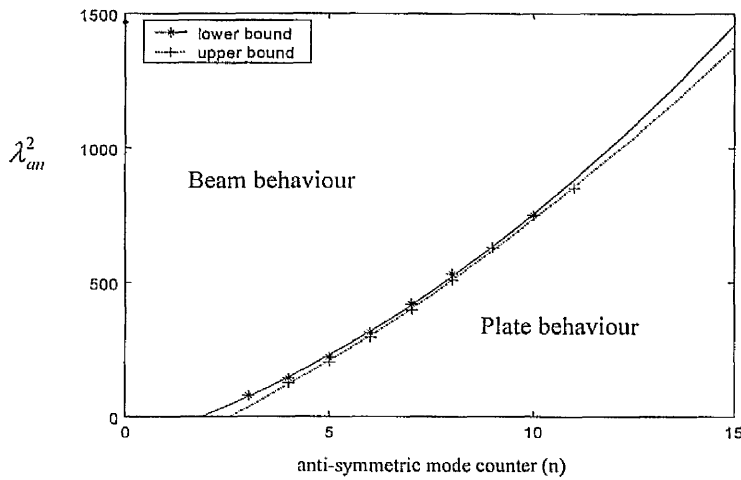


Figure 8.14 Variation of frequency parameter of anti-symmetric modes with anti-symmetric mode counter at transition point for 5% thickness to length ratio free-free beam-plates.

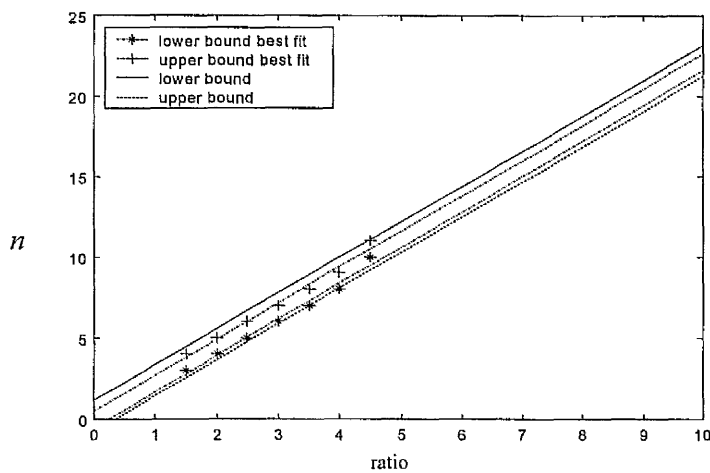


Figure 8.15 Variation of anti-symmetric mode counter at transition point with aspect ratio for 5% thickness to length ratio free-free beam-plates.

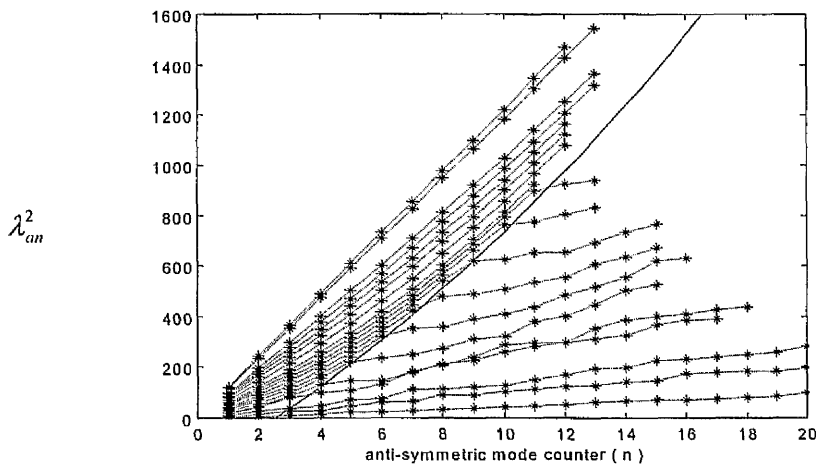


Figure 8.16 Variation of the frequency parameters of anti-symmetric mode with anti-symmetric mode counter (n) for aspect ratios 0.25 to 20.00 for 5% thickness to length ratio free-free beam-plates.

Transition curves for 10% thickness to length ratio beam-plates.

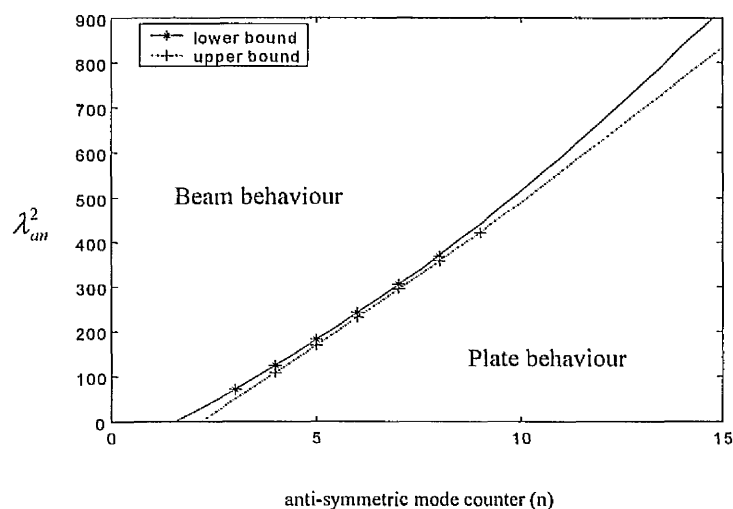


Figure 8.17 Variation of frequency Parameter of anti-symmetric modes with anti-symmetric mode counter at transition point for 10% thickness to length ratio

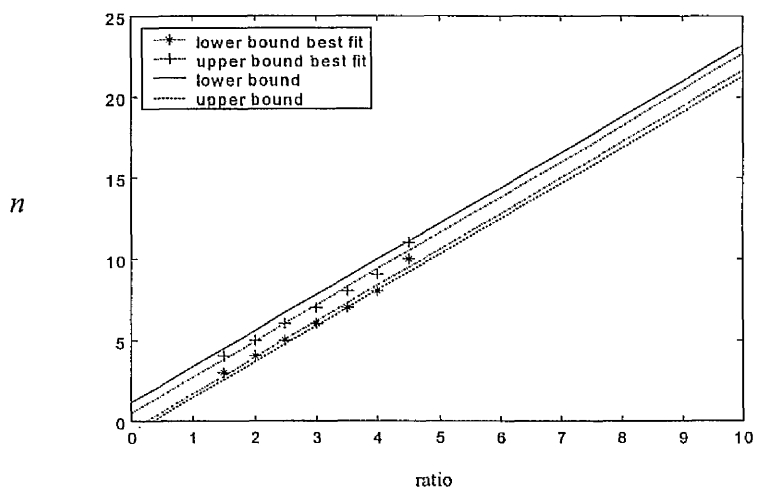


Figure 8.18 Variation of anti-symmetric mode counter at transition point with aspect ratio for 10% thickness to length ratio free-free beams-plates.

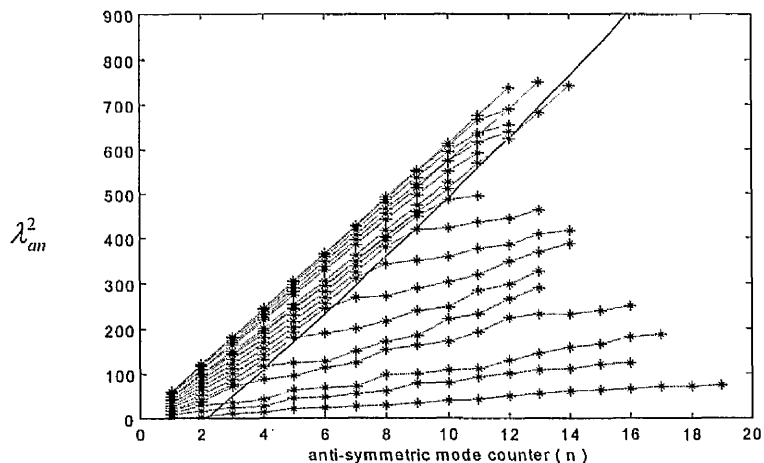


Figure 8.19 Variation of the frequency parameters of anti-symmetric mode with anti-symmetric mode counter (n) for aspect ratios 0.25 to 20.00 for 10% thickness to length ratio free-free beams-plates

8.4 Obtaining the transition curve from anti-symmetric modes for clamped-clamped boundary condition

8.4.1 Deduction from frequency parameter charts

Figure 8.20 shows the variation of the frequency parameters of the anti-symmetric modes (λ_{sn}^2) with the anti-symmetric mode counter (n) for aspect ratios of 0.25 to 3.5. For aspect ratios 0.25 to 1, the figure shows zigzag wavy lines which indicate plate-like behaviour. However as the aspect ratio increases, the curve begins to develop into two distinct line segments. These are a smooth line segment followed by a wavy line segment. The point of intersection of the two line segments is a transition point. For example, consider the beam-plate of aspect ratio of 1.25. It is seen that λ_{sn}^2 varies smoothly with n as n increases from 1 to 3. This section of the curve is associated with beam-like behaviour. However, at $n = 3$, there is a discontinuity in the curve. And as the value of n increases from 3 to 23 the curve becomes a zigzag line. This part of the curve suggests a plate-like behaviour. Therefore we can conclude from this that at $n = 3$ is the transition point from beam-like to plate-like behaviour for ratio 1.25. This value of $n = 3$ represents an upper bound for the transition point. A lower (conservative) bound for the transition point can be defined at a value of $n = 2$.

Figures 8.20 and 8.21 show that for aspect ratios between 3.0 and 6.0 (inclusive), the curve of variation of frequency parameters λ_{an}^2 with n can be divided into 2 sections. In the first section, when $1 \leq n \leq n_t$ where n_t is the value of n at the transition from beam-like to plate-like behaviour, λ_{an}^2 varies smoothly with n .

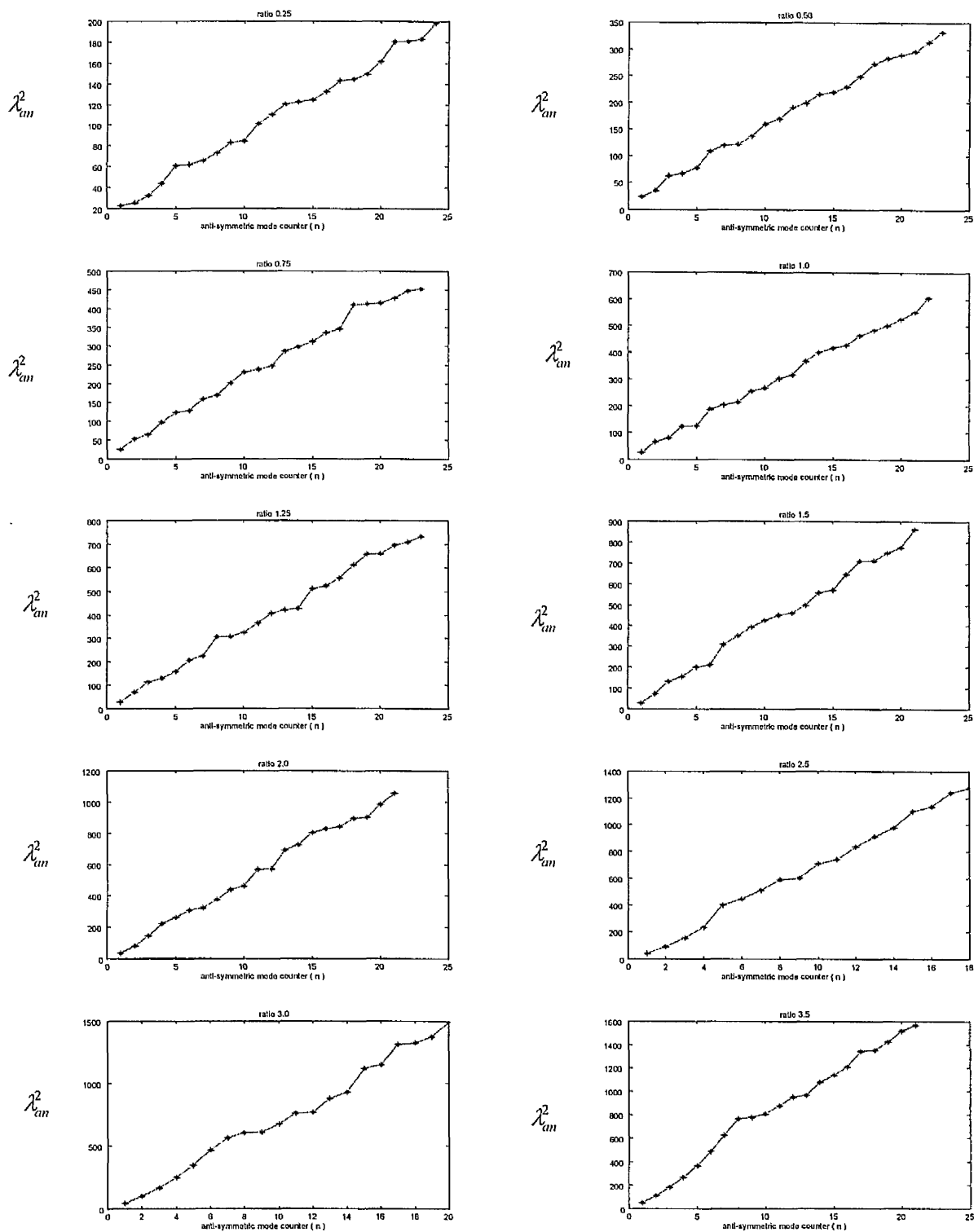


Figure 8.20 Variation of the frequency parameters of anti-symmetric modes with anti-symmetric mode counter (m) for aspect ratio 0.25 to 3.5 for 1% thickness to length ratio clamped-clamped beam-plates.

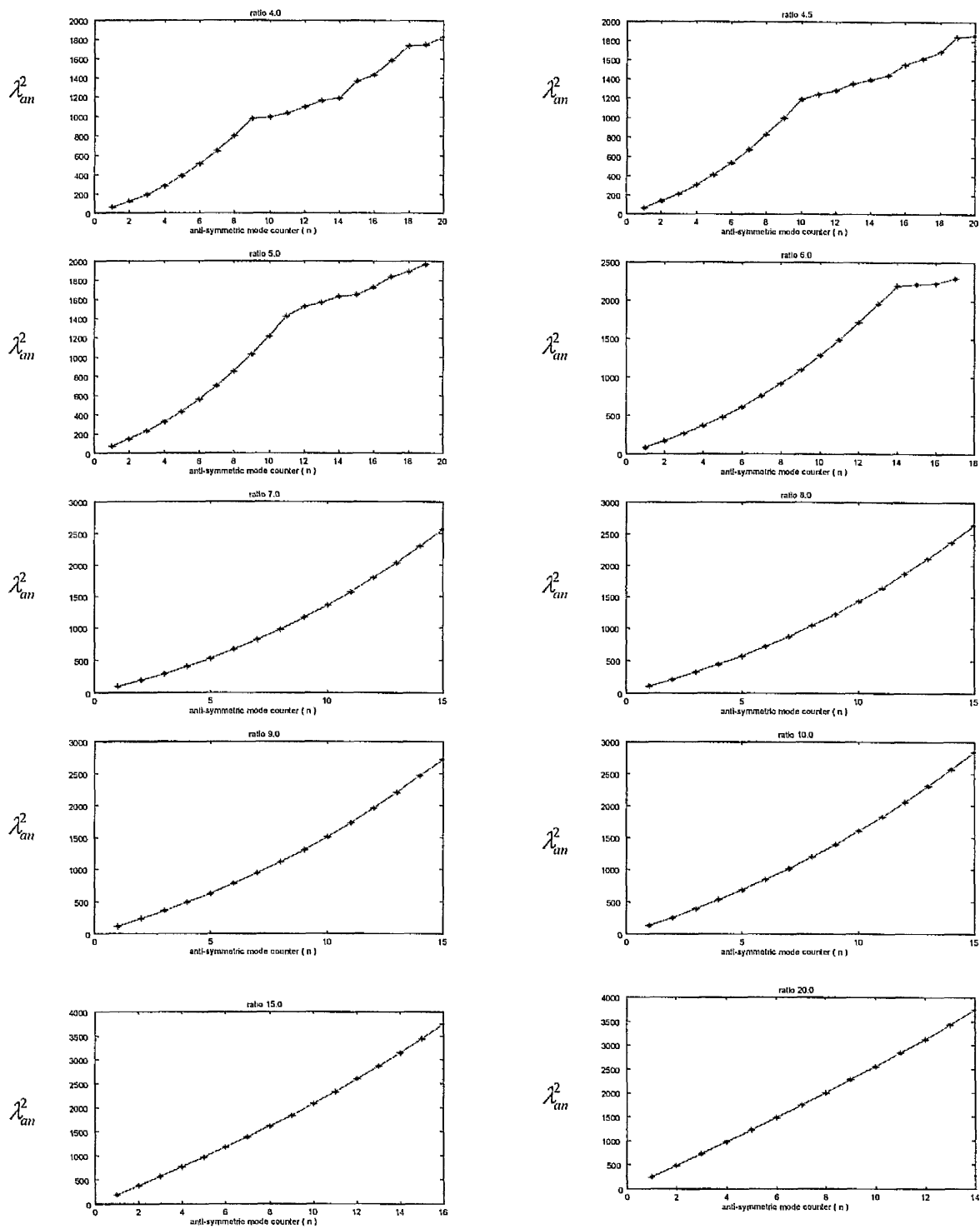


Figure 8.21 Variation of the frequency parameters of anti-symmetric modes with anti-symmetric mode counter (m) for aspect ratio 4 to 20 for 1% thickness to length ratio clamped-clamped beam-plates.

This section of the curve denotes beam-like behaviour. In the second section of the curve, when $n > n_i$, λ_{an}^2 varies in a somewhat zigzag, wavy manner as n increases. This latter section of the curve denotes plate-like behaviour. The upper bound values of n at the transition point from beam-like to plate-like behaviour are deduced from these figures as 6, 8, 9, 10, 11 and 14 for aspect ratios of 3.00, 3.50, 4.00, 4.50, 5.0 and 6.0 respectively. The corresponding lower bound values of n are 5, 7, 8, 9, 10 and 13. For aspect ratios greater than 7.0 the figures show that there is no discontinuity in the curve, and there are no transition points. This is because at these aspect ratios, the first 20 anti-symmetric modes shown in these figures are torsional modes of vibration.

8.4.2 Deduction from mode shapes

This section studies the transition curves using the anti-symmetric modes from the mode shapes. The procedure involves examination of the deformation along the breadthwise or j direction of the beam-plates at different modes of vibration. The modes of vibration for which there is a simple torsional deformation about the lengthwise direction are classed as beam-like behaviour, while modes for which there is a higher torsional deformation about the lengthwise axis or bending along the breathwise direction (j) are classed as plate-like behaviour.

Figures 8.22 to 8.26 shows the selected mode shapes for aspect ratios 0.75, 1.5, 2.5, 5.0 and 20.0 respectively. On examining these modes it is clear that there is a transition mode. Figure 8.22 represents aspect ratio 0.75. This figure shows clearly that there is bending along the breathwise direction (j), this indicates plate-like behavior. This deduction

is confirmed from Figure 8.20, which shows a zigzag variation of the frequency parameters and indicates plate-like behaviour.

Selected mode shapes for aspect ratio 1.5 are shown in Figure 8.23. The figure shows that for $n=1$ to $n=3$, there is only first order deformation in the (j) direction of the beam-plate. This implies fundamental torsional behaviour and indicates beam-like behaviour. However, the figure shows that for $n = 4$ to $n = 8$, there is higher order deformation in the breadthwise (j) direction of the beam-plate, which indicate plate-like behaviour. This statement also agrees with Figure 8.20 which shows that the data points corresponding to the first 3 modes lie on a smooth curve but when $n>3$ the modal points form a zigzag pattern which indicates plate-like behaviour.

The selected mode shapes for aspect ratio 2.50 are shown in Figure 8.24. This figure show that the transition is at mode 5, which again agrees with the deductions from Figure 8.21.

Figure 8.25 shows selected anti-symmetric mode shapes for aspect ratio 5.0. It contains the transition mode shape at mode 11. Again, this agrees with Figure 8.21. Figure 8.26 shows the mode shapes of modes 1 to 8 for aspect ratio 20.0. All modes in this figure are pure torsional mode, which denote beam behaviour. This is also confirmed by the smooth curve shown in Figure 8.21.

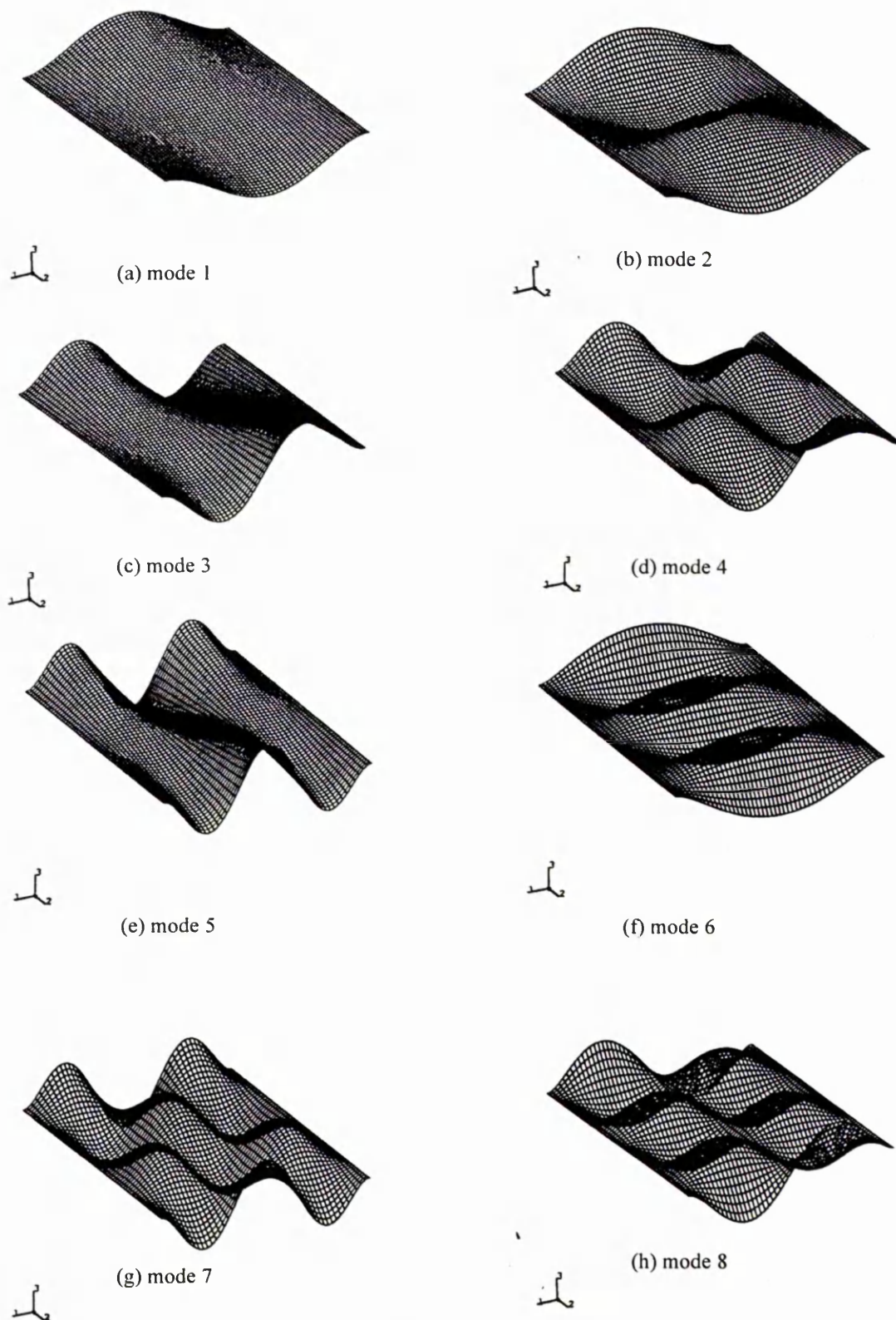


Figure 8.22 Anti-symmetric mode shape for aspect ratio 0.75 for 1% thickness to length ratio clamped-clamped beam-plates.

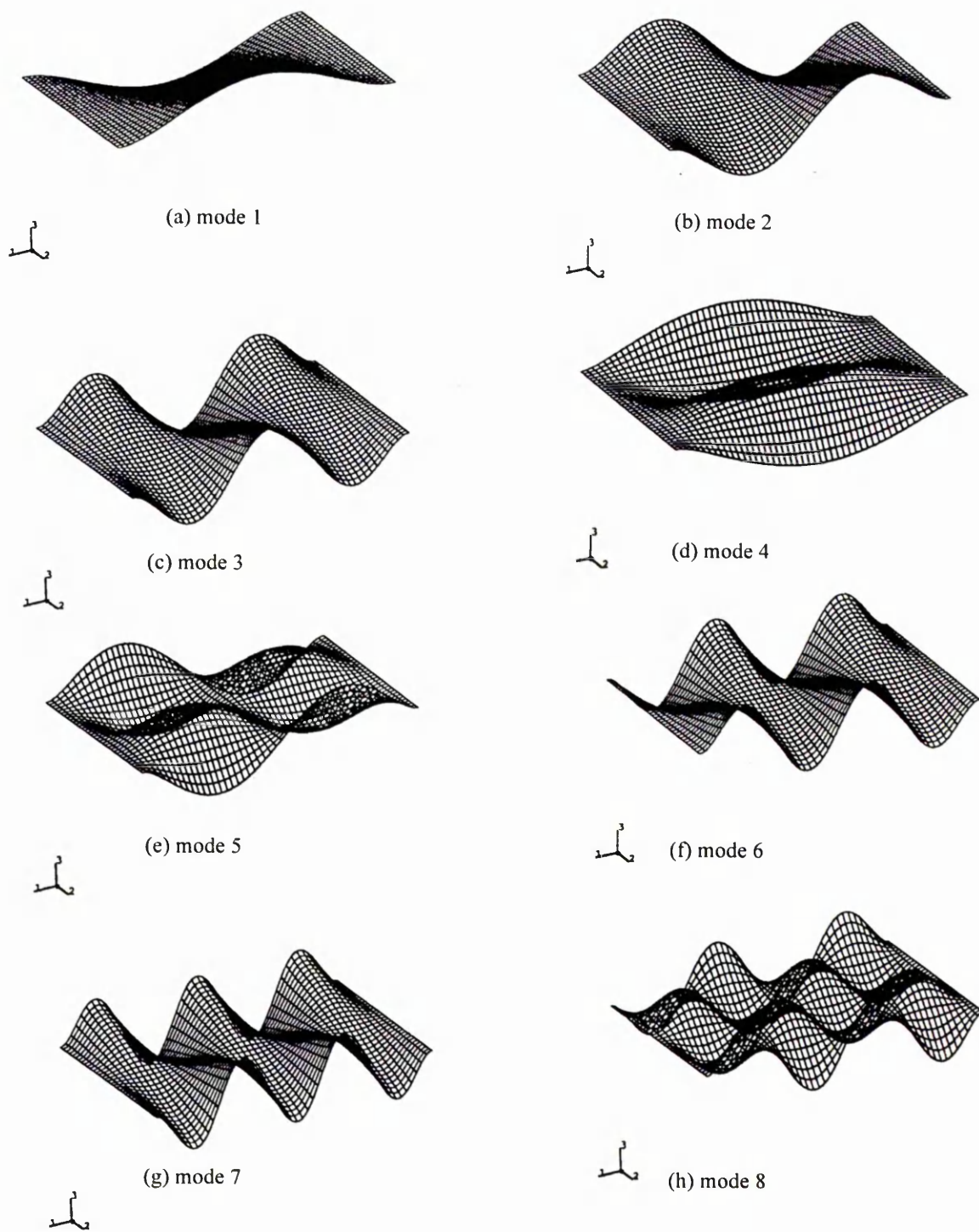


Figure 8.23 Anti-symmetric mode shape for aspect ratio 1.5 for 1% thickness to length ratio clamped-clamped beam-plates.

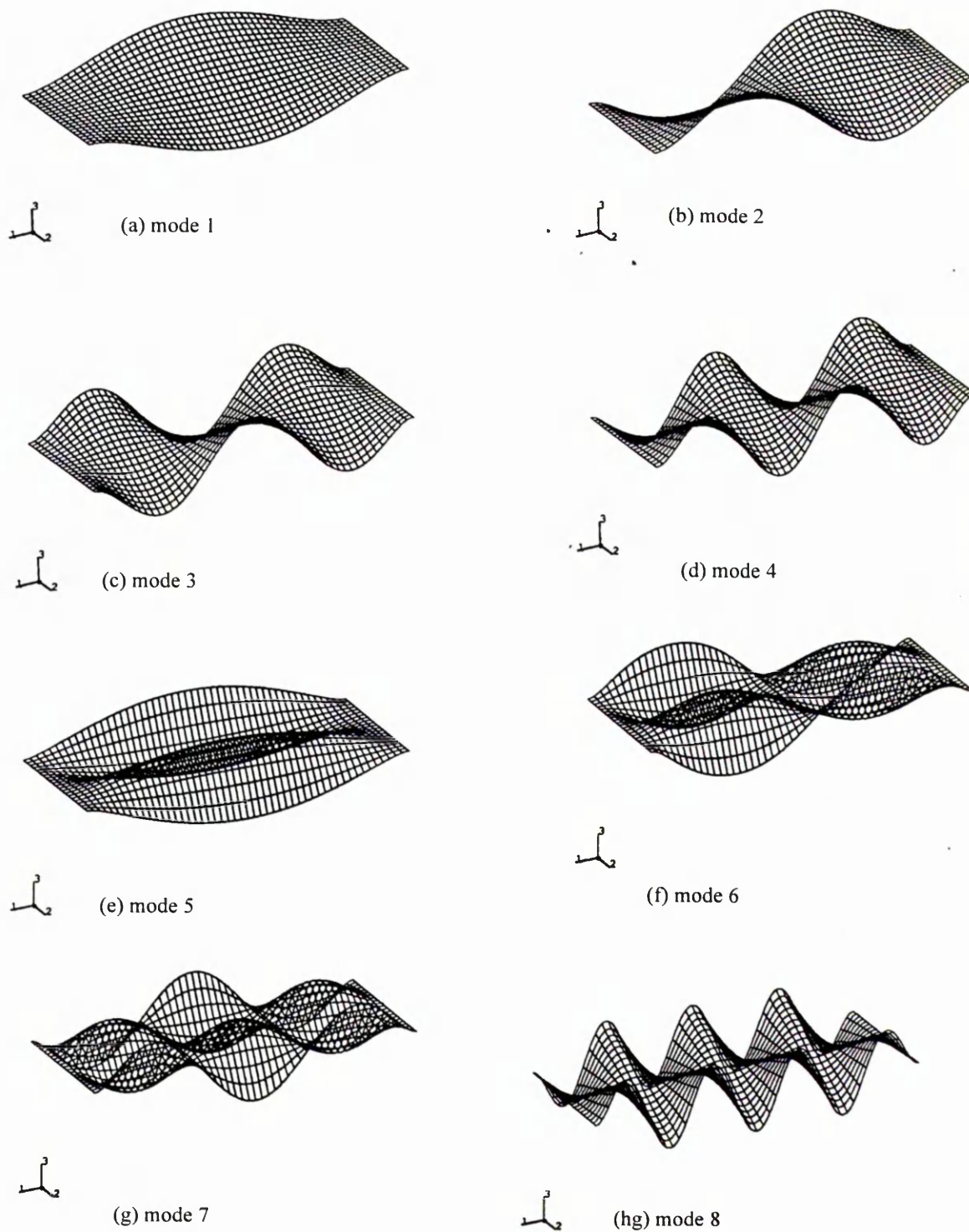


Figure 8.24 Anti-symmetric mode shape for aspect ratio 2.5 for 5 mm thick thickness to length ratio clamped-clamped beam-plates.

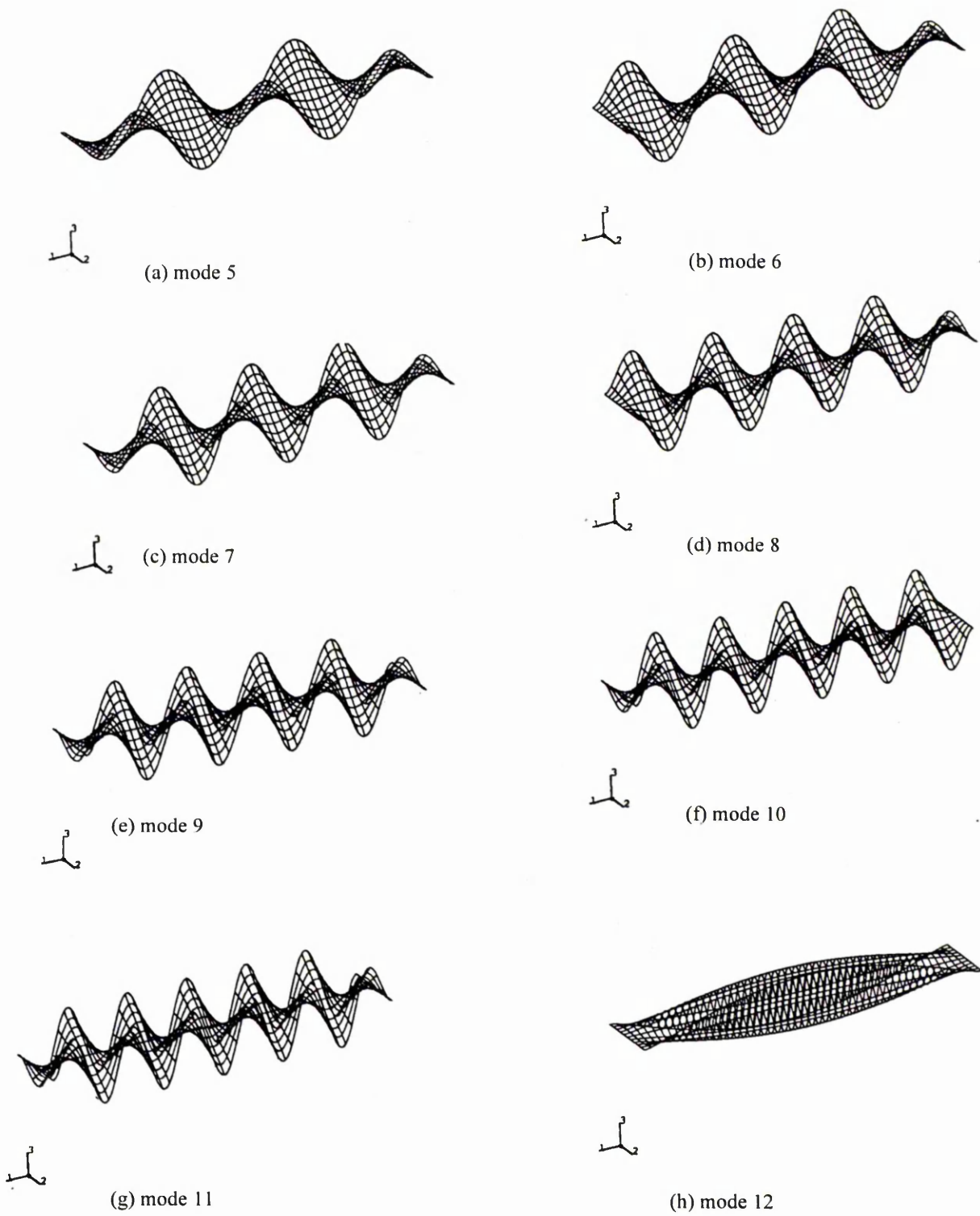


Figure 8.25 Anti-symmetric mode shape for aspect ratio 5.0 for 1% thickness to length ratio clamped-clamped beam-plates.

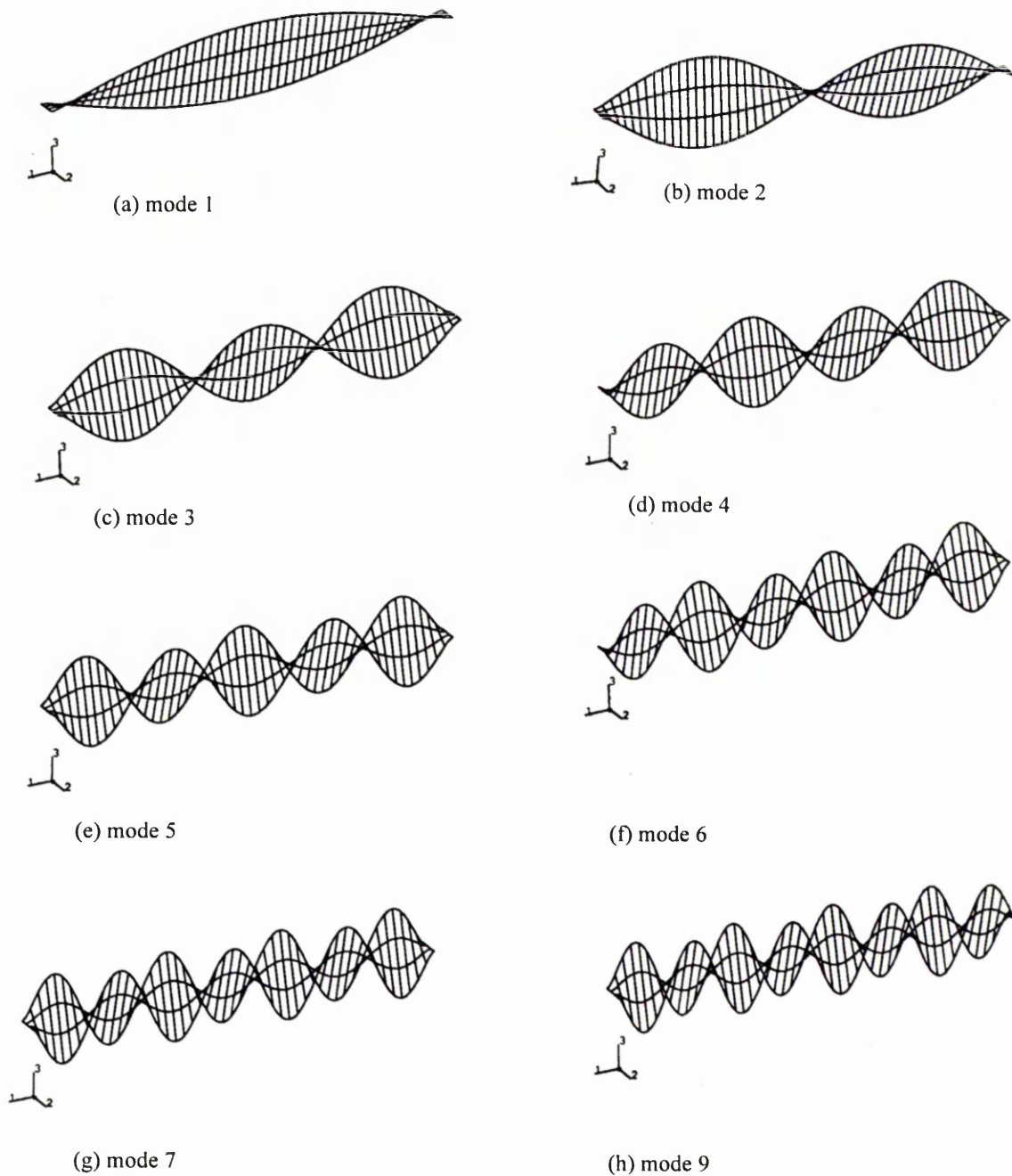


Figure 8.26 Anti-symmetric mode shape for aspect ratio 20.0 for 1% thickness to length ratio clamped-clamped beam-plates.

8.5 Transition curves and equations for clamped-clamped beam-plate

8.5.1 Tables of transition points

Table 8.5 to 8.8 show the transition points for thickness to length ratio 1%, 2%, 5% and 10%

Table 8.5 *Mode counter and frequency parameter of anti-symmetric modes at transition points for 1% thickness to length ratio clamped-clamped beam-plates.*

Aspect ratio	Lower bound values		Upper bound values	
	Mode counter	λ_{an}^2	Mode counter	λ_{an}^2
3.00	5	349.63	6	416.22
3.50	7	622.82	8	761.44
4.00	8	800.01	9	972.14
4.50	9	998.38	10	1188.29
5.00	10	1216.89	11	1424.20
6.00	13	1957.1	14	2190.00

Table 8.6 *Mode counter and frequency parameter of anti-symmetric modes at transition points for 2% thickness to length ratio clamped-clamped beam-plates.*

Aspect ratio	Lower bound values		Upper bound values	
	Mode counter	λ_{an}^2	Mode counter	λ_{an}^2
1.25	2	69.07	3	112.29
1.50	2	72.43	3	131.57
2.00	3	140.84	4	218.37
2.50	4	230.60	5	325.84
3.00	6	452.76	7	580.62
3.50	7	598.59	8	733.21
4.00	8	762.03	9	919.58
4.50	9	941.98	10	1113.02
5.00	10	1136.84	11	1320.47
6.00	13	1776.54	14	1993.38

Table 8.7 Mode counter and frequency parameter of anti-symmetric modes at transition points for 5% thickness to length ratio clamped-clamped beam-plates.

Aspect ratio	Lower bound values		Upper bound values	
	Mode counter	λ_{am}^2	Mode counter	λ_{am}^2
1.50	2	69.18	3	122.84
2.00	3	130.74	4	197.43
2.50	4	207.24	5	284.60
3.00	6	381.71	7	465.65
3.50	7	487.02	8	485.64
4.00	8	598.72	9	701.71
4.50	9	715.48	10	821.97

Table 8.8 Mode counter and frequency parameter of anti-symmetric modes at transition points for 10% thickness to length ratio clamped-clamped beam-plates.

Aspect ratio	Lower bound values		Upper bound values	
	Mode counter	λ_{am}^2	Mode counter	λ_{am}^2
1.50	2	60.96	3	102.78
2.00	3	108.49	4	156.05
2.50	5	213.87	6	267.79
3.00	6	274.55	7	330.04
3.50	7	337.28	8	403.39
4.00	8	401.23	9	458.39

8.5.2 Transition equations:

Transition equation for 1% thickness to length ratio beam-plates.

$$\lambda_{ll}^2 = 9.757 n_{ll}^2 + 26.257 n_{ll} - 30.354 \quad (\text{lower bound, Figure 8.27}) \quad (8.21)$$

$$\lambda_{lu}^2 = 8.949 n_{lu}^2 + 38.326 n_{lu} - 95.213 \quad (\text{upper bound, Figure 8.27}) \quad (8.22)$$

$$n_{ll} = 2.154 r - 2.23 \quad (\text{lower bound, Figure 8.28}) \quad (8.23)$$

$$n_{lu} = 2.514 r - 1.23 \quad (\text{upper bound, Figure 8.28}) \quad (8.24)$$

$$\lambda_{om}^2 = (8.011 + 4.085r - 0.171r^2) + (-4.840 + 11.006r + 0.0273r^2)n + (7.772 - 0.194r - 0.003r^2)n^2 \quad (\text{curve } OA, \text{ Figure 8.29}) \quad (8.25)$$

Transition equation for 2% thickness to length ratio beam-plates.

$$\lambda_{ll}^2 = 8.089n_{ll}^2 + 34.840n_{ll} - 35.146 \quad (\text{lower bound, Figure 8.30}) \quad (8.26)$$

$$\lambda_{lu}^2 = 7.619n_{lu}^2 + 41.450n_{lu} - 72.389 \quad (\text{upper bound, Figure 8.30}) \quad (8.27)$$

$$n_{ll} = 2.349r - 1.411 \quad (\text{lower bound, Figure 8.31}) \quad (8.28)$$

$$n_{lu} = 2.349r - 0.411 \quad (\text{upper bound, Figure 8.31}) \quad (8.29)$$

$$\lambda_{om}^2 = (-21.547 + 7.329r - 0.286r^2) + (17.686 + 7.556r + 0.078r^2)n + (6.459 - 0.185r - 0.004r^2)n^2 \quad (\text{curve } OA, \text{ Figure 8.32}) \quad (8.30)$$

Transition equation for 5% thickness to length ratio beam-plates.

$$\lambda_{ll}^2 = 6.322n_{ll}^2 + 20.022n_{ll} + 30.089 \quad (\text{lower bound}) \text{ From Figure 8.33} \quad (8.31)$$

$$\lambda_{lu}^2 = 6.819n_{lu}^2 + 8.238n_{lu} + 50.731 \quad (\text{upper bound}) \text{ From Figure 8.33} \quad (8.32)$$

$$n_{ll} = 2.428r - 1.714 \quad (\text{lower bound}) \text{ From Figure 8.34} \quad (8.33)$$

$$n_{lu} = 2.428r - 0.714 \quad (\text{upper bound}) \text{ From Figure 8.34} \quad (8.34)$$

$$\lambda_{om}^2 = (-27.26 + 4.672r - 0.174r^2) + (31.190 + 7.410r - 0.158r^2)n + (2.092 - 0.0216r - 0.0035r^2)n^2 \quad (\text{curve } OA, \text{ Figure 8.35}) \quad (8.35)$$

Transition equation for 10% thickness to length ratio beam-plates.

$$\lambda_{ll}^2 = 1.806n_{ll}^2 + 38.828n_{ll} - 24.172 \quad (\text{lower bound}) \text{ From Figure 8.36} \quad (8.36)$$

$$\lambda_{lu}^2 = 1.296m_{lu}^2 + 44.427n_{lu} - 42.673 \quad (\text{upper bound}) \text{ From Figure 8.36} \quad (8.37)$$

$$n_{ll} = 2.457r - 1.590 \quad (\text{lower bound}) \text{ From Figure 8.37} \quad (8.38)$$

$$n_{lu} = 2.457r - 0.590 \quad (\text{upper bound}) \text{ From Figure 8.37} \quad (8.39)$$

$$\lambda_{om}^2 = (-14.482 + 2.100r - 0.076r^2) + (27.853 + 5.696r - 0.233r^2)n + (1.106 - 0.218r - 0.0087r^2)n^2 \quad (\text{curve } OA, \text{ Figure 8.38}) \quad (8.40)$$

8.5.3 Transition curves: Transition curves for 5 mm thick beam-plates

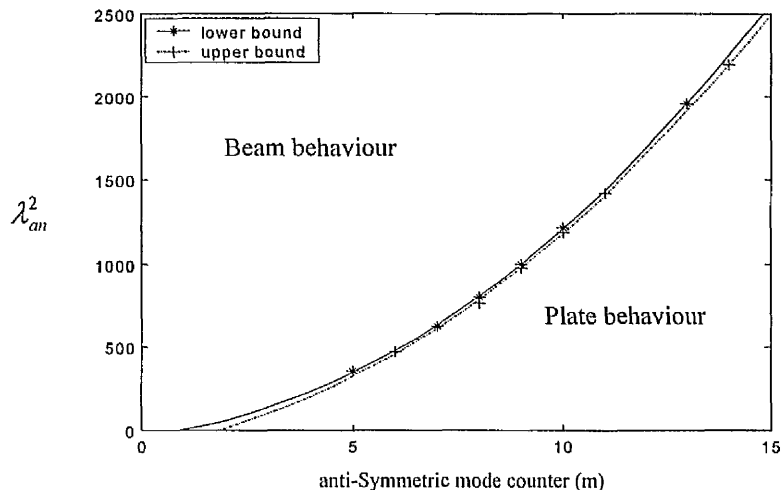


Figure 8.27 Variation of frequency parameter of anti-symmetric modes with anti-symmetric mode counter at transition point for 1% thickness to length ratio clamped-clamped beam-plates.

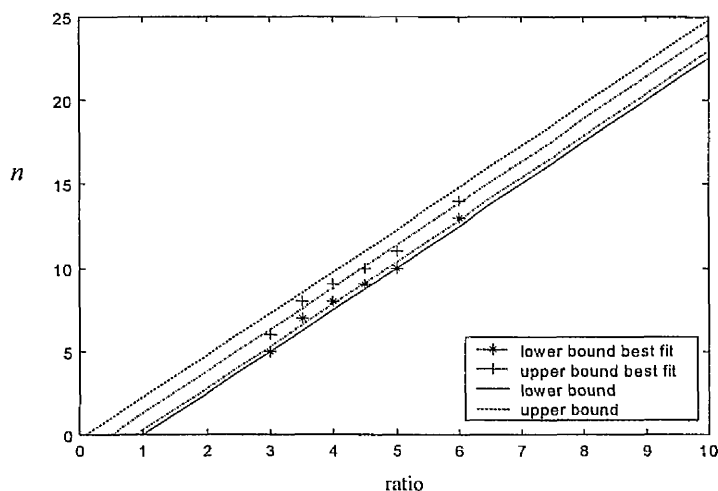


Figure 8.28 Variation of anti-symmetric mode counter at transition point with aspect ratio for 1% thickness to length ratio clamped-clamped beam-plates.

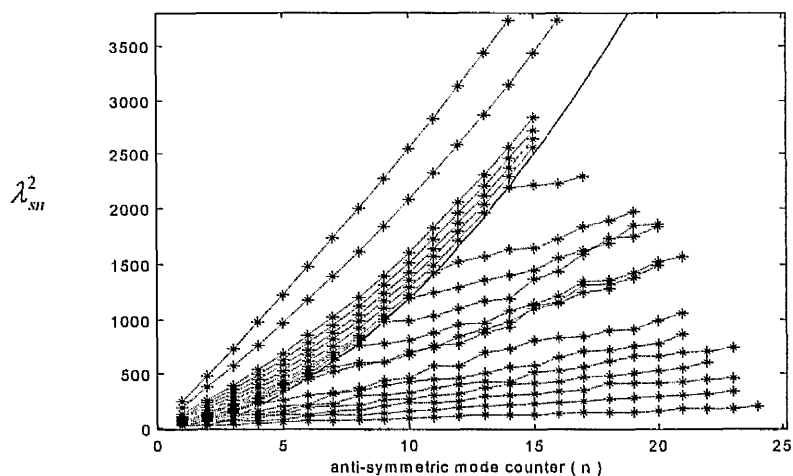


Figure 8.29 Variation of the frequency parameters of anti-symmetric modes with anti-symmetric mode counter (n) for aspect ratio 0.25 to 20.00 for 1% thickness to length ratio clamped-clamped beam-plates.

Transition curves for 2% thickness to length ratio beam-plates

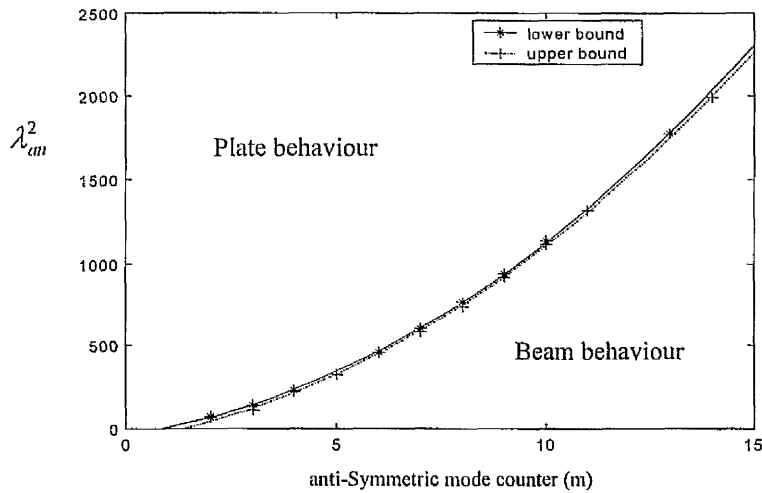


Figure 8.30 Variation of frequency parameter of anti-symmetric modes with anti-symmetric mode counter at transition point for 2% thickness to length ratio clamped-clamped beam-plates.

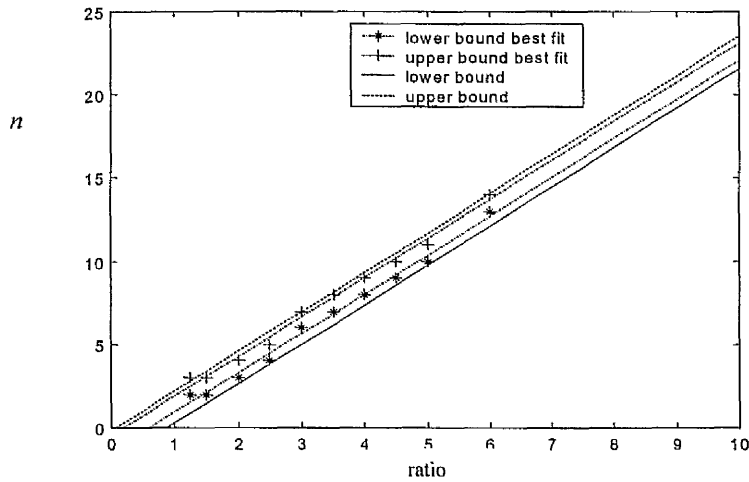


Figure 8.31 Variation of anti-symmetric mode counter at transition point with aspect ratio for 2% thickness to length ratio clamped-clamped beam-plates.

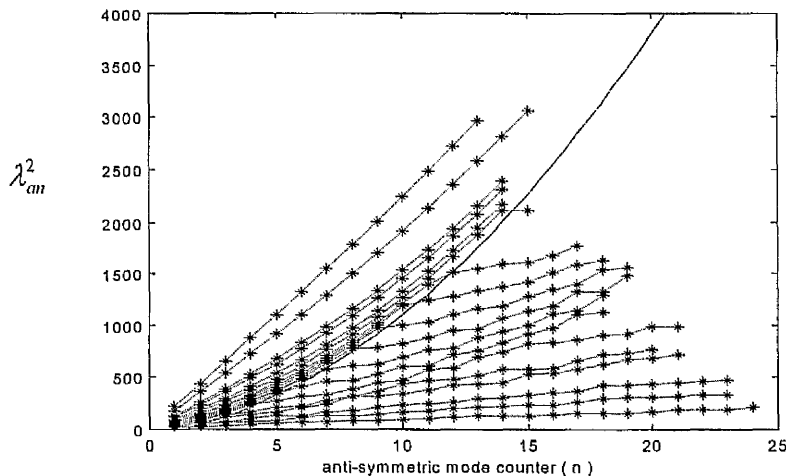


Figure 8.32 Variation of the frequency parameters of anti-symmetric modes with anti-symmetric mode counter (n) for aspect ratio 0.25 to 20.00 for 2% thickness to length ratio clamped-clamped beam-plates.

Transition curves for 5% thickness to length ratio beam-plates

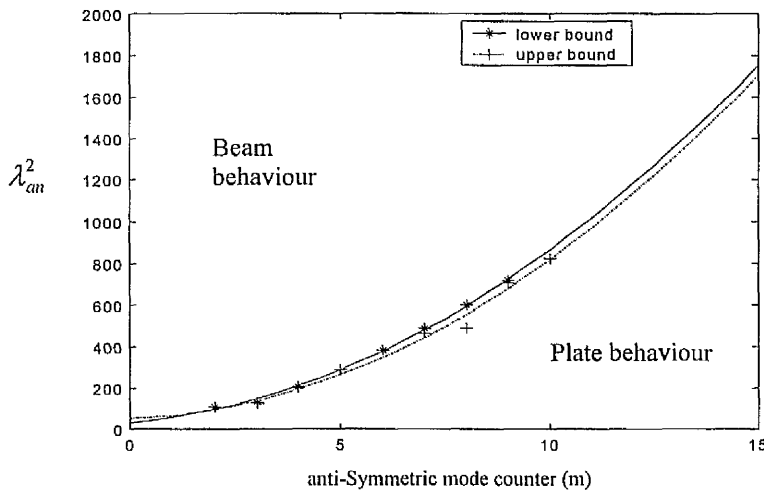


Figure 8.33 Variation of frequency parameter of anti-symmetric modes with anti-symmetric mode counter at transition point for 5% thickness to length ratio clamped-clamped beam-plates.

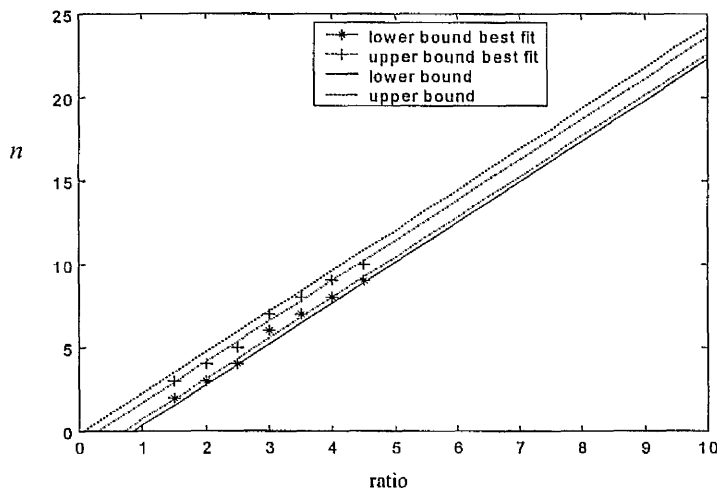


Figure 8.34 Variation of anti-symmetric mode counter at transition point with aspect ratio for 5% thickness to length ratio clamped-clamped beam-plates.

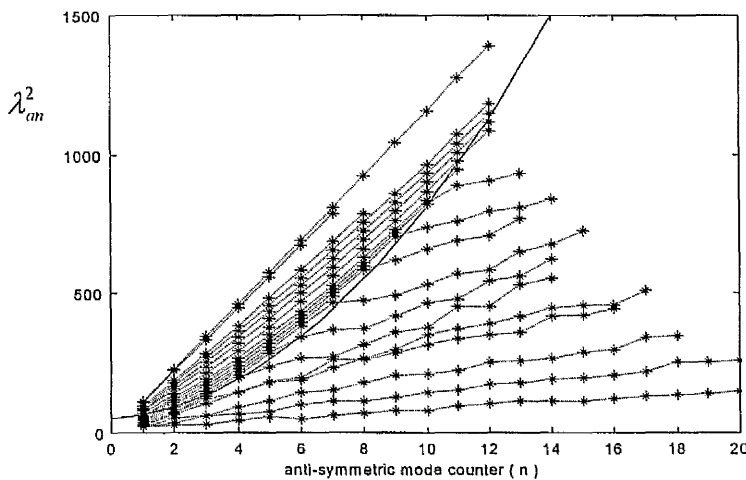


Figure 8.35 Variation of the frequency parameters of anti-symmetric modes with anti-symmetric mode counter (n) for aspect ratio 0.25 to 20.00 for 5% thickness to length ratio clamped-clamped beam-plates.

Transition curves for 10% thickness to length ratio beam-plates

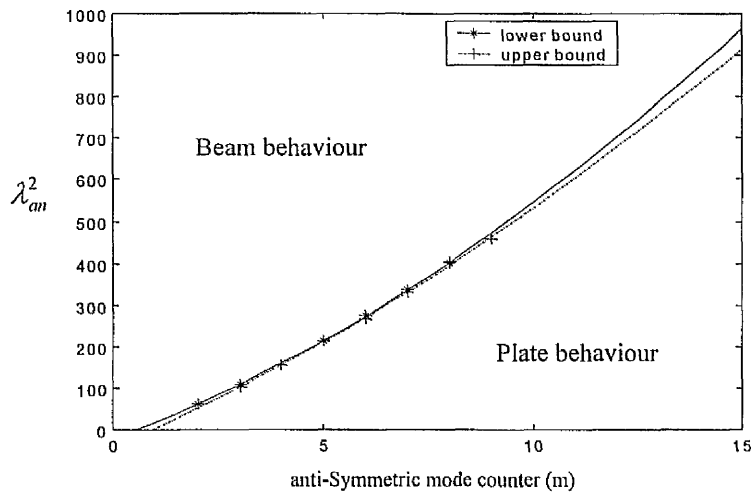


Figure 8.36 Variation of frequency parameter of anti-symmetric modes with anti-symmetric mode counter at transition point for 10% thickness to length ratio clamped-clamped beam-plates.

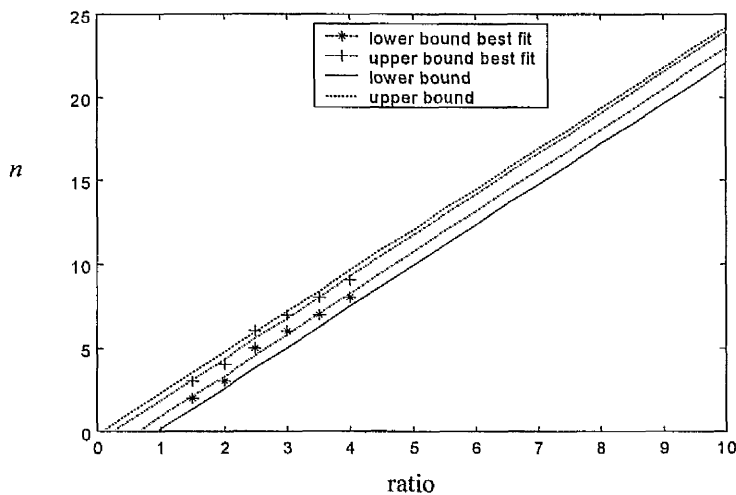


Figure 8.37 Variation of anti-symmetric mode counter at transition point with aspect ratio for 10% thickness to length ratio clamped-clamped beam-plates.

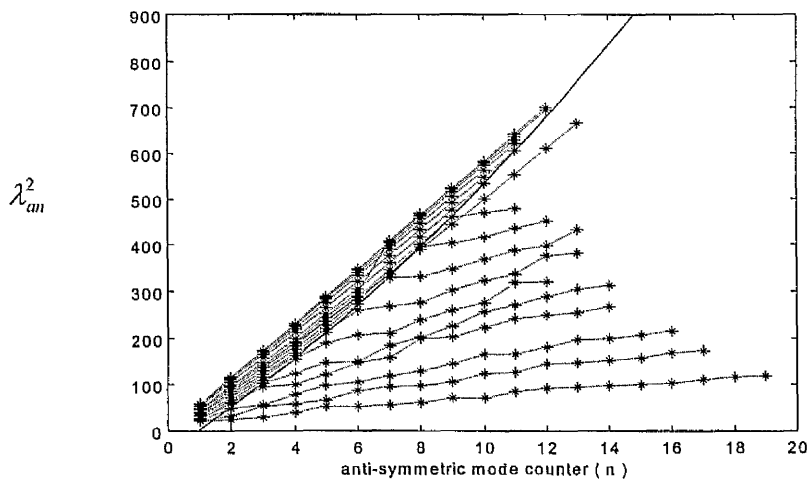


Figure 8.38 Variation of the frequency parameters of anti-symmetric modes with anti-symmetric mode counter (n) for aspect ratio 0.25 to 20.00 for 10% thickness to length ratio clamped-clamped beam-plates.

8.6 Summary

The work presented in this chapter was important in finding the transition curves and equations from beam-like to plate-like behaviour from the anti-symmetric modes for free-free and clamped-clamped beam-plates. The transition curves obtained have defined two regions on the frequency charts. The left region is a region of beam-like behaviour while the right region is a region of plate-like behaviour.

The examination of the mode shapes for some of the aspect ratio for both free-free and clamped-clamped beam-plates has provided further evidence to support the transition points obtained from the frequency charts. This evidence was much clearer in the case of the free-free beam-plates as their breadthwise edges started to bend at the transition point.

The transition curves obtained for both free-free and clamped-clamped beam-plates look very similar. The transition curves for thickness to length ratio 1% has a parabolic shape and as the thickness increases the transition curve becomes almost a straight line.

Chapter 9

Experimental and theoretical modal analysis of clamped-clamped and free–free beam-plates

9.1 Introduction

The determination of the natural frequencies and the mode shapes of a structure is important in order to understand the dynamic behaviour of a structure. This chapter is on the modal testing of selected clamped-clamped and free-free beam-plates of different sizes to determine their natural frequencies and mode shapes. The experimental results obtained are then compared with the FEA results. In addition, the frequency parameter charts are used to identify the modes of vibration from resonance frequencies obtained from measured frequency response functions.

9.2 Finite element modal analysis

Figure 9.1 shows a clamped-clamped plate of length a mm, breadth $b = 250$ mm and thickness $t = 5$ mm. The plate is made of aluminium alloy. The free length a of the plate is varied with the variation of the aspect ratio a/b . An aluminium alloy plate of identical dimensions was used for the free-free boundary conditions. The natural frequencies and mode shapes for the three aspect ratios, $a/b = 1, 2$ and 3 for the clamped-clamped plate, and the three aspect ratios, $a/b = 0.5, 2, 3$ for the free-free plate were calculated using the ABAQUS FE program. Element type S8R5 was used in the FE calculation. The number of elements in the lengthwise (x -) direction of the plate was fixed at a value of 100 ($N_x = 100$) for both cases, while the number of elements along the breadthwise (y -) direction of the plate (N_y) varied according to the aspect ratio a/b . The breadth (b) was fixed at 250 mm, while the length (a) was varied according to the aspect ratio a/b . The ABAQUS FE program was also used to predict the frequency response functions (FRFs) at different locations of the plate.

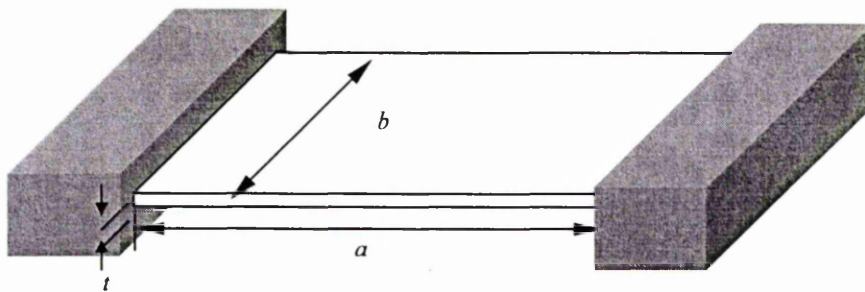


Figure 9.1 Clamped-clamped plate

9.3 Experimental modal analysis

The experimental vibration test on the plates was carried out in order to determine the actual modal characteristics of the plate for both free-free and clamped-clamped boundary conditions. The tests were carried out in the Dynamics and Aeroelasticity Research Laboratory, School of Engineering, University of Manchester. For tests on clamped-clamped plates, two ends of a 1250 mm x 250 mm x 5 mm thick plate were clamped in heavy fabricated supports as shown in Figure 9.2. The support material was steel and was fabricated from short lengths of a 250 mm x 250 mm x 25 mm thick hollow section beam. The top and bottom of the hollow section were welded to solid steel plates of dimensions 325 mm x 325 mm x 25 mm. The support was bolted to a metal bedplate. One of the supports remained fixed at one position while the other support was altered in position to give inter-support distances of 750 mm, 500 mm and 250 mm. These distances enabled clamped-clamped plates of aspect ratios, $a/b = 1, 2$ and 3 to be tested. In the case of the free-free plate, a soft elastic band was used to freely support the plate.

For both the clamped-clamped and free-free beam-plates, an electromagnetic exciter (shaker) was connected to the plate, via a force transducer, at a location which was 20 % of the length of the plate from one end. A band limited random signal was produced digitally in a HP workstation by the LMS CADA-X experimental modal analysis software [60]. The digital signal was converted into an analogue signal by the data acquisition system, amplified by the power amplifier and applied to the shaker to provide a random excitation which was band limited between 0 and 10 kHz. Two accelerometers were fixed to locations on the plates which were defined by a grid of 18 x 24, 27 x 15 and 33 x 12 points for the plate of aspect ratios 1, 2 and 3 respectively and were used to measure the frequency responses of the plate at these points. The outputs of the force transducer and the

accelerometers were connected to a signal conditioner, which amplified, and transducer the force and acceleration signals into voltages. These voltage signals were sampled and digitised by the data acquisition system, which transferred the measured data to a HP computer for processing using the LMS CADA-X modal analysis software.

For a clamped-clamped plate of aspect ratio 3, the predicted mode shape shows that the maximum number of nodes in the lengthwise (x -) and breadthwise (y -) directions are 11 and 4, respectively, or 10 and 3 half sine waves. At least 3 nodes are needed to plot 1 half-sine wave as shown in Figure 9.3. Therefore, for aspect ratio 3.0, FRF measurements need to be made at least at 33 (11x3) and 12 (4x3) nodes or points in the x - and y - directions of the plate. In the same way, the maximum number of half sine waves in the lengthwise (x -) and breadthwise (y -) directions are 9 and 5 for aspect ratio 2, and 6 and 8 for aspect ratio 1. Thus, at least 27 and 15 nodes in x - and y - directions are needed for aspect ratio 2, and at least 18 and 24 nodes in x - and y - directions are needed for aspect ratio 1.

For free-free plates of aspect ratio 3, the predicted modes shapes show that the maximum number of nodes in the lengthwise (x -) and breadthwise (y -) directions are 11 and 4, respectively, for up to 50 modal frequencies. Therefore, FRF measurements need to be made at least at 33 (11x3) and 12 (4x3) nodes for the aspect ratio 3.0. For aspect ratio 2, the maximum number of half sine waves in the lengthwise (x -) and breadthwise (y -) directions are 10 and 5, and 5 and 10 for aspect ratio 0.5. Therefore at least 30 and 15 nodes in the x - and y - directions are needed for aspect ratio 2 and at least 15 and 30 nodes in x - and y - directions are needed for aspect ratio 0.5.

Table 9.1 shows the aspect ratios, length a and breadth b of the clamped-clamped beam-plates tested as well as the locations of the shaker. The table also shows the corresponding numbers of nodes in the lengthwise- (x -) and breadthwise- (y -) directions of

the measured mode shapes of the plates. Similarly Table 9.2 shows the free-free boundary condition.

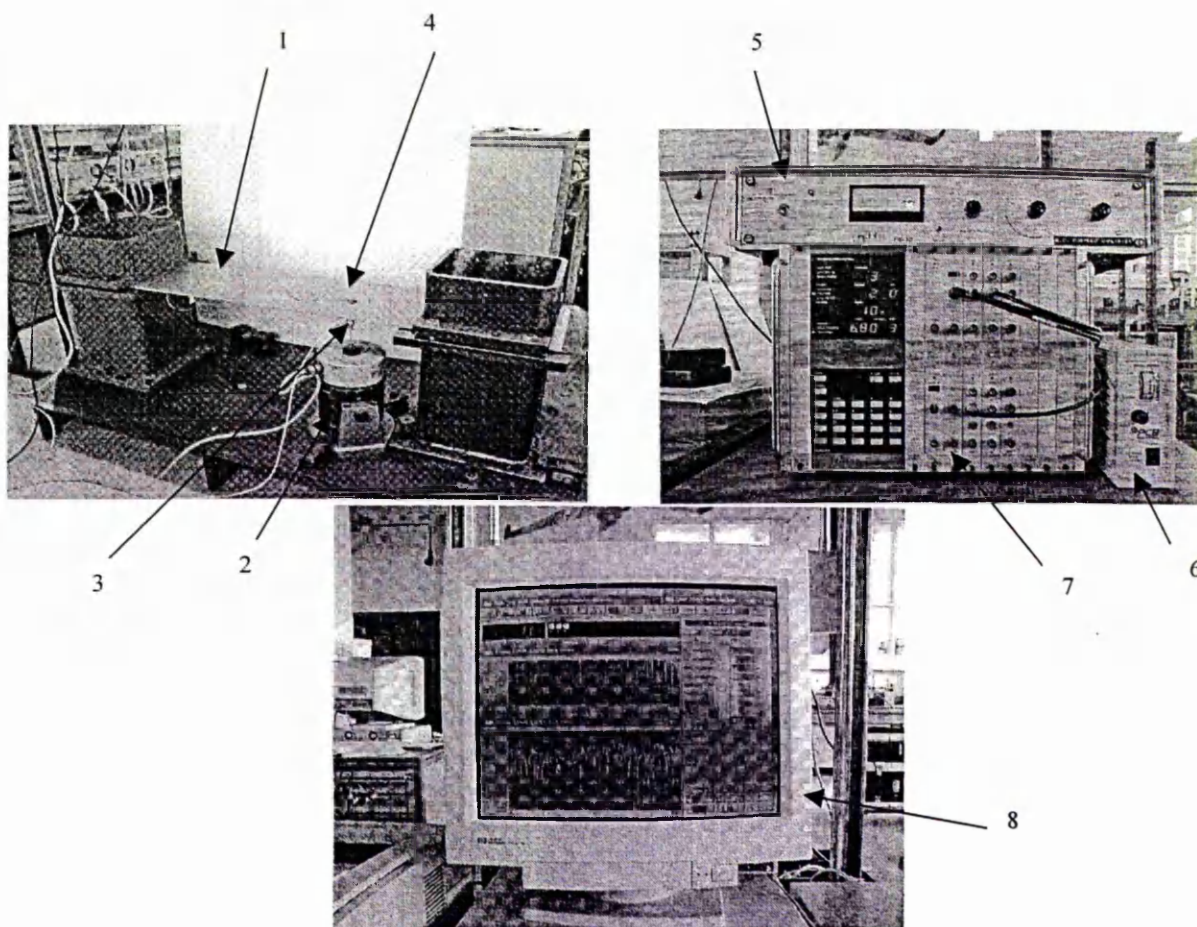
Table 9.1 *Aspect ratios, a , b , number of nodes in x and y directions and position of shaker for the experiment on vibration of clamped-clamped plate.*

Aspect ratio r	a (mm)	b (mm)	Number of nodes in x -direction	Number of nodes in y -direction	Position of shaker
1	250	250	21	21	(95,250)*
2	500	250	31	21	(125,250)
3	750	250	43	21	(150,250)

* Note : 1/5 of length (250 mm) of plate is 50 mm and is too small to install the shaker. Therefore for some aspect ratio 1, the shaker position was more than 1/5 of the free length of the plate.

Table 9.2 *Aspect ratios, a , b , number of nodes in x and y directions and position of shaker for the experiment on vibration of free-free plate.*

Aspect ratio r	a (mm)	b (mm)	Number of nodes in x -direction	Number of nodes in y -direction	Position of shaker
0.5	250	250	15	30	(250,100)
2	500	250	30	15	(100,250)
3	750	250	33	12	(150,250)



- | | |
|--------------------------------------|--------------------------------|
| 1- Clamped-clamped plate | 5- Power amplifier |
| 2 - Electromagnetic exciter (shaker) | 6- Signal conditioner |
| 3- Force transducer | 7- Data acquisition system |
| 4- Accelerometer | 8- HP workstation (computer) |

Figure 9.2 Equipment used in the experiment



Figure 9.3 Half-sine wave represented by 3 nodes.

9.4 Comparison of measured and predicted modal characteristics

Tables 9.3 to 9.5 show the natural frequencies and mode shapes of the free-free plates of aspect ratios 0.5, 2 and 3. The tables also show the percentage error between the measured and computed natural frequencies and the damping ratios derived from the measured FRFs by the LMS software.

The results for the natural frequencies and mode shapes clamped-clamped plates of aspect ratios 1, 2 and 3 are shown in Tables 9.6 to 9.8. However, because the support which clamps the plate ends is not infinitely rigid, the measured modal characteristics of the plate are affected by the finite stiffness of the support. However, in the FE computations, the plate was clamped with infinite support rigidity. Consequently, the experimental results do not compare very well with the FE results obtained.

Therefore, in order to predict more realistic modal properties, the FE computation was repeated for the clamped-clamped plate with supports. The three aspect ratios considered are 1, 2 and 3 with plate dimensions of 250 x 250 x 5 mm, 500 x 250 x 5 mm and 750 x 250 x 5 mm accordingly. The plate material is aluminium. Element type C3D20R was used in the FE analysis for the supports and the clamped-clamped plate.

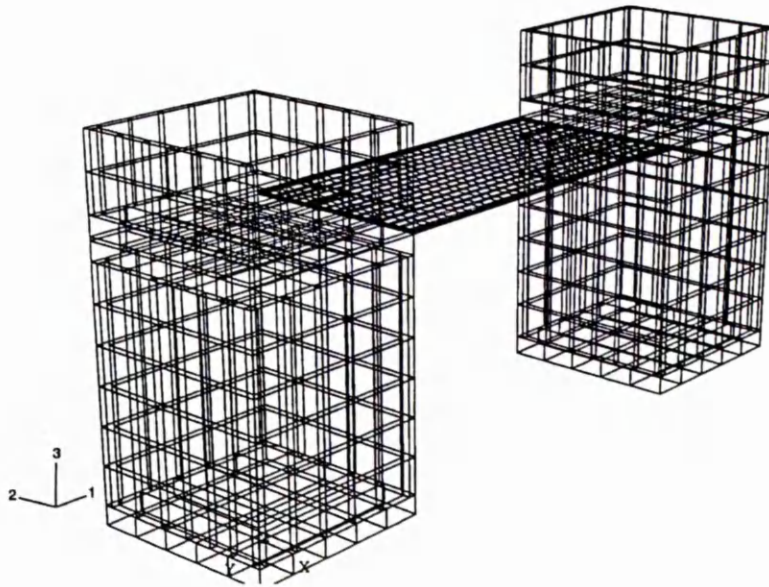


Figure 9.3 FE model of the clamped-clamped plate

From the results obtained in Tables 9.6 to 9.8, it is seen that the natural frequencies of the plate with supports predicted using FEA are closer to the experimental natural frequencies for the same mode shapes than without supports. Also the table shows that the relative errors between the natural frequencies of the plate without supports predicted using FEA and the experimental natural frequencies are higher than with supports. This is due to the fact that in the case of the plate without support, the plate was infinitely rigidly clamped so that the dynamics of the support did not affect the dynamics of the plate. In reality, the dynamics of the support affected the dynamics of the plate. Therefore the FEA predictions for the plate with supports provide closer natural frequencies to the experimentally measured natural frequencies than the FEA predictions for the plate without supports. The residual relative errors between the natural frequencies of the plate with support predicted using FEA and the experimental natural frequencies come from the interaction of the dynamics of the steel bedplate which was not modelled by the FEA.

The natural frequencies of the free-free plates of aspect ratios 0.5, 2 and 3 obtained from FEM are compared with the corresponding experimentally measured natural frequencies as shown in Figure 9.4. Similarly the natural frequencies of the clamped-clamped plates of aspect ratios 1, 2 and 3 with and without supports predicted using FEM are compared with the corresponding experimentally measured natural frequencies as shown in Figure 9.5. The figures show that the natural frequencies of the free-free plate predicted using FEM are closer to the experimentally measured natural frequencies than those of the clamped-clamped plate. This is due to the fact that the dynamics of the support affected the dynamics of the clamped plates.

Figure 9.6 shows the comparison of mode shapes and natural frequencies obtained from experimental measurement and FE analysis for free-free plate of aspect ratio 3. It is seen that the measured and predicted natural frequencies and mode shapes are very close. The percentage errors are relatively small.

Similarly, Figure 9.7 shows the comparison of mode shapes and natural frequencies obtained from experimental measurement and FE analysis for clamped-clamped plate of aspect ratio 3. Again the percentage errors are relatively small between the measure and predicted modal properties.

Table 9.3 Measured and predicted natural frequencies and damping ratios for the free-free plate of aspect ratio 0.5

Mode	FE Natural Frequency	Experimental Natural Frequency	% Error	Damping Ratio
0,2	105.34	105.47	-0.12	0.061
1,1	128.16	125.92	1.79	0.014
1,2	282.77	278.35	1.60	0.006
0,3	292.62	289.61	1.03	0.005
2,0	433.97	419.13	3.42	0.003
1,3	492.38	480.31	2.48	0.004
2,1	509.93	497.18	2.52	0.003
0,4	584.07	579.06	0.86	0.003
2,2	703.1	699.39	0.56	0.006
1,4	779.13	760.46	2.43	0.003
2,3	944.09	905.83	4.08	0.004
0,5	992.44	970.88	2.19	0.001
1,5	1143.1	1055.01	7.73	0.004
3,0	1208.2	1169.39	3.21	0.003
3,1	1282.8	1250.39	2.53	0.002
2,4	1296.3	1274.88	1.69	0.001
3,2	1443	1437.98	0.37	0.001
0,6	1455	-	-	-
1,6	1648.4	1644.40	0.25	0.001
2,5	1707	1709.11	-0.08	0.002
3,3	1734.3	1713.62	1.23	0.003
0,7	2025	2012.05	0.64	0.002
3,4	2103.8	2095.68	0.43	0.005
2,6	2192.2	2178.18	0.68	0.001
1,7	2209.7	2184.65	1.16	0.003
4,0	2368.5	2347.34	0.90	0.002
4,1	2413.1	2372.39	1.70	0.002
3,5	2549.1	2535.67	0.57	0.006
4,2	2580.6	2563.86	0.67	0.003
0,8	2713.6	2676.45	1.38	0.002
2,7	2769.7	2743.25	0.99	0.003
1,8	2868.1	-	-	-
4,3	2884	2869.21	0.54	0.004
3,6	3070.6	3056.46	0.51	0.006
4,4	3239.8	3228.30	0.39	0.007
2,8	3456.3	3393.02	1.86	0.004
0,9	3462.5	3436.06	0.78	0.003
1,9	3611	3563.42	1.34	0.003
3,7	3668	3629.55	1.09	0.003
4,5	3707.5	3706.02	0.08	0.005
5,0	3893.8	3891.74	0.06	0.003

Table 9.4 Measured and predicted natural frequencies and damping ratios for the free-free plate of aspect ratio 2.0

Mode	FE Natural Frequency	Experimental Natural Frequency	% Error	Damping Ratio
2,0	105.34	105.47	-0.12	0.061
1,1	128.21	125.92	1.79	0.014
2,1	282.87	278.35	1.60	0.006
3,0	292.63	289.61	1.03	0.005
0,2	433.98	419.13	3.42	0.003
3,1	492.54	480.31	2.48	0.004
1,2	510.02	497.18	2.52	0.003
4,0	584.11	579.06	0.86	0.003
2,2	703.32	699.39	0.56	0.006
4,1	779.36	760.46	2.43	0.003
3,2	944.37	905.83	4.08	0.004
5,0	992.60	970.88	2.19	0.001
5,1	1143.4	1055.01	7.73	0.004
0,3	1208.2	1169.39	3.21	0.003
1,3	1282.9	1250.39	2.53	0.002
4,2	1296.8	1274.88	1.69	0.001
2,3	1443.3	1437.98	0.37	0.001
6,0	1455.1	-	-	-
6,1	1648.5	1644.40	0.25	0.001
5,2	1707.7	1709.11	-0.08	0.002
3,3	1734.9	1713.62	1.23	0.003
7,0	2025.1	2012.05	0.64	0.002
4,3	2104.7	2095.68	0.43	0.005
6,2	2193.1	2178.18	0.68	0.001
7,1	2210.2	2184.65	1.16	0.003
0,4	2368.6	2347.34	0.90	0.002
1,4	2413.4	2372.39	1.70	0.002
5,3	2550.3	2535.67	0.57	0.006
2,4	2581.1	2563.86	0.67	0.003
8,0	2713.8	2676.45	1.38	0.002
7,2	2770.7	2743.25	0.99	0.003
8,1	2868.7	-	-	-
3,4	2884.8	2869.21	0.54	0.004
6,3	3072	3056.46	0.51	0.006
4,4	3241.1	3228.30	0.39	0.007
8,2	3457.5	3393.02	1.86	0.004
9,0	3462.9	3436.06	0.78	0.003
9,1	3611.9	3563.42	1.34	0.003
7,3	3669.6	3629.55	1.09	0.003
5,4	3709.1	3706.02	0.08	0.005
0,5	3894.1	3891.74	0.06	0.003

Table 9.5 Measured and predicted natural frequencies and damping ratios for the free-free plate of aspect ratio 3.0

Mode	FE Natural Frequency	Experimental Natural Frequency	% Error	Damping Ratio
2,0	46.75	46.20	1.18	0.040
1,1	84.48	84.06	0.50	0.041
3,0	130.02	126.99	2.33	0.013
2,1	178.81	177.31	0.84	0.017
4,0	256.05	254.67	0.54	0.005
3,1	292.25	288.5	1.28	0.009
5,0	417.87	408.57	2.23	0.004
4,1	433.2	424.40	2.03	0.006
0,2	439.47	437.55	0.44	0.004
1,2	480.97	477.31	0.76	0.005
2,2	560.6	557.15	0.62	0.004
5,1	608.24	595.84	2.04	0.004
6,0	649.45	643.30	0.95	0.002
3,2	703.49	694.70	1.25	0.003
6,1	821.13	803.94	2.09	0.003
4,2	879.07	853.08	2.96	0.002
7,0	902.37	891.51	1.20	0.002
7,1	1070.9	1051.01	1.86	0.002
5,2	1086.6	1036.78	4.58	0.002
8,0	1200.3	1187.98	1.03	0.002
0,3	1208.8	1157.99	4.20	0.003
1,3	1240.4	1219.86	1.66	0.004
2,3	1310.5	1300.38	0.77	0.002
6,2	1326.7	1318.39	0.63	0.005
8,1	1390.8	1353.14	2.71	0.002
3,3	1459.3	1432.64	1.83	0.002
9,0	1540.4	1510.24	1.96	0.002
7,2	1601.6	1558.89	2.67	0.002
4,3	1644.7	1734.23	-5.44	0.003
9,1	1716.7	1677.00	2.31	0.002
5,3	1869.8	1734.39	7.24	0.003
8,2	1905.7	1900.35	0.28	0.002
10,0	1928.2	1901.07	1.41	0.001
10,1	2084.7	2033.65	2.45	0.004
6,3	2140.1	2153.55	-0.63	0.004
9,2	2252	2231.38	0.92	0.002
11,0	2334.4	2338.85	-0.19	0.002
0,4	2369.3	2463.24	-3.96	0.003
1,4	2410	2380.00	1.24	0.003
7,3	2414.7	2439.34	-1.02	0.004
2,4	2467.5	2458.96	0.35	0.002

Table 9.6 Measured and predicted natural frequencies and damping ratios for the clamped-clamped plate of aspect ratio 1.00

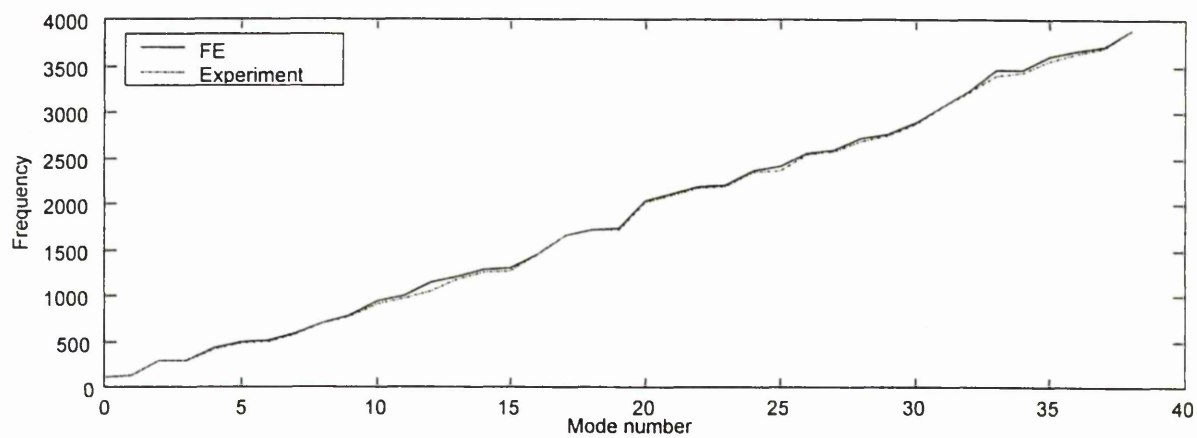
Mode	Natural Frequency			% error		Damping Ratio
	FE		Experiment	Without Support	With support	
	Without support	With support				
0,0	436.74	428.05	342.86	21.50	19.90	0.013
,0,1	516.28	507.95	397.12	23.08	21.82	0.012
0,2	851.31	828.44	692.98	18.60	16.35	0.008
1,0	1201.1	1175.40	988.54	17.70	15.90	0.007
1,1	1312.6	1288.10	1234.4	5.96	4.17	0.012
0,3	1563.2	1513.00	1423.72	8.92	5.90	0.007
1,2	1705.8	1658.00	1676.58	1.66	-1.12	0.026
2,0	2347.5	2292.20	2148.9	8.46	6.25	0.062
1,3	2419.4	2336.00	2248.19	7.08	3.76	0.006
2,1	2468.0	2409.20	2277.87	7.70	5.45	0.016
0,4	2681.3	2591.90	2622.89	2.18	-1.19	0.163
2,2	2900.2	2819.30	2712.24	6.48	3.80	0.002
1,4	3500.7	3370.10	3306.22	5.56	1.90	0.002
2,3	3642.1	3515.00	3341.21	8.26	4.94	0.005
3,0	3862.4	3782.00	3789.21	1.89	-0.19	0.004
3,1	3984.2	3907.70	3830.60	3.86	1.97	0.005
0,5	4190.2	4048.90	4041.31	3.55	0.19	0.003
3,2	4440.1	4317.50	4093.18	7.81	5.20	0.001
2,4	4724.0	4540.50	4379.44	7.29	3.55	0.010
1,5	4964.7	4774.90	4756.39	4.20	0.39	0.006
3,3	5206.1	5028.00	5091.50	2.20	-1.26	0.001
4,0	5734.4	5566.20	5562.76	2.99	0.06	0.002
4,1	5853.4	5728.80	-	-	-	-
0,6	6071.6	5864.70	5618.88	7.46	4.19	0.001
2,5	6165.1	5909.30	5729.27	7.07	3.05	0.003
3,4	6298.7	6049.90	5940.55	5.69	1.81	0.005
4,2	6324.2	6158.30	-	-	-	-
1,6	6705.6	6547.20	-	-	-	-
4,3	7104.5	6867.50	-	-	-	-

Table 9.7 Measured and predicted natural frequencies and damping ratios for the clamped-clamped plate of aspect ratio 2.00

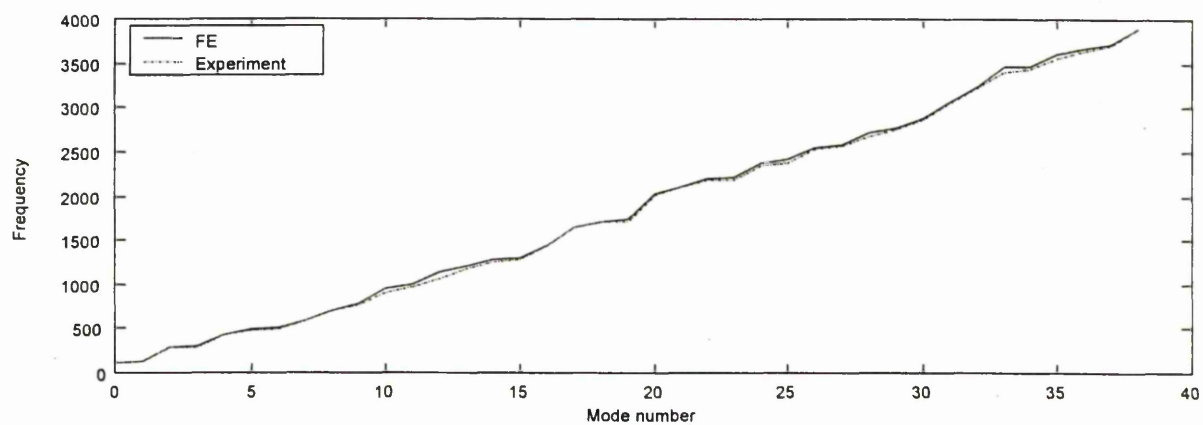
Mode	Natural Frequency			% error		Damping Ratio
	FE		Experiment	Without support	With support	
	Without support	With Support				
0,0	108.64	96.67	93.08	14.32	3.71	0.025
0,1	174.77	163.22	153.30	12.28	6.08	0.015
1,0	299.37	266.62	246.67	17.60	7.48	0.016
1,1	401.61	361.66	342.26	14.78	5.36	0.008
0,2	537.99	475.56	501.09	6.85	-5.36	0.007
2,0	587.91	523.28	541.21	7.94	-3.42	0.013
2,1	707.18	624.46	601.69	14.92	3.65	0.008
1,2	776.36	680.51	679.08	12.53	0.21	0.016
3,0	972.59	865.25	867.84	10.77	-0.30	0.015
2,2	1111.1	959.08	963.83	13.25	-0.50	0.026
3,1	1100.7	964.98	967.44	12.11	-0.25	0.028
0,3	1296.6	1134.30	1158.06	10.68	-2.09	0.007
4,0	1452.7	1290.90	1301.44	10.41	-0.82	0.010
3,2	1531.0	1306.20	1368.50	10.61	-4.77	0.006
1,3	1516.0	1310.90	1323.65	12.69	-0.97	0.009
4,1	1585.2	1388.30	-	-	-	-
2,3	1850.9	1579.30	1615.85	12.70	-2.31	0.008
4,2	2036.0	1727.70	1775.82	12.78	-2.79	0.007
5,0	2027.4	1765.70	1740.58	14.15	1.42	0.010
5,1	2161.6	1893.30	1908.81	11.69	-0.82	0.008
3,3	2283.0	1924.40	1923.07	15.77	0.07	0.007
0,4	2449.5	2139.60	2251.14	8.10	-5.21	0.005
5,2	2627.5	2227.50	2312.33	12.00	-3.81	0.014
1,4	2650.1	2289.20	2369.67	10.58	-3.51	0.013
4,3	2804.0	2341.30		-	-	
6,0	2695.4	2386.90	2455.21	8.91	-2.86	0.019
6,1	2829.8	2469.90	2528.07	10.66	-2.36	0.022
2,4	2969.3	2529.50	2729.42	8.08	-7.90	0.024
6,2	3307.7	2810.10		-	-	
5,3	3411.2	2832.70	3001.49	12.01	-5.95	0.021
3,4	3395.7	2854.60	3076.53	9.39	-7.77	0.010
7,0	3455.5	3078.10	-	-	-	0.002
7,1	3588.7	3458.20	3495.92	2.58	-1.09	0.002
4,4	3918.7	3257.00	3419.24	12.74	-4.98	0.004
6,3	4103.9	3400.60	3611.21	12.00	-6.19	0.004
0,5	3980.8	3472.50	3668.87	7.83	-5.65	0.003
7,2	4075.5	3472.70		-	-	
1,5	4167.0	3601.80	3801.31	8.77	-5.54	0.006
5,4	4532.1	3733.60	4044.74	10.75	-8.33	0.002
2,5	4470.6	3816.70	4109.64	8.14	-7.67	0.003
8,0	4306.3	3923.70	4113.69	4.84	-4.47	0.003

Table 9.8 Measured and predicted natural frequencies and damping ratios for the clamped-clamped plate of aspect ratio 3.00

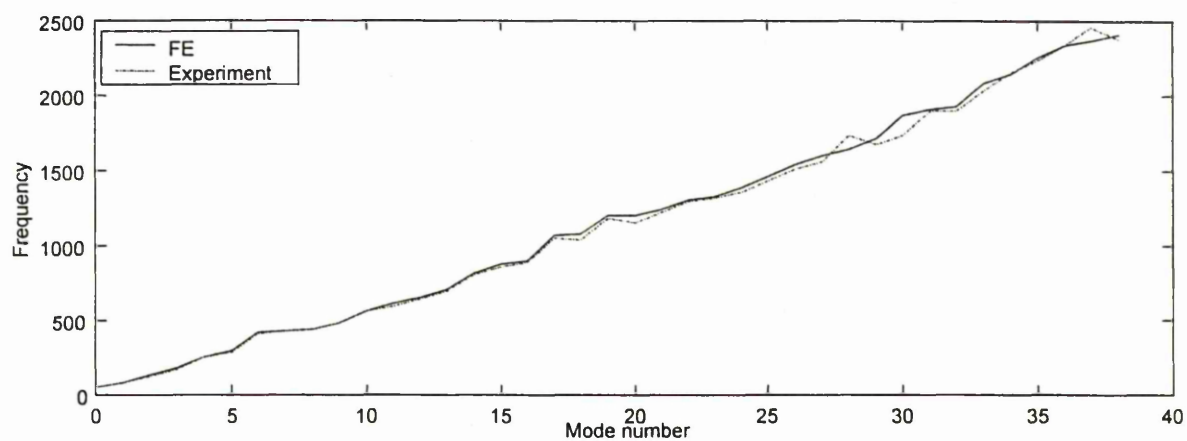
Mode	Natural Frequency			% error		Damping Ratio
	FE		Experiment	Without support	With support	
	Without support	With Support				
0,0	48.05	42.81	44.02	8.39	-2.83	0.006
0,1	102.25	97.95	92.79	9.25	5.27	0.004
1,0	132.37	118.05	119.59	9.65	-1.30	0.007
1,1	221.58	205.95	197.36	10.93	4.17	0.004
2,0	260.15	231.95	228.80	12.05	1.36	0.008
2,1	369.73	334.16	326.18	11.78	2.39	0.004
0,2	483.54	427.20	441.17	8.76	-3.27	0.001
3,0	431.03	384.06	375.22	12.95	2.30	0.011
1,2	593.72	524.40	552.15	7.00	-5.29	0.006
3,1	553.0	490.87	487.83	11.78	0.62	0.004
4,0	644.90	574.20	540.03	16.26	5.95	0.016
2,2	755.67	662.56	586.61	22.37	11.46	0.005
4,1	774.57	681.18	684.78	11.59	-0.53	0.006
3,2	959.05	831.83	-	-	-	-
5,0	901.55	802.42	761.46	15.54	5.10	0.026
5,1	1036.0	907.37	896.66	13.45	1.18	0.008
0,3	1252.1	1098.40	1105.15	11.74	-0.61	0.007
4,2	1200.3	1030.40	-	-	-	-
1,3	1349.0	1176.10	-	-	-	-
6,0	1200.8	1067.90	1073.55	10.60	-0.53	0.012
2,3	1502.8	1299.40	-	-	-	-
6,1	1338.1	1170.50	1130.26	15.53	3.44	0.013
5,2	1478.9	1259.80	1336.97	9.60	-6.13	0.009
3,3	1706.4	1461.1	1461.22	14.37	-0.01	0.005
7,0	1542.2	1370.5	1427.16	7.46	-4.13	0.005
7,1	1681.1	1471.8	1553.67	7.58	-5.56	0.006
6,2	1795.3	1522.10	-	-	-	-
4,3	1954.3	1659.20	1634.05	16.38	1.51	0.005
8,0	1925.7	1707.00	1778.90	7.62	-4.21	0.016
0,4	2410.7	2110.60	2120.87	12.02	-0.48	0.034
5,3	2243.1	1888.50	1957.21	12.74	-3.63	0.012
7,2	2150.1	1819.10	1908.97	11.21	-4.94	0.012
8,1	2065.3	1808.00	1864.84	9.71	-3.14	0.017
1,4	2498.1	2174.90	2299.06	7.97	-5.71	0.034
2,4	2640.9	2280.80	-	-	-	-
6,3	2570.9	2149.40	2115.17	17.73	1.59	0.008
9,0	2350.9	2089.40	2201.58	6.35	-5.37	0.017
3,4	2835.3	2426.00	2516.71	11.24	-3.74	0.009
8,2	2543.8	2151.60	2210.15	13.12	-2.72	0.003
9,1	2490.4	2182.00	2221.83	10.78	-1.83	0.018
4,4	3078.0	2609.20	-	-	-	-



(a) aspect ratio 0.5



(b) aspect ratio 2



(c) aspect ratio 3

Figure 9.4 FEA and experimental natural frequencies versus mode number for free-free plates of aspect ratios 0.5, 2 and 3.

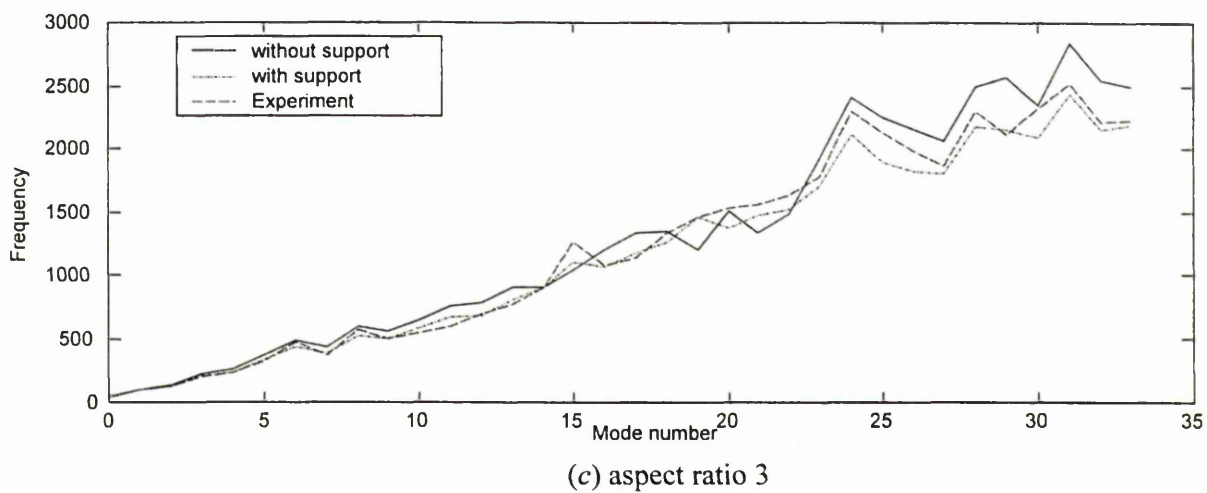
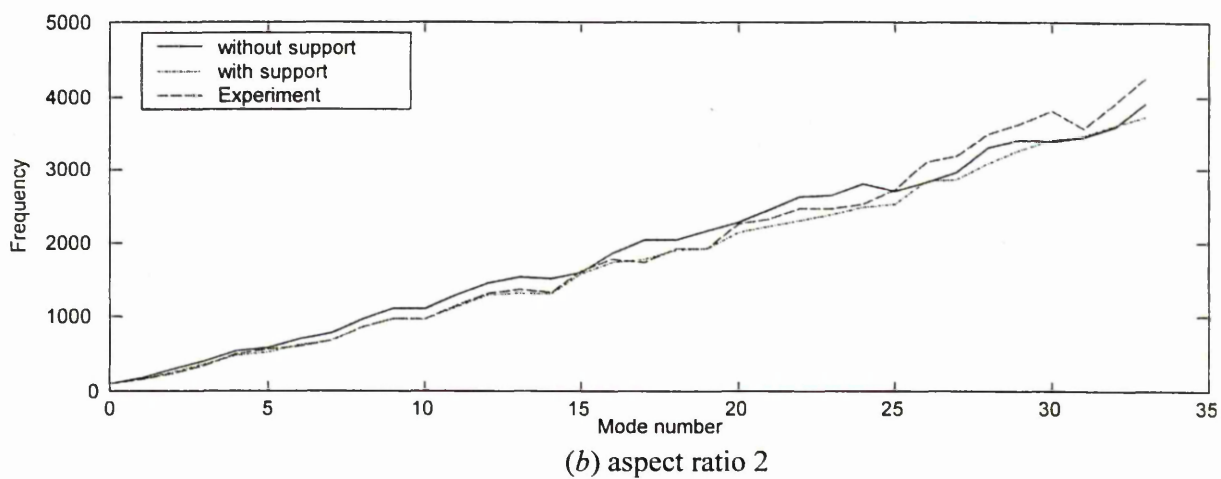
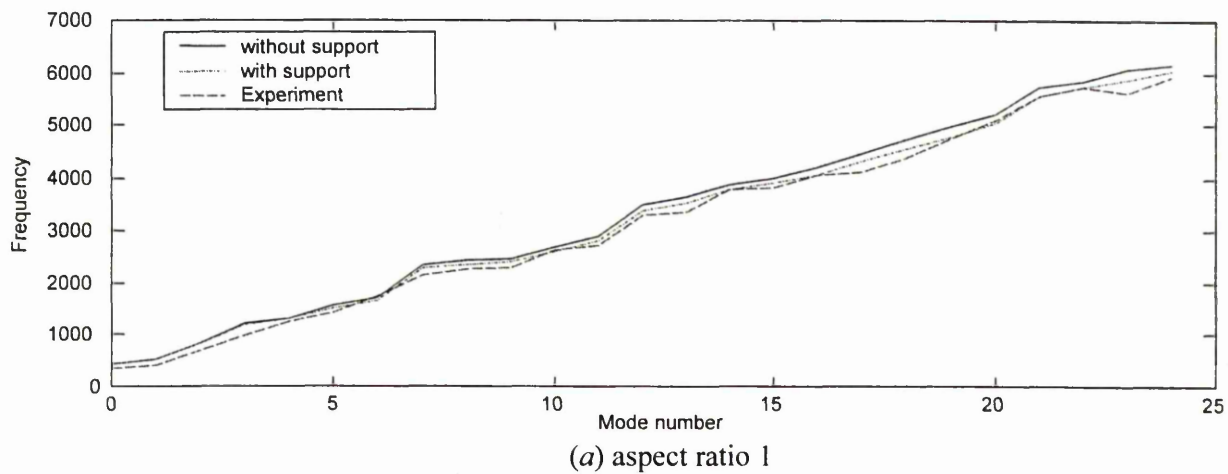


Figure 9.5 FEA and experimental natural frequencies versus mode number for clamped-clamped plates of aspect ratios 1, 2 and 3.

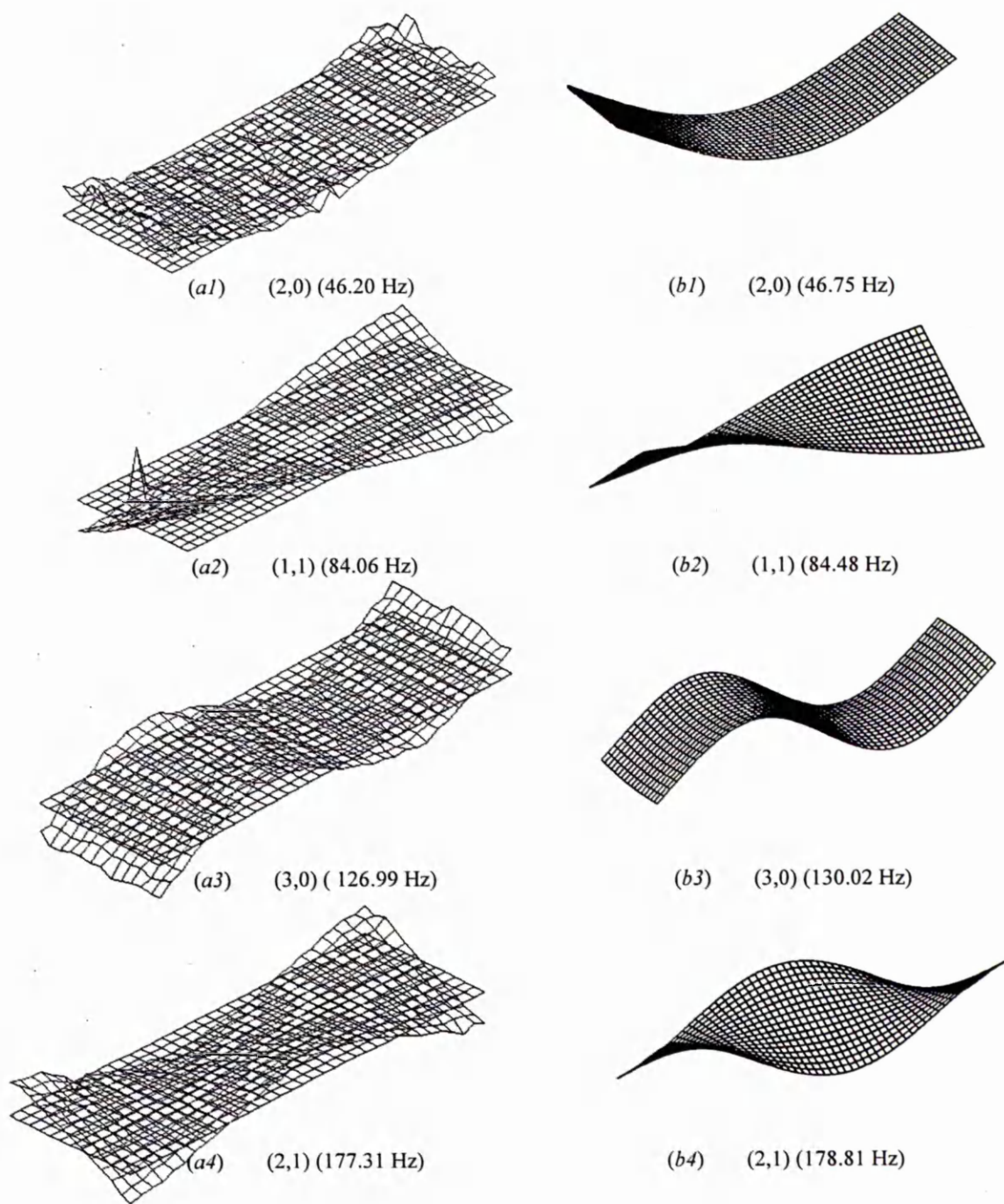


Figure 9.6 Comparison of mode shapes from experimental and FE for free-free beam-plate of aspect ratio 3.

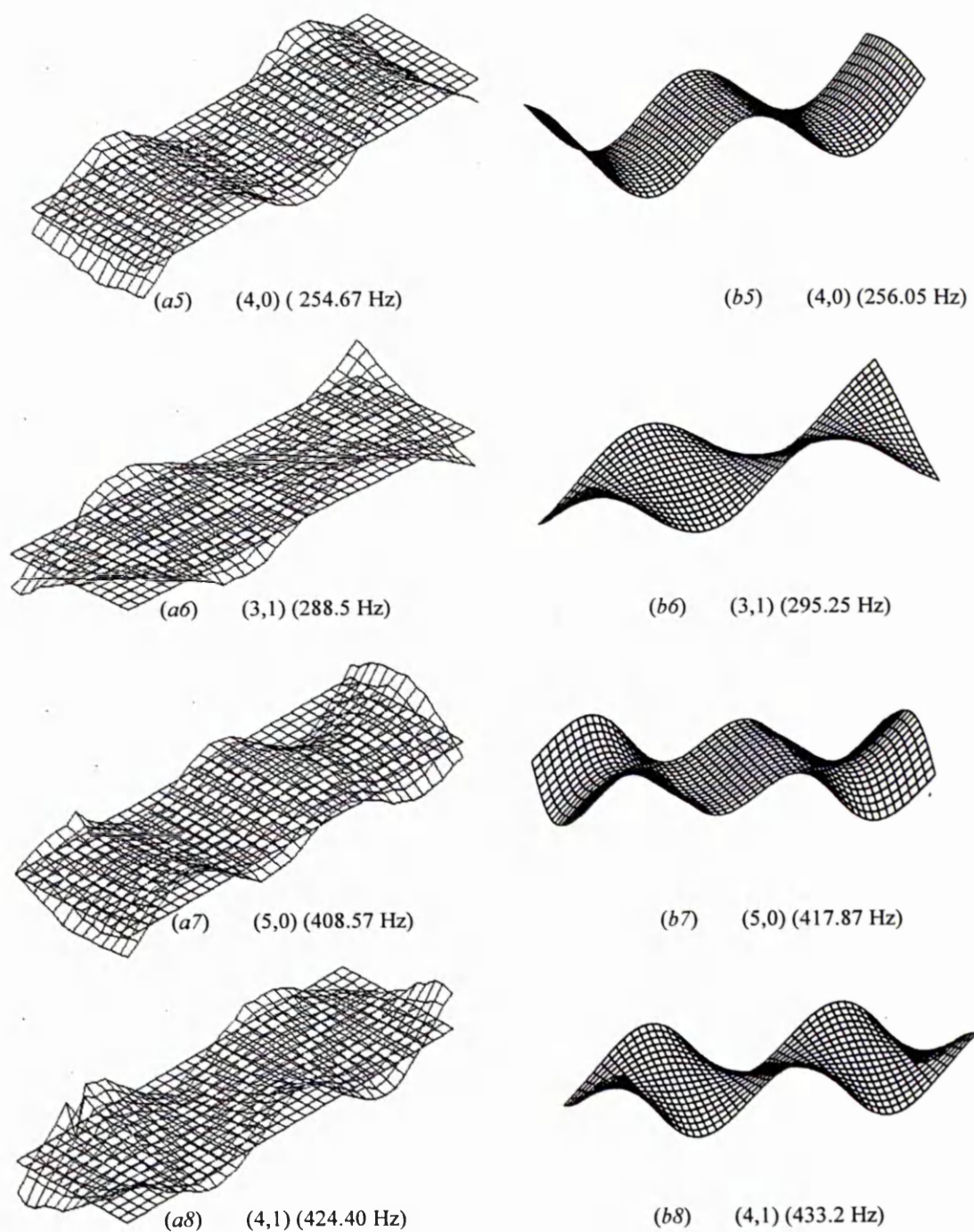


Figure 9.6 (Continued)

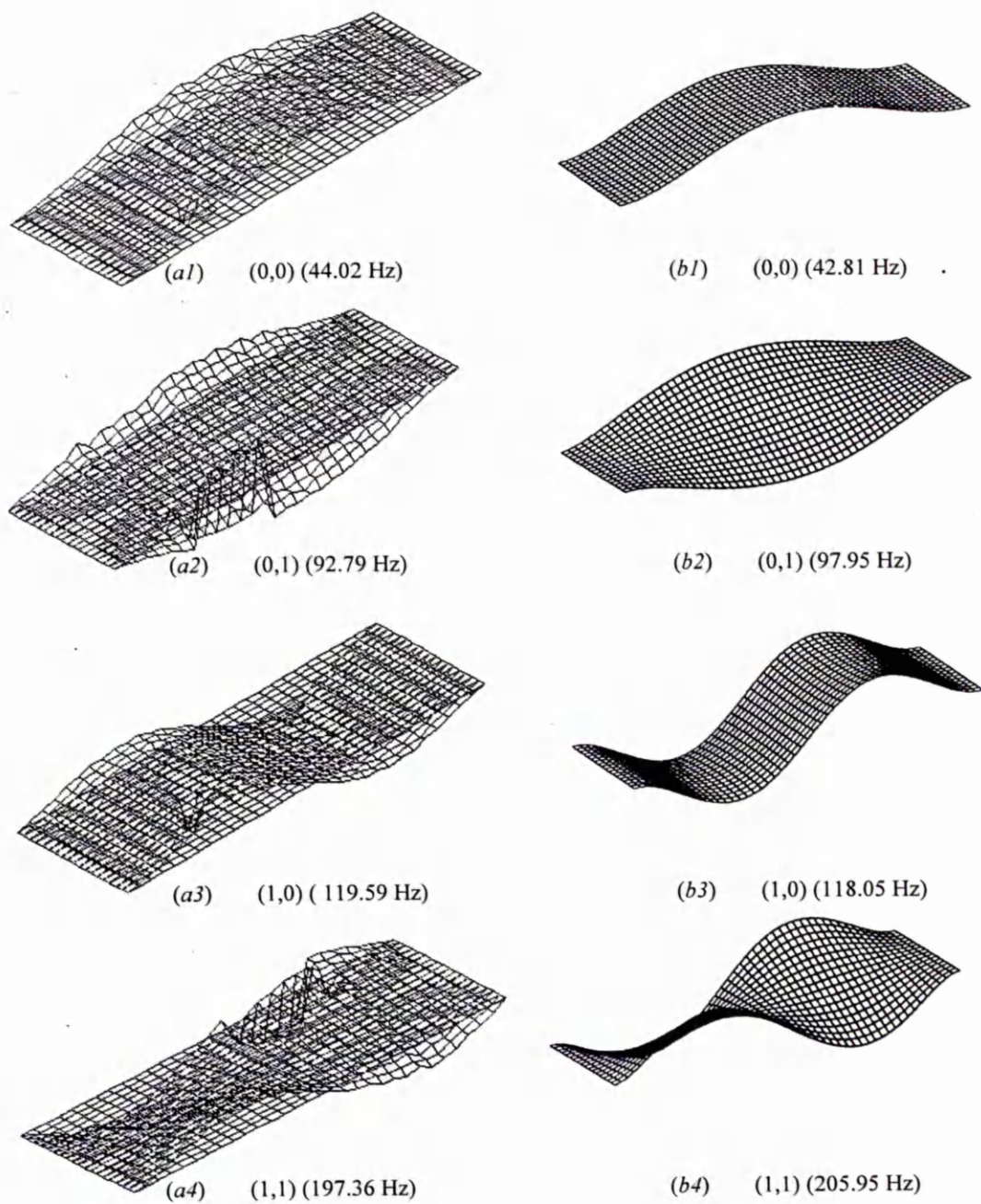
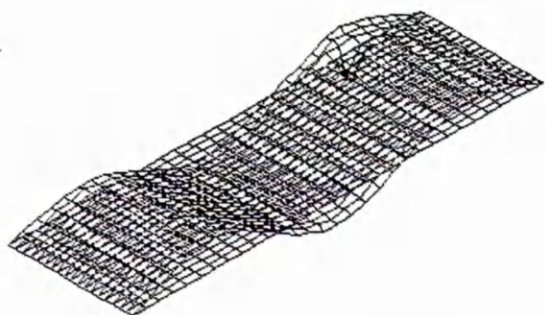


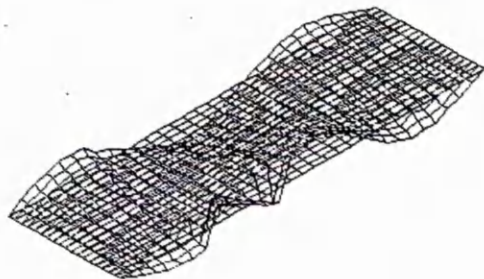
Figure 9.7 Comparison of mode shapes from experimental and FE for clamped-clamped beam-plate of aspect ratio 3.



(a5) (2,0) (228.80 Hz)



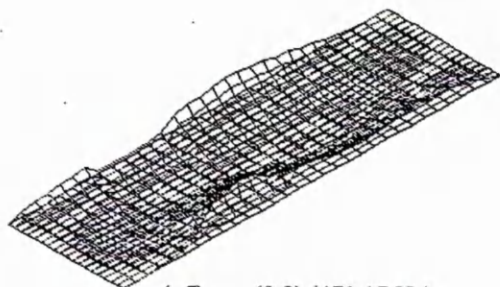
(b5) (2,0) (231.95 Hz)



(a6) (2,1) (326.18 Hz)



(b6) (2,1) (334.16 Hz)



(a7) (0,2) (471.17 Hz)



(b7) (0,2) (427.20 Hz)



(a8) (3,0) (375.22 Hz)



(b8) (3,0) (384.06 Hz)

Figure 9.7 (Continued)

9.5 Comparison of measured and predicted FRFs

A comparison is made between the experimental FRFs and the FEM predicted FRFs carried out for both free-free and clamped-clamped plates. In the case of the clamped-clamped plate, the forced vibration steady-state frequency response functions (FRFs) of the plates with two supports either side were computed for comparison with the experimental FRFs.

The “Steady-State Dynamics” and “Modal Damping” command were used in the ABAQUS FE program in order to predict accurate FRFs. The value of damping ratio obtained from the experiment shown in Tables 9.3 to 9.5 were used in the “Modal Damping” command.

The FRFs were predicted for the free-free boundary conditions as follows. In Figures 9.8 (a) and 9.10, nodes 1, 111 and 221 are the nodes at the 2 corners and centre of one of the free edges of the free-free plate of aspect ratio 0.5. Similarly, nodes 221, 226, 231 in Figures 9.8 (b) and 9.11, and nodes 430, 436, 442 in Figures 9.8 (c) and 9.12, are the nodes at the 2 corners of a free end of the plate, and the centre of one of the free edges of the free-free plate of aspect ratios 2.0 and 3.0 respectively.

The frequency response functions (FRFs) predicted using FEA and measured experimentally at the 2 corners and centre of one of the free edges of the free-free plates of aspect ratios 0.5, 2.0 and 3.0 are compared in Figures 9.10 to 9.12 respectively. In these figures, solid lines denote the FRFs predicted using FEA and dash lines represent the FRFs measured experimentally. It is seen that the measured and predicted natural frequencies and the FRF amplitudes are closer at low modes than at higher mode.

The FRFs were predicted for the clamped-clamped as follows. Nodes 253, 263 and 273 in Figures 9.9 (a) and 9.13 are the nodes at approximately $L/15$ from the centre of the clamped-clamped plate of aspect ratio 1. Similarly nodes 484, 494, 504 in Figures 9.9 (b) and 9.14, and nodes 248, 257, 226 in Figures 9.9 (c) and 9.15, are the nodes at 2 approximately. $L/15$ from the centre of the clamped-clamped plate of aspect ratio 2 and 3.0 respectively.

Figures 9.13 to 9.15 show the overlay of the frequency response functions (FRFs) predicted using FEA and measured experimentally for the clamped-clamped plate. In these figures, solid lines denote the FRFs predicted using FEA and dash lines represent the FRFs measured experimentally. Again these figures shows that the measured and predicted natural frequencies and FRFs at low modes and high aspect ratio are closer than at higher modes or small aspect ratio. This is due to the fact that the dynamics of the supports affect the dynamics of the longer plate than the shorter one.

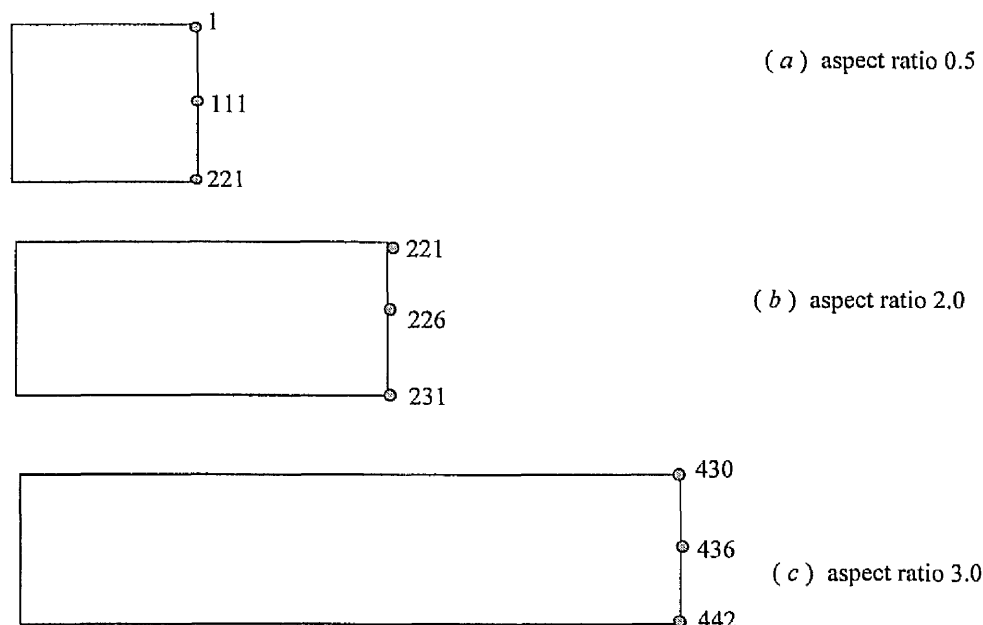
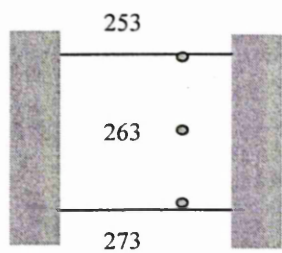
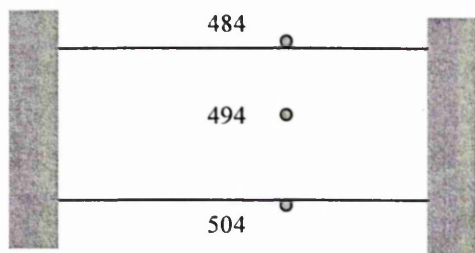


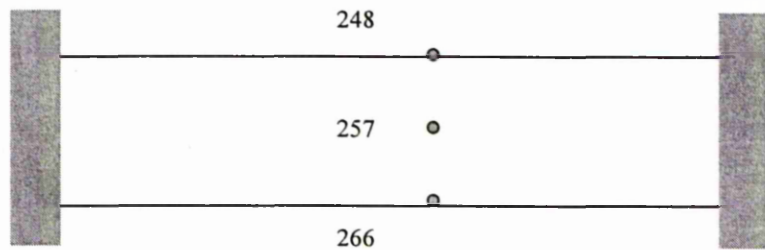
Figure 9.8 Location of nodes at the free edges of the free-free plates of aspect ratios 0.5, 2.0 and 3.0



(a) aspect ratio 1.0



(b) aspect ratio 2.0



(c) aspect ratio 3.0

Figure 9.9 Location of nodes off near centre of the clamped-clamped plates of aspect ratios 1.0, 2.0 and 3.0

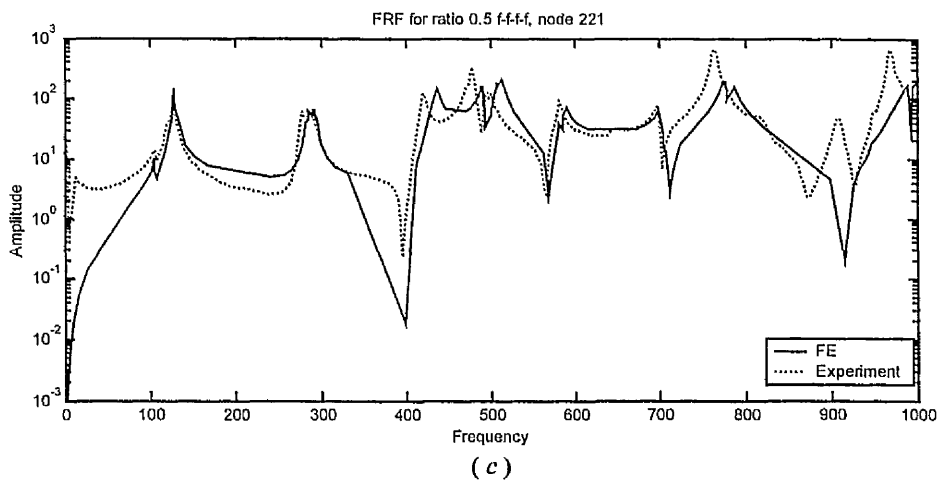
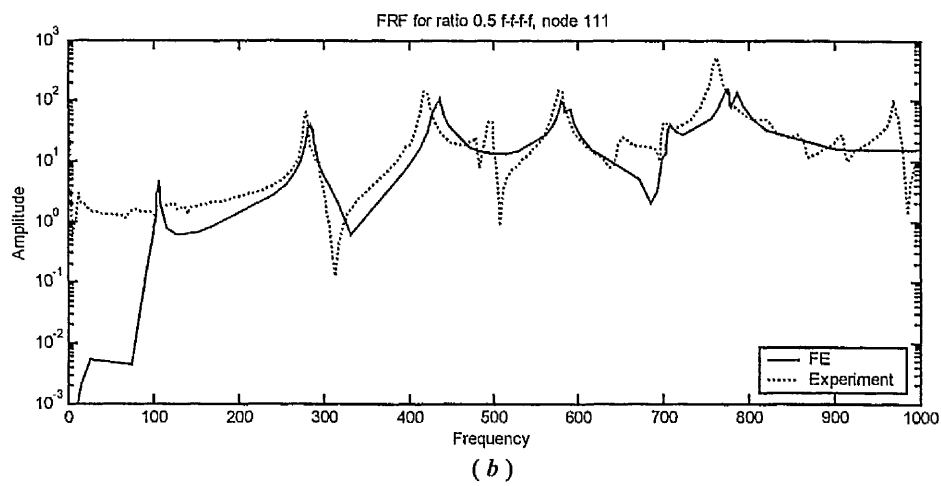
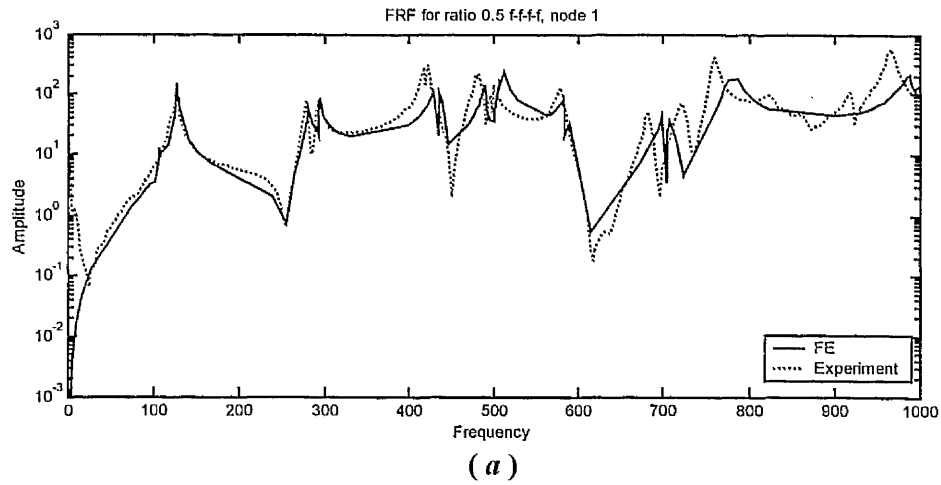


Figure 9.10 FRF between FEA and experiment for free-free plate aspect ratio 0.5 at nodes 1,111 and 221

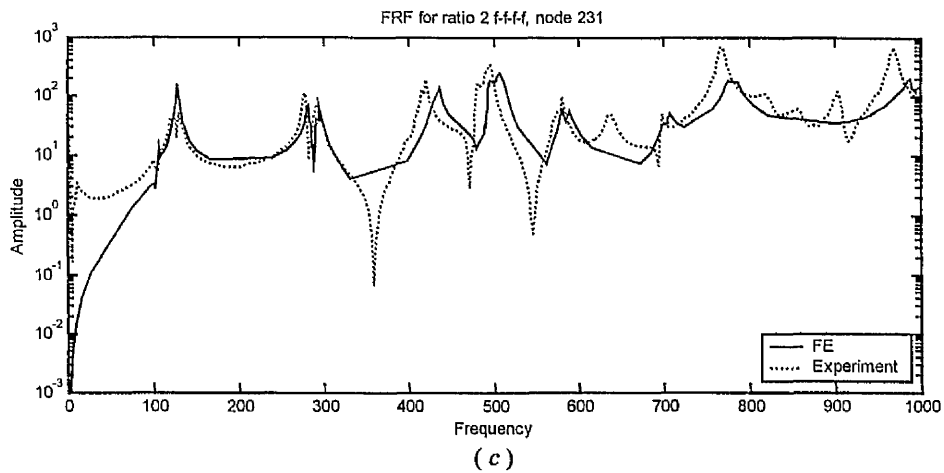
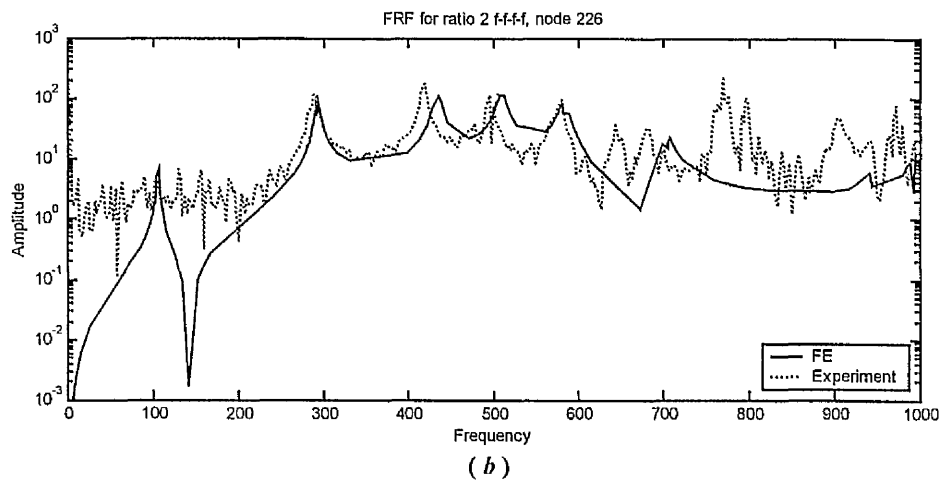
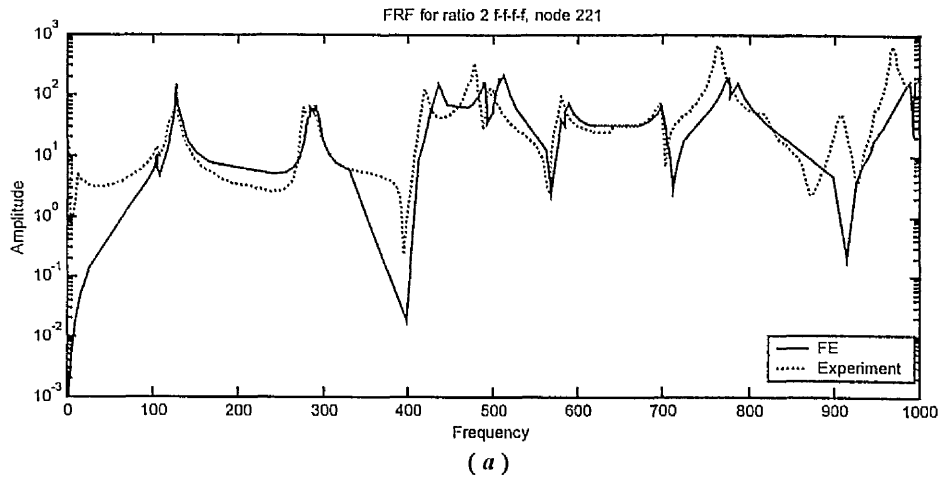
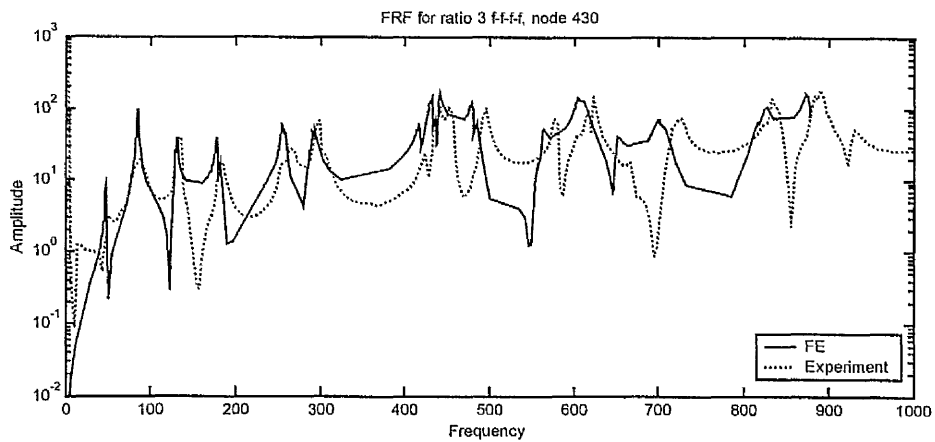
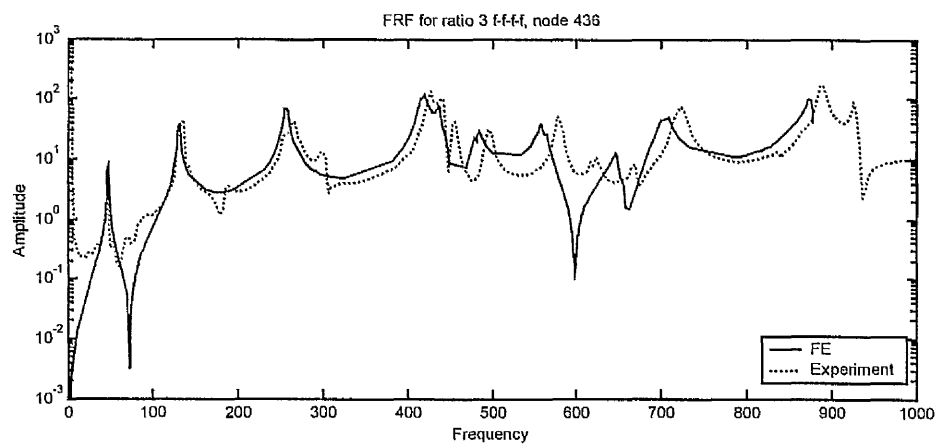


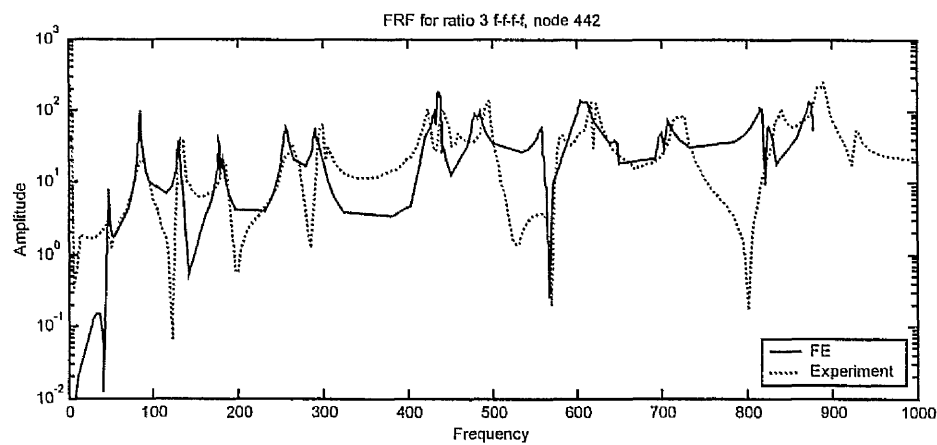
Figure 9.11 FRF between FEA and experiment for free-free plate aspect ratio 2 at nodes 221,226 and 231



(a)

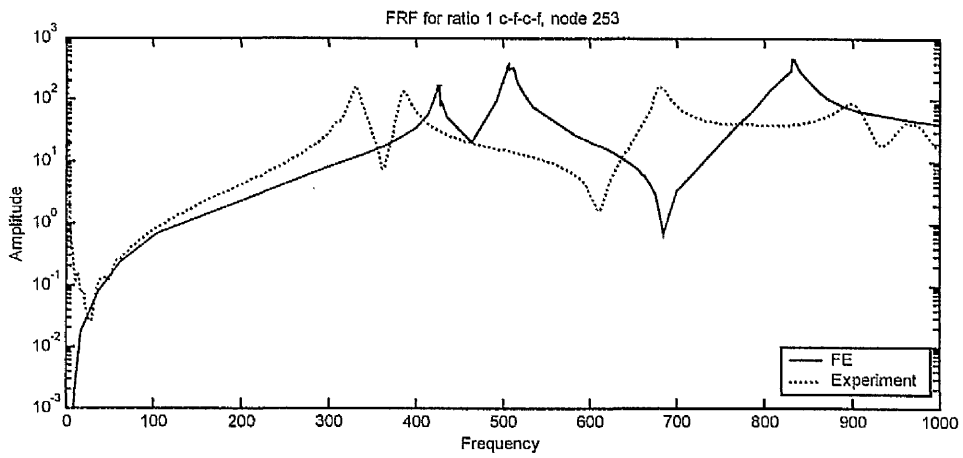


(b)

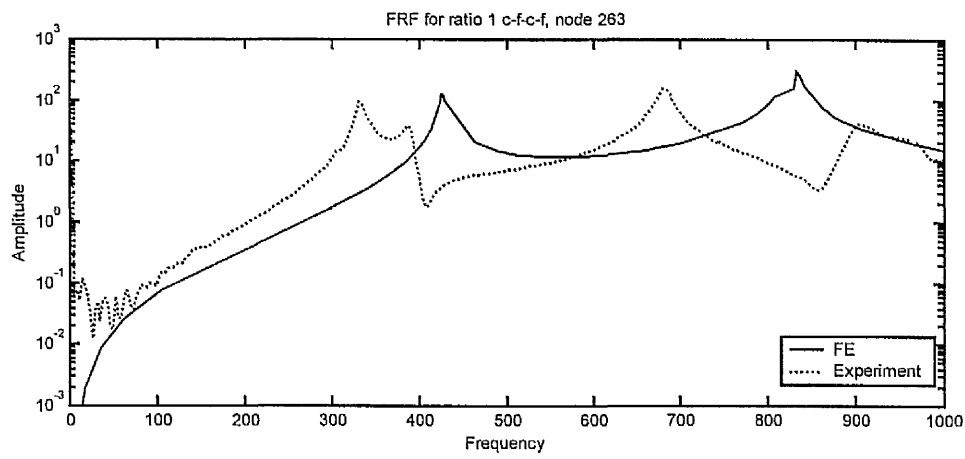


(c)

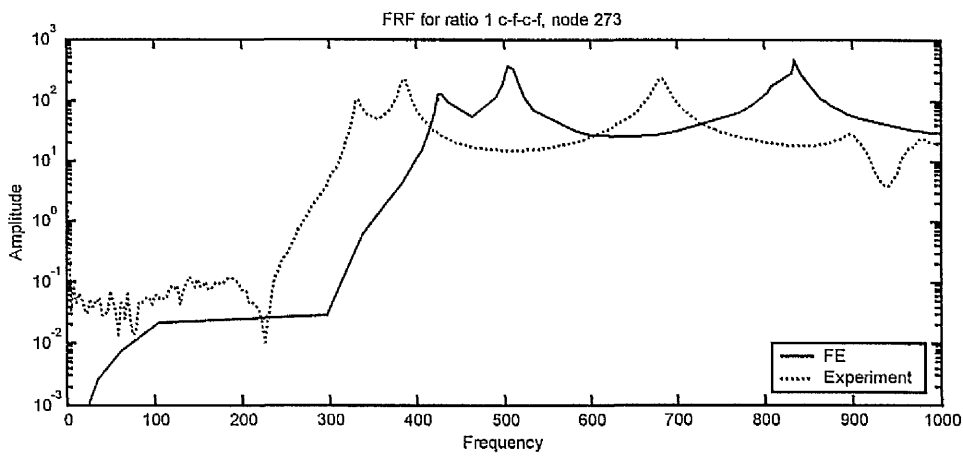
Figure 9.12 FRF between FEA and experiment for free-free plate aspect ratio 3 at nodes 430,436 and 442



(a)



(b)



(c)

Figure 9.13 FRF between FEA and experiment of clamped-clamped plate aspect ratio 1.0 at nodes 253, 263 and 273

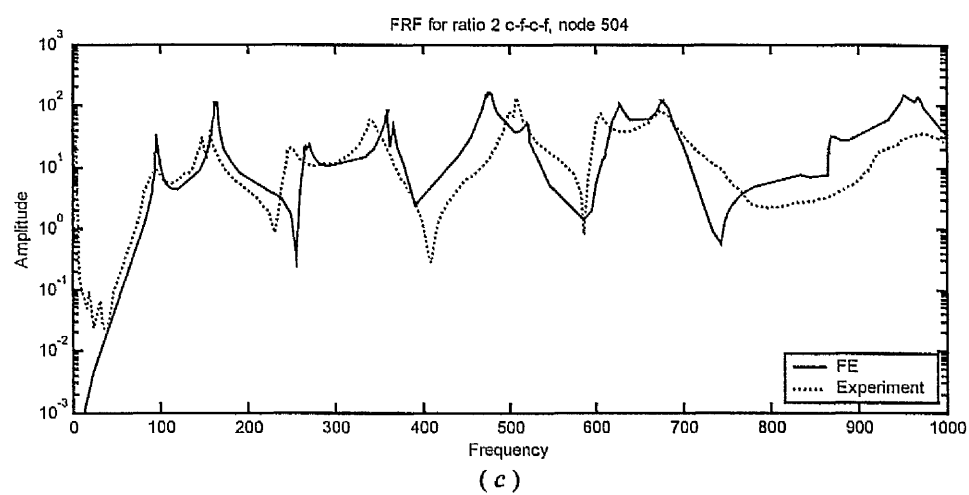
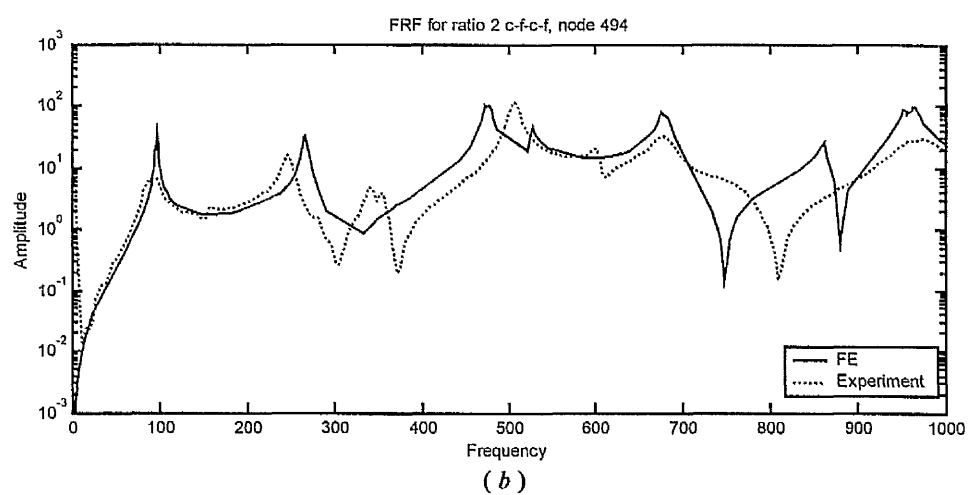
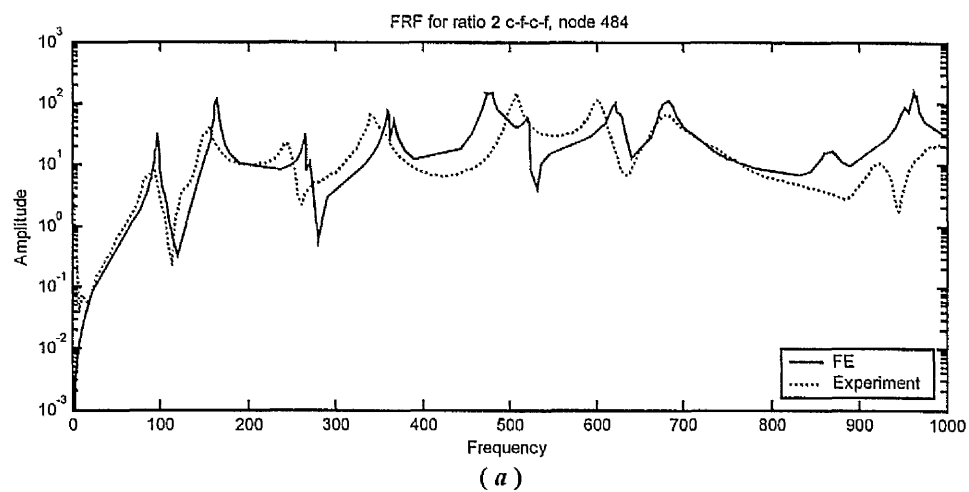


Figure 9.14 FRF between FEA and experiment of clamped-clamped plate aspect ratio 2.0 at nodes 484, 494 and 504

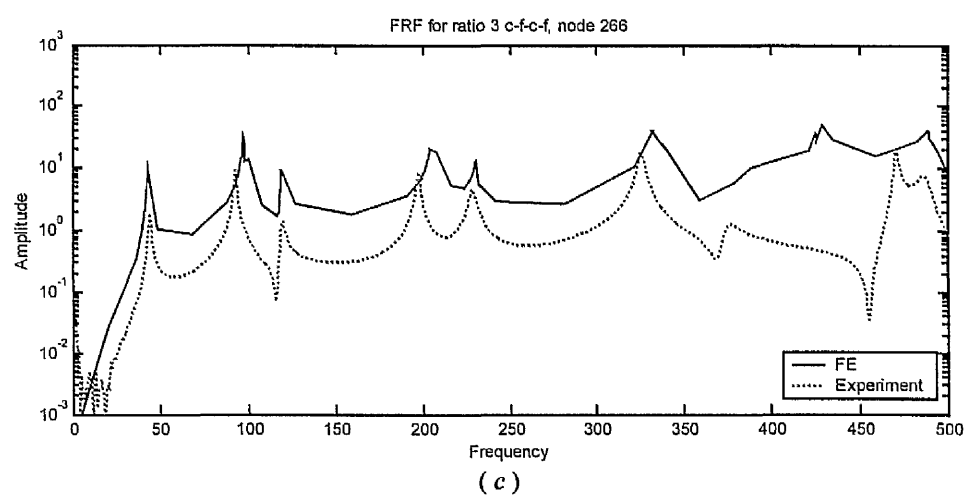
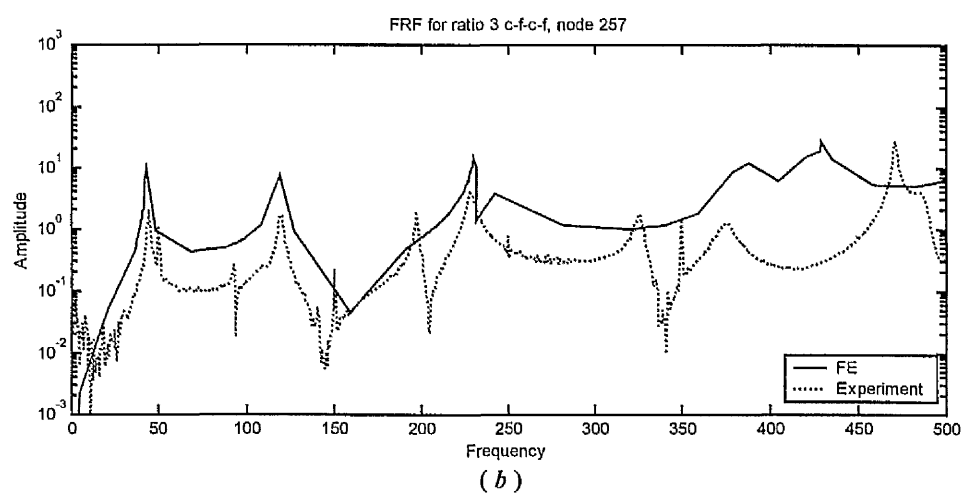
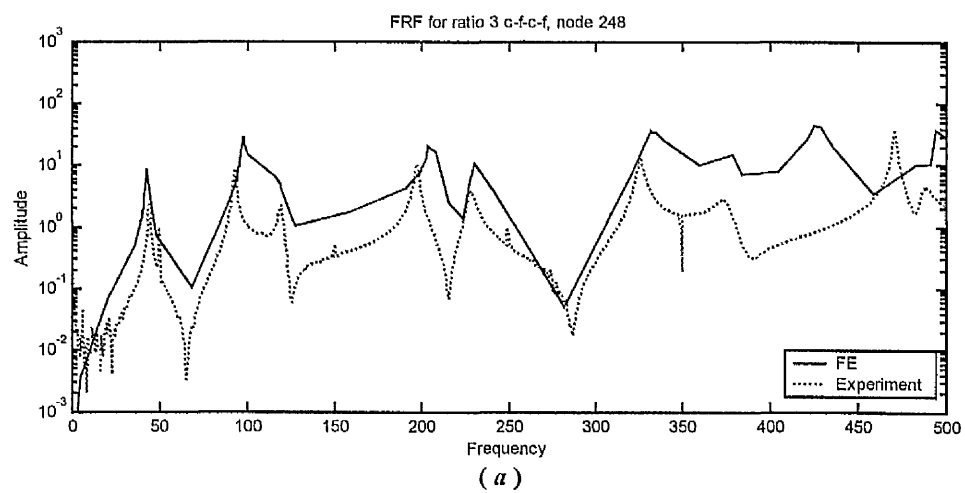


Figure 9.15 FRF between FEA and experiment of clamped-clamped plate aspect ratio 3.0 at nodes 248, 257 and 266

9.6 The use of frequency parameter chart to identify mode types from measured FRFs

By using the frequency charts obtained earlier, it is possible to identify the mode types from measured FRFs. Figure 9.16 shows the frequency response function (FRFs) of the free-free plate of aspect ratio 3 at the corner node of one of the free edge. From this figure, it is possible to estimate the natural frequencies from the peak responses. However this figure does not and cannot indicate the types of modes of vibration which are associated with these natural frequencies. In general, identification of mode types usually requires a full modal analysis to be carried out. This includes the determination of natural frequencies as well as mode shapes. However, to carry out a full modal analysis on a structure is expensive and time consuming as it involves measurement and analysis of FRFs from many locations on the structure. Alternatively, the frequency parameter charts derived in earlier chapters can be used in conjunction with a most typical FRF of the structure. For example considering the frequency parameter chart shown in Figure 5.16c. (Chapter 5). It can be deduced that the first 6 modes of vibration of a plate aspect ratio 3 are B_1 , T_1 , B_2 , T_2 , B_3 and T_3 respectively as shown in Figure 9.17 where B_i denotes bending mode, T_i denotes torsion mode, and i denotes mode number.

The mode types obtained from experimental mode shapes and from the frequency parameter chart for a free-free plate of aspect ratio 3, are compared in Table 9.9. It is seen that all mode types from measured FRF are the same as mode types obtained from frequency chart. Thus, the frequency chart can be used to identify the mode types of a vibrating free-free plate from a measured FRF.

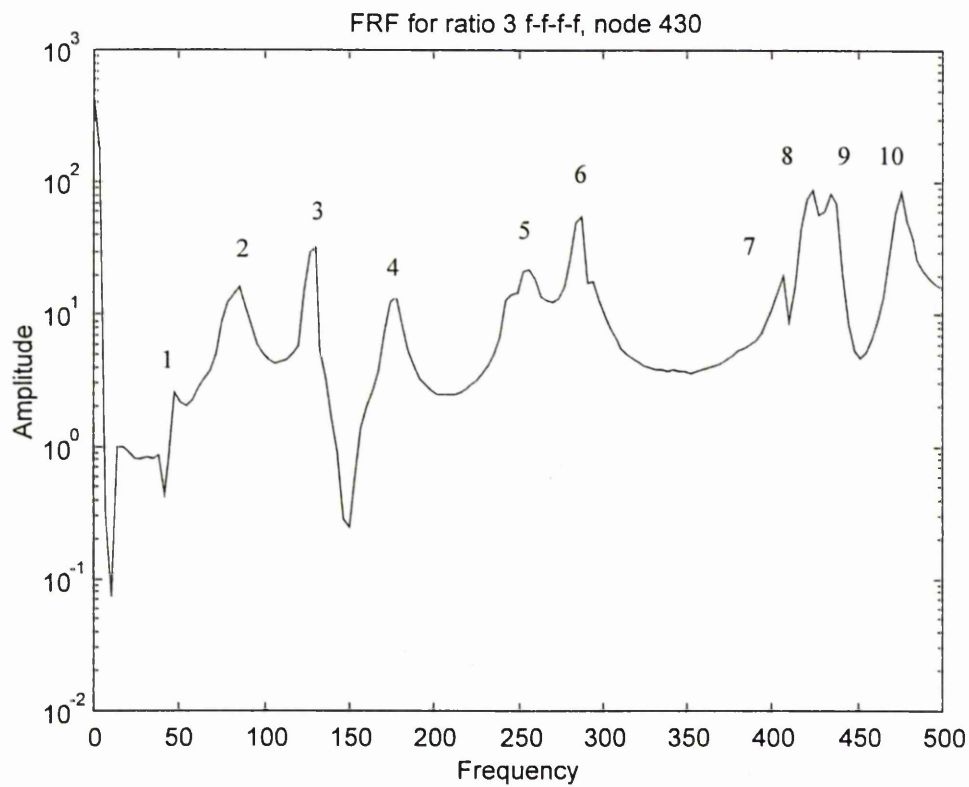


Figure 9.16 FRF of the free-free plate of aspect ratio 3 at the corner node

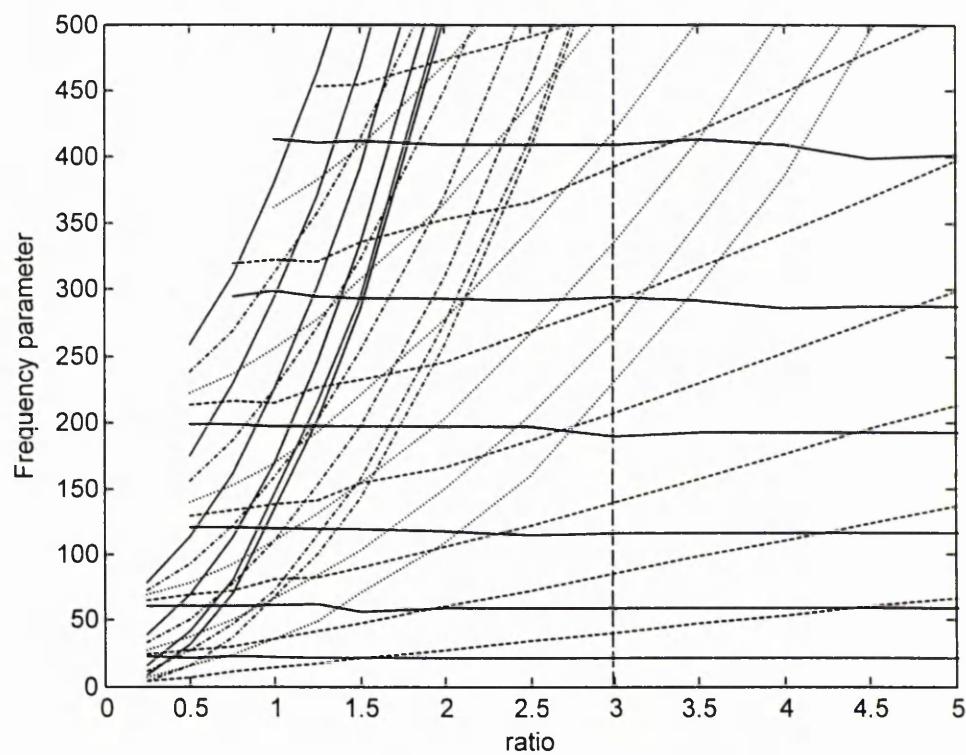


Figure 9.17 Determination of mode type for ratio 3 free-free from FRF using frequency parameter chart

Similarly, Figures 9.18, 9.19 and Table 9.10 shows the natural frequencies and mode types of clamped-clamped plate of aspect ratio 3 obtained from the frequency parameter chart and experiment. It is again seen that the mode types indicated by the frequency parameter are identical to those observed experimentally.

Table 9.9 Natural frequencies, mode types from frequency chart and experiment for free-free beam-plates

Mode Number	Experimental natural frequency (Hz)	Mode type from frequency chart	Mode type from experimental mode shapes	Remark
1	46.20	B_{x1}	(2,0)	First bending mode along x ; 2 nodal lines parallel to y axis
2	84.06	T_1	(1,1)	1 nodal line parallel to x axis and 1 nodal line parallel to y axis
3	126.99	B_{x2}	(3,0)	Second bending mode along x ; 3 nodal lines parallel to y axis
4	177.31	T_2	(2,1)	2 nodal line parallel to x axis and 1 nodal line parallel to y axis
5	254.67	B_{x3}	(4,0)	Third bending mode along x ; 4 nodal lines parallel to y axis
6	288.50	T_3	(3,1)	3 nodal line parallel to x axis and 1 nodal line parallel to y axis
7	408.57	B_{x3}	(5,0)	Fourth bending mode along x ; 5 nodal lines parallel to y axis
8	424.40	T_4	(4,1)	4 nodal line parallel to x axis and 1 nodal line parallel to y axis
9	437.55	B_{x1}, B_{y1}	(0,2)	First bending mode along y -axis; 2 nodal lines parallel to x axis
10	477.31	T_{x1}, B_{y2}	(1,2)	1 nodal line parallel to x axis and 2 nodal line parallel to y -axis

Table 9.10 Natural frequencies, mode types from frequency chart and experiment for clamped-clamped beam-plates.

Mode Number	Experimental natural frequency (Hz)	Mode type from frequency chart	Mode type from experimental mode shapes	Remark
1	44.02	B_{x1}	(0,0)	First bending mode along x ; no nodal lines
2	92.79	T_1	(0,1)	First torsion; 1 nodal line parallel to x axis
3	119.59	B_{x2}	(1,0)	Second bending mode along x ; 1 nodal lines parallel to y axis
4	197.36	T_2	(1,1)	1 nodal line parallel to x axis and 1 nodal line parallel to y axis
5	228.80	B_{x3}	(2,0)	Third bending mode along x ; 2 nodal lines parallel to y axis
6	326.18	T_3	(2,1)	2 nodal line parallel to x axis and 1 nodal line parallel to y axis
7	375.22	B_{x3}	(3,0)	Fourth bending mode along x ; nodal lines parallel to y axis
8	471.17	B_{x1}, B_{y1}	(0,2)	First bending mode along y axis; 2 nodal lines parallel to x axis

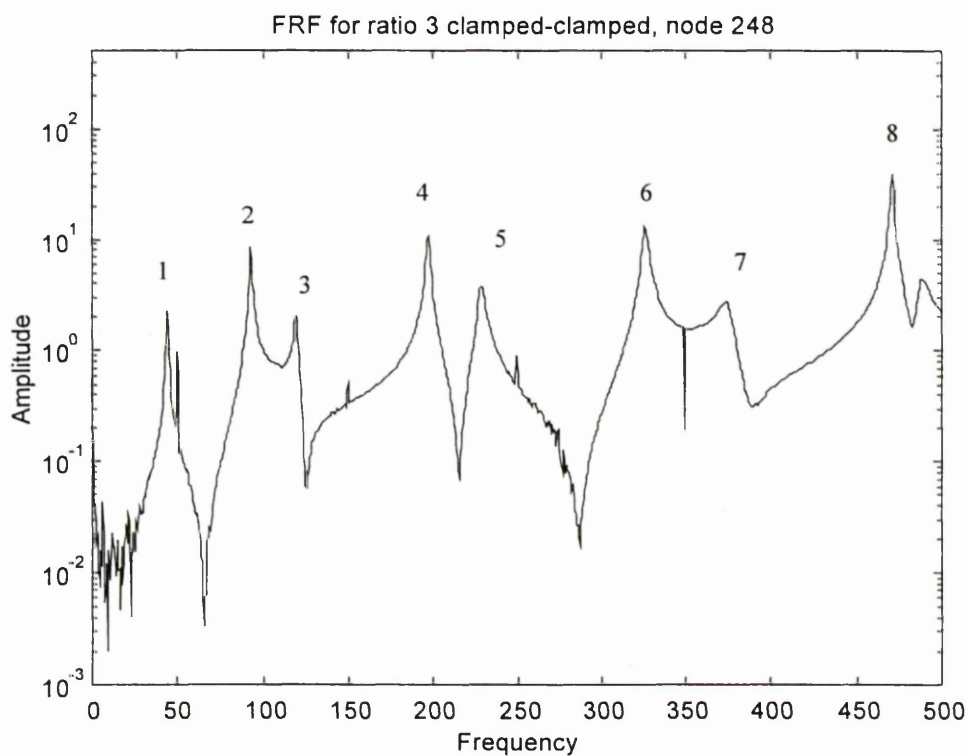


Figure 9.18 FRF of the clamped-clamped plate of aspect ratio 3 at node 248

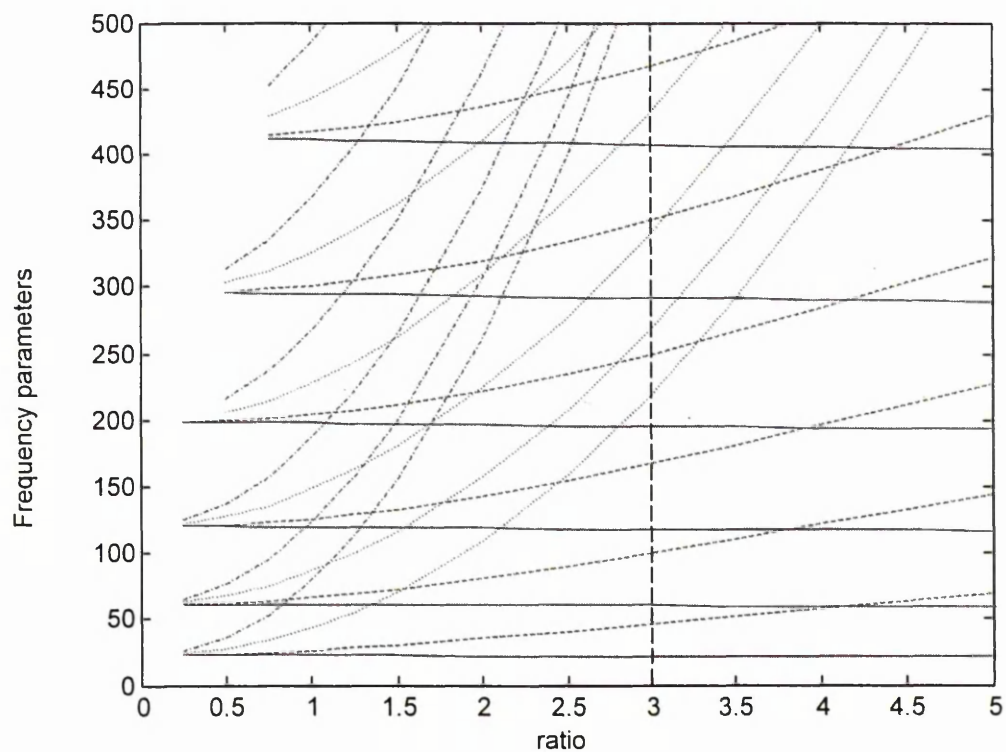


Figure 9.19 Determination of mode type for ratio 3 clamped-clamped from FRF using frequency parameter chart

9.7 Summary

The frequency parameter chart, shown in Chapter 4 for the clamped-clamped beam-plate and in Chapter 5 for the free-free beam-plates, can be used to identify the mode types of vibrating beams and plates from a measured FRF. In the case of the clamped-clamped plate, the natural frequencies of plates with support predicted using FEM are closer to the experimentally measured natural frequencies than the predicted natural frequencies of clamped-clamped plates without support. This is due to the fact that the plate without support was infinitely rigidly clamped, so that the dynamics of the support did not affect the dynamics of the plate. But in reality, the dynamics of the support affected the dynamics of the plate.

The measured and predicted natural frequencies and the FRF amplitudes are closer at lower mode than at higher modes of vibration for both free-free and clamped-clamped beam-plates. The comparison between the experimental measurements and the FEA predictions shows a small percentage error for the natural frequencies at higher aspect ratio and lower modes.

Chapter 10

General summary, conclusions and recommendations

10.1 General summary

The work presented in this thesis has been an investigation of the natural frequencies and mode shapes of free-free and clamped-clamped beam-plates. The study was aimed at obtaining the transition curves or regions from beam-like to plate-like behaviour. This study has also investigated the effect of beam-plate thickness to length ratio on the transition curves for thickness to length ratios 1%, 2%, 5% and 10%. The transition curves and transition equations which define the boundaries between beam-like to plate-like behaviour were obtained for both free-free and clamped-clamped beam-plates of these thickness to length ratio.

The work done and the results obtained from both FE and experiment can be summarised as follows:

1. Finite elements of type S8R5, S8R, S4R and C3D20R of the ABAQUS FEA library were used. It was found that the natural frequencies and mode shapes predicted by

the C3D20R elements agreed closely with the experimentally measured values as expected. It was also found that the thin shell element types S8R and S8R5 predicted modal characteristics that correlated closely with the predictions of the solid element C3D20R only for beam-plates of thickness to length ratio 1%. However, the predictions of element type S8R5 were better than those of element type S8R. On the other hand, the general purpose element type S4R, predicted results that correlated well with the predictions of the solid element for beam-plates of thickness to length ratios 2%, 5% and 10%. Over all, it was found that the S4R element was the best selection of element type for thicker beam-plates. This is because it predicted the closest natural frequencies to those predicted by the solid element than those predicted by the other types of shell elements. Furthermore the S4R element required less analysis time than solid elements and the resultant file size was also smaller than that of the solid element.

2. A mesh study was carried out in order to find the optimum number of elements to use in the lengthwise and breadthwise directions in the FE analysis. It was found that in order to predict the first 50 modes accurately, a minimum number of 50 elements had to be used for the lengthwise direction. The number used for the breadthwise direction depended on the aspect ratio.
3. The frequency parameter charts which represent the variation of frequency parameter with aspect ratio for fixed value of i and j were plotted for all thickness to length ratios investigated. In the case of free-free beam-plates the chart shows that for fixed value $j = 0$, the lines are almost horizontal (zero slope) and for $j = 1$, the frequency parameter increases gradually as the aspect ratio increases, while for $j \geq 2$, the frequency parameter changes rapidly as the aspect ratio changes. The frequency parameter charts can be used to predict the frequency parameters and

types of modes of vibration of beam-plate structures. Similarly for the clamped-clamped beam-plates the chart shows that for fixed value $j = 0$, the lines are almost horizontal (zero slope), and for $j = 1$, the frequency parameter increases gradually as the aspect ratio increases, while for $j \geq 2$, the frequency parameter change rapidly as the aspect ratio changes.

4. The effect of thickness to length ratio on the frequency parameters indicates an inverse relationship i.e. as the plate thickness to length ratio increases the frequency parameter for a fixed aspect ratio decreases. This is because the effect of the increase in bending and torsional stiffnesses of the beams due to the increase in thickness to length ratio is less than the combined effects of increase in mass and mass moment of inertia.
5. The transition curves and equations that determine the boundaries between beam-like and plate-like behaviour for predominantly one-dimensional bending mode of vibration along the lengthwise axis were produced for all thickness to length ratios studied for the free-free beam-plates. The equations were derived by means of the linear least-squares method and were plotted on the frequency parameter charts.
6. The transition curves shown on the λ^2 vs r frequency parameter charts divide the chart into two regions. The left region of the transition curve is the region of plate-like behaviour where a finite element analysis or other numerical methods must be used to predict the behaviour of the plate. On the other hand, the right region of the transition curve is the beam-like behaviour region where the simple beam equations can be used to predict the behaviour of the beam. For the λ^2 vs m and λ^2 vs n frequency parameter charts, for the symmetric and anti-symmetric modes

respectively, the left region of the transition curves on these charts is for beam-like behaviour while the right region is for plate-like behaviour.

7. The effect of thickness to length ratio on the transition from beam-like to plate-like behaviour was studied. This resulted in the derivation of different sets of transition curves and transition equations for each thickness. These equations were combined to give composite equations, which relate the transition frequency parameter to the aspect ratio and thickness. The resulting composite equations give a complete transition equation for free-free beam-plates of thickness to length ratio up to 10% as;

$$\lambda^2 = (-181 - 115r + 8r^2) + (-205 + 7116r - 77r^2)\tau + (3611 - 51186r - 1045r^2)\tau^2 \quad (6.8)$$

where; λ^2 is frequency parameter, r is aspect ratio, τ = thickness to length ratio $(\frac{t}{a})$, t is thickness, a is length

These transition equations can be used with a beam-plate structure which has a different thickness to length ratio within the specified ranges.

However in the case of the clamped-clamped beam-plates, it was not easy to establish the transition curves due to the smoothness of the curves from the one – dimensional bending modes.

8. From the study of the symmetric modes for both free-free and clamped-clamped beam-plates, it was possible to determine transition curves and composite transition equations which relate transition frequency parameter to aspect ratio and mode counter for all the thickness to length ratio investigated. For example, for the 1% thickness to length ratio beam-plates, the composite transition equations are;

$$\lambda_{sm}^2 = (75.89 - 11.75r + 0.364r^2) + (-51.367 + 10.728r - 0.372r^2)m + (15.178 - 0.886r + 0.0284r^2)m^2 \quad (\text{thickness to length ratio } 1\%, \text{ free-free})$$

$$\lambda_{sm}^2 = (17.746 - 3.005r - 0.068r^2) + (2.517 + 1.398r - 0.032r^2)m + (10.339 - 0.165r + 0.004r^2)m^2 \quad (1\% \text{ thickness to length ratio, clamped-clamped})$$

where λ_{sm}^2 = frequency parameter of symmetric mode

m = symmetric mode counter

r = aspect ratio

9. Similarly, transition curves and composite transition equations were obtained from the anti-symmetric modes. For the 1% thickness to length ratio beam-plates, for example the composite transition equations obtained are;

$$\lambda_{an}^2 = (-24.85 + 14.139r - 0.724r^2) + (-5.624 + 4.272r + 0.407r^2)n + (5.532 + 0.361r - 0.034r^2)n^2 \quad (1\% \text{ thickness to length ratio, free-free})$$

$$\lambda_{an}^2 = (8.011 + 4.085r - 0.171r^2) + (-4.840 + 11.006r + 0.0273r^2)n + (7.772 - 0.194r - 0.003r^2)n^2 \quad (1\% \text{ thickness to length ratio, clamped-clamped})$$

where

λ_{an}^2 = frequency parameter of symmetric mode

n = symmetric mode counter

r = aspect ratio

10. The natural frequencies predicted using FEM are much closer to the experimentally measured natural frequencies for free-free beam-plates than for clamped-clamped beam-plates. In the case of the clamped-clamped beam-plates the natural

frequencies predicted by the FEA when supports were considered were closer to the measured frequencies than the natural frequencies without support. This is due to the fact that the plate without support was infinitely rigidly clamped, so that the dynamics of the support did not affect the dynamics of the plate. But in reality, the dynamics of the support affected the dynamics of the plate.

11. For the clamped-clamped beam-plates the natural frequencies measured experimentally are closer to the natural frequencies predicted using FEM for the longer plate than for the shorter plates. This is because the flexibility of the support has less effect on the dynamics of the longer plate than on the dynamics of the shorter plates.
12. The frequency parameter charts can be used to identify mode types from measured FRFs. This approach is quicker and cheaper. The classical approach is to use a multi-channel modal test and analysis system to acquire FRF data from many points on a structure and to derive the natural frequencies and mode shapes from the data. The mode types present in the vibration of the structure are identified by visual examination of the mode shapes. This classical approach is expensive and time consuming.

10.2 Conclusions

1. For the FE analysis of the vibration characteristics of free-free and clamped-clamped beam-plates of thickness to length ratio 1%, the shell element type S8R5 was found to be the most appropriate element type to be used. However, for the thicker beam-plates of thickness to length ratio 2%, 5% and 10% the shell general purpose element S4R was found to be the most appropriate element to be used. This is because these two elements predicted the closest natural frequencies to the natural

frequencies predicted using solid element type C3D20R. But they use less computer memory, less disc storage and less computing time in comparison to the solid element type C3D20R.

2. All frequency parameters charts presented can be used to predict frequency parameters and hence, natural frequencies, and to identify the mode types of free-free and clamped-clamped beams and plates of corresponding thickness to length ratio.
3. The regions of beam-like and plate-like behaviour have been clearly plotted on the frequency charts. In the beam-like regions, the Euler Bernulli or Timoshenko beam equations or the torsion beam equation can be used, where as in the plate-like region, FE analysis or numerical methods need to be used.
4. The effect of the thickness to length ratio of beam-plates was found to be important. Different thickness to length ratio produced different transition curves and transition equations. The effect of increasing thickness to length ratio has been shown to reduce the frequency parameter of the beam-plate. This is due to the fact that as the thickness of the beam plate increases, the effect of the increase in stiffness of the beam-plate is less than the effect of the increased mass of the beam-plate. For thickness-to-length ratios of 2% or less, the transition curves are very close. But for thickness-to-length ratios greater than 2%, there is increase in difference in the transition curves.
5. The FEA results for the clamped-clamped beam-plates show that the dynamics of the supports affect the dynamics of the plate. The dynamics of the support have less effect on the dynamics of the longer beam-plate, which is more flexible, than the dynamics of the shorter plates, which is stiffer.

6. The work presented shows that it was possible to obtain transition curve for the free-free beam-plates from the analysis of one-dimensional bending mode, but for the clamped-clamped it was not possible to obtain transition curves from the one-dimensional bending modes, However from the study for symmetric and anti-symmetric modes it was possible to obtain the transition curves for both clamped-clamped and free-free beam-plates.
7. For both free-free and clamped-clamped beam-plates, the measured and predicted natural frequencies and the FRF amplitudes are closely correlated at lower modes than at higher modes.
8. For the clamped-clamped beam-plates it was found that the FE predictions for a beam-plate modelled with supports are closer to the experimental measurements than without supports.

10.3 Recommendations for future work

1. It would be useful to derive the transition curves and transition equations for other boundary conditions, such as C-C-F-F, C-C-C-F, C-C-C-C, S-F-S-F, P-F-P-F, C-F-P-F, C-F-S-F boundary conditions where C denotes clamped, F denotes free, P denotes pinned, S denotes sliding.
2. Previous work on cantilevered beam-plates can be extended to cover thicker beam-plates, and also to include tapered cantilevered beam-plates with different swept angles, which can be useful in the design of aircraft wings, tail planes and fins.

References

- [1] Tangchaichit K. and Oyadiji S.O., "Transitions in the Free Vibrations of Cantilevered Beams and Plates," *The Integration of Dynamics, Monitoring and Control Conference (DYMAC'99)*, Manchester, 1999.
- [2] Tangchaichit K. and Oyadiji S.O., "Modal Characteristic of Cantilevered Beams and Plates: A Study of Transition from Beam-like to Plate-like Behaviour," *Proceedings of DETC'99: 1999 ASME Design Engineering technical Conference*, Las Vegas, Nevada, 1999.
- [3] Tangchaichit K., A study of transition from beams –like to plate –like behaviour in the free vibration of cantilevered beams and plates, Dynamic and Aeroelastic Research Group, School of Engineering, University of Manchester.
- [4] Rao S.S., *Mechanical Vibrations*, Addison-Wesley Publishing Company, 1995.
- [5] S.P.Timoshenko, History of strength of Materials, McGraw-Hill, New York, 1953
- [6] Szliard R., *Theory and Analysis of Plates: Classical and Numerical methods*, Prentice-Hall, London, 1974.
- [7] Euler, L "De motu vibration tympanorum" *Novi Commentari Acad. Petropolit.*, 10(1766), 243-260.
- [8] Todhunter,I and Person,K "A History of the theory of Elasticity, Vols.1 and 2, Dover publications, Inc New Yory, 1960.
- [9] Kirchhoff, G. vorlesungen vber mathematische physik, Vol 1, B.G. teubner, leipzig, 1876.
- [10] Love, A. E. H., A treatise on the mathematical theory of elasticity, Dover publications, Inc., New York, 1944
- [11] R.D.Mindlin "Influence of rotary inertia and shear on flexural motions of isotropic elastic plates, *Journal of Applied mechanics* 18, 31-38 (1951)
- [12] Reissner,E "The effect of transverse shear deformation on the bending of elastic plates" *J.Appl.Mech.*12 (1954),A69-A77.
- [13] Turner, M.J, Clough, R.W,Martin,G.C, and Topp,L.J."stiffness and deflection analysis of complex structures" *J.Aeron.sci*,23(sept.1956).805-823.
- [14] Inman D. J., *Engineering Vibration*, Prentice Hall, New Jersey, 1994.

- [15] Levinson M. and Cooke D.W., "On the Two Frequency Spectra of Timoshenko beams," *Journal of Sound and Vibration*, vol. 84, no. 3, pp. 319-326, 1982.
- [16] Ku A.B., "Upper and Lower bounds for Fundamental Natural Frequency of Beams," *Journal of Sound and Vibration*, vol. 54, no. 3, pp. 311-316, 1997.
- [17] Shastri B.P. and Rao G.V., "Free Vibrations of Short Beams," *Journal of Sound and Vibration*, vol. 100, no. 2, pp. 305-308, 1985.
- [18] On the transverse vibration of beams and rectangular cross-section, journal of Applied Mechanics, March 1986, Vol.53, 39-44
- [19] Young D., "Vibration of Rectangular Plate by the Ritz method," *Journal of Applied Mechanics*, Trans. ASME, vol. 72, p. 448, 1950.
- [20] Hearmon R.F.S., "The Frequency of Vibration of Rectangular Isotropic Plates," *Journal of Applied Mechanics*, vol. 19, pp. 402-403, 1952.
- [21] Gorman D.J., *Free Vibration Analysis of Rectangular Plates*, Elsevier North Holland. Inc., New York, 1982.
- [22] Gorman D.J., "Solutions of the Levy type for the Free Vibration Analysis of Diagonally Supported Rectangular Plates," *Journal of Sound and Vibration*, vol. 66, n. 2, pp. 239-246, 1979.
- [23] Warburton G.B., "The Vibration of Rectangular Plates," *Proc. Inst. Mech. Eng.*, ser. A., vol. 168, no. 12, pp. 371-384, 1954.
- [24] Love, A. E. H., *A treatise on the mathematical theory of elasticity*, Dover publications, Inc., New York, 1944.
- [25] Blevins R.D., *Formulas for Natural Frequency and Mode Shape*, Van Nostand Reinhold, New York, 1979.
- [26] Leissa A.W., *Vibration of Plates*, NASA SP-160, NASA., 1969.
- [27] T.Sakata and K.Takahashi , Natural Frequencies of Orthotropic Rectangular Plates Obtained by Iterative Reduction of the partial differential equation, , " *Journal of Sound and Vibration*, vol. 189, no. 1, pp. 89-101, 1996.
- [28] K. M. Liew., "Research on thick plate vibration: literature survey". *Journal of Sound and Vibration*, vol. 180, no. 1, pp. 163-176, 1993
- [29] Y.K.Cheune and S.Chakrabarti 1972 *journal of sound and vibration* 21, 277-284. Free vibration of thick, layered rectangular plates by a finite layer method.

- [30] B.S.Al Janabi, E.Hinton and Dj. Vuksanovic 1989 *Engineering Computations* 6, 90-96. "Free vibration of Mindlin plates using the finite element methods", part I:square plates with various edge conditions.
- [31] K.T.S.R.Iyengar and S.K.Pandya 1982 *International journal of structures* 2, 149-156. "Vibrations of orthotropic rectangular thick plates"
- [32] K.S. Sivakumaran. Department of civil engineering and engineering mechanics, McMaster university, Hamilton, Ontario, canada. 1987
- [33] K.M.Liew, K.C.Hung and M.K.Lim "Three-dimensional vibration of rectangular plates:effects of thickness and edge constraints" *Journal of Sound and vibration* 1995, Vol 182(5),709-727
- [34] M. Mukhopadhyay."A semi-analytic solution for free vibration of rectangular plates" *Journal of Sound and vibration* 1978, Vol 60(1),71-85
- [35] C.W.Bert and M.Malik "Frequency equations and modes of free vibrations of rectangular plates with various edge conditions" *Imech E* 1994
- [36] K.M.Liew, K.Y.Lam and S.T.Chow " Free vibration analysis of rectangular plates using orthogonal plate function" Department of mechanical and production engineering, National University of Singapore, 1988
- [37] R.W.Traill-Nash and A.R.Collar 1953 *Quarterly Journal of Mechanics and Applied Mathematics* 6, 186-222. The effect of shear flexibility and rotary inertia on the bending vibrations of beams.
- [38] M.J.Fagan, *Finite Element Analysis*, USA,1992
- [39] ABAQUS, *ABAQUS/Standard user's manual version 5.8*, vol. I, II, III, Hibbitt, Karlsson & Sorensen, Inc., 1996.
- [40] ABAQUS, *ABAQUS/Theory version 5.8*, Hibbitt, Karlsson & Sorensen, Inc., 1996.
- [41] ABAQUS, *Getting Started with ABAQUS/Standard*, Hibbitt, Karlsson & Sorensen, Inc., 1996.
- [42] ABAQUS, *ABAQUS/Post manual version 5.8*, Hibbitt, Karlsson & Sorensen, Inc., 1996.
- [43] ABAQUS, *ABAQUS/CAE user's manual version 2*, Hibbitt, Karlsson & Sorensen, Inc., 1999.
- [44] ABAQUS, *ABAQUS/Viewer user's manual version 0*, Hibbitt, Karlsson & Sorensen, Inc., 1998.

- [45] Gere J.M., Timoshenko S.P., *Mechanics of Materials*, 4th Edition, PWS Publishing company, Boston, 1997.
- [46] Kalnins A., Dym C.L., *Vibration Beams, Plates and Shells*, Dowden Hutchinson & Ross, Inc., 1976.
- [47] Timoshenko S.P., *Vibration Problems in Engineering*, John Wiley & Sons, New York, 1974.
- [48] Rudoulph Szilard, *Theory and analysis of plates*, prentice hall, New Jersey, 1974.
- [49] Benson H. Tongue, *Principles of Vibration*, Oxford University, 1996.
- [50] Leissa A.W., "The Free vibration of Rectangular Plates," *Journal of Sound and Vibration*, vol. 31, no. 3, pp. 257-293, 1973.
- [51] Thomson W.T., *Theory of Vibration with Application*, Prentice Hall, New Jersey, 1993.
- [52] Dickinson S.M., "The Buckling and Frequency of Flexural of Rectangular Isotropic and Orthotropic Plates using Rayleigh's method," *Journal of Sound and Vibration*, vol. 61, pp. 1-8, 1978.
- [53] Leissa A.W., "Recent Research in Plate Vibrations, 1973-76: Classical Theory," *Shock and Vibration Digest*, vol. 9, no. 10, pp. 13-24, 1977.
- [54] Leissa A.W., "Recent Research in Plate Vibrations, 1973-76: Complicating Effects," *Shock and Vibration Digest*, vol. 9, no. 11, pp. 21-35, 1978.
- [55] Leissa A.W., "Plate Vibrations Research, 1976-80: Classical Theory," *Shock and Vibration Digest*, vol. 13, no. 9, pp. 11-22, 1981.
- [56] Leissa A.W., "Plate Vibrations Research, 1976-80: Complicating Effects," *Shock and Vibration Digest*, vol. 13, no. 10, pp. 19-36, 1981.
- [57] Leissa A.W., "Recent Studies in Plate Vibrations: 1981-85, Part I. Classical Theory," *Shock and Vibration Digest*, vol. 19, no. 2, pp. 11-18, 1987.
- [58] Leissa A.W., "Recent Studies in Plate Vibrations: 1981-85, Part II. Complicating Effects," *Shock and Vibration Digest*, vol. 19, no. 3, pp. 10-24, 1987.
- [59] Kim C.S and Dickinson S.M., "Improved Approximate Expressions for the Natural Frequencies of Isotropic and Orthotropic Rectangular Plates," *Journal of Sound and Vibration*, vol. 103, no. 1, pp. 142-149, 1985

- [60] Kim C.S., Young P.G., Dickinson S.M., "On the Flexural Vibration of Rectangular Plates Approached by using Simple Polynomials in the Rayleigh-Ritz method" *Journal of Sound and Vibration*, vol. 143, no. 3, pp. 379-394, 1990.
- [61] Zienkiewicz O.C., *The Finite Element Method*, McGraw-Hill, New York, 1977
- [62] Shames I.H. and Dym C.L., *Energy and Finite Element Method in Structural Mechanics*, McGraw-Hill, 1985.
- [63] Petyt M., *Introduction of Finite Element Vibration Analysis*, Cambridge University Press, Cambridge, 1990.
- [64] Bathe K.J., *Finite Element Procedures in Engineering Analysis*, Prentice Hall, Englewood Cliffs, New Jersey, 1982.
- [65] Gorman D.J., *Free Vibration Analysis of Beam and Shafts*, John Wiley & Sons, New York, 1975.
- [66] LMS International, *LMS CADA-X Modal Analysis Manual*, Interleuvenlaan 68, 3001 Heverlee (Leuven), Belgium, 1991.
- [67] Maarten Vet, "Natural Frequencies of Thin Rectangular Plates," *Machine Design Data Sheet*, pp.183-185, 1965.
- [68] Barton M.V., "Vibration of Rectangular and Skew Cantilever Plates," *Journal of Applied Mechanics*, vol. 18, no. 1, pp. 129-134, 1951.
- [69] Timoshenko S.P., Woinowsky-Krieger S., *Theory of Plates and Shells*, McGraw-Hill, London, 1959.
- [70] Soedel W., *Vibration of Shells and Plates*, Marcel Dekker, Hong Kong, 1981
- [71] Meirovitch L., *Analytical Methods in Vibrations*, Macmillan, New York, 1967
- [72] Meirovitch L., *Elements of Vibration Analysis*, McGraw-Hill, New York, 1986.
- [73] Bhat R.B., "Natural Frequencies of Rectangular-Plates with Free Edges-Comments," *Journal of Sound and Vibration*, vol. 111, no. 1, pp. 171-172, 1986.
- [74] Bhat R.B., "Author's reply on – Natural Frequencies of Rectangular Plates using Orthogonal Polynomials in Rayleigh-Ritz method", *Journal of Sound and Vibration*, vol. 108, no. 1, pp. 167-168, 1986.
- [75] Rossi R.E. and Laura P.A.A., "Symmetric and Anti-symmetric Normal modes of A Cantilever Rectangular Plate : Effect of Poisson's ratio and a Concentrated mass," *Journal of Sound and Vibration*, vol. 195, no. 1, pp. 142-148, 1996.

- [76] Englewood Cliffs, N.J., *The Student Edition of MATLAB [version 4]: the Ultimate Computing Environment*, Prentice-Hall, 1995.
- [77] Biran, Adrian B, *MATLAB for Engineers*, Addison-Wesley, 1995.
- [78] Mackerle-J, *Finite element vibration analysis of beams, plates and shells*
Shock-and-Vibration. vol.6, no.2; 1999; p.97-109.
- [79] Wong-CCK; Vardy-AE, *Finite prism analysis of plates and shells*,
International-Journal-for-Numerical-Methods-in-Engineering. vol.21, no.3; March
1985; p.529-41.
- [80] de-Arantes-e-Oliveira-ER, Completeness and convergence in the finite
element method, *Tecnica*. vol.33, no.403; Dec. 1970; p.109-24.

Appendix 1

Linear least-square method

Consider a numbers of points (r_i, m_i, y_i) . where $i = 1, 2, 3, \dots, n$. The equation that can represent these points can be obtained from the use linear least-square method.

Consider the equation of points is

$$y = (\alpha_0 + \beta_0 R + \gamma_0 R^2) + (\alpha_1 + \beta_1 R + \gamma_1 R^2)M + (\alpha_2 + \beta_2 R + \gamma_2 R^2)M^2 \quad (A1.1)$$

where $\alpha_0, \alpha_1, \alpha_2, \beta_0, \beta_1, \beta_2, \gamma_0, \gamma_1, \gamma_2$ are unknown variables.

The squared error for the Equation (A1.1) is

$$\sum e^2 = \left| y - (\alpha_0 + \beta_0 R + \gamma_0 R^2) - (\alpha_1 + \beta_1 R + \gamma_1 R^2)M - (\alpha_2 + \beta_2 R + \gamma_2 R^2)M^2 \right| \quad (A1.2)$$

Using the least-square method, unknown variables α_i, β_i and γ_i can be obtained by minimising their effects as follows

Differentiating Equation (A1.2) with respect to α_0 gives

$$\sum 2 \frac{\partial e}{\partial \alpha_0} = 2 \sum \left| y - (\alpha_0 + \beta_0 R + \gamma_0 R^2) - (\alpha_1 + \beta_1 R + \gamma_1 R^2)M - (\alpha_2 + \beta_2 R + \gamma_2 R^2)M^2 \right| (-1) = 0$$

$$\sum y = N\alpha_0 + \left(\sum R\right)\beta_0 + \left(\sum R^2\right)\gamma_0 + \left(\sum M\right)\alpha_1 + \left(\sum RM\right)\beta_1 +$$

$$\left(\sum R^2 M\right)\gamma_1 + \left(\sum M^2\right)\alpha_2 + \left(\sum RM^2\right)\beta_2 + \left(\sum R^2 M^2\right)\gamma_2 \quad (A1.3)$$

Differentiating Equation (A1.2) with respect to β_0 gives

$$\begin{aligned} \sum 2 \frac{\partial e}{\partial \beta_0} &= 2 \sum \left[y - (\alpha_0 + \beta_0 R + \gamma_0 R^2) - (\alpha_1 + \beta_1 R + \gamma_1 R^2) M - \right. \\ &\quad \left. (\alpha_2 + \beta_2 R + \gamma_2 R^2) M^2 \right] (-R) = 0 \\ \sum y R &= \left(\sum R\right)\alpha_0 + \left(\sum R^2\right)\beta_0 + \left(\sum R^3\right)\gamma_0 + \left(\sum RM\right)\alpha_1 + \left(\sum R^2 M\right)\beta_1 + \\ &\quad \left(\sum R^3 M\right)\gamma_1 + \left(\sum RM^2\right)\alpha_2 + \left(\sum R^2 M^2\right)\beta_2 + \left(\sum R^3 M^2\right)\gamma_2 \end{aligned} \quad (A1.4)$$

Differentiating Equation (A1.2) with respect to γ_0 gives

$$\begin{aligned} \sum 2 \frac{\partial e}{\partial \gamma_0} &= 2 \sum \left[y - (\alpha_0 + \beta_0 R + \gamma_0 R^2) - (\alpha_1 + \beta_1 R + \gamma_1 R^2) M - \right. \\ &\quad \left. (\alpha_2 + \beta_2 R + \gamma_2 R^2) M^2 \right] (-R^2) = 0 \\ \sum y R^2 &= \left(\sum R^2\right)\alpha_0 + \left(\sum R^3\right)\beta_0 + \left(\sum R^4\right)\gamma_0 + \left(\sum R^2 M\right)\alpha_1 + \left(\sum R^3 M\right)\beta_1 + \\ &\quad \left(\sum R^4 M\right)\gamma_1 + \left(\sum R^2 M^2\right)\alpha_2 + \left(\sum R^3 M^2\right)\beta_2 + \left(\sum R^4 M^2\right)\gamma_2 \end{aligned} \quad (A1.5)$$

Differentiating Equation (A1.2) with respect to α_1 gives

$$\begin{aligned} \sum 2 \frac{\partial e}{\partial \alpha_1} &= 2 \sum \left[y - (\alpha_0 + \beta_0 R + \gamma_0 R^2) - (\alpha_1 + \beta_1 R + \gamma_1 R^2) M - \right. \\ &\quad \left. (\alpha_2 + \beta_2 R + \gamma_2 R^2) M^2 \right] (-M) = 0 \end{aligned}$$

$$\begin{aligned}
\sum yM &= \left(\sum M\right)\alpha_0 + \left(\sum RM\right)\beta_0 + \left(\sum R^2M\right)\gamma_0 + \left(\sum M^2\right)\alpha_1 + \left(\sum RM^2\right)\beta_1 + \\
&\quad \left(\sum R^2M^2\right)\gamma_1 + \left(\sum M^3\right)\alpha_2 + \left(\sum RM^3\right)\beta_2 + \left(\sum R^2M^3\right)\gamma_2
\end{aligned}
\tag{A1.6}$$

Differentiating Equation (A1.2) with respect to β_1 gives

$$\begin{aligned}
\sum 2 \frac{\partial e}{\partial \beta_1} &= 2 \sum \left[y - (\alpha_0 + \beta_0 R + \gamma_0 R^2) - (\alpha_1 + \beta_1 R + \gamma_1 R^2)M - \right. \\
&\quad \left. (\alpha_2 + \beta_2 R + \gamma_2 R^2)M^2 \right] (-RM) = 0 \\
\sum yRM &= \left(\sum RM\right)\alpha_0 + \left(\sum R^2M\right)\beta_0 + \left(\sum R^3M\right)\gamma_0 + \left(\sum RM^2\right)\alpha_1 + \\
&\quad \left(\sum R^2M^2\right)\beta_1 + \left(\sum R^3M^2\right)\gamma_1 + \left(\sum RM^3\right)\alpha_2 + \left(\sum R^2M^3\right)\beta_2 + \\
&\quad \left(\sum R^3M^3\right)\gamma_2
\end{aligned}
\tag{A1.7}$$

Differentiating Equation (A1.2) with respect to γ_1 gives

$$\begin{aligned}
\sum 2 \frac{\partial e}{\partial \gamma_1} &= 2 \sum \left[y - (\alpha_0 + \beta_0 R + \gamma_0 R^2) - (\alpha_1 + \beta_1 R + \gamma_1 R^2)M - \right. \\
&\quad \left. (\alpha_2 + \beta_2 R + \gamma_2 R^2)M^2 \right] (-R^2M) = 0 \\
\sum yR^2M &= \left(\sum R^2M\right)\alpha_0 + \left(\sum R^3M\right)\beta_0 + \left(\sum R^4M\right)\gamma_0 + \left(\sum R^2M^2\right)\alpha_1 + \\
&\quad \left(\sum R^3M^2\right)\beta_1 + \left(\sum R^4M^2\right)\gamma_1 + \left(\sum R^2M^3\right)\alpha_2 + \left(\sum R^3M^3\right)\beta_2 + \\
&\quad \left(\sum R^4M^3\right)\gamma_2
\end{aligned}
\tag{A1.8}$$

Differentiating Equation (A1.2) with respect to α_2 gives

$$\begin{aligned}
\sum 2 \frac{\partial e}{\partial \alpha_2} &= 2 \sum \left| y - (\alpha_0 + \beta_0 R + \gamma_0 R^2) - (\alpha_1 + \beta_1 R + \gamma_1 R^2) M - \right. \\
&\quad \left. (\alpha_2 + \beta_2 R + \gamma_2 R^2) M^2 \right| (-M^2) = 0 \\
\sum y M^2 &= \left(\sum M^2 \right) \alpha_0 + \left(\sum R M^2 \right) \beta_0 + \left(\sum R^2 M^2 \right) \gamma_0 + \left(\sum M^3 \right) \alpha_1 + \\
&\quad \left(\sum R M^3 \right) \beta_1 + \left(\sum R^2 M^3 \right) \gamma_1 + \left(\sum M^4 \right) \alpha_2 + \left(\sum R M^4 \right) \beta_2 + \\
&\quad \left(\sum R^2 M^4 \right) \gamma_2
\end{aligned} \tag{A1.9}$$

Differentiating Equation (A1.2) with respect to β_2 gives

$$\begin{aligned}
\sum 2 \frac{\partial e}{\partial \beta_2} &= 2 \sum \left| y - (\alpha_0 + \beta_0 R + \gamma_0 R^2) - (\alpha_1 + \beta_1 R + \gamma_1 R^2) M - \right. \\
&\quad \left. (\alpha_2 + \beta_2 R + \gamma_2 R^2) M^2 \right| (-R M^2) = 0 \\
\sum y R M^2 &= \left(\sum R M^2 \right) \alpha_0 + \left(\sum R^2 M^2 \right) \beta_0 + \left(\sum R^3 M^2 \right) \gamma_0 + \left(\sum R M^3 \right) \alpha_1 + \\
&\quad \left(\sum R^2 M^3 \right) \beta_1 + \left(\sum R^3 M^3 \right) \gamma_1 + \left(\sum R M^4 \right) \alpha_2 + \left(\sum R^2 M^4 \right) \beta_2 + \\
&\quad \left(\sum R^3 M^4 \right) \gamma_2
\end{aligned} \tag{A1.10}$$

Differentiating Equation (A1.2) with respect to γ_2 gives

$$\begin{aligned}
\sum 2 \frac{\partial e}{\partial \gamma_2} &= 2 \sum \left| y - (\alpha_0 + \beta_0 R + \gamma_0 R^2) - (\alpha_1 + \beta_1 R + \gamma_1 R^2) M - \right. \\
&\quad \left. (\alpha_2 + \beta_2 R + \gamma_2 R^2) M^2 \right| (-R^2 M^2) = 0 \\
\sum y R^2 M^2 &= \left(\sum R^2 M^2 \right) \alpha_0 + \left(\sum R^3 M^2 \right) \beta_0 + \left(\sum R^4 M^2 \right) \gamma_0 + \left(\sum R^2 M^3 \right) \alpha_1 +
\end{aligned}$$

$$\begin{aligned} & \left(\sum R^3 M^3 \right) \beta_1 + \left(\sum R^4 M^3 \right) \gamma_1 + \left(\sum R^2 M^4 \right) \alpha_2 + \left(\sum R^3 M^4 \right) \beta_2 + \\ & \left(\sum R^4 M^4 \right) \gamma_2 \end{aligned} \quad (A1.11)$$

The Equations (A1.3) to (A1.11) can be expressed in matrix form as ;

$$AB = C \quad (A1.12)$$

Where the vectors B and C and the matrix A are defined on the next page.

The vector B which gives the unknown variables α_i, β_i and γ_i can be obtained from Equation (A1.12) by matrix method as

$$B = A^{-1}C \quad (A1.13)$$

The least-squares method outlined above gives the best estimate of the unknown parameters from the available data.

$$A = \begin{bmatrix} N & \sum R & \sum R^2 & \sum R^3 & \sum RM & \sum R^2M & \sum R^3M & \sum R^4M & \sum R^2M^2 & \sum R^3M^2 & \sum R^4M^2 & \sum RM^2 & \sum R^2M^2 & \sum R^3M^2 & \sum R^4M^2 & \sum RM^3 & \sum R^2M^3 & \sum R^3M^3 & \sum R^4M^3 & \sum RM^4 & \sum R^2M^4 & \sum R^3M^4 & \sum R^4M^4 \\ \sum R & \sum R^2 & \sum R^3 & \sum RM & \sum R^2M & \sum R^3M & \sum RM^2 & \sum R^2M^2 & \sum R^3M^2 & \sum R^4M^2 & \sum RM^3 & \sum R^2M^3 & \sum R^3M^3 & \sum R^4M^3 & \sum RM^4 & \sum R^2M^4 & \sum R^3M^4 & \sum R^4M^4 \\ \sum R^2 & \sum R^3 & \sum R^4 & \sum RM^2 & \sum R^2M^2 & \sum R^3M^2 & \sum R^4M^2 & \sum RM^3 & \sum R^2M^3 & \sum R^3M^3 & \sum R^4M^3 & \sum RM^4 & \sum R^2M^4 & \sum R^3M^4 & \sum R^4M^4 \\ \sum RM & \sum R^2M & \sum R^3M & \sum RM^2 & \sum R^2M^2 & \sum R^3M^2 & \sum R^4M^2 & \sum RM^3 & \sum R^2M^3 & \sum R^3M^3 & \sum R^4M^3 & \sum RM^4 & \sum R^2M^4 & \sum R^3M^4 & \sum R^4M^4 \\ \sum R^2M & \sum R^3M & \sum R^4M & \sum RM^3 & \sum R^2M^3 & \sum R^3M^3 & \sum R^4M^3 & \sum RM^4 & \sum R^2M^4 & \sum R^3M^4 & \sum R^4M^4 \\ \sum RM^2 & \sum R^2M^2 & \sum R^3M^2 & \sum RM^3 & \sum R^2M^3 & \sum R^3M^3 & \sum R^4M^3 & \sum RM^4 & \sum R^2M^4 & \sum R^3M^4 & \sum R^4M^4 \\ \sum R^2M^2 & \sum R^3M^2 & \sum R^4M^2 & \sum RM^4 & \sum R^2M^4 & \sum R^3M^4 & \sum R^4M^4 \\ \sum RM^3 & \sum R^2M^3 & \sum R^3M^3 & \sum RM^4 & \sum R^2M^4 & \sum R^3M^4 & \sum R^4M^4 \\ \sum R^2M^3 & \sum R^3M^3 & \sum R^4M^3 & \sum RM^4 & \sum R^2M^4 & \sum R^3M^4 & \sum R^4M^4 \\ \sum RM^4 & \sum R^2M^4 & \sum R^3M^4 & \sum R^4M^4 \end{bmatrix}$$

$$C = \begin{bmatrix} \sum y & \sum yR & \sum yR^2 & \sum yM & \sum yRM & \sum yR^2M & \sum yM^2 & \sum yRM^2 & \sum yR^2M^2 \end{bmatrix}$$

$$B = \begin{bmatrix} \alpha_0 & \beta_0 & \gamma_0 & \alpha_1 & \beta_1 & \gamma_1 & \alpha_2 & \beta_2 & \gamma_2 \end{bmatrix}$$

Appendix 2

Solution of the Timoshenko beam equations for the free vibration of a clamped-clamped and free-free boundary conditions

The coupled equations of free motion from Timoshenko beam theory are given by:

$$\left. \begin{aligned} \kappa \frac{\partial}{\partial x} AG \left(\psi + \frac{\partial w}{\partial x} \right) &= \rho A \frac{\partial^2 w}{\partial t^2} \\ \kappa AG \left(\psi + \frac{\partial w}{\partial x} \right) - \frac{\partial}{\partial x} \left(EI \frac{\partial \psi}{\partial x} \right) &= -\rho I \frac{\partial^2 \psi}{\partial t^2} \end{aligned} \right\} \quad (\text{A2.1})$$

From Equation (A2.1), the frequency equation for the vibration of a **free-free** beam is [7]

$$2 + [(\lambda_1 \alpha_1 / \lambda_2 \alpha_2) - (\lambda_2 \alpha_2 / \lambda_1 \alpha_1)] \sinh \lambda_1 L \sin \lambda_2 L - 2 \cosh \lambda_1 L \cos \lambda_2 L = 0 \quad (\text{A2.2})$$

and for **clamped-clamped** beams [15]

$$2 + [(\alpha_2^2 \lambda_1^2 - \alpha_1^2 \lambda_2^2) / \alpha_1 \alpha_2 \lambda_1 \lambda_2] \sinh \lambda_1 L \sin \lambda_2 L - 2 \cosh \lambda_1 L \cos \lambda_2 L = 0 \quad (\text{A2.3})$$

$$\text{where} \quad \alpha_{1,2} = \left(\frac{\rho \omega^2}{\kappa G} \pm \lambda_{1,2}^2 \right) \quad (\text{A2.4})$$

$$\lambda_{1,2}^2 = \sqrt{\left(\frac{\beta^4 \omega^4}{4} + \delta \omega^2 \right)} \mp \frac{\beta^2 \omega^2}{2} \quad (\text{A2.5})$$

$$\delta = \frac{\rho}{E} \left(\frac{A}{I} - \frac{\rho \omega^2}{\kappa G} \right) \quad (\text{A2.6})$$

$$\beta^2 = \frac{\rho}{E} \left(1 + \frac{E}{\kappa G} \right) \quad (\text{A2.7})$$

L = beam length

Consider a rectangular section aluminum beam of length $L = 0.5$ m., breath $b = 0.5$ m and thickness $t = 0.005$ m, $\rho = 2700$ kg/m³, $\nu = 0.33$, $E = 70 \times 10^9$ N/m², $G = 26.3 \times 10^9$ N/m², $\kappa = 5/6$. Substituting these parameters in Equations (A2.6), (A2.7) yields;

$$\begin{aligned} \delta &= \frac{\rho}{E} \left(\frac{A}{I} - \frac{\rho \omega^2}{\kappa G} \right) = \frac{2700}{70 \times 10^9} \left[\frac{bt}{\frac{1}{12}bt^3} - \frac{2700\omega^2}{\frac{5}{6}(26.3 \times 10^9)} \right] \\ &= 0.0185136 - 4.751 \times 10^{-15} \omega^2 \\ \beta^2 &= \frac{\rho}{E} \left(1 + \frac{E}{\kappa G} \right) = \frac{2700}{70 \times 10^9} \left[1 + \frac{70 \times 10^9}{\frac{5}{6}(26.3 \times 10^9)} \right] = 1.618 \times 10^{-7} \end{aligned}$$

The obtained value for δ, β^2 was then substituted in to Equations (A2.4) and (A2.5) yields;

$$\alpha_{1,2} = 4.2294 \times 10^{-8} \omega^2 \mp \sqrt{1.7948 \times 10^{-15} \omega^4 + 0.0185136 \omega^2}$$

$$\lambda_2^2 = \sqrt{1.7948 \times 10^{-15} \omega^4 + 0.0185136 \omega^2} \mp 0.8090 \times 10^{-7} \omega^2$$

This was then substituted in to Equations (A2.2) and (A2.3), for both free-free and clamped-clamped boundary conditions.

Since L is constant and λ_1, λ_2 are function of ω , therefore Equations (A2.2) and (A2.3) is a function of ω . The solution for these equations can be obtained by using of a MATLAB program using command “fzero”.

The FZERO is a command in MATLAB is used to find the zeros of a function of one variable. FZERO(F,X), where F is a function and X is a scalar value, uses X as a starting guess. FZERO looks for an interval containing a sign change for F and containing X. If no such interval is found, NaN is returned. In this case, the search terminates when the search interval is expanded until an Inf, NaN, or complex value is found. [48,49]

Equations (A2.2) and (A2.3) is in the form $f(\omega) = 0$. Therefore we can use “fzero” command to get the solution for Equations (A2.2) and (A2.3). The angular frequencies from Euler beam equation from Table (2.2) and Table (2.3) for free-free and clamped-clamped respectively shown in Chapter 2 were used as the guess values. The guess values and roots of Equations (A2.2) and (A2.3) is shown in Table A 2.1 and Table A 2.2

Table A 2.1 *Guess values and roots of Equation (A2.2) free-free.*

No.	Guess values, x	Roots
1	22.37	22.35
2	61.67	61.58
3	120.91	120.59
4	199.88	199.04
5	298.58	296.76
6	417.03	413.53
7	555.21	549.08
8	713.14	703.12
9	890.81	875.3
10	1088.01	1065.26

Table A 2.2 *Guess values and roots of Equation (A2.3) clamped-clamped.*

No.	Guess values, x	Roots
1	22.37	22.35
2	61.67	61.54
3	120.91	120.47
4	199.88	198.76
5	298.58	296.29
6	417.03	412.75
7	555.21	547.89
8	713.14	701.40
9	890.81	872.92
10	1088.01	1062.09